

# **Integrated Design Approach for Responsive Solar-Shadings in Double Skin Facades in Hot Arid Climate**

Yomna Saad Abdelraouf ElGhazi

This thesis submitted in fulfilment candidature for Doctor of Philosophy  
School of Architecture, Planning, and Landscape  
Newcastle University  
December 2020





## ABSTRACT

To deliver climate adaptive architecture, current trends in architecture are directed towards *dynamic and responsive building skins*. '*Responsive building skin*' is used to describe the ability of building envelopes to adapt in real time in response to external environmental conditions. Recent attention has focused on '*soft robotics*' approach which uses soft and/or extensible materials to deform with muscle-like actuation, mimicking biological systems. Material embedded actuation can autonomously alter shading systems' morphology stimulated by external environmental conditions. Passively thermally-activated shading systems offer responsive actuation by solar-radiation and stratified hot air in a double skin façade (DSF) without recourse to energy consuming systems.

This research identifies the intersection between bio-inspiration, folding principles and smart materials to integrate the underlying mechanisms in responsive solar-shading systems and assesses their environmental performance. The thesis proposes an interdisciplinary mixed methodology linking hands-on experimentation with environmental performance simulation of responsive building skins. '*Practice-led approach*' is used to explore the design potential of responsive systems using smart materials. '*Computational Fluid Dynamics*' (CFD) numerical methods are used to measure the impact of responsive solar-shading systems on multiple environmental factors in a DSF cavity. This helps the design decisions, selection and customisation of smart materials. Hands-on experimentation is used to explore various prototypes, leading to the selection of a folded prototype, to be simulated for environmental performance. Solar-shading systems are tested within a DSF, in an hot arid climate. Flat and folded solar-shading devices are installed in a DSF cavity with three aperture sizes (30%, 50% & 70%) to represent the responsive system states. Point-in-time simulations are carried at 9:00 am, 12:00 pm and 15:00 pm in peak summer and winter day.

The developed analytical design framework presents different design parameters for responsive solar-shading systems to guide decision-making in research of climate actuated smart shading systems.

**Keywords:** Responsive skins, Adaptive facades, Soft robotics, Bio-inspiration, Origami, Deployable structures, Actuation, Smart materials, Shape memory alloys, Double skin facades, Energy efficiency, Digital simulation, CFD Modelling.



## ACKNOWLEDGMENT

To deliver climate adaptive architecture, current trends in architecture are directed towards dynamic and responsive building skins. 'Responsive building skin' is used to describe the ability of the building envelope to adapt over time in response to external environmental conditions. Recent attention has focused on the 'soft robotics' approach which uses soft and/or extensible materials to deform and extend with muscle-like actuation, mimicking biological systems. Material embedded actuation can alter the shading system's morphology under external stimulation and adapt autonomously to their respective environmental conditions. Passively thermally-activated systems offer actuation for such systems without recourse to mechanically energy consuming actuation systems.

This research identifies the intersection between bio-inspiration, origami principles and smart materials to integrate the underlying mechanisms in responsive solar-shading systems and assesses their environmental performance. The thesis proposes an interdisciplinary mixed methodology to explore the potentials of responsive building skins within their context of operation. A 'Practice-led approach' is used to explore the design potential of responsive systems using smart materials. 'Computational Fluid Dynamics' (CFD) numerical methods is used to measure the impact of responsive solar-shading systems on multiple environmental factors and helps the design decisions, selection and customisation of smart materials. The hands-on experimentation is used to explore various prototypes, leading to the selection of a folded prototype, to be simulated for its environmental performance. Solar-shading systems are tested within a double skin façade DSF, in Cairo, Egypt. Flat and folded solar-shading devices are installed in the DSF cavity and three aperture sizes (30%, 50% & 70%) are modelled to represent the responsive system states. Point-in-time simulations are carried at 9:00 am, 12:00 pm and 15:00 pm in peak summer and peak winter day.

The thesis reflects on design experiments and CFD analysis to develop a design decision making framework. It presents different design parameters for responsive solar-shading systems to guide researchers in a methodology to study climate actuated smart shading systems for future development.



To My Mum  
For all your support and patience

## TABLE OF CONTENTS

ABSTRACT .....	iii
ACKNOWLEDGMENT .....	v
TABLE OF CONTENTS .....	viii
ABBREVIATIONS .....	xiv
NOMENCLATURE .....	xvi
Chapter 1 . INTRODUCTION .....	1
1.2.    Problem Statement .....	3
1.3.    Aims of the Research .....	3
1.4.    Structure of the thesis and chapters .....	4
Chapter 2 . THE CONTEXT FOR RESPONSIVE SOLAR-SHADING SYSTEMS (Literature Review) .....	10
2.1.    Introduction .....	10
2.2.    Overview - Why Responsive Solar-Shading Devices? .....	12
2.2.1.    Definitions, origins and principles .....	17
2.2.2.    Control of adaptive systems .....	21
2.2.3.    Responsive solar shading systems: State of the art .....	24
2.2.4.    Soft robotics .....	32
2.3.    Smart Materials .....	35
2.3.1.    Smart materials classifications .....	37
2.3.2.    Shape memory materials (SMMs) .....	39
2.3.3.    Shape memory alloys (SMAs) .....	40
2.3.4.    The fixation of active and passive materials .....	42
2.3.4.1.    Bending type .....	42
2.3.4.2.    Hinge Type .....	45
2.4.    Bio-Inspired Approach .....	50
2.4.1.    Biomimetic and bioinspired approaches for efficient movement .....	51
2.4.2.    Actuation mechanisms in Plant Movements .....	52
2.4.2.1.    External loads .....	53
2.4.2.2.    Hydraulic mechanisms .....	53
2.4.2.3.    Elastic instabilities and snapping motion .....	54
2.4.3.    Elastic kinetic structures .....	56
2.4.4.    Applications of kinetic solar-shadings .....	57
2.5.    Origami-Inspired Kinetics .....	60
2.5.1.    Folding principles: Straight and Curved Folding .....	61
2.5.2.    Self-folding origami .....	65

2.6.	The Double Skin Façade (DSF) .....	69
2.6.1.	Overview – double skin façade (DSF) .....	69
2.6.2.	DSF classification .....	71
2.6.3.	Cavity-Integrated Shading Devices in DSF .....	72
2.7.	Conclusion .....	73
Chapter 3 . THE METHODOLOGY .....		76
3.1.	Introduction.....	76
3.2.	Practice-Led Approach .....	79
3.2.1.	Practice-related research .....	80
3.2.2.	Hands-on exploration and Material tinkering .....	82
3.3.	Phases of Experimentation .....	85
3.3.1.	Hands-on experimentation and Material tinkering.....	85
3.3.2.	Teaching experiences in designing with kinetic materials .....	89
3.4.	Simulation-Based Method.....	93
3.4.1.	Simulation of DSF .....	94
3.4.2.	Simulation of Adaptive facade .....	96
3.5.	Phases of Building Performance Simulation .....	97
3.5.1.	Environmental Design and Modelling: Validation work (Chapter 5).....	99
3.5.2.	The Simulation of Integrated DSF (chapter 6) .....	102
3.6.	The Design Framework.....	104
3.7.	Conclusion .....	105
Chapter 4 . COMPONENT DESIGN AND PROTOTYPING .....		107
4.1.	Introduction.....	107
4.2.	Forms.....	108
4.3.	Materiality: Passive Light-Weight Materials .....	112
4.4.	Materiability: Active/Smart Material .....	116
4.4.1.	The SMM training .....	116
4.5.	Actuation: Fixations of Active and Passive Materials.....	119
4.6.	System Reversibility .....	123
4.6.1.	Gravity .....	124
4.6.2.	Elastic materials.....	125
4.6.3.	Coupling passive and active elements .....	126
4.6.4.	Two-way training.....	128
4.6.5.	Time.....	128
4.7.	Panelization and Grouping Arrangement.....	130
4.8.	Palette of Models .....	131

4.8.1.	<i>Exploration One: Umbrella units</i>	132
4.8.2.	<i>Exploration Two: Curved folding (two/three/four)</i>	137
4.8.3.	<i>Exploration Three: Single Curved-crease Folding</i>	141
4.8.4.	<i>Exploration Four: Deformed Cylinder</i>	148
4.9.	Experimentation Workflow	152
4.10.	Teaching Experience: Soft Robotics as Design Practice	154
4.10.1.	<i>Prototype A: Sliding hexagons</i>	157
4.10.2.	<i>Prototype B: Folded Flowers</i>	159
4.10.3.	<i>Prototype C: Folded Fins</i>	161
4.11.	Aperture Size as a Main Feature of Responsive Facade	164
4.12.	Form as a Main Feature of Responsive Façade	166
4.13.	Conclusion	169
Chapter 5 .	ENVIRONMENTAL DESIGN AND MODELLING	173
5.1.	Introduction	173
5.2.	Computational Fluid Dynamic Modelling	174
5.2.1.	<i>The nature of coupled fluid dynamics and heat transfer</i>	175
5.2.2.	<i>Method validation</i>	179
	• Validation Case 1: Safer et al. (2005)	180
	• Validation Case 2: Manz et al. (2004)	180
	• Validation Case 3: Mei et al. (2007)	181
5.3.	Case of Mei et al. (2007)	183
5.3.1.	<i>The geometrical model (level of geometrical complexity parameter 3)</i>	187
5.3.2.	<i>Computational domain Size (Parameter 2)</i>	189
5.3.3.	<i>Turbulence Model (parameter 4)</i>	191
5.3.4.	<i>Radiation Model (Parameter 5)</i>	193
5.3.5.	<i>Solar Load Model (solar representation- Parameter 1)</i>	196
5.4.	The Computational Mesh	198
5.4.1.	<i>Independence of Mesh Size</i>	200
5.5.	Numerical Modelling	202
5.5.1.	<i>Solution Method's Set-up</i>	202
5.5.2.	<i>Computational Boundary and Operating Conditions</i>	203
5.5.3.	<i>Materials</i>	206
5.6.	Results	207
5.6.1.	<i>Non-shaded cavity</i>	207
5.6.1.1.	Simulation 1: Solar simulator representation	207
5.6.1.2.	Simulation 2: Domain Size	209



5.6.1.3.	Simulation 3: Radiation model .....	210
5.6.1.4.	Simulation 4: Turbulence model .....	211
5.6.1.5.	Simulation 5: Level of complexity .....	211
5.6.1.6.	Summary .....	212
5.6.2.	<i>Integrated Shaded cavity</i> .....	215
5.7.	Conclusion .....	217
Chapter 6 . INTEGRATED DESIGN AND SIMULATION .....		221
6.1.	Introduction.....	221
6.1.1.	<i>Overview Climate of Cairo City</i> .....	223
6.1.2.	<i>Location and Time conditions</i> .....	225
6.2.	Case Description.....	225
6.2.1.	<i>Geometrical model</i> .....	228
6.2.2.	<i>The shading devices</i> .....	231
6.2.3.	<i>The Materials</i> .....	235
6.3.	The Meshing.....	236
6.3.1.	<i>Mesh independence test</i> .....	239
6.4.	Numerical Modelling.....	240
6.4.1.	<i>Boundary Conditions</i> .....	241
6.4.2.	<i>Solver set-up</i> .....	243
6.5.	Results .....	244
6.5.1.	<i>Scenario 1: Non-shaded DSF</i> .....	244
6.5.1.1.	DSF cavity width .....	244
6.5.1.2.	DSF Façade layering.....	247
6.5.1.3.	DSF domain size.....	247
6.5.1.4.	Non-shaded DSF with time.....	250
6.5.2.	<i>Scenario 2: Flat solar shading</i> .....	254
6.5.2.1.	Temperature Contours.....	255
6.5.2.2.	Airflow rates and Velocity Profiles .....	259
6.5.2.3.	Heat Flux.....	262
6.5.3.	<i>Scenario 3: Origami Folded solar-shading</i> .....	264
6.5.3.1.	Temperature Contours.....	264
6.5.3.2.	Airflow rates and velocity profiles.....	266
6.5.3.3.	Heat Flux.....	268
6.5.4.	<i>Analysis of solar shading</i> .....	268
6.6.	Conclusion .....	275
Chapter 7 . THE DESIGN FRAMEWORK .....		278

7.1.	Introduction.....	278
7.2.	The Design Framework.....	278
7.3.	Experimental Feedback .....	281
7.3.1.	<i>Form and materiality</i> .....	283
7.3.2.	<i>Materiality and actuation</i> .....	284
7.3.3.	<i>Actuation and panelization</i> .....	285
7.3.4.	<i>Panelization and form</i> .....	285
7.3.5.	<i>Materiality and panelization</i> .....	286
7.3.6.	<i>Form and actuation</i> .....	286
7.3.7.	<i>Key factors of experimental performance</i> .....	286
7.4.	Environmental Feedback.....	287
7.4.1.	<i>Airflow analysis and form</i> .....	288
7.4.2.	<i>Airflow analysis and panelization</i> .....	288
7.4.3.	<i>The internal thermal solar gains and materiality</i> .....	288
7.4.4.	<i>The internal thermal solar gains and form</i> .....	288
7.4.5.	<i>The internal thermal solar gains and panelization</i> .....	288
7.4.6.	<i>Solar shading temperature analysis and panelization</i> .....	289
7.4.7.	<i>Solar-shading thermal analysis and actuation</i> .....	289
7.4.8.	<i>Solar-shading thermal analysis and materiality</i> .....	289
7.5.	Conclusion .....	289
Chapter 8 : CONCLUSIONS AND FUTURE OUTLOOK .....		291
8.1.	Introduction.....	291
8.2.	Summary.....	291
8.2.1.	<i>Material-based design approach for responsive solar shading systems (objective 1)</i> .....	291
8.2.2.	<i>The mixed interdisciplinary methodology (objective 2)</i> .....	293
8.2.3.	<i>Hands-on exploration for responsive solar shading components (objective 3)</i> .....	294
8.2.4.	<i>CFD as a tool for assessing integrated DSF (objective 4)</i> .....	298
8.2.5.	<i>Simulation of DSF integrated with responsive solar shading system (objective 5)</i> .....	299
8.2.6.	<i>The design framework (objective 6)</i> .....	302
8.3.	Limitations of the Study.....	304
8.4.	Future Work.....	306
8.4.1.	<i>Materiality and Prototyping</i> .....	306
8.4.2.	<i>Overview of potential applications</i> .....	307
8.4.3.	<i>New software tool</i> .....	308
APPENDICES.....		312
<i>APPENDIX A: Koppen Climate Classification Map World (Beck et al., 2018)</i> .....		313

<i>APPENDIX B: MArch Vertical Technology Studios 2018-19 .....</i>	<i>314</i>
<i>APPENDIX C: Temperature Range of Cairo, Egypt.....</i>	<i>319</i>
<i>APPENDIX D: The Nature of Coupled Fluid Dynamics and Heat Transfer.....</i>	<i>319</i>
<i>APPENDIX E: The Mathematical Model.....</i>	<i>322</i>
<i>APPENDIX F : Surface Temperatures for Flat-shaded Cavities vs Non-shaded.....</i>	<i>325</i>
<i>APPENDIX G: Convergence of Non-shaded Mei et al. (2007) case .....</i>	<i>328</i>
<i>APPENDIX H: Convergence of Case A (non-shaded case) in Cairo, Egypt.....</i>	<i>329</i>
<i>REFERENCES .....</i>	<i>330</i>

## ABBREVIATIONS

Abbreviation	Definition
2D 3D	Two-, Three-Dimensional
BIST	Building- integrated solar thermal
BPS	Building Performance Simulation
BS	Building Simulation
CFD	Computational Fluid Dynamics
CPU	Central Processing Unit
DE	Dielectric elastomers
DES	Detached-eddy simulation
DIY	Do it yourself
DO	Discrete Ordinate Radiation Model
DSF	Double Skin Facades
DTRM	Discrete Transfer Radiation Model
EAP	Electroactive polymers
ES	Energy simulation
LES	Large-eddy simulation
LTR	Length-Thickness Ratio
P1	P1 Radiation Model
PCM	Phase change material
PISO	Pressure-Implicit with Splitting of Operators
PV	photovoltaics
PVT	Photovoltaic/Thermal
RANS	Reynolds averaged Navier-Stokes
RNG	Re-Normalisation Group
RSD	Responsive solar-shading device
RTEs	Radiative intensity transport equations
S2S	Surface-to-surface
SCM	Shape change materials
SIMPLE algorithm	Semi-Implicit Method for Pressure Linked Equations
SMA	Shape memory alloys

<b>Abbreviation</b>	<b>Definition</b>
SME	Shape memory effect
SMH	Shape memory hybrids
SMM	Shape memory materials
SMP	Shape memory polymers
SRM	Stimuli-Responsive Materials
TB	Thermobimetals
TWSMA	Two-way shape memory alloy
URF	under relaxation factor
WWR	Window-To-Wall Ratio

## NOMENCLATURE

<b><math>\rho</math></b>	Air density ( $\text{kg m}^{-3}$ )
<b><math>V</math></b>	Air velocity, (m/s)
<b><math>C_p</math></b>	Specific heat capacity ( $\text{J/kg}\cdot\text{K}$ )
<b><math>k</math></b>	Turbulent kinetic energy
<b><math>\epsilon</math></b>	Turbulence dissipation rate
<b><math>Nu</math></b>	Nusselt Number (Dimensionless Number)
<b><math>P</math></b>	Pressure (Pascal Pa)
<b><math>Ra</math></b>	Rayleigh Number (Dimensionless Number)
<b><math>Re</math></b>	Reynolds Number (Dimensionless Number)
<b><math>T</math></b>	Static temperature (K)
<b><math>cp</math></b>	Specific heat ( $\text{J/K/kg}$ )
<b><math>\sigma</math></b>	Stefan-Boltzmann constant
<b><math>h</math></b>	Heat transfer coefficient $\text{W}/(\text{m}^2\text{K})$
<b><math>k</math></b>	Thermal conductivity ( $\text{W}/(\text{m}\cdot\text{K})$ )
<b><math>q</math></b>	Heat flux ( $\text{W}/\text{m}^2$ )
<b><math>G_k</math></b>	Generation of K due to mean velocity gradients
<b><math>G_b</math></b>	Generation of K due to buoyancy
<b><math>\rho\epsilon</math></b>	Dissipation of k
<b><math>Y_M</math></b>	The contribution of the fluctuating dilatation in compressible turbulence to the overall dissipation rate
<b><math>\alpha^k</math></b>	The inverse effective Prandtl numbers k
<b><math>\alpha^\epsilon</math></b>	The inverse effective Prandtl numbers $\epsilon$
<b><math>Y_+</math></b>	Non-dimensional wall coordinate







## Chapter 1 . INTRODUCTION

The urgent demand for more energy-efficient and sustainable architecture is leading to a growing interest in adaptive skins that can adapt to changing environmental conditions (Fiorito et al., 2016; Kolarevic & Parlac, 2015; Wigginton & Harris, 2013). The term 'Adaptive skins' refers to building envelopes capable of configuration changes due to their geometrical, material and mechanical properties (Adrover, 2015). Recent literature shows that most environmental adaptive skins are based on mechanically operated systems. A mechanical system, such as implemented in the facades of Institut du Monde Arabe in Paris (Figure 1-1) and Al Bahar Towers in Abu Dhabi (Figure 1-2), has the disadvantage of being complex to build, difficult to maintain and requires high energy consumption for the operation of its parts (Karanouh & Kerber, 2015; Meagher, 2015; Reichert, Menges, & Correa, 2015). Recent attention has focused on '*soft robotics*' approach to simplify mechanical designs. '*Soft robotics*' is defined as an approach which uses soft and/or extensible materials that can deform with muscle-like actuation (Bengisu & Ferrara, 2018). Designers, architects and researchers can use *smart materials*, *bio-inspiration* and *origami principles* to move the parts to reduce energy consumption.

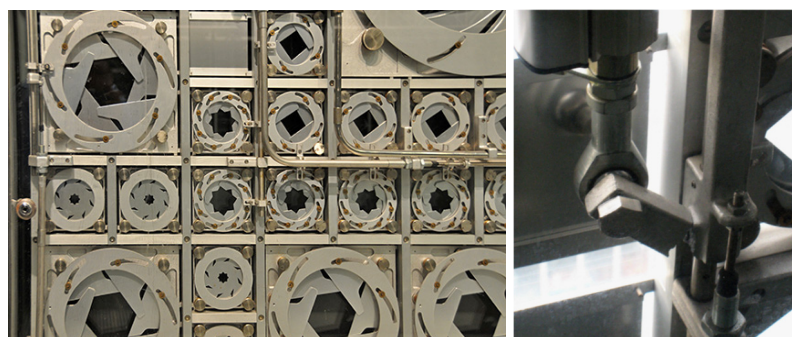


Figure 1-1: Mechanised sunshades at the Institut du Monde Arabe and the damage to the arms in the mechanical diaphragms.

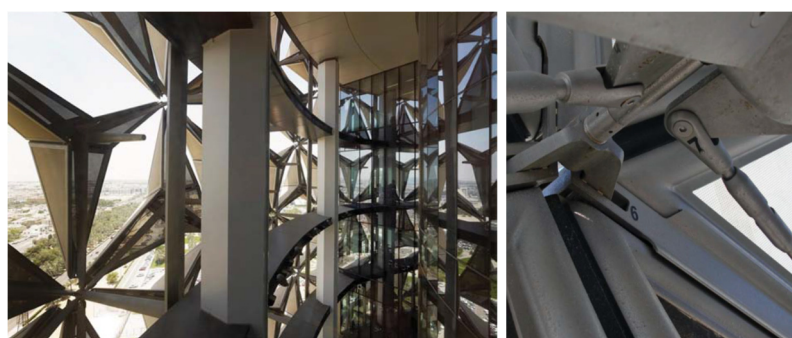


Figure 1-2: The solar screen of the Al-Bahr Towers as seen from the inside and complexity of the mechanical system.

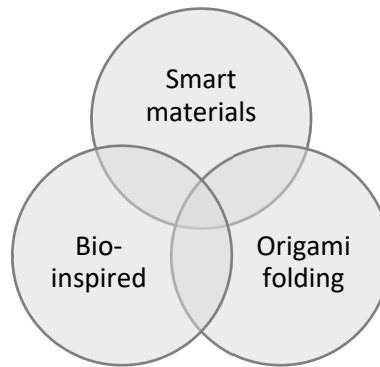
By studying how plant species take advantage of mechanical and structural gradients to perform mobility with minimal energy use, it is possible to learn how to integrate these properties into the design of adaptive skins. Plant tissues can adapt to constantly changing environmental conditions. This is achieved through iterative feedback loops, which sense, record, inform and instruct the fibre composite to alter their current configuration towards an optimised one (Mingallon & Ramaswamy, 2012).

Origami can transform planar sheets to be reconfigurable structures, which has applications in the field of robotics and deployable structures (Edwin, Darren, Richard, & Dimitris, 2014). The generative techniques for soft robotics can draw inspiration from origami principles due to their predictability, controllability, and scalability (Adrover, 2015). They are easily fabricated, assembled, stored, and morphed. Thus origami-inspired structures have a high potential for adaptive skins.

Moreover, Investigation of new responsive smart materials could be an efficient replacement to simplify mechanical actuation (Reichert et al., 2015). Material embedded actuation can alter their morphology under external stimulation and adapt autonomously to their respective environmental conditions (Reichert et al., 2015; Schaeffer & Vogt, 2010). Smart materials have reversible properties which can be triggered by external stimulus such as temperature (Schaeffer & Vogt, 2010). For example, shape memory alloys (SMAs) have great potential to act as actuators to design passive low-tech responsive skins using unsophisticated technology. The activation temperatures of SMAs can be achieved in hot arid climates as a result of the heat transfer through direct solar radiation and convection which can actuate responsive building skins or solar shading systems (Doupoti, Greenberg, & Karatzas, 2010; Fiorito et al., 2016). Thermally activated systems have a high potential for application in hot climates such as Cairo, Egypt, especially when integrated with building skins to moderate temperature and block significant solar radiation. Cairo, as a case study, has a climatic profile and thermal comfort requirements similar to other cities in hot arid climates, as attached in Appendix A, which can use the thermally activated systems.

Materials with embedded responsiveness are still an area of active research, especially on the architectural scale. New material systems in architecture have always produced new design opportunities. The amount of realised architectural projects that use smart materials to propose alternatives to static or mechanised solar-shading systems are somewhat limited.

The research is an extension, to Decker Yeadon (Premier, 2012) and Doris Sung (Sung, 2016) approach to construct responsive solar-shading systems using material-based actuation. Hence, the research is looking at the available resources of architectural projects and the soft robotics' inspiring approach. The thesis proposes an interdisciplinary mixed methodology to explore the potentials of responsive solar shading systems realised with smart materials and understand their behaviour and performance within their context of operation experimentally and environmentally. The thesis tests their potential as a replacement for complex mechanical systems that use electrical input. It identifies the intersection between bio-inspiration, origami principles and smart materials to integrate the underlying mechanisms in responsive solar-shading systems as shown in Figure 1-3 and assess their environmental performance by conducting Computational fluid dynamics (CFD) numerical modelling.



*Figure 1-3: Areas of Intersections for Soft Robotics*

## **1.2. Problem Statement**

The urgent demand for more energy-efficient and sustainable architecture is leading to a growing interest in “Adaptive Skins” that can adapt to changing environmental conditions. The current kinetic mechanical systems rely excessively on technical solutions that are complex to build, difficult to maintain and require high energy input. Responsive systems realised with active materials can replace complex mechanical designs. However, their novelty results in a lack of applied knowledge in the architectural field. Thus, designers and researchers struggle to predict the immanent dynamic activity of smart materials fully. Moreover, architectural research into active materials is done separately from their potential context of operation. All these aspects need to be integrated and analysed relatively to provide a clear design framework that designers can refer to.

## **1.3. Aims of the Research**

The aim of this study is to create a research framework to explore the shading capabilities of a passive environmentally responsive solar shading systems using smart

actuators. Through the design of a prototype as a medium, the study aims to test the performance of the system using building performance simulation and material tinkering.

## **Objectives**

1. To triangulate the intersection between bio-inspiration, folding principles, material science development (smart materials), to study the underlying mechanisms and generative techniques of responsive reversible motion. To explore folding and bio-inspired principles as a source of inspiration that may guide the design of responsive modular systems which respond to environmental stimuli.
2. To explore the mixed interdisciplinary methodology of experimentation, and CFD simulations and investigate how their integration help in the design and assessment of the responsive solar-shading systems.
3. To explore the potential of smart materials, precisely shape memory materials (SMM), in order to understand their immanent dynamic activity, and use bio-inspiration and folding principles to alter complex deployable forms using simple actuation strategies. To test various deployable forms, gain a detailed understanding of smart material behaviour and develop an actual prototype system that can be used in further experiments.
4. To set guidelines for the numerical modelling setup of a DSF integrated with solar-shading system and validate this modelling setup against an experimental case.
5. To environmentally assess, the responsive solar-shading system performance within their potential context of operation and use environmental feedback as a guide to customise the material and design of the responsive system; form and aperture size (Chapter 6).
6. To develop a framework for the design of responsive solar-shading systems informed by experimental and environmental feedback which can be used to generate open-ended design possibilities that can be applied in educational courses and workshops .

### **1.4. Structure of the thesis and chapters**

This thesis responds to some of the challenges faced by the design of responsive architecture, a contemporary discourse inspired by the *soft robotics* approach. An interdisciplinary methodology between physical experimentation and building performance simulations (BPS) is proposed. Physical experimentation is used to explore the design potential of responsive kinetic systems using smart materials, while CFD uses numerical methods to

measure the impact of responsive solar-shading systems on multiple environmental factors and helps the design decisions, selection and customisation of smart materials. The research explores ideas that challenge our present understanding of responsivity in architecture in which the system design is guided by environmental performance of the façade. It aims to illustrate the design process, challenges, constraints and parameters required to realise a responsive solar shading with material-based actuation.

To achieve this, the thesis is divided into seven main chapters as shown in Figure 1-4. The introductory section in *Chapter One* covers the introduction to the topic, research aims, and thesis structure. *Chapter Two* represents the literature review and the theoretical basis of the thesis. *Chapter Three* describes the interdisciplinary methodology between physical experimentation and CFD simulations. The thesis chapters from *Four* to *Seven* form the central body of the research. Finally, *Chapter Eight* provides a conclusion, a reflection on the research contributions and a future outlook of this work.

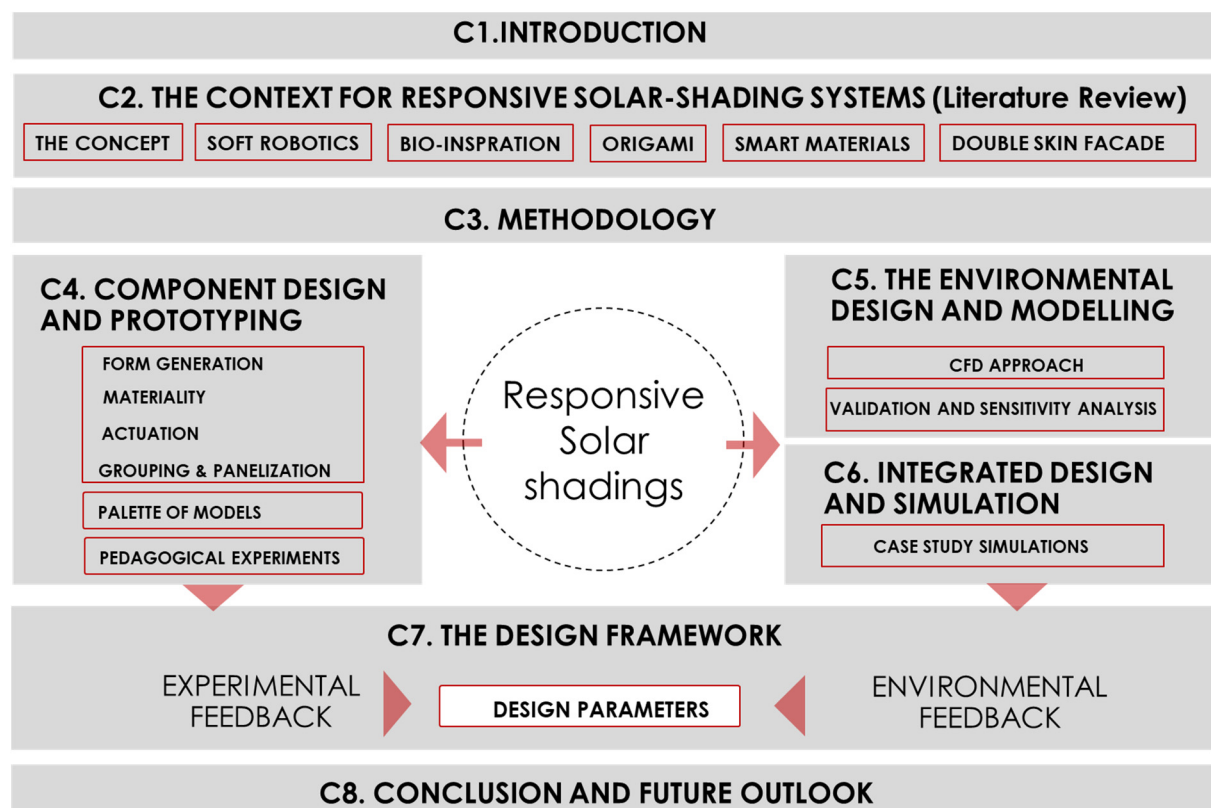


Figure 1-4: The thesis structure.

**Chapter One** introduces the subject broadly and provides general statements that outline the importance of the topic and background information that discuss the gap of knowledge. The introduction chapter discusses the significance of this study by detailing the central argument, the research aims and the structure of the thesis.

**Chapter Two** builds the theoretical groundwork to triangulate the intersection between bio-inspiration, folding principles, and material science development (smart materials), to study the underlying mechanisms and generative techniques of responsive reversible motion. It argues that the *use of* smart materials can reshape our contemporary architecture sustainable solutions to be more responsive. The chapter looks at concepts of adaptivity and responsivity of façades and solar-shading systems in architecture, the available resources of projects and the *soft robotics* inspiring approach. The review analyses plant movement principles and folding techniques for further applications. It covers the concepts and behaviour of smart materials and their applications as actuators which are capable of morphing self-deployable structures. As a cavity-integrated responsive solar-shading system is proposed as a sustainable solution, with the double benefits of a responsive solar shading within a controlled environment, *double skin facades* are reviewed. In doing so, form generation techniques are emerged to find the best working strategies for reconfigurable self-folding structures and to guide the design of responsive modular systems in the experimental component design in *Chapter Four*.

**Chapter Three** represents the methodological approach as a mixed interdisciplinary methodology based on practice-led approach, via hands-on explorations and material tinkering methods, and CFD simulations to design and assess responsive solar-shading systems. This ‘multifaceted’ study aims to understand the behaviour and performance of responsive solar-shadings realised with active materials within their potential context of operation, thus, making design decisions and developing design framework for responsive solar-shading systems. The two methodological approaches are discussed and how the related methods are applied in the thesis. Also, relative teaching experiences are discussed to help to prepare an educational activity module for MArch students during the fall of 2018/2019 to develop responsive shading systems. The experimental practice-led approach and environmental CFD simulations are brought together through the design of a prototype which integrates material thinking and the simulation of real environmental performance developing a demonstrator and design framework for future development in *Chapter Seven*.

In **Chapter Four**, a Practice-led approach through hands-on exploration and material tinkering is adopted to provide design experiments of deployable systems inspired by bio-inspiration and folding principles studied in *Chapter Two*. The ‘*Component Design and Prototyping*’ chapter provides explorations for design possibilities of bio-inspired and origami-

inspired deployable systems that can generate open-ended design outcomes with a wide range of transformation. The learning through making informs the decision-making process. The first set of explorations intends to test lightweight passive materials (fabrics, paper, card, and polypropylene), explore folding forms (straight and curved) and understand the intuition of shape memory materials and how they operate. The second set goes on by providing in-depth analyses of four experimented and actuated models by the researcher. The design process goes through four stages; form generation, materiality, actuation and panelization. This knowledge is further tested with MArch students during the fall of 2018/2019 to test the design process and generate different design possibilities. Each of the case studies features a combination of form and actuation method, which is particularly promising for further upscaling and full system design. The chapter concludes efficient deployable structures, smart material fixation strategies and system reversibility methods. By doing so, an actual prototype system will be selected for further environmental experimentation in *Chapter Six* and an integrative 'Design Framework' will be developed by the end of the thesis in *Chapter Seven* as a reflection on the researcher's and students' experimentation that can be further applied in educational courses and workshops.

**Chapters Five and Six** represent the climate-based approach by conducting Computational Fluid Dynamics (CFD) numerical modelling. It will focus on the simulation of solar-shading devices in their real potential context of operation; encased in a DSF in a hot arid climate. **Chapter Five** starts by introducing CFD simulations as a tool for assessing integrated DSF and reviews critically simulation methods used in literature to environmentally assess DSFs integrated with solar shading devices. It extends to outline the best practice guidelines defining the computational domain, its size, boundary conditions, and mesh. It presents a sensitivity analysis for CFD different geometrical modelling and setup variations in order to set guidelines for the CFD simulation setup to reach results with high accuracy and conclude the most recommended procedure for further investigation by CFD simulation.

Three validation cases are considered, Safer, Woloszyn, and Roux (2005), Manz, Schaelin, and Simmler (2004), and Mei et al. (2007). The CFD modelling will be validated using experimental results from Mei et al. (2007) as an experimental naturally ventilated DSF equipped with shading devices. These CFD variables are, determining the level of geometrical model detailing, extending the domain to include the external environment, representing solar simulator, selection of turbulence and radiation models. In doing so, a recommended

CFD setup will be applied for integrated DSF with responsive solar shading devices in *Chapter Six* to provide architects with environmental-based decisions during the design process.

**Chapter Six** investigates the correlation between responsive solar-shading systems and DSF thermal conditions using CFD coupled thermo-fluid-dynamics models in the hot arid climate of Cairo, Egypt. This chapter uses the recommended CFD modelling setup from *Chapter Five*. The form and aperture size variables are tested environmentally in this chapter. The folded origami prototype is selected from *Chapter Four* as a demonstrator to be simulated for environmental performance. Flat and folded solar-shading devices are installed in the DSF air cavity.

Shaded cases with three aperture sizes are modelled to represent the responsive solar-shading devices' different states tested as a point in time simulations. The shaded cases are compared with the non-shaded base case. The results section analyses two data sets. First, the inner surface temperatures, airflow and heat flux to measure the impact on energy reduction indoors and select optimal range of aperture size to inform solar shading designs. Second, the cavity temperature and solar-shading surface temperature to detect the required activation range for the shape memory material actuators. The chapter informs the design parameters with the required temperature needed for activating the shape memory materials and the optimum solar shading aperture size. In doing so, environmental feedback will be provided to guide the design decisions, and tailor the smart material properties. The synchronisation between the activation temperatures of SMM actuators, the surface temperature of the solar shading and thermal conditions of the cavity is crucial for optimising the operation of responsive solar-shading devices and the resulting aperture size.

**Chapter Seven** integrates and reflects on design experiments from *Chapter Four* and the environmental CFD analysis from *Chapter Six* in order to develop a framework for responsive solar-shading design and decision-making process informed by experimental and environmental feedback. By doing so, different design parameters for responsive solar-shading devices in specific and responsive systems, in general, are related in a way that guides students and researchers in the kinetic field for future development.



**Chapter Eight** outlines the thesis conclusions in terms of a summary, limitations and proposed future work in the field. The chapter discusses the limitations of the work and recommendations for future work in the field, which focuses on an overview of potential applications and new software tool.

## **Chapter 2 . THE CONTEXT FOR RESPONSIVE SOLAR-SHADING SYSTEMS (Literature Review)**

### **2.1. Introduction**

The building façade has a predominant impact on the building's energy balance and insulation (Mirrahimi et al., 2016). Many early research work has been oriented towards understanding the façade performance with respect to building performance and occupants' comfort (Ruck, 1989; Selkowitz, Papamichael, & Wilde, 1986). Research at Lawrence Berkeley National Laboratory sets design guidelines to generate energy-conscious façade design (Bryan & Clear, 1981; Selkowitz et al., 1986). According to the Society of Façades (CIBSE, 2004), proper conversation and collaboration amongst the different disciplines is required to obtain highly energy-efficient façades. Facades deal with climatic conditions that differ diurnally and seasonally. Traditional static façades that deal with dynamic changing environments are not optimally useful all of the time. As facades are the boundaries between interior and exterior spaces, dynamic facades and envelopes have the potential to improve the overall building's performance and human comfort (Kolarevic & Parlac, 2015; Wigginton & Harris, 2013). The desire for reduced energy use initiated the evolution of innovative and performative building envelopes that tend to be more adaptive and interactive with the climate. Adaptive façade systems in hot climates could potentially contribute to total energy reduction in buildings by protecting the façade from solar heat gain, hence reducing the need for cooling energy (Nagy et al., 2016; J. Wang, Beltrán, & Kim, 2012).

To date, most of the automated adaptive façade systems are mechanical solar-shading devices added to the façade externally or internally; or integrated within the façade to reduce the heat gain and regulate the light reflection through mechanical movements and controlling procedures (Barozzi, Lienhard, Zanelli, & Monticelli, 2016). The automated adaptive façade systems, as they are currently designed, are based on complex mechanics which are complex to build, difficult to maintain, liable to break and requires high energy consumption (Drozdowski & Gupta, 2009; Karanouh & Kerber, 2015; Meagher, 2015; Reichert et al., 2015).

Novel approaches of soft robotics can simplify mechanical designs utilised in adaptive facades through smart materials, with few moving parts, by making use of the materials themselves (Kapsali, 2016). Soft robotics use intrinsically soft and/or extensible

materials to deform (Bengisu & Ferrara, 2018). Responsive solar-shading systems can use material-based actuation to achieve dynamic behaviour by means of passive response. This category of responsive solar-shadings are generally soft, flexible and sensitive; therefore it is preferably integrated in a double skin facade (DSF), to be protected from the influences of weather and air pollution. Integration of smart materials for solar-shadings with double skin façade (DSF) systems may exhibit a potential to low-tech adaptive systems.

The generative techniques for soft robotics can draw inspiration from biomimicry, specially plants, and origami which are rich sources of deployable principles (Adrover, 2015). Plants perform mobility with minimal energy use, while origami has the potential to be reconfigurable structures which are easily fabricated, assembled, stored, and morphed.

This chapter builds the theoretical groundwork in order to triangulate the intersection between bio-inspiration, folding principles, material science development (smart materials), to study the underlying mechanisms and generative techniques of responsive reversible motion. It outlines the definition of responsive solar-shading systems and its related terms and strategies in architectural applications. It presents an overview of adaptable envelopes and shading systems applied in contemporary architecture and understands the different adaptive solar shading approaches of classification. It argues that the use of smart materials can reshape our contemporary architecture sustainable solutions to be more responsive. This chapter aims to use soft robotics, bio-inspiration and folding as a source of inspiration to design, develop and test responsive solar shading systems that respond to environmental stimuli. It covers the concepts and behaviour of smart materials and their applications as actuators which are capable of morphing self-deployable structures. In doing so, form generation techniques are emerged to find the best working strategies for reconfigurable self-folding structures and to guide the design of responsive modular systems in the experimental component design in Chapter Four.

## 2.2. Overview - Why Responsive Solar-Shading Devices?

Buildings and construction are responsible for an estimated 36% of worldwide energy consumption (GlobalABC, 2019). In hot arid climates, a range from 70% to 80% of the building's total energy consumption is required to maintain indoor thermal comfort in office buildings (Dabaieh, Wanas, Hegazy, & Johansson, 2015). According to Schaeffer and Vogt (2010), there are four reasons driving the need to raise energy efficiency in buildings. These are the foreseeable exhaustion of fossil fuels, the need to reduce the ecological problems resulting from fossil fuel combustion, the need to massively counteract climate change and reduce political problems resulting from uncertain energy availability in the future.

The *building façades*, vertical faces of buildings, play a predominant role in meeting energy efficiency requirements and interior comfort. Building façades are considered to be responsible for over 40% of winter heat loss and overheating in summer (Barozzi et al., 2016). An accurate façade design and efficient shading system can reduce the whole building energy consumption. The optimisation of *building facade* design positively affects energy consumption and thermal performance. The optimal design of *building façades* should moderate temperature and block significant solar radiation which results in thermal discomfort and unwanted glare. In hot arid climates, such as Cairo, Egypt, the solar radiation passing through windows increases the cooling loads and the energy consumption of buildings (A. Sherif, El-Zafarany, & Arafa, 2012).

In traditional desert architecture, rubble and rammed earth, adobe bricks, and large stone are materials used to increase the mass of wall constructions. Roofs were designed with conventional engineering solutions handed down from generation to generation, such as stone arches and corbelled domes (Z. Zhai & Previtali, 2010).

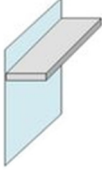
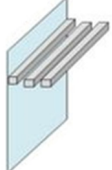
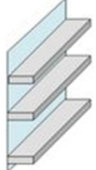
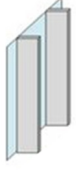













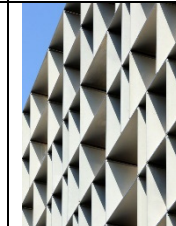
The *building façade* parameters, such as; external walls, glazing area, natural ventilation, window-to-wall ratio (WWR) and solar shading devices have a substantial effect on energy consumption (Mirrahimi et al., 2016). Fenestration plays a critical role in providing optimal lighting levels and thermal comfort in a building (Sadineni, Madala, & Boehm, 2011). The effect of fenestrations on the energy performance of buildings has long been studied since the 1970s. It was found that the optimal WWR results in significant energy savings that reaches more than 50% for heating, cooling, and lighting (Goia, Haase, & Perino, 2013). Tzempelikos and Athienitis (2007) found that a WWR equals to 30% for south-facing facades can

ensure natural daylight illuminance values higher than 500 lux for 76% of the working time in a year. However an appropriate shading control can halve the cooling energy demand compared to non-shaded case (Tzempelikos & Athienitis, 2007).

External window shading is a useful method to keep undesired solar heat gain out from the internal conditioned space (Prowler, 2016). Solar control and shading can be provided by using glazing technologies (Sadineni et al., 2011), by natural landscaping (Tsoka, Leduc, & Rodler, 2021), or by shading devices (Bellia, Marino, Minichiello, & Pedace, 2014) especially for south-facing windows. The south orientation receives the highest levels of solar radiation and controlling the solar gain on this orientation in buildings yields substantial cooling energy-saving results.

Traditionally, landscape elements, such as trees, led to a significant reduction in cooling energy demand, ranging from 11 % to 48% by obstructing solar radiation (Calcerano & Martinelli, 2016). A research project at TU Delft by Stec, Van Paassen, and Maziarz (2005) integrated the double skin facade (DSFs) with plants. They studied thermal performance of the integrated system with plants and argued that the system is more effective shading system than blinds. Glazing technologies include solar control glasses, insulating glass units, low emissivity (low-e) coatings, evacuated glazings, aerogels and gas cavity fills along with improvements in frame and spacer designs (Sadineni et al., 2011). Moreover, shading systems improve the building's thermal efficiency while reducing the amount of natural light it receives (Bellia et al., 2014; Prowler, 2016). The design of a good shading system is highly dependent on the building's use and the façade orientation as well as the local climatic conditions. (Kirimtat, Koyunbaba, Chatzikonstantinou, & Sariyildiz, 2016). Thus the position of the sun and the depth of the shading device become critical. Different types of static solar-shading devices such as overhangs, external roller shades, venetian blinds and internal shadings have always been used to increase building energy efficiency and reduce cooling loads in hot climates (Kirimtat et al., 2016). Different types of external fixed shading devices are included in Table 2-1.

Table 2-1: Types of fixed shading devices.

	Overhang	Overhang Horizontal Louvers	Overhang Multiple Blades	Vertical Fin	Slanted Vertical Fin	Eggcrate
3d view						
Section/ Plan						
Examples						
Best Orientation	South	South	South	West and east	West and east	West and east

Various techniques of passive solar shading have widely been implemented into buildings in Egypt. Throughout history, Middle Eastern buildings used “Mashrabeya” or “Rawshan” as a shading device to protect unglazed openings. As shown in Figure 2-1, they are made of wooden lattice of cylinders connected with spherical joints. Moreover, the latticework offers the chance to visually connect with the outdoor environment, while providing privacy for the occupants indoors, which is a socio-cultural need of communities in the region (Ahmed Sherif, Sabry, & Rakha, 2012). The ancient *mashrabeya* merges cultural, visual and technical aspects. The window screen is often found towards the street to enable discretion and allow cool air to pass through the facade. Several contemporary projects were inspired by the oriental mashrabeya technique and develop solar shadings combined with double-facades to reduce the cooling loads for the interior, such as the Masdar Institute in Abu Dhabi by Foster + Partners (2010) or the Doha Tower in Qatar by Jean Nouvel (2012) (Schielke, 2014).



Figure 2-1: “Mashrabeya” or “Rawshan” screen panels as a shading device to protect openings in middle eastern buildings (Aljofi, 2005).

A. Sherif et al. (2012) argued that external wooden solar screens could provide considerable energy saving that reaches 30% for south-oriented facade compared with a non-shaded window. The study presented the results in terms of depth ratio and perforation percentage. The depth ratio was defined as ‘the ratio between the depth and the width of each perforation opening’ while the perforation percentage was defined as ‘the percentage of the perforation opening area to the whole area of the screen. The study recommended that the optimum solar shadings for south oriented façade should have a depth ratio of 1.00 for large perforation percentage of 90% or depth ratio between 1.25-1.5 for smaller perforation percentage of 80%. This means that the large perforations need thicker/deeper solar screens. Moreover, Datta (2001) optimised the design of external fixed horizontal louvers for south windows to cut off up to 70% of solar gain in summer, and 40% in winter in the weather of Milan. Generally, Exterior solar shadings can reduce direct solar gain by a maximum of 80% (Babaizadeh, Haghighi, Asadi, Broun, & Riley, 2015). Another study by Palmero-Marrero and Oliveira (2010) agreed on the benefits of static solar shadings. The study applied shading devices in three cities; Cairo, Lisbon and Madrid. The louver solar-shadings have an inclination angle equal to latitude of each city on a window height of 1.5 m, the annual energy savings compared to the building without shading systems were 60% in Cairo, 50% in Lisbon, and 9% in Madrid. Although *static solar-shading devices* can reduce cooling demand, they lead to daylight loss and the need for heating over winter.

Current trends in architecture are directed towards *dynamic, adaptive or responsive architecture*, as the key to sustainability (Barozzi et al., 2016). The building *façade* can be animated to act as a living part, a semi-permeable skin, that mediates between the building

and the outer environment (Kolarevic & Parlac, 2015; Wigginton & Harris, 2013). It is a layer or more, where architecture and environmental engineering intersect. It is more than energy barriers; active building skins are able to control energy flows of light and heat dynamically.

Advantages of using *dynamic solar-shading devices* are reported by many researchers (Baldinelli, 2009; Dubois, 2001; Johnsen & Winther, 2015; Nielsen, Svendsen, & Jensen, 2011; Pesenti, Masera, Fiorito, & Sauchelli, 2015; Sauchelli, Lobaccaro, Masera, & Fiorito, 2013). Dubois (2001) examined the impact of an awning on a south-facing office window. According to this study, installing a seasonal awning might result in significant energy savings (about 12 kW h/m<sup>2</sup>/year). However, if a fixed awning was installed, the energy savings would be 11 kW h/m<sup>2</sup>/year. As a result, this result indicated that the shading devices should be removed during the warmer months. In the Mediterranean climate, a study by Sauchelli et al. (2013) compared a *dynamic solar-shaded case* with a non-shaded base case. The completely shaded façade in spring and summer seasons resulted in 80% energy reduction (for cooling), while a 20% shading is recommended in autumn and winter as it positively influences the energy need for heating. Nielsen et al. (2011) investigated the performance of *dynamic solar-shading* in comparison to fixed solar shading and non-shaded case for three window heights. The results reported an increase in the daylight factor and a well-lit area expansion by 70–150%. A 16% difference was found in total energy demand between the worst and the best-performing facade for a given orientation. The dynamic solar-shading recorded a total annual energy demand of (46 kWh/m<sup>2</sup> per year) compared to (50 kWh/ m<sup>2</sup> per year) for fixed solar-shading and (55 kWh/ m<sup>2</sup> per year) for non-shaded windows.

Pesenti, Masera, and Fiorito (2015) optimised a *dynamic origami solar-shading system* for office buildings. The most promising configuration displayed 20.8% Total Energy saving, 18.1% increment of Useful Daylight Illuminance (UDI) percentage and 26.6% Daylight Glare Probability (DGP) compared to the non-shaded facade. All previous findings concluded that the use of *dynamic solar-shading* improves the daylighting availability and optimise the exploitation of free solar energy gains in winter whilst reducing the overheating in hot and warm seasons.

To date, most *dynamic solar-shading* systems are often automated and controlled through central building management systems. For more smart and responsive systems, the *solar-shading* component can develop embedded responsive reaction on its own. Recent



technologies of materials and the latest advances in sensing, controlling and actuation can open up new applications for more *responsive solar-shading systems* with lower levels of cost and complexity. A summary of the main definitions and principles related to *responsive façade and solar-shading systems* will be provided in the next section.

#### 2.2.1. Definitions, origins and principles

This section focuses on the development of new concepts for *energy efficient façades*. As such, it is important to define some of the terms related to the *façade* and its associated properties. Some of the terms are alternative designations or specify the subject on partial aspects. Such terms relevant to this research will be defined.

The '*building envelope*' and '*building shell*' are often used interchangeably and refer to the *façade* (Knaack & Koenders, 2018). Recently, the continuous envelope of the tectonic, environmental and aesthetical relationship between the interior and exterior is called '*skin*'. The '*building skin*' originally derived as an analogy to the human epidermis. Similar to the human skin, the building envelope or skin is understood as a whole entity that can continuously self-regulate between exterior and interior (Wigginton & Harris, 2013). The building skin describes the whole envelope, including the roof and facades, while the *façade* refers to the building's vertical faces.

In the context of adaptive façades, a wider range of terms has been established. Although some of the terms used in the same context, many of them are not clearly defined or even have slightly confusing meanings. The term '*Adaptive*' can be loosely described as 'being adjusted when necessary in order to deal with new conditions' (*Oxford dictionary of English*, 2005). This definition immediately introduces another related term, which is '*Adjustable*'. It encompasses two useful definitions; a) 'alter slightly as to achieve the desired result', and b) 'become used to a new situation' (Hasselaar, 2006). Although adaptive and adjustable are similar terms, they have two different annotations. '*Adaptive*' means the ability to adjust to changing circumstances by itself, while '*Adjustable*' means the ability to adjust by external interference (Hasselaar, 2006). Literature reveals that the terms "smart" and "intelligent" are used interchangeably in relation to materials and systems. The term '*Intelligent*' is the ability to gain information, demonstrate good judgment and comprehend quickly, while the term '*smart*' connotes an informed response, as well as the qualities of alertness and quickness that go with it. There is also a frequent correlation of smartness with

intuitive or intrinsic response (Addington, 2005). There are higher expectations of ‘intelligent structures’ than of ‘smart materials’. Intelligent system can add more control layers to a kinetic system by collecting data, analysing its effect, and responding appropriately to unforeseen circumstances, such as environmental or occupant behaviour (El Sheikh & Kensek, 2011). An intelligent system involves the presence of a central control system or computer to process the data received from sensors and determine the action to be undertaken. ‘Smart’ is associated with materials or smaller components rather than a whole façade system. Intelligent systems involve the realization and networking of smart components. Thus, intelligent building facade can be understood as a system of layers or components which co-operate for multi-functional operability (Böke, Knaack, & Hemmerling, 2018).

‘Responsive’, in this context, can be defined as ‘responding quickly and positively’ (Oxford dictionary of English, 2005). The difference between ‘Adaptive’ and ‘Responsive’ with respect to façades is that *responsive* does not necessarily mean adjusting particular characteristics to the environment, but simply responding to a change (Hasselaar, 2006). Table 2-2 summarises the alternative designations in the field of responsive facades which are sometimes used interchangeably in the same context.

Table 2-2: Alternative designations in the field of responsive facades

Property	Application
<i>Dynamic</i>	<i>Façade</i>
<i>Kinetic</i>	<i>Building Shell</i>
<i>Advanced</i>	<i>Building Envelope</i>
<i>Adaptive</i>	<i>Building Skin</i>
<i>Intelligent</i>	
<i>Smart</i>	
<i>Active</i>	
<i>Responsive</i>	
<i>Performative</i>	

During the past 30 years, the idea of *adaptive building skins* has emerged and described using different definitions, related to how the envelope reacts to environmental conditions and users’ needs as shown in Table 2-2.

The concept of intelligent façades exists since the beginning of the 1980s (Knaack & Koenders, 2018; Wigginton & Harris, 2013). The publication of Mike Davies in 1981 was the first to present the dynamic wall technological system (Kolarevic & Parlac, 2015). He presented

what is called '*polyvalent façade*' where multiple features have been integrated into the façade, each addressing a specific need. Nevertheless, his model became a source of inspiration for architects and many contemporary façade solutions. Afterwards, Hasselaar (2006) defined '*Climate Adaptive Skins*' (CAS) with their ability to adjust their characteristics to mediate between the changing environments. Similarly, R. C. Loonen, Trčka, Cóstola, and Hensen (2013) popularised the term '*Climate adaptive building shell*' (CABS) that refers to the ability of building skins to adapt as a function of the variable climatic conditions and the users' needs. The main aim of CABS adaptive behaviour is the overall energy reduction. This definition is close to *the Adaptive Solar Facade (ASF)*, which was introduced by Rossi, Nagy, and Schlueter (2012). The adaptive facade offers shading and daylight control as well as individual adjustments to the occupants' view in addition to the energy production of the photovoltaics. J. Wang et al. (2012) described the '*Acclimated Kinetic Envelope*' (AKE) as an envelope that respond to variable climatic environments by means of visible physical behaviours of the envelope components. Those kinetic components are integrated into buildings and adapt themselves through changes in reversible ways.

All these definitions fall under '*Performative Adaptive Façades*' and can be further developed by affording bi-directional transmission of energy. According to Addington (2015), the *dynamic smart envelope* shall be smart enough to change for multiple conditions rather than being optimised for a single state, which should indeed resolve the complex changings interactions between the exterior and interior.

Wigginton and Harris (2013) in their book *Intelligent Skins*, argued that responsiveness is the main feature of '*Intelligent Building Skins*' (IBS), and this includes environmental changes as well as human interactions. Recent researches in the field of *adaptive or performative facades* claim that responsive skins are the key to sustainability (Kolarevic & Parlac, 2015). Smart materials that possess the ability to move without mechanical parts started shifting the IBS concept towards '*No-mech Kinetic Responsive Architecture*' (Doumptoti et al., 2010; Kretzer, 2017a; Maragkoudaki, 2013; Ritter, 2007). Experimentation with smart materials, opens up new design possibilities that can be referred to as low or zero energy structures (Maragkoudaki, 2013). Table 2-3 overviews different intelligent façade concepts developed during the past 30 years.

Table 2-3: Criteria and characteristics of intelligent façades

Term	Properties	Reference
<b>Dynamic wall/ polyvalent façade</b>	‘Polyvalent façade’ has multiple integrated features into the façade, each addressing a specific need.	Mike Davies in 1981
<b>Climate Adaptive Skins (CAS)</b>	CASs are building skins with their ability to adjust their characteristics to mediate between the changing environments.	(Hasselaar, 2006)
<b>Climate adaptive building shell (CABS)</b>	CABSs are building skins which are able to adapt themselves as a function of the building users’ needs and the variable climatic conditions. The adaptive behaviour of CABS aims to reduce the overall energy.	(R. Loonen, 2010; R. C. Loonen et al., 2013)
<b>Acclimated Kinetic Envelope (AKE)</b>	AKEs are envelopes with the aptitude to adapt themselves through changes. AKEs are defined as responding to variable climatic environment by means of visible physical behaviours of building envelope components. Kinetic components should be integrated into buildings.	(J. Wang et al., 2012)
<b>Adaptive Solar Facade (ASF)</b>	ASFs offer shading and daylight control as well as individual adjustments to the view by the occupants. Photovoltaics can be integrated for energy production.	(Rossi et al., 2012)
<b>Intelligent Building Skins (IBS)</b>	IBS is an envelope where responsiveness is the main feature, and this include environmental changes as well as human interactions.	(Wigginton & Harris, 2013)
<b>No-mech Kinetic Responsive Architecture</b>	No-mech Kinetic Responsive skins are envelopes with the ability to transform over time by incorporating smart materials that undergo purposeful change in accordance to external, environmental or not, stimuli.	(Maragkoudaki, 2013)

The broad use of the term ‘*building skin*’ is sometimes equated with the ‘*building envelope*’. However, it is not limited to static characteristics of the building envelope, but it goes further to include the smart characteristics of the human skin which has an embedded responsive reaction on its own that can sense, control and actuate. In this thesis, ‘*responsive building skin*’ is used to describe the ability of the building envelope to transform over time by

incorporating smart materials that adapt in response to external or environmental conditions. '*Responsive solar shading system*' represents the responsive skin or layer with embedded responsiveness that is positioned in front or behind the building's glazed surface. Moreover, the '*responsive solar shading system*' can be integrated in-between two glass panels which is called double skin façade (DSF). All these layers can be referred to as an '*adaptive façade*' which tends to be thicker and applied on vertical buildings' surfaces. In this case, not all the layers are responsive but includes one or more responsive layers, such as; electrochromic glazing surface or responsive solar-shading. Both the '*responsive solar shading system*' and the '*adaptive façade*' aim to regulate the internal conditions inside the space, offer shading and provide daylight control, over different periods of time by exhibiting a state of motion and dynamism.

### 2.2.2. *Control of adaptive systems*

These kinetic solar shading systems are considered "active features" which can either be part of an active or passive systems. This thesis aims to develop a passive solar shading system which can control and regulate the internal conditions without the use of electronic or mechanical devices. The material intelligence controls the movement of the shading system's parts when exposed to the solar radiation. On the other hand, the active system can automatically monitor and control the internal conditions through a computerized, intelligent network of electronic devices (Böke et al., 2018).

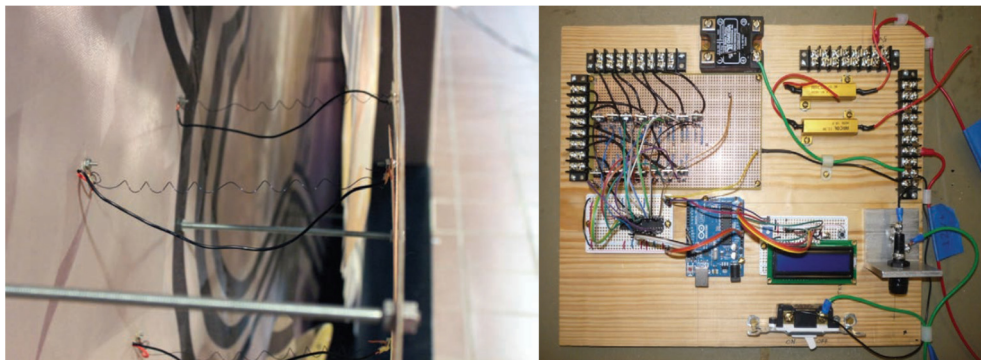
The building management system (BMS), also known as building automation system (BAS), is an overarching control system that is responsible for the automated regulation, maintenance, and control of predefined parameters. BMS is a computer-based control system that should be mounted inside buildings to track and regulate the electrical and mechanical equipment, such as the power system, lighting, and ventilation, in order to ensure sustainability. The main aim of the BMS is to ensure facility operation safety while also controlling and optimising the use and efficiency of its monitored subsystems (Joseph, 2018). A BMS monitors, supervises, manages, and reports on smart building technology (Sinopoli, 2009). It interacts with control hardware in the various mechanical/electrical systems to monitor and modulate the energy used in real time (Minoli, Sohraby, & Occhiogrosso, 2017).

According to Salakij, Yu, Paolucci, and Antsaklis (2016), there are two main research directions in advanced control of building energy management: Learning-based Methods of Artificial Intelligence and Model-Based Predictive Control (MBPC). Learning-based methods include genetic algorithms, fuzzy techniques, and neural networks. The advantage of these methods is that they do not need to know detailed physical information of the system. It is easier to be implemented when many on-site measurements are available, but the subsequent optimization process is not easy since it lacks physical insights and does not deal well with disturbances caused by varying occupants' behaviours or physical changes in a building. Also, the model accuracy depends substantively on the space-resolution of the on-site measurements. Such approach has proven to improve a building's energy efficiency. On the other hand, the Model-Based Predictive Control (MBPC) uses a model to predict the future state evolution of the system and generates a vector of control actions that minimize a certain cost function over the prediction time period in the future in the presence of external disturbances and constraints. It can be regarded as a type of optimal control that is based on a mathematical model with knowledge of the building system. It employs weather and occupancy information to implement optimization in control strategies as a means to minimize the energy consumption, while ensuring comfort conditions.

Before 2003, BMS providers such as Johnson Controls, Siemens, Honeywell, and others have developed and distributed building automation products and services that were closed and proprietary (Mitchell, 2005). There are a few examples that break the closed system of sensor/controller/output to include the user in the monitoring and decision making process (J. Moloney, 2006). Decades of sociological and psychological studies have shown that a sense of control is a strong indicator of physical and mental well-being. A sense of control is widely acknowledged as a significant factor affecting comfort and satisfaction in the built environment (Meerbeek et al., 2014). The control system of the GSW headquarters building in Berlin makes recommendations to users about the selection of natural or mechanical ventilation by means of green or red lights on the window transoms. The user can decide to accept or override the recommendation from the control system, thus enabling a level of interaction (J. Moloney, 2006).

After 2010, the well-established *Internet of Things* (IoT) (Want et al., 2015) facilitated the remote control of building systems through hand held phones and apps that took into account occupant behaviour and usage changes (Makonin, 2016)

In recent years, there is a fruitful convergence for various building technologies and systems to material based responsive systems. These material based responsive systems can be autonomous to direct stimulus exposure or can be electronically controlled. The integration of composite materials with smart materials and Arduino automation control can result in structures that incorporated perceptual and actual motion (Esquivel, Weiser, Hartl, & Whitten, 2013). The control schematic consists of a micro-controller connected to the electronic relay. When the input commands the micro-controller program to activate the actuators, a signal is sent to the relay for activating the actuation cycle. The heart of the electronic control system is the Arduino microcontroller board as shown in Figure 2-2. The Arduino is an open-source hardware and software prototyping platform. Using a series of input and output pins, the Arduino can be programmed to monitor and control an environment using a C/C++ based programming language (Esquivel et al., 2013). In case the electric current required to actuate the SMA wires exceeds the maximum current output of an Arduino pin, some type of transistor is needed to act as a switch for a higher-capacity power supply.



*Figure 2-2: SMA coils attached to the back of the panel and the control system (Esquivel et al., 2013).*

The advantages of the control of active systems signify the MULTI- RESPONSIVE feature to various parameters through a single system where each actuator can be individually controlled through a BMS while the significance of the passive system is its potential to reduce the direct solar exposure, during summers while minimally affecting the day light levels inside the space. The responsive passive system is considered low-cost compared to active systems especially in the running costs. Recently, there is an on-going research on Smarter Smart Material (SSM) by the Institute for Computational Design and Construction (Prof. Achim Menges, Dylan Wood) and HCI Engineering Group systems that effectively and efficiently change-shape via interaction with both humans and the environment which adds a level of control to the highly efficient movements of the materially responsive system.

### 2.2.3. *Responsive solar shading systems: State of the art*

This literal movement of components that incorporate environmental responsiveness, is often used to make buildings appear alive (Kolarevic & Parlac, 2015). This dynamic effect of building facades develop "personality". This argument was supported by Doris Sung in Aouf (2019) as she said:

*"I feel like with my materials, I could make a building facade annoying to you, I can make it pleasant, I can make it happy. We can almost give emotional value to facades by now making them move. People will react to them as if they are alive."*

Research on façade solar-shading systems has usually focused on individual projects rather than clear classification. There is a conventional classification of adaptive facades in terms of solar-shading positioning (Hasselaar, 2006; Oesterle, 2001; Wigginton & Harris, 2013). Also, they can be categorised according to their movement typologies and degree of freedom (Jules Moloney, 2011; Schaeffer & Vogt, 2010). Another more relevant classification can be according to the means of system actuation (Kolarevic & Parlac, 2015; Schaeffer & Vogt, 2010).

Several projects demonstrated that adding kinetic shading devices can achieve an energy demand reduction. Different contemporary case studies are mentioned in Table 2-4 and analysed in Table 2 4 according to the three classification approaches of adaptive systems which are; solar-shading position, movement and actuation mechanism.



Table 2-4: contemporary adaptive envelopes.


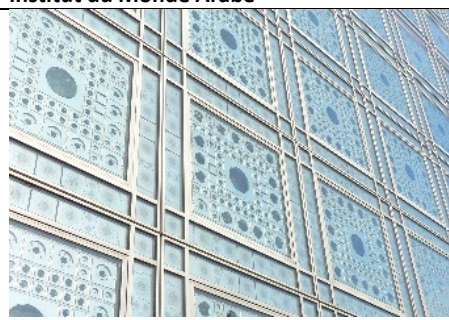
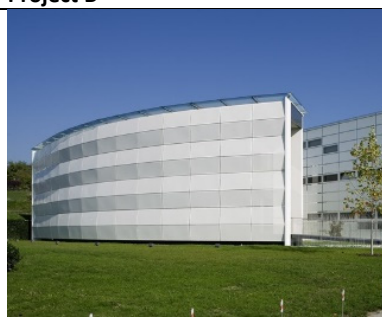


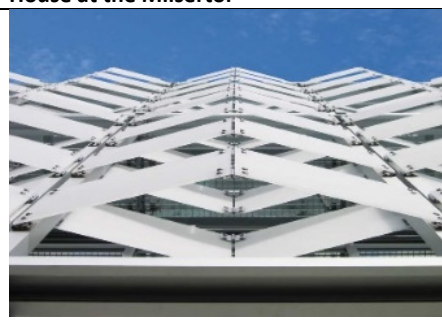


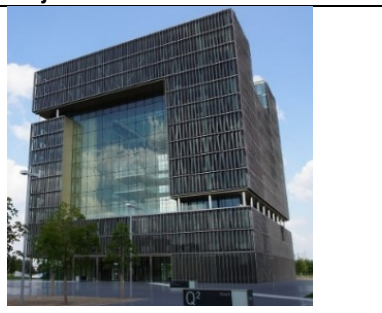
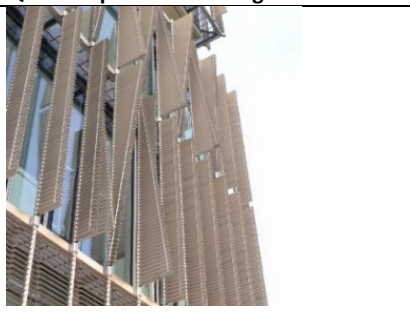

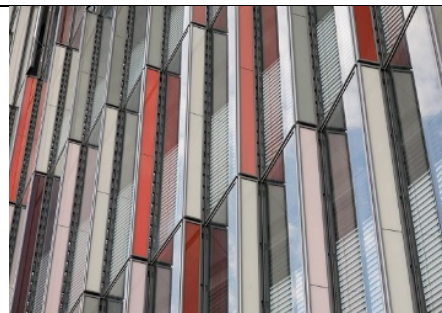
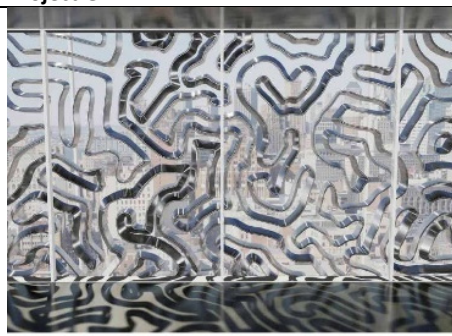
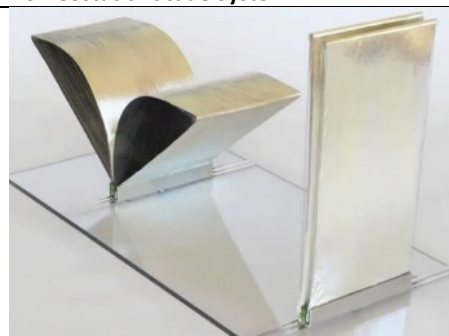

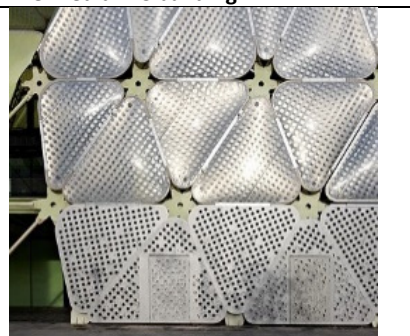

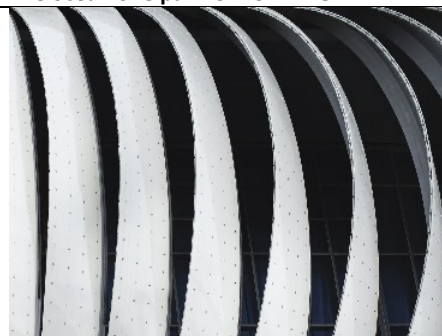
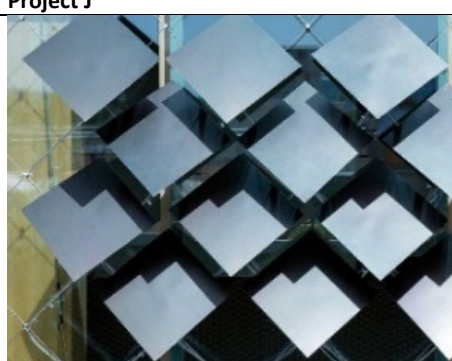

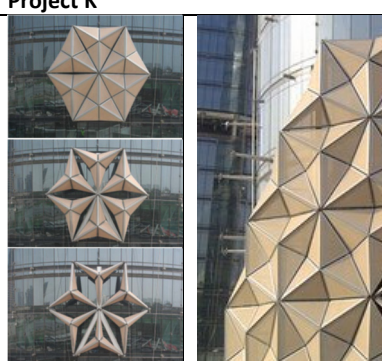
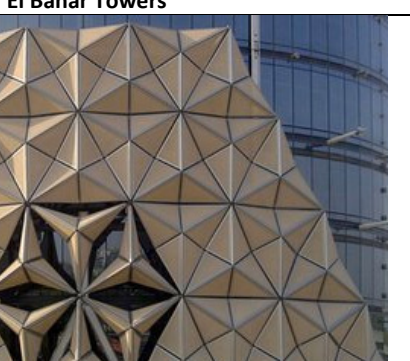
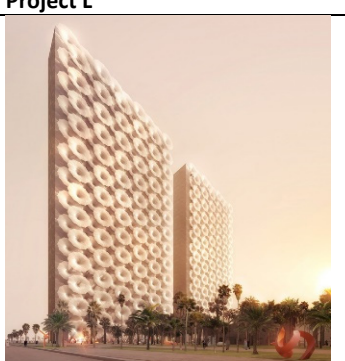
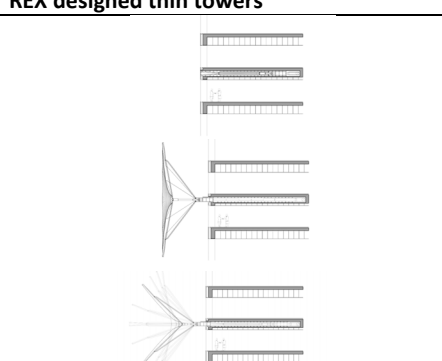
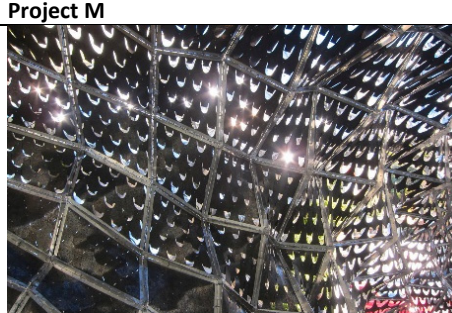
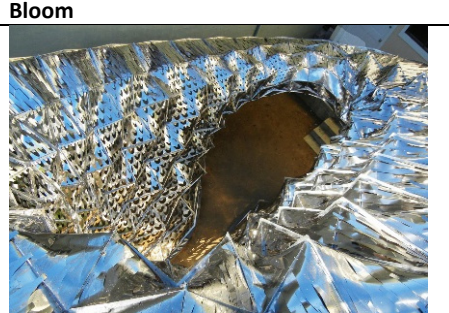

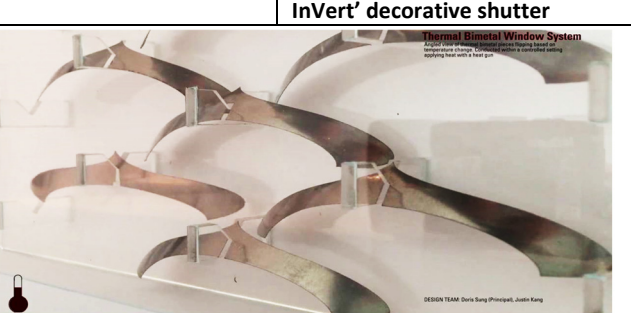
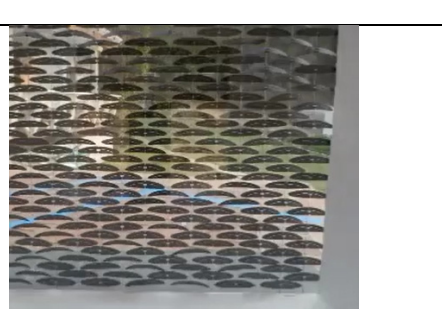
<b>Project A</b> 	<b>Institut du Monde Arabe</b> 	<b>Project B</b> 	<b>Kiefer technic showroom</b> 	<b>Project C</b> 	<b>House at the Milsertor</b> 
<b>Project D</b> 	<b>Adaptive Fritting</b> 	<b>Project E</b> 	<b>Q1 Headquarters building</b> 	<b>Project F</b> 	<b>KfW Westarkade</b> 
<b>Project G</b> 	<b>Homeostatic Facade System</b> 	<b>Project H</b> 	<b>The Media-TIC building</b> 	<b>Project I</b> 	<b>The ocean one pavilion for EXPO</b> 
<b>Project J</b> 	<b>Adaptive Solar Facade (ASF)</b> 	<b>Project K</b> 	<b>El Bahar Towers</b> 	<b>Project L</b> 	<b>REX designed thin towers</b> 
<b>Project M</b> 	<b>Bloom</b> 	<b>Project N</b> 	<b>InVert' decorative shutter</b> 		



Table 2-5: Classification of contemporary adaptive facades

ID	Project Name	Year	Reference	Scale	Façade Type	Movement type	Degree of freedom	Actuation type
A	Institut du Monde Arabe	1987	(Kolarevic & Parlac, 2015)	C	Integrated	Rotation	1	Motor-Based
B	Kiefer technic showroom	2007	(Jules Moloney, 2011)	C	External	Folding, Expansion & Contraction	1	Motor-Based
C	House at the Milsertor	2008	(Schaeffer & Vogt, 2010)	C	External	Folding and sliding	1	Motor-Based
D	Adaptive Fritting	2009	(Drozdzowski & Gupta, 2009)	C	Integrated	Rotation	1	Motor-Based
E	Q1 Headquartes building	2010	(Schaeffer & Vogt, 2010)	C	External	Pivot and flap	1	Motor-Based
F	KfW Westarkade	2010	(Kolarevic & Parlac, 2015)	C	External	Rotation	1	Motor-Based
G	Homeostatic Facade System	2010	(Premier, 2012)	C	Integrated	Expand & Contract, Curl	1	Material-Based actuation
H	The Media-TIC building	2011	(Kolarevic & Parlac, 2015)	C	External	Expansion & Contraction	1	Pneumatic actuation
I	The ocean one pavilion for EXPO	2012	(Schleicher, 2016)	C	Integrated	Rotation and deformation	1	Motor-Based actuation
J	Adaptive Solar Facade (ASF) HIL building ETH Zürich	2012-2016	(Rossi et al., 2012). (Nagy et al., 2016)	C	External	Rotation	2	Pneumatic actuation
K	El Bahar Towers	2012	(Armstrong et al., 2013)	C	External	Folding, Expansion & Contraction	1	Motor-Based
L	REX designed two thin towers	2014	(Kolarevic & Parlac, 2015)	C	External	Expansion & Contraction		Hydraulic actuation
M	Bloom	2011	(Sung, 2016)	C	External	Curling	1	Material-Based actuation
N	'InVert' decorative shutter	2015-2019	(Sung, 2016)	SC	Integrated	Curling	1	Material-Based actuation

Kolarevic and Parlac (2015) argued that there are four means of actuation to produce dynamic effects, which are: a) motor-based; b) hydraulic; c) pneumatic and d) material-based. Common practices in the field of adaptive solar-shading systems, rely on motor-based actuation associated with increased complexity and cost. One of the main challenges for all mechanically motor-based actuation systems is friction, and it is the primary reason of malfunctioning apertures of Jean Nouvel's Institut du Monde Arabe, Project (A), (Kolarevic & Parlac, 2015). There is ongoing experimentation on pneumatic and material-based actuation that promise a more sustainable dynamic building envelopes, not through high levels of cost and complexity.

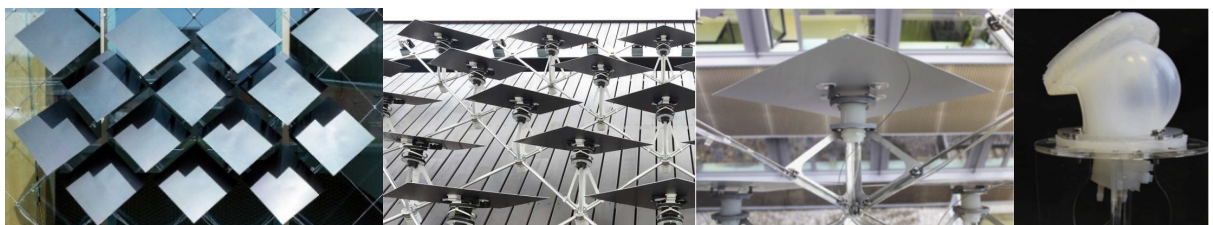
The media-ICT building, Project (G), is designed by the Spanish architect Enric ruiz-geli to be a communication hub as shown in Figure 2-3. The ETFE cladding is inflatable, with up to

three air chambers. The building skin can create shade by means of pneumatic actuation and improve thermal insulation. The first layer is transparent, while the second and third layers have a reverse pattern. This design is responsible for the shade as the second and third layers are joined together when inflated to create a single opaque layer, and the inflatable section only has one air chamber (Kolarevic & Parlac, 2015).



*Figure 2-3: The responsive ETFE cushions in the Media-TIC building smart facade filters solar radiation, imitating nature's adaptive qualities.*

The Adaptive Solar Façade, Project (I), is one of the most significant projects using soft pneumatic actuation applied on the architectural scale, as shown in Figure 2-4. The soft pneumatic actuator is made from elastic materials and energised using compressed air (Nagy et al., 2016). Valves control the airflow by releasing air to deform the actuator and move the solar element selectively. This enables the modules to track the sun's movement and generate power.

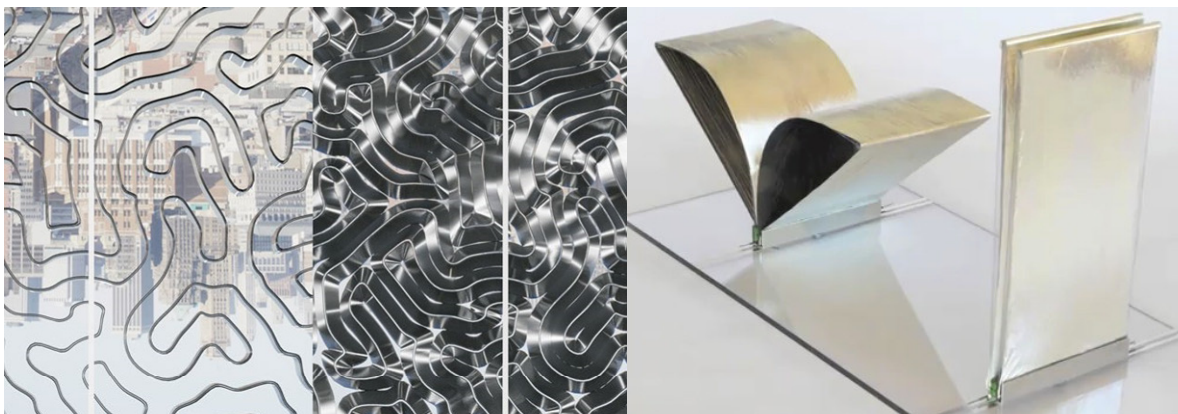


*Figure 2-4: The actuation system of the Adaptive Solar Façade (ASF) is based upon soft pneumatic actuator (Nagy et al., 2016).*

Although pneumatic actuators are fluid-based actuators that have very high power output relative to their size (Schaeffer & Vogt, 2010), they are relatively inefficient compared to electromechanical actuators due to the system flow-resistances. Therefore they require greater input. In general, electromechanical and pneumatic systems have the advantages of coping with changing circumstances from the outside such as; climate change and changing urban environments or from the inside such as; organisational function changes of the building, new space layout, internal thermal and visual conditions. Extrinsic control is considered effective since it allows for advanced automated process techniques and personal control. Moreover, occupants in automated systems could be given some adjustment or

manual override to exploit human intelligence in control (R. C. Loonen et al., 2013). Nevertheless, they need a kind of complex and bulky parts to alter the actuation, and a central building management system to control the system. However, the ongoing experimentation in material-based actuation promises zero energy responsive skins. It has the potential to be easy to build and maintain while requiring less energy consumption.

Homeostatic Façade System project (G) is a leading project of the material-based actuation representing a self-regulating façade system designed by Decker Yeadon. It fits in a DSF which takes advantage of the unique flexibility and low power consumption of dielectric elastomers (Premier, 2012). The façade system incorporates ribbons of the dielectric material across the façade. The actuator is an artificial muscle, created by wrapping the dielectric material over a flexible polymer core. The dielectric elastomer expands by passing electric current over the surface, causing the flexible core to bend, as shown in Figure 2-5.



*Figure 2-5: The façade of Homeostatic Facade System in closed and opened status and a section of the Homeostatic Facade System. <https://www.archdaily.com/533679/how-do-mysterious-memory-materials-work>*

Bloom installation, Project (M) is an example of material-based actuation investigated by the architect Doris Sung. She made use of smart materials, in specific Thermobimetals (TB). It can be defined as a double-layered composite of two metal alloys, in which one expands faster than the other when heated to develop a responsive envelope. Both 'Bloom' installation project (M) and 'InVert' decorative shutter project (N), consist of metal pieces that curl and flip over under sunny conditions, altering how much light and heat can enter a space as shown in Figure 2-6.

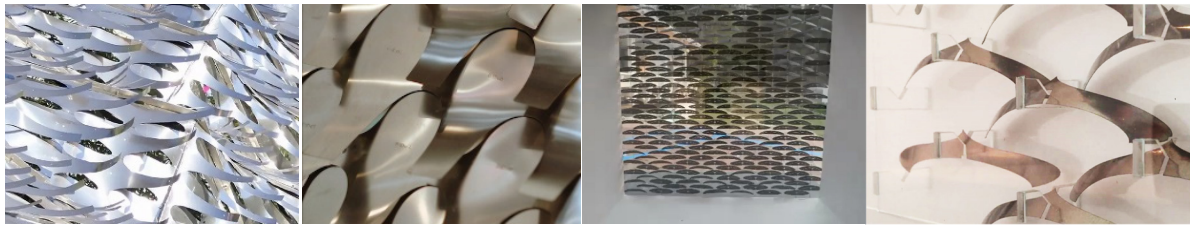


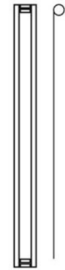


Figure 2-6: The actuation system of Bloom installation and InVert (TM) window shading is based upon thermobimetals. <https://www.tbm-designs.com/watchx>

All motor-based, hydraulic-based and pneumatic based actuation needs kind of complex and bulky parts to alter the actuation, and a central building management system to control the system. These actuation methods could be replaced using the inherited property of the material. It is called the material-based actuation. Material-based responsive systems have the advantage of light-weight and simplicity of manufacture over conventional systems. A key advantage of using smart materials in robotics is their tolerance of large deformations during shape memory cycling. The high performance and low initial cost of conventional materials and mechanisms compared to responsive material systems represent a common obstacle to widespread the use of responsive systems. For these responsive materials to be regarded as technologies in widespread commercial robotic applications, research and development activities must demonstrate competitive performance as well as evaluate potential gains. The research is an extension to Decker Yeadon and Doris sung responsive solar-shading projects to construct an amplified passive motion using material-based actuation. Hence, the study is looking in detail at the material-based actuation and abilities of smart materials in the coming section 2.3 on page 35. The following section is a brief description of the types of solar-shading system positioning.

The solar-shading system positioning typologies can be listed as follows: External, Integrated and Internal solar-shading systems. As shown in Table 2-6, external adaptive shading devices are the most popular due to their efficiency in the summertime, accordingly reducing the cooling loads (Hasselaar, 2006). Recent studies have shown that external solar-shading systems can be 3-5 times more efficient than internal solar-shading systems. However, external solar-shading devices are exposed to harsh weather conditions like rain, wind, water, heat, cold, and pollution (Schleicher, 2016). Therefore they result in high maintenance and cleaning costs due to the exposure of the kinetic system. In this case, integrated solar-shading systems can be considered as efficient. Internal solar-shading systems are less efficient than external and integrated shading systems; especially in hot climates.

Table 2-6: Classification of adaptive envelopes in terms of solar-shading positioning

External solar-shadings	Integrated solar-shadings	Internal solar-shadings
External solar-shadings reflect and emit the heat absorbed from solar radiation to the external environment, reducing the cooling loads in summer. The outdoor elements are exposed, resulting in higher costs for maintenance and cleaning. External devices can be either fixed or kinetic.	Integrated solar-shadings are contained in an enclosed space, generally double skin façade (DSF). Cleaning costs are relatively low. Maintenance costs however, can be higher in cases where the electric motors are also incorporated in the cavity between the panes.	Internal solar-shadings are less effective, as the gained solar heat by the shading device, is trapped by the glass and emitted inside the space. Cleaning and maintaining these devices is considerably easier than exterior and integrated ones, as they can easily be reached.
		

The most common practice for mechanised/ automated venetian blind systems in use today is to house the blind in a DSF system. It is encased between two glass layers, the external glazing protect the elements while the internal glazing protects the shading system from damage or interference with its operation (Hasselaar, 2006). The effectiveness of the integration of automated solar-shading system with DSF has been exemplified in the Institut du Monde Arabe designed by Jean Nouvel, project (A) where the photosensitive diaphragms are sandwiched between two glass sheets. Also, the adaptive fritting Kinetic façade, project (D), is encased between two panes of glass. Besides, the responsive solar-shading systems incorporating material actuation; such as invert project of Doris sung, project (N), and the Homeostatic Façade System, project (G), are integrated within DSFs. An explanation for this integration is to protect the light weight flexible systems from external atmospheric agents, damage and internal interference. The following is a brief description of the movement types of solar-shading devices.

Movement of solar-shading devices can always be categorised into two main types of movement: rotation and translation, or a combination of both (Fiorito et al., 2016; Jules Moloney, 2011; Schaeffer & Vogt, 2010). In translation movement (linear), the object in space moves parallel to the coordinate axes in a consistent planar direction. In rotation movement, the object changes its spatial orientation by rotating around the coordinate axes. Rotation can be divided into three typologies: swivel (restricted rotation), revolving (free rotation), and

swing (off-centre rotation). A different set of movements can be represented by combining rotation and translation, such as folding, expanding and contracting (Fiorito et al., 2016). For each of these kinds of movement, one may define three degrees of freedom, depending on how the direction or orientation of an object shifts with respect to one, two or three coordinate axes as shown in Figure 2-7. Typologies of motion are defined by the number of degrees of freedom (Fiorito et al., 2016).

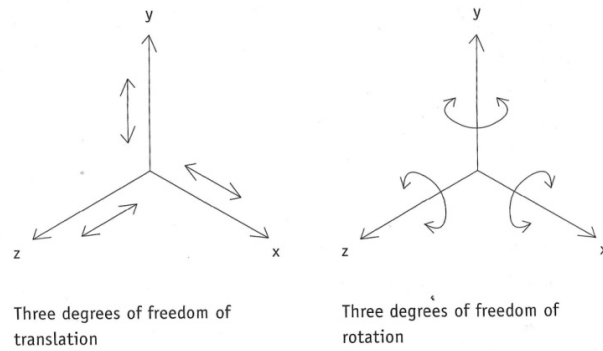


Figure 2-7: Degrees of freedom for translation and rotation motion (Werner, 2013).

Jules Moloney (2011) classified movements of kinetic surface components into translation, rotation, scaling movements, and, material deformation, as shown in Figure 2-8. Scaling movements describes expansion or contraction in size, while the deformation motion is achieved through material change.

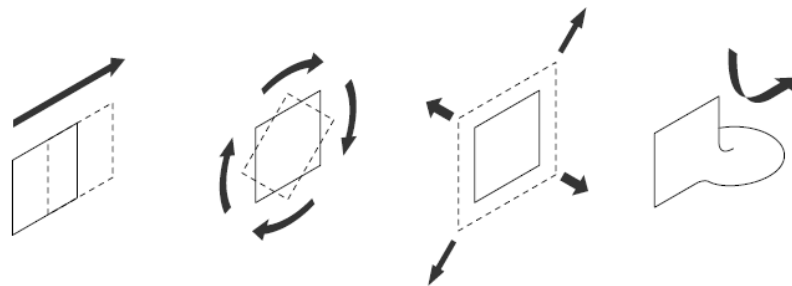


Figure 2-8: Movement through three geometric transformations in space – translation, rotation, scaling and movement via material deformation (Jules Moloney, 2011) .

As examples of the *translation* movement, the Adaptive Fritting, Project (D), achieved translational shift through utilising a parallelogram linkage system through the panels themselves used as the linkages. The mechanism converts a rotational motion into a translational motion delivering a *scaling* effect (Drozdowski & Gupta, 2009). The kinetic motion of Project (B) Kiefer Technik, is a vertical translation incorporated with a folding joint that also enables a *scaling* effect. The major considerations for the translational motion become friction and inertia.

There are a large number of projects that use *rotation* movement, in particular those that use adjustable louvers to provide dynamic effect (Jules Moloney, 2011). For example, the Institut du Monde Arabe, project (A), represents a particular *scaling* kinetic. The south facade is composed of a  $24 \times 10$  grid of square bays. Each bay contains a circular central shutter surrounded with a grid of smaller circular shutters. The actual movement is the *rotation* of flat sheets over each other, similar to the mechanism of a camera lens. Moreover, Q1 Headquarters building façade, project (C), represents a *rotational* movement of the cantilevered fins. Each side of the stud can be twisted separately, as the arms rotate from widely open ( $0^\circ$ ) to parallel ( $90^\circ$ ). Rotation and/or translation movements define opening ratios or aperture size at the component scale, which are relative to the geometrical shapes proposed for each project (Fiorito et al., 2016).

Examples on *deformation* motion were investigated on a prototype level and can be found in the work of C. K. Khoo and F. D. Salim (2013) and Begle, Luna, Luna, and Ardila (2013) when they applied shape memory alloys in conjunction with silicon or tensile skins. This can be found later in section 2.3.4 page 45.

The most common practice for the movement of responsive solar-shading systems in use today is *rotation* movements and the combination of the *translation* and *rotation* movements. This is in addition to some innovative explorations in *material deformation* using lightweight flexible and/or elastic materials. Having discussed the different terminologies and typologies of adaptive facades and responsive solar-shading systems, the next section will describe the soft robotics approach to simplify mechanical designs utilised in adaptive facades.

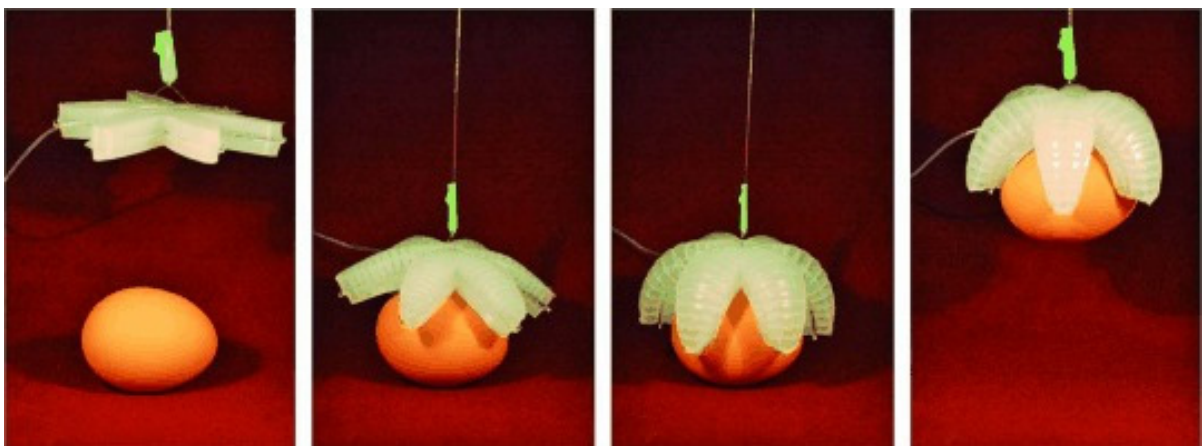
#### 2.2.4. *Soft robotics*

*Soft robotics* use intrinsically soft and/or extensible materials that can deform with muscle-like actuation that mimic biological systems (Bengisu & Ferrara, 2018). They absorb much of the energy arising from a collision and generate little resistance to compressive forces (Rus & Tolley, 2015). *Soft robots* have the advantage of distributed deformation with a relatively large number of degrees of freedom (Rus & Tolley, 2015; Trivedi, Rahn, Kier, & Walker, 2008). Also, they promise to be able to bend and twist with high curvatures and to deform their bodies continuously and thus achieve movements that emulate biology. *Soft robotics* promise to adapt their shape to the environment, employing compliant motion and thus manipulate objects (Rus & Tolley, 2015). They are robots with physically flexible-bodies



and electronics or AI technologies. Thus it includes extensible materials which can be pneumatically actuated, hygroscopic materials and smart materials. It is experimented to simplify mechanical actuation using pneumatic or material-based actuation to achieve dynamic behaviour.

Pneumatically-driven McKibben-type actuators are considered among the most advanced soft actuators. They can be fast and have a length-load dependence similar to that of muscle. They consist of a bladder or a pouch covered in a shell of braided, strong, inextensible fibers. Each actuator can only contract and extend when pressurisation changes. Complex movements require multiple actuators acting in series or parallel. A similar procedure was done using 'Origami-Inspired Artificial Muscles'. Each muscle consists of an outer bag that is made of plastic or textile, filled by air or fluid and surround an inner folded skeleton. This fluid is sucked out of the bag to initiate the muscle's movement by causing the skin to collapse onto the inner folded skeleton, creating tension that drives the motion (Burrows, 2017). They argue that the 'Origami-Inspired Artificial Muscles' are soft, strong, cheap and scalable. Other researchers, Ilievski, Mazzeo, Shepherd, Chen, and Whitesides (2011), used embedded pneumatic networks of channels in elastomers to provide a broader range of behaviours and complex motion as shown in Figure 2-9.



*Figure 2-9: Soft-robotic 9 cm tip-to-tip PneuNet gripper grabs a chicken egg.*

The Tangible Media Group researchers at MIT Media Lab's developed a project 'Aeromorphs' inflatables which is transforming basic flat sheets into complex inflatables. Pouches made out of plastic, paper or fabric are blown up into a spherical shape like a balloon, to form different three-dimensional shapes determined by the seam pattern that is pressed into them as shown in Figure 2-10 (Aouf, 2017).

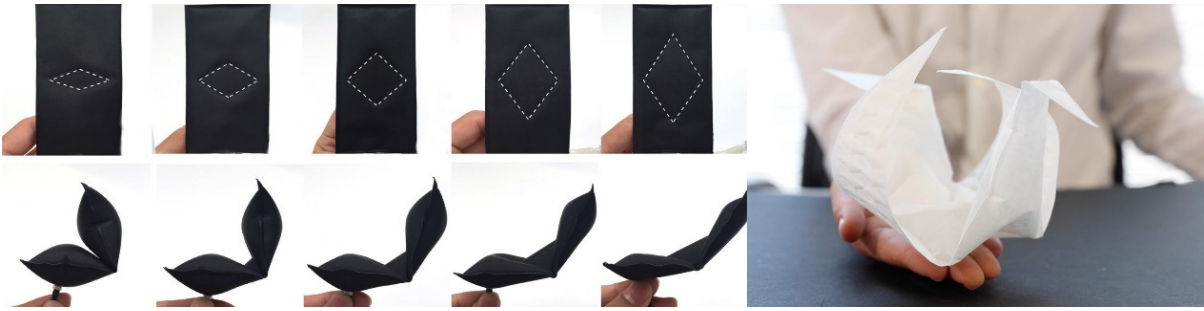


Figure 2-10: Aeromorphs inflate into different shapes, determined by the pattern of seams that is pressed into them.

Investigation of new responsive smart materials, could be an efficient replacement to mechanical joints as they have the potential to work as muscles with even less complexity than pneumatic muscles. Material embedded actuation can alter their morphology under external stimulation and adapt autonomously to their respective environmental conditions (Reichert et al., 2015; Schaeffer & Vogt, 2010). Bio- and origami-inspiration are rich sources of inspiration for deployable principles (Adrover, 2015). Soft robotics can draw inspiration from biomimicry to perform as a muscle-like actuation that mimic biological systems. Additionally, Origami can be turned into self-folding structures which can automatically fold and/or unfold itself by embedding smart materials. Thus, Smart materials, Bio-inspiration and Origami can be considered as key factors of soft robotics approach. Each of these factors will be studied sequentially in the following sections to discover deployability concepts and means of actuation, as shown in Figure 2-11.

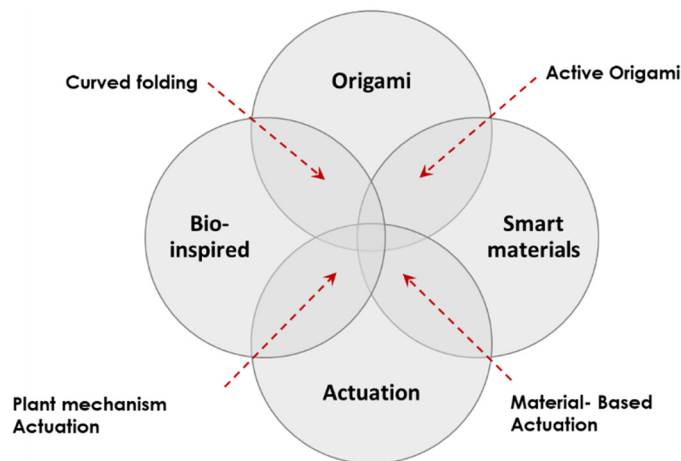


Figure 2-11: Areas of Intersections for Soft Robotics.

Having defined what is meant by soft-robotics, the next section will explain the smart materials types, characteristics and means of attachment. Smart materials are used as material-based actuation to achieve dynamic behaviour by means of passive response.

### 2.3. Smart Materials

Materials are the key players in the design process. In all different architectural stages from schematic design to the project construction, the material involvement is inevitable (Kretzer, 2017a). Architecture is defined by physical components, materials to convey specific architecture expressions. In the 19th century, William Morris mentioned that, “the subject of material is clearly the foundation of architecture”. When a material is used in novel and unforeseen ways, or when its properties are presented in an unconventional setting, the design level is improved (Bell, 2014). The industrial revolution reshaped the relationship between materials and architecture. Through advances in computer aided design and computer aided manufacturing (CAD/CAM) technologies, engineering materials such as aluminium and titanium can now be efficiently employed as building skins, allowing for a new variety of building façade forms. Designers consider materials as part of the design process, from which materials are selected for their functional, compositional and visual properties. Materiality has emerged as a powerful concept influenced by developments in digital fabrication and digital science in recent years (Loschke, 2016). Hence, all the design professions have been influenced by the materiality concept and experienced renaissance in materials which are clearly reflected through the leading exhibitions and publications that highlight the role of materials in design (Oxman, 2010).

To better understand the emerging materiality concepts nowadays, researchers should study material properties, abilities and their effect on design. Menges (2012) claimed that material properties, characteristics and behaviour can now be employed as active design generators that guide and inform the design. In architecture, materials at both microscale and macroscale can now be understood as a continuum of reciprocal behavioural characteristics and performative capacities. In the same vein, Oxman (2010) claimed that modern design culture is experiencing a shift to material aware design. She is calling for material-based design computation where material precedes shape, and it is the structuring of material properties that generates design form. Oxman (2010) has proposed a novel definition of ‘*New Materiality*’ as ‘*a non-hierarchical association between form, structure and material*’ which appears to have a diverse and complex influence upon contemporary design. Other researchers have highlighted how literally active materials could reshape our built environment.

In 2011, the concept of '*Materiability*' had been introduced by Prof. Ludger Hovestadt to highlight the design using new active and smart materials. Kretzer (2017a) defined it as '*the ability to create materials with abilities*'. Materiability addresses the potential to control and design matter at a nano- or micro-scale and construct materials that are dynamic, active, and responsive to environmental conditions (Kretzer & Hovestadt, 2014). Programmable matter, an older term introduced by Toffoli and Margolus (1991), refers to matter or materials which inherently have the ability to change their physical properties, like shape, colour, temperature, density, conductivity, opacity, etc., according to internal or external action in a controlled and direct way (Kretzer, 2017a). The concept aims to create synthetic materials with performative abilities liberated from a materialistic and mechanistic point of view (Kretzer, 2017a).

Recently, considerable literature has grown around the theme of smart materials that could be passively efficient and replace energy-intensive mechanical actuation. Material embedded actuation can alter their physical appearance under external stimulation and adapt autonomously to their respective environmental conditions (Reichert et al., 2015; Schaeffer & Vogt, 2010). Smart materials, according to NASA, are 'materials that "remember" configurations and can adapt to them when exposed to a certain stimuli' (Addington, 2005). Smart materials and structures are defined in the Encyclopedia of Chemical Technology as 'entities that detect environmental events, process sensory data, and then act on the environment' (Mabermann & Kroschwitz), 1991). The smart materials are also known as Stimuli-Responsive Materials (SRMs). Stimuli-responsive materials are defined as the materials that change one or more of their properties under a defined stimulus (Sun et al., 2012). Smart Materials or Stimuli-Responsive Materials have permanently reversible properties which are triggered by external physical and chemical influences such as temperature, light, pressure, electrical, magnetic or chemical stimulus (Schaeffer & Vogt, 2010).

In the field of smart materials, current projects are driven by research in engineering, medical sciences, and human-computer interaction, while only a few projects are undertaken in architecture, product design, and fashion design domains. The progress occurring in the area of smart-materials can provide a relevant contribution and bring real benefits to the design and architectural practice and industry (Oxman, 2010).

According to Addington (2005), Transiency, selectivity, immediacy, self-actuation, and directness are the five fundamental characteristics that differentiate smart materials from more traditional materials. These characteristics are defined as follows:

- Immediacy – have real-time responses.
- Transiency – they respond to more than one environmental state.
- Self-actuation – intelligence is intrinsic to the material rather than external to it.
- Selectivity – their reaction is discrete and predictable.
- Directness – the response is local to the triggering event.

#### 2.3.1. *Smart materials classifications*

Based on the general approach described above, smart materials may be easily classified in two basic ways. The first group of smart materials is comprised of materials that undergo changes in one or more of their properties – chemical, mechanical, electrical, magnetic or thermal – in direct response to a change in the external stimuli associated with the environment surrounding the material. Among the materials in this category are thermochromic, magnetorheological, thermotropic and Shape memory. The second group of smart materials is comprised of those that transform energy from one form to an output energy in another form. Among the materials in this category are piezoelectrics, thermoelectrics, photovoltaics, pyroelectrics, photoluminescents and others. Another classification was presented by (Sun et al., 2012) who classified stimulus-responsive material (SRM) according to their change in their properties; physical and chemical. For shape-changing solar shadings, the physical change of smart materials are the best option (Fiorito et al., 2016). Focusing on the physical phenomenon of smart materials that convert external stimuli into kinetic force and change their shape correspondingly, these materials can be classified into two types: *shape change materials* (SCMs) and *shape memory materials* (SMMs) as shown in Figure 2-12 (Sun et al., 2012).

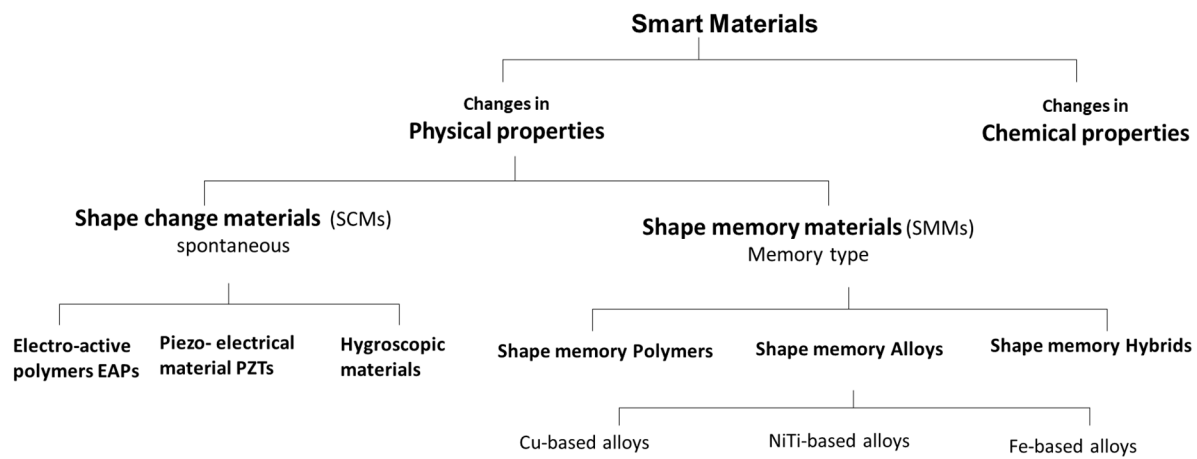


Figure 2-12: Classification of smart materials.

*Shape change materials* (SCMs) are able to change their shape at the presence of the right stimulus (Fiorito et al., 2016). Some relevant examples of SCMs are the electro-active polymers EAPs, piezo- electrical material PZTs and hygroscopic materials as shown in Figure 2-12. Electroactive polymers (EAP), also known as dielectric elastomers (DE), are ‘*smart*’ materials capable of undergoing deformations in response to suitable electrical stimuli (Carpi, Kornbluh, Sommer-Larsen, & Alici, 2011). The main weakness with such electroactive material deformation is that it requires high energy consumption and demonstrates a lack of physical strength (Carpi et al., 2011; Reichert et al., 2015). The wooden sheets with hygroscopic actuation, which are similar to plant cones that react to humidity levels, are considered SCM (Reichert et al., 2015). Chromoactive materials are characterized by its ability to change colour, to reduce direct solar radiation but they affect the levels of daylight and colour rendering of the internal space, when faced with an external stimulus. The kinetic nature of a shading system offers more individual control on the levels of daylight without change to the interior colour rendering. However, another problem with this category of smart materials is that it is limited to a ‘*change*’ in their physical/chemical properties (Sun et al., 2012). On the other hand, *Shape memory materials* (SMMs) are able to ‘*change*’ their physical properties as well as to “*remember*” a specific “*memorized*” shape they were “*trained*” to adopt (Bengisu & Ferrara, 2018). Some relevant examples of (SMMs) are Shape Memory Alloys (SMAs), Shape Memory Polymers (SMPs) and Shape Memory Hybrids (SMHs) (Fiorito et al., 2016). A more detailed account of shape memory materials is given in the following section for their good potential to actuate solar-shading systems.

### 2.3.2. *Shape memory materials (SMMs)*

SMMs are ideal for an integrated responsive system, that can sense and then produce reactive motion as pre-programmed, in which "the material is the machine" (Sun et al., 2012). These materials can be activated by a difference in temperature, which can be triggered by direct sunlight exposure and converted into kinetic force (Fiorito et al., 2016). Features found in SMM enables enthusiasts to design SMMs with tailored properties/features for a particular application without the aid of experts following a do-it-yourself (DIY) manner (W. M. Huang et al., 2010). In the shape memory materials (SMMs), the temporary shape can be virtually held forever unless the right stimulus is applied to trigger the shape recovery.

All SMMs are characterized by the shape memory effect (SME), which is defined as the ability to recover the original shape at the presence of the right stimulus, after being severely and quasi-plastically distorted (Sun et al., 2012). This characteristic makes them the most appropriate choice for activating smart morphing solar-shading devices with the thermal effect of incident solar radiation. The SME can be utilized in deployable structures (W. M. Huang et al., 2010). Although, the SME can be traced back to 1932 when it was detected in AuCd alloys, later it was observed in other alloying systems.

Fiorito et al. (2016) argue that smart materials, Shape Memory Alloys (SMAs), Shape Memory Polymers (SMPs) and Shape Memory Hybrids (SMHs), have been shown to possess the characteristics to work as actuators, either separated or integrated into shading components. Among the SMMs, which have been developed so far, SMAs and SMPs are the most important. SMAs are featured by the ability to recover their original shape upon changes in temperature, stress, or magnetic field via a reversible martensitic transformation (Bengisu & Ferrara, 2018). On the other hand, SMPs have limited SME, which means they are only capable of a certain level of shape recovery. Although SMPs have lower densities than SMA, they have low cost as a raw material and also in fabrication (Sun et al., 2012). On the other hand, SMPs can be pre-programmed to desired shapes. A shape recovery is exhibited when a specific critical temperature is exceeded. They can be applied to hinges which differs from the rest of material allowing the hinges to respond to a uniform stimulus (Liu, Boyles, Genzer, & Dickey, 2012). Moreover, SMHs which represents the newest type of SMMs, are composed of easily available, inexpensive materials such as silicone rubber loaded with paraffin. They share the same mechanism as SMPs but don't have any SME as an individual (Sun et al., 2012).

Through their memory shape effect and speed of actuation, these actuators are able to produce ranges of movement and responsiveness suitable to be applied in dynamic solar-shading systems. Thermal triggering has been discovered as the most significant method for activating shape memory alloys. Commonly, those materials are activated by a difference in temperature, which can be triggered by direct sunlight exposure (Fiorito et al., 2016).

The activation temperatures for (SMMs) have been exemplified by some researchers; such as (Fiorito et al., 2016) and (Sun et al., 2012). Doumptoti et al. (2010) have tested the activation temperatures of embedded SMAs that allows for integrated sensing and actuation. It was designed to have an actuation temperature of 35-40 degrees Celsius, a temperature easily achieved through direct solar exposure. Another project carried by Lignarolo, Lelieveld, and Teuffel (2011) implemented a composite of SMA and SMP. The SMAs are applied as an actuator material, which is implemented in a SMP matrix and enable the deformation of the element when reaching more than 90 °C. Overall, these cases support the view that activation temperatures of Embedded SMAs can be achieved in hot arid climates through direct solar contact and can be applied for responsive solar-shading system.

### *2.3.3. Shape memory alloys (SMAs)*

SMAs, also referred to as shape memory metals or memory metals, composed of at least two metallic elements (Ritter, 2007). Till now, SMAs have mainly been classified into three types; Nickel-Titanium alloys (NiTi-based), copper-based alloys (Cu-based) and iron-based alloys (Fe-based). Among them, Cu and Ni-based alloys are more suitable for engineering applications and have extensive practical usability, but the latter has better mechanical properties (Sun et al., 2012). In 1962, the shape memory effect (SME) was found in Nickel-Titanium (NiTi) alloys, which are known as Nitinol (Kretzer, 2017a). They are the most diffuse SMAs, due to their relatively high recoverable strain (around 7%), high actuation stress (up to 500 MPa) and high corrosion resistance (Fiorito et al., 2016). NiTi-based SMAs are more reliable and can be highly biocompatible (Sun et al., 2012). They have been extensively employed as passive/active control systems and as smart/adaptive materials because of their unique thermomechanical characteristics, good output/weight ratio, sensing and actuating capability and good damping properties (Sun et al., 2012). NASA's folded satellite dish was among the first users of SMAs that folded out under the influence of solar radiation (Ritter, 2007).



Thermo-responsive SMAs can exist in two different phases, with three different crystal structures (i.e. twinned martensite, detwinned martensite and austenite) and six possible transformations as shown in Figure 2-13 (Ritter, 2007; Sun et al., 2012). The NiTi-based alloys recover its original shape after being deformed when heated above an austenite finish temperature (Mestre, Riofrio, & Shin, 2014). This SME is associated with the phase transformation between the martensite phase and austenite phase (Mestre et al., 2014). Since the austenite–martensite inter-phase is fully coherent to ensure high reversibility during transformation, there is a definite relationship between the orientation of an austenite crystal and that of a neighboring martensite crystal (Sun et al., 2012). The reversibility of NiTi SMA occurs due to the solid-to-solid phase transformation from a high symmetry austenite to a lower symmetry martensite phase (Tadayyon et al., 2016).

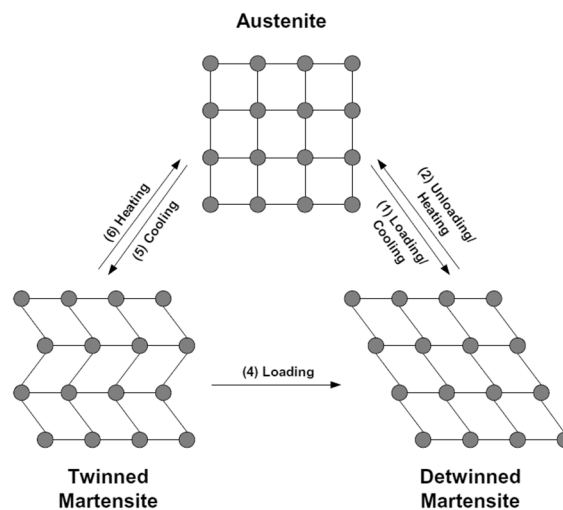


Figure 2-13: Change in lattice structure (Sun et al., 2012).

The SME in SMAs provides the possibility to achieve “*the material is the machine*”. As a machine, it is ideal that the motion of a SMA follows a prescribed sequence in a programmable manner, which requires some intermediate shapes or positions to be reached. Some special mechanisms can be used to achieve multiple SME (i.e., with multiple intermediate shapes/positions). A SMA wire can reach two or three positions depending on how it is joule heated (Sun et al., 2012).

The ordinary SMA have one-way SME, which enables it only to remember the high temperature (austenite) shape. On the other hand, the *two-way shape memory alloy* (TWSMA) remembers both high temperature and low temperature shapes during thermal cycling. It is believed that the training process plays a key role in the introduction of the *two-way SME* which originally has only *one-way SME*, i.e., only the high temperature austenite

shape can be recovered (that is intrinsic) (W. Huang & Toh, 2000; Sun et al., 2012). On the other hand, the *two-way SME* is achieved by means of introducing an elastic stress field at micro-scale for reversible shape switching. It is introduced into the SMA by means of thermomechanical training (Sun et al., 2012).

#### *2.3.4. The fixation of active and passive materials*

Many practices in the field of self-folding origami and robotics tend to attach or use 'patching' strategies between smart materials and rigid structures. This approach has been criticized by Oxman (2010) and Kretzer and Hovestadt (2014), encouraging a more holistic approach to understand and implement materials design which is customized through formal, structural and material heterogeneity (Oxman & Rosenberg, 2007). Kretzer and Hovestadt (2014) argued that the first approach is used to replace technologies and devices without addressing material-specific characteristics or apply them in superficial, sensational contexts. He claimed that those systems require much energy to operate, and are typically maintained by global control. However, those 'patching' strategies can be low cost and achieve material and energy reductions when being thoroughly studied. Sterman, Demaine, and Oxman (2013) argued that embedding or attaching smart materials within a passive material substrate could achieve integrated properties. It is an interplay or a dialogue between passive and active materials to create an autonomous system or structure which takes advantages of both material properties. It is rather a balance of forces and not only embedding a sensor or actuator. All the decisions on the form, locations of the sensor/actuator, the patterns of attachments, and exposure to stimulus affect the motion and performance. Methods of attachment of how the active and passive parts are fixed together or printed on top of each other can result in various outputs, allowing the emphasis of very different aspects of the composition. Edwin et al. (2014) conducted a survey and analysis of prior work on active self-folding using active materials. The study classified those concepts into two categories: hinge type and bending type.

##### *2.3.4.1. Bending type*

The direct bending approach without hinges may offer the advantage of larger foldability (Edwin et al., 2014). This approach of self-folding mainly depends on the bi- or multi-layering concept. It allows for folds in both directions relative to the sheet normal based on the direction of the driving field gradient as shown in Figure 2-14 (Edwin et al., 2014). The bilayer concept is highly related to bio-inspiration similar to the hygroscopic materials studied

by (Holstov, 2018; Holstov, Bridgens, & Farmer, 2015; Reichert et al., 2015). Also, bimetals fall under the bilayer concept, which flex reversely in response to a change in temperature due to the differential expansion of the two tightly bonded metals (Kretzer, 2017a). The concept of bilayering was explored by Sung (2016) in some kinetic systems; such as ‘bloom’ and ‘invert’, using thermobimetal with pieces that bend and curl upon heating. Thermobimetals (TB) are defined as ‘*laminated composite materials and consist of at least two components, made from metals with different thermal expansion coefficients, which are permanently bonded to one another*’ (Ritter, 2007). The component with the lower thermal expansion coefficient is called passive, while the component with the higher coefficient is called active, as shown in Figure 2-15. The material deforms when heated or cooled (Sung, 2016), and it takes up a curved shape (Ritter, 2007).

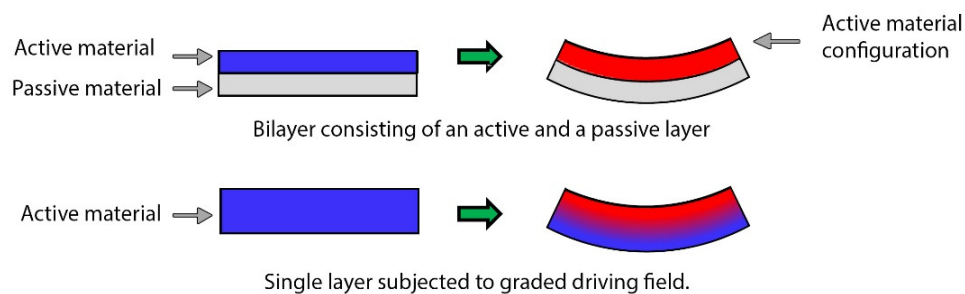


Figure 2-14: Bilayer consisting of an active and a passive layer (Edwin et al., 2014).

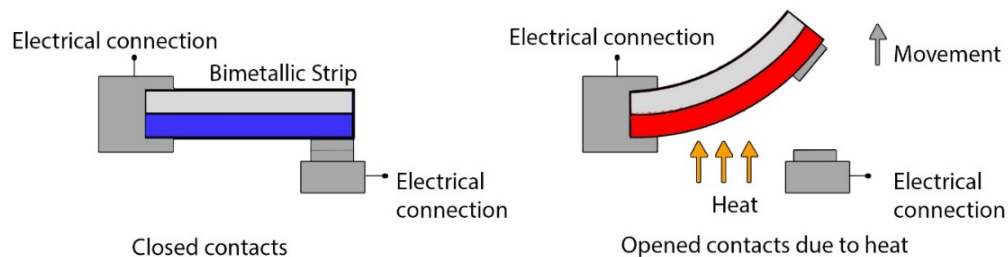


Figure 2-15: Schematic diagram of the working principle of a bimetallic strip as used in early thermostats (Kretzer 2015)

Electroactive polymers (EAPs) are mostly used as bending actuators with strong bending capabilities where high forces are required but have a rather slow response speed (Kretzer, 2017a). The ‘*ShapeShift*’ final prototype exhibited at the Gallery StarkArt in Zurich, employs bending motion upon the action of Dielectric elastomers (DE) thin film, which belongs to the second group of EAPs (Kretzer, 2017b; Kretzer & Rossi, 2012a). The ‘*shape shift*’ project represented a major shift to the material-based actuation by exploring the potential application of electro-active polymer (EAP) at an architectural scale. It is an ultra-lightweight,

flexible, aesthetically interesting material with the ability to bend without the need for mechanical actuators, as shown in Figure 2-16 (Kretzer, 2017b). In 2012, *'Animated Textiles'*, a one-week workshop, held at the Swedish School of Textiles in Borås by Kretzer, Damjanovic and Dumitrescu investigated the use of dielectric elastomers based on the same bilayered bending motion. During this workshop, the participants created animated surfaces, structures, and assemblies from combining dielectric elastomers with various lightweight textiles, as shown in Figure 2-17 (Kretzer, 2017a).

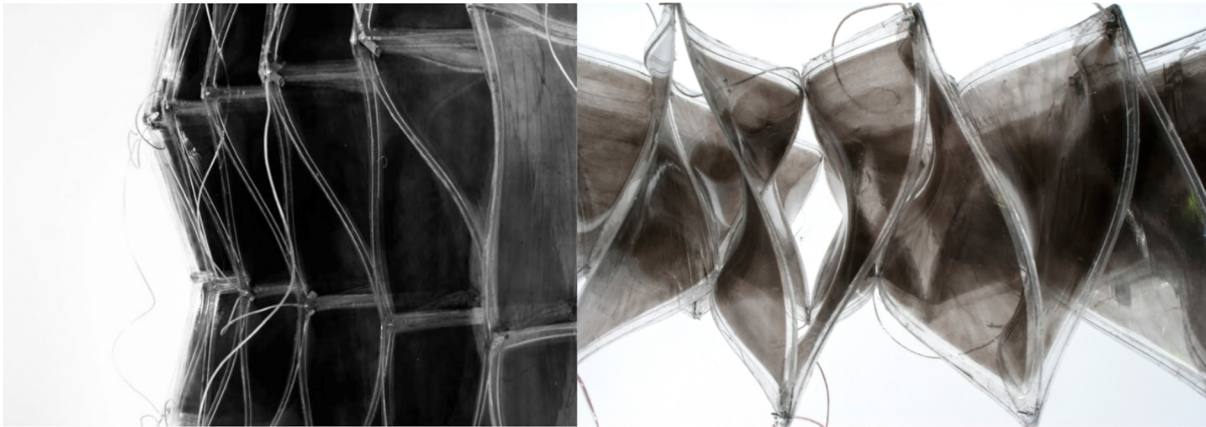


Figure 2-16: *'ShapeShift'* final prototype exhibited at the Gallery StarkArt in Zurich, which consisting of 36 individual EAP elements (Kretzer, 2017b).



Figure 2-17: Combining custom electroactive polymers with lightweight fabrics was one goal of the *Animated Textiles Workshop* (Kretzer & Damjanovic, 2012).

The multi-layering concept has been investigated by researchers through self-folding composite (S. M. Felton, Becker, Aukes, & Wood, 2015; Tolley et al., 2014). Tolley et al. (2014) presented a self-folding origami consisting of shape memory composites that are activated with uniform heating in an oven. The self-actuated surface depends on the contraction of a heat-activated SMP layer material sandwiched between two structural layers. The SMP layer is fixed with two additional adhesive layers to hold the laminate together. Similarly, S. M. Felton et al. (2015) presented a self-folding composite consists of three materials comprising

seven layers bonded with an acrylic adhesive. Those functional materials are the substrate, the polyolefin SMP and the polyimide flexural layer. This composite was programmed with self-folding hinges by activating the SMP, causing it to contract, as shown in Figure 2-18 from position (a) to (b). The composite can also be programmed using passive hinges that allows the structure to bend repeatedly as shown Figure 2-18 from (c) to (d).

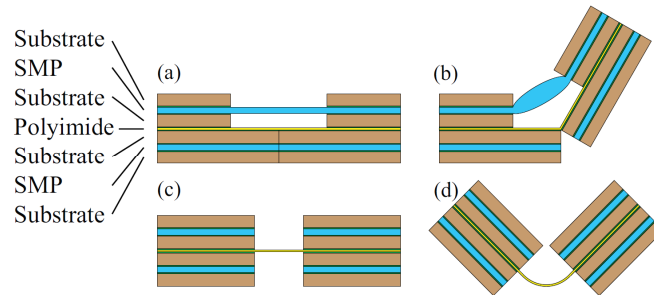


Figure 2-18: Self-folding composite consists of seven layers and programmed with self-folding hinges (S. M. Felton et al., 2015).

#### 2.3.4.2. Hinge Type

Hinge mechanism can deploy different forms and folds actuated by a SMM, SMA wire or spring or SMP. Edwin et al. (2014) classified the hinge active fold into three basic concepts as shown in Figure 2-19, which are: (a) extensional (variable length linear actuator that connects two faces, active rod or spring), (b) torsional (active element with twisting abilities at the hinge), (c) flexural (the active element with pre-set folded or bended shape).

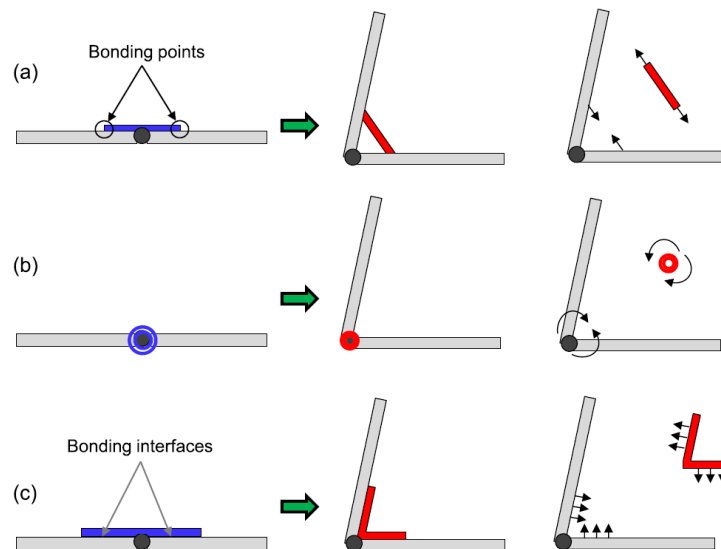


Figure 2-19: The Hinge type basic active fold concepts (Edwin et al., 2014).

Some research prototypes used the hinged connections to actuate their models, such as ("Air Flow(er)," 2018; Gianluca, Fiorito, & Vallati, 2018; C. K. Khoo & F. Salim, 2013; Pesenti, Masera, & Fiorito, 2015). Pesenti, Masera, Fiorito, et al. (2015) actuated a cardboard origami model that has a Ron Resch pattern with NiTi SMA wires (720 mm length and 150  $\mu\text{m}$  thickness) stimulated by Joule heating 16 V electricity as shown in Figure 2-20. The extensional SMA wires resulted in a non-sufficient deformation percentage, and it was reported that a further deformation multiplication is needed for this new generation of engineered materials.

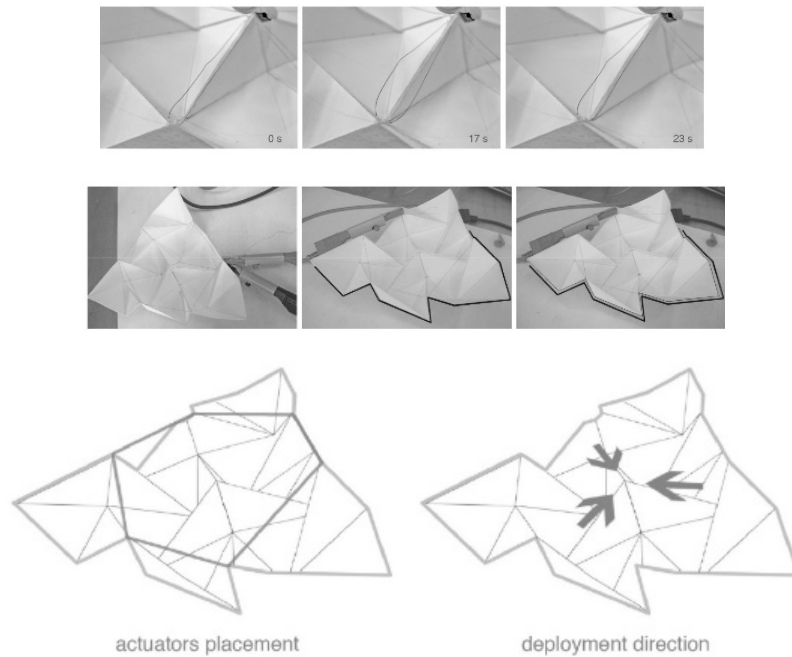


Figure 2-20. A cardboard origami model is actuated with NiTi SMA wires (Pesenti, Masera, Fiorito, et al., 2015).

The significance of SMA springs as actuators was exemplified in work undertaken by C. K. Khoo and F. D. Salim (2013). An extensional type actuator using a SMA spring is used to actuate a blind with multiple eye-like apertures to allow light penetration, as shown in Figure 2-21. The blind can be programmed to accept data input for visual communication. The elastic nature of silicone rubber 'closes' the 'eye' apertures when SMA springs are not heated.



Figure 2-21: Eye- like apertures actuated by a single linear actuator (C. K. Khoo & F. D. Salim, 2013).



Another example is a master project by Dulce Luna, Iker Luna, Juan Diego Ardila, and Moritz Begle in the Institute for Advanced Architecture of Catalonia (IAAC) (Begle et al., 2013). The project developed an adaptive solar radiation façade that rotates according to the sun position, depending on a single diagonally exposed SMA spring.

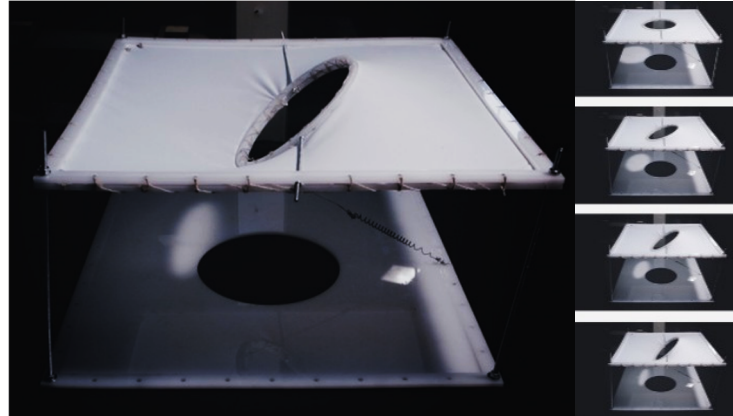


Figure 2-22: An adaptive solar radiation façade rotates depending on a single diagonally exposed SMA spring (Begle et al., 2013).

Also, Lift architects developed a four leaf prototype with a name Air Flow(er) device which is actuated by a suspended extensional SMA wire to open the leaves for ventilation. In a small wooden box, a heat gun was used to heat the wires to contract and the panels to open. The wires start cooling off after the heat is removed, and the elastic cords gently pull each panel back into its closed location. ("Air Flow(er)," 2018).

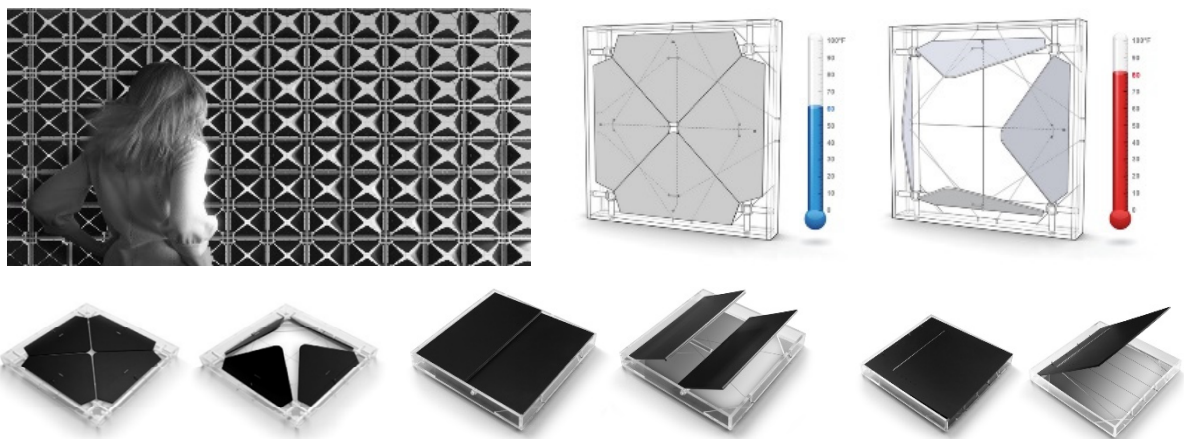
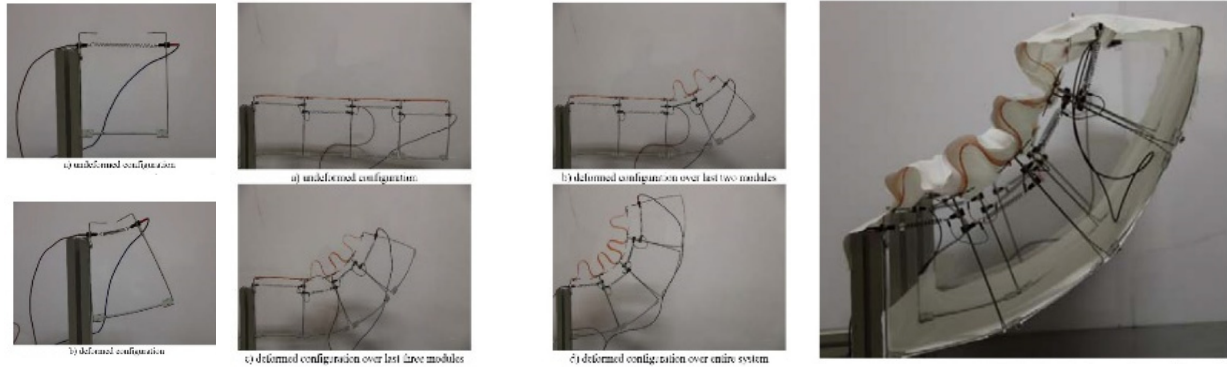


Figure 2-23: Air Flow(er) device which is actuated by a suspended SMA wire to open the leafs for ventilation("Air Flow(er)," 2018).

Recently, Gianluca et al. (2018) developed an adaptive shading device structurally morphed using (SMA) springs combined with flexible structural components. The structure consists of three parallel modular systems covered by a lycra fabric placed around a thin-metal skeleton, as shown in Figure 2-24. The shading structure moves from an initial configuration to a deformed shape by the actuation of SMA springs through heating. The SMA springs

shorten upon heating and resulted in elastic deformations in the structural components. The particularity of the proposed system is that, upon cooling of the SMA springs, the shading device returns to its 'cool' configuration by releasing the flexural elastic strain stored in the deformed conditions.



*Figure 2-24: An adaptive shading device structurally morphed using (SMA) springs combined with flexible structural components (Gianluca et al., 2018).*

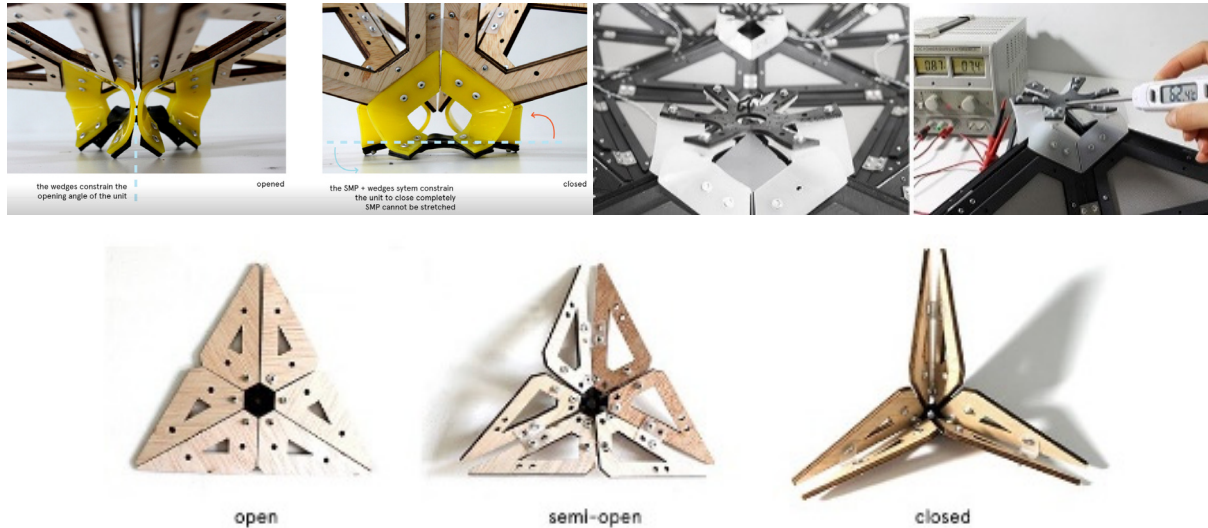
A responsive experimental installation, Hylozoic Series by Philip Beesley, explores responsive spaces which are based on the philosophical notion of hylozoism, believing that everything is animated and inseparably linked to life (Kretzer, 2017a). His installations achieved a caressing, clamping, and swelling motions, by means of SMA. The thin SMA actuators, which have the ability to contract when thermally activated, represent the muscles. A transparent structure is made of flexible and transparent material components, lily-shaped ribbed vaults and basket-like columns, where SMA actuators are embedded in the structure to animate it as shown in Figure 2-25 (Bengisu & Ferrara, 2018).



*Figure 2-25: Beesley's installation is made of flexible and transparent material components, lily-shaped, which is animated by means of countless embedded electronics and a myriad of glands and bladders.*



The integration of SMPs as actuators has been employed in a master project in the Institute for Advanced Architecture of Catalonia (IAAC) by (Baseta, Tankal, & Shambayati, 2014). A responsive architectural material system was created using flexural joints made of SMP, as shown in Figure 2-26.



*Figure 2-26: IAAC students create a responsive architectural material system.*

After reviewing a number of precedents for shading devices integrated with smart materials, the result highlighted that most of the case studies have seldom gone beyond a prototypical state. Only a few examples like the above-mentioned projects have reached the testing stage. Thus, the amount of realized architectural projects that use smart materials and proposes alternatives to conventional or mechanized solar-shading systems is rather limited. This is due to a general lack of knowledge and limited access to architectural information material products and above all, the low-cost culture in respect to building materials (Kretzer, 2017a).

Taken together, responsive shading projects based on material actuation with bending technique, such as 'Invert decorative shutter' (Sung, 2016) and 'Homeostatic Facade System' by Decker Yeadon can be considered as material consuming compared to hinged technique. However, it depends on the materials' cost and the characteristics of both passive and active materials. The recent explorations of actuator hinged types are more flexible to design motion. The hinged connections can move a single shading unit or connect more than one to enable the system to work collectively.

To conclude, the literature identifies the potential of SMMs as thermo-responsive materials capable of physical changing with the interesting ability of being pre-programmed

and customized. NiTi-based alloys are reliable as being the most diffuse SMAs, due to their relatively high recoverable strain (around 7%), high actuation stress (up to 500 MPa) and high corrosion resistance (Fiorito et al., 2016). SMAs features shape memory effect (SME), superelasticity, and high- damping capacity (Liu et al. 1999). SMAs has been applied in infrastructure like bridges, and robust behavior was demonstrated under dynamic loads (Cismaşiu and Amarante dos Santos 2008). The use of NiTi as wires (Formentini and Lenci 2018) and springs (Gonzales and Shreyas 2015 ; Khoo et al. 2011b, 2011a ; Khoo and Salim 2013, 2012) can be applied in more stiff and robust panels skins. However, the fixing is a critical component to provide robustness and stability to the façade. Moreover, the material's performance, life cycle assessment and the potential gains are still under investigation. Nitinol wires and springs which are available in the market can be programmed and embedded in a skeletal tensegrity structure to activate solar-shading systems. Thus, explorations with SMA actuators and fixation types will be tested later in *Chapter Four, 'Component design and prototyping'* chapter, page 119, using the physical experimentation.

Having defined the smart materials' types, characteristics and means of attachment, the coming section will discuss bio-inspiration as a form generative technique to understand how the form and materiality together can facilitate the motion. Drawing inspiration from biomimicry, specially plants, follows Adrover (2015) insights who argued that biomimicry and origami are rich sources for deployable principles.

## **2.4. Bio-Inspired Approach**

The possibilities of responsive architecture from the biological paradigm point of view make the mechanical paradigm seems dated (Fox & Kemp, 2009, p. 246; Jules Moloney, 2011). In relation to kinetics and movement, Fox and Kemp predict "the end of mechanics" as a "paradigm shift from the mechanical to the biological in terms of adaptation in architecture." Soft robotics can use plant actuation principles to develop reversible motions. Some studies have attempted to explain the actuation principles of plant movements, such as; (ElGhazi, Hamza, & Dade-Robertson, 2017; Fiorito et al., 2016; Poppinga et al., 2017; Schleicher, 2016; Schleicher, Lienhard, Poppinga, Speck, & Knippers, 2011). Plant flexibility is achieved through the adaptive behaviour that changes its morphological features by acting as living hinges and allowing for elastic deformations. They are able to move with low energy use, due to the fibre elasticity composition and integration of sensing and actuation capabilities into their system (Fiorito et al., 2016).

#### 2.4.1. *Biomimetic and bioinspired approaches for efficient movement*

Some designers and researchers argue that nature is the best, most influencing and the guaranteed source of innovation. As we know, imitating something that has already been known to function well may increase the probability of producing a successful analogous system. Biomimicry is the study of imitating and mimicking nature, where it has been utilized by designers to help in solving human problems. The term '*Biomimetics*', which was introduced in the 1960s, originally is a combination of two words; *Biology and mimesis* (imitation). Although terms like 'biologically inspired' or 'bio-inspired' are sometimes used instead of 'biomimetic' (Speck & Speck, 2008), they are different. Biomimetics is kind of limited to mimicking or copying natural solutions that work but might not be the simplest or the best answers and might have restricted technological implementation (Zhao et al., 2014). Bio-inspiration transfers from basic science to applied engineering without obvious resemblance to the biological prototypes. It extracts fundamental principles from biological systems to produce solutions that differ from the original biological prototypes. In this thesis, bio-inspiration, specifically, plant inspiration, will be used to understand the folding mechanisms and their actuation.

Plants can be a promising inspiration source to learn soft mechanics (Schleicher, Lienhard, Poppinga, Speck, & Knippers, 2015). Suitable analogues can be developed into responsive movements' production that meet design and sustainability demands. Plants show the capability of responding to a wide range of signals and efficiently adapt to changing environmental conditions. In particular, the bending and folding mechanisms of leaves and petals demonstrate how the number of mechanical parts can be reduced by making use of flexible and elastic material properties and allow reversible deformations (Poppinga et al., 2010; Schleicher et al., 2015).

For biologists, the classification of plant movements is a critical aspect to understand how plants develop morphogenesis (Boudaoud, 2010), and especially how they respond to environmental stimuli. Plant biologists distinguish between '*nastic*' and '*tropic*' movements. The movement in nastic responses is independent of the spatial direction of a stimulus, whereas '*tropic*' movements are influenced by its direction (Burgert & Fratzl, 2009; Schleicher, 2016). Generally, '*nastic*' movements occur due to the swelling and shrinking of motor cells and result in reversible movements that could be of high interest in responsive solar-shading applications (Poppinga et al., 2010; Ueda & Nakamura, 2006). In order to understand how

plants' movements develop in general, they will be analyzed on mechanical and structural levels. For example, the opening movement of *Lilium* (Liliaceae) is driven by a differential growth that appears between the rapidly expanding edges and the tepals inner lamina, as shown in Figure 2-27. It is relevant to look at the location of the motion triggers, which can resemble the actuator. Schleicher (2016) suggested recreating this opening mechanism by increasing the temperature in the tepal edges and thus enforcing a local expansion.

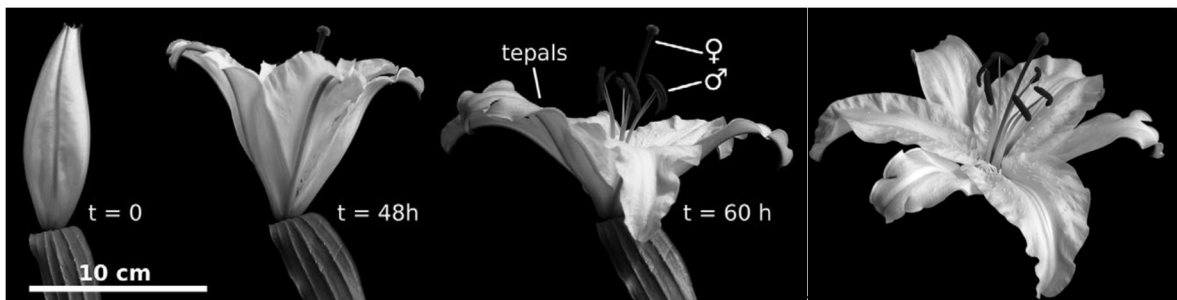


Figure 2-27: Opening movement of *Lilium* is driven by a differential growth (Schleicher, 2016).

#### 2.4.2. Actuation mechanisms in Plant Movements

Numerous studies have attempted to classify plant movements. Poppinga et al. (2010) developed a wide-ranged matrix focusing on the actuation systems found in active or passive nastic plant movements in response to environmental stimuli. The study distinguished between 'autonomous' and 'non-autonomous' movements as well as the 'active' and 'passive'. 'Non-autonomous' movements are often reversible deformations induced in pre-stressed structures by the release of stored elastic energy or triggered by external mechanical forces. Similarly, Schleicher (2016) distinguished between frequently encountered drivers like *external loads, growth processes, hydraulic mechanisms, and elastic instabilities*.

Accordingly, a more detailed structure of 'nastic *non-autonomous*' reversible movements is given, as shown in Figure 2-28. Reversible plant movements can be actuated either *hydraulically in an active way by turgor changes, or in a passive way by hygroscopic swelling and shrinking*. Other mechanisms use *the release of stored elastic energy after an external trigger* or by *direct application of mechanical forces*. The next section will discuss the actuation mechanisms derived by external loads, hydraulic mechanisms, and elastic instabilities.

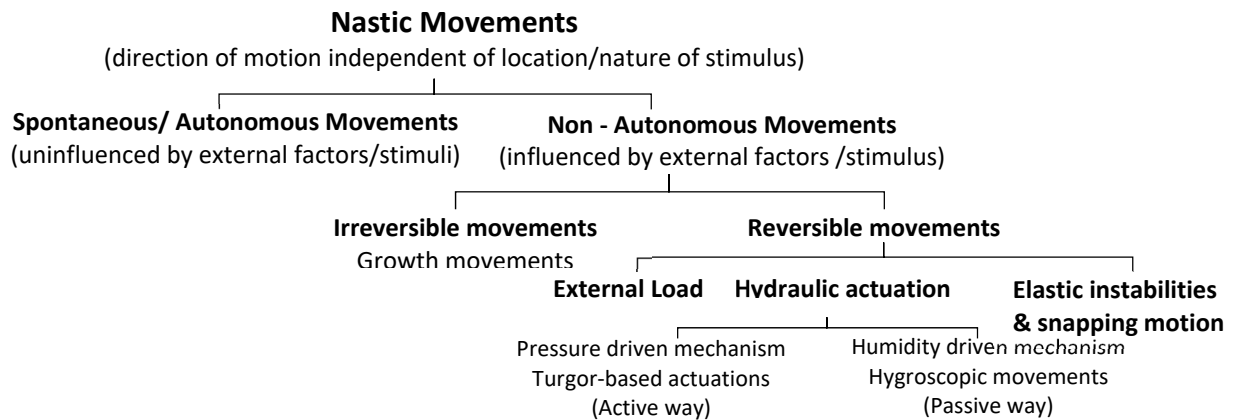


Figure 2-28: Classification of nastic plant movements.

#### 2.4.2.1. External loads

The motion of plants can be a response to the direct application of mechanical forces. This movement follows an external influencing factor passively rather than been driven by the plant itself. A plant can be affected by various loads, such as flowing water, wind gusts, contact with pollinating insects or natural predator attacks. An external drive may either cause immediate deformation or be redirected to initiate secondary transformation processes according to the composition of the plant (Schleicher, 2016). For example, the Bird-of-paradise movement is caused by a locally applied load at a specific point due to the pollination mechanism, as shown in Figure 2-29 (c).

#### 2.4.2.2. Hydraulic mechanisms

Hydraulic mechanisms in plant movements can be actuated either actively by ‘turgor changes’ that lead to reversible movement or passively by ‘hygroscopic swelling and shrinking’. ‘Osmotic actuation’ is a ubiquitous plant-inspired actuation technique that has a very low power consumption but is capable of producing efficient movements in a wide range of environmental conditions (Sinibaldi, Argiolas, Puleo, & Mazzolai, 2014). A living plant cell can produce inner hydrostatic/turgor pressure by sustaining an osmotic gradient between its cytoplasm and the ambient environment (S. Li & Wang, 2016). Turgor pressure variations allow plants to perform volumetric changes and rapid movements (Burgert & Fratzl, 2009; Schleicher, 2016). For example, *Mimosa pudica* responds rapidly and defensively to external stimuli, by closing the leaves and bending the pulvinus. Motor cells, which are classified into flexor and extensor cells on the ventral and dorsal side of the leaf as shown in Figure 2-29 (a), control the volume and shape according to its turgor pressure (Guo et al., 2015). The water-based, pressure-driven actuation system in plants is related to hydraulic and pneumatic

actuators that allow volumetric changes (S. Li & Wang, 2016). They are attractive for adaptive structures applications.

Other than the pressure-driven mechanism, plants can passively achieve reversible movements by '*hygroscopic swelling and shrinking*'. Plants also exploit a '*humidity driven mechanism*' to achieve shape change and actuation. The plant cell wall is a hydrophilic material, so it shrinks in volume when exposed to a dry atmosphere due to evaporation. This process can occur in both living cells and dead cells in the sclerenchyma tissues (S. Li & Wang, 2016). For example, a change in the relative humidity causes a closed, tightly packed Pine cone to open gradually. The mechanism relies on the bilayered structure, the active outer layer of tissue, closely packed long parallel thick-walled cells respond by expanding longitudinally when exposed to humidity and shrinking when dried, while the inner passive layer does not respond as strongly as shown in Figure 2-29 (b) (Reyssat & Mahadevan, 2009). But to be consistent with the scope of this review, this mechanism is only applicable in humid climates.

#### 2.4.2.3. Elastic instabilities and snapping motion

'*Elastic instabilities and snap-buckling*' effects are methods for translating small stimuli into large and amplified movements. The results of 'snap-buckling' intensify motions above the limitations set by simple hydraulic systems. These elastic instabilities are special mechanical failure modes characterized by a sudden deformation of a structural element. The structural unit withdraws from high tensile or compressive stresses by deflecting into a less strained but geometrically deformed condition. Particular carnivorous plants, like the Venus Flytrap, seem to master this technique (Schleicher, 2016). Interestingly, leaf closing tends to require a kind of 'memory' (Ueda & Nakamura, 2006). The '*bistable, doubly curved*' arrangement of the leaves, which snap-buckle to reverse their Gaussian curvature when closing, is the primary cause of the fast closure as shown in Figure 2-29 (d) (Guo et al., 2015). The movement of the Venus flytrap is hydraulically driven by a central surface with a midrib, which induces a bidirectional transition. Schleicher (2016) mimicked the cellular actuation of the Venus flytrap with Finite Element Modelling (FEM) simulation by applying heat to the lower side of the trap lobes surfaces. Five ribs were added to the trap lobes as an auxiliary construction. When these ribs get exposed to the same differential heat actuation as the trap lobe surfaces, however, they expand along their longitudinal axis and provide an additional impulse, with which it was possible to trigger the desired snap-through buckling.

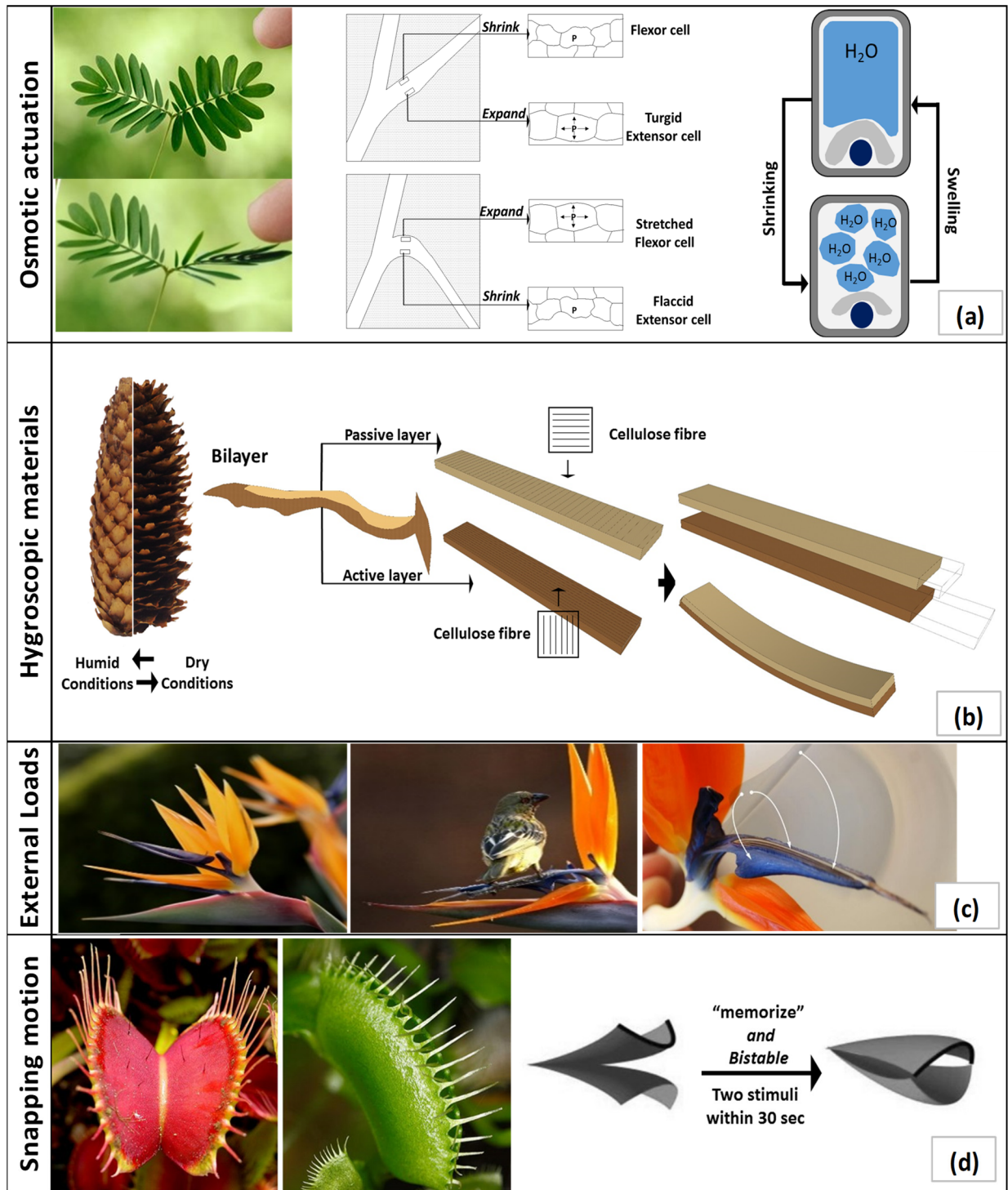


Figure 2-29: Reversible movements in the plant kingdom (a) *Mimosa pudica* rapid closure of leaves (Guo et al., 2015) (b) Pinecone hygroscopic swelling and shrinking (Holstov et al., 2015) (c) the Bird-of-paradise movement (Schleicher, 2016) (d) Actuation of the Venus flytrap (Guo et al., 2015)

This concept of ‘elastic instabilities and snap-buckling’ could have great potential in responsive systems. It can be adopted to achieve amplified and reversible movements. By looking at these methods of plant-folding mechanisms and their actuation, ideas can be generated on how to actuate kinetic structures and where to put the actuators. It can inspire both the form and material selections which will be explored later in *Chapter Four*.

#### 2.4.3. Elastic kinetic structures

The employment of elasticity within a structure not only facilitates the generation of complex geometries but also the creation of elastic kinetic structures. Plants' flexibility represents a compliant mechanism that reduces the number of mechanical parts by an integrative design (Schleicher, 2016). Howell (2001) defined '*Compliant Mechanisms*' as mechanisms that gain their motion from the deflection of elastic members and transforms the kinetic energy to strain energy in the members and then transforms it back to the kinetic energy (Howell, 2001). '*Compliant Mechanisms*' combine strength with elasticity and gain some of their mobility from flexible members' deflection rather than only from movable joints (Howell, 2001; Schleicher, 2016). In '*pliable systems*', the behaviour of individual components is limited by their adjacent components. The linking of these components enables the transmission of forces and torque (Schleicher et al., 2011). Thus, the deformation of one component will result in the deformation of the adjacent component. It is possible to use the connections of the pliable systems to generate a cascading deformation movement. '*Pliable structures*' are built on elastic deformation as well as the ability to convert between various stable configurations (Aline Vergauwen, Laet, & Temmerman, 2017).

'*Bending-active structures*' are *pliable structures* that generate their geometrical form and system rigidity by elastically deforming their components (Schleicher et al., 2011). Julian Lienhard (2014) defined '*bending-active structures*' as structural systems that include curved beam or shell elements based on the elastic deformation of their geometry from the initially planar configuration. Yet, most *bending-active structures* are designed to bear loads and to be stiff only in their final configuration (Julian Lienhard, 2014). However, various types of adaptive and elastic kinetic structures are often distinguished by bending-active structures. In the previously mentioned example of the Venus trap, the movement is acquired by the kinematic coupling of the midrib bending and the snap buckling trap closure. The bending of the midrib transforms the structure to be bending active. The use of '*curved-line folding*' to combine '*folding*' and '*bending*' may have the same potential for bending-active structures that can be used to build an effective kinetic system. Kinetic systems based on '*curved-line folding*' are '*pliable structure*' (Aline Vergauwen et al., 2017). This concept of pliability can inspire deployable structures on the component and grouping level of the responsive solar-shading system.



By studying how plant species perform mobility with minimal energy use, it is possible to learn how to integrate these properties into the design of responsive solar-shading devices. Plant movement principles highlighted '*bi-layering*', '*bi-stability*' and '*pliability*' as efficient strategies used to develop hinge-less responsive skins.

'*Bi-stability*' principle provides the leaf with a kind of '*memory*' which appears to be involved in its closure (Ueda & Nakamura, 2006). The fundamental cause of the fast closure is the leaves' bistable, doubly curved structure, which snap-buckles after closing to reverse their Gaussian curvature. At the same time, the concept of '*bi-layering*' relies on two layers, an active outer layer of tissue that expands upon its exposure to a particular stimulus, while the inner passive layer does not respond (Reyssat & Mahadevan, 2009). Also, the concept of '*pliability*' can have a major benefit for deployable systems based on the elastic deformation which helps the structure to convert between different stable configurations (Aline Vergauwen et al., 2017). In '*pliable systems*', the linkage between elements leads to the transfer of motion from one element to their adjacent/ neighbouring elements (Schleicher et al., 2011). Thus, it is used to build up a cascading deformation, that begins in one part of the system with a small and simple actuation and then translated into a large yet stable deflection of another (Schleicher et al., 2011). Those concepts work best with soft robotics incorporating flexible and lightweight materials.

#### 2.4.4. *Applications of kinetic solar-shadings*

Some projects linked kinetic design with biomimicry; from the selection and investigation of plant movements to the abstraction methods which were developed to translate plant movements into hinge-less elastic kinetics for deployable structures.

A research group in the Institute of Building Structures and Structural Design (ITKE) in Stuttgart University is interested in plant-inspiration as concept generators for deployable compliant mechanisms. The Flectofin® façade was developed by the Institute of Building Structures and Structural Design (ITKE) team in collaboration with Plant Biomechanics Group (PBG). A sun-shading system for complex building facades was inspired by the elastic deformation behaviour of the Bird-of-Paradise flower. It is based on the valvular pollination mechanism of the Bird-of-Paradise flower. The fins' deformation is a reaction to the bending of the attached beam that initiates the successive lateral-torsional buckling and forces the fins into a bending mode. The fins bend up to 90° in relation to its initial position, as shown in Figure 2-30. In each position of the buckling process, the deformation results in a new double

curved surface with higher stiffness using curved-line folding. It was discovered accidentally from manufacturing tolerances but is understood as a key function of the mechanism (Julian Lienhard, 2014; J. Lienhard, Poppinga, Schleicher, Speck, & Knippers, 2010; J. Lienhard et al., 2011).



*Figure 2-30: Flectofin® sun-shading system.*

The One Ocean - Thematic Pavilion at the EXPO 2012 trade-fair in Yeosu, Korea, project (I), was inspired by the Flectofin® concept. It was proven that the up-scaling of the basic principle is possible. It is magnified to the large scale of 108 individual GFRP lamellas with varying heights that are deformed by controlled buckling, as shown in Figure 2-31. The facade can therefore adapt to light and physical building conditions (Schleicher, 2016)



*Figure 2-31: The up to 14 m high lamellas can be opened and closed individually and thus enable an impressive transformation of the building envelope.*

Hygroskin project was developed by a team from the Institute for Computational Design (ICD). Achim Menges in collaboration with Oliver David Krieg and Steffen Reichert, presented a comprehensive development of smart skins based on the biomimetic transfer of hygroscopic actuation of plant cones, as shown in Figure 2-32. The shape change of wood was utilized to develop a humidity responsive integrated technical system (Reichert et al., 2015).



Figure 2-32: Hygroskin project by Achim Menges (Reichert et al., 2015).

Holstov et al. (2015) studied the same mechanism of hygromorphic (moisture-sensitive) materials to produce low-tech, low-cost adaptive systems by deploying materials with embedded responsive properties. They developed two prototypes, an overlapping cladding module of hygromorphic panels and a responsive umbrella canopy that consists of triangular panels with seven different types of active layers, as shown in Figure 2-33.

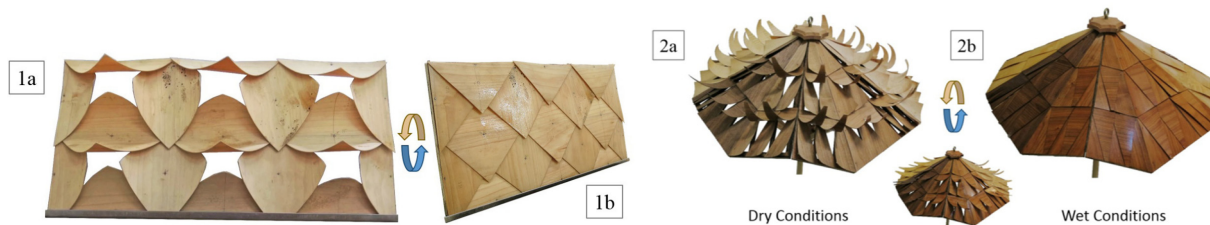


Figure 2-33: (1) a & b) the prototype of a cladding module panels, and (2) a & b) the prototype of a responsive umbrella canopy (Holstov, 2018; Holstov et al., 2015).

Inspired by the pinecone hygromorph biomimetic model, moisture responsive textiles were developed by Scott (2016). She examined the potential for knitted fabrics to exhibit environmentally responsive shape-changing behaviour through differential swelling upon changes in moisture level, as shown in Figure 2-34 (Scott, 2013, 2016). Two knitted prototypes were developed to demonstrate how to program specific shape change behaviours in knitted fabrics that are composed of natural fibres.



Figure 2-34: Fabric actuated using cold water spray (Scott, 2016).

On the whole, the structural behaviour and material properties have a great responsibility towards the actuation system, thus making it easier to be triggered by the smart material. Plants as biological kinetic structures could inspire a new pattern of thought on how to respond to environmental changing conditions. The integration of smart materials with bio-inspired compliant mechanisms may exhibit potential to low-tech strategy and open up new fields of applications in solar-shading systems.

Having looked at how plant structures and movements can inspire work for soft-robotics and deployable structure, the following section will discuss the origami as a source of inspiration that may guide the design of responsive modular systems for their potential as reconfigurable structures (Adrover, 2015) and how is it related to biomimicry.

### **2.5. Origami-Inspired Kinetics**

The folding surface applications for building facades are currently an active research area (Jaksch & Sedlak, 2011; Pesenti, Masera, & Fiorito, 2015; Sharaidin, 2014). Due to their high-performance capabilities in lightweight surface materials, the fold stiffening property is strongly leveraged for building facades (Sharaidin, 2014). Origami presents innovative ways to fabricate, assemble, store, and morph structures (Edwin et al., 2014). Potential advantages are the reduced material consumption and creation of structures with improved strength-to-weight ratios (Tolley et al., 2014). Folding has many benefits over traditional manufacturing techniques, including a reduction in manufacturing complexity (Mueller, Kruck, & Baudisch, 2013) fast and inexpensive methods of production, and practicality in storage and transportation (Callens & Zadpoor, 2018; Liu, Genzer, & Dickey, 2016).

Recent developments in the field of robotics, deployable structures and adaptive façades have led to a renewed interest in origami-inspired structures for their potential to be reconfigurable structures (Edwin et al., 2014). Origami is applicable across different scales ranging from nano-scale to large-scale deployable structures of space explorations. Due to their predictability, controllability, and scalability, origami techniques have benefited many engineers to develop self-folding robots, deployable structures and stretchable electronics (Callens & Zadpoor, 2018).

Folding principles transform two-dimensional planar geometries into three-dimensional forms (Callens & Zadpoor, 2018; Samuel M. Felton et al., 2013). It requires stretching and bending over regular folds to create new typologies (Epps & Verma, 2013). This state of transformation is specifically what makes folding an interesting area of exploration

for kinetics. The shape of the folded structure is defined by the crease pattern, folding directions, folding magnitude, and folding sequence (Edwin et al., 2014). Creases, which are defined by their endpoints, bound faces. Folding is based on creases, in specific the ‘mountain-valley’ assignment, which is used to determine the direction of the fold (Edwin et al., 2014; Epps & Verma, 2013). Folded geometrical forms vary according to the type of crease lines; whether ‘straight’ or ‘curved’. The type and pattern of crease lines and their relationship are the main factors that define the behaviour of the folded surface. Folded geometries using curved folds inherit a structural strength and show better performance compared to straight folded geometries (Epps & Verma, 2013).

#### 2.5.1. *Folding principles: Straight and Curved Folding*

In Biology, plants and tree leaves can be modelled as thin surfaces that fold in various ways to perform mobility. ‘*Straight-line folding*’ was observed in hornbeam leaves (Kobayashi, Kresling, & Vincent, 1998; Mahadevan & Rica, 2005) as they have a regular corrugation pattern, as shown in Figure 2-35. On the other hand, ‘*Curved-line folding*’ is presented in the rapid trap closure mechanism of the carnivorous plants (Schleicher et al., 2011).

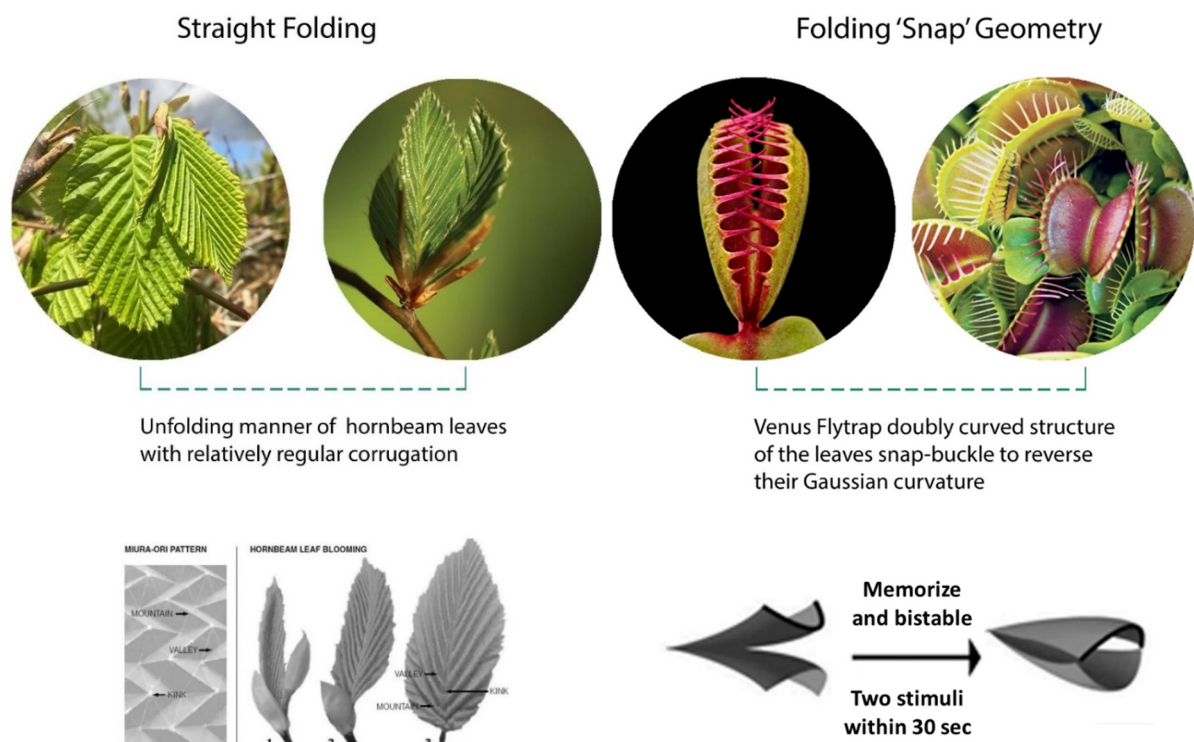


Figure 2-35: Straight and curved folding principles in plants.



Figure 2-36: Straight and curved folding crease lines applied on paper (Epps & Verma, 2013).

In architecture, an example of the '*straight crease folding*' is shown in the responsive façade of albahar towers designed by Aedas Architects. External triangular 1049 origami units operate as a fully automated and actuated shading screen, as shown in Figure 2-37 (a) (Attia, 2018; cimento, 2012; Wood & Henry, 2014). Sharaidin (2014) developed a kinetic shading made of '*straight-line folded*' panels that demonstrated the arch shape movement as shown in Figure 2-37 (b). The Un-Fold prototypes were integrated with the idea of a pulley system to maximise the opening and closing of the units (Sharaidin, 2014). On a smaller scale, a kinetic sculpture tyvek '*straight crease origami*' umbrellas expand and collapse in beautifully rhythmic patterns. The 'Diffusion Choir' is a kinetic sculpture which uses 400 folding elements arrayed on a three-dimensional grid to reveal the movements of an invisible flock of birds (Sterling, 2016). It is inspired by the way birds stow their wings and jellyfish gently fold into themselves, as shown in Figure 2-37 (c). Similarly, the Kinetic Façade of the CJ R&D Center in Seoul, south Korea by Yazdani Studio of Cannon Design used the umbrella mechanism which depends on a single linear actuator that could gather the pleated membrane like an umbrella to vary aperture based on time and user preferences (Krymsky, 2011).



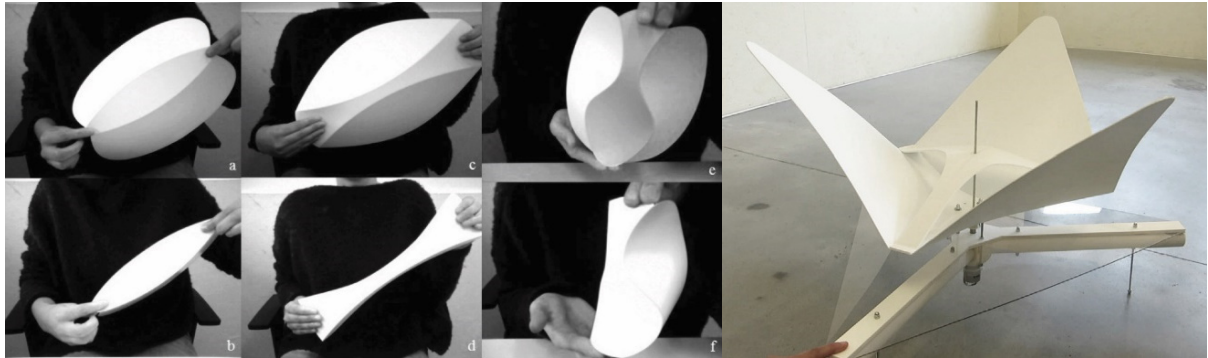


When discussing curvature and origami, it is natural to also consider *curved-crease origami*. Although origami has interested artists for several decades, *curved creasing* remains relatively underexplored (Callens & Zadpoor, 2018; Koschitz, Demaine, & Demaine, 2008). Most origami, both practical and mathematical, have been primarily limited to straight creases (Callens & Zadpoor, 2018; Koschitz et al., 2008). On the other side, *curved creases* offer a variety of new possibilities for design. '*Curved-line folding*' is defined as '*the act of folding paper along with a curved crease pattern in order to create a 3D shape using a combination of folding (plastic deformation) and bending (elastic deformation)*' (A. Vergauwen, De Temmerman, & Brancart, 2014). In curved-crease origami, the surfaces close to the curved crease must bend in order to accommodate the folding motion (Callens & Zadpoor, 2018). The principles of '*curved-line folding*' can be used to create bending-active kinetic systems (A. Vergauwen et al., 2014).

Not only the curved creases have a significant potential to achieve complex geometries, but also to be used in kinetic architecture applications (Callens & Zadpoor, 2018). Some researchers such as A. Vergauwen et al. (2014) and Bende et al. (2015) combined folding and bending using curved-line folding to design efficient kinetic system. A. Vergauwen et al. (2014) demonstrate how the resulting kinetic mechanism is influenced by the choice of the crease pattern composition, the curvature of the creases and the length-thickness ratio. The curved folds develop complex double-curved three-dimensional models that could afford shading from plain sheets. They have significant potential as kinetic applications for their simplicity and inherited return mechanism characteristics (Aline Vergauwen, Alegria, Roovers, & De Temmerman, 2013; A. Vergauwen et al., 2014; Aline Vergauwen, De Temmerman, & De Laet, 2014; Aline Vergauwen et al., 2017). However, A. Vergauwen et al. (2014) argued that systems which have more than two-creases need elastic deformation for more than one surface to fold it to the compact state. This leads to a loss of the bending-active properties and the system behaves more like a mechanism in this case. Therefore, the two-crease curved forms is able to store enough elastic energy in the deformed model to return it to the initial state. The researchers collected data experimentally by manually folding physical models to select the best range of the Length-Thickness Ratio (LTR) as shown in Figure 2-38. They found that when LTR is higher than 400, the structure is very stiff and the deployable system loses its reversibility. When the LTR is lower than 300, the structure is reversible but very flexible, which is a drawback for responsive solar-shading systems. LTR between 300 and 400 have a



good balance between the structural stiffness and the actuation forces, which means the transformation is reversible. This range of medium stiffness from LTR results was achieved by two creases/ flaps physical models made of polypropylene with Length between endpoints of the crease between 268 and 558mm and thickness between 0,8 and 1,8mm.



*Figure 2-38: On the left, an exploration of various two-creases patterns (A. Vergauwen et al., 2014). On the right, a physical model, actuated with a linear actuator (Aline Vergauwen et al., 2017).*

Origami principles are applied to develop various deployable structures later in the ‘*Component design and prototyping*’ chapter using physical experimentation. More details of coupling folding principles with SMM are investigated in the following self-folding section and the hands-on exploration in Chapter 4, page 107.

### *2.5.2. Self-folding origami*

Coupling origami principles with active materials allows engineers to create self-folding structures. Self-folding structures can be found in nature at different scales, such as organic molecules, winged insects, brains, and tree leaves (Mahadevan & Rica, 2005; Tolley et al., 2014). Based on inputs, they can automatically fold and/or unfold itself, without being controlled by external forces (Stermann et al., 2013; Tolley et al., 2014). A key study introduced the material-based approach to origami folding is that of Hawkes et al. (2010), in which the creation of a foldable object is promoted by materials embedded within the material substrate to have integrated properties. Hawkes et al. (2010) developed a unique concept of self-folding origami or self-actuated surface with universal crease patterns that is scalable (in the number and size of elements) and less complex. An integrated approach for designing ‘*Programmable matter*’ was demonstrated by integrating folding material and electronics in a self-actuated surface (Hawkes et al., 2010; Stermann et al., 2013). A single sheet consisting of interconnected triangular parts utilizes this method. The sheet can fold into a set of predetermined shapes using embedded actuation. The system computes an optimized design for a single fabricated sheet (less than 0.5 mm thick) and multiple controllers to create self-folding sheets capable of

realizing various shapes (boat and an aeroplane) using embedded actuation as shown in Figure 2-39 (Hawkes et al., 2010). A thin foil of Nitinol shape memory alloy (SMA) (100  $\mu\text{m}$ ) is used as the actuator material. The three components of the programmable material are: the tiled composite sheet, thin-foil actuators, and flexible electronics.

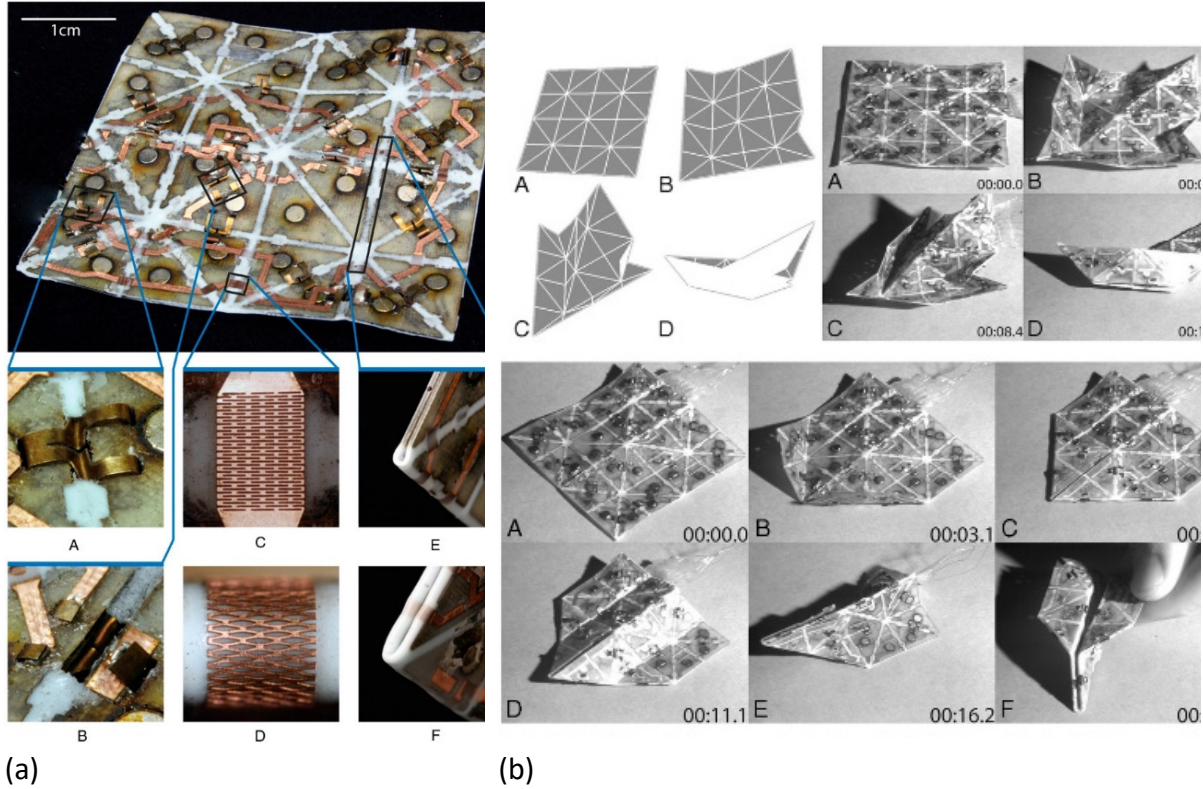
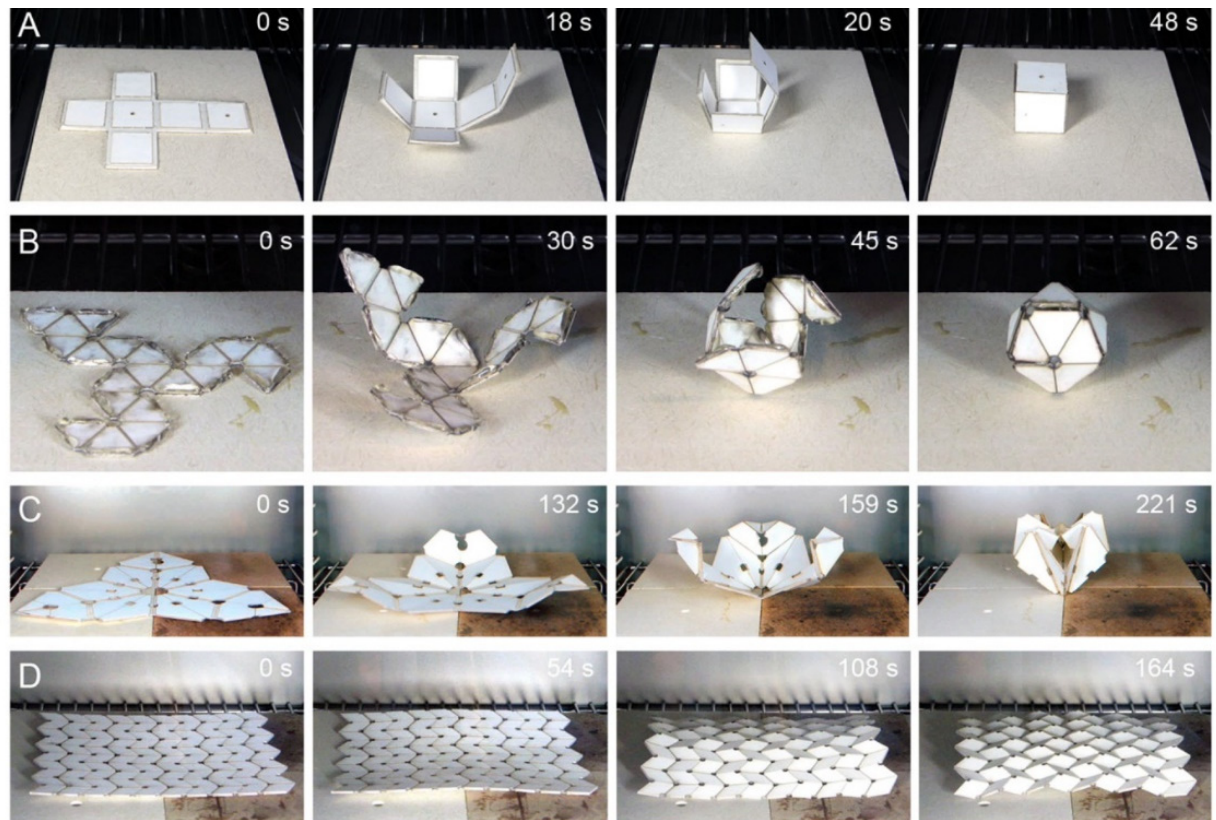


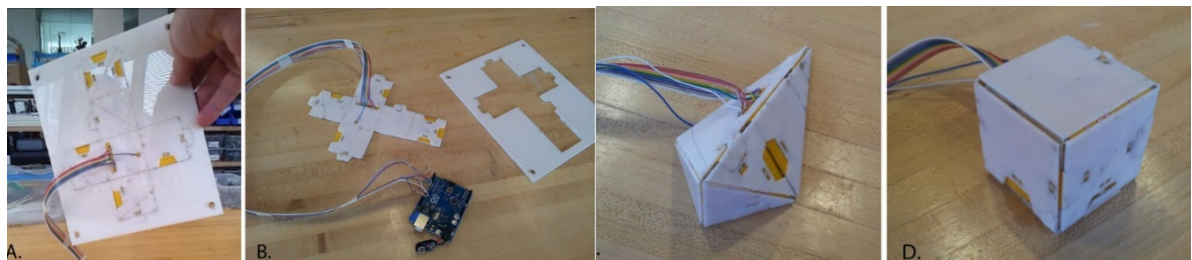
Figure 2-39: (a) 32-tile self-folding sheet which can achieve two shapes (a boat and an aeroplane) (Hawkes et al., 2010), (b) Sequential Folding of a flat sheet realizing multiple shapes (boat and an aeroplane) (Hawkes et al., 2010)

Tolley et al. (2014) presented a self-folding origami which consists of shape memory composites (SMC) that are activated with uniform heating in an oven. The study demonstrated four self-folding shapes based on shape memory polymer (SMP) sheet in-plane contraction as shown in Figure 2-40. The self-actuated surface depends on the contraction of the heat-activated SMP layer sandwiched between two structural layers, with two additional adhesive layers holding the laminate together.



*Figure 2-40: Self-folding experiments (Tolley et al., 2014)*

Sterman et al. (2013) created a self-folding origami by embedding a laminated printed circuit board (PCB) between two sheets of machined acrylic plastic to create an interactive folding experience and to generate foldable objects with added functionalities as shown in Figure 2-41.



*Figure 2-41: The fabrication and folding of flexible printed circuit boards (PCB) which laminated between two acrylic sheets (Sterman et al., 2013).*

Liu et al. (2012) applied a simple approach to achieve folding using homogeneous 2D pre-strained polymer sheets with inkjet-printed hinges on a planar surface as shown in Figure 2-42 (Liu et al., 2012; Liu et al., 2016). The pre-strained polymer sheet is a type of SMP that shrinks in-plane when heated uniformly. Black toner which was patterned on the surface provided localized absorption of light, which heated the underlying polymer to temperatures above the glass transition temperature to induce the local shrinkage of the polymer so that the planar sheet folded into a 3D shape (Liu et al., 2012).



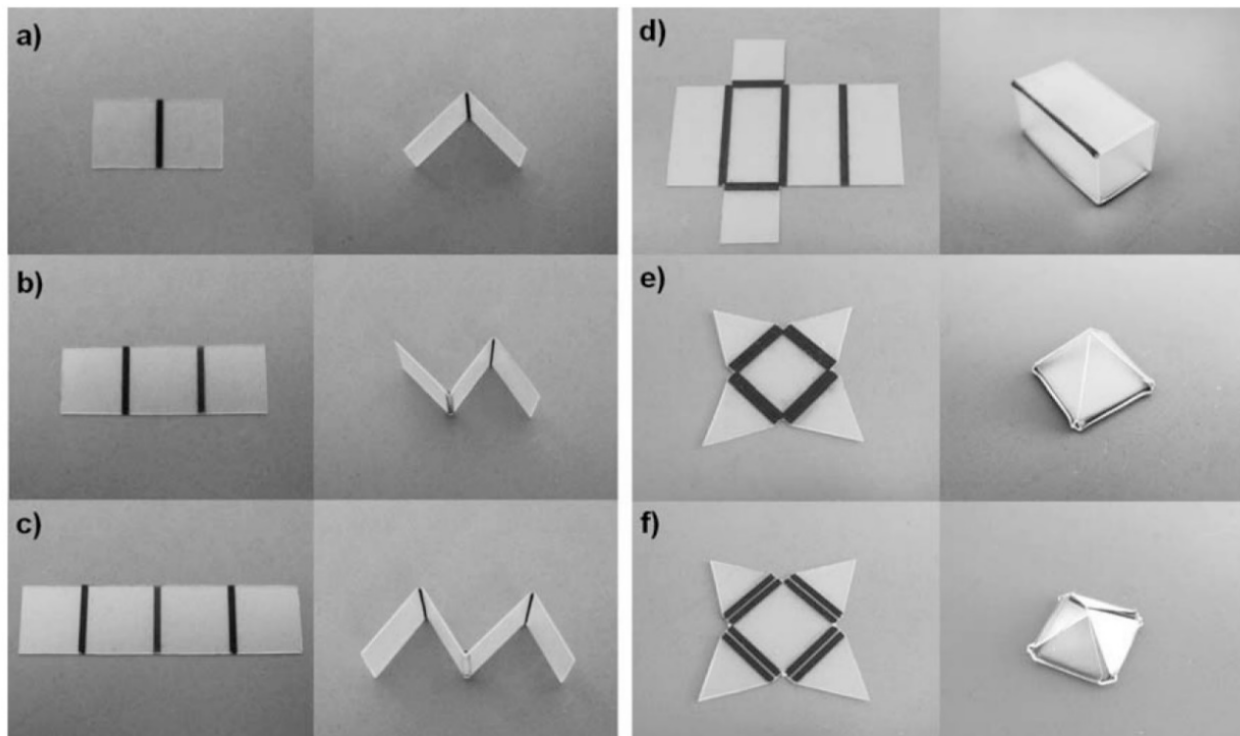


Figure 2-42: Photographs of 3D structures created by self-folding of Shrinky-Dinks patterned with a desktop printer (Liu et al., 2012)

In conclusion, most examples of self-folding surfaces employ embedded smart materials or hinges that actuate when they receive inputs or are exposed to an external stimulus. Some examples developed sequential folding which allows for more complex geometries, but generally folding all hinges is more reliable. All previously mentioned self-folding examples coupled simple straight crease folding with material actuation. Also, they were applied on a small scale using hands-on experimentation. Thus, explorations with self-folding structures will be tested later in *Chapter Four, 'Component design and prototyping'*, page 131, to test the potentials of coupling origami and SMMs.

As mentioned earlier that many projects depending on material-based actuation such as invert project of Doris sung and Homeostatic Façade System of Decker and Yeadon are encased in double-skin façade DSF system to protect the lightweight, flexible solar-shading system from external atmospheric agents, damage and internal interference. The integration has relatively low cleaning and maintenance cost. Moreover, the most common practice for mechanized/ automated solar-shading system currently in use house the blind in a DSF system. In order to protect the responsive skin for more efficiency and durability and to achieve the activation temperatures needed to activate the SMM, the use of double skin facade (DSF) has been considered.

## 2.6. The Double Skin Façade (DSF)

The double skin façade (DSF) offers protection to the shading system from potential damage and interference internally and protection from atmospheric agents; such as bad weather and pollution externally. It has the potential to decrease cooling energy demand in hot arid areas (Hamza, 2004). Cavity-Integrated responsive shading system, is a sustainable solution, with double benefits of a responsive façade under a controlled environment. According to Gratia and De Herde (2007) and Hazem, Ameghchouche, and Bougriou (2015), management of solar-shading devices and ventilated channels are the two most effective strategies to reduce undesirable solar loads inside interior spaces, especially during warm periods. Moreover, the integration of solar-shading devices in DSF system has many advantages in hot climates (Gratia & De Herde, 2007). First, It is developed to take advantage of the benefits of a typical DSF in winter conditions while it limits cooling loads in the warm season (Baldinelli, 2009; Hashemi, Fayaz, & Sarshar, 2010). Second, it modifies the airflow into the channel (Baldinelli, 2009). Third, the shading system is thus protected from atmospheric agents; such as weather and pollution (Gratia & De Herde, 2007).

This notion of responsive solar-shading systems could present a modern version of the traditional solar screens in a more adaptive way by using smart materials. The proposed system positions the responsive solar-shading in the cavity of a DSF in order to increase the kinetic system efficiency and responsivity.

### 2.6.1. Overview – double skin façade (DSF)

Double-skin facades (DSFs) are known for their attractive aesthetics as well as reducing energy consumption (Ghaffarianhoseini et al., 2016; Velasco, Jiménez García, Guardo, Fontanals, & Egusquiza, 2017). DSFs are generally composed of multiple layer skins; an external skin, an intermediate space and an inner skin (Wong, Prasad, & Behnia, 2008). The inner and external skins could be of either single glaze or double glazed glass panes of float glass or safety glass (Shameri, Alghoul, Sopian, Zain, & Elayeb, 2011). There are various definitions of the DSF system. Safer et al. (2005) have provided a clear inclusive definition of DSF, who wrote: *'Double-skin facade is a special type of envelope, where a second skin, usually a transparent glazing, is placed in front of a regular building façade'*. The in-between air space, is called the channel, can be up to 1.0 m. In general, the channel is ventilated (naturally, mechanically, or using a hybrid system) in order to diminish overheating problems in summer and to contribute to energy savings in winter. The gap between the outer and inner layers of

a double configuration, allows for a safe installation and maintenance of shading systems (Oesterle, 2001). This realization underpins the rationale behind considering the retrofitting of solar-shadings into an existing double skin facade as a refurbishment option.

Most DSFs are built in Europe and America's temperate climates. Over the last decade, there has been a growing trend in other areas of the world with differing temperatures, such as the hot humid climates, hot arid climates and the Mediterranean, to adopt this façade technology (Hamza & Qian, 2016). A number of recent findings are reported in the literature pertaining to the thermal performance of DSFs in hot arid areas. Cairo, the capital of Egypt, is situated in a hot arid climate, with increasing cooling loads in office buildings to maintain suitable work environments. The energy consumption used to maintain indoor comfort represents a range from 70% to 80% of the total energy consumption and grows by 7-8% in commercial buildings sector annually (Hamza & Underwood, 2005). In hot arid climates, DSF is estimated to reduce indoor cooling loads between 12-30% based on the size and configuration of the building (Hamza, 2008, Hamza and Qian, 2016). Besides, DSFs promise to deal with direct solar radiation as a shading system; decrease the cooling loads by lowering the temperature via nocturnal ventilation and act as an acoustic barrier (Hamza & Qian, 2016; Hashemi et al., 2010). A movable solar-shading device is usually installed at the intermediate space of the DSF for thermal controls (Ghaffarianhoseini et al., 2016; Gratia & De Herde, 2007; Wong et al., 2008). The hypothesis that integrated smart shading could be used to improve both winter and summer energy efficiency was backed by a study conducted by Baldinelli (2009). Similarly, variation of venetian blind's slat angle integrated with DSF, proved to be energy-efficient solution. Iyi, Hasan, Underwood, and Penlington (2014) and Iyi (2013) deducted that the variation of the venetian blind's slat angle reduces the solar transmittance into the interior environment by 85%. Accordingly, the proposed system will position the responsive solar-shading devices in the DSF cavity as shown in Figure 2-43 (a). This research will optimize the positioning of the shading system within the cavity to achieve the activation temperatures needed to actuate the SMM.

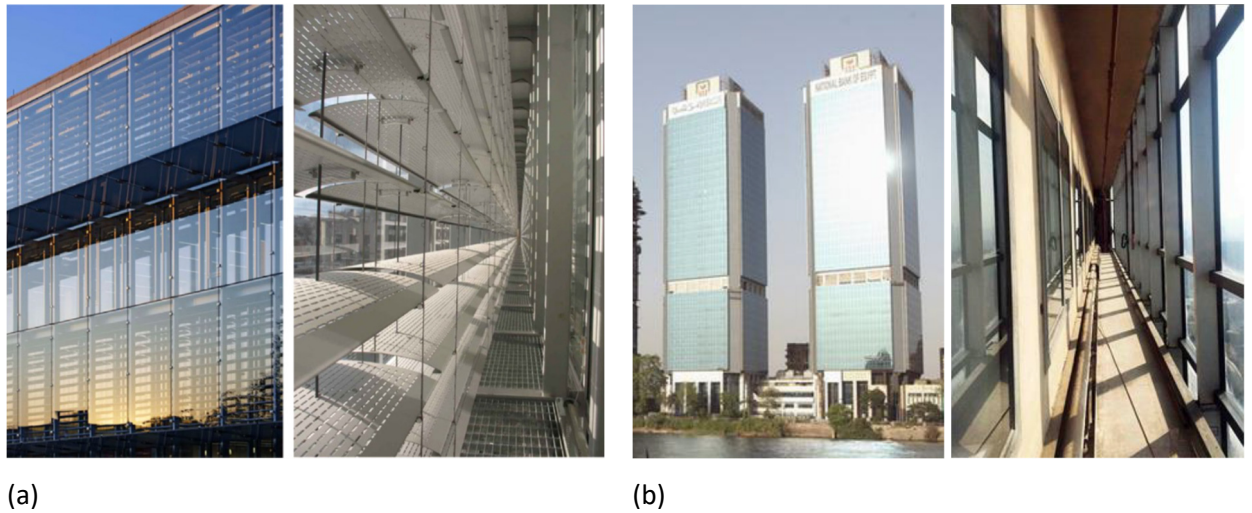


Figure 2-43: Double skin façade examples (a) Shaded cavity in Cambridge public library, USA. (b) Non-shaded cavity in Al ahly bank, Egypt.

### 2.6.2. DSF classification

DSF typologies are classified according to their ventilation strategies. The performance of the DSF depends closely on the chosen ventilation means within its intermediate space (Gratia & De Herde, 2004; Shameri et al., 2011; Wong et al., 2008). The principal purpose is to exchange contaminated air with clean, fresh air (Ghaffarianhoseini et al., 2016). DSF is categorized according to ventilation type of the cavity into three basic kinds of ventilation modes: natural (buoyancy-driven), forced (mechanically driven) or hybrid (both natural and forced). Chan, Chow, Fong, and Lin (2009) showed that air-tightened DSF improves the building thermal insulation in the wintertime while ventilated DSFs reduce the heat gain in the summertime. The ventilated cavities encourage the exhaustion of heated air with the means of buoyancy. In contrast, unventilated cavities prevent the heated air exhaustion, which is not beneficial for a hot arid climate (Gratia & De Herde, 2007). Naturally ventilated cavities diminish overheating problems in summer and contribute to energy savings in winter.

Another well-known DSF classification of Oesterle (2001) is according to the partitioning of the air cavity. It is categorized into four type, *box window*, *corridor facades*, *shaft box facades*, and *multi-story facades*, as shown in Figure 2-44.

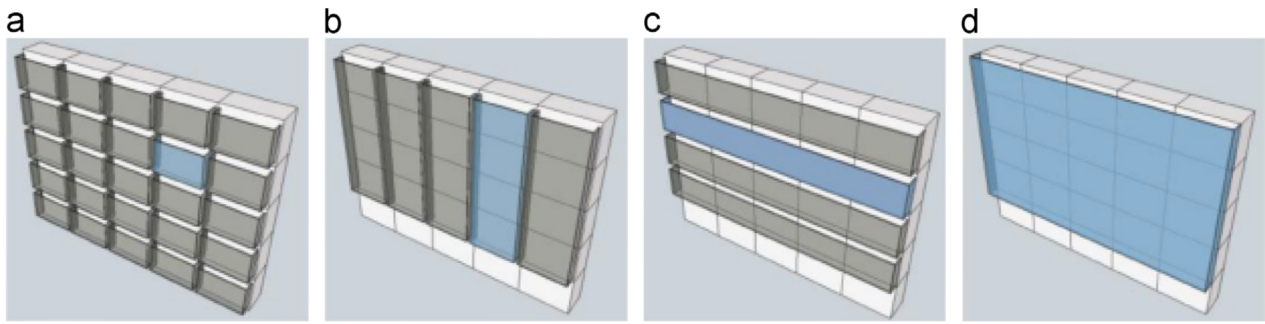


Figure 2-44: DSFs' categorization: (a) Box window, (b) shaft-box, (c) corridor and (d) multi-storey double skin façade.

### 2.6.3. Cavity-Integrated Shading Devices in DSF

As discussed above, movable solar-shading devices have many advantages in hot climates. A study carried out by Baldinelli (2009) supported the hypothesis that the cavity-integrated smart shading device could be used to optimize both winter and summer energy performance. Baldinelli (2009) tested a DSF equipped with integrated movable solar-shading devices and found that it significantly improves the building energy behaviour through the entire year. The investigated solution is made up of external laminated glass (two layers of 5-mm float glass divided by a 0.37-mm film of polyvinyl butyral) coupled with aluminium shading device. The inner skin is made up of transparent surfaces assembled with the coupling of the same laminated glass used for the external layer plus 4-mm float glass; the two panes are divided by a 10-mm air gap. The proposed system recorded improvements that reaches up to 60 kWh/m<sup>2</sup> per year compared to opaque walls facade.

Gratia and De Herde (2007) examined the influence of the position and colour of the solar-shading device integrated in the cavity on the cooling consumption of an office building with a DSF in Uccle, Belgium. The study highlighted the importance of the opening of the double-skin to reduce cooling loads. Light coloured solar-shadings placed at the mid of the cavity can significantly reduce the cooling consumption. Moreover, the solar-shading devices placed against the external skin achieved a good reduction compared to solar-shading devices which are placed against the internal skin. The results of Gratia and De Herde (2007) and Baldinelli (2009) demonstrated that the use of light coloured and high reflection shading devices reduce cooling loads in summer and allows a satisfactory solar gain in winter in warm climates.



After considering the previously mentioned benefits of using this integrated system, the proposed system positions the responsive solar-shading in the cavity of a DSF in order to increase the kinetic system efficiency and responsivity. It is recommended to position the solar-shading device in the range between the mid of the cavity and the external skin, taking into consideration the highest temperature profile of the cavity to activate the smart system thermally. Light-coloured and high reflective shading devices are recommended.

As located in the hot arid climate of Cairo, Egypt, the responsive solar-shading system is intended to produce movements by means of solar exposure, cavity temperature and changing the aperture size. The thermally triggered SMMs in the solar-shading device, which is positioned in the cavity, need to perform in specific cavity temperature ranges. The conditions in the DSF cavity; cavity temperature contours for an empty cavity will be measured to detect the highest temperature profile to install the shading screen and to activate the smart system thermally. Afterwards, the inner surface temperatures and airflow will be measured to test the DSF performance efficiency. Then, the solar-shading surface temperature is measured to detect the required activation range for the SMM. A more detailed account of DSF performance is given in Chapters Five and Six.

## **2.7. Conclusion**

Collectively, this review outlines the critical role of adaptive and responsive solar-shading systems. Most buildings still have adaptive façades with hinged and louvered shutters fixed outside the windows. The future challenges lie in the development of responsive systems which require low-tech with unsophisticated technology to perform but have high potential in their technical uses. Interestingly, this notion of façades that change; every day, and every hour is turning into a dynamic sculpture that continuously shows a new “face”.

All of the studies reviewed here support the hypothesis that soft robotics and smart materials can present a possible alternative for conventional building skins and envisions the concept of a futuristic and soft, flexible architecture. Soft robots are similar to natural organisms which are often composed of soft materials like skin or muscle tissue. The flexibility of soft materials enable them to produce soft deformation movements like bending swelling and curling motion which are not possible with rigid materials. Soft robots have the advantage of distributed deformation with a relatively large number of degrees of freedom and deformation through controllable variance in material properties. Thus, this chapter argues

that it is within the soft creative sciences, the next advancements in adaptive deployable skins may emerge. The important theme emerging from the studies discussed so far is that soft robotics with embedded material-based actuation can use '*plant-inspired*' and '*origami-inspired*' principles as form generators. '*Smart materials*', '*Bio-inspiration*' and '*Origami*' can be integrated to develop responsive solar-shading systems applications as shown in Figure 2-11.

*The science of 'Smart Materials'* is still an area of active research, especially on the architectural scale. This research is an extension to Decker Yeadon, Sung (2016) and Kretzer (2017a), (2017b) approach to construct an amplified passive motion using material-based actuation. The literature identifies the potential of SMA; specifically NiTi-based alloys, that can be used to mimic reversible plant motions. Nitinol Wires and springs can be embedded within a skeletal tensegrity structure to activate the solar-shading systems. Smart materials based actuators have the capability of morphing self-deployable structures repetitively and continuously. To conclude this section, the literature identifies the potential of using SMAs in conjunction with light-weight structures and tensile skins using hinged or bilayered fixation types. The hinged actuators are more flexible to design motion and can move a single shading unit or connect more than one to enable the system to work collectively. Also, SMP can be considered taking into consideration their low density and limited SME, which means they are only capable of a certain level of shape recovery.

*'Bio-inspiration'* principles highlighted bi-layering, bi-stability and pliability as efficient strategies that can be used to develop hinge-less responsive systems. Coupling of elastic instabilities and snap buckling with bending active structures have great potential to be applied to kinetic systems. Kinetic systems based on '*curved-line folding*' are '*pliable structure*' that perform in a similar manner to bending active structure. Pliability concept can inspire deployable structures on the component and grouping level of the responsive solar-shading system.

*'Origami-inspired'* structures have a great potential for reconfigurable structures, especially self-folding robots, due to their predictability, controllability, and scalability. Origami has other advantages of reduced material consumption, creation of structures with improved strength-to-weight ratios, reduction in manufacturing complexity (Mueller et al., 2013), fast and inexpensive methods of production and practicality in storage and

transportation (Callens & Zadpoor, 2018; Liu et al., 2016). It was found that most of the self-folding examples coupled simple straight crease folding with material actuation. Straight folding can achieve a high range of deployability and aperture sizes. Adding extra folds helps the module to achieve more contractions and improve rigidity. However, the principles of curved-line folding can be used to create bending-active kinetic systems (A. Vergauwen et al., 2014) despite being relatively underexplored. They have significant potential as kinetic applications for their simplicity and inherited return mechanism characteristics.

This category of responsive solar-shadings are generally soft, flexible and sensitive. Therefore it is preferably integrated in a DSF, to be protected from the influences of weather and air pollution. Also, DSF can help in achieving the activation temperatures needed to activate the shape memory materials. Integration of smart materials for solar-shadings with DSF systems may exhibit a potential to low-tech adaptive systems. Besides, DSFs promise to deal with direct solar radiation as a shading system; decrease the cooling loads by lowering the temperature via ventilation and act as an acoustic barrier (Hamza & Qian, 2016; Hashemi et al., 2010). Positioning the solar-shading inside the cavity modifies the airflow into the channel (Baldinelli, 2009). On the whole, cavity-integrated responsive shading devices is a sustainable solution, with double benefits of a responsive façade under a controlled environment which is naturally ventilated to diminish overheating problems in summer and contribute to energy savings in winter.

## **Chapter 3 . THE METHODOLOGY**

### **3.1. Introduction**

The methodological approach taken in this study is a mixed interdisciplinary methodology between experimentation for physical exploration and CFD simulations for environmental assessment of responsive solar-shading systems. The integrated methodological approach is chosen to explore the potentials of responsive solar-shading systems realised with smart materials and understand their behaviour and performance within their context of operation experimentally and environmentally as shown in Figure 3-1. This chapter explores the practice-led approach, and CFD simulations and investigates how their integration helps in the design and assessment of responsive solar-shading systems. This work seeks to explore the relationship between the Design thinking (DT) and engineering systems thinking (EST) concepts, using the Learning through making for design thinking to create innovative solutions while using the simulations as a system engineering methodology to evaluate technical systems interactions. Design thinking (DT) and engineering systems thinking (EST) are two complementary approaches aims at understanding the different factors that affect the design and performance of the responsive solar-shading systems. Design thinking is a method for creating creative and user-centred products that has its origins in psychology, industrial design, and product development. In contrast, systems thinking has been restricted to the viewpoints and techniques of systems engineering, management science, and quantitative decision-making.

Practice-led approach is used to explore the design potentials of responsive kinetic systems using smart materials, while CFD simulation used numerical methods to environmentally assess the responsive system performance within their potential context of operation. The mixed interdisciplinary methodology aims to bring experimental and environmental together through the design of a prototype which integrates material thinking and the simulation of real environment performance, developing a demonstrator and design framework for future development.

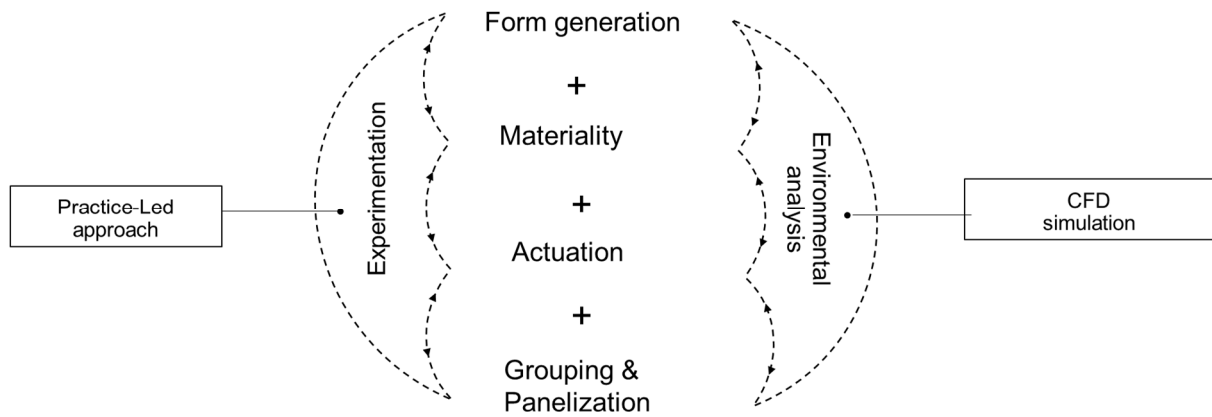


Figure 3-1: The two approaches testing the responsive systems

**Component design and prototyping Chapter (Chapter 4)** adopted the ‘Practice-led concept’, through ‘Hands-on’ experimentation, and the creative practice of ‘*Material Tinkering*’ to explore the potential of smart materials (SMMs) in order to understand their immanent dynamic activity, and use bio-inspiration and folding principles to alter complex deployable forms using simple actuation strategies. Prototypes are explored by using an open-ended design approach to explore a design space rather than finding an optimal solution. A four-stage design process is proposed relied on the layered investigation of façade kinetics that includes; form generation, materiality, actuation and panelization as shown in Figure 3-1. This design workflow represents an experiential knowledge and gained insights into the responsive system which is subjected to test and validation through an educational activity module of 6 weeks with MArch students during the fall of 2018/2019. The ‘Practice-led’ process highlights the design process and variables to develop an actual prototype system for further environmental experimentation in chapter six and an integrative ‘Design Framework’ by the end of the thesis in chapter seven.

The methodology of climate-based design, which is applied in chapter five and six, adopted CFD as a method for energy modelling and analysis. CFD analysis is used to predict the DSF performance in terms of coupled thermal and airflow behaviour. It is carried on two phases; validation and simulation of integrated DSF.

The ‘**Environmental Design and Modelling**’ Chapter (Chapter 5) represents the ‘validation phase’ which includes sensitivity analysis to set guidelines for the CFD setup of a DSF integrated with solar-shading devices and validate this CFD modelling setup against an experimental case conducted by Mei et al., (2007). The chapter discusses the challenges met

during the simulation process of a DSF, including solar simulator representation, domain size, selection of radiation and turbulence models and the level of model detailing and meshing.

The **‘Integrated Design and Simulation’** Chapter (Chapter 6) represents the ‘simulation phase’ which includes an assessment of: 1) non-shaded cavity as a base case; 2) an integrated DSF with simplified flat solar-shading at three aperture sizes; (30%, 50%, & 70%), and 3) an integrated DSF with folded origami solar-shading at three aperture sizes (30%, 50%, & 70%) as shown in Figure 3-3. Measurements of surface and air temperatures, airflow and heat flux are collected to environmentally assess the proposed responsive solar-shading devices performance within their potential context of operation and use environmental feedback as a guidance to customise the material and design the responsive system; form and aperture size. The main aim behind assessing such variables is to test the DSF performance efficiency and optimise the solar-shading aperture ranges at different times.

In the **‘Design Framework’** Chapter (Chapter 6), the findings from the creative practice in chapter four and scientific approach of CFD simulations in chapter six are collectively analysed to reflect the impact of experimental and environmental factors on the responsive solar-shadings’ design. Both of the practice-led approach and CFD simulation guided the formulation of the design framework presented in chapter seven, as shown in Figure 3-2.

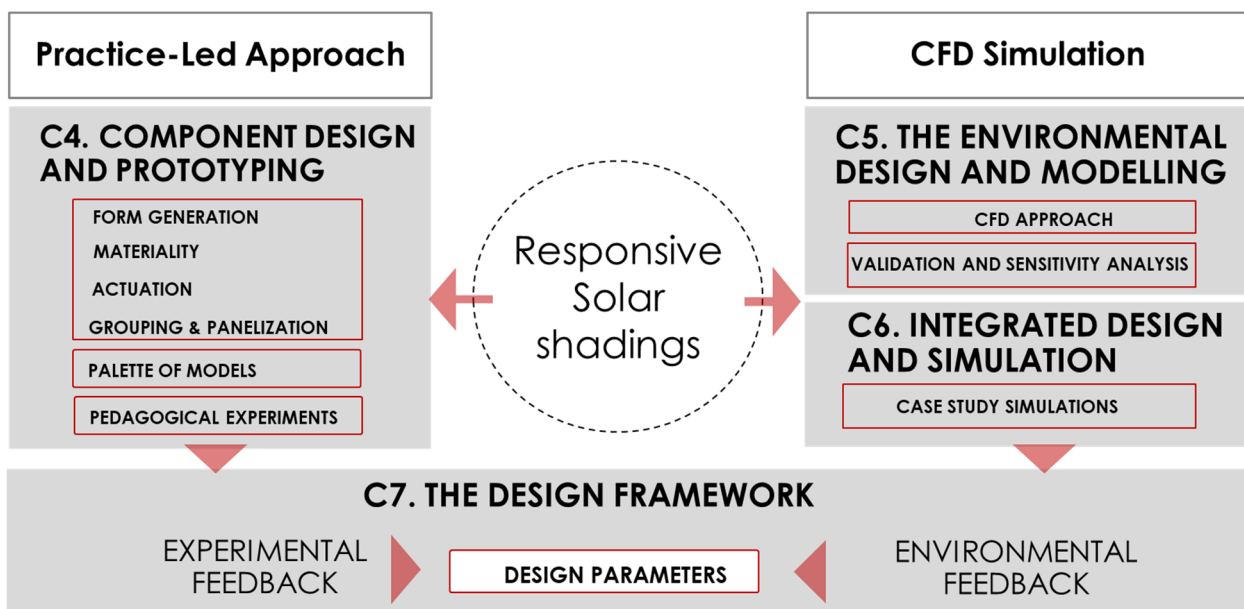


Figure 3-2: The two methodological approaches merging into integrative feedback, informing the design of responsive solar-shadings.

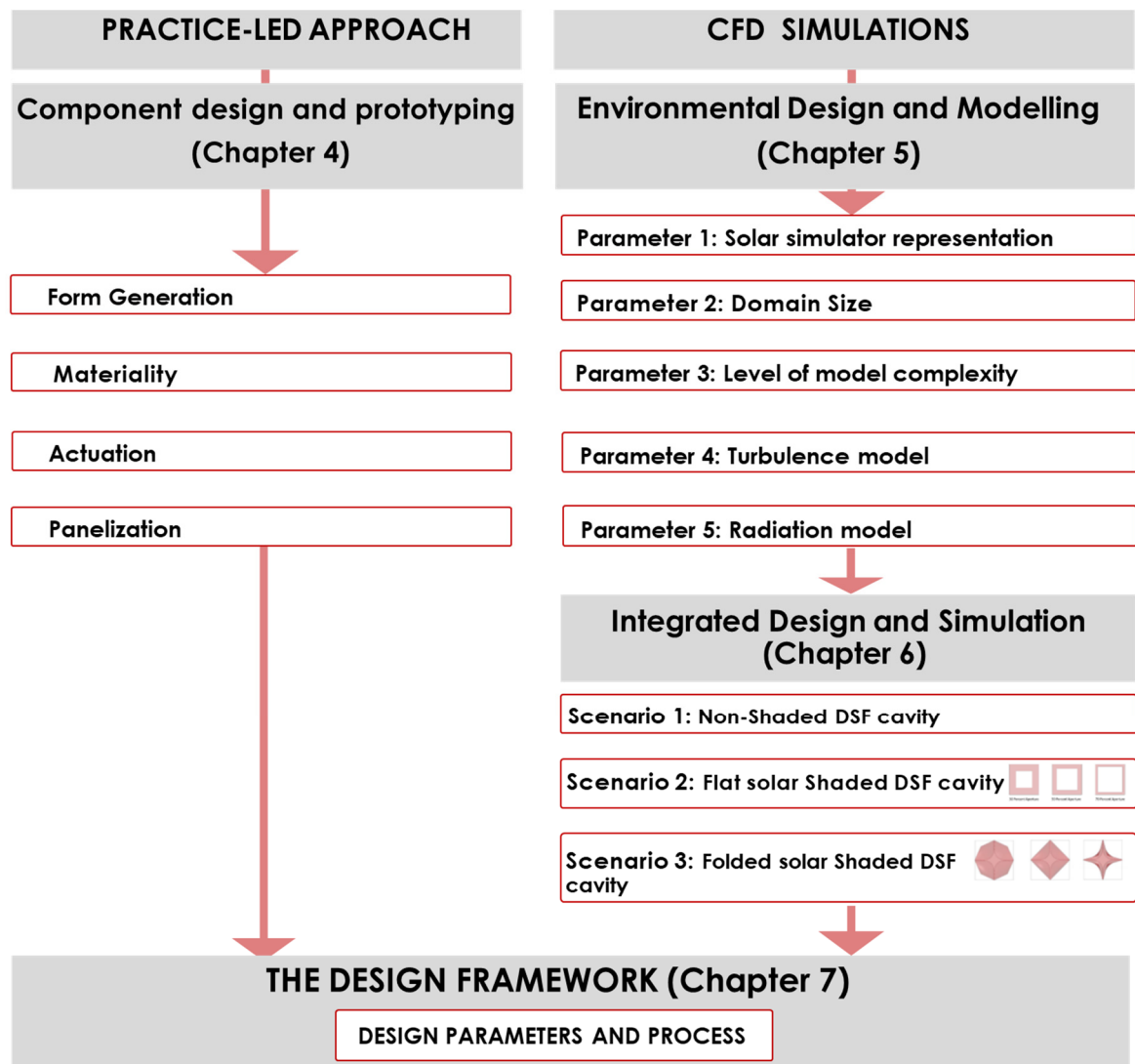


Figure 3-3: Methods used for practice-led approach and Building performance simulations.

A summary of the mixed interdisciplinary methodology, together with the aims, is provided in the introduction. The next sections describe the procedures and methods used in this thesis in detail.

### 3.2. Practice-Led Approach

The novelty of soft-robotics approach and smart materials, resulted in a lack of applied knowledge in the architectural field and limited knowledge of responsive structures' design process and smart material behaviour. Generally, designers in the field of kinetics, interactive or responsive systems are likely to use a Practice-led approach to test the resulting motion, actuation mechanisms and embody novel materials (Kretzer & Damjanovic, 2012; Kretzer & Rossi, 2012b; Sung, 2016). Concepts as Practice-led and learning-by-doing and methodologies as Hands-on experimentation and the creative practice of Material Tinkering, help designers to explore in the field of kinetics and understand the behaviour of smart materials. Thus,

Practice-led approach is adopted in 'component design and prototyping' chapter using Hands-on experimentation and 'Material Tinkering' to explore the potential of smart materials (SMMs) and investigate the origami abilities for deployable forms for forward and reverse motion. The Material Tinkering is used as purely exploratory experiments. It is applied in SMMs testing and their training process which aims to control their geometric and mechanical properties. Later some potential prototypes or artefacts for four different ideas are developed, discussed and compared to develop a design framework which can be used to generate different design possibilities.

The following sections will discuss the concept of Practice-related research as the basis of the contribution to knowledge, Craft as a drive for practice-led research, and the range of related concepts and terms as well as the role of the artefacts.

### 3.2.1. *Practice-related research*

Towards a more explorative and practical approach, Practice-based, and Practice-led researches are adopted by relevant researchers in the field. The movement of practice-related research has drawn inspiration from Bauhaus didactic notion of 'learning-by-doing' (Wick & Grawe, 2000). As noted by Niedderer and Roworth-Stokes (2007), the varied terminologies of Practice, Practice-based, and Practice-led are used to label different forms of using practice within the research. The term Practice is used to refer to '*practice or processes in professional and creative practices to produce work for any purpose other than the acquisition of knowledge*' (Niedderer & Roworth-Stokes, 2007). The Practice-based research aims to generate knowledge by undertaking original artefact creation, which distinguishes the researcher from the practitioner (Candy, 2006; Scrivener, 2002). The creative artefact in Practice-based research is the basis of the contribution to knowledge which arises from a structured process. In the Practice-led research, the investigation leads primarily to new understandings about practice (Candy, 2006). The 'Practice-led' research is considered one of the new ways of doing research affected by the process of accumulation of knowledge (Mäkelä, 2007). The importance of this approach lies in the new knowledge of operational significance resulted in that practice (Candy, 2006). The output of the Practice-led research includes artefacts as well as a written text to explain and reflect on the practice (Candy, 2006; Nimkulrat, 2013). According to Nimkulrat (2013) and Choi (2016), Practice-led approach highlights the active role of creative practices in the art and design research process, due to



the generation of new or enhanced understandings of the expressive potential of materials in art and design.

The idea of knowing-through-making in the field of design and materials highlighted the role of the artefact. The terms knowing-through-making and learning-by-doing are often used interchangeably to refer to the hands-on approach to learning. The understanding and reflection of the artefact and its making process present a body of knowledge (Cross, 1982, 2001; Mäkelä, 2007; Parisi, Rognoli, & Sonneveld, 2017; Rognoli, Ayala-García, & Parisi, 2016; Scrivener, 2002; Scrivener & Chapman, 2004). The making of the artefact, even if intuitive, determine the direction of the Practice-led research process (Mäkelä, 2007; Scrivener & Chapman, 2004). Mäkelä (2007) suggests that an artefact can embody a greater range of roles as answers to research questions and argumentation on the topic. Artefacts can be seen as a method for understanding and collecting information (Mäkelä, 2007). In the field of Practice-led research, the making process is conceived as the driving force behind the research and even the creator of ideas in specific modes (Mäkelä, 2007). This making concept differs from conventional research, which is regarded as consequent to thinking as experiments, are carried out to test a particular assumption (Mäkelä, 2007; Scrivener & Chapman, 2004). During this creative process, the designer may rearrange several ideas, beliefs and conceptions, and thus advance her or his knowledge, understanding and insight (Mäkelä, 2007). The creative practitioner thus brings to the academy new dimensions of what knowledge itself consists of and how this contributes to learning.

The concept of “making with own hands” relates between the tinkering and the practice of crafting (Nimkulrat, 2012, 2013; Parisi et al., 2017; Rognoli et al., 2016). Craft in contemporary design is used as an inspirational and creative driver to enhance and qualify design using self-made, hands-on, and experimental approach (Parisi et al., 2017). Craft is perceived as a mean for logically thinking through the senses (Nimkulrat, 2012). Hence, this sensorial understanding of objects and artefacts is a way for designers to carry out research (Gray & Burnett, 2009; Nimkulrat, 2012; Rognoli et al., 2016). Another related concept regarding craft notion is presented by Gray and Burnett (2009) who perceived crafting as “a dynamic process of learning and understanding through material experience”. Accordingly, the craft can drive a Practice-led research process (Nimkulrat, 2012). In many material designated disciplines, such as textiles, the *Craft* is understood not only as a means of hand-

making but also as a way of thinking by manipulating materials by hand (Nimkulrat, 2012; Rognoli et al., 2016).

*“Nothing is a mistake. There’s no win and no fail. There’s only make.”*

*Kent and Steward (1992, Learning by Heart, p. 176) (Barth, 2002)*

As design is considered a practice-based branch of knowledge, novel applications of methods should be considered for carrying out research in the field of smart materials (Rognoli et al., 2016). Due to the novelty of smart materials, there is a lack of applied knowledge in the architectural field (Hovestadt & Kretzer, 2014; Kretzer, 2017a). Designers struggle to fully predict the inherited dynamic behaviour of smart materials which vary radically from traditional materials. In 1991, Toffoli and Margolus (1991) invited suggestions for experiments on the programmable matter that will make significant use of its novel capabilities. Hence, *‘Practice-led approach’* is adopted to reveal the behaviour of such smart materials and responsive kinetic structure. A PhD research by Winters (2017) in soft matter examined how the emerging role of the ‘material designer’ can enrich the design process in the fields of soft robotics, as well as programmable materials. Her *‘Practice-led’* research concluded that a designer could create a fertile ground for a polyvalent imagination by thinking through physical prototyping and bodily engagement with materials. The work carried in the ‘Component design and prototyping’ chapter follows the Practice-led approach using a straight forward experimentation methodology.

### *3.2.2. Hands-on exploration and Material tinkering*

To be able to work with smart materials and use them for actuation, it is necessary to understand the behaviour of these materials over time (Kretzer, 2017a). Two knowledge sets are required to gain an experience with smart materials; first a theoretical understanding of their mechanical and chemical characteristics, internal processes, working principle and composition as well as practical instructions on how to train or anneal them. Second, their physical behaviour and transformative capabilities in response to energy fields. Therefore, experiencing materials through direct and creative engagement with materials are carried out experimentally to understand the material behaviour through its direct manipulation.

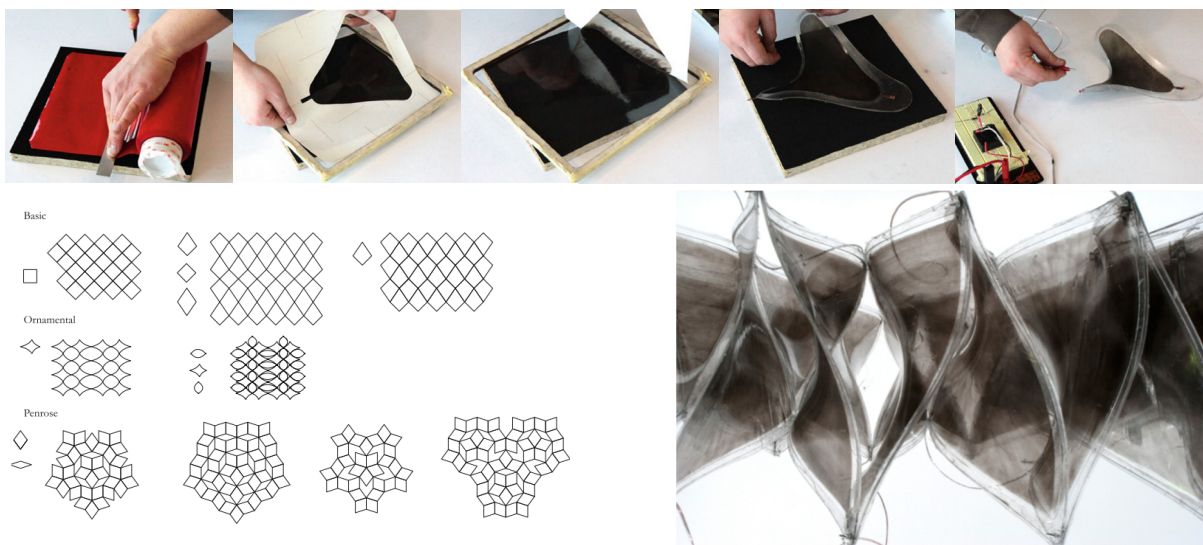
Methodologies for materials exploration are experimental, explorative and practical (Parisi et al., 2017). This practice of direct, creative, and iterative experimentation on materials is referred to as “Material Tinkering” (Cermak-Sassenrath & Møllenbach, 2014; Jacobsson, 2013; Parisi et al., 2017). The term *‘Tinkering’* originated in the field of Human-Computer

Interaction (HCI) that refers to physical manipulations of materials in a direct, naive, playful, and creative way (Cermak-Sassenrath & Møllenbach, 2014; Parisi et al., 2017). It is a practice that may drive innovation and uniqueness in design (Parisi et al., 2017). The importance of the tinkering approach lies in its implications in the designer's experiential learning and engagement with the material (Niedderer & Roworth-Stokes, 2007; Nimkulrat, 2013; Parisi et al., 2017). Jacobsson (2013) positioned '*tinkering*' as an essential attitude that is part of an overall design process in interaction design research where the design of artefacts depends on the relationship between the actuators and the direction of heat stimulus. Rognoli et al. (2016) argued that by following a conscious method of research through material tinkering, the designer is able to create a vision with the material that becomes for certain, a valuable contribution to create meaningful material experiences for the further projects. Accordingly, playful, and creative way of material manipulations are carried through testing pre-trained and trained shapes, experimenting different training procedures and testing the system reversibility.

On the architectural scale, Beasley Studio research focuses on aesthetics, technology and Craft of responsive envelope systems including the digital fabrication of extremely lightweight, flexible component arrays containing embedded sensors and actuators. Philip Beesley's architectural installations have inspired Manual Kretzer to explore more about the soft matter. He initiated the *materiability research network* in 2012 (renamed into materiability) (<http://materiability.com/>). Under the slogan '*What I Hear I Forget- What I See I Remember- What I Do I Understand*', the online platform and hub encourages architects and designers to participate with experiments carried using active materials. Projects and tutorials are executed with a hands-on approach by architects and designers to learn using and qualifying active materials potential (Kretzer, 2017a). The website provides hands-on tutorials to self-produce them and promotes their assembly in speculative spatial installations and artistic explorations (Kretzer, 2017a).

Moreover, Kretzer in his book '*Information Materials Smart Materials for Adaptive Architecture*' demonstrated explorations carried in courses and workshops to mediate the smart materials properties and their potential in the context of adaptive architectural systems (Kretzer, 2017a). In the process of physical making through hands-on experience, the materials are fabricated following simple rules. Instructions were given to provide direct experience of a smart material by breaking down scientific processes into easily understandable steps

(Kretzer, 2017a). Electroactive polymers have been tested during ShapeShift (Kretzer, 2017b) and Animated Textiles (Kretzer, 2017a) projects. Work can be classified on a component scale and then on a grouped scale. The steps started with 'Shape design' which includes designing the desired shape using a graphical computer program that exports laser-ready files. Secondly, the membrane, and powder making phase which are followed by the stretching of materials. It can be called 'materiality'. Thirdly, the electronic connection and power were applied to test the motion which can be called 'actuation'. Finally, the shapeshift structure grouped 36 unit, which can be called 'grouping and panelization' as shown in Figure 3-4.



*Figure 3-4: Developing a component unit of Electroactive polymer material and then grouping them as seen in 'ShapeShift' final prototype, which consists of 36 individual EAP elements.*

Moreover, some responsive skin prototypes discussed in the literature chapter used two main performative components, folding geometry and smart actuator ("Air Flow(er)," 2018; Gianluca et al., 2018; C. K. Khoo & F. Salim, 2013; Pesenti, Masera, & Fiorito, 2015). The process of physical making can be analysed as four steps.

- 1- Fabrication of the folding geometry,
- 2- Fabricating or training the kinetic smart material actuators,
- 3- Fixing or layering them together to work as an integrated system,
- 4- Testing the dynamic movement.

Thus, a four-stage design process is conducted using a straight forward experimentation methodology. It includes form generation, materiality, actuation and panelization. These phases of experimentation will be discussed in detail in the following section.

### 3.3. Phases of Experimentation

The experimentation work in the ‘Component design and prototyping’ chapter is informed by bio-inspiration and folding principles to explore design possibilities of deployable systems. The design goals of the experimentation work are as follows: (1) to develop a lightweight system which provide the least friction possible, (2) to use simple actuation methods (3), to achieve a high range of aperture size (4), and to achieve a forward and backward motion. The work experimented some of the analysed principles of the natural-driven plant motion, such as; elastic kinetic approach, bilayering, pliable structures and curved folding. The interesting connections between bio-inspiration’ and ‘origami’, which was studied in Chapter Two, is reflected during the four design stages using folding principles and actuation techniques. The experimentation work is carried on four design phases as shown in Figure 3-5. Experimentation is driven by curiosity, excitement and skills of the researcher to guide this practice of knowledge production and not the attribute of a finished product. Later some potential prototypes or artefacts for four different ideas are developed, followed by *the teaching experience* with the students to test the design process.

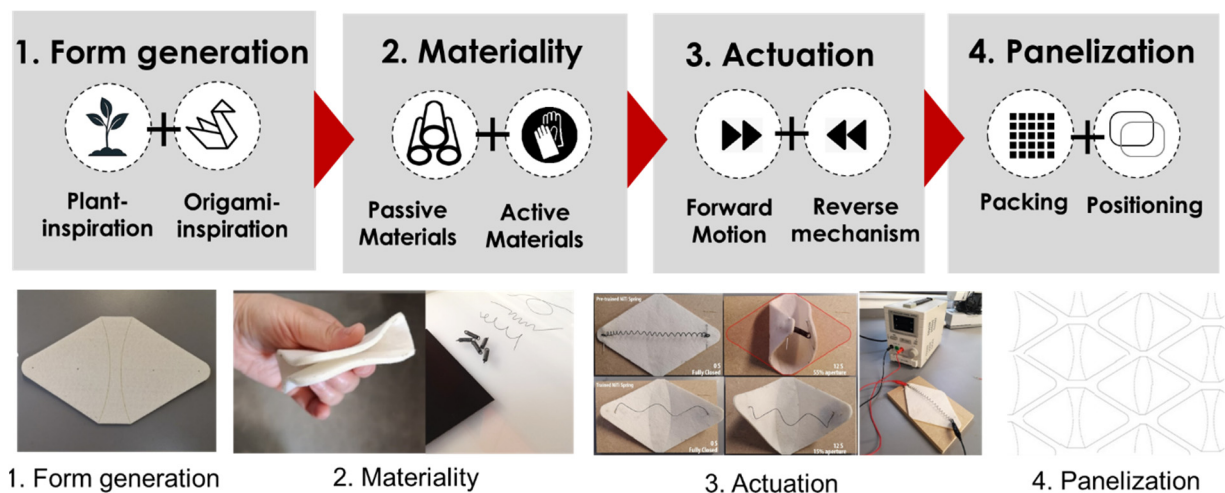


Figure 3-5: A Four-stage design process proposed by the researcher to design responsive solar-shading systems.

#### 3.3.1. Hands-on experimentation and Material tinkering

Each design stage is discussed below in terms of objective, general approach, methodology and methods.

#### In the Form generation stage

- The objective is to find the best folding deployable forms that are contractible and can be easily actuated using simple actuation strategies.

- The general approach is practice-led.
- The methodology is an experimental methodology using hands-on practices through manually manipulated physical models in which different patterns are tested against one another with an evaluation of the contraction and aperture size. This playful investigation and creative design of deployable forms aims to explore their dynamic aesthetical qualities and transformation states.
- The specifics are tested using several different straight and curved crease patterns. Straight and curved-line folding patterns are applied within individual units of lightweight materials. Step-by-step procedures are demonstrated for the form transformation.

**In the Materiality phase ‘active’ and ‘passive’ materials are tested separately as follows:**

**Experimenting with ‘passive’ materials**

- The objective is to find the best passive material to provide little resistance whilst also allowing for a natural return mechanism.
- The general approach is Practice-led and computational
- The methodology is an experimental methodology in which different material configurations are tested against one another with an evaluation of the best results by measuring flexure and response and their ability to hold crease patterns.
- The specifics are tested using a number of different configurations which are consistently applied to each type. Different lightweight materials are tested; such as; fabrics woven (e.g. linen) and non-woven (e.g. felt), paper, card, and polypropylene sheets. Preliminary samples with dimensions of 10 cm x 10 cm were chosen for testing, as they are handy and easily manipulated and controlled.

**Experimenting with ‘active’ materials (Materiality)**

- The objective is to test SMMs’ different shapes and training procedures to achieve high range of transformation in forward motion.
- The general approach is Practice-led.
- The methodology is an experimental methodology in which material tinkering is applied in SMMs testing and their training process which aims to control their geometric and mechanical properties.
- The specifics are tested using a number of different types of nitinol wires, shapes and training techniques, which are consistently compared to one another. Nitinol SMA

wires and springs, are purchased from Fuxus Germany, and two-way nitinol springs, from nexmetal, with various diameters (0.15, 0.375, 0.5 and 1.0 mm) and activation temperatures (from 30°C to 70°C) are tested. Material experimentation was first carried through testing the original shape of the materials and their activation temperature. It was immersed in boiling water to measure its initially remembered high temperature shape following instructions of Sun et al. (2012), W. M. Huang, Goh, and Li (2002). SMAs are trained to memorised shapes. Nitinol samples are annealed at temperatures of approximately 500 °C from 10 to 25 minutes and followed by cold water quenching upon retrieval. The trained form is tested by immersing it again into boiling water or by direct Joule heating by passing an electrical current through it. SMAs are trained using three fixation methods to shape the wires into flat springs (zigzag wires), helical springs, curve-shaped, star-shaped and 3D wires. These methods are: (1) using a metal perforated aluminium jig; (2) using a screw to train a helical spring, and (3) using a CNC carved mould of casted plaster.

#### **In the Actuation stage**

- The objective is to acquire forward and backward motion and achieve a high range of transformation using simple geometries and simple smart material actuators.
- The general approach is Practice-led.
- The methodology is an experimental methodology in which hands-on explorations are carried to test some of the fixation techniques developed by Edwin et al. (2014) mentioned in Chapter Two to fix ‘active’ and ‘passive’ materials.
- The specifics are tested using a number of different fixation patterns and actuation means. The SMMs are attached, linked or embedded within the previously investigated deployable structures to be developed into some potential artefacts/prototypes. Four methods of attachment and fixation techniques are tested to achieve forward motion (a) weaving with fabric material, (b) knitting the wire with the material, (c) suspended/ hinged connections, and (d) Bilayering. To achieve system reversibility, the study considers four return mechanisms, (a) the gravity, (b) coupling passive and active elements, (c) the elastic passive material, and (d) the two-way training for SMM. Material activation took place by the Heat gun or by direct Joule heating by passing an electrical current through it.

•

### In the Panelization phase

- The objective is to create different patterns and maximise the range of aperture size.
- The general approach is Practice-led.
- The methodology is digital and physical experimentation in which different pattern manipulations are tested against one another with an evaluation of their effect on aperture size.
- The specifics are tested using different packing: straight and staggered, and the three key manipulations: translation, reflection, and rotation to create different patterns. The pattern and sequence of repetition can alter many alternatives each with different range of aperture size.

All the tested experimentation parameters are presented in Figure 3-6.

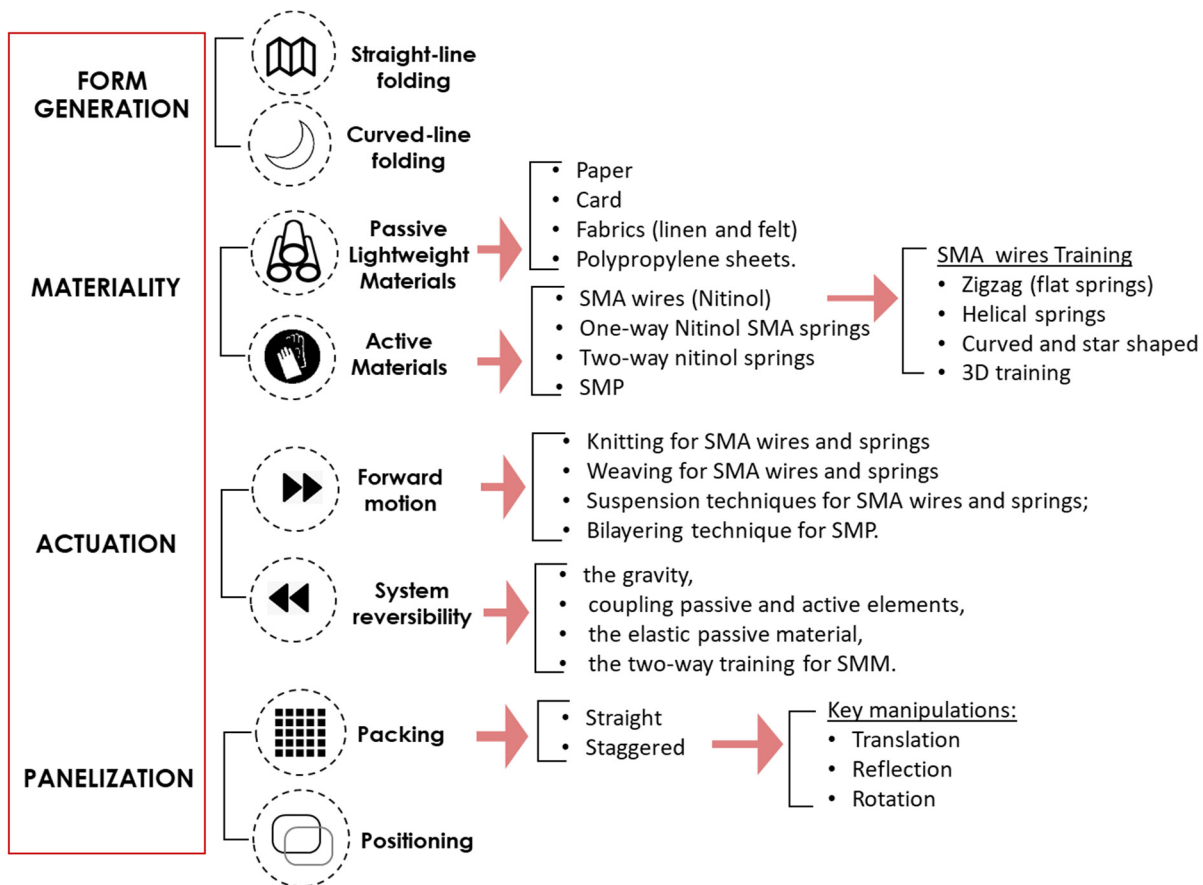


Figure 3-6: The tested parameters of responsive solar-shading systems using hands-on practice & material tinkering

The developed prototypes or artefacts combine different parameters of forms, materials and fixation techniques to investigate their potential as design outcomes with high range of transformation. Prototypes for four ideas are developed and compared based on return mechanism and deployability to reach robust, responsive reversible systems.



### **In the researcher's explorations**

- The objective is to develop an actual prototype system that can be used in further experiments.
- The general approach is Practice-led, Design-led and Creative practice.
- The methodology is an experimental methodology in which a combination of different parameters of forms, materials and fixation techniques are experimented to investigate their potential as design outcomes with high range of transformation.
- The specifics are tested using a number of different configurations which combines selected form, material, actuation and panelization technique. Prototypes for four different ideas are developed and compared based on return mechanism and deployability to reach robust, responsive reversible systems.

Finally, reflections on the prototype making process and outcome formulated a design process. A four-stage linear design process is proposed; which includes form generation, materiality, actuation and panelization. This proposed design flow is tested with MArch students to facilitate the reflection and articulation of knowledge generated from the students as being designers doing a creative practice. After observing the creative practice process and analysing the output of the course, the design process and parameters are reorganised to form an open-ended design approach which will be discussed in chapter seven. The next section will discuss the teaching experience in detail.

#### *3.3.2. Teaching experiences in designing with kinetic materials*

Design research in the field of kinetics and soft-robotics often use a material-centric approach (Bengisu & Ferrara, 2018). The ever-increasing amount of new technologies and smart materials require innovative teaching methods, to prepare students for upcoming challenges and uncertainties (Kretzer, 2017a). Researchers such as; (Oxman), (Bell) and (Kretzer), call for a more holistic and integrative educational approach in relation to materials which leads to a basic but broad understanding of materiality and/or materiability. In design and architecture schools devoted to learning soft robotics, multidisciplinary activities are carried out in labs or workshops to involve students in experimenting with smart materials (Bengisu & Ferrara, 2018). According to Drew (2007), Practice-based learning is a way of conceptualising and organising student learning, where the tutor encourages students to manage projects involving complex problem-solving skills, which are set in the context of professional practice. Practice-based learning in designing with kinetic materials stresses the

value of physical making and hands-on experimentation, which encourages students to understand and emphasise dynamic material properties and develop (adaptive) architectural solutions in relation to time and space (Kretzer, 2017a). The practice-led educational approach is used as a way of thinking through material (Nimkulrat, 2012; Parisi et al., 2017) to create awareness among young designers of possibilities provided by new technology (Bengisu & Ferrara, 2018).

Many courses and workshops are following this approach and encourage students to experience materials through a hands-on experimentation. For example, some courses in the research units of architecture schools devoted to advanced research and learning such as, MIT Media Lab, Interactive architecture lab and ICD/ITKE University of Stuttgart, follows this experimental hands-on approach. Also, the projects and workshops that emerge from the materiability approach led by Manuel Kretzer, such as ShapeShift, Phototropia, Animated Textiles, or Dynamics in Extreme Environments, followed a hands-on approach which encouraged the participants to physically engage with smart materials' intrinsic properties (Kretzer, 2017a; Kretzer & Damjanovic, 2012; Kretzer & Hovestadt, 2014; Kretzer & Rossi, 2012a, 2012b).

A description of the educational approach of materiability was presented by Kretzer (2017a) in his book 'Information Materials Smart Materials for Adaptive Architecture'. His educational framework is refined during numerous experimental student projects, the above-mentioned workshops, as well as the materiability research network. The framework followed a process-oriented model for physical making, hands-on experience and design-through-making that focus on exploration rather than a final product.

The developed educational framework of the materiability approach by Kretzer (2017a) contains a series of successive activities, which are:

- A basic theoretical understanding of their working principle and composition;
- Studying the respective materials in more detail;
- Gaining first-hand insights in fabrication procedures and assembly details in an early introductory workshop;
- Getting theoretical information on the materials' functionality and practical instructions on how to self-make them. (introductory phase);
- Physically experiencing the functionality of materials, comprehend their working principles, the relationship of fabrication procedures and materials' behavior, and finally extract and emphasise one or more particularly exciting material phenomena;

- Working in small teams, the students think about architectural situations related to the overarching theme of the course, without a direct correlation to the available materiality;
- Delivering lectures on the topic, with selected readings and literature, as well as a vast collection of sample projects;
- Bringing together the two approaches, the bottom–up material exploration and the top–down situational scenario, through a speculative spatial intervention;
- Grouping scaled components to express a specific architectural relevance. Designing the whole system for a selected situation requires further structural and aesthetical investigations more than individual elements.

To evaluate such designed projects, Kretzer (2017a) divided the criteria of success into two scales: the material scale; and the project scale. On the material scale, the criteria of success is developing particular design answers to achieve specific motion, while on the project's scale, the criteria of success is measured by the balance between the aestheticisation of the material phenomena and the effect of the system on the selected situation.

### **In teaching experiences**

- The main purpose is to test the generated design process developed over the investigation phase and to facilitate the reflection and articulation of knowledge generated from the students as being designers doing a creative practice. This knowledge is used to develop a design framework for responsive solar shading with material-based actuation. The course aimed to encourage the students to develop and articulate new areas of design and to deal effectively with innovative materials change.
- The general approach is practice-led.
- The methodology is an experimental methodology using hands-on experimentation as a practical and *creative* approach to design education regarding materials for design. This method fosters students' creativity and educates them to understand the material abilities along with the form to design motion. By knowing materials, their technical properties, their fabrication and training processes, designers can select the suitable actuation mechanism to get an amplified motion result.
- The specifics of the six-week design project are tested using the four-stage design process. The MArch students went through a proposed design process for responsive solar-shading systems. The six-week design project required the students to understand the behaviour of smart materials; shape memory alloys and polymers, to design solar shading systems in which the smart material are employed as thermos-

responsive actuators. Experimenting with a class of 10 MArch students during the fall of 2018/2019, three teams managed to prepare 15 design variants with finally actuated three models. The students worked in groups of three to develop a responsive solar shading module fits in a 0.5 m x 0.5m. The act of learning through making proved to be an effective way to intellectually engage the students and help them to discover the best working strategies.

As shown in Appendix B, the course structure follows the following steps, where each activity is carried in a separate session.

- Delivering lectures on Origami and Bio-inspiration as form generative techniques as well as smart materials, with selected readings and literature, as well as a vast collection of sample projects to help the students to get started.
- Working in small teams (3-4 students), Gaining first-hand insights in deployable structures using origami principles and physical models that are manually manipulated;
- Getting practical instructions on how to train SMA and test their behaviour in an early introductory workshop
- Physically experiencing the fixation of active and passive materials to develop one moving unit
- Working in small teams of three, the students developing a responsive solar shading module fits in a 0.5 m x 0.5m

The researcher's proposed linear design process is instructed to the students' following the below flow of activities, as shown in Figure 3-7, which are carried using the hands-on exploration.



*Figure 3-7: Design Process of responsive solar shading.*

Further reflections of the researcher's experience as a co-leader, tutor and observer are included over the educational experience, and the students' output to develop a design framework for responsive solar shading systems in Chapter Seven. So far, this chapter has discussed experimentation as a significant and valuable methodology for gaining knowledge from physical exploration. The next part of this chapter will discuss the CFD simulations as a methodology for environmental assessment of responsive solar-shadings within their potential context of operation and use the feedback to customise the material and design of

the system. A design of an origami prototype is selected from the experimental material thinking to be tested in the environmental performance.

### **3.4. Simulation-Based Method**

Climate-based design is a methodology for designing high-performance building facades through systematic investigations of different design options (Aksamija, 2016). Building performance is a guiding design principle similar to form making. It covers a broad domain from spatial to structural, thermal and technical aspects (De Wilde, 2018). Methods of energy modelling and energy analysis, study the effects of design decisions on energy consumption, occupants' comfort, and the environment. These effects are investigated and quantified using Building Performance simulations (BPS), to identify an optimal solution based on the requirements of location, climate and building type (Aksamija, 2016). BPS in architectural design can play an essential role in addressing the issue of environmental sustainability. Recent progress in computer science and sustainability requirements offers simulation-based methods that could be applied in the building sector. The simulation tools become widely available, which positively affects the way by which the buildings are being designed, analysed and constructed (Crawley, Hand, Kummert, & Griffith, 2008; Malkawi, 2004). Façade design is a significant contributor in determining building performance (Aksamija, 2016; Tzempelikos, Athienitis, & Karava, 2007). Façade analysis guides the design decisions to control solar gains and reduce the consumption of heating, cooling and electric loads while maintaining a comfortable and efficient indoor environment (Tzempelikos et al., 2007). Design decisions can only be justified by comparing the performance of various design alternatives on total energy consumption and the indoor environment in the early design phase (Nielsen et al., 2011).

The proposed responsive solar-shading systems are generally soft, flexible and sensitive. Therefore it is preferably integrated within a Double skin facade (DSF). It is thus protected from atmospheric agents; such as bad weather and pollution (Ghaffarianhoseini et al., 2016; Gratia & De Herde, 2007), and can make use of both the direct sun and greenhouse effect as an actuating force to transform energy into movements that open and close the solar-shading system. Such a system has two main façade characteristics that need special attention when selecting a proper simulation tool. These characteristics are, the *dynamic property of the solar-shading and the DSF; either naturally or mechanically ventilated*.

A variety of tools and simulation programs with different modelling capabilities have been developed during the past few decades to environmentally assess building designs in

areas, like lighting, thermal, acoustic, structural, etc. (Attia, Beltrán, De Herde, & Hensen, 2009; Crawley et al., 2008; Malkawi, 2004). One study by Crawley et al. (2008) compared the capabilities of twenty Building Performance simulations (BPS) programs, which are: BLAST, BSim, DeSTm DOE-2.1E, Ecotect, Ener-Win, Energy Express, Energy-10, Energy Plus, eQuest, ESP-r, IDA ICE, IES VE, HAP, HEED, PowerDomus, Sunrel, TAS, TRACE, and TRNSYS. No single simulation program can address all design aspects of high-performance facades, thus multi-domain integration in different BPS tools is required to investigate the facade systems behaviour (Aksamija, 2016), especially adaptive building facades (R. C. Loonen, Favoino, Hensen, & Overend, 2017). Besides, different stages of the design process may require different simulation tools (Aksamija, 2016).

A considerable amount of literature has been published to select the energy performance of solar-shading systems by using simulation tools (Kirimtat et al., 2016). Despite the regular updates of these BPS tools and the extension of their modelling capabilities, these tools are developed for conventional shaded building facades. Thus, It may restrict the options for modelling the dynamic property of the adaptive building skins (R. C. Loonen et al., 2017) as well as the multiple coupled physical phenomena that occur in the complex 3D geometry of DSF (Kim & Park, 2011).

#### *3.4.1. Simulation of DSF*

Several building simulation tools can be used for DSFs' energy performance assessment, such as, EnergyPlus, ESP-r, TRNSYS, TAS, IDA ICE, VA114, BSim, etc. (Kim & Park, 2011). However, there is an accountability issue as to whether such tools can accurately describe the transient heat and mass transfer phenomena that occur in the complex 3D geometry of DSFs. For example, EnergyPlus can properly handle simulations of any whole building and its subsystems, but are ill-suited for particular domain simulations, such as for DSFs. Difficulties and limitations in performance simulation of a DSF with EnergyPlus have been reported by Kim and Park (2011). The study found significant variations in the behaviour of DSFs in both thermal and airflow between the measurements and EnergyPlus simulation predictions. Significant simulation errors were found in the prediction of the inner glazing temperature.

To overcome the above disadvantages of general simulation tools, several in-house simulation models (MATLAB language) were developed in previous studies (Yoon, Park, & Augenbroe, 2011; Zanghirella, Perino, & Serra, 2011). These in-house models were calibrated

and, when compared to whole building simulation programs, proved to be reasonably accurate in describing DSFs. One of the major drawbacks of this approach is that it has difficulty handling building and system simulation models. Moreover, Modelica is an object orientated, equation-based language that can describe physical systems in various domains (Wetter, 2009). It supports transient thermal modelling and allows it to be combined with a customised control strategy for seasonal adaptive solar gain management. Modelica is a free open-source language for modelling of systems that are described by differential, difference and algebraic equations (Wetter, 2009). In the context of adaptive facades, it allows for high-resolution multi-domain analysis, rapid extension of modelling capabilities, as well as smooth interactions with other building integrated energy systems. However, the development of Modelica for building performance simulation has not yet reached a mature phase (R. C. G. M. Loonen, Favoino, Hensen, & Overend, 2016).

Additionally, there are some component-based softwares which could be used in modelling building envelope components such as windows, skylights, walls, roofs. It is done for energy, moisture and structural performance. Several industry standard tools employed this modelling, such as THERM, WINDOW, and WUFI. THERM is a computer program developed at Lawrence Berkeley National Laboratory (LBNL) which can be use by building component manufacturers, engineers, educators, students, architects, and others interested in heat transfer. Therm is a 2D finite element heat-transfer analysis tool, with a steady-state conduction algorithm known as CONRAD. THERM can be used to simulate 2D heat transfer effects in building components with thermal bridges. THERM's heat-transfer analysis allow the evaluation of the product's energy efficiency and local temperature patterns, which may relate directly to problems with condensation, moisture damage, and structural integrity. THERM's calculation routines evaluate conduction and radiation (Pelaz, Blanco, Cuadrado, Egiluz, & Buruaga, 2017). Additionally, WUFI software enables one-dimensional investigation of the hygrothermal performance of building components for various effects such as built-in moisture, solar radiation, long-wave emissions, and summer condensation. Although, the tool permits a simulation over a complete year, it has some modelling limitations, when some layers differ in size along the wall (Zirkelbach, Schmidt, Kehrner, & Künzle, 2007).

CFD analysis is one of the most powerful tools to predict DSF behaviour and assist architects with environmental-based decisions during the design process (Pasut & De Carli, 2012). A considerable amount of literature has used CFD to study the behaviour, features and energy consumption of DSFs such as; (Baldinelli, 2009; Hamza, Cook, & Cropper, 2011; Hamza & Underwood, 2005; Ioannidis, Buonomano, Athienitis, & Stathopoulos, 2017). Specifically, over the last two decades, most research in buoyancy-driven flow has emphasised the use of CFD due to the growing demand for detailed quantitative knowledge of heat transfer processes in buildings, and accordingly the heating and cooling demands. Fluent has a User-Friendly Interface for a fluid simulation software. It is known for its advanced physics modelling capabilities and ability to analyse a variety of fluids phenomena. It has high capabilities from visualization to mesh generation and solvers which enable users to design from scratch for different purposes. Many researchers in the field of DSF used Fluent to couple convective and radiative heat transfer and fluid flow in the DSF (Amaireh, 2017; Guardo, Coussirat, Valero, Egusquiza, & Alavedra, 2011; Hazem et al., 2015; Iyi et al., 2014; Y. Li, Darkwa, & Kokogiannakis, 2017; Parra, Guardo, Egusquiza, & Alavedra, 2015; Safer et al., 2005; Velasco et al., 2017).

#### *3.4.2. Simulation of Adaptive facade*

The potential of adaptive facade system, or what Tzempelikos et al. (2007) called dynamic fenestration is quantified by using integrated simulations that adopt energy demand, the indoor air quality, daylight availability, and visual comfort (Nielsen et al., 2011). Such systems have changeable building façade shape and/or material properties that need to be considered during the simulation run-time in these tools (R. C. Loonen et al., 2017). R. C. Loonen et al. (2017) found that the integration of modelling and simulation of adaptive facades performance has the potential to provide:

- Informed decision-making to support the design process;
- Prediction of energy-saving potential;
- Virtual rapid prototyping to identify promising future alternatives;
- Exploration of high-potential control strategies;
- HVAC system sizing and fine-tuning of the system interaction with other building services;
- Virtual testing of the robustness of adaptive facade systems.



For these reasons, modelling and simulation of adaptive facades can bring insights into their performance benefits and the development of innovative technologies in general (R. C. Loonen et al., 2017).

Parametric and generative design tools, as well as computational optimisation using Rhino/Grasshopper platform, have high potential to simulate adaptive building facades (El Ahmar & Fioravanti, 2015; Eltaweel & Su, 2017; Mahmoud & Elghazi, 2016; Roudsari, Pak, & Smith, 2013; Sharaidin, 2014; Wagdy, Elghazi, Abdalwahab, & Hassan, 2015). Diva, ladybug and Honeybee as engines to EnergyPlus, Radiance and Daysim provide designer-friendly interactive graphics to support the decision-making process (Roudsari et al., 2013). Butterfly is an under development plugin that enables designers to connect to OpenFoam and run CFD simulation (Roudsari et al., 2013). Although this might seem very promising, it is still under development and doesn't allow the simulation of complex geometries compared to Ansys CFD capabilities.

Although modelling and simulation of adaptive facades have to accurately represent the time-varying states or properties of building skins or solar-shadings, a simplified simulation strategy has been developed to reduce computational time and cost. This discrete approach subdivides the simulation period into several simulation runs with shorter periods which works well with long (seasonal) adaptation cycles. Additionally, separate models for the adaptive facade different states can be tested over the whole simulation period or as a point in time simulation. Given that the inputs should be set accurately at the initiation of each simulation.

### **3.5. Phases of Building Performance Simulation**

For the purpose of the study, single-storey south-orientated office room with Cavity-Integrated responsive solar-shading devices is assessed to set selection criteria for appropriate smart materials, to select the optimal range of aperture size and to test the Cavity-Integrated responsive solar-shading devices performance and reduction of internal solar gains. Therefore, Chapters Five & Six present a systematic procedure to gather numerical simulation to quantitatively assess the integrated DSF system, as shown in Figure 3-8.



BUILDING PERFORMANCE SIMULATIONS	
Environmental Design and Modelling (Chapter 5)	Integrated Design and Simulation (Chapter 6)
<b>Parameter 1: Solar simulator representation</b> <ul style="list-style-type: none"> <li>Two different modelling methods are used to represent the solar generator.</li> </ul>	<b>Scenario 1: Non-Shaded DSF cavity</b> <p>The non-shaded DSF variables are tested on the 15<sup>th</sup> of July at 12:00 pm</p> <ul style="list-style-type: none"> <li>the DSF cavity width (0.4, 0.6, 0.8, 1m)</li> <li>The façade layering (single &amp; double inner glazing)</li> <li>The domain size (0.4 vertical section and full cavity).</li> </ul> <p>Simulations are tested on 15<sup>th</sup> of July and 15<sup>th</sup> of January at 9:00, 12:00 pm and 3:00 pm</p> <ul style="list-style-type: none"> <li>Simulation runs will measure the inner glazing surface temperature (and the solar flux) and the airflow in the cavity relative to screen aperture sizes.</li> </ul>
<b>Parameter 2: Domain Size</b> <ul style="list-style-type: none"> <li>With and without external environment</li> </ul>	<b>Scenario 2: Flat solar-shaded DSF cavity</b>  <ul style="list-style-type: none"> <li>Simulations are tested on 15<sup>th</sup> of July and 15<sup>th</sup> of January at 9:00, 12:00 pm and 3:00 pm</li> <li>Simulation runs will measure the inner glazing surface temperature (and the solar flux) and the airflow in the cavity relative to aperture sizes.</li> </ul>
<b>Parameter 3: Level of complexity</b> <ul style="list-style-type: none"> <li>A full detailed model vs an abstracted version</li> </ul>	
<b>Parameter 4: Turbulence model</b> <ul style="list-style-type: none"> <li>SST K-omega vs RNG k-epsilon</li> </ul>	
<b>Parameter 5: Radiation model</b> <ul style="list-style-type: none"> <li>DO radiation models vs P1 radiation model</li> </ul>	<b>Scenario 3: Folded solar-Shaded DSF cavity</b>  <ul style="list-style-type: none"> <li>Simulations are tested only 15<sup>th</sup> of July and 15<sup>th</sup> of January at 12:00 pm</li> <li>Simulation runs will measure the inner glazing surface temperature (and the solar flux) and the airflow in the cavity relative to aperture sizes.</li> </ul>
	<b>Solar-shading surface temperature analysis</b>

Figure 3-8: The tested parameters of the numerical Building performance simulation

The behaviour of DSF is complex because multiple coupled physical phenomena take place inside the cavity. These phenomena are air movement and heat convection, conduction, short- and long-wave radiation (Safer et al., 2005). The flow inside the cavity could be laminar, turbulent or a combination of all the flow regimes (Z. J. Zhai, Zhang, Zhang, & Chen, 2007). CFD modelling has achieved success in predicting airflow and thermal performance in DSFs cavity as reported by several studies over the past two decades (Baldinelli, 2009; Coussirat et al., 2008; Safer et al., 2005; Z. J. Zhai et al., 2007). For the airflow study in indoor environments, the mean airflow parameters are more effective than instantaneous turbulent-flow parameters. Hence, the interest is stronger in solving the RANS equations with turbulence models that can quickly predict air distributions. Despite the challenges associated with turbulence modelling, the RANS approach is popular in modelling airflows in enclosed environments due to its significantly smaller requirements of computer resources and user skills (Z. J. Zhai et al., 2007). CFD code (Ansys-Fluent®v18.1) model heat transfer and

turbulence for performance prediction. Simulation runs will measure the inner glazing surface temperature, the heat flux, and the airflow in the cavity relative to screen aperture sizes.

Three-dimensional models are proposed for the DSF vertical section. The 3D approach has been adopted mainly for three reasons:

1. It is able to use the solar load model, which is only available in the 3D solver of ANSYS Fluent;
2. It has better accuracy as the 2D model slightly underestimates the flow rate;
3. It allows assessment for more complex solar-shading forms.

All 3D cases were modelled in CAD software and exported as step files to be further processed in Ansys software package, as shown in Figure 3-9. Navier-Stokes equations along with the energy conservation equation were solved using CFD code Ansys Fluent® v18.1 to simulate the studied cases. At present, the commercial CFD code allows coupled thermo-fluid-dynamics problems to be solved using turbulence and radiation sub-models.



*Figure 3-9: Software programs used for modelling, meshing and simulation.*

#### *3.5.1. Environmental Design and Modelling: Validation work (Chapter 5)*

Simulations must be validated by comparison with data of a similar experimental apparatus. An Experimental case from literature is used for the validation of DSF numerical modelling. Three validation cases are considered, Safer et al. (2005), Manz et al. (2004), and Mei et al. (2007). Mei et al. (2007) is selected as an experimental naturally ventilated DSF equipped with shading devices which is similar to the proposed DSF integrated with a responsive solar-shading system in terms of natural ventilation and integrated shading. Safer et al. (2005) and Manz et al. (2004) cases are excluded because Safer et al. (2005) case is a 3D simulation which was carried in absence of experimental tests while Manz et al. (2004) case is an experimental mechanically ventilated DSF. Thus, Mei experimental case was reproduced numerically and simulated.

### **In the Validation phase**

- The objective is to set guidelines for the Computational fluid dynamics (CFD) numerical modelling setup of a DSF integrated with solar-shading system and validate this CFD modelling setup against an experimental case.
- The general approach is computational approach.
- The methodology is Building Performance simulations/ simulation methodology in which the results of a CFD numerical model are compared against the experimental physical real case of Mei et al. (2007).
- The specifics are tested using several variables, which are: determining the level of geometrical model detailing, extending the domain to include the external environment, representing solar simulator, and the selection of turbulence and radiation models.

Chapter Five discusses the challenges of validation of DSFs. Different methods from literature for modelling DSF equipped with integrated shading devices are discussed. Turbulence and radiation sub-models selection, as well as coupling and decoupling of external environment, are compared with Mei experimental results. Coupling Radiation and turbulence models have always been a problem addressed by researchers in different ways. Although CFD allows for detailed numerical modelling of the interactive physical phenomena inside DSF cavities, its simulation setup has many challenges associated with turbulence modelling and conjugate heat transfer. Sensitivity analysis is defined as a process of determining the rate of change in model output with respect to changes in model inputs (parameters) (Arnold et al., 2012) The simulation process is explained in Chapter Five, including solar simulator representation, the level of geometrical model detailing, domain size, and selection of turbulence and radiation models, as shown in Figure 3-10. These tests work as a sensitivity analysis to find the optimised setup for the simulations and conclude the most recommended procedure for further investigation of the performance of DSF integrated with responsive solar-shading system in Chapter Seven.

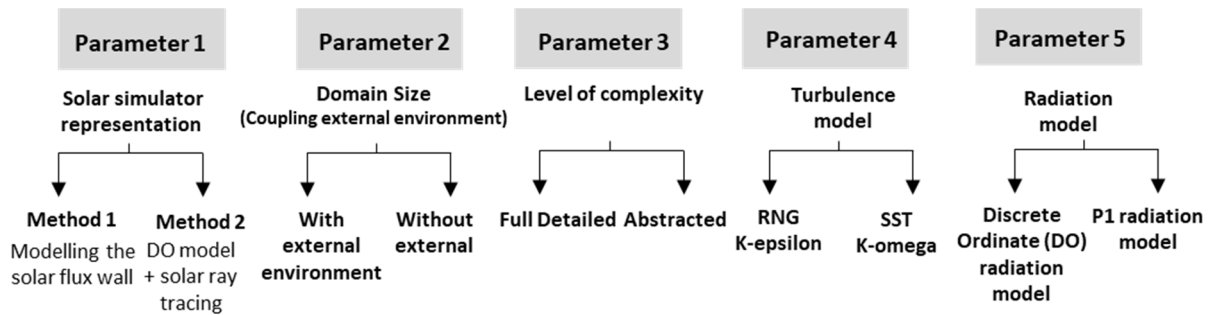


Figure 3-10: Sensitivity analysis for the Validation Case

- Two different modelling methods are used to represent the solar generator. A solar flux of  $715 \text{ W/m}^2$  is applied to a wall surface representing the solar generator, and the simulated solar flux using a two-band non-gray DO radiation model and solar ray tracing.
- Two different domain size are compared, coupled and decoupled DSF cavity with the external environment. The DSF cavity domain is extended to include an external domain of 0.6m which is the original distance between the cavity and the solar simulator
- The level of complexity of the model is tested by comparing a full detailed model with an abstracted version without grilles. The concept of levels of detailing is similar to the concept of level of development/detail (LOD) in Building Information Modeling (BIM) which represents the total amount of information contained in the BIM element. Two different turbulence modelling are compared, SST K-omega and RNG k-epsilon turbulence models coupled with discrete ordinate (DO) radiation model.
- Two different radiation modelling are compared, (DO) radiation model and P1 radiation model coupled with RNG k-epsilon turbulence models

The setup of the best agreement with the experimental measurements will be applied for Mei's shaded cavity, which is equipped with white blinds at angle  $45^\circ$ . Temperature profile of the mid cavity at 1.1m is studied to be compared with Mei's experimental measurements. Afterwards, the setup of the best agreement in the validation phase is processed in integrated case studies in Chapter Six.

### 3.5.2. The Simulation of Integrated DSF (chapter 6)

Performance assessment of movable solar-shadings is a complex mission which is used to inform the design decision making of the responsive system. The best performing setup from Chapter Five is used in the chapter for the three cases of DSFs which are shown in Figure 3-11.

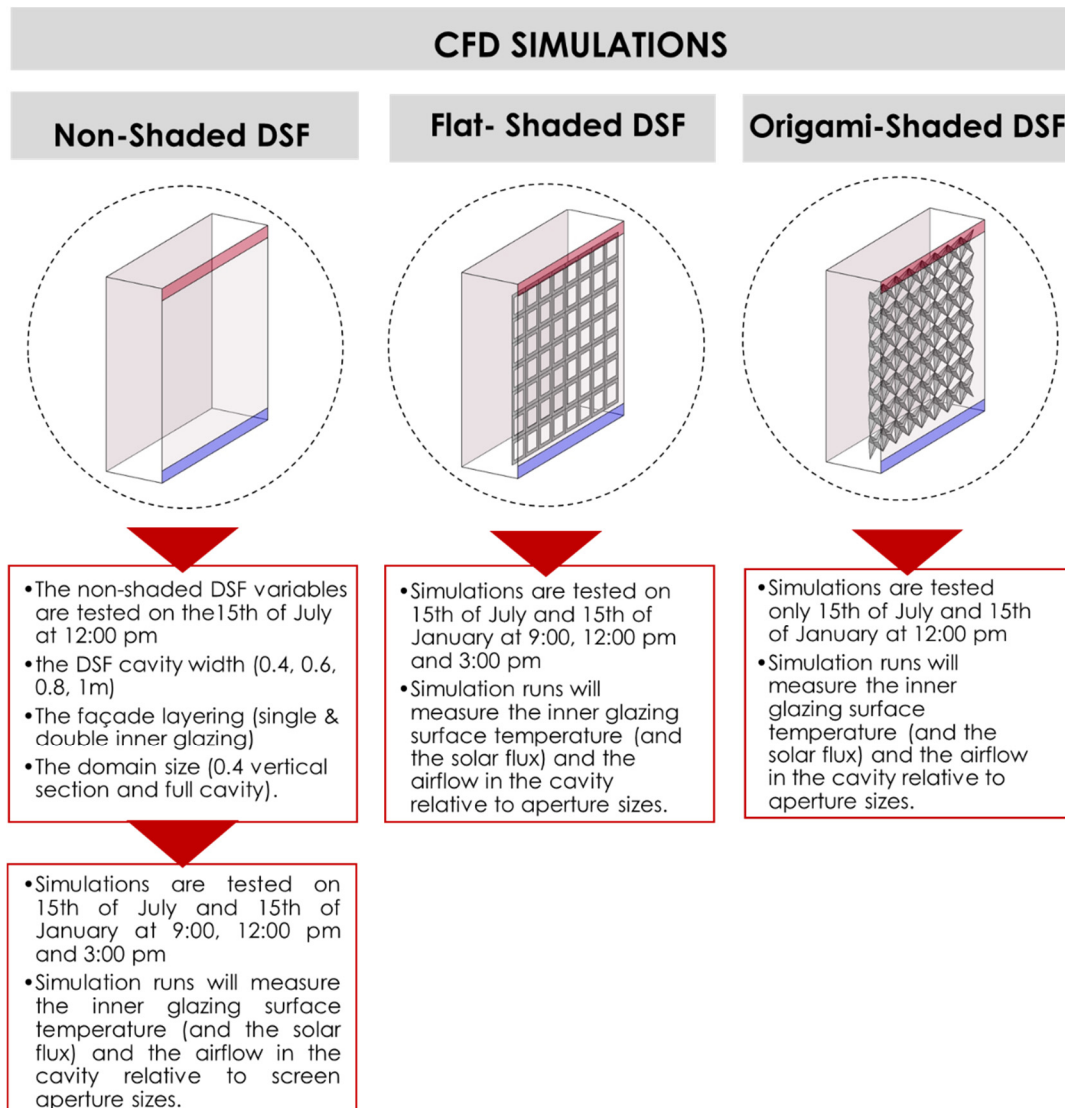


Figure 3-11: The three cases of DSFs, non-shaded, flat-shaded and origami-shaded DSFs

#### In the Simulation phase

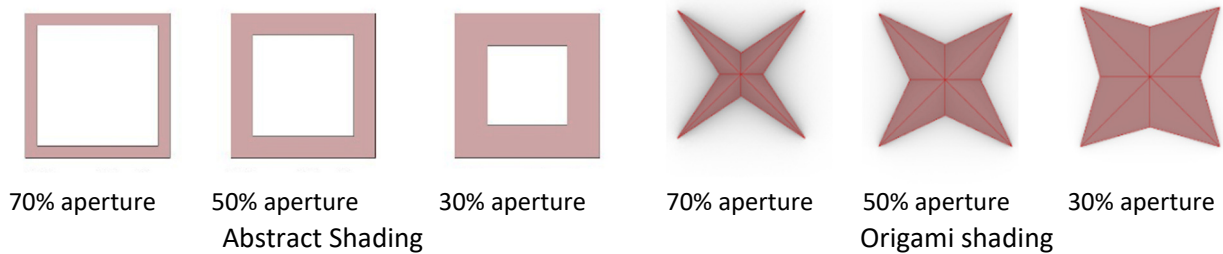
- The objective is to inform the design decision making of the responsive system.
  - 1) To set selection criteria for appropriate smart materials, activation temperatures and their thermal requirements,
  - 2) To select optimal range of aperture size/percentage of the shade opening to inform the solar-shading designs,

- 3) To test the Cavity-Integrated responsive solar-shading devices performance and reduction of internal solar gains.
- The general approach is computational approach.
  - The methodology is Simulation methodology in which (CFD) numerical modelling is used to assess single storey south-oriented DSF with and without solar-shadings in Cairo, Egypt
  - The specifics are tested using variables of the aperture size and the form of solar shading devices. Flat and folded solar-shading devices are installed in the air cavity of the DSF and compared with the non-shaded base case.

First, non-shaded cavity is studied as a base case at 9:00 am, 12:00 pm and 15:00 pm in peak summer and peak winter day; 15<sup>th</sup> of July and 15<sup>th</sup> of January. July in Cairo, Egypt, is known as the hottest month as shown in Appendix C. DSF geometrical variables which can impact the efficiency and effectiveness of DSF are tested. These variables are: the DSF cavity width (0.4, 0.6, 0.8, 1m), the façade layering (Single and double inner glazing), and the domain size (0.4 vertical section and full cavity). The 3D vertical segment of 0.4m deep which can include one solar shading modules is compared with full DSF cavity modelling (3.2m deep) which contains eight solar shading modules as shown in Figure 3-12. Conditions of the non-shaded DSF cavity, temperatures' contours, are measured to detect the highest temperature profile to install the shading screen to thermally activate the responsive system by solar exposure and cavity temperature.

In the second set of simulations, the proposed responsive kinetic solar shading system is measured at three different apertures; 30, 50 and 70 opening percentages. A minimum opening percentage of 30% is considered as a minimum aperture to ensure appropriate natural daylight illuminance values for south-facing office spaces as per recommended by (Mahmoud & Elghazi, 2016; Tzempelikos & Athienitis, 2007; Wagdy et al., 2015). A simplification of complex solar-shading forms into flat screen with the same aperture size is carried to guide us of the general system performance in peak summer and winter days with less computational power. The flat solar-shading devices with the three aperture sizes are installed inside the DSF cavity and tested at the same previously mentioned times and dates of peak summer and peak winter day. A set of studies analyses the surface and air temperatures, airflow and heat flux to test the DSF performance efficiency and optimise the screen aperture ranges at different times.

In the third set of simulations, a complex folded origami solar-shading devices are tested numerically with the same three aperture sizes (30%, 50%, & 70%) at 12:00 pm on 15<sup>th</sup> of July (peak summer day). Finally, a focused analysis is carried on the heat distribution of solar shadings; the flat and folded.



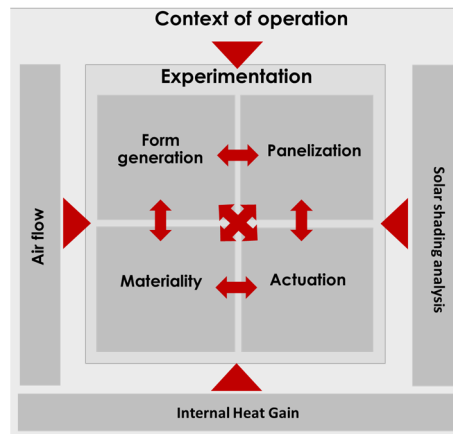
*Figure 3-12: Flat and Origami Solar shadings with 3 apertures sizes; 30%, 50% & 70%.*

### **3.6. The Design Framework**

Chapter seven integrates and reflects on the design experiments of the researcher and the MArch students presented in chapter 4 and the environmental data from CFD analysis in chapter 6 using an open-ended design approach. Chapter seven aims to develop a framework for responsive solar-shading design informed by experimental and environmental feedback. The design framework represents an experiential knowledge and gained insights into the responsive system through the researcher's different identities as a designer as well as tutor and observer in the educational experience. The design framework opens up possibilities by leaving spaces of freedom for designers to re-appropriate the design of the responsive system by changing their context of operation and design approach. The design framework is identified as an Open-ended Design approach (OeD) which is defined as a project capable of changing, as per the changing context (Ostuzzi, De Couvreur, Detand, & Saldien, 2017). The framework attempts to provide a rich platform for independent self-development which encourages thinking in terms of dynamic processes rather than static attributes. The framework is inspired by the didactic model presented by (Kretzer, 2017a), which is referred to as the materiability approach. This type of framework goes beyond traditional architectural forms of expression by incorporating cooking instructions, recipes, or tutorials (Kretzer, 2017a). The materiability approach was inspired by Yona Friedman who promotes the development of a universal language in the form of cooking instructions, recipes to democratize design incentives. Another study by Schleicher (2016) inspired the framework. Schleicher (2016) created a diagram that depicts a potential transition process that begins with biological role models and progresses through bio-inspired mechanisms to prototypes and mock-ups. The presented framework rearranged the main four aspects of the design of



the responsive structure; which are: form, materiality, actuation and panelization into a network of entities related to their context of operation that can be approached differently by each designer as shown in Figure 3-13. The relationships between entities are analysed in the chapter informed by all the gained knowledge from the physical experimentations and CFD simulations.



*Figure 3-13. Entities in the experimental and contextual domains*

### 3.7. Conclusion

A mixed interdisciplinary methodology and integrated methods are adopted in this research to understand the performance of responsive solar-shading systems on multiple levels (experimentally and environmentally) and how the design parameters are affected by each other when studied collectively by the end of the thesis. It opens the discussion of the importance of examining all these aspects relative to each other and looking for tools to achieve this goal for more sustainable futures.

The Practice-led approach is adopted in Chapter Four using Hands-on experimentation, and Material Tinkering methodologies to explore the potential of smart materials (SMM), and use bio-inspiration and folding principles to alter complex deployable forms using simple actuation strategies. The hands-on exploration is carried to investigate the origami abilities, both straight and curved folding, for deployable forms in forward and reverse motion. As the materials and its physicality are the key players of the design activity of responsive solar shading, the researcher acquires experience by working directly with the smart materials, through ‘hands-on’ explorations and Material tinkering. Material tinkering is used to predict the immanent dynamic activity of smart materials in a purely exploratory way. The ‘Material tinkering’ application includes the annealing processes,

training different geometric shapes (Star shape, curves, flat spring and helical spring), using different types of SMAs (wires and springs). Through this, the design of materials become an explorative process of learning characterised by unexpected and surprising discoveries provoked from the direct interactions and experiments.

The Teaching Experiments with MArch students is performed to test the design process. The educational experience is designed in a similar structure to Kretzer (2017a) guidelines. The experience with a real-world problem offered an action-based method of advancing the student's knowledge.

The Climate-based design scientific approach is adopted in Chapters Five & Six using CFD simulations to measure the impact of responsive solar-shading systems on multiple environmental factors. It helps the design decisions, selection and customisation of smart materials. The CFD coupled thermo-fluid-dynamics models investigates the correlation between responsive solar-shading devices and the DSF thermal conditions in the hot arid climate of Cairo, Egypt as their context of operation. Validation of the simulation method is carried in Chapter Five. The simulations results are compared with data of a similar solar-shaded DSF experimental case from literature; Mei et al. (2007). The recommended CFD modelling setup from chapter five is applied in Chapter Six. A simplified simulation strategy is developed to reduce computational time and cost. A discrete approach subdivides the simulation period into several simulation runs with shorter periods. An origami folded prototype is selected as a demonstrator for environmental analysis from the experimental '*Practice-led*' approach to bring both experimental and environmental aspects together. Thus, flat and folded solar-shading devices are installed in the DSF air cavity and compare it with the non-shaded base case. Three aperture sizes are modelled to represent the responsive solar-shadings different states. The cases are tested as point in time simulations on a peak summer and winter days, 15<sup>th</sup> of July and 15<sup>th</sup> of January at 9:00, 12:00 pm and 3:00 pm respectively. Measurements of surface and air temperatures, airflow and heat flux, are collected to environmentally assess the proposed responsive solar shading devices performance within their potential context of operation. The environmental feedback is used as a guide to customise the material and design the responsive system; form and aperture size.

The Open-ended Design approach is adopted in Chapter Seven to open up possibilities by leaving spaces of freedom for designers to re-appropriate the responsive system's design by changing their context of operation and design approach

## Chapter 4 . COMPONENT DESIGN AND PROTOTYPING

### Experimentation in Responsive Solar-shading (Learning through making)

#### 4.1. Introduction

This chapter adopts a Practice-led approach through hands-on experimentation and material tinkering to explore the potential of smart materials (SMM) in order to understand their immanent dynamic activity and use bio-inspiration and folding principles studied in *Chapter Two* to alter complex deployable forms using simple actuation strategies. The '*Component Design and Prototyping*' chapter provides explorations for design possibilities of bio-inspired and origami-inspired deployable systems that can generate open-ended design outcomes with a wide range of transformation. The design process goes through four stages; form generation, materiality, actuation and panelization. This knowledge is further tested with MArch students during the fall of 2018/2019 to test the design process and generate different design possibilities. Each of the case studies features a combination of form and actuation method, which is particularly promising for further upscaling and full system design. By doing so, an actual prototype system will be selected for further environmental experimentation in *Chapter Six* and an integrative 'Design Framework' will be developed by the end of the thesis in *Chapter Seven* as a reflection on the researcher's and students' design process that can be further applied in educational courses and workshops.

The explorations for the design possibilities in the '*Component design and prototyping*' chapter is carried on two sets by the researcher and a third set by the students.

- Exploring deployable components made of flexible, lightweight passive materials (fabrics, paper, card, and polypropylene) to test folding forms (straight and curved) and tinkering with SMAs to understand the intuition of smart materials and how they operate.
- In-depth analyses of four experimented and actuated models carried by the researcher to explore a design space rather than finding an optimal solution.
- Teaching experiences with MArch students to analyse how other designers may produce with movable forms by following a design workflow

Information about bio-inspiration and folding principles, as well as smart materials properties, is transferred to MArch students during the fall of 2018/2019 to gain lessons learnt

from hands-on application and explore best working strategies. As a reflection on the researcher's and students' process of design, the forms and aperture sizes are discussed as an important parameter for the responsive system efficiency to be tested environmentally in Chapter Six. This chapter identifies combined structures and materials that support dynamic forms suitable for responsive solar shadings with minimal material and energy consumption. On the whole, the chapter concludes efficient deployable structures, smart material fixation strategies and system reversibility methods for solar shading systems application.

From the reviewed literature in Chapter two about soft robotics and responsive solar shading systems, some core areas are found important for the workability of the system. These areas are form, materiality, materiability, actuation, system reversibility and panelization. The next sections will discuss these areas sequentially.

#### **4.2. Forms**

Recently, the experimentation with soft matter and textile-like materials has exposed the need to develop our methods and practices (Oxman, 2010; Ritter, 2007). The concept of *soft robotics* or what Kretzer (2017b) called *new softness* incorporate flexible and soft materials which allow the body to bend, twist, and deform. These types of movement using material deformations are difficult for traditional hard robots with rigid bodies. For example, various textile materials realized with smart materials have been used in functional clothing. Grado Zero Espace has used SMAs to obtain a fabric used for the manufacturing of a shirt, called Oricolco, with long sleeves that roll up on hot days (Ritter, 2007). Similarly, special qualities of soft robotics integrated with lightweight materials can be used for architectural applications such as solar shadings. Soft materials are the key enablers for creating soft robot bodies (Rus & Tolley, 2015). It is similar to natural organisms which are often composed of soft materials like skin or muscle tissue. Rus and Tolley (2015) defined soft robots as systems that are capable of autonomous behaviour, and that are primarily composed of materials with moduli in the same range of soft biological materials. Compliant materials can also lead to improved mobility over soft substrates (Rus & Tolley, 2015). The experimentation explores self-deployable or self-folding structures that integrate lightweight materials which can bend or fold with SMA actuators. The behaviour of folded surfaces largely depends on the properties of the material in which folding is done, particularly its thickness and flexibility.

Thickness is an issue for compound folds in particular; when folding multiple layers of material at once, hence sometimes stretchable materials are used for the crease joints to ease

the movement. When looking for an appropriate material for elastic kinetic structures, it is particularly useful to consider the ratio of a material's strength to its Young's modulus. Table 4-1 categorizes some potential materials based on their strength-to-modulus ratio. In general, materials with a greater ratio can withstand significantly bigger deflections and achieve smaller bending radii before plastic deformation and failure than materials with a lower ratio. The group of plastics and polymers has the highest values which makes them well suited for compliant mechanisms and elastic kinetic structures. Experimentation takes into account the material properties; elasticity, stiffness and strength. Different lightweight materials are tested; fabrics (woven and non-woven), paper, card and polypropylene sheets.

*Table 4-1: Categorization of polypropylene, felt and plywood based on their strength-to-modulus ratio (Julian Lienhard, 2014)*

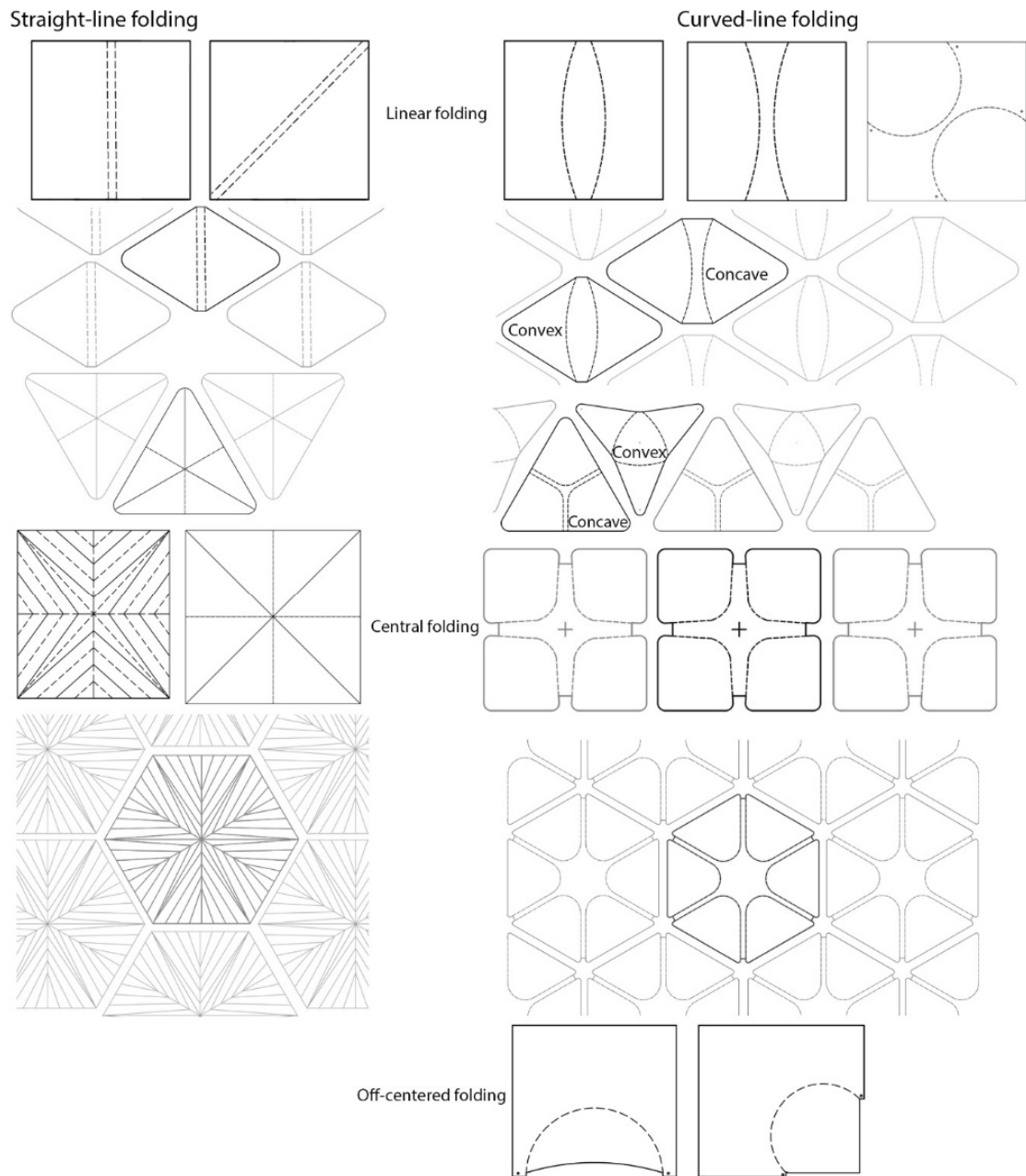
	Flexural Young's Modulus [GPa]	Flexural strength [MPa]	Strength-to modulus
Polypropylene	1.5	55	36.7
Felt	5.63	109.6	19.5
Plywood	11	51	4.6

Paper is the primary folded medium and most related material to origami models which is defined as the art of paper folding. Yet real-life applications require materials that can provide the necessary strength and stiffness to achieve the desired functionality (Lauff et al., 2014). The card is formed in the same way as paper but is thicker and denser, giving it higher strength and structural properties. It can be safely laser-cut, marked, and engraved. Both paper and card can fold well and retain their shape. Paper is used only as a primary folded medium and most related material to origami models. Card is used in the exploration as a stronger material than paper, however it is not durable for application in practice.

Polypropylene sheets with a thickness of 0.8mm are used. It has adequate material properties to work as elastic kinetic structures. It can be safely laser-cut, marked, and engraved. It is a lightweight, flexible material with good resistance to fatigue (A. Vergauwen et al., 2014). The material can be creased using a cold or hot creasing technique. The resulting 'hinges' can be folded many times without the material breaking, which makes it possible to create living hinges. As a polymer, polypropylene embodies the potential for exploring lightweight bending-active structures. Its elasticity can be used for compliant mechanisms inspired by plants. The material has high elasticity and could work as return mechanism. Polypropylene sheets which were used in the initial prototyping is intended to be used in practice.

Different fabrics, woven and non-woven, are tested. Non-woven fabrics are long fibers which are strongly bonded autogenously and/or adhesively using some sort of heat, chemical, or mechanical treatment (Pourmohammadi, 2013). Non-woven fabrics, such as felt, are tested for its durability and resistant to wear and tear. It is an outstanding insulator for both sound and temperature. As a non-woven fabric, it holds its edges and does not unravel when laser-cut. These advantages, along with its natural beauty and versatility, make felt represents good potential for such solar shading systems. Additionally, lighter woven fabrics like linen and denim are tested for exploring soft material deformation such as stretching, bending, twisting and rolling movements.

Paper, card, plastic and felt are materials that can sustain bending without stretching or tearing. Both elastic and stiff materials can be precisely shaped into deployable foldable units that can be reconfigured by a linear actuator. Preliminary ideas were tested using paper models and passive materials which are manually actuated then integrated with SMM actuators. SMMs are embedded within different passive lightweight materials to activate it. The hands-on experimentation intends to explore, understand and analyse the movement that can be achieved by folding and/or bending different lightweight passive materials and how to make such structures move. It is an open exploratory stage where the researcher plays around with deployable forms and materials to explore the resulting motion with time in space. Preliminary samples with dimensions of 10 cm x 10 cm were chosen for testing, as they are handy and easily manipulated and controlled. Later, it can be doubled or up-scaled. These samples are integrated with SMM which are embedded, hinged or bi-layered in different patterns. Some origami patterns are applied, as shown in Figure 4-1.



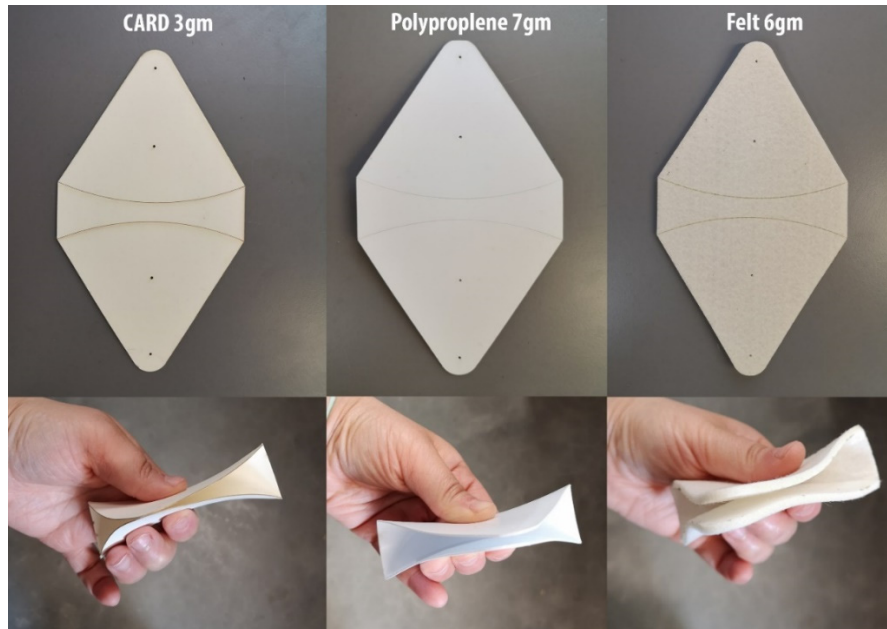
*Figure 4-1: Straight and curved crease folding patterns.*

Many explorations are applied to create surfaces that expand and contract. This experimentation explored straight and curved creases origami for their potential in the field of kinetics with a focus on curve crease explorations for their inherited return mechanism characteristics that they present to help shape-memory performance.

The concepts of straight and curved folding are applied in this research using individual units with different light-weight materials. Hands-on experimentation of such folding principles are tested for different materials to explore the resulting deformation movement and its workability and aesthetical qualities as shown in Figure 4-2. The deployability of such units depends on both the form and materiality which needs to be explored together.

#### 4.3. Materiality: Passive Light-Weight Materials

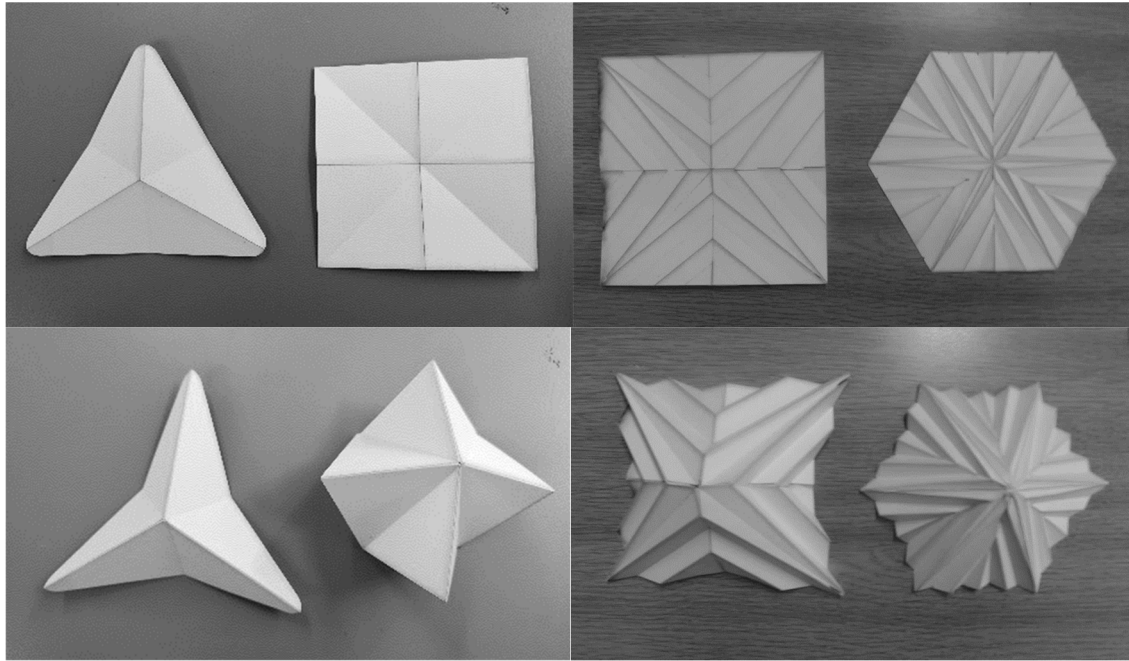
Straight and curved foldings are applied to the card (280 gsm/grams per square meter), polypropylene (0.8 mm), and felt (3 mm). A crease pattern is implemented to illustrate the curved folds. Mountain and valley folded lines were laser cut, each on the side of the material.



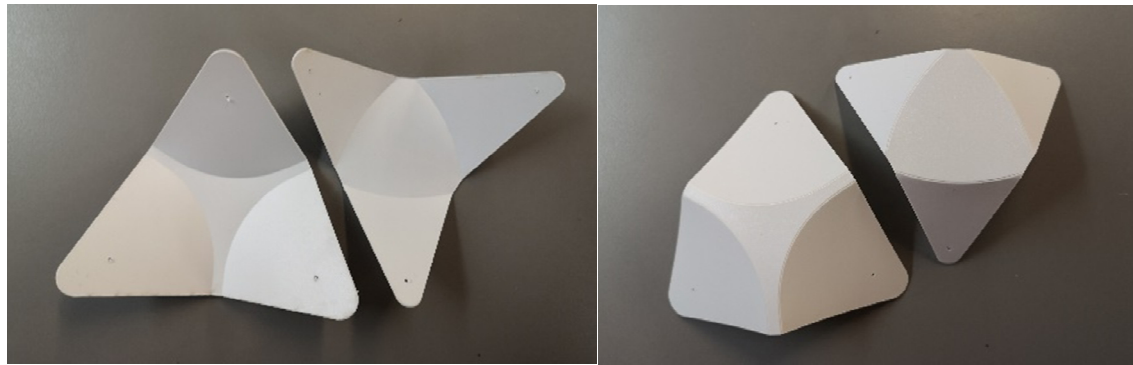
*Figure 4-2: Hands-on experimentation of curved folding for card, polypropylene and felt (author investigation).*

The card is found to have the best behaviour in straight folds for its rigidity. Various shape 'hands-on' experimentation led to an understanding of how to improve rigidity by adding folds. It is also found that adding extra folds helps the module to achieve more contractions, as shown in Figure 4-3. Additionally, the card performs well with curved crease folding. However, it is less flexible than polypropylene and may tear under high bending. Interestingly, polypropylene behaves best with curved folding for its smooth motion, fine laser-cut creases and the elasticity that helps the system reversibility, as shown in Figure 4-4. The felt didn't perform effectively in straight crease folding due to its flexibility. It barely managed to fold and bend with simple curved crease fold. It performs best in hingeless soft deformation.



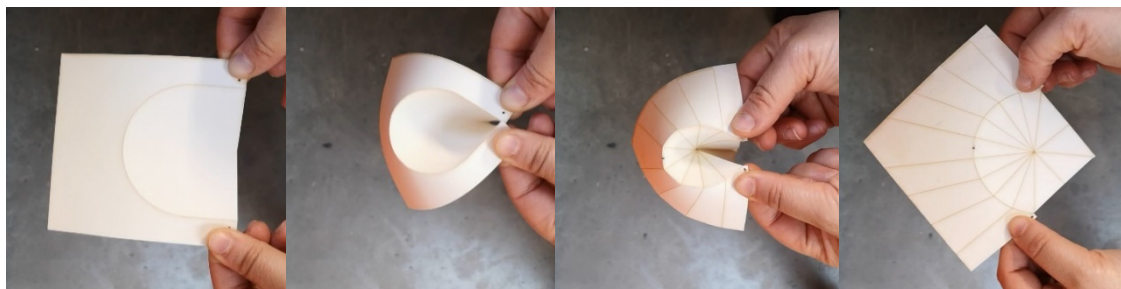


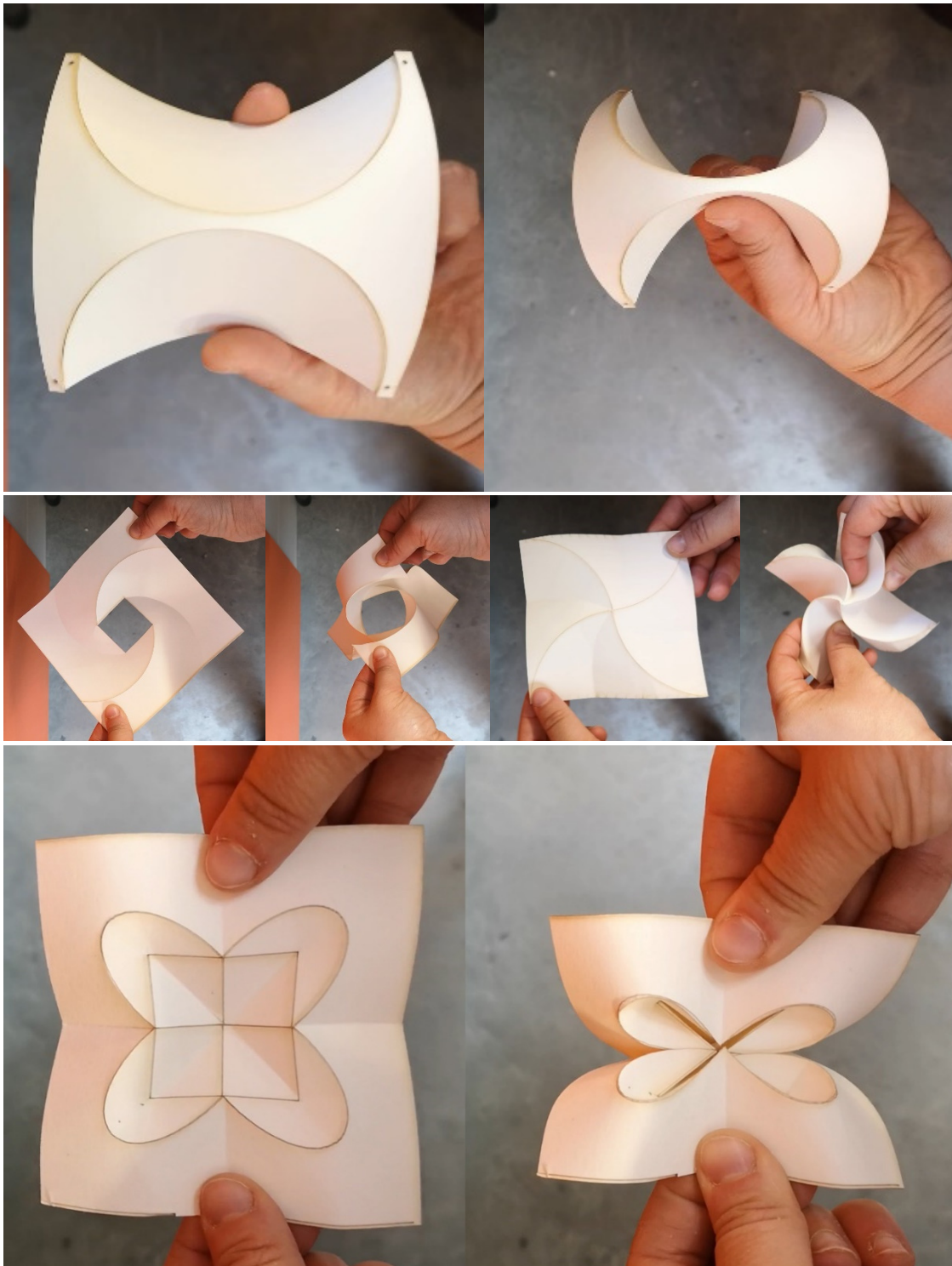
*Figure 4-3: Explorations of the straight folding (author investigation).*



*Figure 4-4: Explorations of the Curved-line folding (author investigation).*

The manual folding of curved creases models shows a range of design possibilities for kinetic architecture applications, as shown in Figure 4-5. Based on A. Vergauwen et al. (2014), the curved-line folding can offer double-curved interesting self-shaded solar-shading modules by combining folding and bending motion. The resulting bending-active kinetic structures have inherited reverse mechanism property, especially when an elastic material, polypropylene is used. It was found that models of one or two curves are easier to be moved and thus actuated.





*Figure 4-5: Hands-on explorations of the Curved folding with card (author investigation).*

Based on Plant-inspired principles tested in Chapter Two, Page 56, 'curved-line folding' result in 'Bending-active structures' and 'pliable structures', which generate their geometrical form and their system rigidity by elastically deforming their members and have high potential to achieve reversible movements. Thus, 'Hands-on' exploration focuses on curved-line folding applied on lightweight materials to achieve self-deployable structures which can bend and fold. Although these structures start with basic planar geometry, the behaviour is complex to

understand or predict unless manually experimented. Even it is a hard task to model their actual movement digitally model. Thus the hands-on exploration is significant. Figure 4-5 shows the experimentation with one, two, and four curved creases on a planar surface where each pattern generates a different three-dimensional form. It was found that single curved crease results in two points of actuation which make these models easier to actuate. Models of one or two curves are easily moved and actuated compared to three and four crease models. Models with more than two creases require more actuation points and force, to fold all the surfaces that need elastic deformations and the system loses its bending-active properties. Additionally, high curvature crease patterns require small displacements, which might need shorter linear elements.

To explore movements through *material deformations*; such as stretching, bending, twisting and rolling movements, some fabrics are tested. Fabrics, such as denim, and linen, are woven soft fabrics that can't hold shapes or creases, as shown in Figure 4-6. In this case, the SMA wires are embedded in the textile structures following some patterns to facilitate mobility resulting in a swelling, curling motion, as shown in the next section. The thick felt has different behaviour as a non-woven fabric. Felt is used for bending motion and soft deformation. It has a high potential for architectural applications.

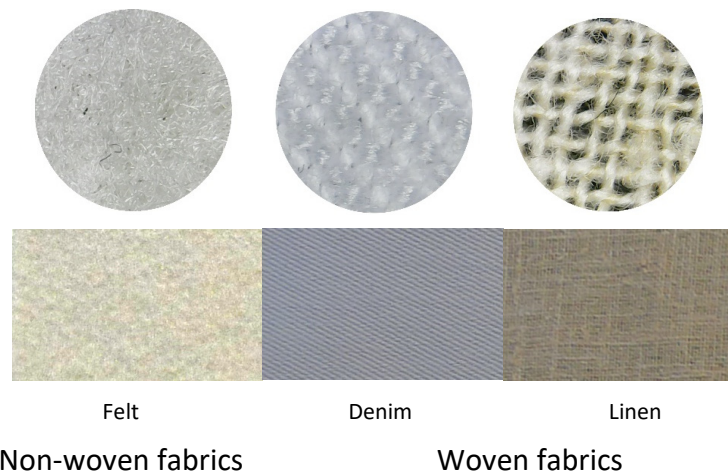


Figure 4-6: Three fabric types used in experimentation & illustrated in details (author investigation).

More details of coupling folding principles with SMM will be investigated in the following sections. The following part moves on to describe the material properties of SMAs and how they can be customized. The specific objective of this section is to determine whether the soft mechanics' approach that uses smart materials and folding principles can acquire a high range of motion and replace the traditional mechanical systems. It aims to achieve a high range of deformation and complex forms using simple geometries and actuation methods.

#### **4.4. Materiability: Active/Smart Material**

Due to the novelty of smart materials, there is a lack of applied knowledge in the architectural field (Hovestadt & Kretzer, 2014; Kretzer, 2017a). Designers and researchers struggle to fully anticipate and predict the immanent dynamic activity of smart materials which are fundamentally different from traditional materials. To bridge this knowledge gap, the '*hands-on*' experimentation aims to understand material behaviour by defining their active and variable properties. This knowledge help designers to avoid ignoring or simplifying their abilities to make them fit into existing design palettes. SMMs possess the characteristics to work as actuators, either separated or integrated into shading components. Their memory shape effect (SME) and speed of actuation, enable them to produce ranges of movement and responsiveness suitable for kinetic solar shading applications. Generally, actuators must be low profile, simple to attach, and easy to create in quantities of tens or hundreds (Hawkes et al., 2010). SMA based actuators are outstanding in terms of high power/weight ratio over other types of actuators (Sun et al., 2012). They are typically energy-dense, geometrically simple (Edwin et al., 2014; Frecker, 2003) and silent (Ritter, 2007).

The research excludes materials as the Dielectric Electro Active Polymers (DEAP) that need electronic control to work and have durability and scalability problems (Kretzer, 2017a); and shape memory hybrids (SMH), that can be affected by external weather conditions. The shape memory polymers (SMP) have good potential, but they have durability issues as reported by Pesenti, Masera, Fiorito, et al. (2015) and limited SME. On the other hand, the research used Shape memory alloys (SMAs) which have great potential to act as a servo-actuators to design low-tech responsive skins. SMAs can be attached at one or both ends, manually or mechanically weaved and repeatedly installed.

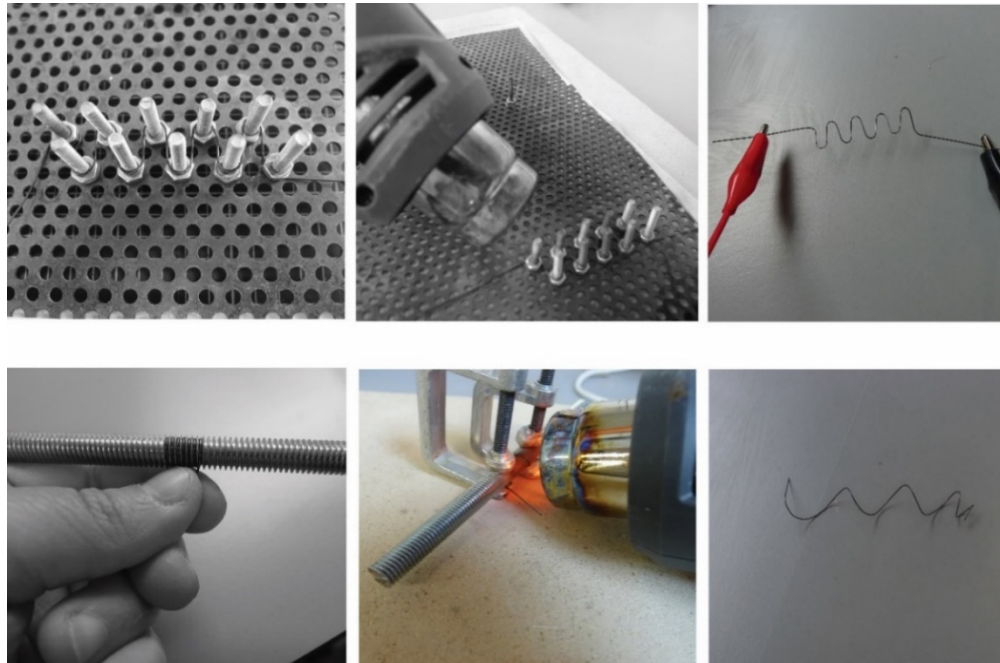
##### *4.4.1. The SMM training*

Thermo-responsive SMAs can exist in two different phases. It recovers its original shape after being deformed when heated above the activation temperature. To function properly, SMAs must be "trained", "annealed" or "programmed" to have a preferred shape under certain conditions to be able to act as an actuator (Sun et al., 2012; Tadayyon et al., 2016; Zanaboni, 2008). The material tinkering is used in the training process of SMAs, which aims to control their geometric and mechanical properties. The training procedure of SMAs can be reconstructed following annotated step-by-step instructions as recommended by (W. Huang & Toh, 2000; Sun et al., 2012). Thus, experiments are carried on SMA wires (Nitinol)



with various diameters (0.15, 0.375, 0.5 and 1.0 mm) and activation temperatures (from 30°C to 70°C) supplied by Smart wires.

In order to train the nitinol wire, it is necessary to fix it in the desired shape and condition it to high temperatures. Three fixation methods are tested: (1) using a metal perforated aluminium Jig where the wire is fixed around screws as shown in Figure 4-7; (2) using a screw where the wire is trained as a helical spring as shown in Figure 4-7; and (3) using a CNC carved mould of casted plaster and fixed with clamps as shown in Figure 4-8. The third fixation method has the benefit of getting smooth curves and wires without kinks. The heat treatment process, normally required to memorize a certain shape, is carried out using a heat gun. The experiments which are carried out to train the SMA wires took into consideration the temperature and duration of the heat required for annealing indicated by the supplier. To test the pre-trained material shape, it was immersed in boiling water to measure its initially remembered high-temperature shape. Nitinol samples should be annealed at temperatures of approximately 500 °C from 10 to 25 minutes and followed by cold water quenching upon retrieval. Time taken to anneal in this study depended on the wire diameter. For example, the 0.5mm wire may take time up to 20 minutes. The trained form was then tested by immersing it into boiling water, by heat gun or by direct Joule heating by passing an electrical current through it.

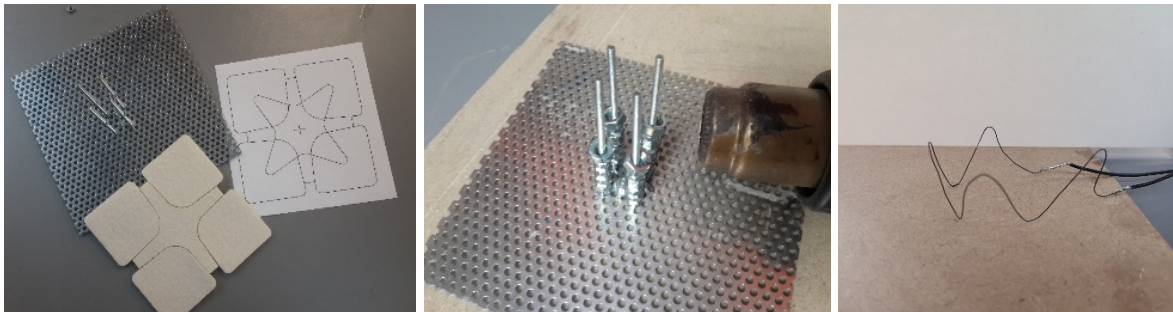


*Figure 4-7: The wire is fixed on a metal perforated Jig and around screws. It is trained by a heat gun (author investigation).*



*Figure 4-8: The wire is fixed in the negative mould of casted plaster and fixed with clamps (author investigation).*

Also, 3D wire training is experimented to generate 3D forms from planar surfaces upon attachment and activation. The wire was fixed around four screws with four high points and four lower points. It was trained using a heat gun, and then the shape is tested by electric current as shown in Figure 4-9.



*Figure 4-9: The wire is fixed in 3D shape (author investigation).*

SMA actuators can be trained in a one-way or two-way in the desired form to be integrated within lightweight materials to form deployable self-folding structures. The zigzag wires which are called flat springs and helical springs are found to be the most effective trained form as they gave the longest travel distance in a linear direction. This simple linear actuators can be integrated with different planar folded surfaces and fixed at specific points to give more complex 3D forms.

#### 4.5. Actuation: Fixations of Active and Passive Materials

The actuation phase focuses on how smart materials operate the solar-shading structure. Methods of attachment of how the active and passive parts are fixed together or printed on top of each other can result in various outputs, allowing the emphasis of very different aspects of the composition. Different fixation patterns are investigated as part of the materials' *hands-on* experimentation. Knitting, weaving and suspension techniques are used for SMA wires and springs; (trained and with pre-trained manufacturer setting) and bilayering technique for SMP.



*Figure 4-10: Materials tested SMA wires and springs and SMP (author investigation).*

The first experimentation set starts by embedding pre-trained nitinol wires, with the pre-trained manufacturer setting, into different fabrics to understand the SMA behaviour. At the primary stage, material deformation is explored using two fixation patterns, knitting and weaving, as shown in Figure 4-11. The electric current is used at this point of the experiment to activate the wires. In the beginning, the SMA wire is weaved through the pores of linen fabric, as shown in Figure 4-12. The weaved technique slightly swells the knitted fabric but failed to show a significant motion changes as the wire is slightly fixed to the fabric and the pre-trained motion of the wire is not fully transferred to the material as shown in Figure 4-12. Then, the knitting technique was implemented to give the wires extra fixation and attachment with the fabric. SMA with 0.5mm diameter was knitted in the centre of two ribbons made of linen and felt materials with 30 cm long, as shown in Figure 4-13. Felt showed a regulated bending motion along the length of the strip compared to the linen, which was so soft to hold a form and crumpled up. Although the knitting procedure resulted in recognized motion, it added a degree of insulation and partially restricted the wire's movement.





Figure 4-11: Three joining techniques were tested, (a) weaving with fabric material (b) knitting the wire with the material, and (c) fixing the wire at the ends (author investigation).

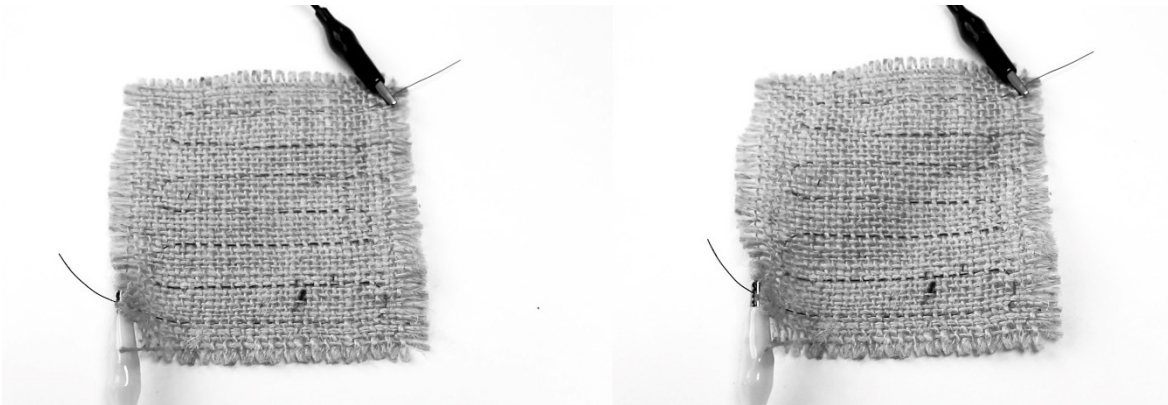


Figure 4-12: The weaving technique between 0.5 SMA wires & linen material activated by electric current (author investigation).

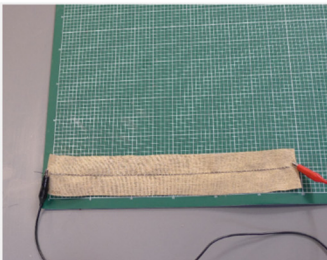
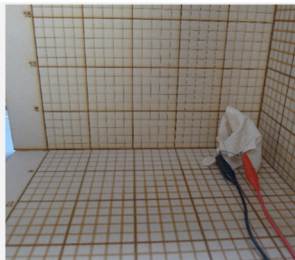
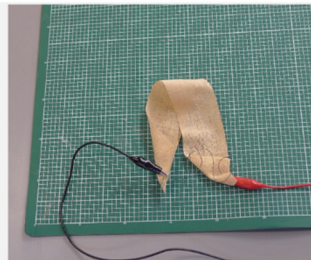
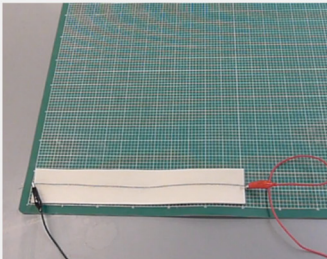
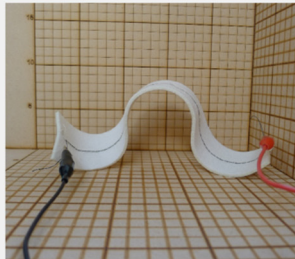
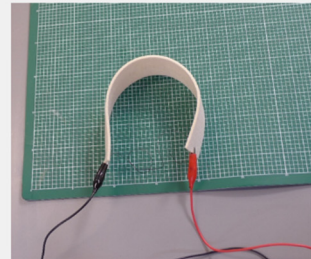
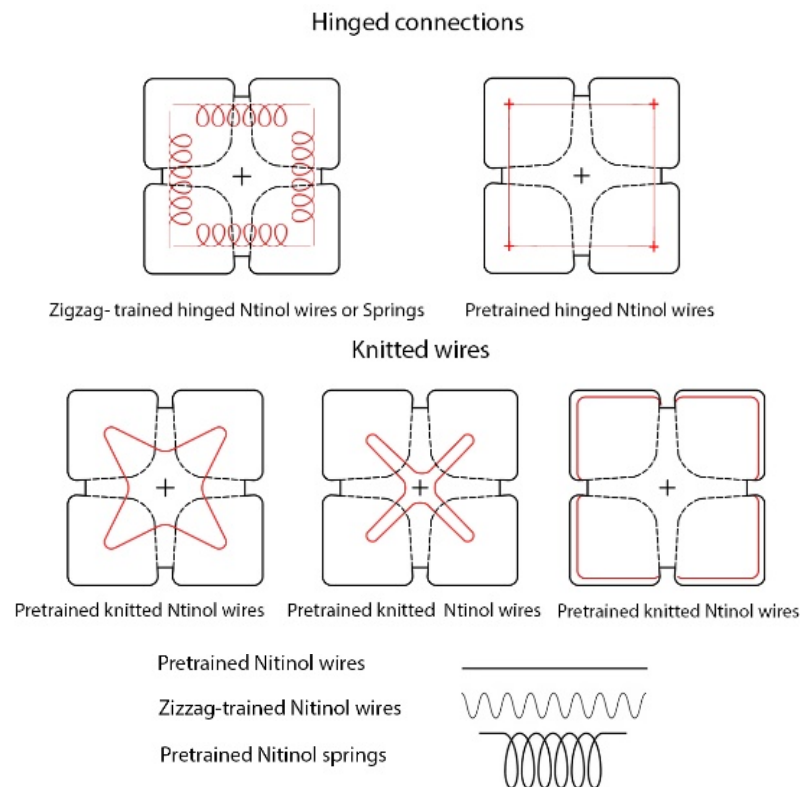
	Pretrained Nitinol stitched (0.5mm $\varnothing$ and 70° activation temp.)	Re-trained Nitinol stitched (spring shaped) (0.5mm $\varnothing$ and 70° activation temp.)	Re-trained Nitinol at ends (spring shaped) (0.5mm $\varnothing$ and 70° activation temp.)
Linen			
Felt (3mm thickness)			

Figure 4-13: The Knitting technique between wires & unit material activated by electric current; (a) Linen (b) Felt (3mm thick) (author investigation).

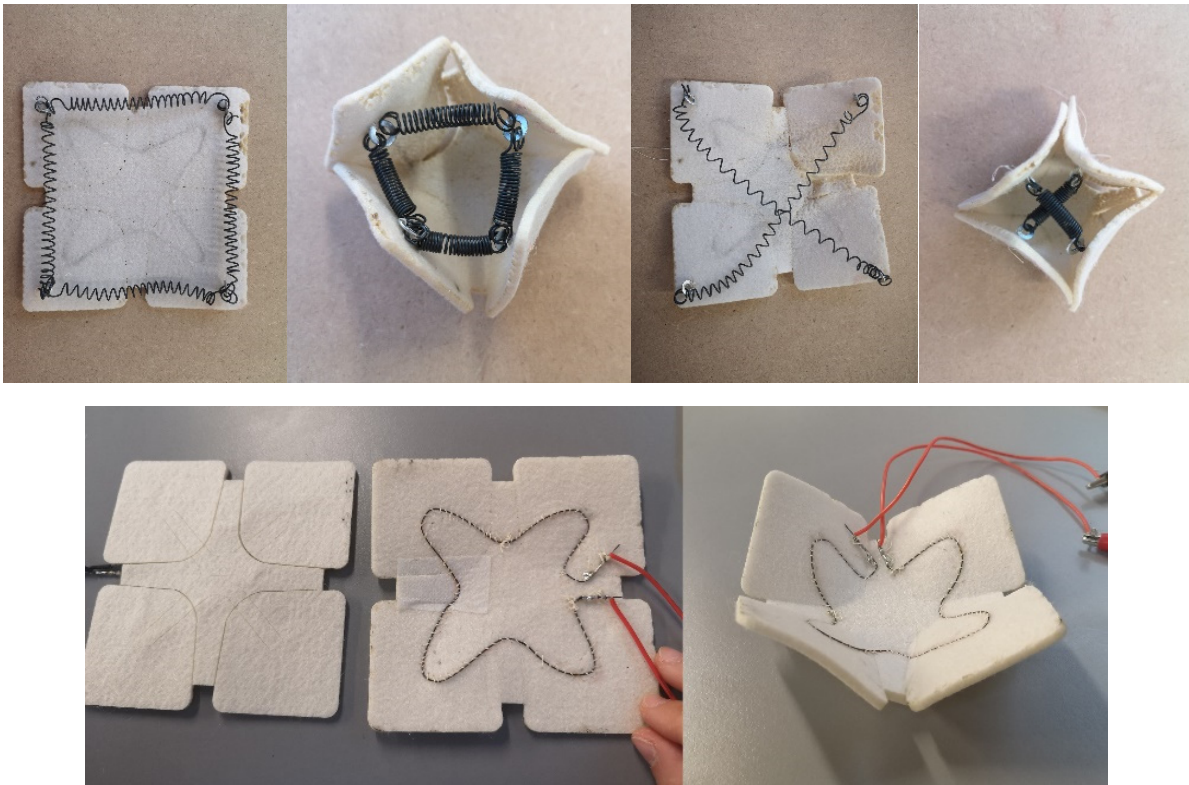


Hence, the wires are tested as suspended with the only fixation at the endpoints, which brings parts of the surface together. This technique is referred to as ‘extensional’ by Edwin et al. (2014). It works with thicker materials that can hold forms like thick felt, card and polypropylene. Additionally, origami-inspired forms can guide specific kind of motion that is simply actuated by linear SMA elements. SMA spring actuator that connects two faces is considered as hinge-type active folds that have variable length. The fixation of the actuator only at the unit’s ends, gives the wire the freedom to move and be highly exposed to the heat source. On the other hand, the wire knitting or stitching results only in a small range of deformation. This happens because of the strong attachment between the wire and unit material that absorb part of the temperature and stops the wire from achieving the required range of deformation. The freedom of the hinged or suspended actuators can better sense environmental conditions and trigger motion.

In agreement with some prototypes mentioned earlier in the literature, the hinged type actuators are more flexible to design motion. It is capable of moving a single shading unit or connect different units to work collectively as a system. A four curved crease model can be actuated by different fixations, as shown in Figure 4-14. A four curved crease model is actuated using knitted and hinged connections, as shown in Figure 4-15, and it was found that the crossing springs was the most significant transformation.



*Figure 4-14: Possible wires and springs fixations to actuate a four curved crease model.*



*Figure 4-15: Application of knitted and hinged connections to a four curved crease model (author investigation).*

Architectural applications may require longer travel distances (Ritter, 2007). Springs proved to achieve the longest travel distance. Zigzag trained wires or springs work better in this case with maximum deformation or contraction. The trained springs' range of motion depends on the pitch and the spring mandrel size (spring inner diameter). Springs with smaller pitch decreases the stiffness and increases the travel distance. This type of springs is defined as Helical-spring when the spring mandrel size equal and bigger than 4.75mm. Different spring types can be custom made or ordered from manufactures such as [kelloggsresearchlabs](http://kelloggsresearchlabs.com). The helical springs are able to make the largest travel distance. It can reach 15 cm at cool conditions and contracts to 2 cm at activation temperature (original length). The trained helical springs are able to achieve a contraction third their original length from 15 cm to 5 cm. The pre-trained manufactured helical springs was able to fully fold a two-flaps curved crease model compared to the trained spring, as shown in Figure 4-16. However, trained springs with small pitch dimension should be able to achieve more contraction close to the manufactured ones. Similarly, flat springs were able to achieve a contraction third their original length from 15 cm to 5 cm depending on the wavelength.

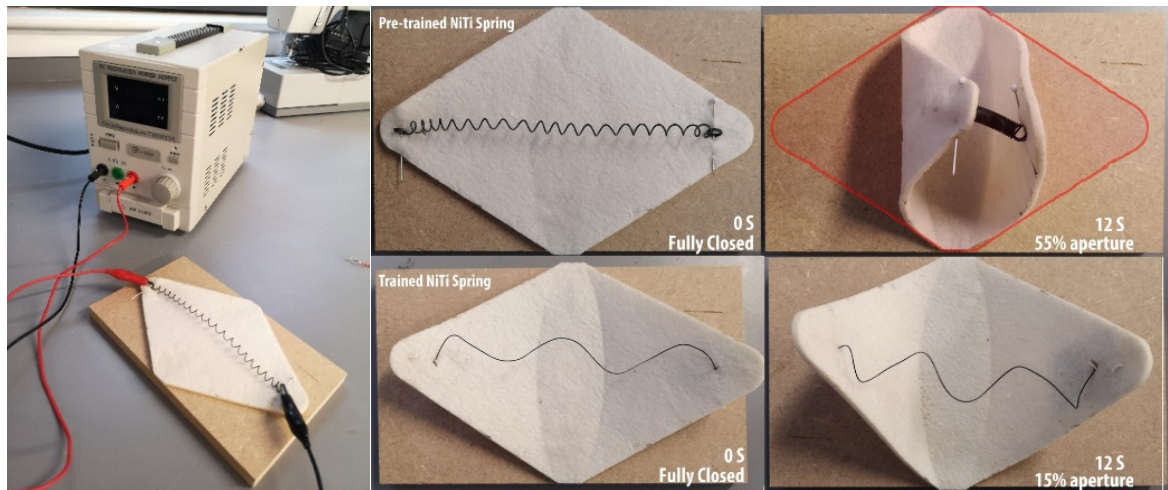


Figure 4-16: Folding the two-flaps curved crease model using a hinged spring SMA actuator, the pre-trained and the trained SMA spring (author investigation).

These fixation methods aimed to animate the models upon being activated electrically when joule heated or being exposed to heat sources to achieve forward motion; however, the return mechanism is as important to enable the structures to repeat these dynamic movement over and over again. The next section will discuss methods to achieve reverse motion.

#### 4.6. System Reversibility

Return mechanism is one of the major aspects that should be considered to design an efficient, robust system. Although most of the investigated forms and fixation techniques made the units move, it was a one-way motion. As shown in Figure 4-17, the study considers four main mechanisms as return mechanisms, as shown in Figure 4-17. The four return mechanisms are:

- (a) Gravity,
- (b) Coupling passive and active elements,
- (c) Elastic passive material,
- (d) Two-way training for SMM.

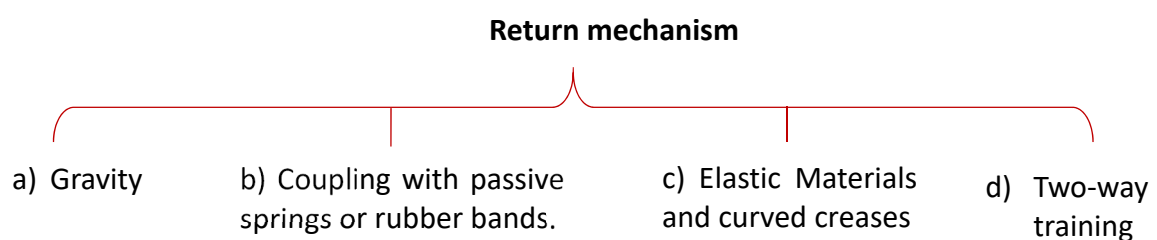
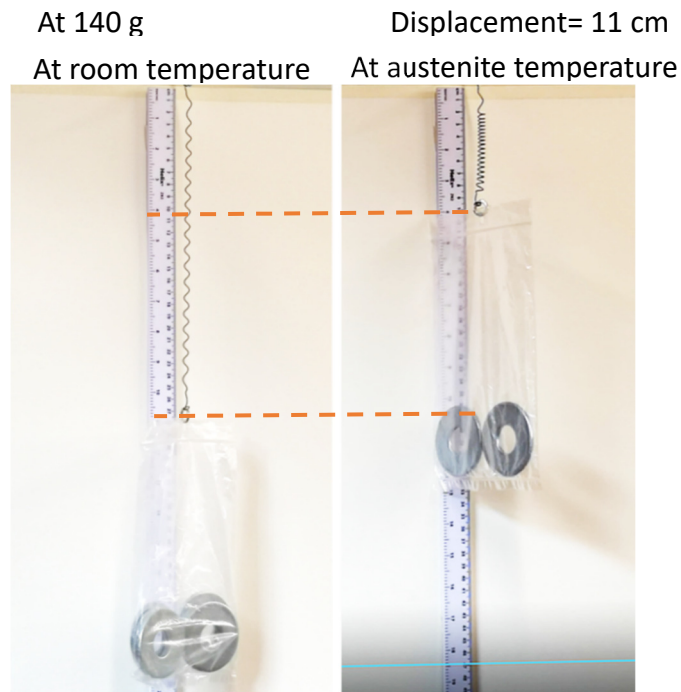


Figure 4-17: The tested return mechanisms

#### 4.6.1. Gravity

Gravity as a return mechanism is used to enable the form to fall back to its original position under the effect of its own weight or added weight. Gravity can be designed with high sensitivity considering a balance between the force of the wire or spring and the weight of the material in relation to time. Using gravity as a return mechanism, the system is activated by actuators that change form by heat and move the unit against gravity, when the temperature drops the unit reverts to its original position under its weight. Gravity has a significant impact on forces acting on structures, especially in the kinetic movement. Gravity can be used with little energy input to move planar horizontal shading devices compared to a system of counterweights or high energy level for the vertical position (Schaeffer & Vogt, 2010). Thus, this mechanism is simple and efficient in the horizontal position of panels or inclined position. The reversibility of the system depends on the balance between the force of the wire (the diameter of the wire and its specifications) in relation to the weight of the material. The self-weight of the shading units has great importance along with the direction of motion. The SMA spring is tested under different weights 140 gm, 280 gm and 420 gm, as shown in Figure 4-18. The used SMA spring is a one-way Nitinol SMA spring (0.5mm) with activation temperature 65 °C purchased from Fuxus Germany.

The spring actuated fast under the 140 gm (20sec) compared to the 420 gm (35sec). On the contrary, the reverse motion for the 420 gm (180 sec) is faster than the 140 gm (240sec). Thus, there is an observed correlation between the weight of the material and the time for actuation and reverse motion. The lighter weights result in fast actuation (20sec) and slow reverse motion (240sec) and vice versa. The stretched wire shrinks fast upon activation as it is tied to a light weight which slowly reverts the wire back to the stretched position. These findings show that the faster the actuation, the slower the return mechanism.



*Figure 4-18: Testing the SMA under 140 gm weight (author investigation).*

It was found that the spring was deformed after being stretched under the heavy weight of 420 gm and didn't fully revert to the original size (3cm) and only reverted to (8cm) instead in high temperature. Thus, the 240 gm can be considered the maximum weight a single spring can carry or actuate without deformation (240gm per spring). This capacity of nitinol spring to pull this force reversibly during its transformation makes it an ideal candidate as a kinetic joint.

#### *4.6.2. Elastic materials*

Elastic materials for shading units can be used as a return mechanism. This technique has been used by C. K. Khoo and F. D. Salim (2013), as shown in Figure 2-21, where the elastic nature of silicone rubber 'closes' the 'eye' apertures when the SMA spring not heated. Some plastics; such as polypropylene, are considered materials with high elasticity and could help in returning the unit to its initial form. As shown in Figure 4-19, the SMA spring clamped at the ends of 10cm polypropylene sheet shrunk from 10cm to 3cm upon heating from position (a) to (c). The polypropylene material stretched the spring back from 3cm to 8cm in 6 mins time from position (c) to (e). Although this return action doesn't bring the unit to the fully flat position but rather a slightly deformed unit, as shown in Figure 4-19, it presents an adequate material to act as living hinges. Further size and material tests can be carried to balance the force of the spring to achieve a flat position. The material as a return mechanism was found to be very efficient.



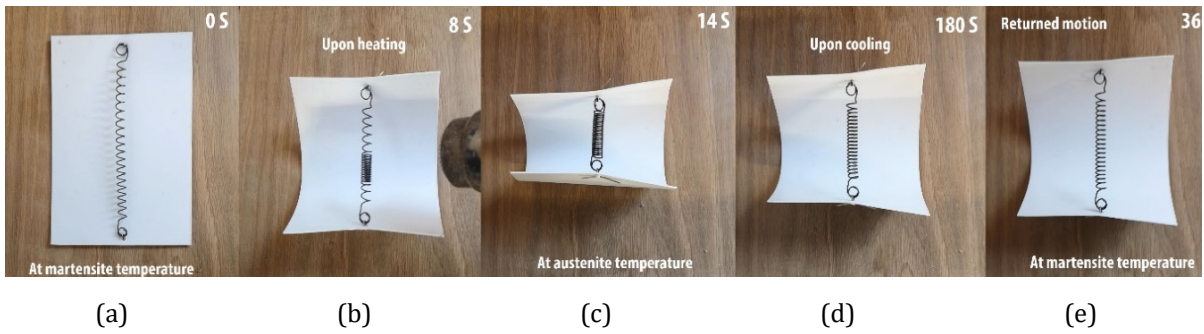


Figure 4-19: Elastic Materials (system of counterweight) as a return mechanism (author investigation).

Moreover, when a curved folding is applied over an elastic material, they work together to help the return mechanism characteristics.

#### 4.6.3. Coupling passive and active elements

One of the efficient return mechanisms used previously by researchers was coupling the active members with passive springs or rubber bands, as shown in Figure 4-20. The achieved displacement depends on the pulling force of each of the Nitinol (active) spring and zinc (passive) spring or rubber band. Upon actuation, the SMA spring contracts pulling the passive spring or rubber band. Upon cooling, the passive spring or rubber band draws the SMA spring back. The rubber band results in a fast initiation/activation time for the spring (15sec) compared to the zinc spring (35sec). On the contrary, the reverse motion for the zinc spring (180sec) is faster than the rubber band (240sec). Similar to the gravity conclusions, strong counter elements result in fast reverse and slow actuation and vice versa. The rubber band which is more elastic achieved a higher displacement of 8 cm, as shown in Figure 4-23, compared to 6.5 cm achieved by the zinc tension spring, as shown in Figure 4-22.



Figure 4-20: Nitinol SMA tension spring and zinc spring (author investigation).

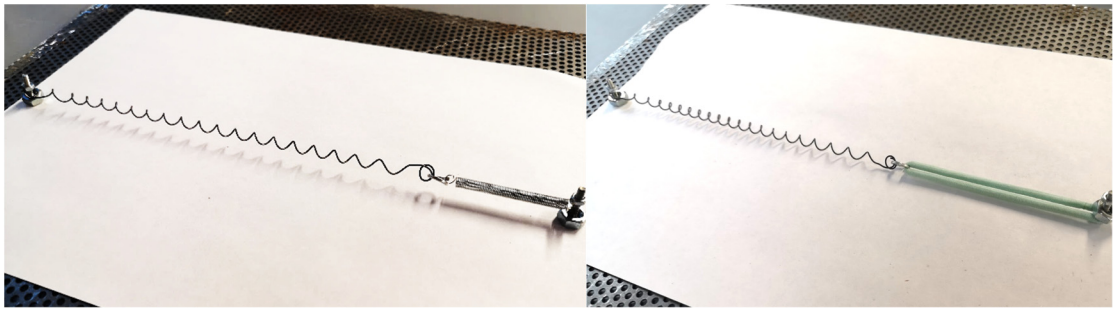


Figure 4-21: Using Counter-weights as a return mechanism by coupling the SMA springs with passive springs or rubber bands (author investigation).

- Time taken for actuation= 25 sec	- Return 0:30 mins= 30 sec
------------------------------------	----------------------------

At austenite temperature

Displacement= 6.5 cm

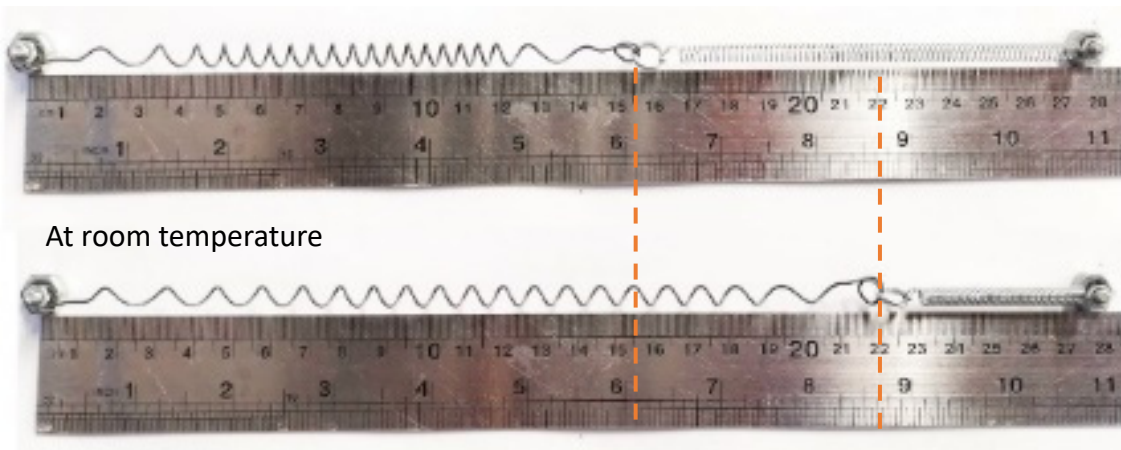


Figure 4-22: Using Zinc tension springs for a Counter-weight return mechanism with SMA springs (author investigation).

- Time taken for actuation= 15 sec	- Return 2:30 mins= 150 sec
------------------------------------	-----------------------------

At austenite temperature

Displacement= 8 cm

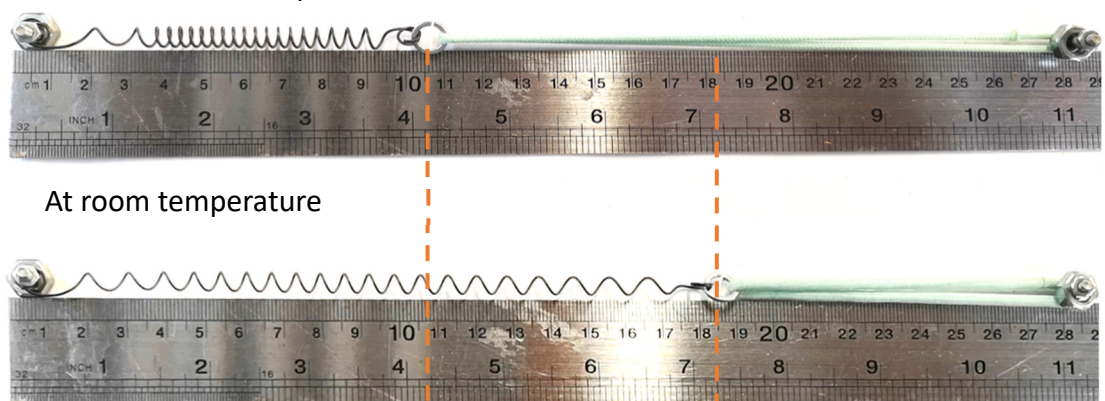


Figure 4-23: Using rubber bands for a Counter-weight return mechanism with SMA springs with passive springs (author investigation).

#### 4.6.4. Two-way training

Although SMAs are predominantly with one-way characteristics, some studies argued that they can be trained in a two-way to return to its original form in response to a thermal stimulus. Some manufacturer's customize springs to work as two-way springs which automatically resets itself when cooled, eliminating the need for a biasing force. It is argued by some manufacturers that the reduction in components offsets the higher cost of the two-way springs for many applications ("Kelloggs Research Labs," USA). The wire can be trained in a two-way motion as suggested by some researchers in the field where the wire remembers its shape at both high and low temperatures (W. Huang, 2002; W. Huang & Toh, 2000; W. M. Huang et al., 2002; Sun et al., 2012; Zanaboni, 2008). A two-way nitinol spring purchased from nexmetal was tested at martensite temperature (30°C) and austenite temperature (60°C). An original length of 1.5 cm was measured at room temperature which extends to be 4.5 cm at austenite temperature (60°C) as shown in Figure 4-23. It was quickly actuated in less than 4 sec and reverted in 70 sec when cooled down to below (30°C). Two-way springs are a standalone reversible action which is able to bring the structure back to its original position upon cooling. The similar concept can be applied by coupling two reversible active spring that works alternatively (Sun et al., 2012).

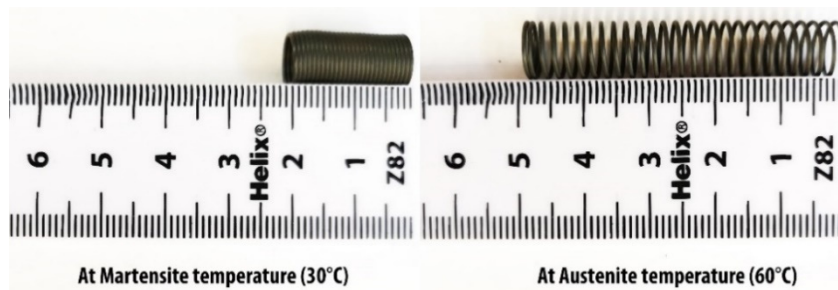


Figure 4-24: Two-way spring at martensite temperature (30°C) at austenite temperature (60°C) (author investigation).

So far, this section analysed the four potential return mechanisms where the material as a return mechanism seems simple and promising. However, the balance of forces in the kinetic system is the key to proper functionality. It has to be designed with high sensitivity considering a balance between the force of the wire and the weight of the material in relation to time.

#### 4.6.5. Time

The time factor is important and differs from one method to another. The system used to create the balance of the forces affects both times of initiation and reverse. When both forces



are equal, time taken for initiation and reverse are equal. All of the time taken by the four experimented reverse mechanisms is recorded in Table 4-2 using Nitinol spring with 0.5 mm diameter. All the experimented return mechanisms are considered successful. However, gravity is better for the horizontal position. Depending on material as a return mechanism is best for achieving individual unit movement, while coupling with passive springs or rubber bands is good for linked units. The coupled counterweight exhibits the fastest return mechanism actuation. Time in the return mechanism depends mainly on the weight, elasticity of the material or the force of the counterweight elements. So far, this section has focused on smart materials' properties and its training techniques for actuation as well as the proposed return mechanism.

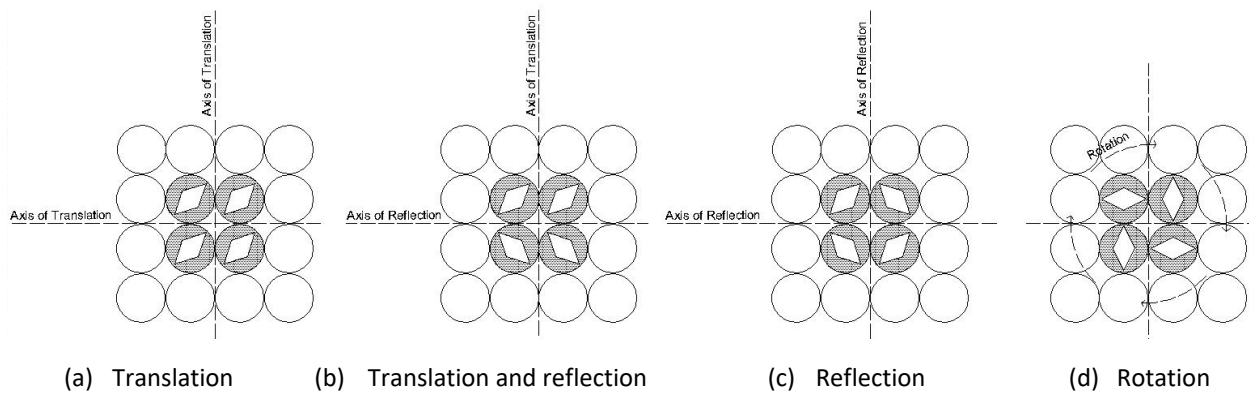
*Table 4-2: Comparison of reverse mechanism techniques*

Return mechanism	Gravity (different weights)			Coupled springs (different strength and length)		Coupled material & curved creases	Two-way SMA spring
	140 gm	280 gm	420 gm	Zinc spring	Rubber band	Polystyrene with single crease	
Time taken for initiation	20 sec	30 sec	35 sec	25 sec	15 sec	8 sec	4 sec
Time taken for reverse	240 sec	200 sec	180 sec	30 sec	150 sec	1320 sec	70 sec
Max displacement	11 cm	14 cm	15 cm	6.5 cm	8 cm	5 cm	3cm

Having discussed the potential of forms, lightweight materials, smart materials, actuation methods and return mechanisms, the next section move on from the design of the single component to clustering and grouping of units.

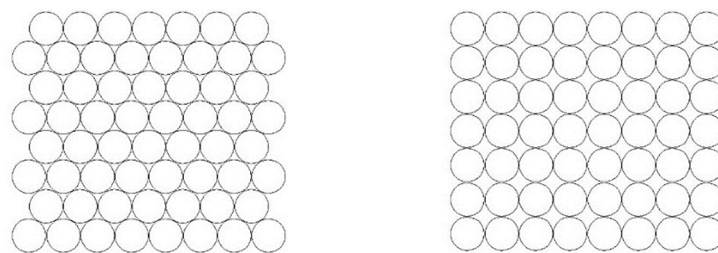
#### 4.7. Panelization and Grouping Arrangement

The single component can be attached to a panel in various ways, and multiple components can be repeated in different types of tessellations. Changing the references allows for three key manipulations: translation, reflection, and rotation in creating patterns (Schleicher, 2016). By applying these three key manipulations on the circular pattern, different patterns can be created, as shown in Figure 4-25.



*Figure 4-25: The application of the three key manipulations: translation, reflection, and rotation in pattern making.*

These models have the freedom to add solid fixed connections in-between the circular modules to achieve higher levels of opaqueness. Open connection areas will maximize the opening percentage and aperture size to more than 90% but also may not reach over 50% closure maximum. A staggered pattern can also be applied, as shown in Figure 4-26. Form, pattern and sequence of repetition can all alter many alternatives each with different range of aperture size.



*Figure 4-26: Staggered and straight circular patterns*

Methods of actuation and location of actuators highly affect the resulting pattern and its aesthetical qualities. In case of using gravity, elastic material or two-way SMA spring as a return mechanism, the unit is independent of any neighbours, and a wide range of arrangements can be applied taking the gravity as a force in consideration.

Other concepts of grouping depend on connecting smaller components to work together. The concept of pliability can have a major benefit for deployable systems based on elastic deformation. In pliable systems, the linkage between elements leads to the transfer of motion from one element to their neighbouring elements (Schleicher et al., 2011). Thus, it is used to build up a cascading deformation, that starts with a small and simple actuation in one part of the structure and then translate it into a large yet stable deflection of another (Schleicher et al., 2011). Every unit could wake another neighbour through active or passive material connections. The arrangement of components in clusters can generate major synergy effects (Schleicher, 2016). The clustering strategy facilitates the allocation of actuators or counter action members in-between the units to effectively drive an entire group.

Depending on the chosen mechanism, some patterns are more suitable than others. A possible explanation for this might be that some components require a specific orientation or position in order to function properly as sun protection. Another reason may be that only a specific arrangement ensures a high sun exposure for the actuators. So far, it becomes increasingly clear that the arrangement of the responsive units has a huge impact on their functionality and efficiency. It is highly related to both the location of actuators and the resulting aperture size.

Having discussed the potential of forms, materials, actuation methods and grouping strategies, the next section brings these ideas together through the design of prototypes by using an open-ended design approach to explore a design space rather than finding an optimal solution. The next section will discuss the experimental design compositions which have good potential for solar-shading to develop a framework design for future development in chapter seven.

#### **4.8. Palette of Models**

Coupling origami and bio-inspired principles with data collected from experimentation of materials behaviour and methods of actuation may alter a wide range of design possibilities. The aim of this section is to put all gained knowledge together to develop and test design compositions through different approaches which have good potential for solar shading application. Experimentation through direct and creative engagement with forms and materials is carried to produce responsive solar shading systems. The *'hands-on'* experimentations focus on the selection of type, form and location of actuator integrated with form and type of passive material that result in deployable solar shading with efficient

aperture range, reverse mechanism and time. It explores the design of motion and its aesthetical qualities. The explorations aim to alter 3D forms that might be complex, aesthetically pleasing but easily fabricated and deployed by linear actuation. In short, the main aim is producing a low-cost system working with minimum energy and smart material use. This phase of the research focuses on hands-on practices, demonstrating step-by-step procedures for transforming 2D surfaces into 3D forms.

In the previous section, Hands-on explorations were carried on the component level. It focused on how forms and materiality can work together to facilitate forward and backward motion for deployable structures. Previous explorations highlighted some insights for responsive systems, which are:

- a) the potentials of straight-line folding where extra folds can improve deployability, rigidity and contraction,
- b) the potentials of curved-line folding coupled with elastic materials,
- c) the potentials of SMA spring actuators for their large travel distances,
- d) the potentials of soft deformation using fabrics especially felt, and
- e) the potentials of materials as a return mechanism.

All these gained knowledge helped to explore the parameters of the responsive solar shading systems to develop some potential prototypes. In this section, in-depth analyses of four experimented and actuated models are provided by the researcher which includes exploration through physical and digital models and sketches. Each of the case studies features a combination of form and actuation method, which is particularly promising for further upscaling and full system design.

#### *4.8.1. Exploration One: Umbrella units*

A responsive system can act like little umbrellas that expand to afford solar shading for the glazed surfaces. They could be located either in a horizontal or a vertical position, as shown in the researcher's primitive sketches in Figure 4-27.

- Form

Each shading unit represents an umbrella; a folding canopy that opens and closes.

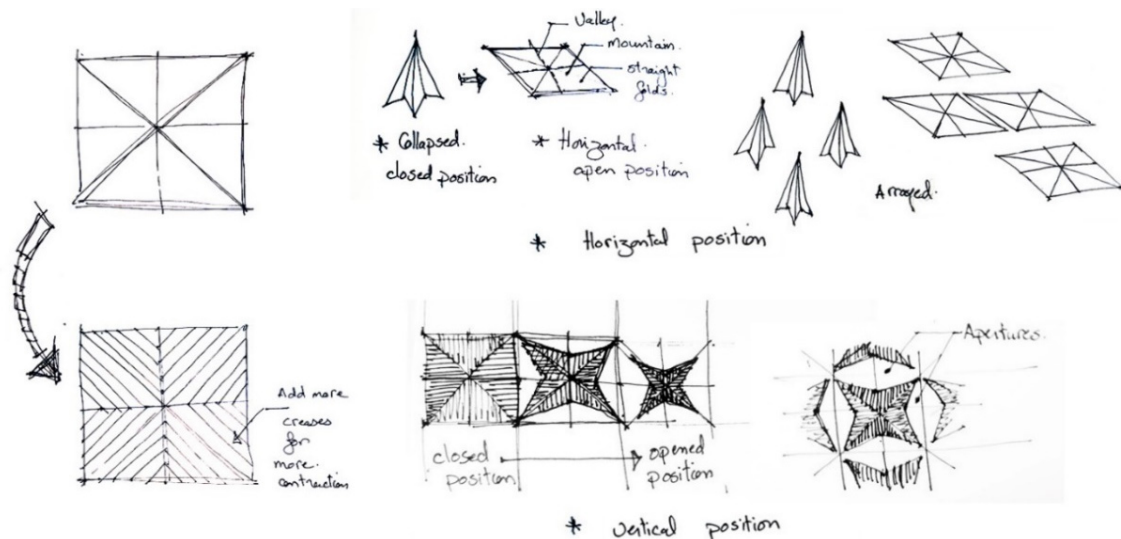


Figure 4-27: Primary researcher's sketches exploring Umbrella units horizontally and vertically (author investigation)

- Materiality

Soft Fabrics; Linen and denim, are embedded with Nitinol wire in a star-like shape with a knitted stitch to achieve the desired form; a horizontal sheet upon activation and a collapsed form below activation temperature. The behaviour of the soft materials is compared to folded card paper as a more rigid material to achieve a more regulated motion, as shown in the below section.

- Actuation

Early explorations started by knitting Nitinol wire in a star-like shape on a square piece of fabric; with the intension of opening upon actuation, as shown in Figure 4-28. This prototype expands to form a horizontal shade that acts as a louver and then collapses in a closed vertical position. The initial intention was to use gravity as a return mechanism. It was found that the Linen fabric ( $600 \text{ gm/m}^2$ ) was too light for the wire and lifted part of the fabric more than  $90^\circ$  as shown in Figure 4-29. An extra weight of 8gm was added at each of the four fabric corners to balance the wire's force, as shown in Figure 4-30. The same technique is used for a denim fabric of ( $1800 \text{ gm/m}^2$ ) which was found heavy for the 0.5mm diameter Nitinol wire and only lifted it around  $45^\circ$ . In all cases, the motion was unpredicted and unregulated or uniformly distributed. A possible explanation for this might be that the fixation of the electric current clamps and the added weight of soldered wires at the two ends of the Nitinol wire affected the load distribution as shown in Figure 4-29. The activation using electric current differs from the distributed heat of exposed solar radiation and positioning the surface horizontally prevent the direct sun exposure of the knitted wire. Also, as mentioned earlier, the knitting technique added a degree of insulation and restricted the movement of the wire.



Figure 4-28: knitting Nitinol wire in a star-like shape to square flexible fabrics; linen and denim (author investigation).

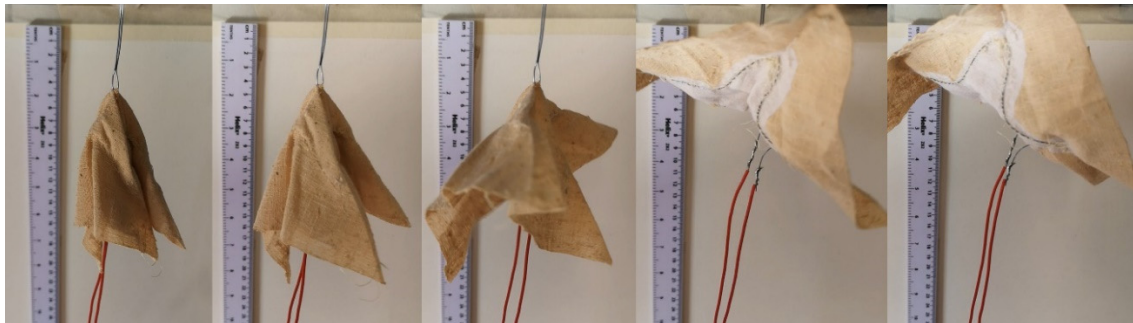


Figure 4-29: The linen fabric ( $600 \text{ gm/m}^2$ ) knitted with star-like Nitinol wire (author investigation).

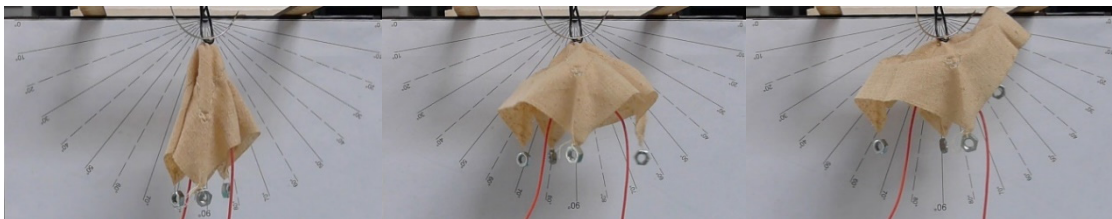


Figure 4-30: The linen fabric ( $600 \text{ gm/m}^2$ ) knitted with star-like Nitinol wire with extra added weight to balance the force (author investigation).

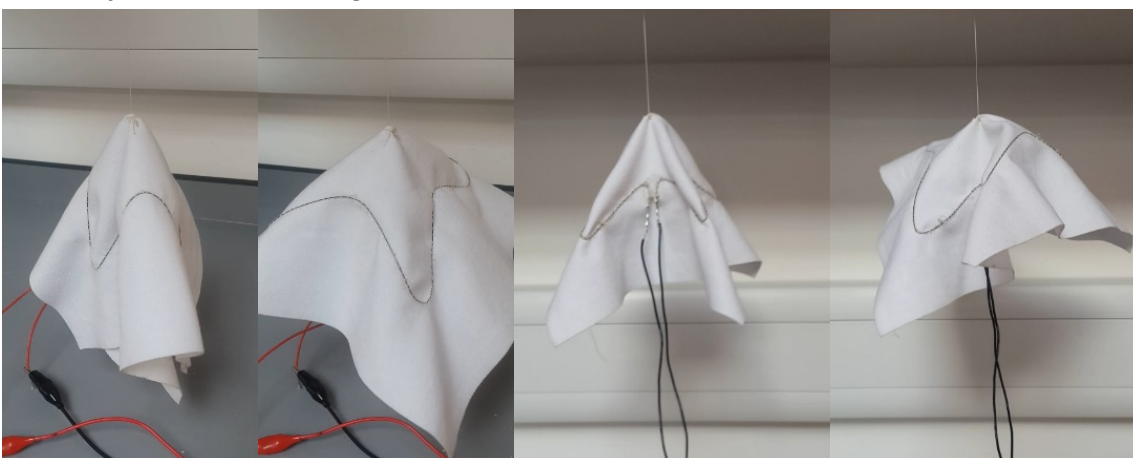
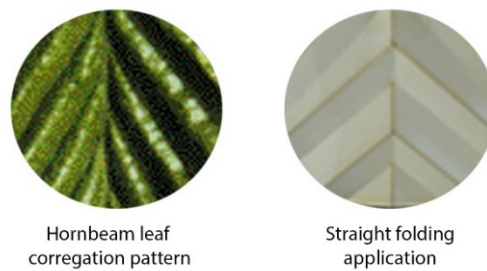


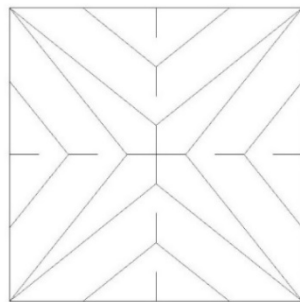
Figure 4-31: The denim fabric ( $1800 \text{ gm/m}^2$ ) knitted with star-like Nitinol wire (author investigation).



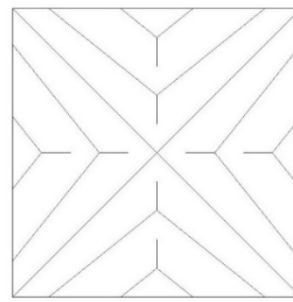
The resulting unmanageable motion of these fine fabrics needed to be controlled and regulated either through reinforced seam lines or by applying folds to thicker materials. Hence, straight-folding is adopted to regulate the motion using solid bodies. The straight folding was applied as a regular corrugation pattern inspired by the hornbeam leaves where its bud started as a Miura-ori folded pattern Figure 4-32. Similar straight folding concepts have been adopted by Sosolimited, Hypersonic, and Plebian Design in the Diffusion Choir, Pesenti, Masera, Fiorito, et al. (2015) and Arup in albahar towers. A star-like crease pattern is implemented to illustrate the folds. Mountain and valley folded lines were laser cut on both sides of card paper material, as shown in Figure 4-33. It has been realized that more creases result in a more compact structure.



*Figure 4-32: Bio-inspiration of using the regular corrugation pattern of the hornbeam leaves.*



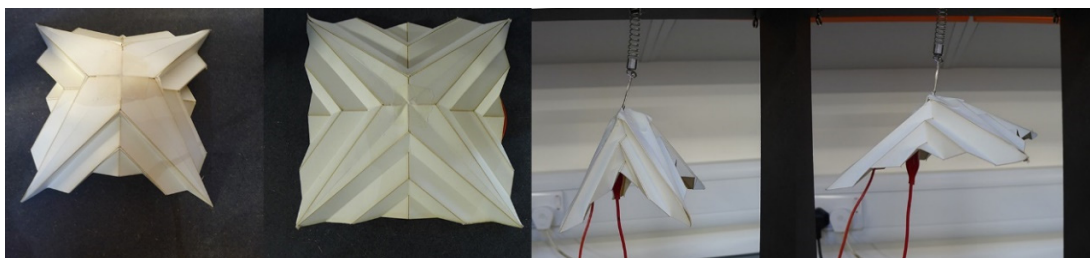
(a) mountain line laser cut on the front



(b) valley lines laser cut on the back

*Figure 4-33: Laser-cut square unit of 10cm x 10cm and applied Mountain and valley folded lines.*

The pre-trained Nitinol wire (0.5 mm) is fixed on the inner side of the surface. When the Nitinol wire is activated, it expands and triggers the folded surface to open. The resulting motion is more regulated and looks like little umbrella canopies.



*Figure 4-34: A star-like laser cut folded surface that acts like a little umbrella that expands to afford solar shading (author investigation).*

The horizontal position of umbrella canopies has the disadvantage of unexposed SMA that cannot be easily actuated by direct solar radiation but can be actuated electrically. Also, the actuator suffers from the high attachment with the passive material and part of the heat is absorbed by the material and thus limiting its motion power.

- Return mechanism

The return mechanism proposed for this system is the gravity which is simple and efficient; it gets back to its original collapsed or closed position under the weight of the material. Those models can also be located in a vertical position coupled with a different reverse mechanism. An inclined position can be considered to make use of higher closure and still use gravity as a reverse mechanism.

- Grouping

The responsive components can be either located horizontally or vertically. The horizontal position can afford shading with minimal view blockage. It doesn't achieve small apertures or high closure under high temperature but can act as a large horizontal louver which breaks the direct sunlight. In the horizontal position, the rhythm of repetition can change to achieve more closure, but it needs to take the range of motion into consideration. Additionally, the components can be organized in a staggered pattern. In the vertical position, the umbrella-like components can be positioned vertically to achieve a higher range of deformation and smaller aperture size, as shown in Figure 4-35. A more detailed account of this approach is tested by the students in section 4.10.2. It ranges from a fully closed state to 91% opening. The components can be individually actuated using two-way springs, or the counterweight reverse mechanism of coupling active and passive springs. These passive elements either the zinc tension springs or rubber bands elongate the spring back to flatten the surface.



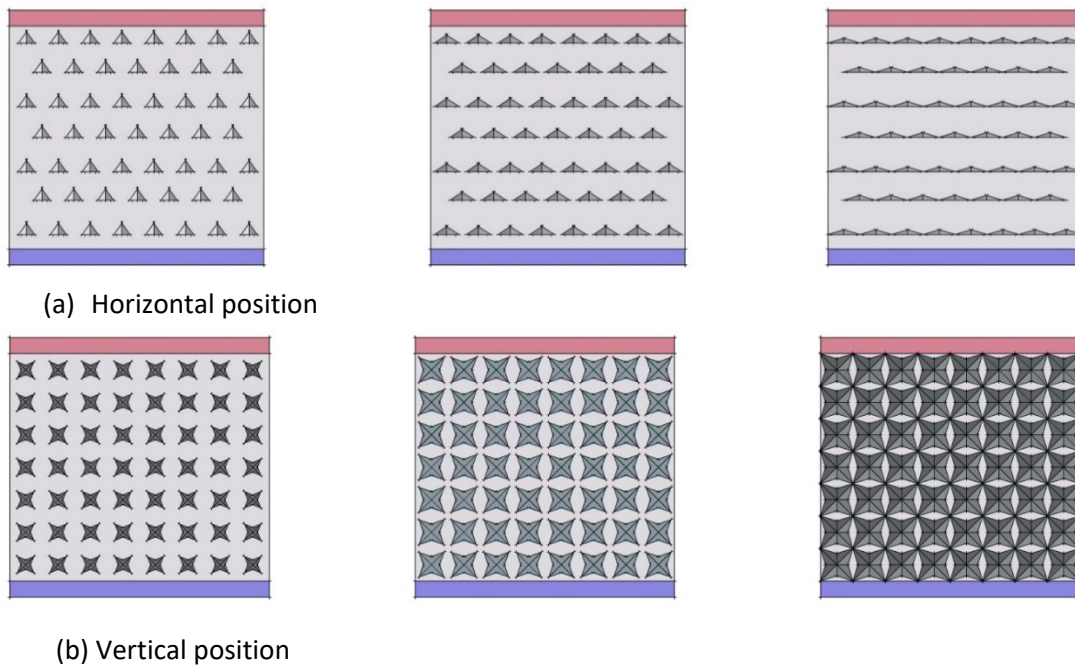


Figure 4-35: Arraying umbrella units horizontally or vertically.

#### 4.8.2. Exploration Two: Curved folding (two/three/four)

Curved folding was applied to create bending-active kinetic systems which base their geometry on the elastic deformation from the planar configuration. Inspired by the carnivorous plants like the Venus Flytrap, the two flaps curved folding can resemble the bistable, doubly curved structure of the leaves, which snap-buckle to reverse their Gaussian curvature upon closing. The two-flap surface is one of the simplest kinetic geometries with great potential either by using straight or curved line fold, as shown in Figure 4-36.

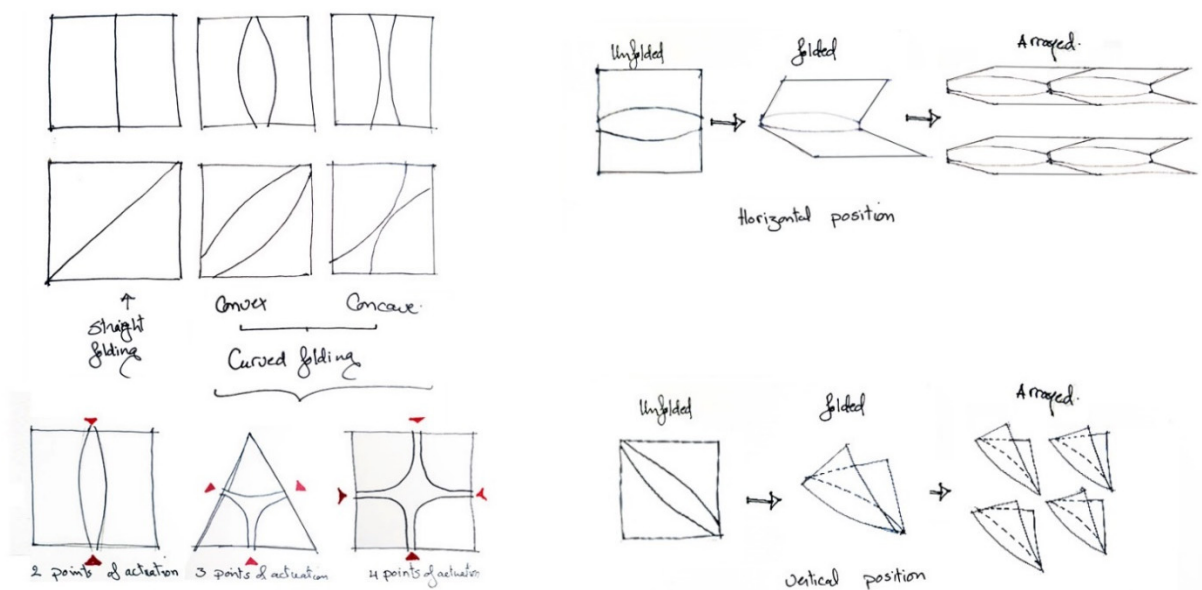
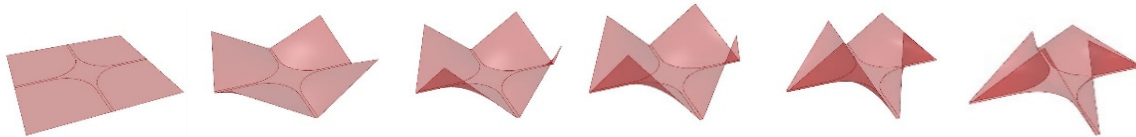


Figure 4-36: A sketch of two-flap surfaces which is one of the simplest geometries with great potential using a curved line fold.

- Form

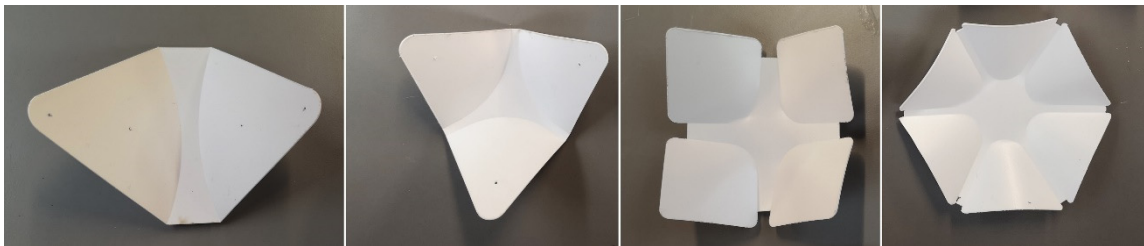
Four curved creases result in a double curved surfaces with intrinsic abilities of reverse motion which are similar to the previous umbrella folded structures as shown in Figure 4-37. Applying two, three or four curves to the module would make a major change in forming a double-curved surface, as shown in Figure 4-38. Generating patterns with concave or convex central area results in a bending-active kinetic system that folds in one direction (A. Vergauwen et al., 2014).



*Figure 4-37: Transformation of one unit of four curved creases.*

- Materiality

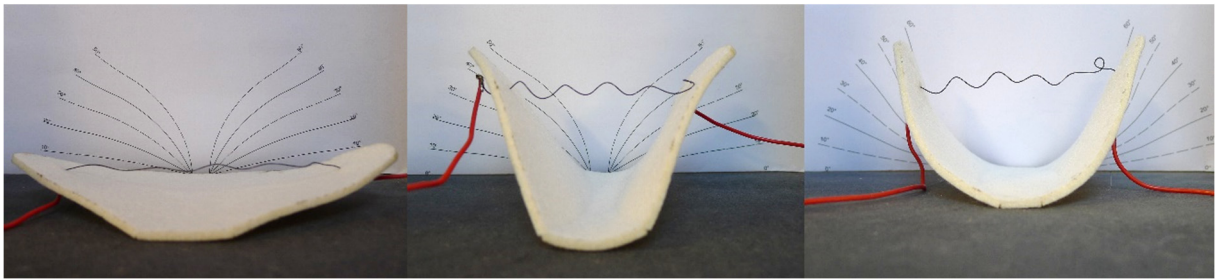
Card paper, polypropylene and thick felt fabric of 3 mm thickness can be used in these set of models. The flaps are easily actuated by an exposed trained Nitinol wire, either flat or helical springs, suspended between the flaps transforming them to complex morphologies



*Figure 4-38: Applying two, three or four curves to a polygon works in similar manner (author investigation).*

- Actuation

The two concave or convex curves result in two flapped form that can fold together in the middle. The model can be actuated by trained spring as shown in Figure 4-39 (a) or pre-trained spring, as shown in Figure 4-39 (b). By changing the location of the pre-trained spring, it was found that fixing the spring at the far ends achieved higher deformation as shown in Figure 4-39 (b). However, fixing the springs at a lower level results in an acceptable range of deformation achieved with shorter springs, thus less material consumption. As shown in Figure 4-39 (a), the hinged wire was trained to shrink from 15cm to 7cm resulting in flaps' rotation up to 50-60°. The axial spring actuator along the core can fully transform the surface from opened to fully closed with a minimal contraction of the spring from 10 cm to 9 cm, as shown in Figure 4-40, resembling the Venus trap by actuating the rib.



(a)



(b)

Figure 4-39: Convex and concave two-curved cease surface with hinged actuator (author investigation).

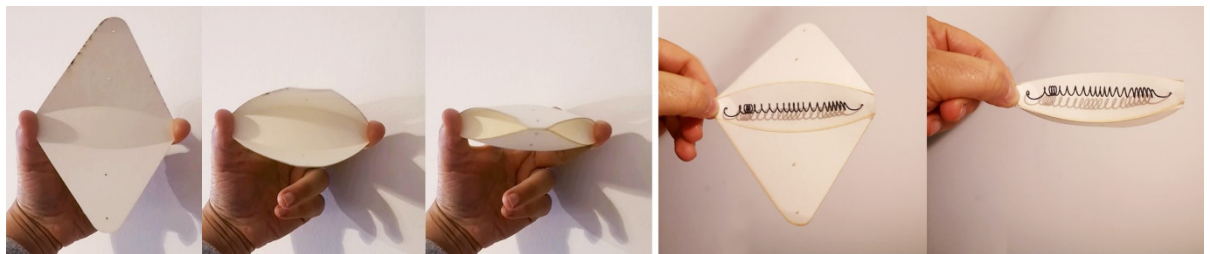


Figure 4-40: Two-curved cease moves using axial actuator with minimal contraction (author investigation)

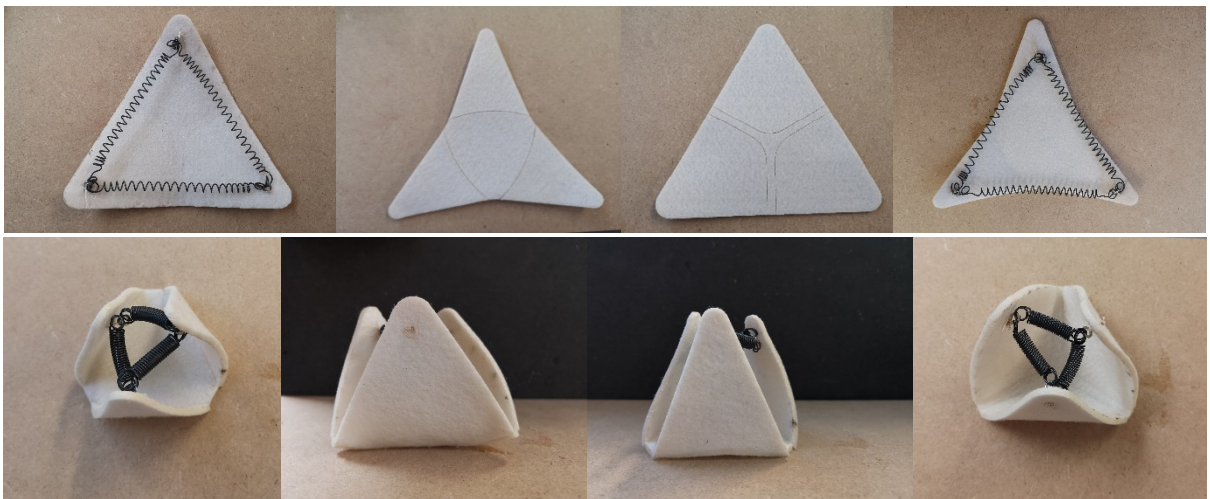


Figure 4-41: Comparing convex and concave three-curved cease surface (author investigation).

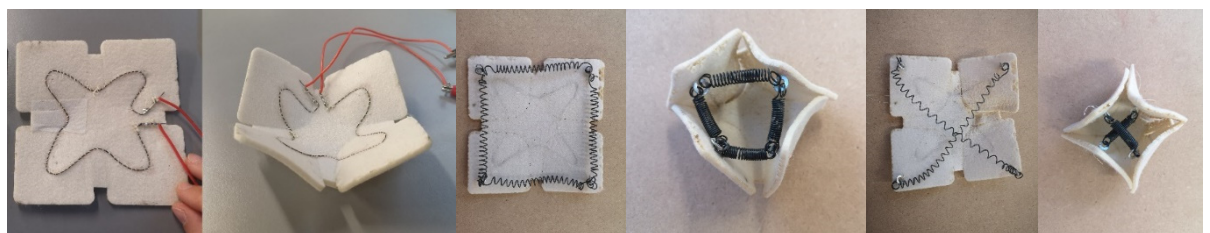


Figure 4-42: Actuation of four curved creases unit using Nitinol wire or springs (author investigation).



During the *experimental* investigations, a resemblance of the motion triggers in the opening process of Lilium, inspired the allocation of the actuators at the periphery of the passive material to change the surface curvature upon expansion. This was carried by knitting the wires at the periphery of a triangular piece of fabric. This model has the flower motion effect; however the knitted wires only work well with light fabrics and couldn't achieve high deformations for thick felt. All these motions are one way, and a reverse mechanism needs to be integrated.

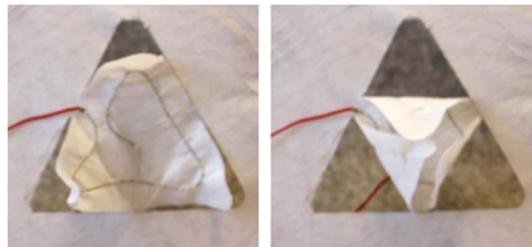


Figure 4-43: The opening process of Lilium, inspired the allocation of the actuators at the periphery of the passive material (author investigation).

- **Return mechanism**

This model has the potential of using the elasticity of polypropylene material as a return mechanism. Also, the system can work with two-way actuators to achieve a full individual action, as shown in Figure 4-44. A counterweight reverse mechanism of coupling active and passive springs can also be considered for this model which works by connecting units with zinc tension springs that elongate the spring back to flatten the surface.

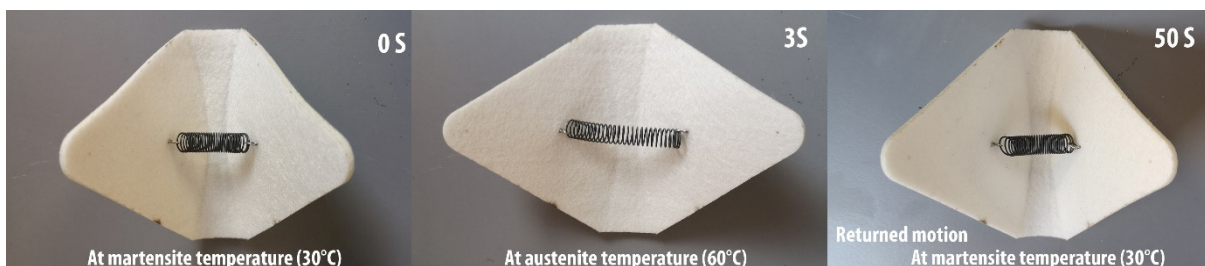


Figure 4-44: Two-way Nitinol spring attached to a two-flap form made of felt (author investigation).

- **Grouping**

The concept of curved folding can be applied to cells with any polygonal shape and arrayed on triangular, rectangular, pentagonal or hexagonal tessellations. The vertical positioning of the components allows them to achieve high range of motion and aperture size around 70% as shown in Figure 4-45.

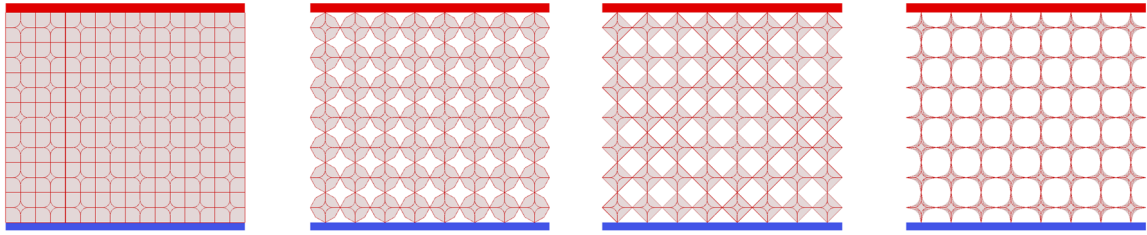


Figure 4-45: Solar shading range of transformation of four curved creases modules (author investigation).

#### 4.8.3. Exploration Three: Single Curved-crease Folding

Applying one curve to a flat surface would make a major change in forming an active bending structure and a double-curved surface, as shown in Figure 4-46 and Figure 4-47. The choice of the crease location and curvature affects the final form dramatically. Card paper, polypropylene and felt can be laser cut to engrave crease lines that illustrate the folds.

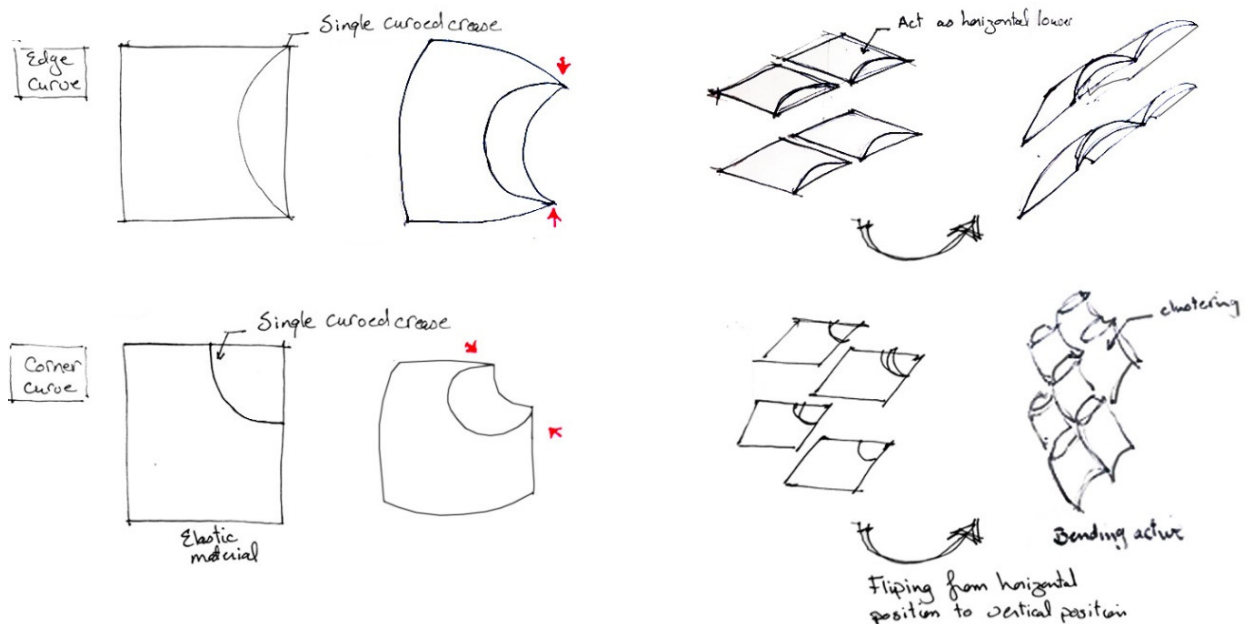


Figure 4-46: Researcher's sketches of single-crease curves transformation.

- Form

The single curve is applied to a square unit of (10cm) size. Two models are tested, the first has the curve engraved along one of the edges, and the second is engraved at the corner, as shown in Figure 4-48. The single curve transforms the flat surface to complex morphologies activated by a linear actuator.

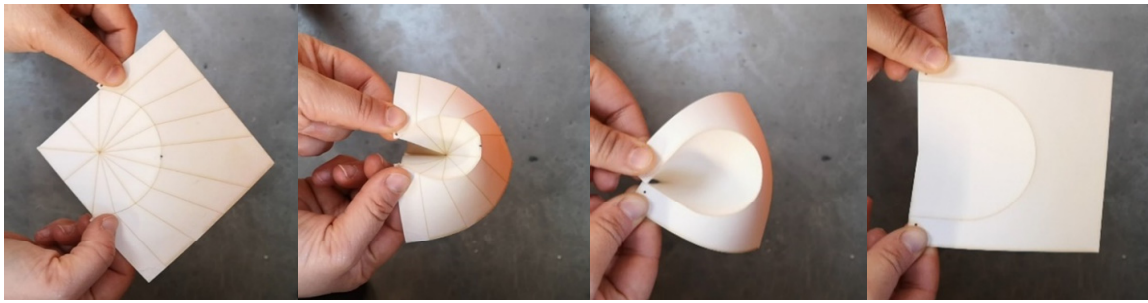


Figure 4-47: Single-crease curve is laser cut and engraved to the square unit (author investigation).

- Materiality

Card paper, polypropylene (0.8mm) and thick felt fabric (3 mm) are fabricated in these set of models. It was found that the felt can't hold the curved crease compared to card paper and polypropylene. Polypropylene performed best for the smooth movement and return mechanism.

- Actuation

These single curve models have two points of actuation, which make it easy to be actuated with a single linear actuator. A linear SMA actuator can be fixed at both ends of the curved crease. As shown in Figure 4-48, the nitinol SMA spring shrinks when heated transforming the planar horizontal form into a double-curved surface. The SMA actuator is activated primarily by electric current, and then a heat gun is used to activate the wires and free the unit from the wiring loads and clamps that may affect the motion behaviour. The heat gun resembles the external heat stimulus of direct sun exposure.

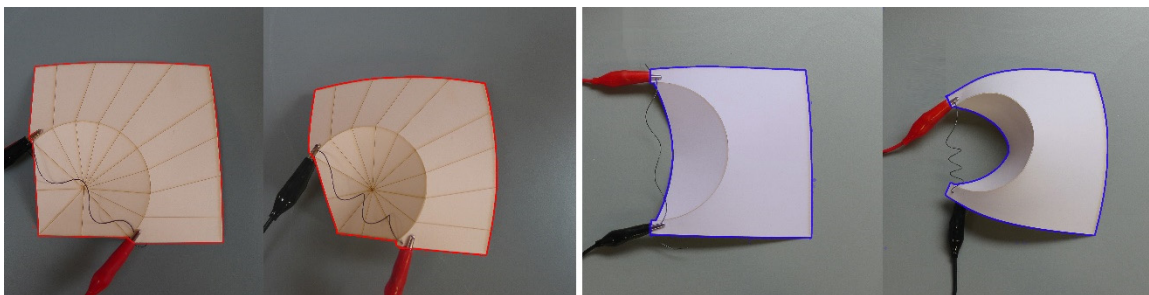


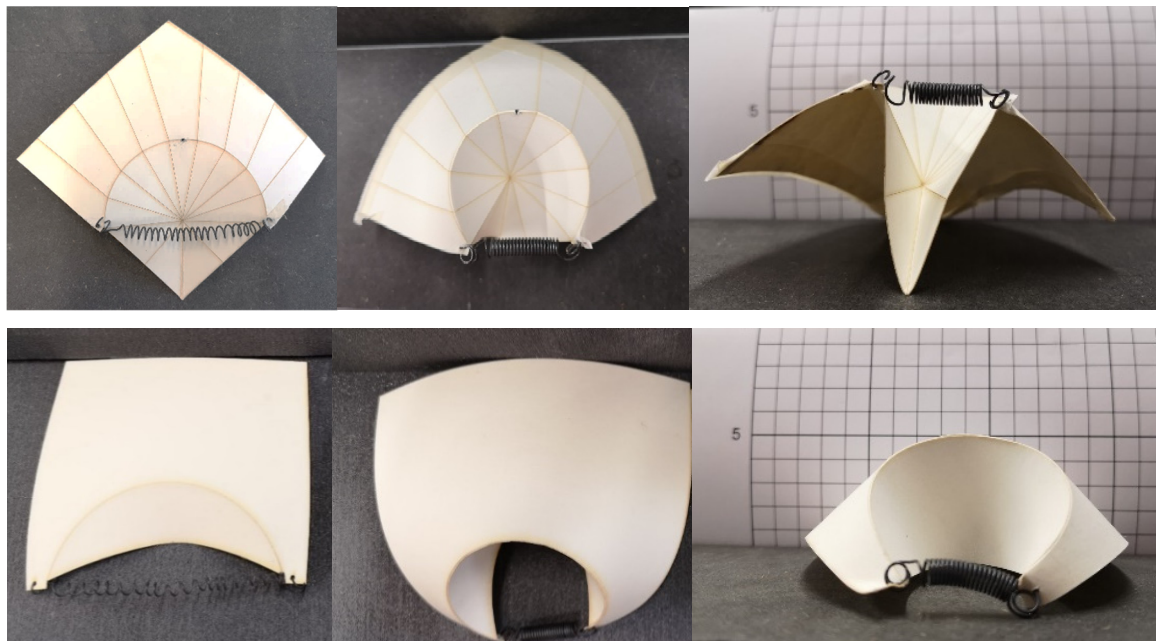
Figure 4-48: Electric current is used to activate the simple linear SMA actuators which are fixed at both ends of the curved crease (author investigation).

This exploration with a single curved crease surface and exposed single actuator result in a high surface deformation with a minimal number of actuators. Smaller springs can even result in higher deformation. One of these exploration advantages is that the single spring helps each unit to work individually. Although all of them are exposed to similar conditions, each unit alters its motion individually, which seems like swarm algorithm and flocking behaviour that is working together, but each unit has full control over its motion. Technically

speaking, when any of the springs is not working to its full range, it is not affecting a neighbouring unit and preventing the part-to-part interactions, thus produce pattern consistency.

- Return mechanism

This model has the potential of using the elasticity of polypropylene material as a return mechanism which could make it one of the most successful experimented prototypes. The use of polypropylene material with high elasticity coupled with curved crease form results in a return action. The unit stretches the spring back from 3cm to 7cm in 20 mins time for the edge curve model, as shown in Figure 4-49. The return action doesn't bring the unit to a fully flat position but rather a slightly deformed unit. Although A. Vergauwen et al. (2014) stated that the curved cease models have embedded return mechanism, the card model barely succeeded to move the spring back 1cm. Hence, the polypropylene sheets present adequate material to act as living hinges for its flexibility and good resistance to fatigue. The system can work with a reverse material mechanism or two-way actuator to achieve a full individual action. The horizontal position of the components can use gravity as a reverse mechanism when flapping the unit upward upon spring shrinkage then flatten back under its self-weight. Although the counterweight reverse mechanism of coupling active and passive springs may work by connecting units with zinc tension springs that elongate the spring back to flatten the surface, it has the risk of a resulting inharmonious motion.



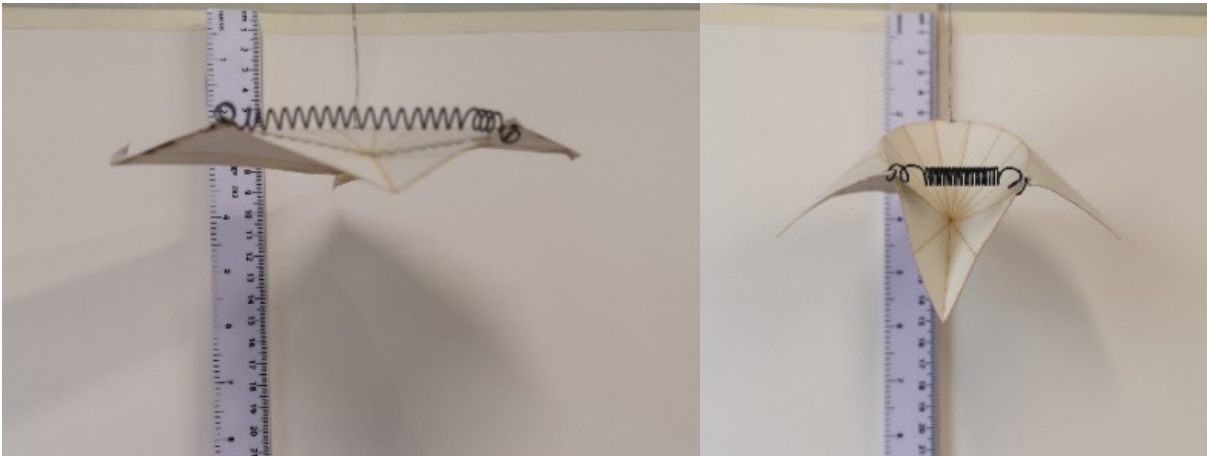
*Figure 4-49: Single curved cease surface results in high deformation in the X-, Y- and Z-direction; corner single crease at the top and edge single crease at the bottom (author investigation).*

*Table 4-3: Comparing time taken and displacement for edge and corner curved creases of 10cm x 10cm polypropylene material.*

	Polypropylene material with curved creases	
	Edge single crease	Corner single crease
<b>Time taken for initiation</b>	8 sec	8 sec
<b>Time taken for reverse</b>	1,320 sec	1,200 sec
<b>Max actuator displacement</b>	5 cm	3 cm

By comparing the edge curve and corner curve models as shown in Figure 4-49 and Table 4-3, it was found that both models are actuated in the exact same time. However, the edge curve model reversed the motion by the elastic material in a slightly longer time than the corner curve by 120 sec. Also, it was found that the form with corner curve can be more efficient as it can use shorter actuator while altering higher deformation and height that reached (7cm) compared to (5cm) for edge curve.

Fixing these models structurally is kind of challenging as all vertices are moving and all surfaces deformed. A vertical structure; rods, cables or strings, can pass through the units to be hanged loosely or fixed with clamps from its centre of gravity as shown in Figure 4-50.



*Figure 4-50: The single curved unit is hanged loosely from its centre by vertical strings giving a light flying effect (author investigation).*



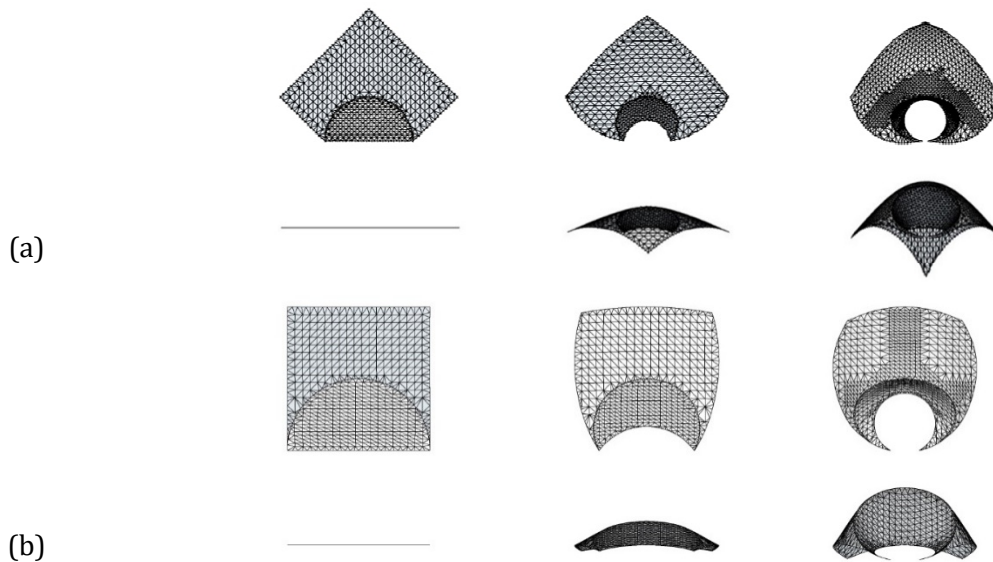


Figure 4-51: Single curved cease units top & front view; (a) corner single crease (b) edge single crease (author investigation).

- **Grouping**

Being in the horizontal position, the models have the freedom of adding more horizontal layers to achieve higher levels of opaqueness. The in-between spacing of rows can be adjusted with overlapping to achieve up to 90% closure or less than 10% aperture size. Hypothetically, the models can achieve 100% openness in the flat horizontal position but realistically speaking from physical explorations, the models are slightly deformed when stretched back after the reversible material motion to 80% openness.

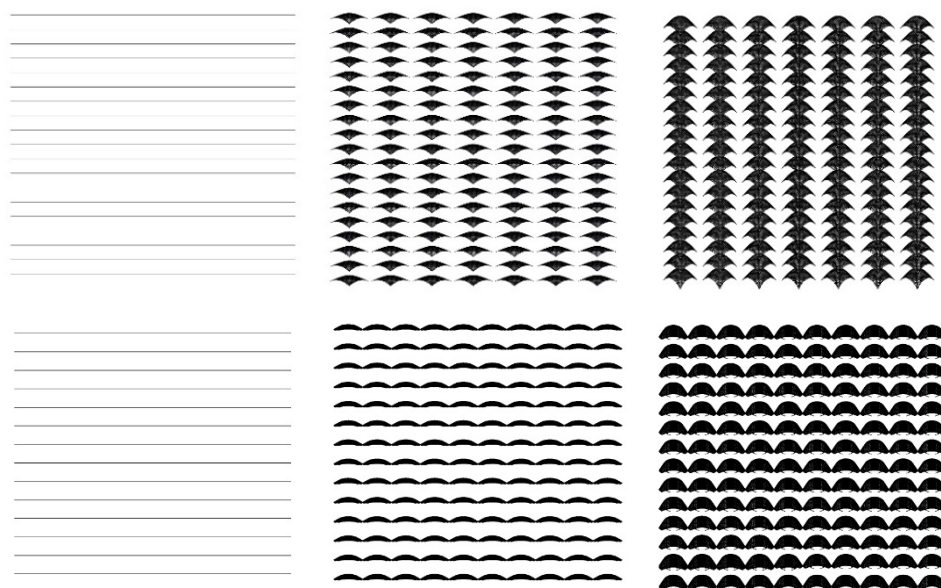
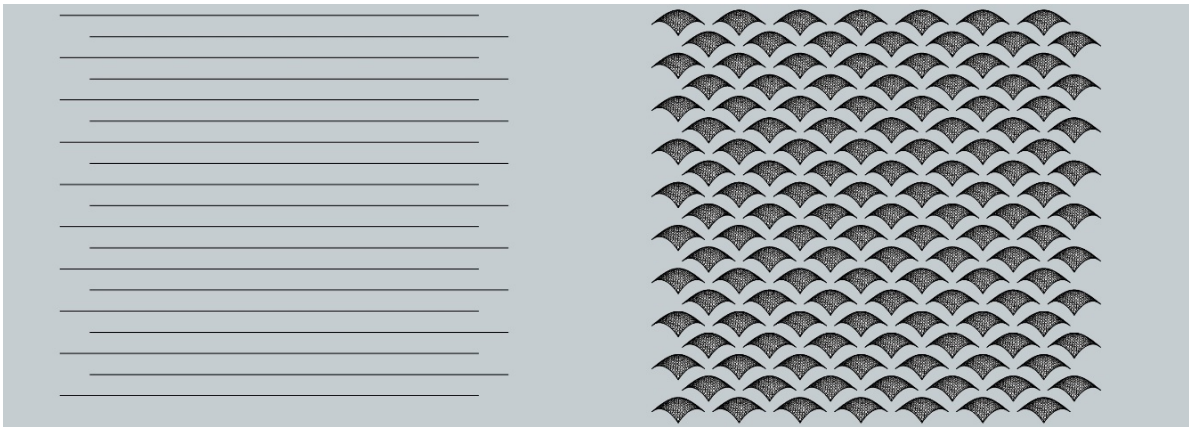
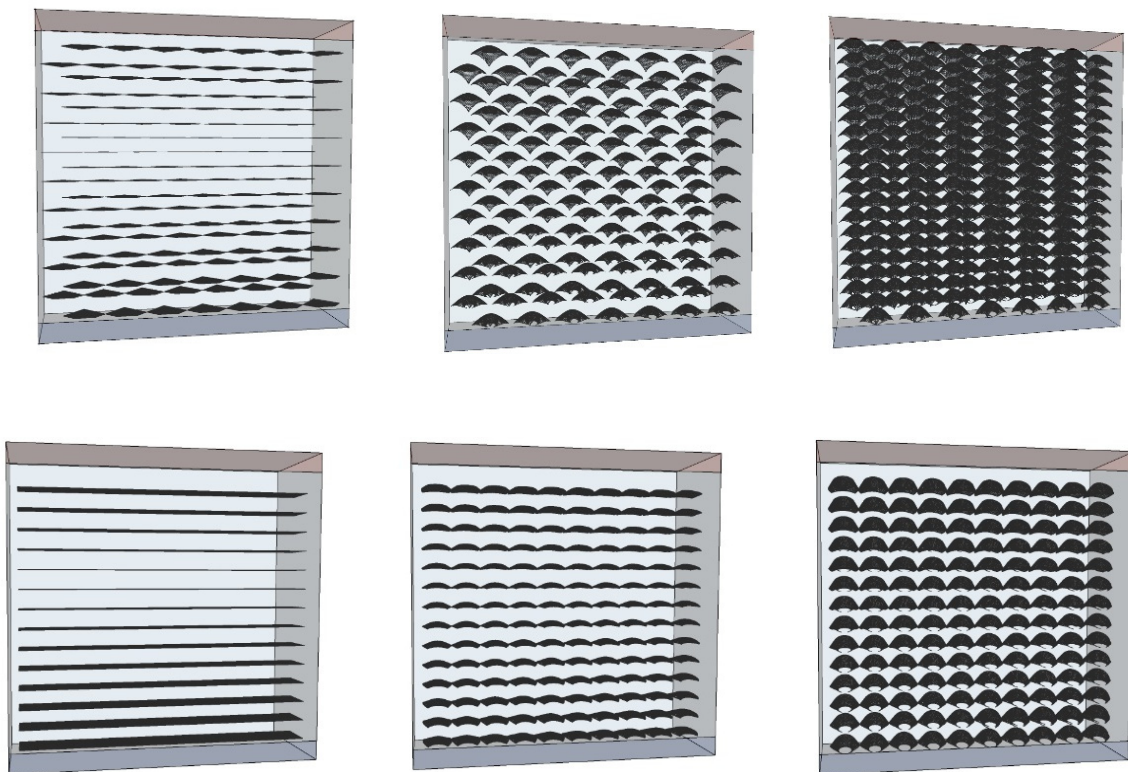


Figure 4-52: Arraying edge single curved cease acting as horizontal louvers (author investigation).

Additionally, the units can act as continuous louvers or organized in a staggered pattern. All previously mentioned variables can alter many design alternatives to select the required range of aperture size.

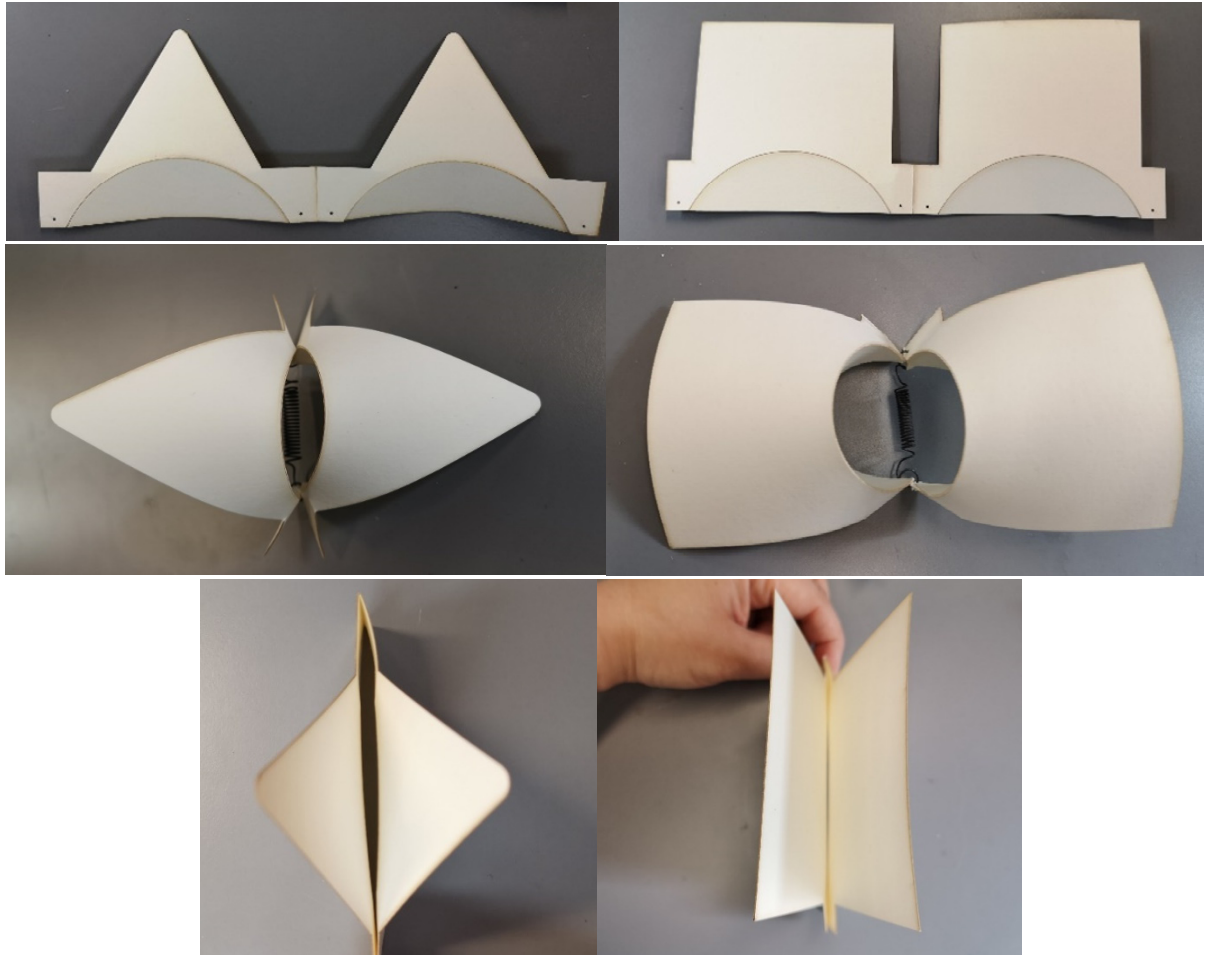


*Figure 4-53: Corner curved crease units arranged in a staggered pattern to achieve higher levels of opacity (author investigation).*

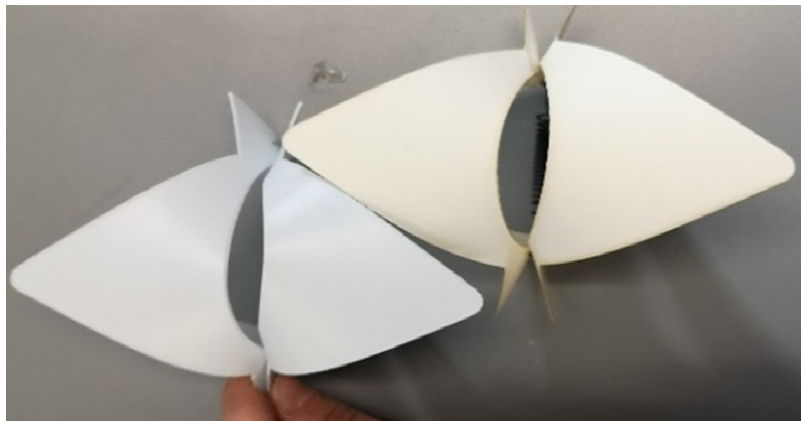


*Figure 4-54: 3D explorations of the solar shading system of single curved crease unit transformations (author investigation).*

Further exploration based on the same technique intended to couple two single curved-crease units back to back and actuate them with an intermediate SMA spring. The units are positioned vertically, and when the spring is actuated, it shrinks to open up the flaps and afford sun protection, as shown in Figure 4-55. This coupled vertical exploration has the potential of being applied on different patterns and tessellations altering different effects.



*Figure 4-55: Two single curved-crease units are attached back to back and actuated with one SMA spring (author investigation).*



*Figure 4-56: Grouping of the coupled single curved-crease system (author investigation).*

#### 4.8.4. Exploration Four: Deformed Cylinder

The capabilities of the textile-like materials and the resulting deformation motion may represent a driving force for the new generation of soft robotics application in architecture. This exploration is inspired by the deformation motion that can be achieved by felt when stretching two or more points. The sound-proof wall coverings made with woollen felt by Anne Kyyrö Quinn is based on three-dimensional technique inspired by organic shapes and expressed in simple yet elegant compositions as shown in Figure 4-57 (Quinn, 2018). This sculptural approach can be applied to architectural solar shading systems to achieve mobility through the deformation motion of textiles or elastic materials.

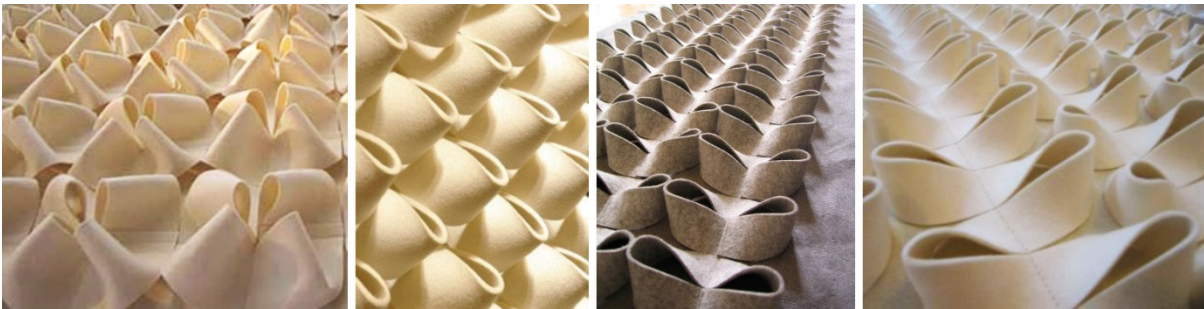


Figure 4-57: Felt Wall Coverings by Quinn (2018).

- Form

A circular pattern made of an array of uncapped cylinders can transform to rosette pattern by actuating 4 points on the upper circular periphery of the cylinders. Linear actuators can connect two pairs of opposite points to achieve the required material deformation. The resulting flower-like aperture depends on the rotation motion of the cylinder's side surface from vertical to a horizontal position. The simple linear contraction motion coupled with the deformation of material results in a transformation from an open to a closed configuration, as shown in Figure 4-58 with smaller apertures that can afford more shading. The resulting peanut-like aperture is interesting and can be arranged in different ways by key manipulations or using different basic cells.



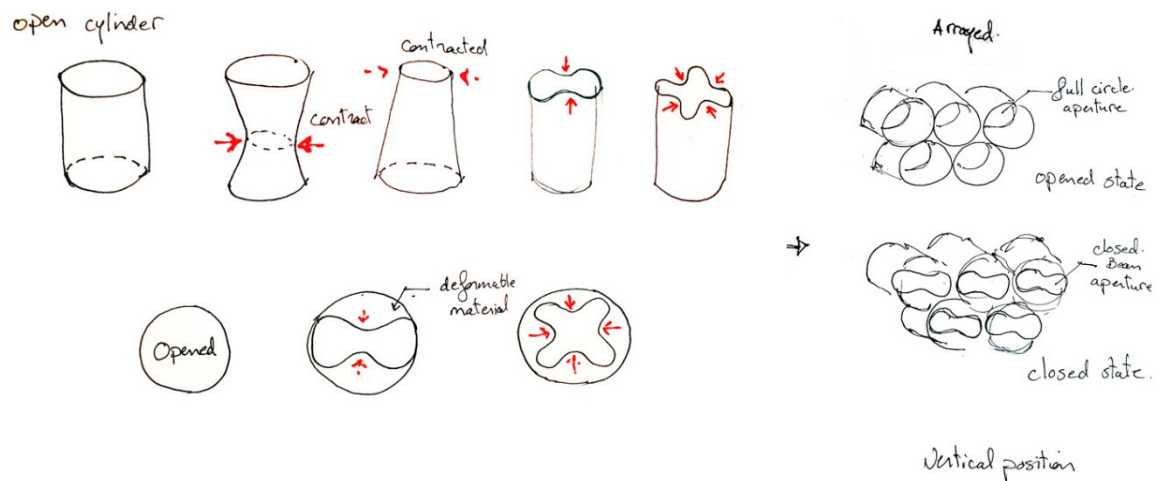


Figure 4-58: Researcher's sketches of Flower or peanut-like apertures achieved by connecting 2 or 4 points.

- Materiality

The use of felt material coupled with linear actuation resulted in a peanut - or flower-like aperture, which has high aesthetical values. The technique is very simple yet aesthetically pleasing and has high potential as soft deployable structure. Other rubber-like materials and polymers can deform similarly in addition to the intrinsic return mechanism capabilities such as used by Begle et al. (2013) and C. K. Khoo and F. Salim (2013) in section 2.3.4 page 45.

- Actuation

A suspended nitinol SMA springs are proposed for actuation. They can make high advantage of sun exposure and direct radiation, as shown in Figure 4-59.



Figure 4-59: Peanut- or flower-like aperture actuated with suspended nitinol SMA springs (author investigation).

The spring may be located on the outside for maximum sun exposure but also can be located on the inside of the solar shading or suspended diagonally. Single spring actuator results in a peanut-like aperture, while the two springs results in the rosette pattern as shown in Figure 4-59. Four springs instead of two can be used for smaller travel distances as shown in Figure 4-60.

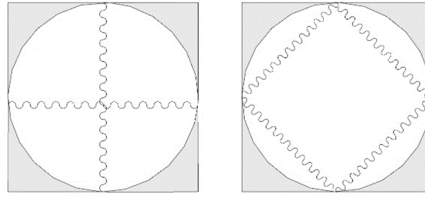


Figure 4-60: Four springs or two crossed springs can be used to produce the Rosette pattern.

- Return mechanism

The proposed reverse motion is a counterforce with zinc springs in-between the cylinders. It can also be achieved using elastic materials that are capable of bringing the circular patterns back similar to (C. K. Khoo & F. Salim, 2013). The model has the advantage of enabling each component to work individually by using linear exposed two-way SMA springs.

The aperture size depends on the travel length of the linear actuator and its proportion to the scale of the model. The ratio between the radius of the circular pattern and depth of the unit has to be 1:1 to achieve a full closure with tiny springs.

- Grouping arrangement

Form, pattern and sequence of repetition can all alter many alternatives each with different range of aperture size, as shown in Figure 4-63. The scale of the model, together with the actuator size control the minimum aperture size that this typology can reach. The aperture size for the regular rosette pattern with in-between fixed solid areas can reach a minimum of 30% and a maximum of 78.5%, as shown in Figure 4-61.

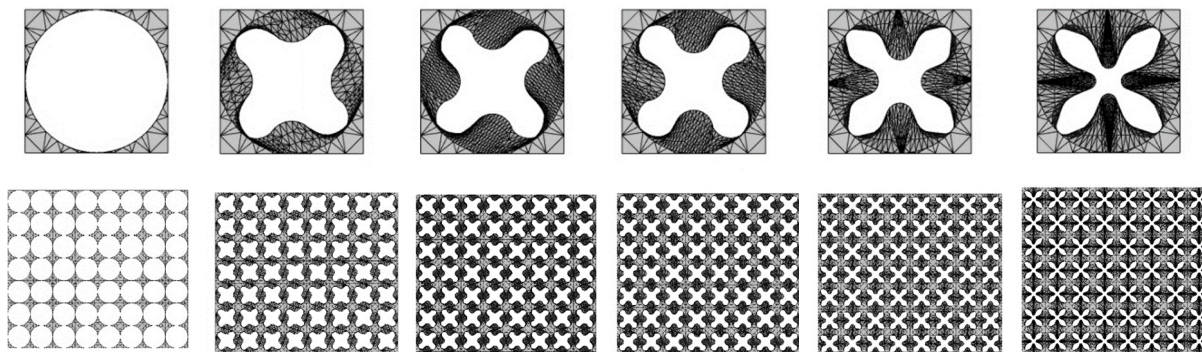


Figure 4-61: The aperture size of rosette pattern ranges from 30% to 78.5%.

These models have the freedom to add solid fixed or open connections, in-between the circular components to control the levels of openness, as shown in Figure 4-62. Open connections can maximize the opening percentage and aperture size to more than 90% but also may not reach over 50% closure maximum. The circular staggered pattern can also be applied, as shown in Figure 4-63 (c) & (f).

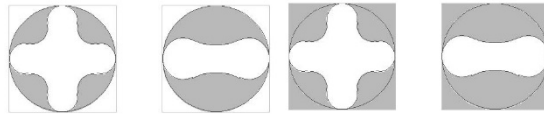


Figure 4-62: Alternatives of Flower or peanut-like apertures achieved through one or two suspended springs with opened or closed connection area.

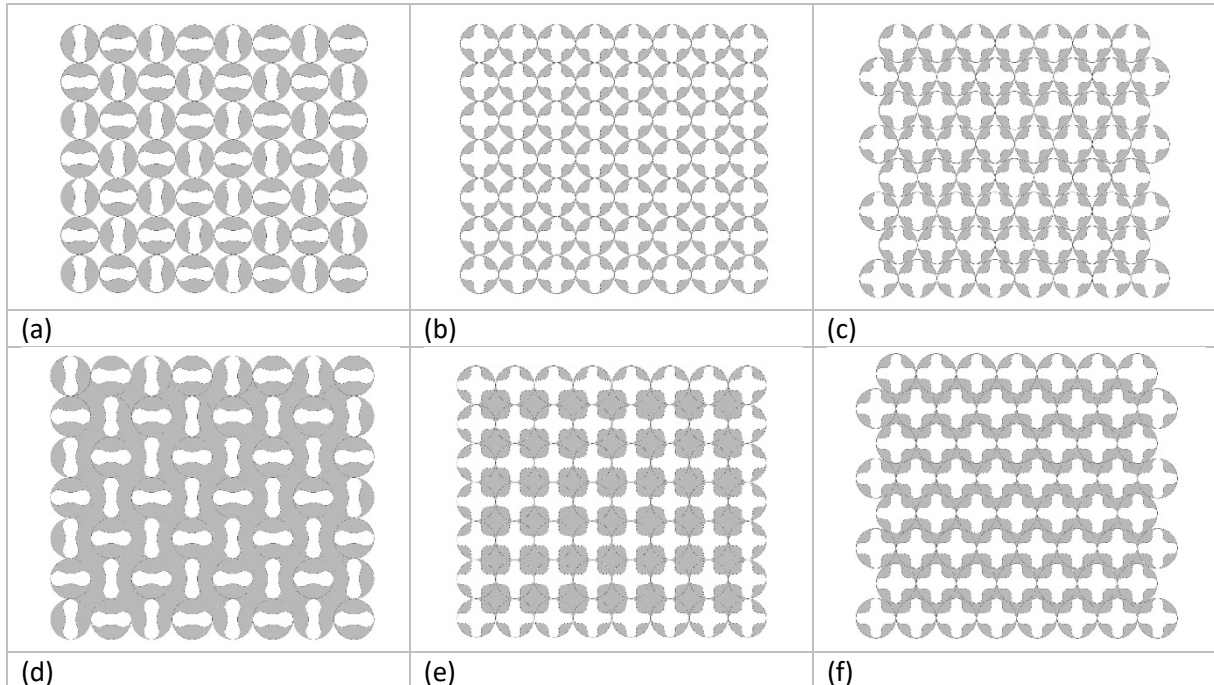


Figure 4-63: Alternatives of deformed circular patterns (a) with one SMA spring (b) with two SMA springs (c) staggered pattern of two SMA springs (d) with one SMA spring with closed connections (e) with two SMA springs with closed connections (f) staggered pattern of two SMA springs with closed connections.

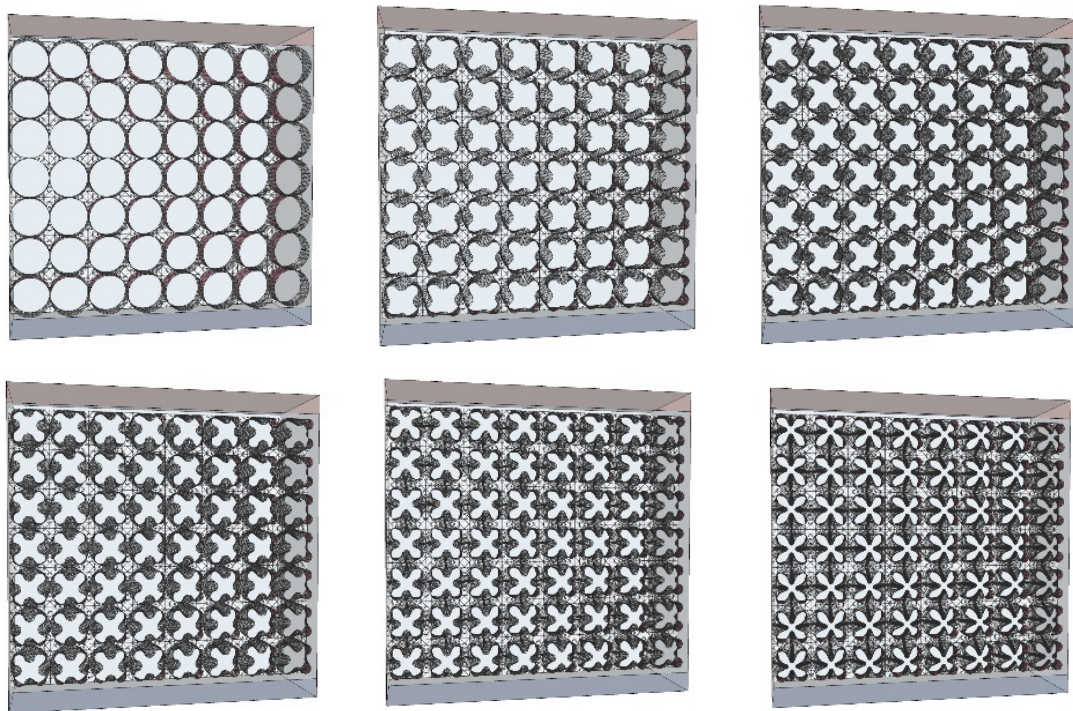


Figure 4-64: 3D explorations of rosette pattern transformations for solar shading system application.



The combination of natural felt and three-dimensional forms can enhance airflow and reduce ambient noise levels. Although the model has the advantages of a simple fabrication and actuation, it still needs to be studied structurally.

Thus far, the set of researcher's explorations investigated the coupled strategies of origami and bioinspired principles with SMM actuators through the hands-on exploration to show their potential as responsive solar shading systems. This exploration presented some actuated components involving trade-offs between materials, forms and structures which are promising for further upscaling; however, they aim at investigating the design process and exploring the design space rather than finding an optimal solution. The next section will present the design process.

#### 4.9. Experimentation Workflow

By reflecting on the hands-on explorations carried by the researcher in the previous sections, it can be seen that the design process relied on a layered investigation of the system kinetics that includes; form generation, materiality, actuation and panelization as shown in Figure 4-65. This design process workflow represents an experiential knowledge and gained insights into the responsive system which will be subjected to test and validation through the educational experiences in the coming section. Through this linear process, parameters of responsive solar shading can be tested to develop an integrative design framework by the end of the thesis.

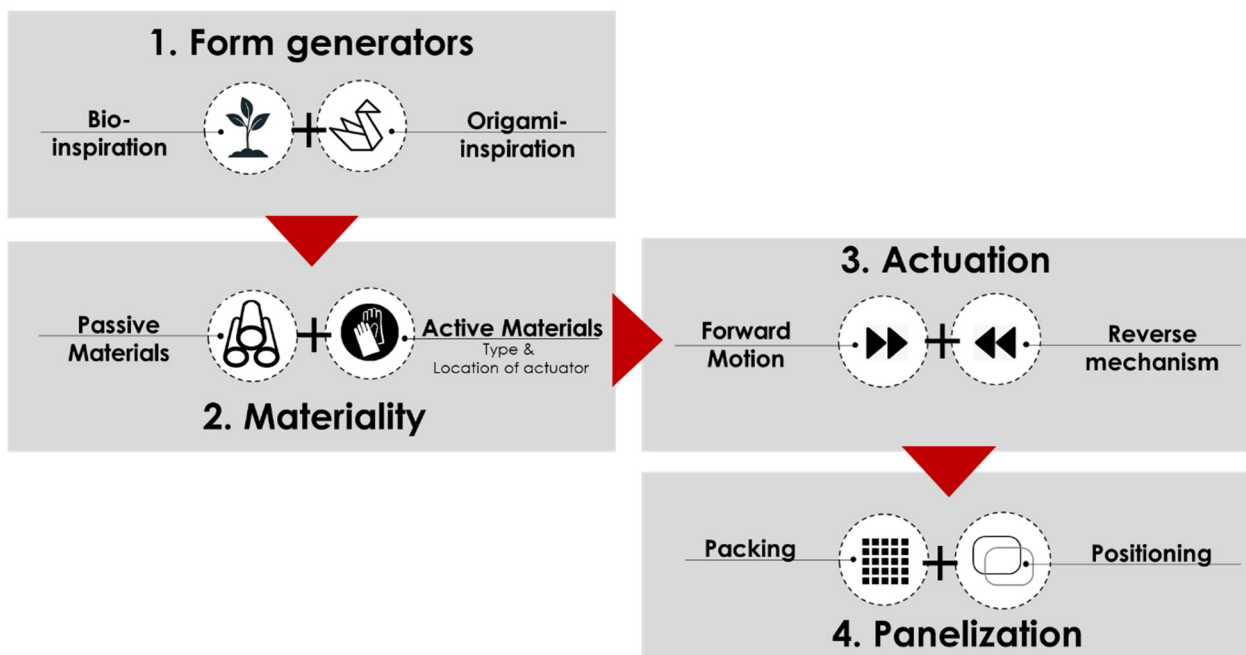




Figure 4-65: This diagram presents the experimentation workflow and outlines a possible transfer process from bio- and origami-inspired models to artefacts and prototypes


The workflow diagram includes important key concepts in the design process of responsive solar-shadings. The role of each of these concepts in the design process is summarized below.


**FORM GENERATION** represents the starting point of the workflow. It is finding inspiration from nature or origami art driven by the potential of acquired motion, aesthetics of form and interest of the designer.

-  **BIO-INSPIRATION** highlights a sensitive observation of biological processes and their transfer into novel design methodologies for the creation of innovative architectural explorations (Hovestadt & Kretzer, 2014).


-  **ORIGAMI-INSPIRATION** transforms two-dimensional forms to three-dimensional forms by bending over regular creases to create new reconfigurable typologies.


**MATERIALITY** addresses the potential to control and design matter at a nano- or micro-scale by understanding their behaviour and characteristics.

-  **PASSIVE MATERIALS** addresses the potential to control and design with materials that are flexible, elastic or rigid to serve or generate the form.


-  **ACTIVE MATERIALS (MATERIABILITY)** addresses the potential to design with materials that are dynamic, active, and responsive to environmental conditions.


**ACTUATION** operates the solar-shading unit by material activation which took place by the Heat gun and electric current. The actuation phase aims to achieve forward and backward motion.

-  **FORWARD MOTION** is the way in which the active material drives the motion of the system under specific environmental conditions.

-  **SYSTEM REVERSIBILITY** balances the design of the system where the unit returns to its original shape. It has a strong connection with active and passive material properties.

**PANELIZATION** is the action of grouping units together which might include joining units via actuators, or joining counteraction members that brings the system back to its original shape.

-  **PACKING** is the action of tiling, tessellating a surface, or selecting the grouping pattern.

-  **POSITIONING** addresses the relative positioning of the component to gravity and façade.

This knowledge is transferred to MArch students during the fall of 2018/2019 to use *teaching experiences* as a method to test the different parameters and validate the design process workflow. Students tested parameters of the design framework which are; form generative techniques; Bio- and Origami-inspiration, materiality and materiability, actuation and system reversibility, and panelization. During the course, we were able to use hands-on experimentation, play around with deployable forms and tinker around with active SMA actuators through physical modelling.

To analyse how other designers may produce with movable forms by following this design workflow, the next section will go further transferring the previously gained knowledge to an educational research domain for MArch students as creative practitioners.

#### **4.10. Teaching Experience: Soft Robotics as Design Practice**

(Lessons learnt from teaching soft robotics approach to designers)

The practice-led educational approach is used as a way of thinking through the material (Nimkulrat, 2012; Parisi et al., 2017) to facilitate the reflection and articulation of knowledge generated from the students as being designers doing a creative practice. These teaching experiences serve the main aim of the experimental explorations which is developing an actual prototype system for further environmental experimentation in *Chapter Six* and an integrative 'Design Framework' by the end of the thesis in *Chapter Seven*. The experimentation was done with Stage 5 students as a part of MArch Vertical Technology Studios 2018-19 in Newcastle University. A six-week design project based on a brief, as shown in Appendix B, to develop a responsive system that is actuated by SMM to open and close an aperture according to changing temperature levels. The outcome of the course is a final prototype that fits in a 0.5 m x 0.5 m for an exhibition display.

In line with the educational framework of Kretzer (2017a) mentioned in the '*Methodology*' chapter section 3.3.2, the course structure follows the following steps, where each activity is carried in a separate session as shown in Figure 4-66.

- Delivering lectures on Origami and Bio-inspiration as form generative techniques as well as smart materials, with selected readings and literature, as well as a vast collection of sample projects to help the students to get started.
- Working in small teams (3-4 students), Gaining first-hand insights in deployable structures using origami principles and physical models that are manually manipulated; (Form)
- Getting practical instructions on how to train SMA and test their behaviour in an early introductory workshop (Materiality)
- Physically experiencing the fixation of active and passive materials to develop one moving unit (Actuation)
- Working in small teams of three, the students develop a responsive solar shading module that fits in a 0.5 m x 0.5m (Panelization)



*Figure 4-66: Experimentation workflow.*

The students were introduced to Bio-inspiration; particularly plant actuation, and folding principles in the form generation stage to achieve geometrical deployability. They were assigned to design primitive prototypes to achieve deployable forms. Primitive paper models were developed to test the form, structure, motion and different modes of change. Figure 4-67 shows some of the paper models produced by the students. Some origami-inspired and Plant-inspired models were developed as well as sliding layers, and umbrella-like mechanism. Some explorations used the doubly curved structure of the leaves, which can snap-buckle to reverse. This model was further compared to a similar origami-inspired straight folding model to explore both motions and their potential for actuation and reverse mechanism as shown in Figure 4-67.a. Other explorations tested the idea of translational and sliding motion, as shown in Figure 4-67.b. Students tested many 2D and 3D Origami models with straight folding, as shown in Figure 4-67.c,d. Also, three-dimensional rotating origami models or flexagons with different tetrahedron numbers are investigated. Although the motion of rotating origami is fascinating, it didn't achieve large size apertures and hard to be fixed, as shown in Figure 4-67.d. Some experimentations developed an umbrella-like mechanism. Some of these models were selected for further fabrication and actuation based on their efficiency, aesthetic and potential for actuation.

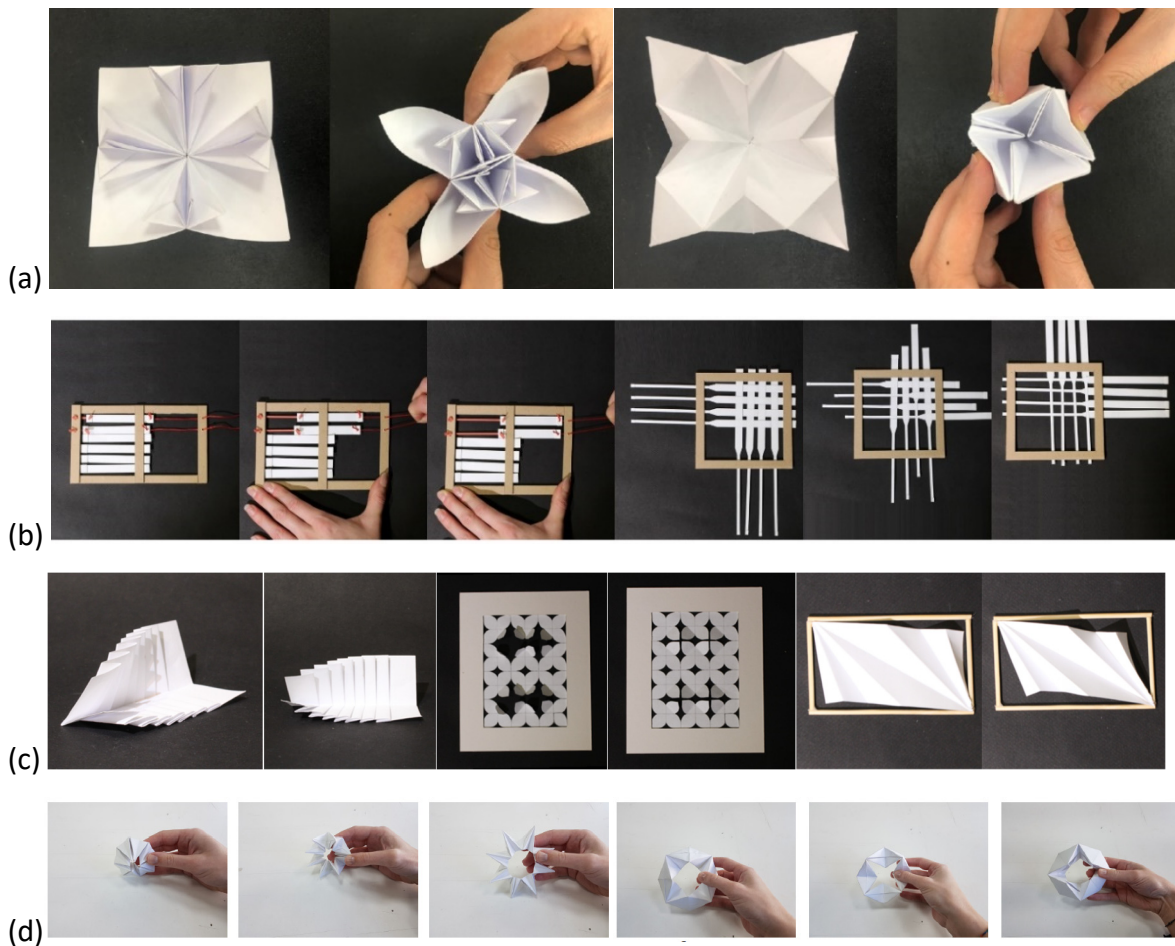


Figure 4-67: Early stage explorations of deployable models using paper (NCL MArch students stage 5, 2018-19).

The integration of passive and active materials and the selection of efficient return mechanisms have been thought of as key factors to achieve a robust, responsive system. The designers determined to keep the experimented systems as simple as possible to put these factors together. Students experimented and compared different materials to select the most promising deployable motion. Mountain and valley creases of origami-based structures are scored in thin materials. While, for thicker materials such as plywood, students connect solid rigid surfaces with an intermediate textile layer or joining the solid surfaces with metal hinges, as shown in Figure 4-68.



*Figure 4-68: Development and fabrication of primitive models and sketches of Prototype B (NCL MArch students stage 5, 2018-19).*

The next sections will provide in-depth analyses of the three experimented models by the MArch students demonstrating step-by-step procedures for transforming 2D surfaces into 3D forms. Each of these case studies features a combination of form and actuation method, which is particularly promising for further upscaling and full system design.

#### *4.10.1. Prototype A: Sliding hexagons*

This group of students started working on an eight-piece shifting octagonal model; as shown in Figure 4-69, which can compress into an eight-point star shape, as shown in Figure 4-70. The group simplified this idea into a linear sliding movement. The shading system consists of two layers; a front moving layer and a back fixed layer. The front shading layer moves back and forth to open and close the facade. The front moving layer is controlled through horizontal strings connected to a separate group of SMA springs on the left, as shown in Figure 4-71. The system is meant to be coupled with another group of compression springs on the other side to achieve the reversible movement. Looking at how the students clustered their units, students of Prototype A used passive material; strings; to connect units horizontally depending on the group of actuator located at the ends.



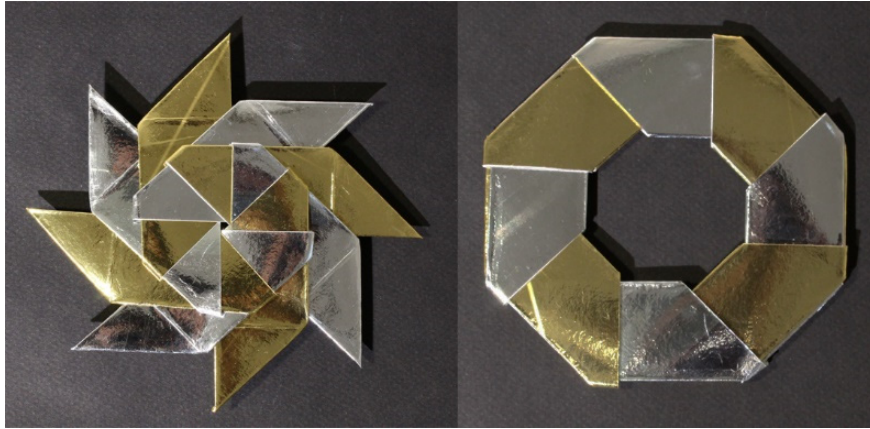


Figure 4-69: Eight point star-shaped closes and opens (NCL MARCH students stage 5, 2018-19).

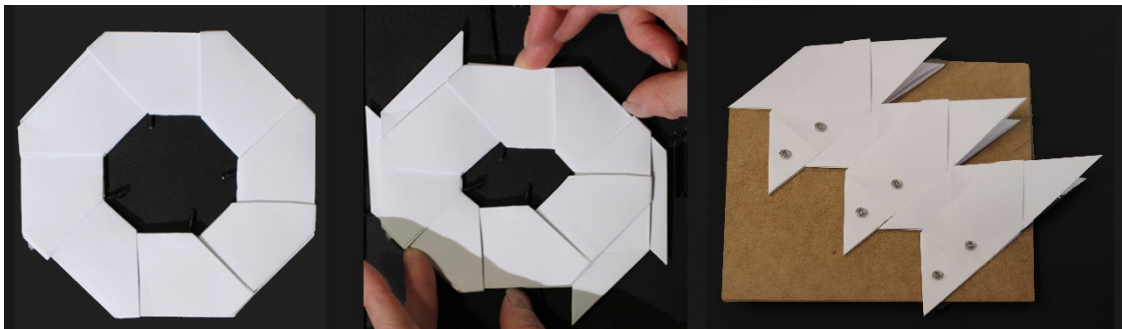


Figure 4-70: Simplification of eight-piece shifting circular model to shifting grids of Prototype A (NCL MARCH students stage 5, 2018-19).

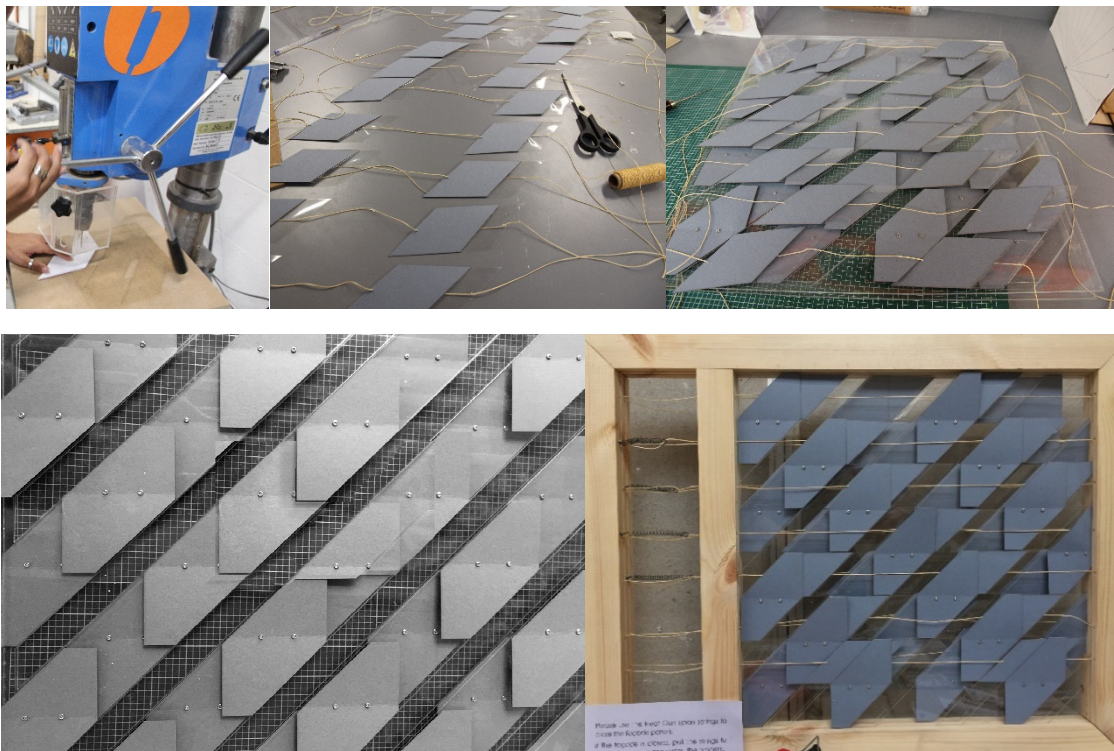


Figure 4-71: Final model development of Prototype A (NCL MARCH students stage 5, 2018-19).



The form of the sliding layers informed the actuation. The coupling smart and zinc springs can animate the structure to achieve forward and backward motion. A clear relationship between panelization and actuation has shown in this kind of exploration. Panelization informs the location of actuators' which shows that it is not a linear one-way design process.

#### *4.10.2. Prototype B: Folded Flowers*

This group of students developed a folding geometry similar to the vertical umbrella-like structure investigated earlier by the researcher. The students laser-cut plywood and connected the solid rigid surfaces with small metal hinges. The operation of the system relies on coupling four conventional compression springs or rubber bands with four opposing (SMA) springs, as shown in Figure 4-74 and Figure 4-75. The design group tried different types of compression springs and rubber bands to reach an equilibrium of forces between the conventional compression springs and the (SMA) springs. The system was designed that the conventional springs keep the folded unit closed at low temperature, while, the SMA springs contracts when the temperature rises resulting in an expansion of the folded unit and a closed aperture. This mechanism worked efficiently for a single square unit of 15 cm and in a fully reversible manner. When it was grouped in a set of four to fit the frame of 0.5 m x 0.5 m, SMA springs were used as connectors between deployable units. Although the actuation method was fully working on the component level, it failed to achieve the previously tested transformation when grouped. A possible explanation of this discrepancy is that each individual unit should have been properly fixed on a secondary structure from the centre of the units to achieve the required motion. Further modifications need to be carried to reach an equilibrium of forces.

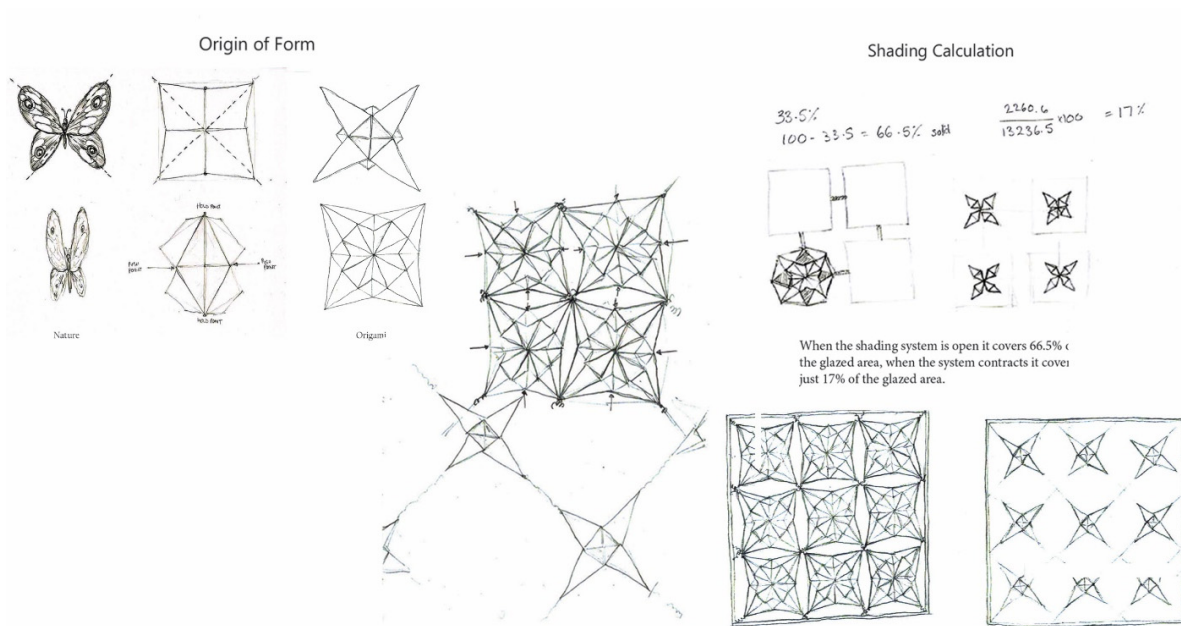


Figure 4-72: Students' sketches starting form generation of single unit to grouping and panelization

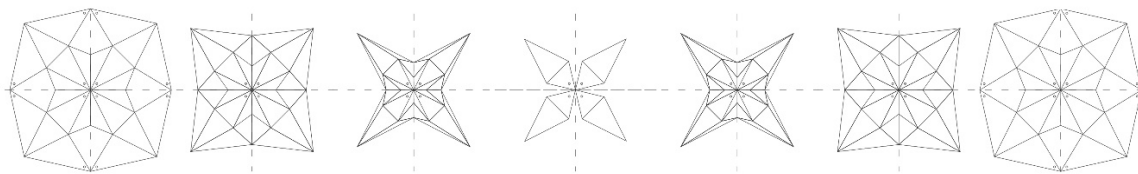


Figure 4-73: Diagrams of the transformation of the folded unit (NCL MArch students stage 5, 2018-19).



Figure 4-74: Students testing counter-weight reverse mechanism (NCL MArch students stage 5, 2018-19).

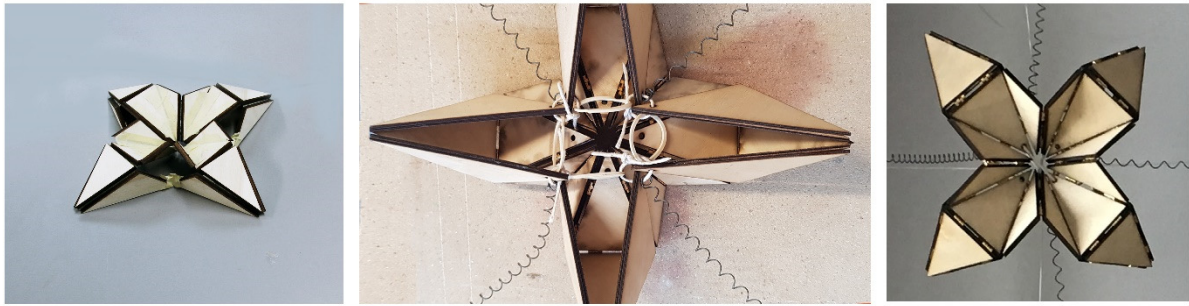


Figure 4-75: Fabrication and actuation of a single folded unit (NCL MArch students stage 5, 2018-19).

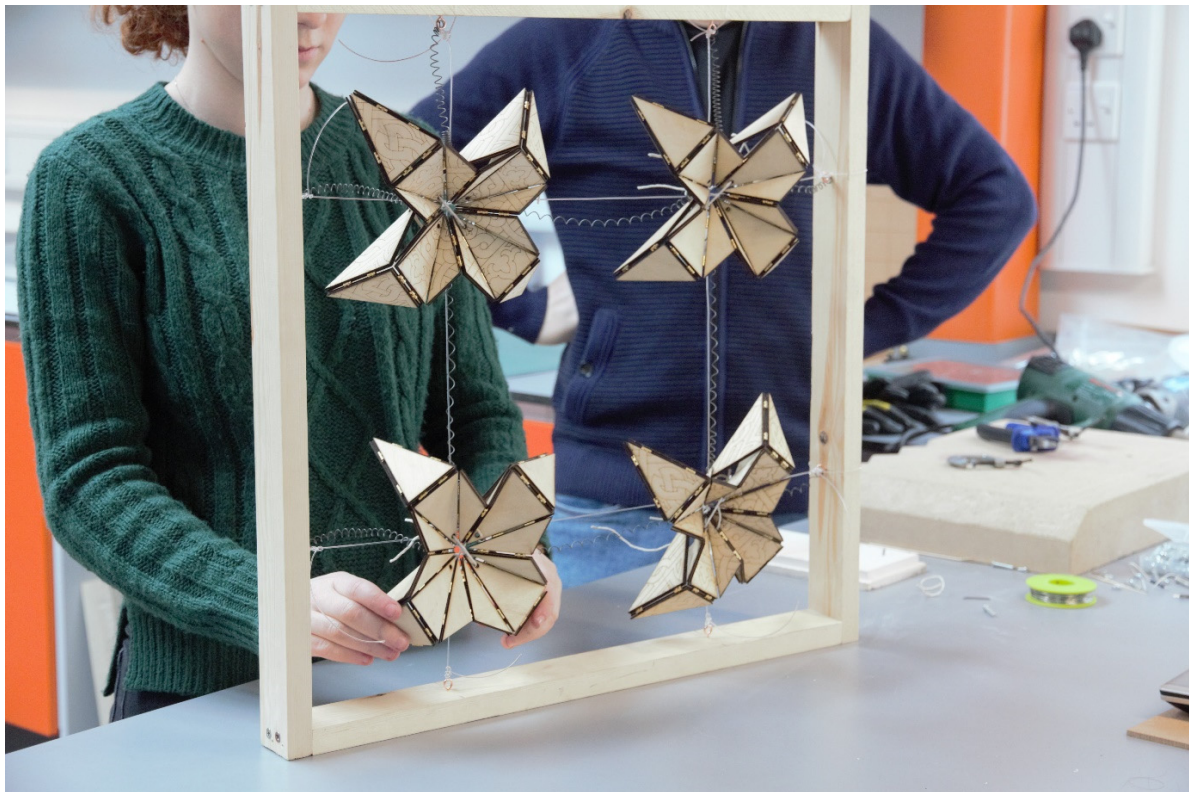


Figure 4-76: Final model development of Prototype B (NCL MArch students stage 5, 2018-19).

#### 4.10.3. Prototype C: Folded Fins

In Prototype C, The solar-shading is made up of multiple fan-shaped origami units, repeated vertically to form a fin, as shown in Figure 4-79. This idea is similar to the Chinese paper lanterns. Each fin is supported by a vertical post fixed from the upper and the lower to the window frame. The vertically grouping concept aims to facilitate the actuation mechanism. In the preliminary phase, students succeeded to actuate the fin using a bilayer fixation technique. They attached a layer of SMP; as shown in Figure 4-78, which expanded the folded structure to shade upon heating. The students intended to couple a rubber band as a counterweight reverse mechanism but they didn't manage to produce a reversible motion. Another trial was made by coupling two SMA springs that work alternatively to achieve system reversibility, as shown in Figure 4-80. The vertical stacking of the folded units using one rigid connector; a vertical rod was a successful choice, but the model failed to



achieve system reversibility. Other ways of return mechanism should be considered, such as material as a return mechanism or applying curved folding to achieve bending active structures. In this case, actuation would inform the form or materiality for proper system workability.

A clear benefit of this prototype is that it can achieve large apertures as the structure totally collapsed into a thin fin or louver. Additionally, it can be positioned horizontally or vertically according to the façade orientation.

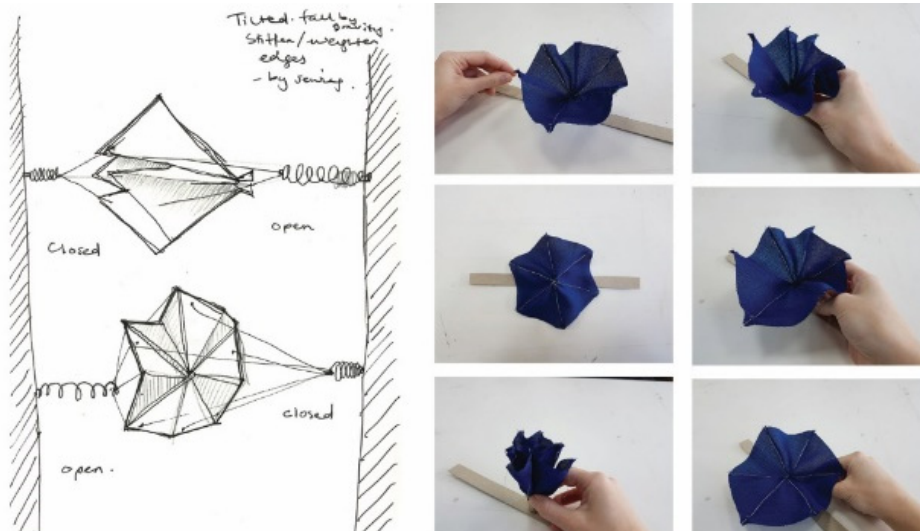


Figure 4-77: Students' sketches and primary models (NCL MArch students stage 5, 2018-19).



Figure 4-78: Multiple fan-shaped origami units and trails of actuation by joining SMP (NCL MArch students stage 5, 2018-19).

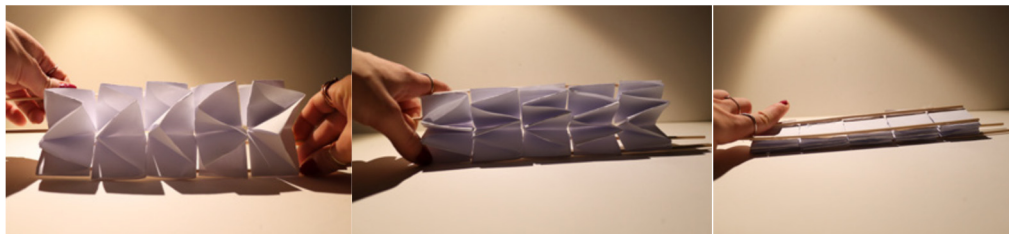


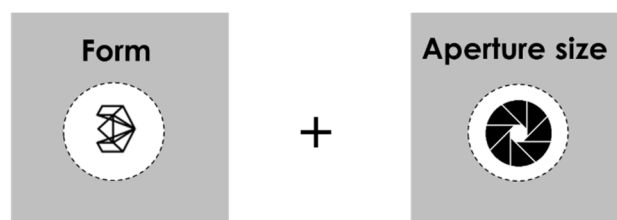
Figure 4-79: Transformation of the vertical fan-shaped origami (NCL MArch students stage 5, 2018-19).



*Figure 4-80: Final model development of Prototype C (NCL MArch students stage 5, 2018-19).*

All the students' models are found successful at one level or another but mostly need some refinements to overcome any discrepancy. It was found that the students didn't dig deep in bio-inspiration as a source of form generation and mainly used origami-inspired forms. The actuation phase, including forward and reverse motion, was the most challenging and needed thorough experimentation. On the whole, more time devoted to actuation and balance of forces for forward and reverse motion can overcome any prototype discrepancy. However, it is found that the process of designing responsive systems is not linear, and different parameters can inform each other in loops until a fully working responsive system is achieved. The linear design process will be further rethought to develop a design framework in chapter seven. The modified design framework intends to leave spaces of freedom for designers to reappropriate the design of the responsive system according to the changing context.

The form and the resulting aperture size are found to be significant variables that can highly affect environmental performance. The form and aperture size variables of an actual prototype system will be selected for the further environmental assessment using CFD simulations in chapter six.



*Figure 4-81: Form and aperture size as tested variables*

#### 4.11. Aperture Size as a Main Feature of Responsive Facade



Variation in aperture size is a key variable for efficient environmental performance for kinetic systems. The solar-shading components vary between two extreme positions, opened and closed modes, with a continuous transition between the two positions. The system should be able to have small apertures to block direct solar radiation which results in thermal discomfort and unwanted glare. Otherwise, the solar-shading units should open autonomously through large apertures to enable external views and daylighting.

The 'aperture size' or the 'opening size' has always been referred to in the environmental studies of static facades as a window-to-wall ratio (WWR). WWR is an important contributor to building energy usage and cooling loads. A. Sherif et al. (2012) used the term 'perforation percentage' to indicate the same definition but on solar screens. It can be defined as *'the percentage of the opening area to the whole area of the facade'*. A. Sherif et al. (2012) evaluated the external wooden solar screens in terms of perforation percentage and depth ratio. Thus, the perforation percentage and depth ratio variables are studied as two different parameters without taking in consideration the sun angles.

The aperture size is a result of the deployability of solar shading component in a specific position. The motion type impacts the range that can be achieved. For example, the traditional louvers or Venetian blinds with one-degree rotation motion can achieve a high range of motion reaching 90% opening with 90° rotation angle when swapped from vertical to horizontal position.

The experimented sliding motion explored in section 4.10.1 achieved an aperture size of 50% maximum due to having a fixed layer behind the activated one. This percentage may change relative to the form and number of flat surfaces that overlap on each other. It can go up to around 85% in case of having a multi-layered sliding screen. Nevertheless, the translational motion has the disadvantage of having friction between layers and represents a flat solar shading which doesn't totally diffuse the direct sunlight.

The vertical folded fins explored in section 4.10.3 achieved the largest aperture of 90% as the structure collapsed into a thin fin and can achieve a fully closed status upon opening. The vertical position of the Umbrella-like mechanisms using straight folding was explored in section 4.10.2, and the curved folding explored in section 4.8.2. The straight crease folding can achieve larger aperture size than the curved folding of four flaps model, as shown in Table 4-4. The straight-crease umbrella-like mechanism can achieve more than 90% aperture size as in Figure 4-82 (a) compared to 70% recorded by curved folding module, as in Figure 4-82 (b).

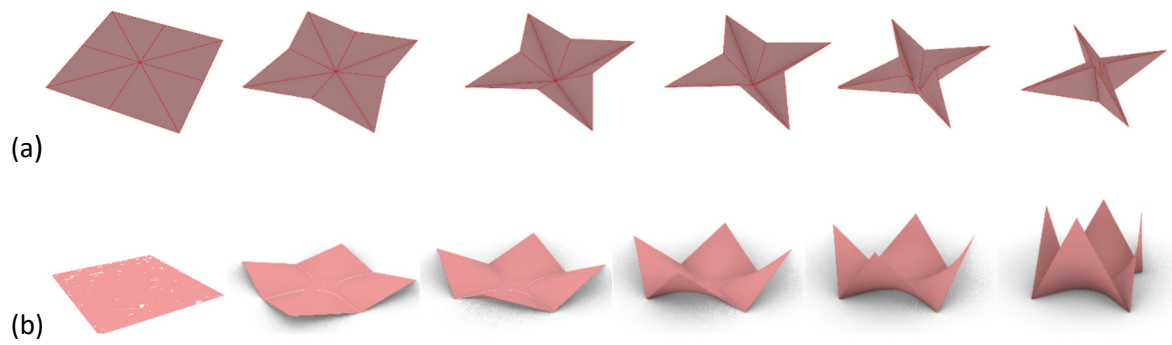


Figure 4-82: Straight line folding and Curved-line folding between opened and closed status.

The vertical circular pattern transforming into rosette pattern explored in section 4.8.4 can achieve 80% aperture size maximum with closed connection areas and a minimum of 35%. The horizontal position of single curved units explored in 4.8.3 has the freedom of adding more horizontal layers to achieve higher levels of opaqueness. The in-between spacing of rows can be minimized with overlapping to achieve less than 10% aperture size. These models can achieve more than 90% aperture size.

Table 4-4: Aperture size from the closed configuration to the opened configuration.

	Steps from closed configuration to opened configuration								
Curved folding									
	0% (Fully Closed)	1.5%	6%	13.4%	23.4%	35.7%	50%	62.1%	70.1%
Umbrella-like									
	0% (Fully Closed)	2%	31.5%	42.2%	52.8%	63.1%	73	82.5	91%
Single curved folding									
	56.15%	61.64%	67.12%	72.6%	78.08%	83.56%	89.04%	94.32%	100%
Soft deformation									
	35%	38.3%	45.8%	48.6%	54.3%	63.6%	60.6%	67.5%	78.5%



The aperture size of the system is a result of all the parameters integrated including; the geometry of the surface, the type of motion, its actuation, its position and the grouping arrangement. However, the required range of aperture can be customized for the responsive solar shading to achieve higher levels of opaqueness or openness by controlling some factors in the actuation and panelization stages; such as:

- Strength of the springs and counter weight reverse mechanism
- In-between spacing between components (rows & columns)
- Using straight or staggered pattern
- Using in-between solid or void connections

These variations can alter many alternatives with different range of aperture size. All these models can be designed to achieve a high range aperture size. The folded straight-crease origami model showed a high range of aperture size. The model can contract to achieve more than 90% aperture size and expand to fully close, which seems promising for environmental performance. Thus, it is selected as an actual prototype for the further environmental assessment using CFD simulations in chapter six.

#### **4.12. Form as a Main Feature of Responsive Façade**



Forms can initially start from a two-dimensional surface or three-dimensional component. Each component can move by rotation, translation or their combinations in specific directions to form the entire façade kinetic composition. Sliding layers or translational movement of components is a valid approach although smaller cellular components are more appropriate for the material-based actuation for aspects related to scale and power of actuators. Internal applied crease patterns enable the units to fold. The outer shape of the surface and the inner crease pattern define the geometrical characteristics of these two-dimensional folding surfaces. The folding approach is popular, simple and derived from origami and bio-inspiration. It should be studied in all states from opened to closed and the intermediate states. Therefore, the form is more than the geometry of the surfaces it extends to include the 'movement itself'; the motion type and direction. It is the most crucial parameter in the design of the system and has a high impact on its aesthetics, workability and environmental performance.

So far, this chapter emphasized the potential of folding throughout its sections. Folded origami units are investigated in this research as they have a high potential as deployable structures as explored in albahar towers designed by Aedas Architects and Un-Fold prototypes (Sharaidin, 2014). Straight-line folded origami was tested by the students in *'folded flowers'* (prototype B) in section 4.10.2 and the researcher in *'Umbrella units'* (exploration one) in section 4.8.1. Similar four-flap curved-line folding with the potential of intrinsic return mechanism was tested by the researcher in 4.8.2. A model is chosen for environmental assessment according to the following criteria:

- High range of aperture size
- Successfully achieve forward and backward motion
- Simple actuation methods
- Simple geometry to be digitally and numerically modelled

Despite of the great potentials of curved folding, the choice of model which will be numerically modelled was limited to a simplified form as the double curved surfaces of soft models require more mesh cells which will be hard to process with the available computational power. As a result, the geometrically simplified version of the umbrella units will be assessed environmentally using fewer creases, as shown in Figure 4-83 and compared with a flat screen.

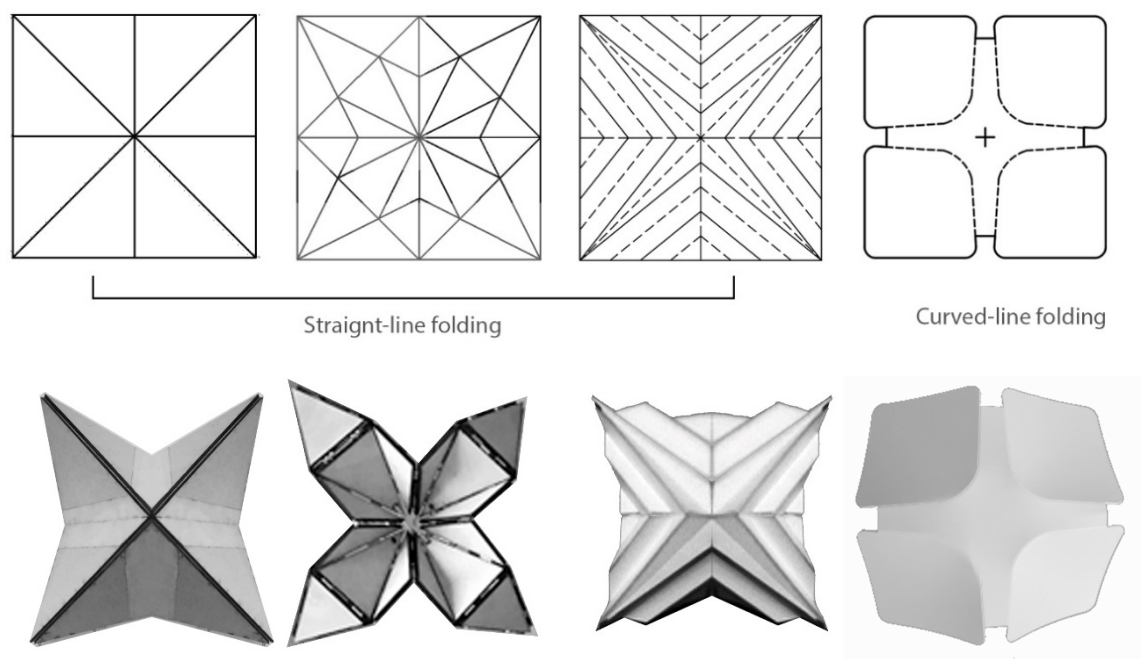


Figure 4-83: Folded origami was tested by the students in *folded flowers* (prototype B) and the researcher in *Umbrella units* (exploration one).

By reflecting on the origami shading modules, the actuators can be located in different locations, as shown in Figure 4-84. (1) Suspended linear actuators, such as Nitinol SMA springs, can be located in-between units coupled with counterweight elements for the reverse mechanism (2) Linear two-way actuators can be located at the wings. (3) SMP attached as a bi-or multi-layered at the crease lines as proposed by Tolley et al. (2014), and Liu et al. (2012), (4) An axial actuator (expand upon heated) can work like a piston as applied in the Kinetic Façade of the CJ R&D Center (Krymsky, 2011).

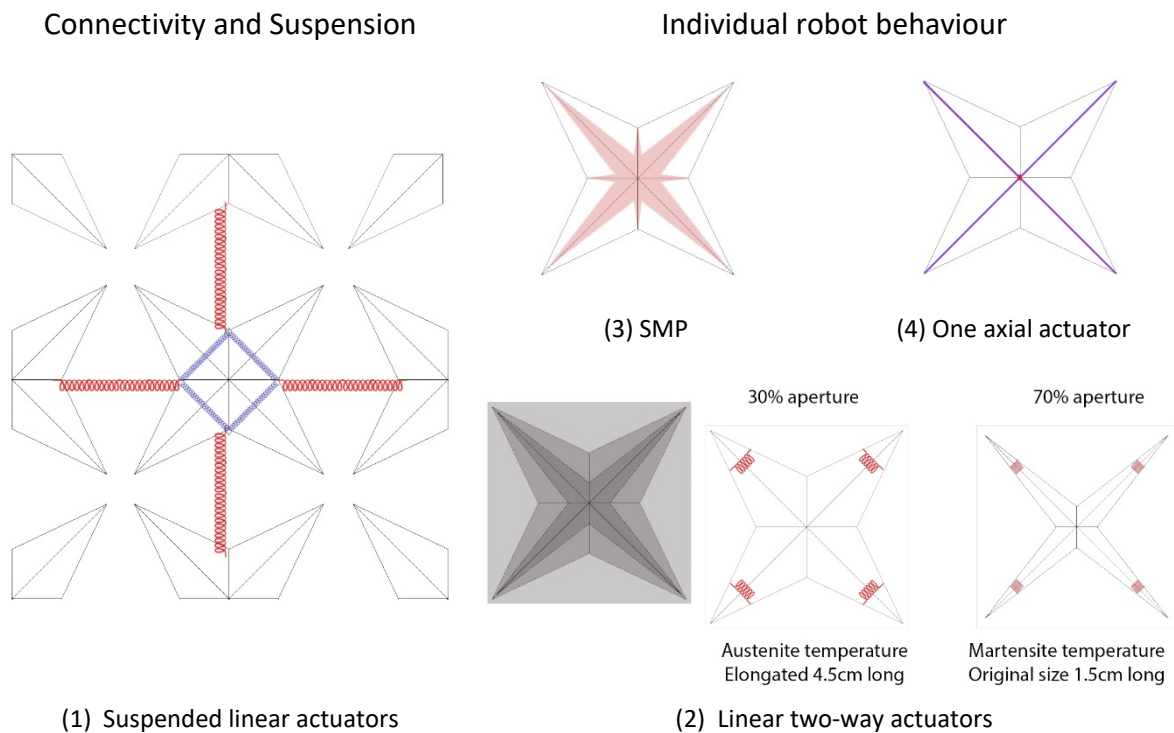


Figure 4-84: Actuation means of Origami star-like solar-shading unit.

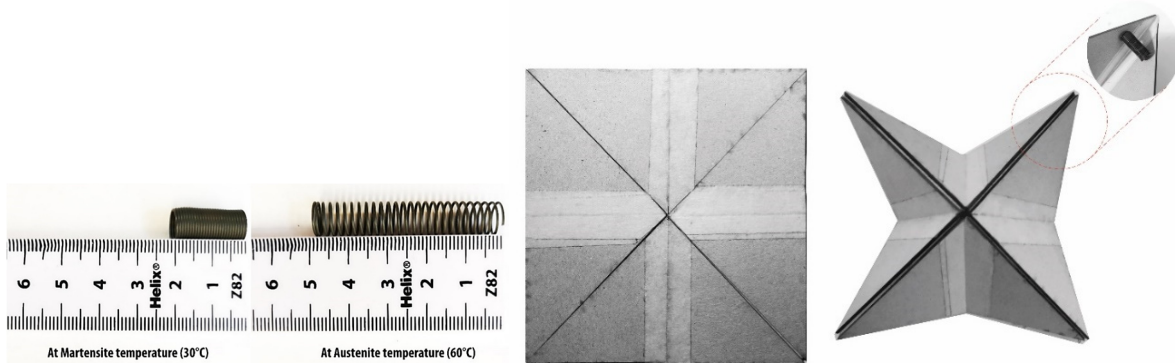


Figure 4-85: Two-way spring actuators at martensite temperature (30°C) at austenite temperature (40°C). They can be located at the four wings of the simulated Origami solar-shading unit.

Apparently, the two-way exposed springs with intrinsic return mechanism have the benefits of maximum sun exposure, high range of motion and allows the solar-shading unit to

act individually as a robot. Besides, components achieve a standalone reversible action which is able to bring the structure back to its memorized position upon cooling. The two-way actuators can elongate from 1.5cm to 4.5cm to transform the unit from opened configuration (70% aperture) to closed configuration (30% aperture) as shown in Figure 4-85. Accordingly, three aperture sizes (30, 50 and 70%) of the origami folded-shading will be modelled numerically to represent the responsive solar-shading system different states for further environmental assessment in chapter six.

#### **4.13. Conclusion**

The creative design processes carried individually by the researcher or as part of the educational activity with students led to a richer experience and deeper understanding of the system potentials and parameters. The chapter explored the technicalities of designing SMA actuators and its integration to activate solar-shading components where the sensors, actuators and structure, are all designed to work in harmony to develop a design framework for responsive solar shading with material-based actuation. This chapter has addressed various approaches and solution techniques using an open exploration by the researcher and the students to overcome the complexity of the interactions between the subsystems in dynamic situations and develop an actual prototype system that can be used in further experiments. The hands-on explorations led to the development of a design process or sequence of activities for designing responsive solar shading. The four proposed design stages are; form generation, materiality, actuation and panelization. However, it is found that the process of designing responsive systems is not linear, and different parameters can inform each other in loops until a fully working responsive system is achieved. The linear design process will be further rethought to develop a design framework in chapter seven. These stages can be summarized as follows:

- FORM GENERATION: Deployable forms can be inspired by nature and origami art which are driven by the potential of acquired motion, aesthetics of form and interest of the designer.

- Plants are inspiring models at any of the four discussed stages. On the geometrical form level, straight folding inspired by the hornbeam leaves can achieve significant contraction while curved folding can create bending-active kinetic systems. On the material selection level, the strong but flexible, pliable and elastic properties of plant leaves led to selections like polymers, polypropylene and felt. On the actuation level, the way the plants are actuated, would guide the type and location of actuators

needed to move, roll and fold the deployable structure. Actuators can be located on the outer edge/periphery of a light-weight soft surface or on the inner ribs or core coupled with bistability principles. On the grouping level, pliable systems encourage the linkage between elements to transfer the motion from one element to their neighbouring elements.

- By applying the *Folding principles*; straight and curved, it was found that the curved folding develops more complex and interesting models from very simple plain sheets and linear actuation. The curved-line folding has the ability to transform a flat surface into a curved 3D shape producing an interesting transformation process. The principles of curved-line folding or curved folding are related to bio-inspiration. They are used to create bending-active kinetic systems similar to plants. Their simplicity and inherited return mechanism characteristics enhance the shape memory performance. On the other hand, the straight crease folding proved to achieve better contractions and higher ranges of motion.

-MATERIALITY: Paper, card, plastic and felt are light-weight passive materials that can sustain bending without stretching or tearing. These type of materials can be precisely shaped into deployable foldable units that can be easily reconfigured by linear actuation. The card is used for straight and curved crease folding. Other rigid thin materials; such as plywood, are connected with flexible joints or metal hinges to be able to fold. Also, polypropylene can be folded into origami and has the advantage of being moisture-resistant and having embedded properties that help the system reversibility. When the curved folding is applied over an elastic material, they work together to help the return mechanism. On the other hand, the flexibility of textiles presents a new generation of soft robotics. Felt proved to have a great potential to be used for bending and soft deformation. Other soft fabrics fixed with wires are capable of producing swelling and curling motion. However, it might not suit the large scale of solar shading application.

-MATERIABILITY: Smart memory alloys can automatically animate a solar-shading component to shade, self-assemble, and change shape. They succeeded to act as material-based actuators which can be tailored to alter complex behaviour. SMA actuators are geometrically simple and silent. They can be clamped at one or both ends, installed as endless, and weaved manually or mechanically. They are simple to attach and easy to create in quantities of tens or hundreds. The challenges of using SMA actuators are: reaching an

equilibrium of forces, making the soft structures structurally stable and identifying their performances in terms of durability, and life cycle assessment.

- ACTUATION: By looking at the fixation methods, the weaving technique failed to achieve major movement changes as the wire is slightly fixed to the unit material and the pre-trained motion of the wire is not transferred to the material. The Knitting technique added a degree of insulation and relatively restricted the movement of the wire. On the other hand, a fully suspended SMA spring actuator that has variable length has a great potential to work as living hinges. The freedom of the hinged actuators can better sense environmental conditions. Springs proved to achieve the best travel distance. The axial spring actuator along the core was able to fully transform the surface from opened to fully closed with a minimal contraction of the spring. Models were activated using electric current and heat gun. Future work can investigate their performance in a real context and direct sun exposure.

- SYSTEM REVERSIBILITY: Four return mechanisms were implemented, (a) the gravity, (b) coupling passive and active elements. (c) The passive elastic material, and (d) the two-way training for SMM in the experimental models. The gravity and material as a return mechanism are simple and promising. It has to be designed with high sensitivity considering the balance between the force of the wire and the weight of the material. These techniques enable the single unit to act on its own without affecting other neighbour units. Gravity can be only considered in the horizontal position where the active material moves it upwards and uses the gravity to bring it back to its original position. Hence it doesn't suit vertical applications.

- PANELIZATION: It became increasingly clear that the arrangement of the responsive components has a huge impact on their functionality and efficiency. The method of actuation and location of actuators highly affect the resulting pattern, its aesthetical qualities and workability. In case of using gravity, elastic material or two-way SMM as a return mechanism, each unit can move independently from any neighbor unit. On the other hand, connecting smaller components enables the system to work collectively. This takes place by allocating actuators or counter elements in-between the components or joining them with solid connectors.

In conclusion, this chapter proved that the adoption of lightweight and elastic materials integrated with material-based actuation is a significant solution to perform a movement in

solar shading devices. This chapter highlighted some insights for responsive systems, which are:

- a) the potentials of straight-line folding where extra folds can improve deployability, rigidity and contraction,
- b) the potentials of curved-line folding coupled with elastic materials,
- c) the potentials of SMA spring actuators for their large travel distances,
- d) the potentials of soft deformation using fabrics especially felt, and
- e) the potentials of materials as a return mechanism.

The prototypes were studied on small units of 10cm x 10cm which can be 'doubled or up-scaled' later. Issues of scalability might be preventing the application of smart materials on large architectural scale. There are limitations due to material characteristics of lightweight passive materials and smart materials. The size and characteristics of such actuators are limited to the market availability and manufacturers production. This limitation can be overcome by increasing the number of embedded or attached actuators which are needed to acquire the required motion and achieve the system balance at larger scale. Even though such systems may have a limitation for a maximum module size but it can be repeatedly and endlessly arrayed.

An integrated DSF system is proposed to protect the responsive solar shading system from the potential damage of atmospheric agents; such as bad weather and pollution, and internal interference for more efficiency and durability. Moreover, DSFs can help the system to achieve the activation temperatures needed to activate the SMM.

From the hands-on exploration, the '*form*' and the resulting '*aperture size*' are found to be significant variables that can highly affect environmental performance. An actual prototype of origami folded solar-shading with three aperture sizes (30, 50 and 70 %) is selected to bring experimental and environmental together through the integration of material thinking and simulation of real environment performance. Moving on now from experimental component design to environmental design and simulation to environmentally assess the responsive solar shading system performance within their potential context of operation; encased in a DSF in a hot arid climate and evaluate the effects of different aperture sizes and forms of the system, through coupled simulations, on cavity airflow and internal glazing thermal gain.



## Chapter 5 . ENVIRONMENTAL DESIGN AND MODELLING

### Computational fluid dynamic modelling and method validation

#### 5.1. Introduction

Chapters five and six represent the climate-based approach by conducting CFD numerical modelling. They will focus on the simulation of solar-shading devices in their context of operation; encased in a DSF in a hot arid climate. The behaviour of DSF is complex due to the multiple coupled physical phenomena that take place inside the cavity. These phenomena are air movement and heat convection, conduction, short- and long-wave radiation (Safer et al., 2005). These combined phenomena can lead to laminar, turbulent or a mixture of flow regimes inside the cavity (Z. J. Zhai et al., 2007). CFD analysis is one of the most significant tools to predict the DSF behaviour and assist architects with environmental-based decisions during the design process (Pasut & De Carli, 2012). Considerable literature used CFD to study the behaviour, features and energy consumption of DSFs (Baldinelli, 2009; Coussirat et al., 2008; Hamza & Underwood, 2005; Hazem et al., 2015; Ioannidis et al., 2017; Iyi, 2013; Iyi et al., 2014; Ji et al., 2007; Y. Li et al., 2017; Parra et al., 2015; Pasut & De Carli, 2012; Safer et al., 2005; Velasco et al., 2017). Specifically, over the last two decades, most research in buoyancy-driven flow has emphasized the need to use CFD to provide numerical predictions of airflow and detailed quantitative knowledge of heat transfer processes in buildings, and accordingly the heating and cooling demands.

This chapter starts by introducing Computational fluid dynamics (CFD) simulations as a tool for assessing integrated DSF and reviews critically simulation methods used in literature to environmentally assess DSF integrated with solar shading devices; specifically Venetian blinds. The simulation of kinetic folded shading systems is similar to simulation concept of Venetian blind shading system which examine the change of the blind position and the slat tilt angle, however it is applied to different form, motion and resulting aperture. It extends to outline the best practice guidelines defining the computational domain, its size, boundary conditions, and mesh. It presents a sensitivity analysis for CFD different geometrical modelling and setup variations in order to set guidelines for the CFD simulation setup to reach results with high accuracy.

The well-cited experimental case of Mei et al. (2007), which was conducted using a large-scale simulator at Loughborough University, is used for validating this study. Numerical

modelling is carried as a code validation for this case. It tests the main variables affecting the performance of the shading system in the DSF to conclude the most recommended procedure for further investigation by CFD simulation. These variables are, determining the level of geometrical model detailing, extending the domain to include the external environment, representing solar simulator, and the selection of turbulence and radiation models. *In doing so, the best working* CFD setup will be applied for integrated DSF with responsive solar shading devices in *Chapter Six* to provide architects with environmental-based decisions during the design process.

## **5.2. Computational Fluid Dynamic Modelling**

In general, CFD predicts turbulent flows through three approaches: direct numerical simulation (DNS), large-eddy simulation (LES), and Reynolds-averaged Navier-Stokes (RANS) equation simulation with turbulence models (Z. J. Zhai et al., 2007). For the airflow study in enclosed cavities, the mean air parameters are more effective than instantaneous turbulent-flow parameters. Hence, the interest is stronger in solving the RANS equations with turbulence models that can quickly predict air distributions. The RANS approach calculates Reynolds-averaged variables statistically and uses different turbulence models to study the mean airflow. Despite the challenges associated with turbulence modelling, the RANS approach is commonly used in modelling airflows in enclosed environments due to its significantly smaller requirements of computer resources (Z. J. Zhai et al., 2007).

The rectangular cavity of DSF with differentially heated walls generates a buoyancy-driven flow in the cavity. Predicted results depend on the appropriate selection of turbulence modelling method, which will directly affect the simulation accuracy and efficiency. In DSFs, the large exposed glass areas increase the total transmitted solar gains (g-value). The g-value of glass is the coefficient that measures the solar heat allowed in through the glazing or what is called the solar energy transmittance. Focusing on the heat transfer in DSF, it has been found that the cavity's net heat gain is mostly dominated by transmitted solar radiation (Mei et al., 2007). The radiation effects should be accounted for when it is equal or greater than the convective and conductive heat transfer rates. Therefore the turbulence modelling should be coupled with radiation modelling. The heat exchange between the glazing elements and the surrounding by conduction, and convection are discussed in Appendix D, while the following section will focus on radiation as the main contributor to the heat transfer problem rather than conduction and convection.

### *5.2.1. The nature of coupled fluid dynamics and heat transfer*

Radiation energy is created by the atoms or molecules of the material moving and being transmitted in the form of electromagnetic waves. Heat exchange occurs from higher temperature to lower temperature and is not bound to a medium. The process depends on the temperature distribution, the optical properties and the surface geometry. Generally, using glass with large exposed areas for buildings in hot climates would increase total transmitted solar gains (g-value) by several means. Practically, transmitted rates depend strongly on several factors, including properties of the glass (transmittance, reflectance & conductance) and ambient conditions (solar irradiance, incident angles). Optical properties of glass rely on the angle of incidence as solar transmissivity would decrease by increasing this angle (Baldinelli, 2009). On the other hand, solar irradiance relies considerably on the site's coordinates, season and daytime. Solar irradiance consists of the beam and diffuse components (Amaireh, 2017).

The selection of the radiation model depends on several factors; such as the optical thickness, the presence of scattering effects, the emissivity, and the nature of the surface and the fluid involved (Coussirat et al., 2008). To account for radiation, radiative intensity transport equations (RTEs) are solved. Local absorption by fluid and at boundaries couples these RTEs with the energy equation. The selection of the radiation model enables radiative heat transfer. Five radiation models are available in FLUENT as will be discussed later in section 5.3.4. The importance of radiation phenomena in the heat transfer mechanism present in these surfaces is greater than the contribution of the conduction and convection phenomena. This conjugate heat transfer problem that includes solar radiation fields along with convection and conduction fields is solved using a ray-traced solar model coupled with longwave radiation model.

The complex behaviour of DSF results from the coupled physical phenomena of airflow and heat transfer within the cavity as shown in Figure 5-1. As shown on the right, the heat exchange between the glazing elements and the surroundings occurs by conduction, convection and radiation, while the airflow can be laminar, turbulent or a mixture of flow regimes inside the cavity as shown on the left. These coupled physical phenomena result in buoyancy-driven flow in DSF cavity.

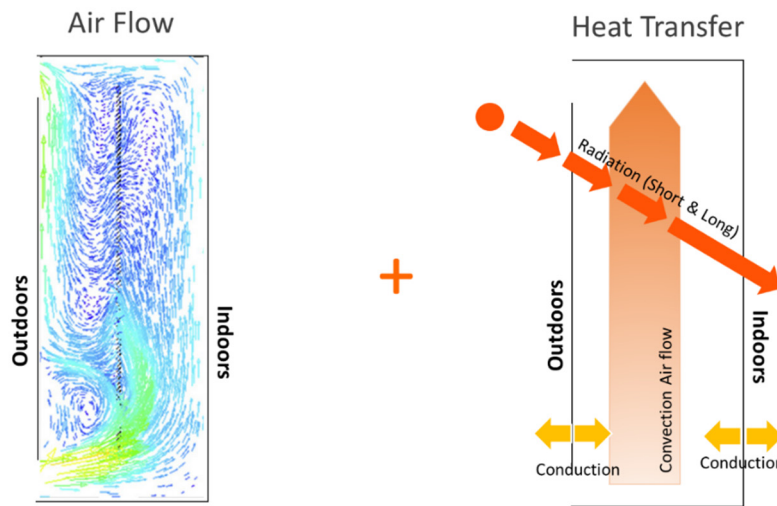


Figure 5-1: The coupled physical phenomena of airflow and heat transfer within the cavity. On the right, the heat exchange between the glazing elements. On the left, the airflow which can be laminar, turbulent or a mixture of flow regimes.

The literature review has shown many different approaches in numerical simulations of DSF equipped with solar shadings. This is due to the high range of possible DSF and solar-shading geometrical configurations as well as the different heat transfer modes, such as; natural or forced convection, with or without radiation participation (Safer et al., 2005). Some researchers couple Building Performance simulation with CFD (L. Wang & Wong, 2009) while others depend on coupled thermo-fluid-dynamics problems using sub-models of radiation and turbulence to capture the various thermophysical properties of DSF configurations and turbulence models (Coussirat et al., 2008).

For the performance investigation of the proposed integrated, responsive solar-shading system and how factors such as aperture size, and form may influence the heat transfer problem and turbulence in the cavity, the simulation tools, their setup and setup for similar cases from the literature will be studied. Extensive research has been conducted on DSF equipped with solar shadings; specifically Venetian blinds; using CFD. These researches proved that factors such as blind position (Gratia & De Herde, 2007; Jiru, Tao, & Haghighat, 2011) slat tilt angle (Safer et al., 2005), colour and form of the blind (Amaireh, 2017; Gratia & De Herde, 2007) and material of the blind, have influenced the airflow and heat transfer in the cavity.

Ye, Harrison, Oosthuizen, and Naylor (1999) studied the influence of the position of blinds inside the DSF's air cavity and the slat tilt angles. The results have shown that the presence of the Venetian blinds led to a 75% reduction in internal heat loads and 35%

enhancement in natural ventilation flow. However, the results cannot be easily generalised because the simulations were carried out for the laminar flow only. Although the Global heat transfer coefficients were also obtained, the study ignored the radiation exchange between the internal glazing and solar shading as well as the solar energy absorption of the solar shading. Similarly Safer et al. (2005) conducted numerical simulation for a mechanically ventilated DSF equipped with Venetian blinds to investigate the influence of the slat tilt angles in the range of 0 - 60°, numerous blind positions inside the DSF channel, and the impact of the different air outlet positions on the airflow and heat transfer within the cavity. The study used the realizable k- $\epsilon$  turbulence model but didn't take solar radiation into account of heat transfer modelling.

Pasut and De Carli (2012) simulated the DSF performance using CFD with RNG k- $\epsilon$  and SST k- $\omega$  for turbulence modelling, but the solar radiation was not directly simulated. Alternatively, the study used the surface temperatures measured by the experimental apparatus as boundary conditions.

L. Wang and Wong (2009) argued that coupled simulations between building simulation (BS) and CFD can effectively improve the speed and accuracy in predicting indoor thermal environment for natural ventilation studies. The study compared between coupled simulation and full CFD simulation. The study performed coupled simulations between FLUENT and ESP-r for the single-zone scenario. The coupling strategy between BS and CFD program depends on feeding the surface temperatures for each wall from BS into CFD simulation. Standard k- $\epsilon$  two-equation model is used for indoor CFD simulations, and realizable k- $\epsilon$  two-equation model is used for full CFD simulation. The study concluded that coupled simulation can better predict the indoor airflow simulation than BS program alone and agreed well with the full CFD simulation. However, there is a gap in computing speed between energy simulation (ES) and CFD programs. Z. Zhai, Chen, Haves, and Klems (2002) developed simplified coupling strategies to minimize the number of CFD runs. The study used simpler turbulence models (zero-equation turbulence model) to reduce the computing time of CFD programs directly. The study discussed the application of 'Virtual Dynamic Coupling', presented by Qingyan and Van der Kooi (1988), between CFD program with the energy simulation program, where temperatures are one of the information exchanged between the two software. The coupling strategies have been implemented by using the EnergyPlus and MIT-CFD program.

A different approach of coupling radiation and turbulence in CFD modelling was investigated for more accurate results. Coussirat et al. (2008) compared different radiation and turbulence models. From the results, the RNG k- $\epsilon$  turbulence model and standard k- $\epsilon$  turbulence models seem to perform better than the other turbulence models while the P-1 radiation model seems to better predict the temperature of the solid surfaces present in the double façade.

Jiru et al. (2011) investigated the airflow and heat transfer for a DSF system equipped with a Venetian blind using the RNG k- $\epsilon$  turbulence model for a three-level combination of slat tilt angle and blind position. The thermal radiation heat transfer between the facade and the blind surfaces is calculated using surface-to-surface (S2S) radiation model assuming gray-diffuse surface. Their results show that the presence of Venetian blinds influences the surface heat transfer coefficients and the temperature and the air distribution in the DSF system. Also, the change in the blind position (outer, middle, and inner) has more effect on the distribution of temperature, velocity, and heat transfer compared to the change in the slat angles (0°, 45°, 90°). Another research by Manz et al. (2004) coupled surface-to-surface (S2S) radiation model with revised k- $\epsilon$  turbulence model to assess the cavity performance and compare it with the experimental database.

As will be mentioned later in the validation section, Ji et al. (2007), Iyi et al. (2014) Varughese and John (2016) and Amaireh (2017) coupled the turbulence models with discrete ordinate (DO) radiation non-gray model with two bands, solar and thermal, from 0-2.7mm and 2.7-1000mm to represent the spectral radiation. Parra et al. (2015) and (Velasco et al., 2017) used P1 radiation model for coupling radiation in Ansys. This coupling method was also applicable for more recent investigations of innovative solar shading materials to implement renewable energy resources. Lamnatou, Mondol, Chemisana, and Maurer (2015) who reviewed the literature of building-integrated solar thermal (BIST); such as (photovoltaics PV) and (Photovoltaic/Thermal: PVT), found that a wide range of methods have been adopted covering from finite-difference and CFD to ray-tracing tools for optical simulation. Liao, Athienitis, Park, Collins, and Poissant (2005) studied the conjugate heat transfer with a 2D CFD model while the realizable k- $\epsilon$  model was used to simulate the turbulent flow and convective heat transfer in the cavity, in addition to buoyancy effect. A recent innovative integrated system by Y. Li et al. (2017) presented an integrated DSF with phase change material (PCM) solar shading system. The study simulates the airflow and temperature distributions in the

integrated DSF system using ANSYS FLUENT 14.0 where the RNG k- $\epsilon$  turbulence model and discrete ordinates (DO) radiation model were selected. The materials' properties of the phase change material (PCM), as a thermal energy storage medium were taken in consideration. The study found that the PCM blind can absorb large amount of excessive heat in the cavity compared to the aluminium blind. These (PCM) solar shading system is able to minimize the overheating effect in DSFs.

Having discussed how researchers in literature represented radiation participation and coupled it with turbulence modelling in CFD, the next section will discuss CFD validation criteria and methods for similar problems.

#### *5.2.2. Method validation*

CFD simulations are embedded with uncertainties and approximations. The digital model is a computational version used to simulate a solution of a modelled real problem. The accuracy of the simulated results can be affected by the uncertainties in the CFD simulation. Additionally, all computers do their operations with limited precision, and the number of significant digits degenerates as operations are performed. As a result, errors and uncertainties are accumulated. However, a discrepancy or error margin is acceptable. Summers, Hanson, and Wilson (1986) suggested a 20% discrepancy as an acceptable error in environmental design. The study argued that this level of accuracy can be used as a rough accuracy measure expected in a numerical simulation which is the same discrepancy between wind-tunnel and full-scale measurement. A model accuracy criteria was set by Zhang, Zhang, Zhai, and Chen (2007) to evaluate the difference between experimental data and CFD results in enclosed environments. The model quantifies the relative error between prediction and measured points. If this error is less than 10% the results are good, (A), and between 10% and 30% the results are acceptable (B). Pasut and De Carli (2012) added a B+ rating for the results between 10% and 20% to improve the results' legibility. Zhang et al. (2007) suggested a 30% discrepancy as an acceptable error in enclosed environments. Due to the errors and uncertainties in CFD simulations, validation studies are essential for assessing the quality of the results and reducing the uncertainties in CFD simulations. It can be argued that reproducing the naturally ventilated DSF of Mei, 2007 experimental case numerically would be adequate for validating similar CFD simulation results later in this research.



Validation assessment determines whether the simulation agrees with measurements of a real physical case. Thus, CFD simulations must be validated by comparing simulation results with measurements of the experimental apparatus. Some reference cases from literature are used for the validation purposes of naturally and mechanically ventilated DSF with Venetian blind; Safer et al. (2005) as numerical mechanically ventilated case, Manz et al. (2004) as experimental mechanically ventilated case, and Mei et al. (2007) as experimental naturally ventilated case, and

- Validation Case 1: Safer et al. (2005)

Safer et al. (2005) conducted a 3D simulation with a CFD for a DSF equipped with Venetian blinds. Although his research was carried in the absence of the experimental tests, it is a main reference in the field. A homogeneous porous media model was used to represent the effect of the shading system presence to reduce the number of cells, thus the computing time. The research conducted comprehensive numerical modelling of radiative and convective heat transfer of a compact DSF equipped with Venetian blind. The results found that the radiative heat transfer was very important for the regulation of transmitted solar radiation to the inside. Hazem et al. (2015) validated Safer et al. (2005) model. The study used the realizable  $k-\epsilon$  turbulence model and discrete ordinates (DO) radiation method. The DO was applied using a two-band spectral model to solve the RTE and to quantify the solar and thermal radiation. The study tested the solar transmission as a result of variation in the solar radiation, the incidence angle, the slat angle and the material emissivity.

- Validation Case 2: Manz et al. (2004)

Manz et al. (2004) carried an experimental study for mechanically ventilated facades, supported by a well detailed CFD simulation. The experimental case by Manz et al. (2004) has been used for validation by a research group from Polytechnic University of Catalonia. Coussirat et al. (2008) studied the performance and influence of numerical models on CFD simulations to validate Manz case in Mediterranean climates. A pressure-based double-precision solver was selected in Ansys fluent. The study compared five different turbulence models and three different radiation models. The results recommended the P-1 radiation model for its better prediction of the solid phases' temperature present in the DSF and the RNG  $k-\epsilon$  and standard  $k-\epsilon$  turbulence model.

Consequently, Guardo et al. (2011), Parra et al. (2015) and Velasco et al. (2017) used the same method to investigate the effects of different parameters of integrated DSF with Venetian blinds. Mainly their research coupled RNG k- $\epsilon$  and P1-Radiation using a pressure-based double precision transient solver in Ansys Fluent. In these cases, the solar radiation dynamics that include direct, diffuse and ground-reflected radiation were directly linked with the solar calculator.

- Validation Case 3: Mei et al. (2007)

Mei et al. (2007) investigated the performance of naturally ventilated DSF box window experimentally under good control of the key environmental factors. The experimental case tested the DSF in a full-scale solar simulator at Loughborough University. The solar simulator, which is located in front of the facade generates the solar heat flux. The DSF consists of a single outer glazing element; Venetian blinds and double inner glazing.

A series of publications by (Ji et al., 2007, 2008; Mei et al., 2007) were published by the research group to compare the experimental case with CFD tested cases. These represent benchmark test cases. Ji et al. (2007) coupled k- $\omega$  based turbulence model with Monte Carlo (MC) radiation model using (Ansys CFX 2005). Other researchers, such as; Pasut and De Carli (2012), Iyi et al. (2014), Varughese and John (2016) and Amaireh (2017) used Mei et al. (2007) well-documented case for the validation of their numerical models.

As seen in Table 5-1, a considerable amount of literature has been published on assessing DSF performance of the three cases using CFD. Table 5-1 reviews the setup used by different researches to validate the three cases in terms of the solver setup, the size of the domain, the applied turbulence and radiation model.

By looking at the three cases, Safer et al. (2005) case is a 3D simulation which was carried in the absence of experimental tests, Manz et al. (2004) case is an experimental mechanically ventilated DSF, while Mei et al. (2007) case is an experimental naturally ventilated DSF equipped with shading devices. Mei's case is similar to the proposed DSF integrated with a responsive solar-shading system case in terms of natural ventilation and integrated shading. The naturally ventilated DSF is chosen to diminish overheating problems in summer and contribute to energy savings in winter. Hence, the validation work will be carried on Mei et al. (2007) experimental case.

Table 5-1: Overview of CFD simulation modelling for integrated DSF with shading devices.

Case 1 used for Validation (Numerical): (Safer et al., 2005)						
Ref.	3D/2D	External environment	Turbulence modelling	Radiation modelling	Solver	solution scheme
(Hazim, A. et al., 2015)	2D	Indoor Modelling	Realizable k- $\epsilon$ turbulence model	Discrete Ordinate Model	Steady-state simulation	SIMPLE solution algorithm
Case 2 used for Validation (Experimental): (Manz et al., 2004)						
Ref.	3D/2D	external environment	Turbulence modelling	Radiation modelling	Solver	solution scheme
(Manz et al., 2004) *	2D	Indoor Modelling	Revised k- $\epsilon$ model	Surface-to-surface radiation model	Steady-state simulation	SIMPLE solution algorithm
(Coussirat et al., 2008)	3D (1 cell)	Indoor Modelling	RNG k- $\epsilon$ model	P1 radiation model	Transient simulations (time step=1h)	PISO pressure velocity coupling
(Velasco et al., 2017)	3D	Indoor Modelling	RNG k- $\epsilon$ model	P1 radiation model	Transient simulations (time step=120 s)	PISO pressure velocity coupling
(Parra et al., 2015)	3D	Indoor Modelling	RNG k- $\epsilon$ model	P1 radiation model	Transient simulations (time step=600 s)	PISO pressure velocity coupling
Case 3 used for Validation (Experimental): (Mei et al., 2007)						
Ref.	3D/2D	external environment	Turbulence modelling	Radiation modelling	Solver	solution scheme
(Ji, et al. 2007), (Ji, et al. 2008)	2D	Indoor	k- $\omega$	Monte Carlo (MC)	Steady-state simulation	SIMPLE solution algorithm
(Pasut and De Carli, 2012)	2D & 3D	Indoor / coupled Indoor and outdoor	RNG k- $\epsilon$ with enhanced wall function and SST k- $\omega$	Applied Mei's surface temperature as boundary conditions	Steady-state simulation	SIMPLE solution algorithm
(Iyi, et al. 2014)	3D	Indoor / coupled Indoor and outdoor	lauder-sharma low-Re	Discrete Ordinate Model	Steady-state simulation	SIMPLE solution algorithm
(Varughese and John, 2016)	2D	Indoor Modelling	k- $\epsilon$ model	Discrete Ordinate Model	Steady-state simulation	SIMPLE solution algorithm
(Amaireh, I., 2017)	2D	Indoor / coupled Indoor and outdoor	RNG k- $\epsilon$ model with enhanced wall function and SST k- $\omega$	Discrete Ordinate Model	Steady-state simulation	SIMPLE solution algorithm

As shown in Table 5-1, Mei et al. (2007) case study was validated in several studies; thus there is a good amount of data available on the case experimentally and numerically. The following part discusses the challenges met during the simulation process, including solar simulator representation, the level of geometrical model detailing, domain size, selection of turbulence and radiation models.

### 5.3. Case of Mei et al. (2007)

Mei et al. (2007)'s naturally ventilated DSF is discussed thoroughly to be simulated later in the next section. The experimental case tested the DSF in a full-scale solar simulator located in front of the facade as shown in Figure 5-2. The DSF consists of a single outer glazing element; Venetian blinds and double inner glazing. The outer skin of the facade is a single 12mm thick clear glass pane. The external glass area is 1.28m and 1.91m high. The inner glazing consists of double glass panes each 6mm thick, separated by an air cavity of width 16mm. The dimensions of the inner skin are 1.38m  $\times$  2 m and the glass area is 1.22m  $\times$  1.85m. Both the air intake and exhaust of the DSF are designed as a commercial grille arrangement to permit airflow through the cavity. The grilles are 0.24m high and 1.45m wide. Each grille (inclined at 30° to the horizontal line) has three 0.045m high spaces for air ingress and egress. The sun-shading blind is a Venetian type blind. It is made of aluminium and is 2.1m high and 1.45m wide. The blind blades are 80mm wide and located at one third of the cavity width as measured from the outer skin. Table 5-2 and Figure 5-3 illustrates the geometrical dimensions and configuration of the cavity.



*Figure 5-2: On the left: Large Scale Solar Simulator, showing lamp array. On the right: The white blinds installed inside the cavity (Mei et al., 2007).*

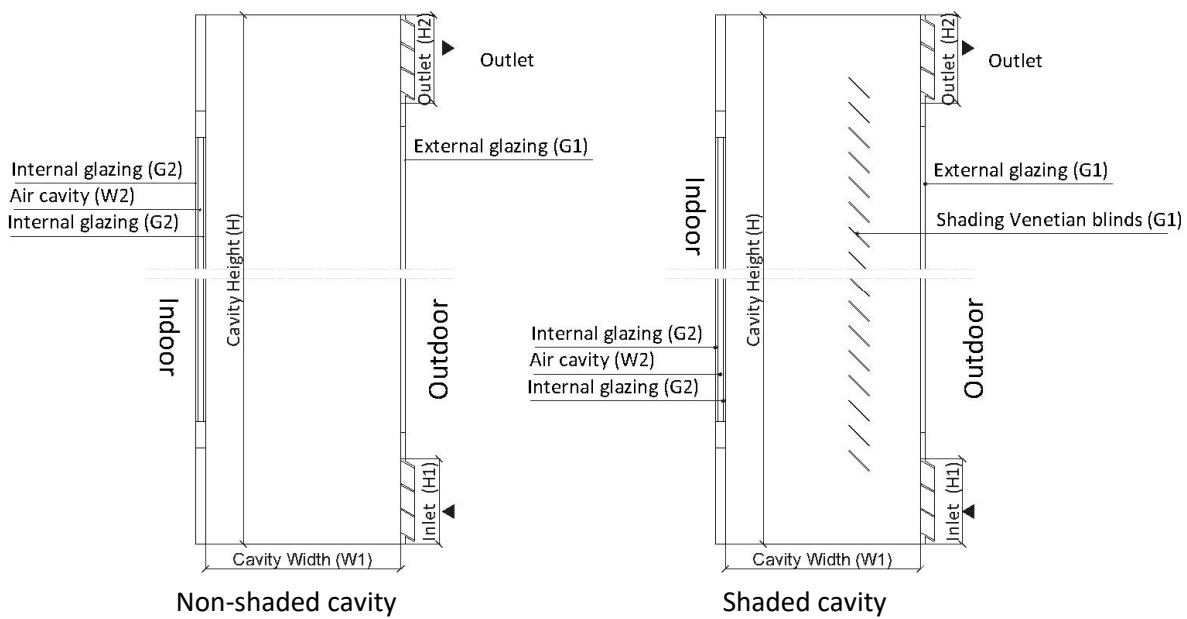


Figure 5-3: Geometrical model of non-shaded and shaded cases of Mei et al. (2007) DSF.

Table 5-2: Dimensions of Mei et al. (2007) DSF.

Cavity height	Cavity width	Inlet height	Outlet height	External glazing thickness	Internal glazing thickness	Air cavity	Internal glazing thickness
H (mm)	W1 (mm)	H1 (mm)	H2 (mm)	G1 (mm)	G2 (mm)	W2 (mm)	G3 (mm)
2450mm	550mm	240mm	240mm	12mm	6mm	16mm	6mm

The experimental study explored the DSF performance under many parameters, as shown in Table 5-3. In the experiments, measured irradiances were varied from 187 W/m<sup>2</sup> to 715 W/m<sup>2</sup>. The outdoor air temperature was set at 12°C, 20°C and 30°C, while the indoor air temperature was set to 20°C.

Table 5-3: Mei's experiment parameters.

Study parameters	
Irradiance	187 W/m <sup>2</sup> , 360 W/m <sup>2</sup> , 540 W/m <sup>2</sup> , and 715 W/m <sup>2</sup>
Outdoor temperature	12°C, 20 °C, & 30°C
Indoor temperature	20°C

A series of publications by the research group were published to compare the experimental case with CFD tested cases (Ji et al., 2007, 2008; Mei et al., 2007). This represent a benchmark test case. Ji et al. (2007) coupled k- $\omega$  based turbulence model with Monte Carlo (MC) radiation model using (Ansys CFX 2005).

Other researchers, such as; Pasut and De Carli (2012), Iyi et al. (2014), Varughese and John (2016) and Amaireh (2017) used Mei et al. (2007) case for the validation of their numerical

models. Pasut and De Carli (2012) compared RNG  $k-\epsilon$  and SST  $k-\omega$  turbulence models and imposed the surface temperatures measured by the experimental apparatus as boundary conditions in CFD. The study recommended using RNG  $k-\epsilon$  turbulence model for good results and good simulation stability. Iyi et al. (2014) and Amaireh (2017) have coupled the turbulence models with DO radiation model using Ansys fluent to compare the results with Mei et al. (2007) experimental data. Both of the researchers used the fixed temperature of 20°C for indoor and outdoor temperatures and fixed solar radiation 715  $\text{W/m}^2$  to validate their numerical models and compare the results of different tilt angles with the case recorded results. They used DO radiation non-gray model with two bands, solar and thermal, from 0-2.7 $\mu\text{m}$  and 2.7-1000 $\mu\text{m}$ . The simulations were carried under relaxation factors using SIMPLE algorithm. Iyi et al. (2014) used lauder-sharma low-Re model. Amaireh (2017) compared standard  $k-\epsilon$ , RNG  $k-\epsilon$ , realized  $k-\epsilon$ , standard  $k-\omega$  and SST  $k-\omega$  and recommended both RNG  $k-\epsilon$  and SST  $k-\omega$  for such problems, which are generally recommended for natural convection in cavities. Iyi et al. (2014) used solar load model to simulate the direct illumination effects resulting from solar simulator.

Varughese and John (2016) modelled turbulence using low Reynolds number of  $k-\epsilon$  model and solar radiation using DO model. The semi-transparent glazing elements have been modelled by “Two Band” spectrum model. The first represented the solar band (0 – 2.7 $\mu\text{m}$ ) and the second represented the thermal band having wavelength greater than 2.7  $\mu\text{m}$ . All materials were participating in radiation. The solar radiation for the solar band is taken as 720 $\text{W/m}^2$ . The researcher considered only direct radiation and neglected the diffuse radiation and the scattering effect. The study identified the influence of the inlet velocity variation on airflow and heat transfer. It analysed the heat flux penetrating through the inner surface under five different inlet velocity, ranging from 0.07 to 0.35 m/s. The results found that the increase in the inlet velocity decreases the slat temperature. Figure 5-4 shows the apparatus setup of Mei et al. (2007) and the boundary condition setup by Ji et al. (2007), Iyi et al. (2014), Amaireh (2017), and Varughese and John (2016).

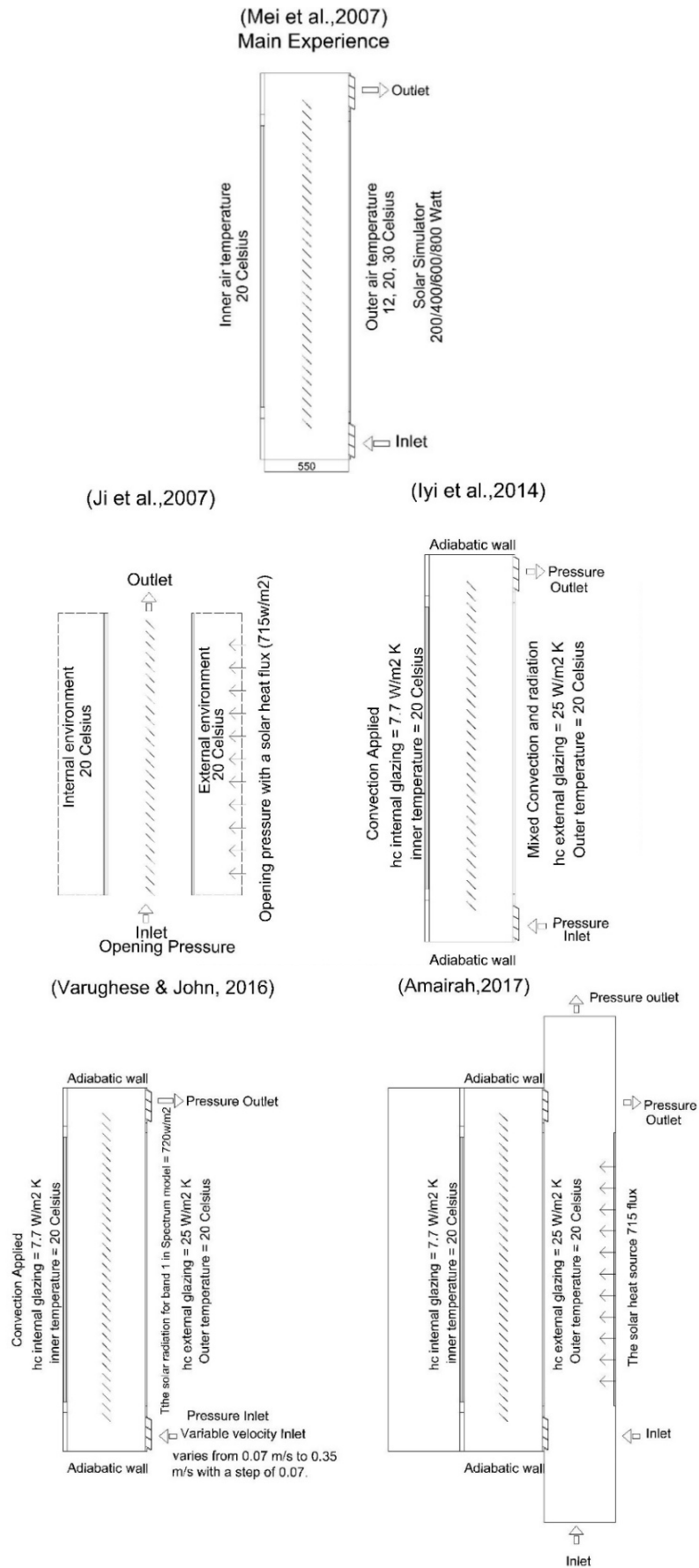


Figure 5-4: The boundary condition setup of some validation work in Literature carried on Mei et al. (2007).



As shown in Figure 5-4, a good amount of data is available on the numerical setup of Mei et al. (2007) case. Although CFD allows for detailed numerical modelling of the interactive physical phenomena inside DSF cavities, its simulation setup has many challenges associated with turbulence modelling and conjugate heat. The following part discusses the challenges met during the simulation process including solar simulator representation, the level of geometrical model detailing, domain size, selection of turbulence and radiation models, as shown in Figure 5-5. It presents a comparative study for different methods for modelling DSF equipped with shading devices.

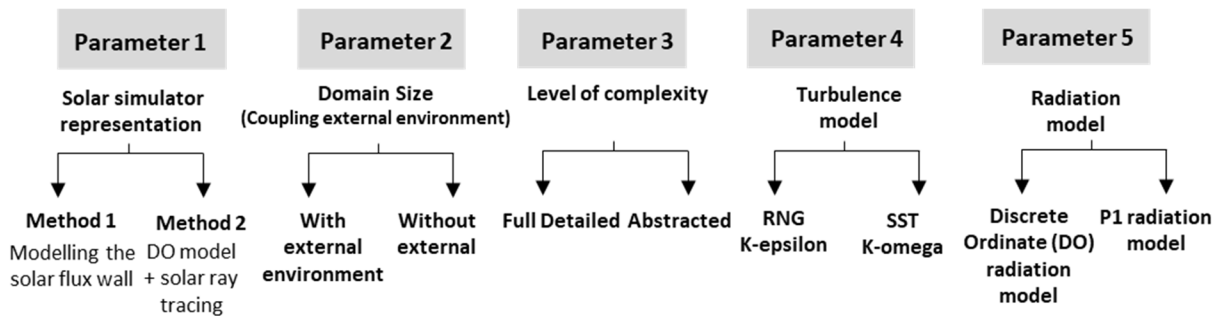


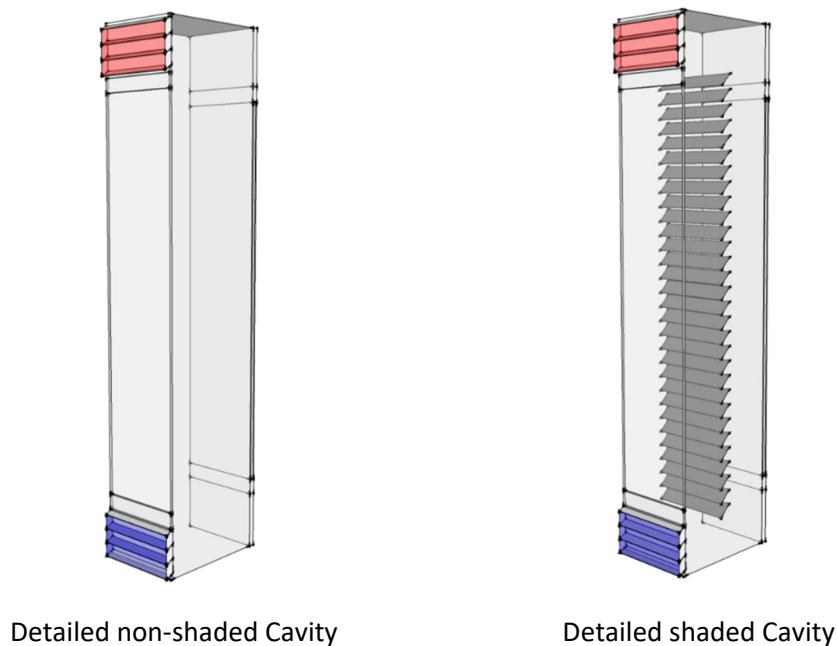
Figure 5-5: Different CFD setup parameters.

#### 5.3.1. The geometrical model (level of geometrical complexity parameter 3)

This study uses 3D modelling based on the following analytical literature review. The geometric model should represent the real problem with affordable CPU demand and without affecting the accuracy of the results. Thus, the level of complexity of the model needs to be sensitively selected. Most of the studies simplified the problem using 2D simulations to study the conjugate heat transfer. Ji et al. (2007), Liao et al. (2005) and Amaireh (2017) used 2D numerical simulation to study the coupled convective, and radiative heat transfer through the DSF integrated with shading devices. Other researchers, such as Velasco et al. (2017) and Parra et al. (2015) simulated a 3D model for the whole cavity. Detailed comparisons of 2D & 3D simulations with experimental results by Baldinelli (2009) and Safer et al. (2005) showed that the 3D simulations are more accurate while the two-dimensional model marginally underestimates the flow rate. One of the important advantages of 3D models is its ability to use the solar load model, which is only available in the 3D solver of ANSYS Fluent. Nevertheless, 3D simulations consume large computing power and time. One approach by Safer et al. (2005) represented the solar shadings by a homogeneous porous media model to reduce the number of cells and save computing time. Another approach by (Coussirat et al., 2008) limited the three-dimensional model to a cell size to compute the turbulent mixing appropriately with the proposed geometry.

A single-storey double skin cavity is modelled to minimize the computational timing and the problem resolved. A 3D approach is adopted mainly for two reasons: it is able to use the solar load model, which is only available in the 3D solver of ANSYS Fluent; it has better accuracy as the 2D model slightly underestimates the flow rate. For the purpose of further research investigation, a vertical section with 0.4 m deep and assigned symmetry condition at both sides is used. This depth represents the solar shading module. Dimensional considerations are taken according to the limitations of lightweight materials controlled with SMM actuators. This is inspired by the size of a single panel of Adaptive Solar Facade (ASF) installed in HIL building ETH Zürich which is 40cm moved with pneumatic actuators and the thermobimetals (TB) units of (Sung, 2016) ‘Bloom’ which are 30cm. The modelling of the 3D vertical section allows for complex form assessment with a reduced computational cost.

This study will cover both modelling of the non-shaded cavity and integrated shaded cavity with blinds at angle 45° as shown in Figure 5-6. The exact geometrical dimensions of the cavity section were replicated as in Table 5-2 and Figure 5-3, including cavity height, width, single external skin, internal double skin, inlet, outlet, Venetian blinds and grills.



*Figure 5-6: Schematic description of the model.*

Previous research simplified the geometrical model detailing to minimize the computational timing and the problem resolved. Ji et al. (2007) simplified the validated geometry by ignoring the curvature and swapping the ventilation inlet and outlet from one side to top and bottom. This simplification changed the airflow inside the cavity, but it resulted in the same thermal behaviour with a substantial reduction in the mesh size, leading to a

reduction in the CFD calculation and computational cost. Amaireh (2017) tested the geometrical level of simplification for the validated cavity and how it influenced the predicted airflow and thermal behaviour. Four different levels were examined, which are; (1) full detailed representation including vents/grilles and cavity's bottom and top meshes, (2) detailed representation for cavity vents/grilles, (3) cavity with no grilles at all, and (4) simple cavity structure with two vertical glazed walls with vertical inlet and outlet. All scenarios, except simple cavity, were able to predict surface temperatures in good agreement with experimental cases. Thus, CFD modelling will compare a full detailed model with an abstracted version without grilles. Figure 5-7 shows the full detailed model and the simplified version without grilles.

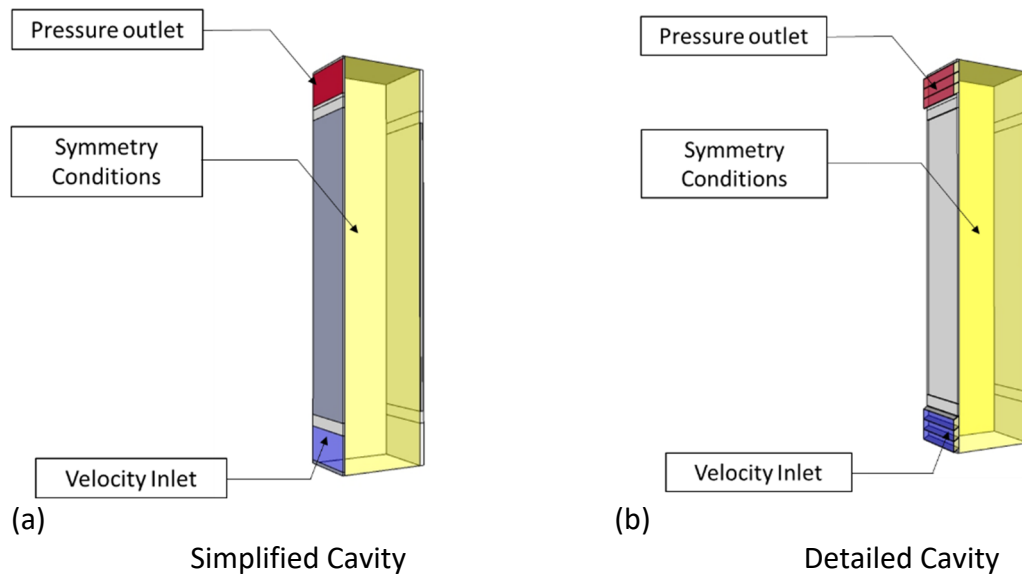


Figure 5-7: The boundary conditions on the full detailed model of DSF and the abstracted model without grilles.

### 5.3.2. Computational domain Size (Parameter 2)

The size of the computational domain is important for simulation accuracy. The computational domain is bounded by edges (2D) or faces (3D) on which boundary conditions are applied. Most studies in similar cases simulated a single storey DSF adiabatically to minimize the computational timing and the problem resolved. Pasut and De Carli (2012) compared the DSF cavity model with another DSF model coupled with the external environment. The study found that the results' accuracy is improved by modelling an outdoor ambient environment. Iyi et al. (2014) evaluated the influence of the different modelling strategies based on coupling and/or decoupling of the external and/or internal environmental conditions with the DSF channel flow and heat transfer as shown in Figure 5-8. Four modelling strategies were compared; which are (a) coupling with the internal space and external

environment, (b) coupling with the external environment only, (c) decoupling with the internal space and external environment, and (d) coupling with the external environment only. However, the study proceeded with the DSF cavity coupled with the internal environment only because of their interest in evaluating key parameters in the indoor environment.

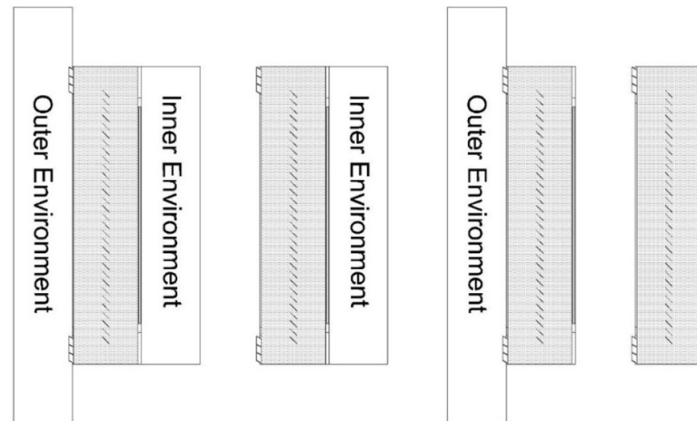


Figure 5-8: Different modelling strategies based on coupling and/or decoupling of the external and/or internal environmental conditions by (Iyi et al. 2014).

Amaireh (2017) tested a 2D DSF cavity coupled with external and internal environments. The study applied a sensitivity analysis for the external domain dimension for proper modelling of the ambient environment. But, it was found that the extension of the external domain did not result in any further improvement of the results and the best case was only the original distance of 0.6m between the solar simulator and the cavity. All previous studies detected a slight improvement by modelling outdoor ambient environment. Other studies applied the simulations on the whole building and façade model, such as Hassanli, Hu, Kwok, and Fletcher (2017). Nevertheless, the cases were extremely simplified without integrated solar shading systems.

Amaireh (2017) and Pasut and De Carli (2012) argued that extending the computational domain to include part of the external environment may eliminate any possible restrictions and boundary conditions' simplifications and allows for proper modelling of the ambient environment. Thus, the study will simulate the coupled and decoupled DSF cavity with the external environment. The DSF cavity domain is extended to include an external domain of 0.6m which is the original distance between the cavity and the solar simulator located in front of the facade as shown in Figure 5-9 (b). The location of the inlet and outlet boundary conditions are the main difference. In the coupled DSF, the inlet and the outlet are assigned on the surfaces of the extended domain, as shown in Figure 5-9 (d). Pressure outlet is assigned as the outlet boundary condition while velocity inlet is assigned as the inlet boundary condition.

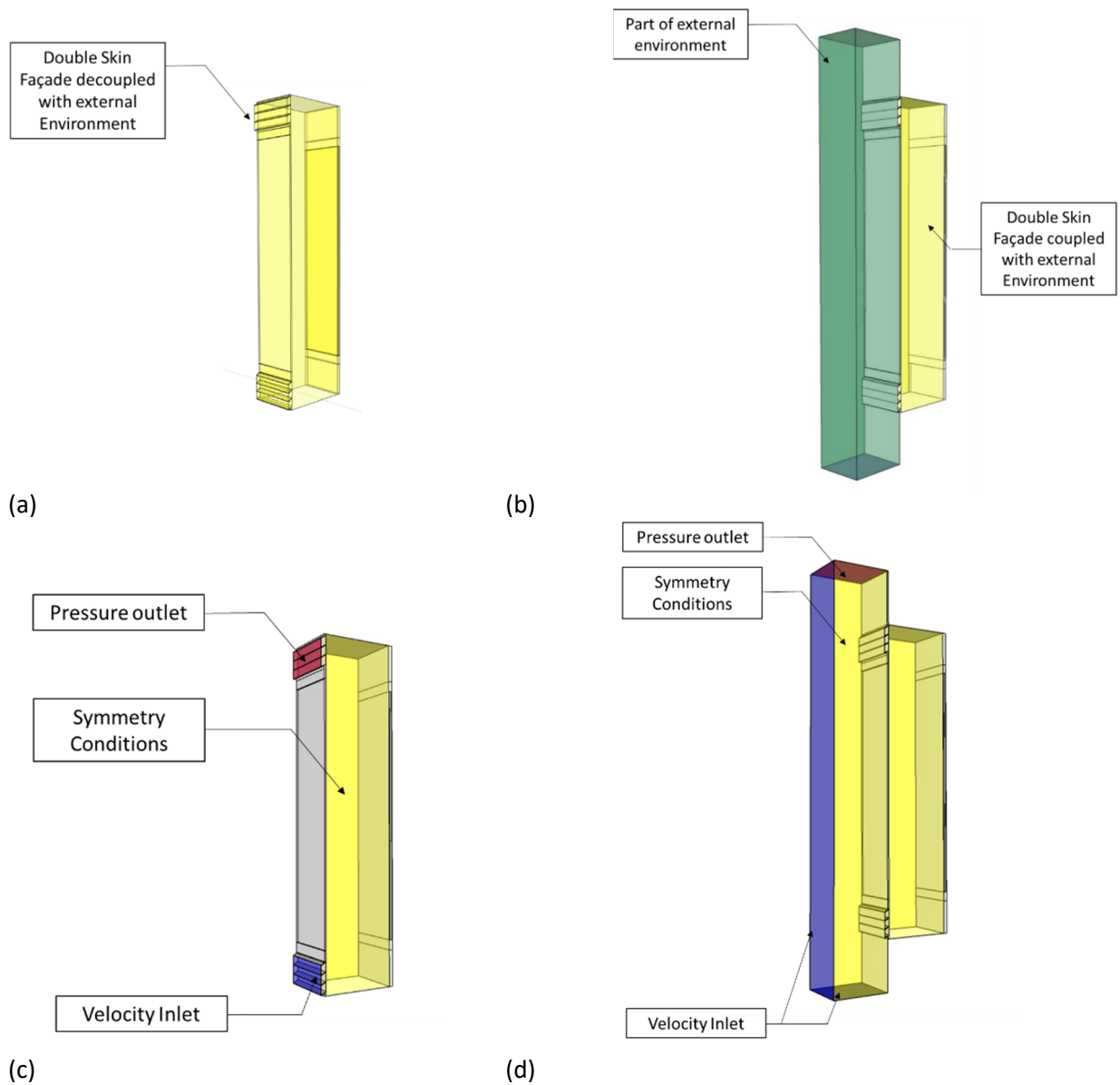


Figure 5-9: Domain size presentation (a) decoupled DSF cavity with the external environment, and (b) coupled DSF cavity with the external environment.

### 5.3.3. Turbulence Model (parameter 4)

This study uses RNG  $k-\epsilon$  and SST  $k-\omega$  turbulence models. Turbulence models, potentially suitable for indoor airflow, are available in a wide range of CFD approaches. It includes Reynolds averaged Navier-Stokes (RANS) modelling, large-eddy simulation (LES), and hybrid RANS /LES, which is called detached-eddy simulation (DES) (Zhang et al., 2007). RANS modelling can quickly predict air distributions with good accuracy compared to LES, which provides the most detailed flow features but requires substantial computing resources.

$k-\epsilon$  is RANS turbulence eddy-viscosity model that belongs to the subcategory called Two-Equation (Pasut & De Carli, 2012; Z. J. Zhai et al., 2007; Zhang et al., 2007). The “standard”

k- $\epsilon$  model by Launder and Sharma (1974) is one of the most prevalent models for indoor airflow simulation due to its simple format, robust performance, and wide validations. The RNG K-epsilon model by Yakhot and Orszag (1986) is an alternative to the standard model that includes some refinements that improve the turbulent flow accuracy. According to a review carried by (Pasut & De Carli, 2012; Z. J. Zhai et al., 2007), the k- $\omega$  models present new potential for modelling indoor environment with good accuracy and numerical stability. Some recent studies indicated that the SST model by (Menter, 1994) has better overall performance than the standard model. Zhang et al. (2007) evaluated the generality and robustness of the turbulence models for various indoor airflow scenarios in terms of accuracy and computing cost. These results proved that the RNG and a modified k- $\epsilon$  v2 f- model perform the best overall in all studied cases. This view is supported by Pasut and De Carli (2012) who recommended using the RNG k- $\epsilon$  turbulence model for good results and good simulation stability. Coussirat et al. (2008) compared five turbulence models, which includes standard k- $\epsilon$ , realizable k- $\epsilon$ , RNG k- $\epsilon$ , standard k- $\omega$  and SST k- $\omega$ , for validation purposes of DSF. The RNG k- $\epsilon$  turbulence model proved to perform better than the other tested turbulence models in the prediction of heat transfer, especially in the low velocities of DSF.

The RNG k- $\epsilon$  model is similar in form to the standard k- $\epsilon$  model, but includes the following refinements (Pasut & De Carli, 2012):

- The RNG model has an additional term in its  $\epsilon$  equation that significantly improves the accuracy for rapidly strained flows.
- It has modifications responsible for improving predictions of near wall flows with the enhanced wall treatment option
- RNG model enhances accuracy for swirling flows by including the effect of swirl on turbulence.
- The RNG theory provides an analytical formula for turbulent Prandtl numbers, while the standard k- $\epsilon$  model uses user-specified, constant values.
- While the standard k- $\epsilon$  model is a high-Reynolds-number model, the RNG theory provides an analytically-derived differential formula for effective viscosity that accounts for low-Reynolds number effects. Effective use of this feature does, however, depend on the appropriate treatment of the near-wall region.

All three turbulent models, standard k- $\epsilon$ , RNG k- $\epsilon$  and SST k- $\omega$ , satisfactorily predict the main qualitative features of the flow in indoor environments, especially in hot climates. The selection of a suitable model depends on the accuracy needed and computing time afforded. Both RNG k- $\epsilon$  and SST k- $\omega$  models have good accuracy for modelling the indoor environment

(Amaireh, 2017; Coussirat et al., 2008; Pasut & De Carli, 2012; Zhang et al., 2007). It was argued that the RNG k- $\epsilon$  has a better prediction for heat transfer when there are zones of low velocities in the façade configuration (Coussirat et al., 2008) as well as better simulation stability. The turbulence model should properly represent the turbulence phenomenon inside the DSF cavity thus would better predict both airflow and thermal performance of the DSF. The full buoyancy effect in the RNG k-epsilon turbulence model should be turned on during the simulations. The Enhanced Wall Treatment is adopted for the RNG k- $\epsilon$  model. Air is chosen as the simulation fluid, for which the constants are available in the software database. The fluid is set to be incompressible ideal gas and in a turbulent flow regime to make variables temperature-dependent. The study investigates two different turbulence models under this validation work to select the suitable model: RNG k- $\epsilon$  and SST k- $\omega$ . Mathematical equations for turbulence modelling are included in Appendix E.

#### 5.3.4. Radiation Model (Parameter 5)

This study couples radiation models with turbulence models. To account for radiation, radiative intensity transport equations (RTEs) are solved. Local absorption by fluid and at boundaries couples these RTEs with the energy equation. The selection of the radiation model enables the radiative heat transfer. Five radiation models are available in FLUENT, which are: Discrete Ordinates (DO) model, Discrete Transfer Radiation Model (DTRM), P-1 Radiation Model, Rosseland Model, and Surface-to-Surface (S2S). In Previous research solving the similar problem of DSF, Manz et al. (2004) and Jiru et al. (2011) used *Surface-to-Surface* (S2S) radiation model in which the thermal radiation occurs only as a surface phenomenon. Although it assumes that the fluid medium is transparent to radiation, it permits the solution of radiation problems involving non-participating media. However, some applications require consideration of *participating media* such as in the case of DSF. The term “*participating media*” has been used to refer to media lying between the radiating surfaces that can absorb, emit, and/or scatter thermal radiation. The DO and P-1 radiation models deal with cases with the *participating media* and multiple domains that contain both transparent fluids and semi-transparent solids. The glazing surfaces are modelled as "semi-transparent" medium/solid zone to participate in radiation as part of the boundary condition setup. These radiation models deal with the surface emissions; however, solar raytracing should be enabled to calculate the radiation effects from the sun's rays that enter the computational domain.



Discrete Ordinates (DO) model transforms the radiative transfer equation into a transport equation for radiation intensity in the spatial coordinates, solving as many transport equations as there are direction vectors associated with a number of discrete solid angles. The solution method is identical to that used for the fluid flow and energy equations (Coussirat et al., 2008). DO radiation model has been used widely as it suits both low and high optical thickness. Furthermore, DO model proved its superiority in solving RTE with participating medium with spectral absorption coefficient, at semi-transparent walls, by using the non-gray model and at a moderate computational cost (Amaireh, 2017; Hazem et al., 2015). The DO model is used to simulate the effect of incident solar radiation on the glazing surfaces, grills and solar-shading.

The P-1 radiation model is the simplest case of the more general P-N model, which is based on the expansion of the radiation intensity into an orthogonal series of spherical harmonics, in order to solve the RTE (Coussirat et al., 2008). The P-1 radiation model integrates the directional dependence in (RTE), resulting in a diffusion equation for incident radiation. It has the advantage of including the effect of scattering. Furthermore, it proved its superiority in solving (RTE), easily and with little CPU demand.

The P1 radiation model only works reasonably well for applications with large optical thickness, while DO is more inclusive and applicable to a wide range of optical thicknesses. The key problem with coupling the radiation models is the high computational costs. The main advantage of solving with the P-1 radiation model is the ease to solve with small computational power. On the other hand, the DO model is CPU-intensive to analyse a large number of ordinates. One drawback of the P1 radiation model is that it tends to over-predict radiative fluxes which may result in loss of accuracy, especially with complex models. The accuracy of DO model can be increased with applying finer discretization. Table 5-4 presents a comparison between DO and P-1 radiation models showing the pros and cons of each model. In summary, the DO model is the most comprehensive of all models, which takes into account the scattering effects, semi-transparent media, specular surfaces, and wavelength-dependent transmission using the banded-gray option.

Table 5-4: Comparison between DO and P-1 Radiation models

Model	Discrete ordinates (DO)	P-1 Radiation model
<b>Features</b>	The DO model transforms the RTE into a transport equation for radiation intensity in the spatial coordinates, solving as many transport equations as there are direction vectors associated with a number of discrete solid angles (Coussirat et al., 2008).	The P-1 radiation model is the simplest case of the more general P–N model, which is based on the expansion of the radiation intensity into an orthogonal series of spherical harmonics, in order to solve the RTE (Coussirat et al., 2008).
<b>Optical thickness</b>	DO is more inclusive and applicable to a wide range of optical thicknesses.	P-1 radiation model works reasonably well for applications with large optical thickness.
<b>Accuracy</b>	The accuracy of DO model can be increased with applying finer discretization.	P-1 radiation model tends to overpredict radiative fluxes.
<b>CPU demand</b>	It requires small CPU usage.	It is CPU-intensive.

In previous research concerned with DSFs simulation, DO radiation model is the most popular assuming that the problem has a low optical thickness and negligible scattering coefficients for its medium (air). However, some studies used P-1 radiation model upon (Coussirat et al., 2008) recommendation for its better prediction of solid phases temperature. Therefore, the study compares DO radiation model and P-1 radiation model. Mathematical equations for radiation modelling are included in Appendix E.

Surface emission is an important factor in our study; therefore, the radiation model is implemented in conjunction with the *solar ray tracing* options of the solar load model. *Solar ray tracing* is used to calculate radiation effects from the sun rays that enter the computational domain. It predicts the direct illumination energy source that results from incident solar radiation. It applies the incident solar radiation beam to walls and/or inlet/outlet boundary zones and performs a face-by-face shading analysis. The *non-Gray Model* was set for both the P-1 and the Discrete Ordinates (DO) radiation models.

For cases, like a semi-transparent medium (glass), non-gray behaviour is important, and few bands are necessary. The semi-transparent glazing elements are spectrum selective of radiation transfer, i.e., short wave radiation (solar) has a very high transmittance while longwave (thermal) radiation has a very low transmittance. Two bands will frequently suffice, and their wavelength intervals are set to be ‘Solar’ (0-2.7  $\mu\text{m}$ ) and ‘Thermal’ (2.7-1000  $\mu\text{m}$ ) as shown in Table 5-5. A fine angular discretization can be specified to better resolve the influence of small geometric features but larger divisions will add to the cost of the

computation. Besides, the setting of 3x3 pixilation is recommended for semi-transparent boundaries to achieve acceptable results (Amaireh, 2017; Iyi et al., 2014). It is recommended that the Angular Discretization settings, Theta & Phi Divisions, are both set to 6 as shown in Table 5-5. All glazing surfaces are set as participating in radiation, to enable transmission and absorption of radiation inside the cavity. Since radiation is the dominant mode of heat transfer in the computational domain, therefore, the flow iterations per radiation iteration are specified as 5 as recommended by (Iyi et al., 2014).

*Table 5-5: Energy bands for Non-Gray radiation model and Angular Discretization characteristics.*

	Start	end
Solar	0	2.7
Thermal	2.7	1000
	Angular Discretization	
	Theta	Phi
Divisions	6	6
Pixels	3	3

### 5.3.5. Solar Load Model (solar representation- Parameter 1)

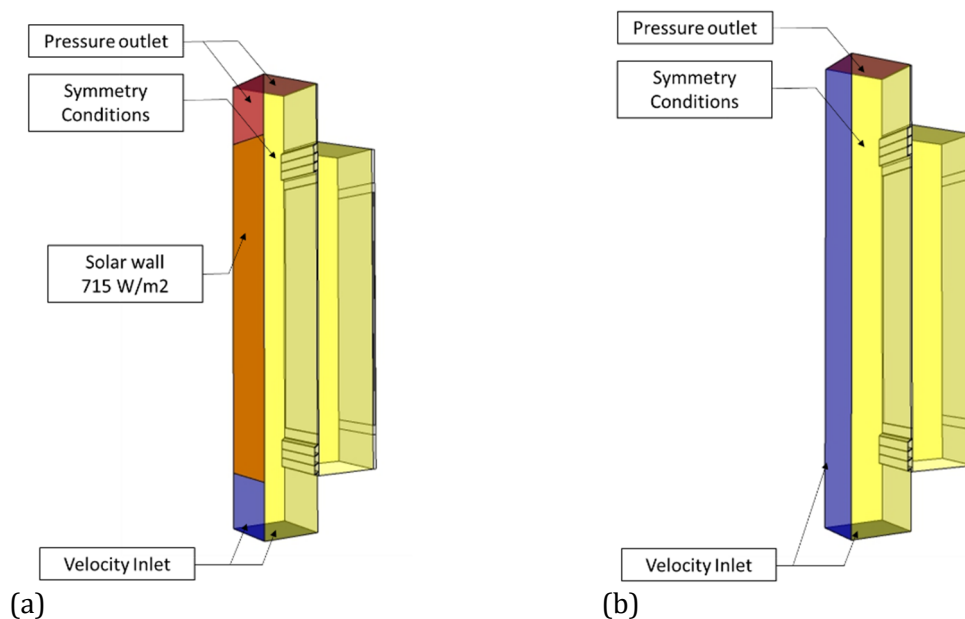
The main challenging aspect with Mei model is how the solar simulator radiative flux is represented in the domain. As stated by the research team (Ji et al., 2007), the solar generator which is the main source of the solar heat flux was located at a distance of 0.5m from the front of the facade.

Ji et al. (2007) used CFX Opening pressure for entrainment with a solar heat flux ( $715\text{w/m}^2$ ) as the boundary source for radiation modelling to simulate the external environment. They used a radiation model based on Monte Carlo (MC) techniques. Amaireh (2017) represented the solar heat source by a vertical plane opposite to the front face of the structure. Iyi et al. (2014), Varughese and John (2016) coupled *Solar load model with DO radiation non-gray model* with two bands, solar and thermal, from 0-2.7mm and 2.7-1000mm to represent the spectral radiation.

*Solar load model* is available in the 3D solver of ANSYS Fluent, which can be used to calculate the radiation effects from the sun rays that enter the computational domain. *Solar Ray Tracing* is not a participating radiation model. It does not deal with emissions from the surfaces. The reflecting component of the primary incident load is distributed uniformly across

all surfaces rather than being local to the surfaces reflected to. The radiation model (P-1 or DO radiation model) is coupled with the *solar ray-tracing* model to deal with emission from surfaces, and the reflecting component of the primary incident load through the computational domain (Iyi et al., 2014). Two options are available for the model: *solar ray tracing* and *DO irradiation*. The (DO) model calculate radiation effects within the domain; an option is available to supply outside beam direction and intensity parameters directly to the DO model. Also, it includes a solar calculator that is used to construct the position of the sun in a given time, day and location. The solar load model in the Radiation Model is enabled by selecting Solar ray-tracing. The set solar calculator computes the solar beam direction, Direct and Diffuse Solar Irradiation. It defines the global position by Longitude, Latitude and Time zone. As the solar load model is limited to 3D modelling, Amaireh (2017) applied alternative methods to calculate the direct and diffuse radiation for 2D modelling. Therefore, 3D modelling is a more comprehensive approach for its inclusion of the solar raytracing option

Two different modelling methods are used in this study to represent the solar generator. In the first method, a full-height wall was modelled, as shown in Figure 5-10. A solar flux of  $715 \text{ W/m}^2$  is applied to the wall surface representing the solar generator coupled with DO radiation model, as shown in Figure 5-10 (a). The second model simulated the solar flux using a two-band non-gray DO radiation model and solar ray tracing. The solar radiation for the 'solar' band with wavelength ( $0\text{-}2.7 \mu\text{m}$ ) is set to  $715 \text{ W/m}^2$  as shown in Figure 5-10 (b).



**Figure 5-10: Methods of Solar simulator representation in this study (a) the first method modelled a full-height wall with a solar flux of  $715 \text{ W/m}^2$  coupled representing the solar generator. (b) The second method applied the solar flux using a two-band non-gray discrete ordinate model.**

Having discussed different CFD parameters that affect the simulation of DSF integrated with shading devices, the next section will now move on to simulate these parameters including a description of mesh creation and numerical modelling

#### **5.4. The Computational Mesh**

In this study, non-shaded and shaded cases are modelled in AutoCAD and exported as step files to be meshed. Mesh creation is one of the main factors affecting the quality of the CFD simulation. The choice of proper mesh type, size and quality are essential for converged reliable simulations. The good quality mesh shall limit highly skewed elements or large aspect ratio elements. Generally, hexahedral mesh proved to be the best in terms of quality, flow analysis and time consumed to reach convergence. Complex forms would need tetrahedral mesh, especially for fluid zones.

Beyond hexahedral and tetrahedral meshing, there are tools for hybrid meshing with combined hexahedral and tetrahedral regions or bodies. In hybrid models, conformal or non-conformal meshes can be generated at common interfaces ("ANSYS Meshing Solutions," 2014). Inflation layers around all solid surfaces are recommended to model the thermal boundary layers created at the solid-fluid surface contacts (Hazem et al., 2015; Iyi, 2013; Pasut & De Carli, 2012).

Creating the contact layers and meshing the interface between bodies is essential in DSF modelling for proper heat transfer and solar ray tracing/solar load analysis. Slitting walls into coupled walls results in shadow zone creations for glass surfaces that face the fluid zone. The coupled wall with shadow zones is responsible for proper radiation and solar load modelling. Conformal mesh has the characteristics of bodies sharing common nodes at the interface. It is achieved by gathering all parts into one by using the (Form New Part) functionality in the ANSYS DesignModeler application before moving to the ANSYS Meshing application. Thus, a conformal mesh where bodies share common nodes at the interface is used to enable solar ray tracing analysis which only works with conformal mesh.

The number of cells affects the simulation accuracy and computational time. Therefore, Mesh independency tests are done through series refinements to select the optimal size taking in consideration the  $Y^+$  value. The  $y^+$  is a non-dimensional distance refers to the size of the mesh near the wall compared to the fluid behaviour (Iyi et al., 2014). This number indicates the location of the first cell centre compared to the boundary layer

thickness. The parameter  $y^+$  is critical to the correct use of turbulence models (Pasut and De Carli, 2012). Accurate presentation of the flow in the near-wall region determines the successful prediction of wall-bounded turbulent flows.  $Y^+$  calculator is normally used; however, values of  $y^+ \approx 1$  are most desirable for near-wall modelling as advised by previous practice in the same problem (Hazem et al., 2015; Iyi, 2013; Pasut & De Carli, 2012).

Meshes with high skewness always result in solution divergence. Mainly skewness mesh metric is considered acceptable for the simulation with a maximum value of 0.94 as shown in Table 5-6. The average orthogonal quality should be checked in the acceptable ranges. It also ranges from 0 to 1, where values close to 1 correspond to good quality.

*Table 5-6: Skewness and orthogonal quality ranges for mesh creation.*

<b>Skewness</b>	<b>Orthogonal Quality</b>
0 to 0.25: Excellent	0 to 0.001: Unacceptable
0.25 to 0.5: Very good	0.001 to 0.14: Bad
0.5 to 0.8: Good	0.15 to 0.2: Acceptable
0.8 to 0.94: Acceptable	0.2 to 0.69: Good
0.95 to 0.97: Bad	0.7 to 0.95: Very good
0.98 to 1.0: Unacceptable	0.95 to 1.0: Excellent

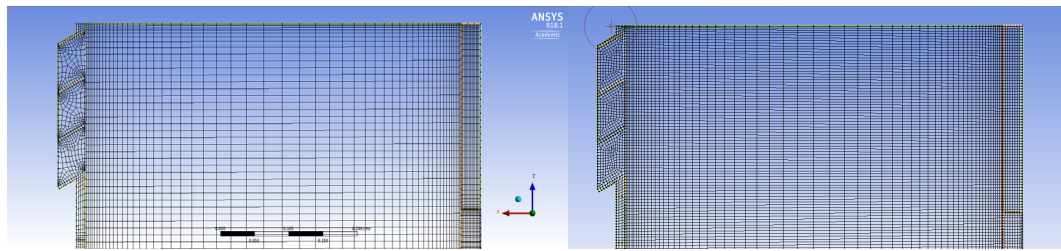
The meshing is built within ANSYS Meshing application, and different parts are given named selection without any overlapping to guarantee successful mesh transformation to fluent. In this study, general recommendations for the mesh generation are adopted from previous relevant work and current practice as follows:

- Create named selection without any overlapping to guarantee successful mesh transformation to fluent.
- Create equidistant mesh cells while refining the mesh near solid surface for proper analysis of complex flow phenomena and heat transfer
- Generate prism/Inflation layers across bodies (use  $Y^+$  calculator)
- Do not exceed a ratio of 1.3 between two consecutive cells in case of stretched cells.
- Generate conformal mesh to enable solar ray-tracing analysis. It is achieved by gathering all parts into one by using the (Form New Part) functionality in the ANSYS DesignModeler application before moving to the ANSYS Meshing application.
- Slit interface walls into coupled walls, to create a shadow zone for surfaces facing the fluid zone. This is responsible for proper radiation and solar load modelling.

#### 5.4.1. Independence of Mesh Size

The meshing is processed in Ansys software package. At early stages of simulation, several trials were done using ICEM meshing, but it was not successful in creating interface walls. Thus, the meshing is built using ANSYS meshing. The non-shaded cavity is meshed using hexahedral mesh, as shown in Figure 5-11. The shaded cavities are meshed with a hybrid meshing of combined hexahedral and tetrahedral cells where conformal meshes are generated at common interfaces. Inflation layers are generated along surfaces to increase boundary layer resolution perpendicular to the wall. Mesh independency tests were done through series refinements to select the optimal size taking in consideration  $Y^+$  value. Values of  $y^+ \approx 1$  are most desirable for near-wall modelling. Acceptable values of  $Y^+$  distribution are achieved by using inflation elements along the walls to better capture the sharp gradients near the wall with an exponential distribution of the cell blocking near the walls (of the ratio of 1.3).  $Y^+$  was checked for different meshes. Three different mesh densities are tested for the non-shaded Mei case (mesh 1=95,400, mesh 2=598,300 cell and mesh 3=1,185,000 cell). The finer meshes have smaller cells and more inflation layers. The two finer meshes obtain similar results in terms of mid cavity temperature, as shown in Figure 5-11. The hexahedral cavity mesh of 598,300 cells (mesh 2) is selected for the simulation of the non-shaded cavity of Mei's case. The non-shaded case convergence is attached in Appendix G.





Mesh 1

Mesh 2

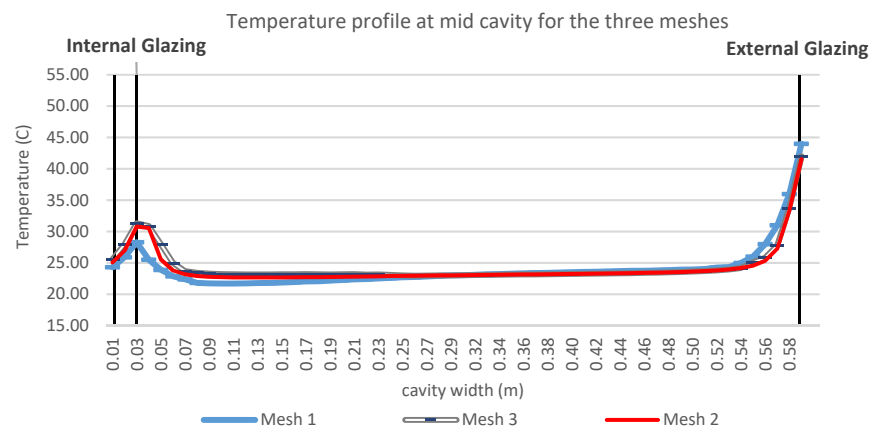
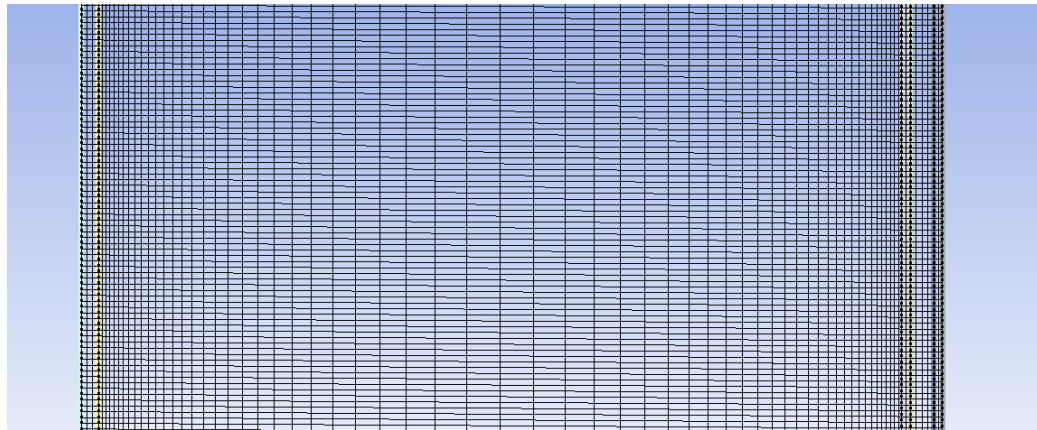


Figure 5-11: Hexahedral Meshing of the non-shaded cavity of Mei et al. (2007) case- Mesh 1 & 2.

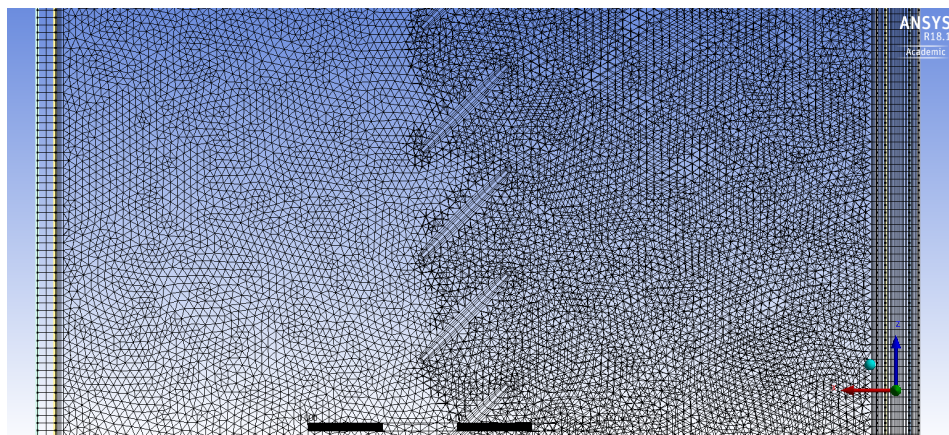


Figure 5-12: Hybrid meshing of combined hexahedral and tetrahedral cells for the shaded cavity of Mei et al. (2007).

## 5.5. Numerical Modelling

In this section, the solution method setup, the boundary conditions and materials are discussed. The study is conducted through 3D modelling using CFD code Ansys Fluent package to simulate the airflow and associated heat transfer (coupled convective, conductive and radiative) through the DSF. In order to simulate the studied cases, Navier-Stokes equations together with the energy conservation equation were solved using CFD code Ansys Fluent® v18.1. At present, the commercial CFD code allows coupled thermo-fluid-dynamics problems to be solved using turbulence and radiation sub-models. Some mathematical equations are included in Appendix E.

### 5.5.1. Solution Method's Set-up

All the cases in this study are solved using Fluent code with double precision for better accuracy. The SIMPLE algorithm (Semi-Implicit Method for Pressure Linked Equations), is used for coupled pressure and velocity. The PRESTO! (PREssure STaggering Option) discretization scheme is adopted for pressure and Second order upwind discretization schemes are imposed on all the transport equations as shown in Table 5-7. The model's numerical convergence is checked based on the normalized numerical residuals of all computed variables. The criteria used for defining convergence is i) all the maximum residuals for each equation are lower than  $5 \times 10^{-4}$  for the last 100 time steps and ii) All residuals dropped for less than  $1 \times 10^{-3}$  for all solved equations except energy to  $1 \times 10^{-6}$ . The number of iterations was doubled to be sure of the stability of the results.

Table 5-7: Set-up for solution methods in fluent; and Discretization.

Parameters	Discretization
Pressure	PRESTO!
Density	-
Body Forces	-
Momentum	Second Order Upwind
Turbulent Kinetic Energy	Second Order Upwind
Specific Dissipation Rate	Second Order Upwind
Turbulent Viscosity	Second Order Upwind
Energy	Second Order Upwind
Discrete ordinates	Second Order Upwind
P-1 radiation	Second Order Upwind

Due to the complexity of hybrid meshes, it was recommended to test the cases under the zero-equation model as initial condition (Zhang et al., 2007) or Under Relaxation Factors (URF) initial conditions (Amaireh, 2017; Iyi et al., 2014) to achieve convergence. Moreover, Ji et al. (2007) recommended running the simulations under a small relaxation factor (URF=0.2) for the energy equations in the solid domains to achieve the convergence. Therefore, low values for URF are initially set until convergence to achieve good solution stability and then default URF values were set for fast convergence as shown in Table 5-9. URF is used to further relax the radiation equation. URF reduces solution oscillations and helps to keep the computation stable. This may slow down the speed of convergence but increases the stability of the computation, i.e. it decreases the possibility of divergence or oscillations in the solution zones.

*Table 5-8: Set-up for solution methods in fluent; Initial Under-Relaxation Factors (Amaireh, 2017; Iyi, 2013; Iyi et al., 2014; Ji et al., 2007).*

Parameters	Initial Under-Relaxation factors	Default Under-Relaxation factors
Pressure	0.2	0.3
Density	0.8	1
Body Forces	0.8	1
Momentum	0.5	0.7
Turbulent Kinetic Energy	0.5	0.8
Specific Dissipation Rate	0.5	0.8
Turbulent Viscosity	0.8	1
Energy	0.9	1
Discrete ordinates	0.8	1
p-1	0.8	1

Numerical simulations were performed using HP Z420 workstation with a Quadro 2000 graphics card, 16gig ram using a Xeon e5-1650 3.2 ghz processor. Simulation times ranged between 40 to 60 hours, depending on the studied case.

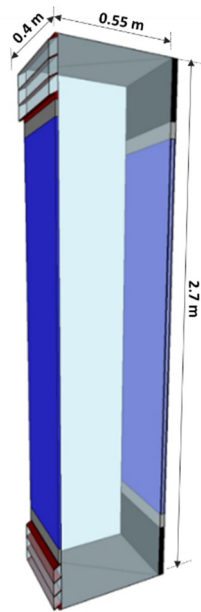
#### *5.5.2. Computational Boundary and Operating Conditions*

The computational domain refers to a simplified form of the physical domain both in terms of geometrical representation and boundary condition imposition ("Computational Domain," 2008). The geometrical representation should retain all physically important features of the problem but can ignore minor details. Thus, boundary conditions are assigned to the boundaries of the computational domain to simulate the physical quantities in the real flow problem. Assigning these physical quantities to the boundaries is important for the

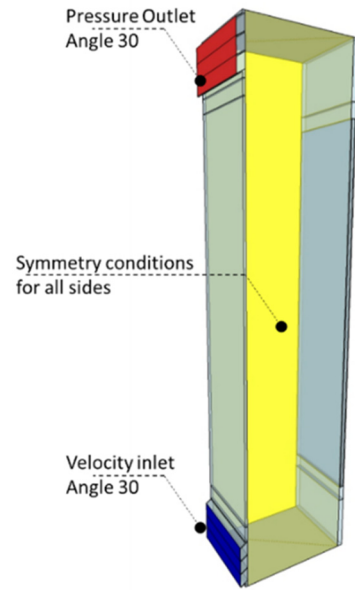
simulation accuracy as well as the solution stability and convergence speed. The boundary conditions are divided into five main boundaries which are assigned to faces or edges of the domain. These are the inflow boundary condition, outflow boundary condition, bottom boundary condition, top boundary condition and the side boundary conditions.

Considering the influence of wind pressure on DSF ventilation, the inflow section of the external environment or cavity inlet can be either set as a velocity inlet or as a pressure inlet boundary with the gauge total pressure equal to 0. In naturally ventilated DSF cases in real environments, the parameters should be set according to local meteorological parameters and the generalized logarithmic law of gradient wind. The velocity inlet should have a magnitude and direction either normal to the boundary condition or with an angle.

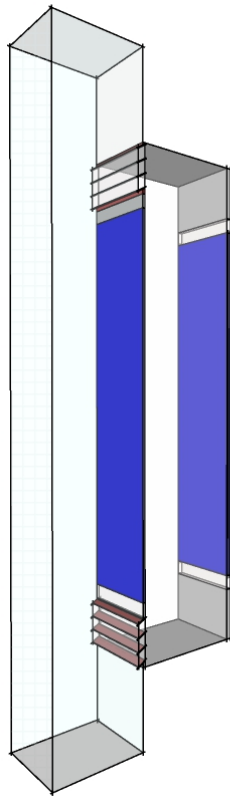
While simulating Mei et al. (2007) case, boundary conditions are set as close as possible to the experimental operating conditions. For studying a buoyancy-driven flow, the pressure outlet should be set as a pressure outlet boundary with the same gauge total pressure equal to 0. On the other hand, the inlet condition can be either pressure inlet (Iyi et al., 2014; Pasut & De Carli, 2012) or velocity inlet (Hazem et al., 2015; Iyi, 2013; Varughese & John, 2016) which is unknown Mei et al. (2007) case. Varughese and John (2016) examined the effect of the change in the inlet velocity of the airflow and argued that the increase in the inlet velocity led to a reduction of slats temperature. The temperature and airflow contours were evaluated under five different Inlet velocity, ranging from 0.07 to 0.35 m/s, with a 0.07m/s step. In this study, the temperature and airflow contours are evaluated under an inlet velocity of 0.4 m/s. The air direction for the inlet, which matches the grill angle, was always used by many researchers to improve the resulting quality for the air direction. The solid-fluid interfaces, such as the inner glazing and the blind surfaces, are treated as a coupled wall. The bottom and top boundary conditions are mostly treated in the same way. They are considered adiabatic, and they do not participate in the solar ray tracing. In 3D cases, the lateral section can be set as adiabatic walls or as a symmetric boundary. As studying a vertical section with 0.4 m deep, the lateral walls are set as symmetric boundaries, as shown in Figure 5-13 (b) & (d).



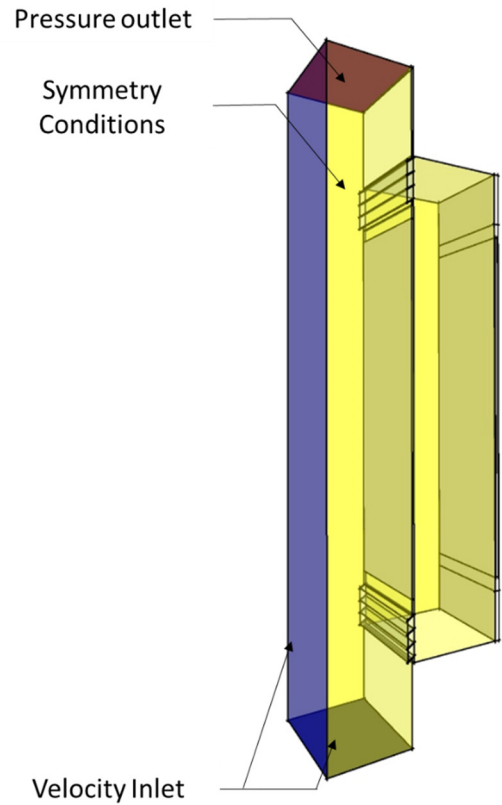
(a) Decoupled DSF cavity with the external environment.



(b) Boundary conditions of the decoupled DSF cavity



(c) Coupled DSF cavity with the external environment.



(d) Boundary conditions of the coupled DSF cavity.

*Figure 5-13: Boundary conditions of the decoupled and coupled DSF cavity with the external environment based on boundary conditions used by researchers in Figure 5-4.*

A fixed temperature of 20 degree Celsius (293 K) was set for the internal space and outside environment. A fixed solar radiation of  $715 \text{ w/m}^2$  was set to validate the numerical method and compare the results of the non-shaded and shaded (45 degree inclination) cavities with the recorded results from the literature. Thermal boundary conditions for the exterior and interior layers were imposed as a mixed condition (radiation and convection).

Convection coefficients are set to 25 W/m<sup>2</sup>K and 7.7 W/m<sup>2</sup>K for the outdoors and indoors glazing surfaces respectively as advised by the research group (Ji et al., 2007, 2008). DO and P1 radiation models were applied and compared in conjunction with the Solar Ray-tracing options of the solar load model. Two bands ‘Solar’ and ‘Thermal’ were set for the Non-Gray model. The solar band corresponds to wavelengths smaller than 2.7 μm, and the thermal band to wavelength larger than 2.7 μm. The Angular Discretization was set to 6x6 divisions and a pixilation of 3x3.

### 5.5.3. Materials

Semi-transparent solids are set for all glazing materials in the simulations, while opaque solids are set for blinds and passive walls. Physical and optical properties for solid materials are set as shown in Table 5-9 and Table 5-10. The air is set as a transparent media and air density is set as a function of temperature using the Boussinesq approximation method. This method treats density as a constant value in all solved equations, except for the buoyancy term in the momentum equation (equation (3) in Appendix E).

Table 5-9: Physical properties of DSF elements.

	Single glazing (outer)	Double glazing (inner)	Grills	Passive walls
ρ (kg/m <sup>3</sup> )	2500	2500	2719	2100
C <sub>p</sub> (J/kg·K)	840	840	871	1100
K (W/m·K)	1.7	1.7	202.4	0.8
Absorption coefficient	30*	30*	-	0.58
	3000**	1285.7**	-	
Emissivity	0.84	0.84	0.7	0.58
Refractive index	1.5	1.5	1.4	1

\*\* For wavelength 0–2.7 micrometers and \* for wavelength 2.7–1000 micrometers.

Table 5-10: Solar radiation properties of materials.

		Absorptivity (α)	Transmissivity (τ)
Outer glass	Visible	α <sub>V</sub> = 0.09	τ <sub>V</sub> = 0.83
	Infrared	α <sub>IR</sub> = 0.09	τ <sub>IR</sub> = 0.83
	Diffuse hemispherical	α <sub>D</sub> = 0.1	τ <sub>D</sub> = 0.75
Inner glass	Visible	α <sub>V</sub> = 0.49	τ <sub>V</sub> = 0.3
	Infrared	α <sub>IR</sub> = 0.49	τ <sub>IR</sub> = 0.3
	Diffuse hemispherical	α <sub>D</sub> = 0.49	τ <sub>D</sub> = 0.32
Grills	Visible	α <sub>V</sub> = 0.5	-
	Infrared	α <sub>IR</sub> = 0.75	-

This section explained the numerical CFD setup carried for the CFD simulations. The next section will discuss the results of the simulated cases.

## 5.6. Results

The study covers the analysis of a DSF with and without blinds. The five parameters stated previously as simulation parameters are tested on the non-shaded cavity. The setup of the best agreement with the experimental measurements will be applied for the shaded cavity which is equipped with white blinds at angle 45°. The experimental data of Mei's case were collected with seven TSI Omni directional anemometers located at 1.1m from the bottom of the DSF cavity (the middle height of the cavity). Accordingly, CFD analysis are collected along a line at 1.1 m from the internal to the external glass pane. Temperature profiles of the mid cavity is studied to be compared with (Mei et al., 2007)'s experiment measurements.

### 5.6.1. *Non-shaded cavity*

The different runs covering the five parameters are tested sequentially in the following order: (1) solar simulator representation, (2) domain size, (3) selection of radiation model, (4) selection of turbulence model and (5) level of geometrical detailing. The mid cavity temperature profile is measured, compared and matched with the data documented in Mei et al. (2007).

#### 5.6.1.1. Simulation 1: Solar simulator representation

Two different modelling methods are used to represent the solar generator. In the first method (1), a solar flux of 715 W/m<sup>2</sup> is applied to the wall surface, while the second method (2) simulated the solar flux using a two-band non-gray DO radiation model and solar ray tracing.



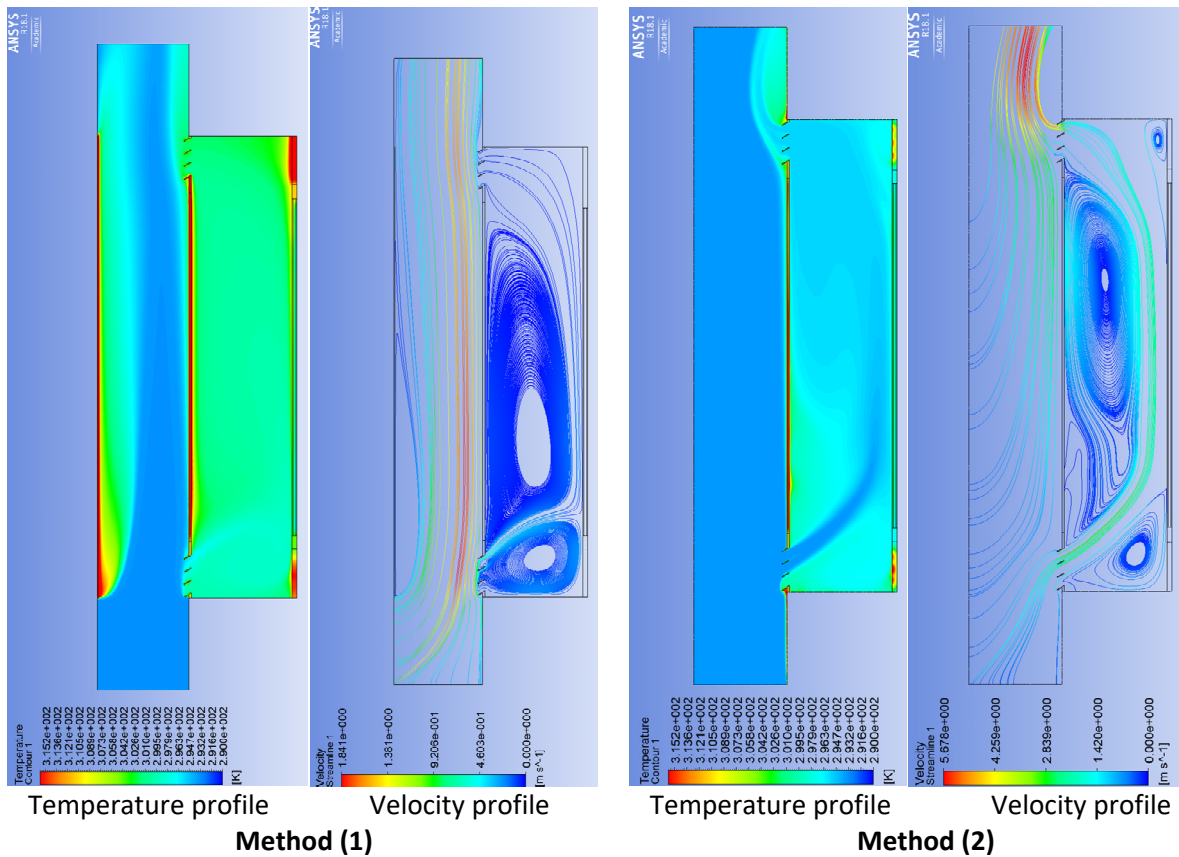


Figure 5-14: Results of Solar simulator representation methods (1) full-height wall with a solar flux of  $715 \text{ W/m}^2$  representing the solar generator, (2) solar flux using a two band non-gray discrete ordinates with solar raytracing.

As shown in Figure 5-14, Method (1) adopted in this research resulted in a lower variance of  $5^\circ\text{C}$  in mid cavity temperatures and an increase of  $7^\circ\text{C}$  in surface temperature of the outer glazing layer compared to experimental results. Although air temperature in the cavity is closer to the experimental results, the simulation predicts higher surface temperatures on the outer skin. On the other hand, method (2) which applied DO radiation model with solar load model predicted external glazing with higher accuracy recording  $45.25^\circ\text{C}$ , while a variance of 8% was found on the back of the inner glazing (facing the inner space) recording  $25.65^\circ\text{C}$  compared to experimental data recording  $27.85^\circ\text{C}$ . A variance of 20% was found on the front of the inner glazing (facing the cavity)  $32^\circ\text{C}$  compared to experimental data  $40^\circ\text{C}$ . RNG k-epsilon turbulence model with full buoyancy effect and Enhanced Wall Treatment was adopted.

### 5.6.1.2. Simulation 2: Domain Size

Two Domain sizes are compared, the coupled and decoupled DSF cavity with the external environment, as shown in Figure 5-15.

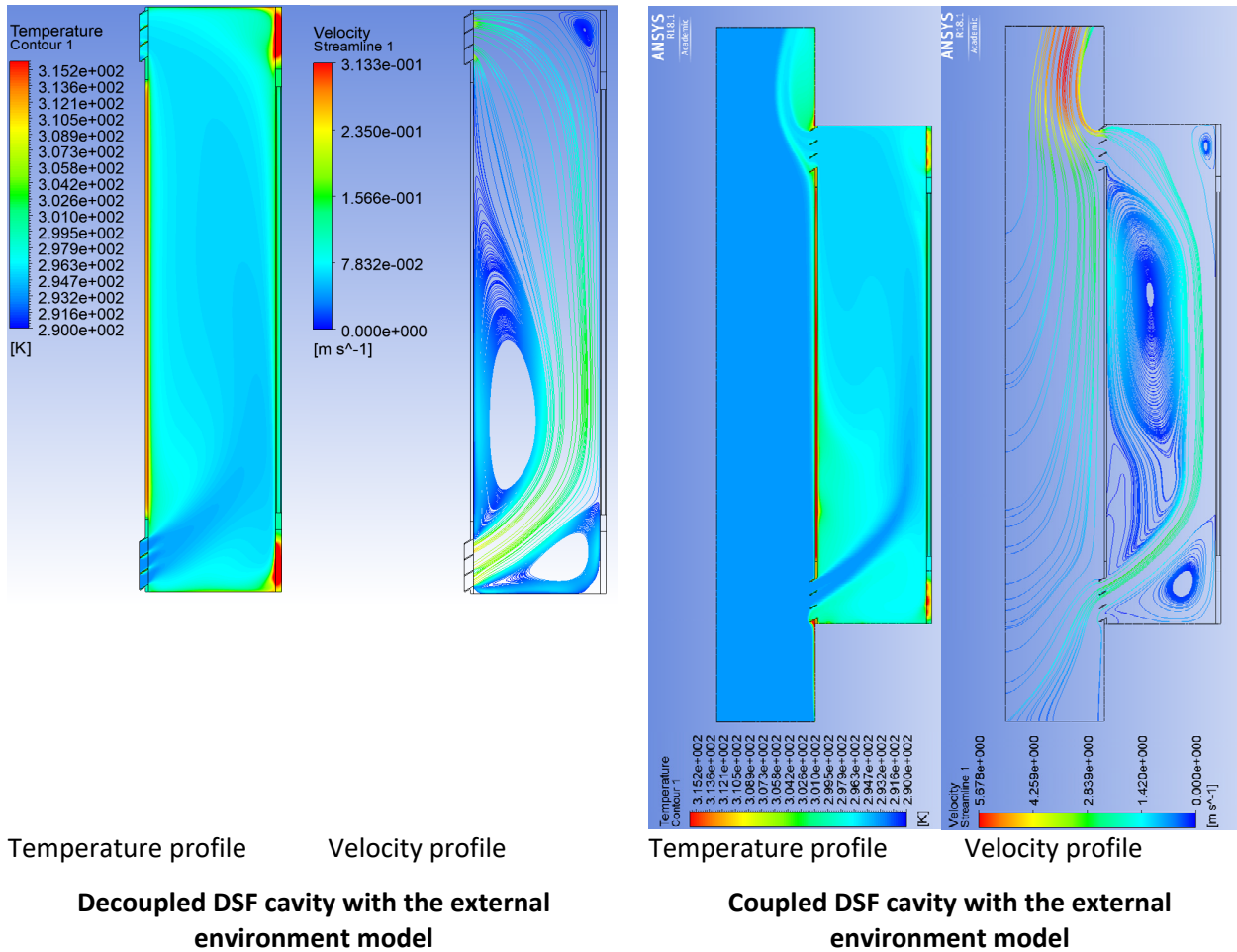


Figure 5-15: Results of coupled and decoupled DSF cavity with the external environment.

As shown in Figure 5-15, a coupled computational domain to include a part of the external environment of 0.5m is compared with a decoupled model. DO radiation model with solar load model and RNG k-epsilon turbulence model with full buoyancy effect and Enhanced Wall Treatment was adopted. In agreement with (Amaireh, 2017; Pasut & De Carli, 2012), the extension of the computational domain to include part of the external environment, allows the modelling of the ambient environment. The coupled modelled resulted in higher external glazing temperature of 45.2°C, which matches the experimental result recording 44.85°C, while the decoupled model resulted in 42.5°C, which represents a 7% variation than the experimental. Also, the coupled model resulted in higher back internal glazing temperature 25.6°C, which is closer to the experimental result recording 27.8 °C while the decoupled resulted in 25.1 °C. Although the results of the coupled cavity with the external environment showed a 1°C higher air cavity temperatures, the difference is small and can be negligible.

### 5.6.1.3. Simulation 3: Radiation model

The P-1 and DO radiation models are compared. Two bands ‘Solar’ and ‘Thermal’ were set with non-gray option for both models. The solar band corresponds to wavelengths smaller than 2.7  $\mu\text{m}$ , and the thermal band to wavelength larger than 2.7  $\mu\text{m}$ .

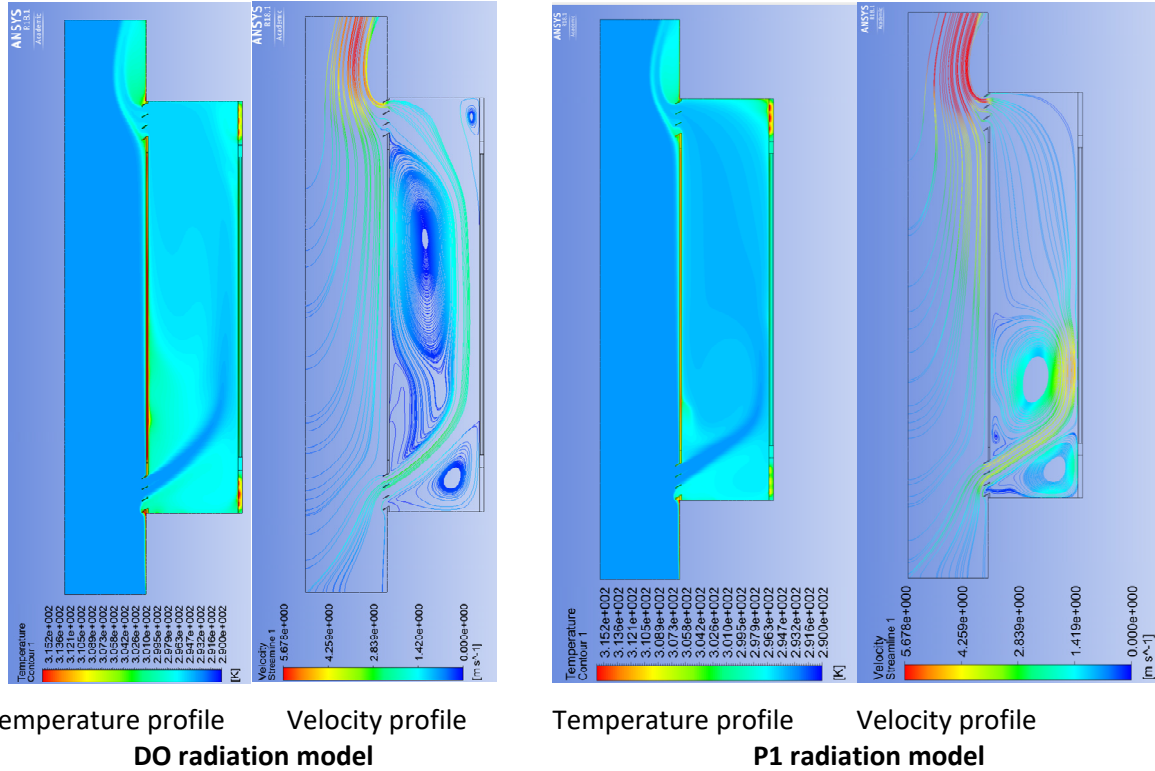


Figure 5-16: Results of P1 radiation models and DO radiation model.

As shown in Figure 5-16, it was found that P-1 radiation model reached convergence faster than the DO Model, but the DO radiation model showed better agreement with the experimental results both for surface and air temperatures. As mentioned in the previous section, DO resulted in around 7% variation on the external glazing and 10% on the back internal glazing. P1 radiation models resulted in around 11% variation on both the external and back internal surface temperatures. Moreover, it underestimates the air temperature in the cavity by 3°C compared to DO radiation model. These results are contrary to that of Coussirat et al. (2008) who found that the P-1 radiation model seems to predict solid phases temperature better and showed a better fit to Manz et al. (2004) experimental results. It is found that the DO Radiation Model is more accurate but requires higher computational facilities. The DO Radiation Model is recommended for further validation and simulation work.

#### 5.6.1.4. Simulation 4: Turbulence model

SST K-omega and RNG k-epsilon turbulence models are compared. Both turbulence models are coupled with discrete ordinate (DO) radiation model. RNG resulted in around 7% variation on the external glazing and 10% on the back internal glazing. SST k- $\omega$  resulted in a surface temperature of 39.9°C for the external glazing, which represents 11 % variance. The back of the inner glazing has a temperature of 24 °C compared to experimental data recording 27.85°C, which represents a 14% error. A 30% discrepancy was found on the front of the inner glazing recording 28°C compared to 40°C recorded by Mei's experimental measurements. Thus, SST K-omega results deviated with large error margin from experimental results. In agreement with (Coussirat et al., 2008), it was found that the RNG k- $\epsilon$  has a better prediction for heat transfer when there are zones of low velocities in the façade configuration. In all cases, RNG k- $\epsilon$  turbulence model with full buoyancy effect and 'Enhanced Wall Treatment' resulted in the best agreement for the simulations. It proved to have better simulation stability and achieve convergence faster than SST k- $\omega$ .

#### 5.6.1.5. Simulation 5: Level of complexity

This section examines the influence of the level of complexity or simplification of the validated structure on heat transfer and airflow predictions. As shown in Figure 5-17, two different levels are examined: (a) abstracted model replaced the grill with an opening (b) full detailed modelling of the structure and grill. Both models used DO radiation model with solar load and RNG k- $\epsilon$  turbulence model with full buoyancy effect and Enhanced Wall Treatment.

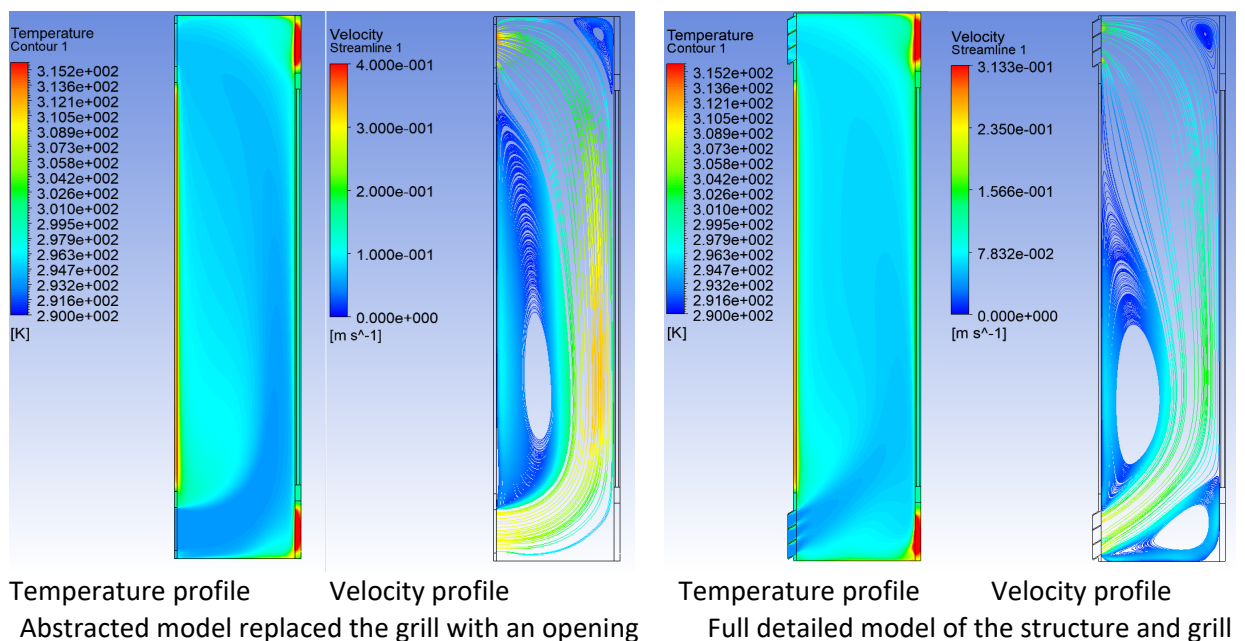


Figure 5-17: Results of the two levels of Complexity.

As shown in Figure 5-17, the cool air enters from the bottom inlet and slowly rises inside the cavity moving from the inner glass to the external glass. This phenomenon can explain why the temperature measured on the right side of the gap is always lower than the temperatures measured on the left side of the gap. The detailed modelling of grills resulted in a directed airflow entering the domain at 30 degrees (inclined at 30° to the horizontal line), a controlled volume of air, and a minimized air velocity at the inlet. On the other hand, the abstracted model resulted in higher air velocity near the inner glazing, which decreases the temperature of the front internal glazing surface by 1°C and slightly reduces the air cavity temperature. Although the full detailed model resulted in a more accurate airflow analysis, the abstracted model predicted the exact same external and internal glazing surface temperatures.

#### 5.6.1.6. Summary

Surface and mid cavity temperatures for previous parameters are measured and compared with the data documented in Mei et al. (2007) as shown in Figure 5-18 and Figure 5-19.

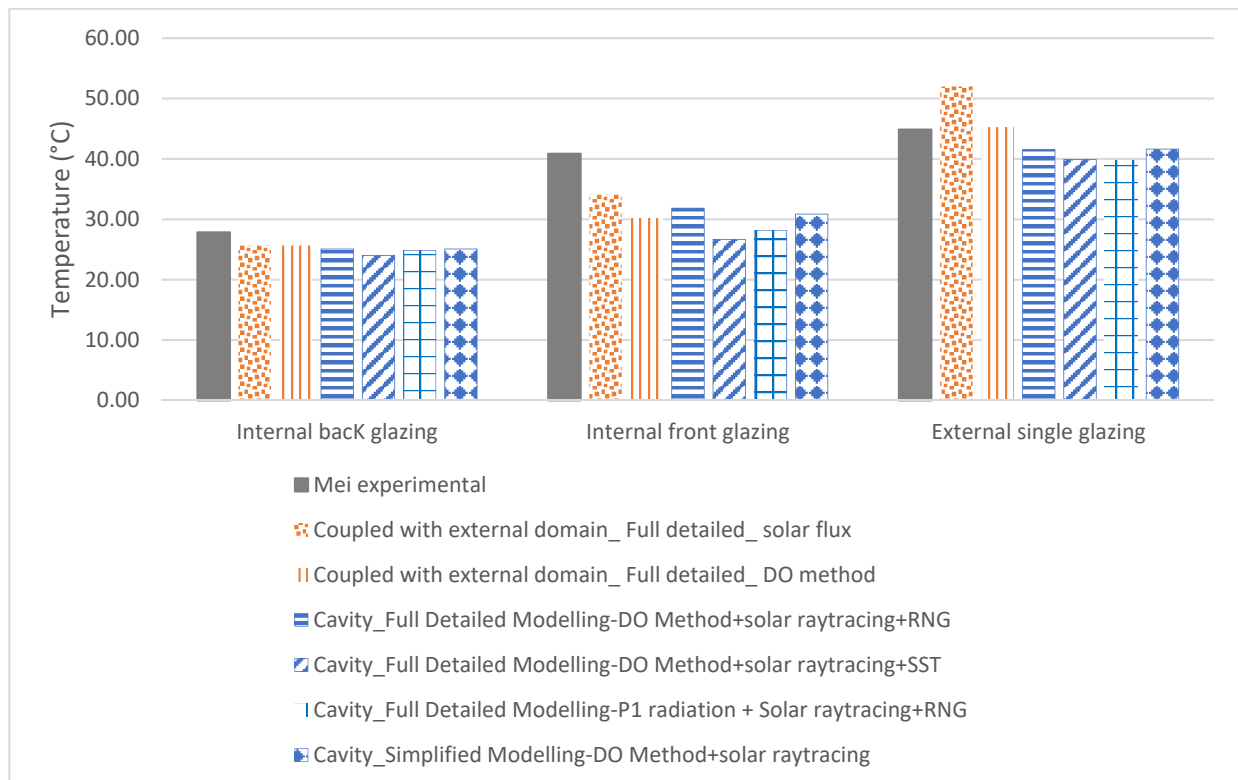


Figure 5-18: Comparing surface temperatures of cases

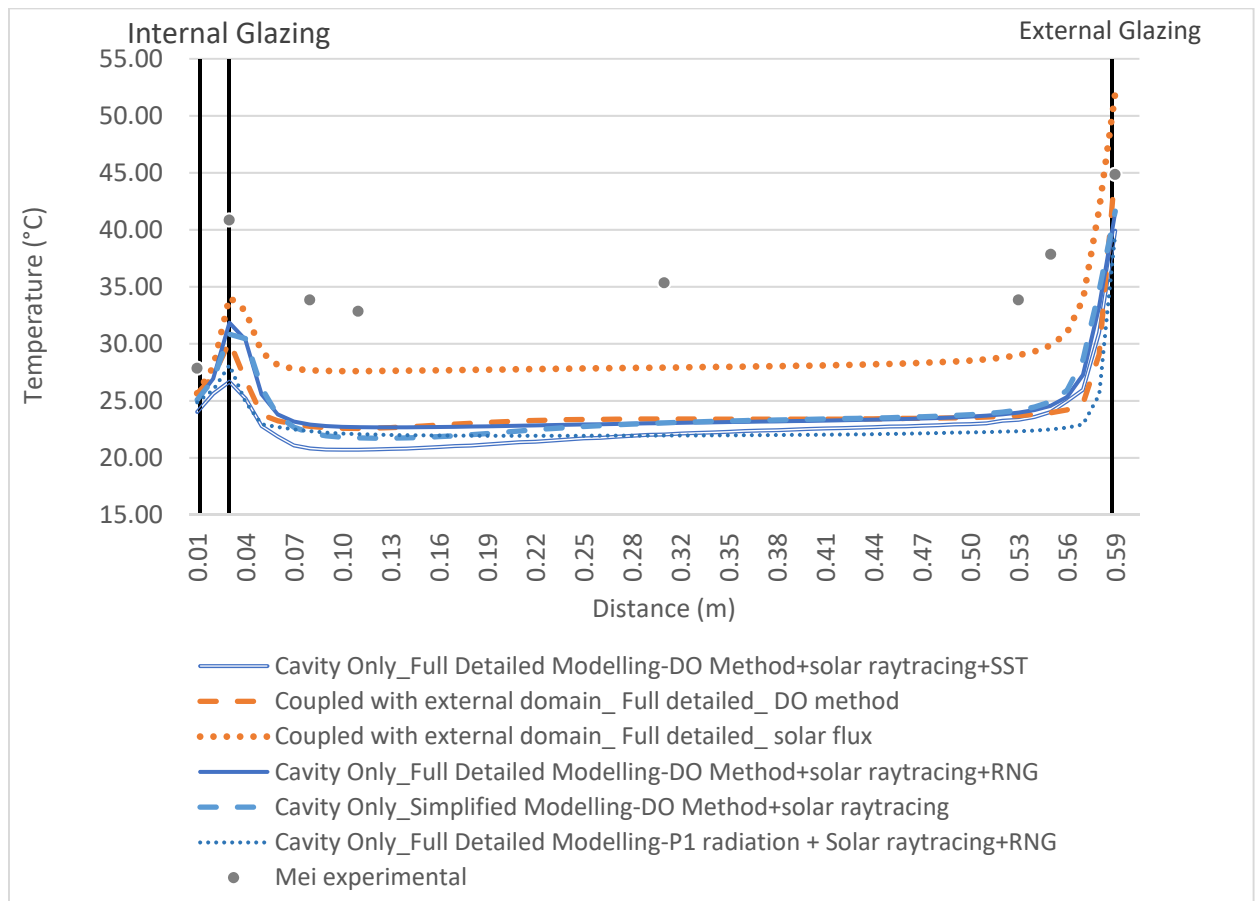


Figure 5-19: Comparing mid cavity temperatures at 1.1m

In all cases, RNG k- $\epsilon$  turbulence model with full buoyancy effect and Enhanced Wall Treatment resulted in the best agreement for the simulations. It proved to have better simulation stability and achieved convergence faster than SST k- $\omega$ . Both turbulence models are coupled with discrete ordinate (DO) radiation model. RNG resulted in around 7% variation on the external glazing and 10% on the back internal glazing. SST k- $\omega$  resulted in a surface temperature of 39.9°C for the external glazing, which represents 11 % variance. The back of the inner glazing has a temperature of 24 °C compared to experimental data 27.85°C, which represents a 14% error. SST k- $\omega$  results in 30% discrepancy on the front of the inner glazing recording 28°C compared to experimental data 40°C as shown in Figure 5-18 and Figure 5-19. Thus SST k- $\omega$  resulted in the highest discrepancy and slowest convergence. In agreement with Coussirat et al. (2008), it was found that the RNG k- $\epsilon$  has a better prediction for heat transfer when there are zones of low velocities in the façade configuration. In all cases, RNG k- $\epsilon$  turbulence model with full buoyancy effect and Enhanced Wall Treatment resulted in the best agreement for the simulations.

It is found that the DO Radiation Model is more accurate than P1 radiation but requires high computational power. The P1 radiation model reached convergence faster than DO Model, but the DO radiation model showed better agreement with the experimental results both for surface and air temperatures. DO resulted in around 7% variation on the external glazing and 10% on the back internal glazing. P1 radiation models resulted in around 11% variation on both the external and back internal surface temperatures. Moreover, it underestimates the air temperature in the cavity by 3°C compared to DO radiation model. These results contradict Coussirat et al. (2008), who found that the P1 radiation model seems to better predict solid phases temperature and showed a better fit to (Manz et al., 2004) experimental results. DO radiation model was implemented in conjunction with the Solar Ray Tracing options of the solar load model. Two bands 'Solar' and 'Thermal' were set for the Non-Gray DO model. The solar band corresponds to wavelengths smaller than 2.7  $\mu\text{m}$ , and the thermal band to wavelength larger than 2.7  $\mu\text{m}$ . The Angular Discretization was set to 6x6 divisions and a pixilation of 3x3. The DO Radiation Model is recommended for validation and simulation work.

The level of complexity of the model directly affects the computational timing and the problem resolved. It was found that the full detailed model resulted in a more accurate airflow analysis, but the abstracted model was able to predict the exact same external and internal glazing surface temperatures. The addition of the grills details does not show an appreciable difference in the results. It means that it is not worthy of making a full detailed model.

The recorded errors could be due to:

1. It is worth mentioning that solar radiation value used in the simulation was 715W/m<sup>2</sup> as reported from the experimental work and also recommended through related validation work (Ji et al., 2007, 2008). However, the value 715W/m<sup>2</sup> refers to the measured value at the outer glass skin while its nominal value was 800W/m<sup>2</sup>, which was produced by the solar simulator and was thus 12% higher.
2. The seven (TSI Omni-directional Model 8475) has an accuracy of  $\pm 3.0\%$  for a temperature range of 20°-26°C.
3. The undefined inlet boundary condition.



The setup of the best agreement with the experimental measurements will be applied for the shaded cavity which is equipped with white blinds at angle 45°

### 5.6.2. Integrated Shaded cavity

Detailed shaded DSF equipped with white Venetian blinds at angle 45° is simulated using RNG k –  $\epsilon$  model and DO radiation model with non-gray specification as shown in Figure 5-21. The model is decoupled from the external environment. The simulation results are compared with the experimental results Mei et al. (2007) as well as Pasut and De Carli (2012) and Ji et al. (2007) numerical simulation results as shown in Figure 5-20.

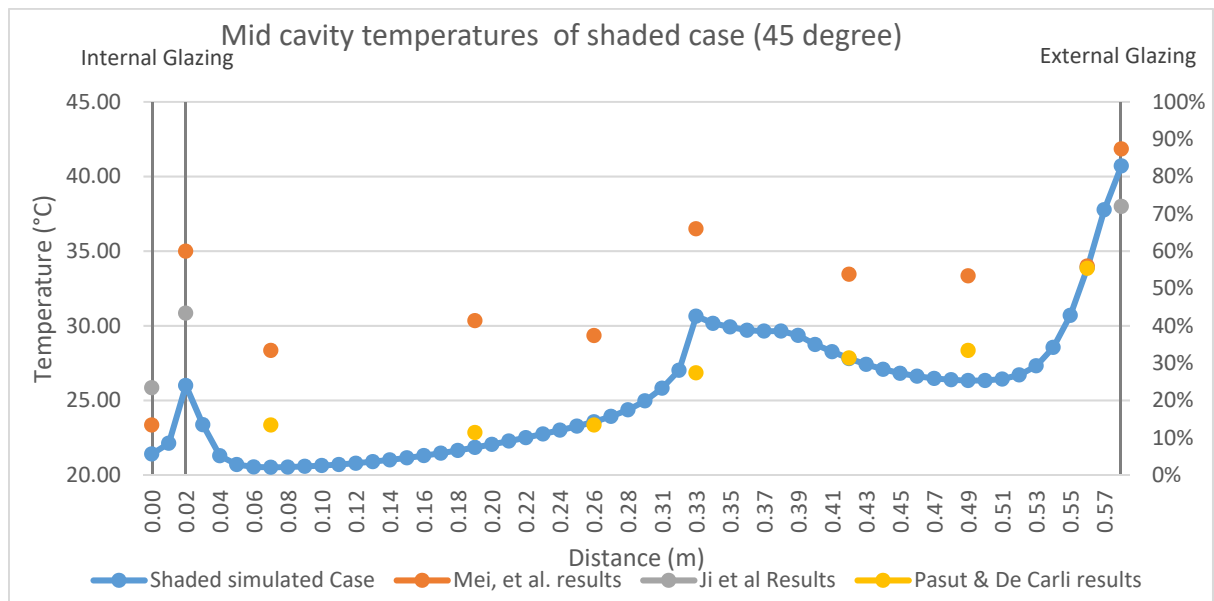


Figure 5-20: Mid cavity temperatures of the shaded case (45 degrees) compared with (Mei et al., 2007) experimental results as well as (Ji et al., 2007) and (Pasut & De Carli, 2012) numerical simulation results.

As shown in Figure 5-20, the surface temperature of the external glazing of the integrated DSF recorded 40.7°C compared to 41.85°C recorded by Mei et al. (2007) and 38°C recorded by Ji et al. (2007). The internal glazing facing the space recorded 21.4°C compared to 23.3°C recorded by Mei et al. (2007) and 25.85°C recorded by Ji et al. (2007). The internal glazing facing the cavity recorded 27°C compared to 35°C recorded by Mei et al. (2007) and 30.85°C recorded by Ji et al. (2007). The computed air temperature generally agrees well with the measured data of Mei et al. (2007). The results of air temperature matched Pasut and De Carli (2012) to a great extent. The 5°C variations in air cavity temperature compared to the experimental results of Mei et al. (2007) has been reported by the research group (Ji et al., 2007). The under-prediction of air temperature could be due to geometry simplification. Less than 5% discrepancy was found on the external glazing and around 10% on the internal glazing as shown in Figure 5-20. 20% discrepancy was found on the front inner glazing (27°C)

compared to (35°C) experimental data. According to Zhang et al. (2007) and Pasut and De Carli (2012) 30% discrepancy is an acceptable margin of a discrepancy between CFD and experimental results in enclosed environments. Despite the reported variations, there is a consistency of the data trend between the simulations' results and all previous experiments as shown in Figure 5-20.

As shown in Figure 5-21, comparing shaded with non-shaded cavity models showed that the use of Venetian blinds at 45 degrees resulted in a significant difference in the temperature of the inner double glazing which was reduced from 24 °C to 21.4°C. These results indicate that the CFD model succeeded to represent the shading effects provided by the Venetian blinds. The simulations predict that the inner double glazing temperature can be substantially reduced by solar shading systems.

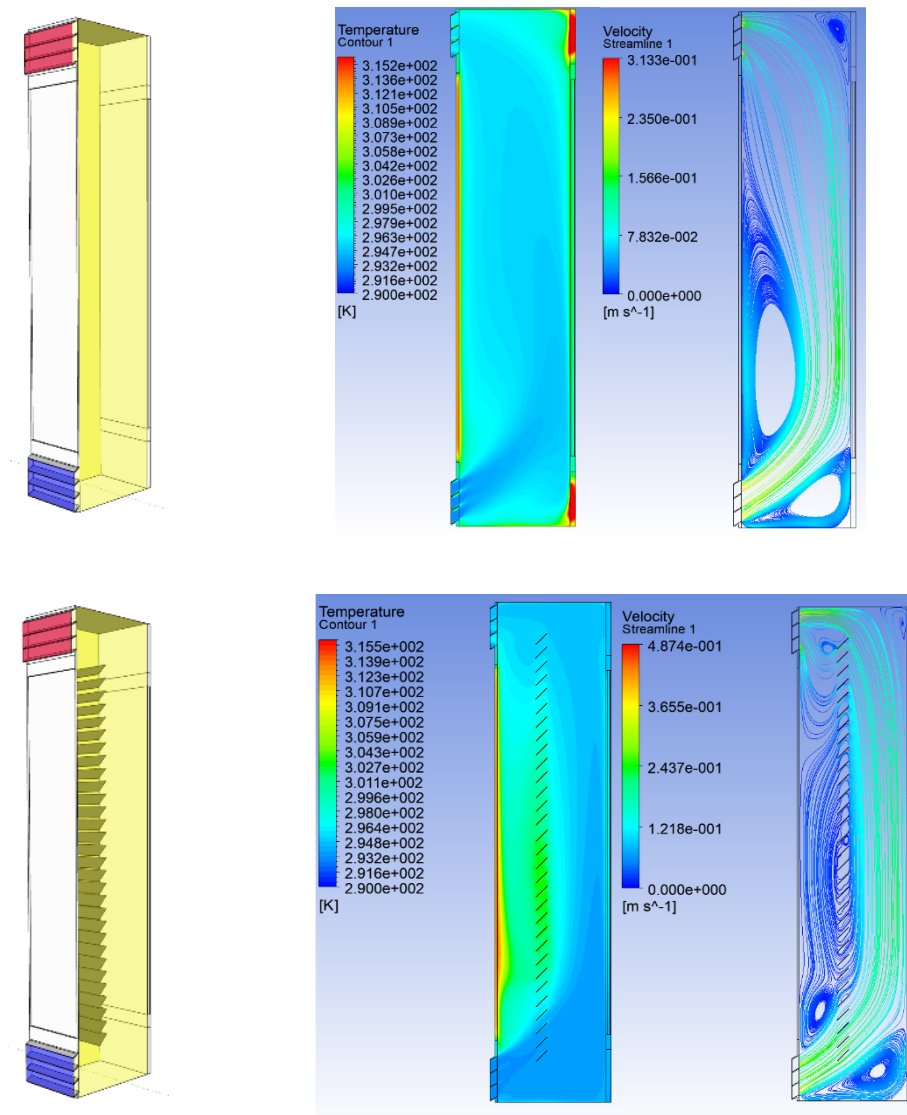
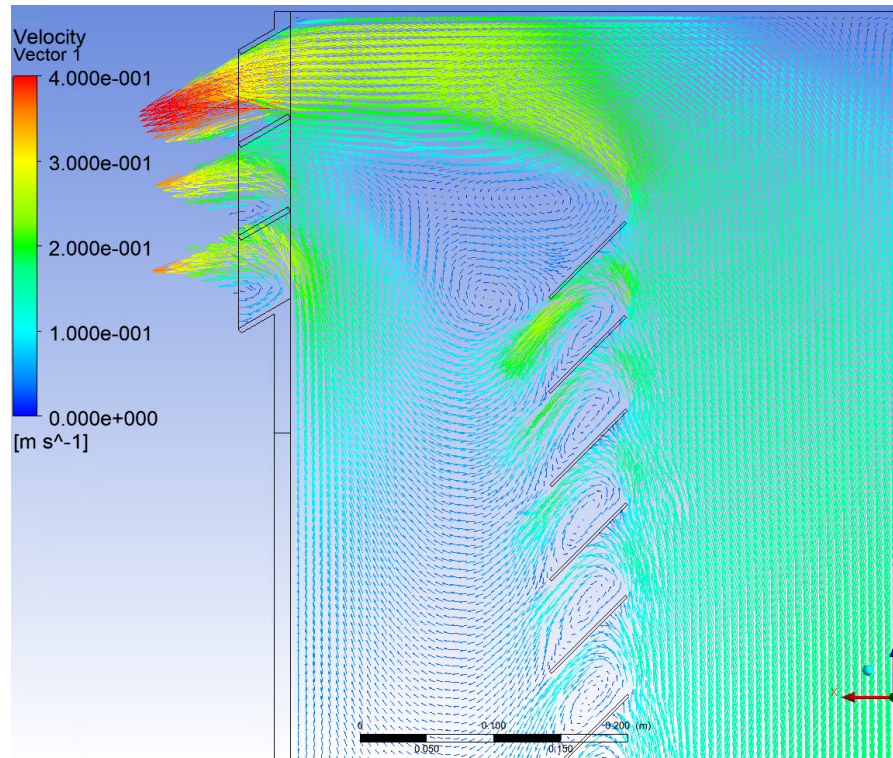


Figure 5-21: Cavity temperatures and airflow of non-shaded and shaded case.

As shown from the airflow in Figure 5-22, the cavity flow was largely enhanced with the presence of the Venetian blinds. The blinds absorbed part of the incident radiation which heated them up to 30.65°C resulting in an additional source for buoyancy-driven flow in the cavity and improved buoyancy around them. The velocity of the air is very slow through the blind, and no eddy is produced before and after the blind as shown in Figure 5-22.



*Figure 5-22: The airflow velocity [m/s] field close to the Venetian blind.*

## 5.7. Conclusion

This chapter represents the general methodology of the numerical work. After briefly reintroducing the problem, a detailed discussion is provided for the computational domain, boundary conditions, computational mesh and fluent setup. The chapter reviews critically methods used in literature to assess both naturally and mechanically ventilated DSF and discusses the challenges met during the simulation process including the level of geometrical model detailing, domain size, solar simulator representation, and selection of turbulence and radiation models.

A CFD model for the natural ventilated DSF was developed using Ansys Fluent. The model can predict the surface temperatures, air temperature and air velocity distributions, and heat flux. The model was validated using Mei. et al. experimental data collected in a full-scale DSF. The computed velocity, surface and air temperatures were in good agreement with the measured data.

It was found that modelling a full-height wall with an applied solar flux of  $715 \text{ W/m}^2$  achieved higher external glazing surface temperature than the experimental results. Despite achieving higher air cavity temperatures, it is over expecting the outer glazing temperature by the physical representation of the heat source in the domain. On the other hand, the application of the Discrete Ordinate (DO) model with non-gray specification and solar raytracing achieved good agreement of glazing surfaces with the experimental case.

RNG k-epsilon turbulence model with full buoyancy effect resulted in the best agreement for the simulations. The Enhanced Wall Treatment was adopted for the RNG k-epsilon model. It proved to have better simulation stability and achieve convergence faster than SST k-omega.

It was found that the DO radiation model is more accurate than P1 radiation model but requires high computational facilities. P-1 radiation models resulted in around 11% error on external and internal surface temperatures. It underestimated the air temperature in the cavity by  $3^\circ\text{C}$  compared to DO model. These results are contrary to that of (Coussirat et al., 2008) who found that the P-1 radiation model seems to predict solid phases temperature better and showed a better fit to (Manz et al., 2004) experimental results. DO radiation model was implemented in conjunction with the solar ray-tracing options of the solar load model. DO radiation model is responsible for calculating surface emissions while the solar ray tracing solar load model was used to calculate radiation effects from the sun's rays that enter a computational domain. Two bands 'Solar' and 'Thermal' were set for the Non-Gray Discrete Ordinates (DO) model. The solar band corresponds to wavelengths smaller than  $2.7 \mu\text{m}$ , and the thermal band to wavelength larger than  $2.7 \mu\text{m}$ . Although, a fine angular discretization of  $6 \times 6$  was recommended,  $4 \times 4$  achieved acceptable results and is chosen for further implementation as the larger divisions highly added to the cost of the computation. Besides, a pixilation of  $3 \times 3$  achieved acceptable results. The DO Radiation Model is recommended for further validation and simulation work.

In agreement with Amaireh (2017) and Pasut and De Carli (2012), the extension of the computation domain to include part of the external environment, allows proper modelling of the ambient environment. Thus, the results of coupled cavity with the external environment showed better agreement with the experimental results. A slightly higher cavity temperature was recorded but almost the same surface temperatures. Although the results of coupled cavity with the external environment showed a slightly higher air cavity temperatures, the difference is small and can be negligible. Therefore, modelling the cavity without external environment will be further applied to minimize the computational time.

Level of complexity of the model directly affected the computational timing and the problem resolved. It was found that the full detailed model resulted in a more accurate airflow analysis while the abstracted model predicted the exact same external and internal glazing surface temperatures. Adding the grills details does not show an appreciable difference in the results. It means that it is not worthy of making a full detailed model.

Finally, The settings for fluent setup are presented, where RNG  $k - \epsilon$  turbulence model and Discrete Ordinate (DO) model with non-gray specification with two bands, solar and thermal, from 0-2.7mm and 2.7-1000mm to represent the spectral radiation are preferable. It is recommended to use velocity inlet, which matches the reality conditions for naturally ventilated cavities. After setting guidelines for the CFD numerical modelling setup through the validation against Mei et al. (2007) naturally ventilated DSF case. The CFD setup will be used in Chapter six to environmentally assess the responsive solar-shading system performance within their potential context of operation.



# Chapter 6 . INTEGRATED DESIGN AND SIMULATION

## 6.1. Introduction

This chapter compares the thermal performance of DSF integrated with responsive dynamic solar-shading system (Flat and folded) having three aperture sizes with the non-shaded case. Ventilated Double Skin Façade (DSF) integrated with solar-shadings in hot and subtropical climates proved efficient in substantially decreasing indoor heat gains and thus the building cooling loads (Amaireh, 2017; Bellia et al., 2014; Chan et al., 2009; Ghaffarianhoseini et al., 2016). DSF equipped with kinetic solar-shadings significantly improves the building energy behaviour through the entire year (Baldinelli, 2009), and provides architects with more freedom to integrate advanced technologies in their practice. This chapter investigates the correlation between responsive solar-shading devices and DSF thermal conditions using CFD coupled thermo-fluid-dynamics models in the hot arid climate of Cairo, Egypt. It uses the recommended CFD modelling setup from chapter five. Flat and folded solar-shadings are installed in the DSF air cavity and compare it with the non-shaded base case. Three aperture sizes (30, 50 and 70 %) are modelled to represent the responsive solar-shadings different states.

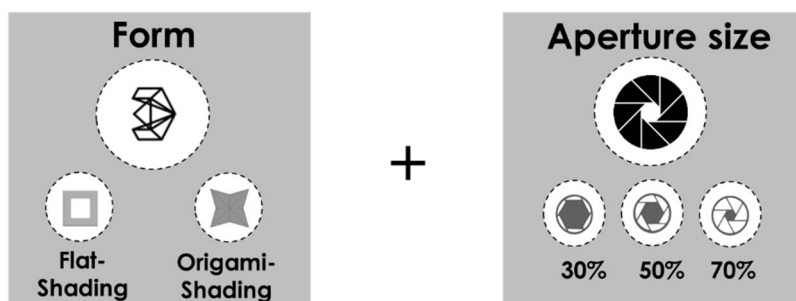


Figure 6-1: Form and aperture size tested variables.

The results section analyze two aspects. First, the inner surface temperatures, airflow and heat flux are analyzed to measure the impact on energy reduction indoors and select optimal range of aperture size/percentage of the shade opening to inform solar shading designs. Second, the cavity temperature and solar-shading surface temperature are analyzed to detect the required activation range for the SMM actuators. The chapter informs the design parameters with the required temperature needed for activating the SMMs and the optimum solar shading aperture. *By doing so*, environmental feedback will be provided to guide the design decisions, and tailor the smart material properties. The synchronization between the activation temperatures of SMM actuators, the surface temperature of the solar shading



materials and thermal conditions of the cavity is crucial for optimizing the operation of responsive solar-shading devices and the resulting aperture. The thermal simulations can guide two groups of decisions; one related to the solar shading unit and the other related to smart materials (actuators).

In this Chapter, three scenarios of the DSFs are studied as follows; non-shaded DSF, flat-shaded and origami-shaded DSF, as shown in Figure 6-2.

In the first scenario, the non-shaded cavity is studied as a base case. The conditions of the non-shaded DSF cavity, temperatures' contours are measured to detect the highest temperature profile to install the shading screen to activate the responsive system thermally. The analysis of non-shaded DSF parameters, which included DSF cavity width, the façade layering and the domain size, leads to the next level of investigation with solar shading apertures and forms.

In the second scenario, flat solar-shading devices are installed inside the DSF cavity. The flat solar-shadings have three aperture sizes (30%, 50% and 70%) which represents a simplified simulation method for responsive kinetic solar shading system. A set of studies analyses the surface and air temperatures, airflow and heat flux to test the DSF performance efficiency and optimize the screen aperture ranges at different times in peak summer and winter day. Moreover, the solar shading surface temperature is measured to detect the required activation range for the SMM.

In the third scenario, more complex forms of folded origami shading are tested numerically with the same three aperture sizes (30%, 50%, & 70%) and compared at 12:00 pm in a peak summer day. Analyses of surface and air temperatures, airflow, and heat flux aim to test the effect of the change of form from flat to folded shading. The solar-shading surface temperature is analysed to allocate SMM actuators and detect their required activation range.

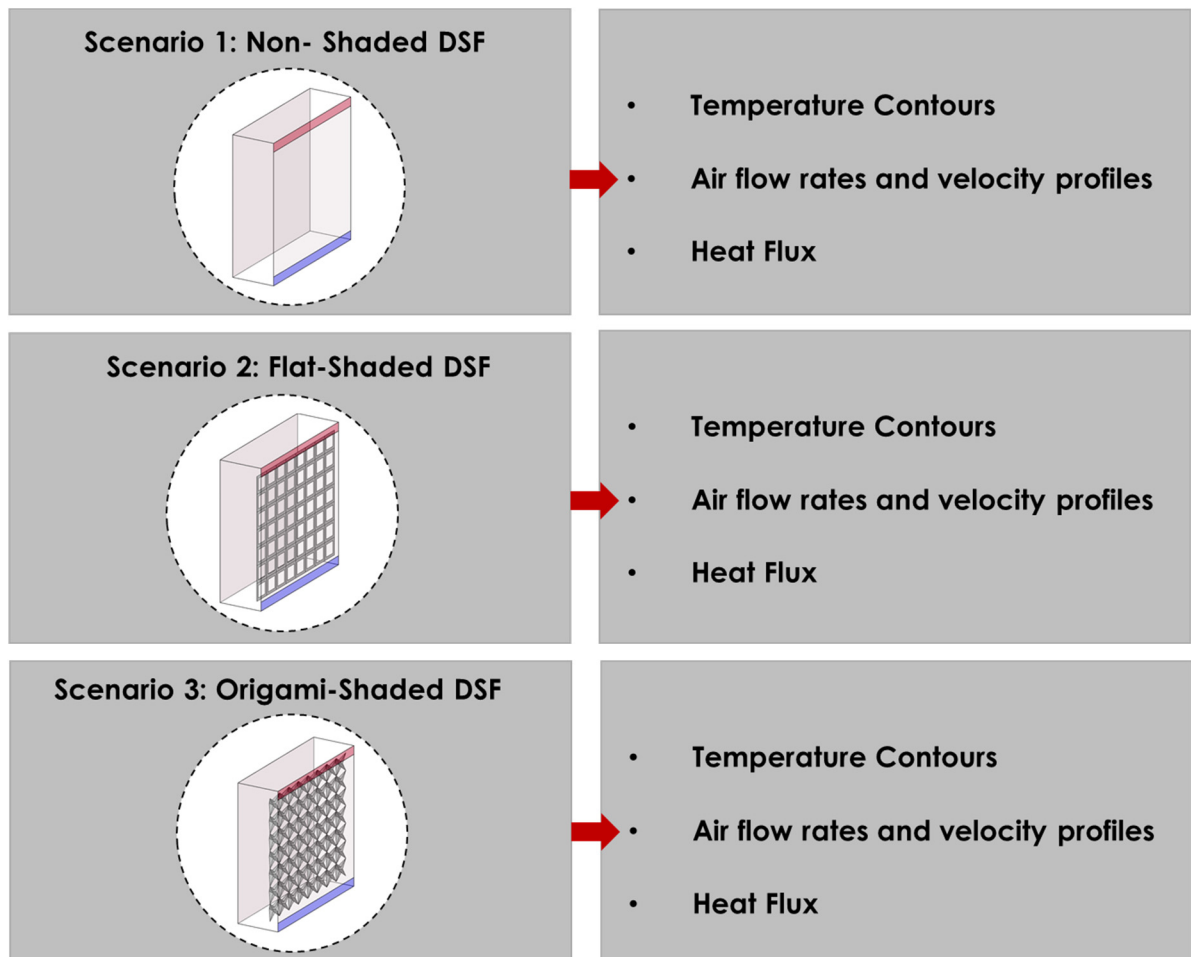


Figure 6-2: The three studied scenarios.

#### 6.1.1. Overview Climate of Cairo City

Cairo, the capital of Egypt, is situated in a hot arid climate, with increasing cooling loads in office buildings to maintain suitable work environments. Cairo as a case study has a climatic profile and thermal comfort requirements similar to other cities in hot arid climates according to updated Köppen climate classification (Beck et al., 2018; Kottek, Grieser, Beck, Rudolf, & Rubel, 2006) as shown in Appendix A.

Climatological information of Cairo was taken from the Egyptian Meteorological Authority report, which is based on monthly averages for the 30-year period (1976 – 2013). The report suggested that the annual average temperature is 22.4 °C. In July, the peak summer, has a maximum average temperature of 35.4 °C and a minimum average temperature of 20 °C, while in January, the peak winter, a maximum average temperature of 18 °C and a minimum average temperature of 10.2°C based on the standard EnergyPlus Weather files (.EPW) and climate consultant which is attached in Appendix C (Liggett et al., 2016).

Despite office buildings in Cairo dating back to the 1880s, contemporary office buildings have been adopting the 'international style' with excess usage of glazed facades irrespective of the bioclimatic conditions (Hamza, 2004). A range from 70% to 80% of total energy consumption is used for the cooling system (Dabaieh et al., 2015). In hot climates, the management of solar-shadings and ventilated channels are the two most effective strategies to reduce undesirable solar loads inside interior spaces, especially during warm periods (Gratia & De Herde, 2007; Hamza & Underwood, 2005; Hazem et al., 2015). These two most effective strategies are merged in DSFs integrated with solar-shading devices. Moreover, solar shadings can be more responsive to changing environmental conditions to achieve more energy reductions. This hypothesis is supported by (Baldinelli, 2009), who argued that the integrated movable solar-shading device could be used to optimize both winter and summer energy performance.

The proposed responsive solar-shading skins could present a modern version of the traditional solar screens in a more adaptive way, using the soft mechanics' approach. The proposed system positions the responsive solar-shading in the cavity of a DSF in order to increase the kinetic system efficiency and responsivity. Safer et al. (2005) found that positioning the blind at 15cm from the external glazing is the best configuration for the external ventilation of the channel, particularly in summer conditions. It is recommended to position the solar-shading device in the range between the mid of the cavity and the external skin (Gratia & De Herde, 2007; Hamza & Underwood, 2005; Safer et al., 2005), taking in consideration the highest temperature profile of the cavity to activate the smart system thermally. Light- coloured and high reflective shading devices are recommended as they allow considerable cooling load reductions in summer and satisfactory solar gain in winter (Baldinelli, 2009).

Due to high direct solar radiation in the hot arid climate of Cairo, Egypt, responsive solar-shading system can be thermally activated to produce movements and change its aperture size. The thermally triggered SMMs of the solar-shading device positioned in the cavity need to perform in specific cavity temperature ranges. Temperature contours for the empty cavity are measured to detect the highest predicted possible temperature profile to install the shading screen to activate the smart system thermally. Then the solar shading surface temperature is measured to detect the required activation range for the shape memory materials.

### 6.1.2. Location and Time conditions

The study is conducted as point in time simulations for summer and winter; where the day of peak conditions (air temperature and solar radiation) is considered. For these selected days, investigation and simulation are conducted at 9:00 am, 12:00 pm and 15:00 pm. The south-oriented DSF is located in Cairo, Egypt (30.044° N and 31.34° E) as shown in Table 6-1. Climatic data for outdoors temperature for a peak summer day (15<sup>th</sup> of July) and a peak winter day (15<sup>th</sup> of January) is taken from based on Egyptian Meteorological Authority report and the standard EnergyPlus Weather files (.EPW). A difference of 46.8° was found in the sun angle between summer and winter in Cairo by recording 83.4° in summer and 36.6° in winter (Gadelhak, 2013). Temperature ranges in Cairo are generated from climate consultant and attached in Appendix C (Liggett et al., 2016).

The solar calculator of Ansys Fluent is manually updated every simulation with time and date with linked external ambient temperature. Then solar calculator of Ansys Fluent automatically updates the sun direction vector and solar irradiation values on boundary conditions.

Table 6-1: Location settings, date and time.

Site	Longitude	31.34° E	
	Latitude	30.044° N	
Date	15 July		
Time	9:00	12:00	15:00
Sun Direction Vector	X: -0.0113, Y: -0.6594, Z: 0.7518	X: -0.1487, Y: -0.0024, Z: 0.9888	X: -0.0136, Y: 0.6561, Z: 0.7545
Date	15 Jan		
Time	9:00	12:00	15:00
Sun Direction Vector	X: -0.6358, Y: -0.6711, Z: 0.3813	X: -0.7781, Y: -0.0167, Z: 0.6279	X: -0.6470, Y: 0.6477, Z: 0.4023

## 6.2. Case Description

For the purpose of the study, 3D Models of one storey south-oriented DSF similar to the experimental case of Mei's 2007 (chapter 5: page 187) is studied numerically with and without solar shading. The configuration has been used for several reasons: it increases the natural ventilation contribution; provides a high level of daylighting and sound insulation; reduces cooling load considerably when equipped with the solar-shading system, and provides good

protection from wind and pollutants. The study is carried for three scenarios, *non-shaded DSF*, *integrated DSF with flat solar-shadings* and *integrated DSF with folded solar-shadings*.

- *Non-shaded DSF base case (Scenario 1)* studies the impact of non-shaded DSF geometrical variables (DSF cavity width, the façade layering and the domain size) on the internal glazing surface temperature. A set of simulation runs are carried for the cavity without solar-shading for peak summer and winter day to study where to locate the solar shading devices best.

- *Flat solar-shading DSF (Scenario 2)* studies the impact of different aperture sizes of flat solar shading on the internal glazing surface temperature and heat flux to optimize the solar shading apertures. The temperature on the solar shading is recorded to customize the temperature needed by the smart material to be activated and perform responsively.

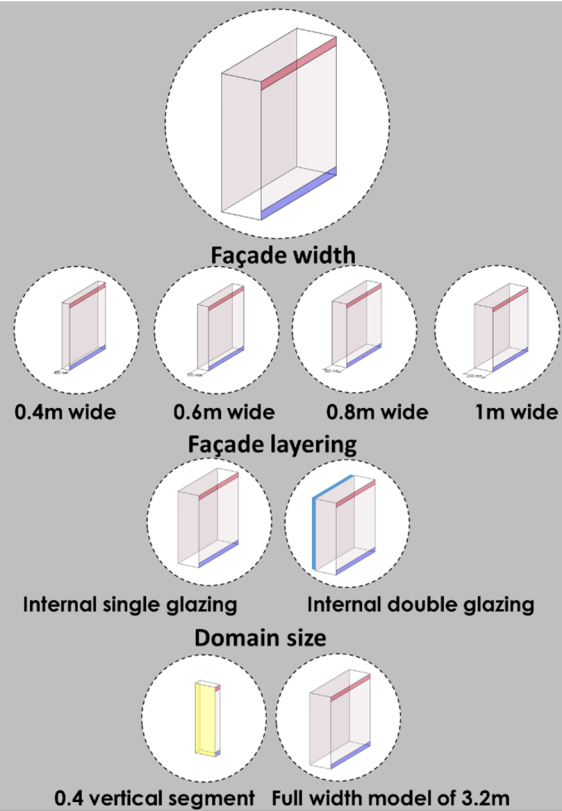
- *Folded solar shading DSF (Scenario 3)* studies the impact of different aperture sizes of folded origami solar shading on the internal glazing surface temperature and heat flux to optimize the solar shading apertures.

Table 6-2 and Figure 6-3 shows the tested variables which include; DSF width, façade layering, size of the domain, solar-shading aperture, and solar-shading form.

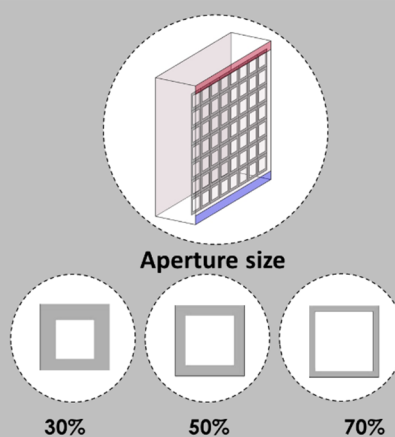
Table 6-2: Variables of DSF and solar shading

Space Parameters	
Climate Zone	Hot Arid
Orientation	South-oriented
DSF type	Corridor type
Scenario 1: DSF geometrical parameters (non-shaded cavity)	
Cavity's width	0.4, 0.6, 0.8, 1.0 m
Façade layering	Single glass of 6 mm thickness Double panels glass each pane is 6 mm thickness with 16 mm air gap.
DSF domain size	3D vertical segment of 0.4m and full DSF cavity of 3.2m
Solar-shading Parameters	
Scenario 2: Flat solar-shading Parameters	
Aperture size	30%, 50%, 70%
Scenario 3: Folded solar-shading Parameters	
Aperture size	30%, 50%, 70%

**Scenario 1:**  
Non- Shaded DSF



**Scenario 2:**  
Flat-Shaded DSF



**Scenario 3:**  
Origami-Shaded DSF

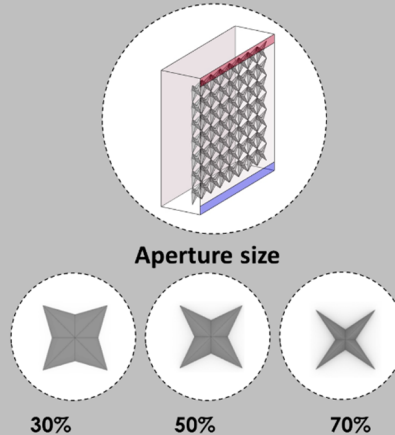


Figure 6-3: Tested variables for each scenario.

### 6.2.1. Geometrical model

Naturally ventilated one storey south-orientated DSF in Cairo, Egypt is studied numerically in this chapter with and without solar shading. The cavity is naturally ventilated through the inlet and outlet. The position of inlet/outlet on the outer DSF surface provides homogeneous horizontal ventilation (Guardo et al., 2011). Based on Guardo et al. (2011), this configuration indicated better performance in buoyancy induced air movement over bottom/top arrangements. The outside air is drawn from the bottom inlet of the cavity at 0.2m and the outlet of 0.2m at the top of the façade configuration as shown in Figure 6-4. The system consists of an external single pane glass surface of 12 mm thickness of toughened clear glass, a main air cavity of (0.4, 0.6, 0.8, 1m), a single inner glass of 6 mm thickness or double panels glass each pane is 6 mm thickness with 16 mm air gap in between. Table 6-3 shows the geometrical dimensions of the cavity and material thicknesses. Figure 6-4 represents the three cavities, *non-shaded DSF*, *integrated DSF with flat solar-shadings* and *integrated DSF with folded solar-shadings*.

Table 6-3: Geometric Parameters of DSF.

Cavity height	Cavity depth (3D domain)	Cavity width	Inlet height	Outlet height	Shading thickness	External glazing thickness	Internal glazing thickness	Air cavity	Internal glazing thickness
H (mm)	D (mm)	W1 (mm)	H1 (mm)	H2 (mm)	S1	G1 (mm)	G2 (mm)	W2 (mm)	G3 (mm)
3200	400, 3200	400,600,800 1000	200	200	8mm	12mm	6mm	16mm	6mm



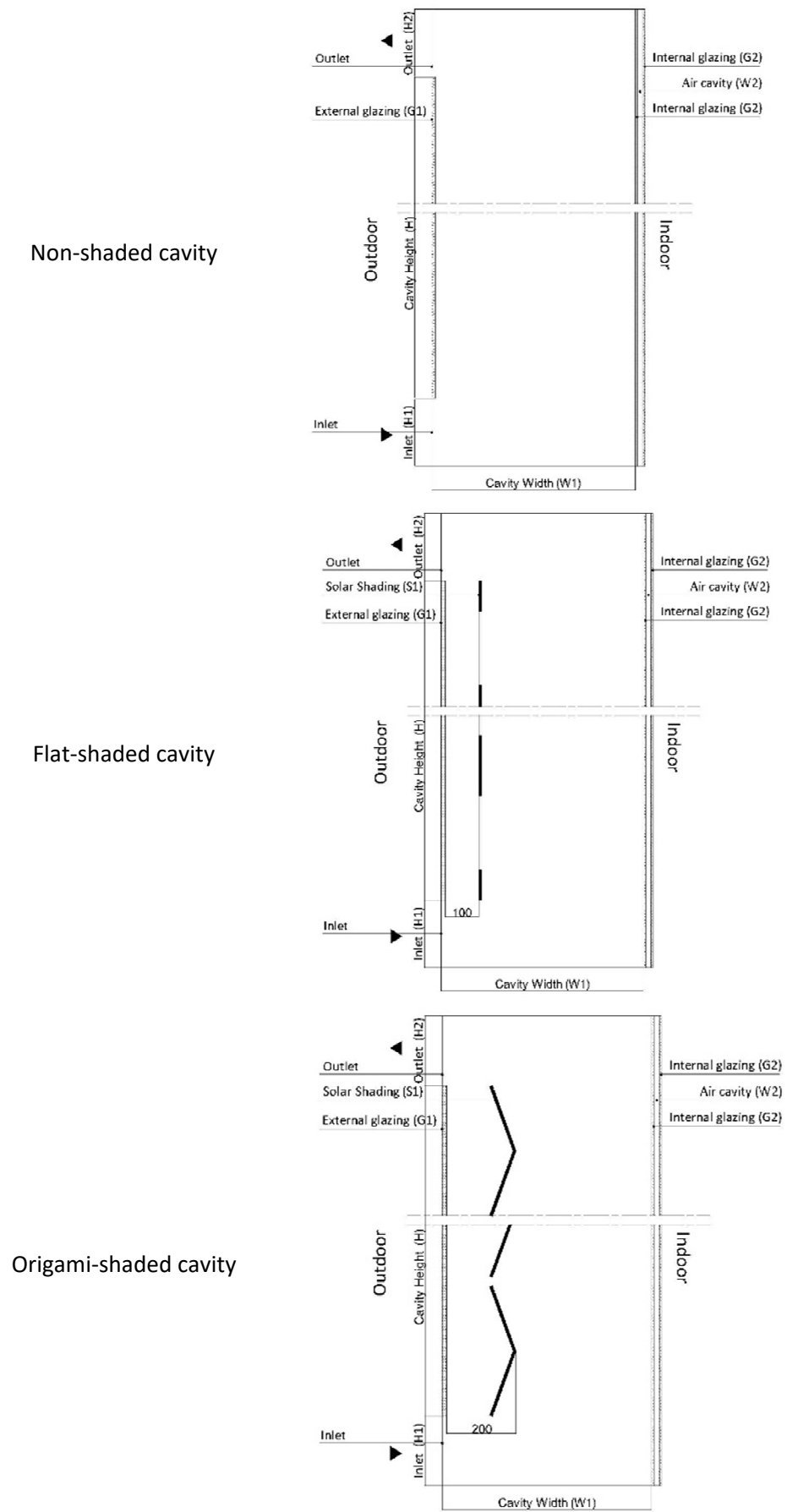


Figure 6-4: Geometrical model of non-shaded and shaded DSF.

In *Scenario 1*, some analysis are performed to examine the impact of the different parameters of DSFs, including cavity width, type of inner glazing, and the domain size on the DSF system performance and the temperature profiles.

- The impact of the change of **cavity width** is studied on the surface temperature of the inner wall. It has been stated in the literature that decreasing the cavity width, increases the heat gains on the inner façade surface as it reduces the global heat transfer coefficient of the module (Velasco et al., 2017). As seen in Figure 6-5, four different cavity depths of 0.4, 0.6, 0.8 and 1m are compared in terms of temperature and velocity fields.

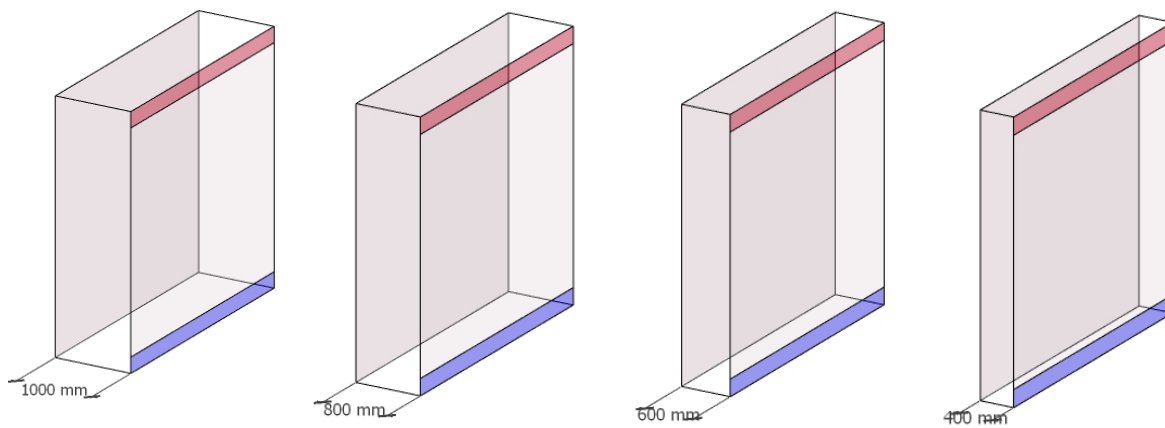


Figure 6-5: The four different cavity depths (0.4, 0.6, 0.8 and 1m).

- The impact of the **type of inner glazing (single & double)** is studied on the surface temperature of the inner wall. In warm summer temperatures, it was argued that increasing the *number of glazing layers* on windows of the interior wall to double clear glazing, did not offer major reductions in cooling loads (Hamza, 2004). Elarga, Zarrella, and De Carli (2016) reported that double inner glass layer with ventilation technique attained the lowest daily cooling sensible energy needs 669 kWh/day, on the other hand using single inner layer has increased the sensible cooling energy to 826 kWh/day. Accordingly, the study hypothesized that increasing inner glazing layers can improve conduction to the indoor environment. Two inner skin configurations; single and double inner glazing; are compared. A single glass panel with 6 mm thickness is compared to double-pane glass each pane is 6 mm thickness with 16 mm air gap.
- The impact of **domain size** is studied on the surface temperature of the inner wall. Different *DSF model sizes* are tested. Initially, a 3D vertical segment of

0.4m deep which represents the width of one solar shading module is modelled. This depth represents the solar shading module which can have more complex forms rather than an extruded solar-shading section. Further modelling of a full DSF cavity (3.2m deep) which includes eight solar shading modules is modelled to compare the two methods, as shown in Figure 6-6.

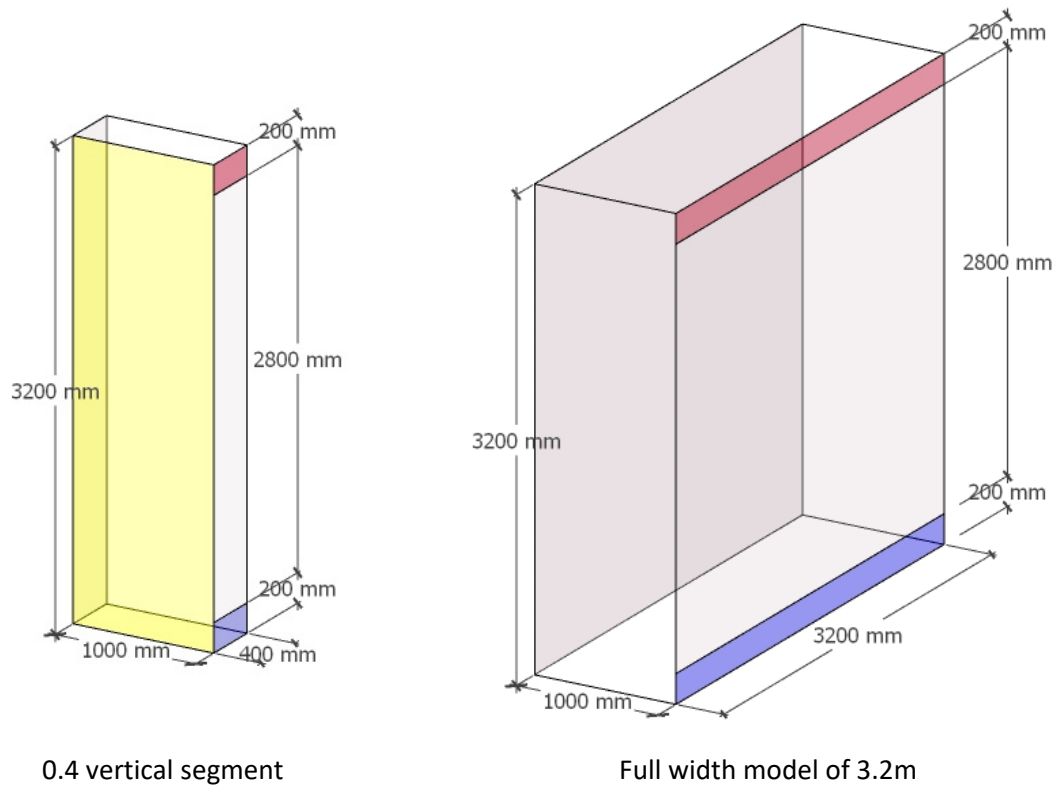


Figure 6-6: Domain Size.

### 6.2.2. The shading devices

The solar shading device within the DSF separates the cavity into two vertical zones, 'Frontal Zone' and 'Back Zone'. The solar-shadings have a significant influence on the thermal and airflow performance of the façade (Amaireh, 2017; Kirimt et al., 2016; Mei et al., 2007). The responsive shading screen with different forms and opening ratios is located at the highest temperature range of the cavity to heat and activate the actuators as well as to block the direct solar irradiation. A minimum opening percentage of 30% is considered to allow minimum required daylighting office spaces as per recommended by (Mahmoud & Elghazi, 2016; Wagdy et al., 2015).

From chapter four, the straight-line folding origami units showed potential as deployable structures, as shown in sections 4.8.1 and 4.10.2. The vertical position of the umbrella-like mechanisms using straight folding was explored in section 4.10.2, and the curved folding explored in section 4.8.2. It can achieve a high range of transformation resulting in aperture size between 0% (fully closed) and 90% (fully opened), as shown in Figure 6-7. Three aperture sizes (30%, 50% & 70%) are separately modelled to represent the different states of *responsive solar-shadings* for the simulations as shown in Figure 6-8. The proposed *responsive solar-shadings* are simplified into flat squares with aperture sizes of; 30%, 50% & 70% as shown in Figure 6-9, to cut down the computational cost and use this primary data for further system refinement.

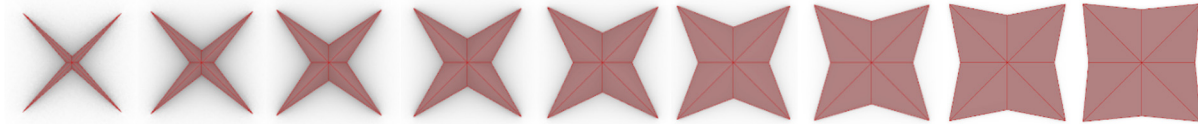


Figure 6-7: Steps of origami module kinetic motion.

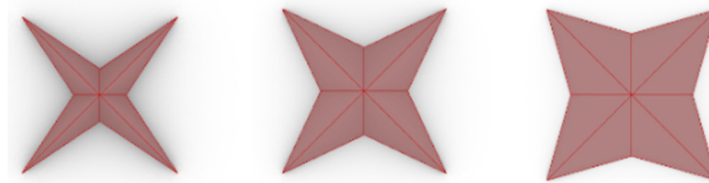


Figure 6-8: Selected aperture size (30%, 50% and 70%) of origami module kinetic motion.

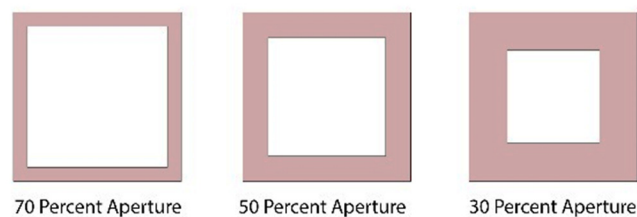


Figure 6-9: Abstraction of selected aperture sizes (30%, 50% and 70%).

The 0.4m vertical segment domain contains seven shading modules (0.4m X 0.4m) stacked vertically, as shown in Figure 6-10. The full cavity model is composed of an array of the module (0.4m X 0.4m). Seven shading modules are arrayed vertically, and eight shading modules are arrayed horizontally, as shown in Figure 6-11.

Screen positioning takes into consideration:

- The solar screen doesn't block the inlet and outlet of the cavity to facilitate airflow in the back zone to reduce the inner glazing temperature.
- The solar shading device will be located in the highest temperature within the cross-section of the cavity to benefit from the temperature resulting from direct solar irradiation to heat and activate the actuators.
- Dimensional considerations are taken according to material-based actuation limitations. The solar shading module can have an average size of 0.4m for a light material controlled with SMM actuators. This is inspired by the size for a single panel of Adaptive Solar Facade (ASF) installed in HIL building ETH Zürich which is 40cm moved with pneumatic actuators and the thermobimetals of (Sung, 2016) 'Bloom' 30cm and 'InVert' decorative shutter.
- A folded form is chosen to contain the heat inside the folding, reducing energy transmittance to inner façade layers for extra energy savings and for shape memory material activation.
- The folded origami form is chosen as one of the working models from the experimental explorations in chapter four in sections 4.8.1 (page 132) and 4.10.2 (page 159) and according to the selection criteria in section 4.12.

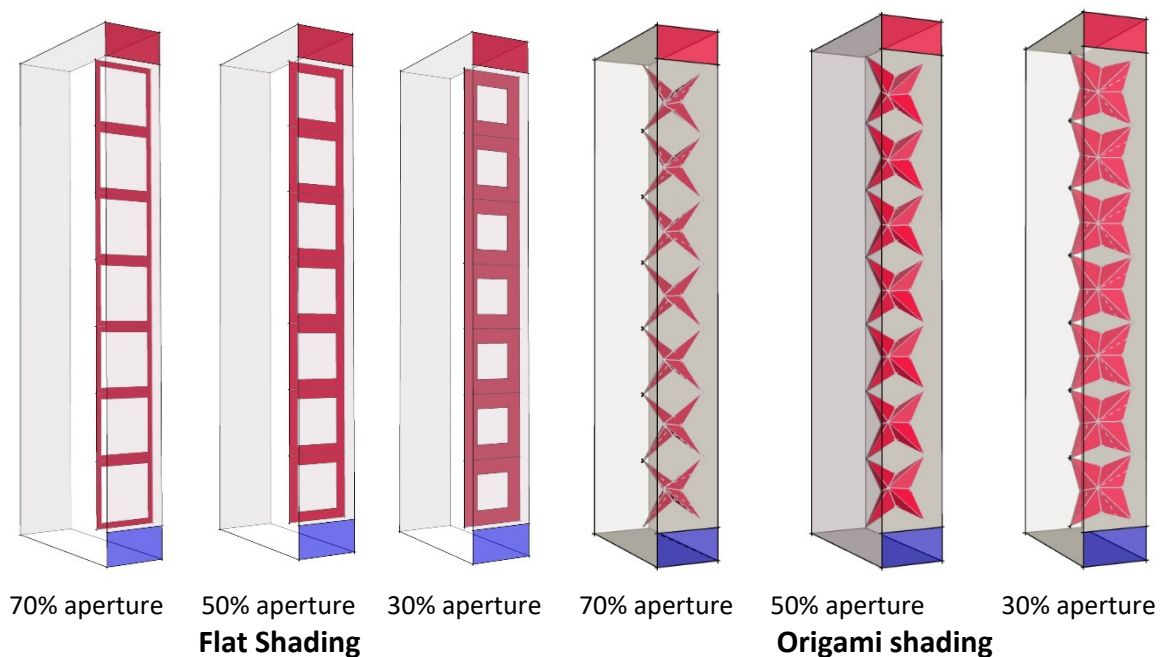
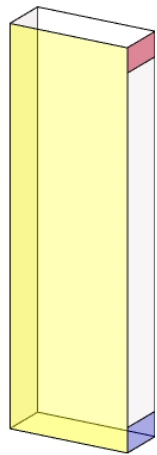
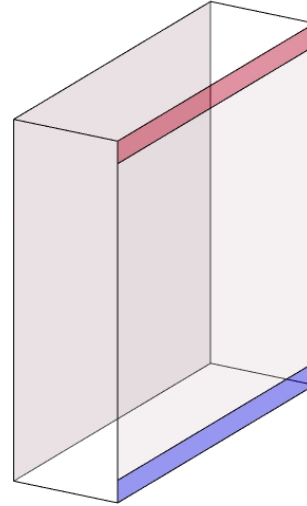


Figure 6-10: Flat and Origami Solar shadings with 3 apertures sizes; 30%, 50% & 70%.

Non-shaded Cavity

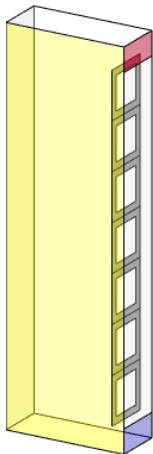


(Case A)

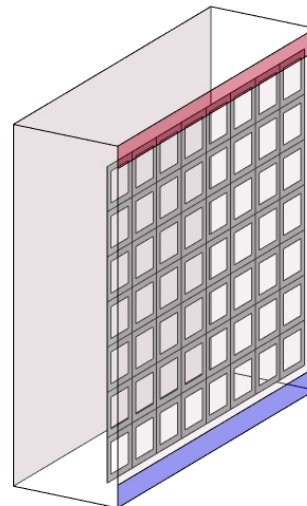


(Case B)

Flat shaded cavity

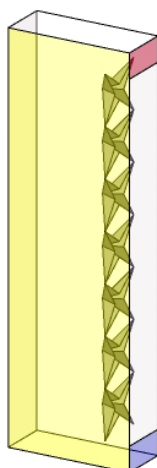


(Case C)

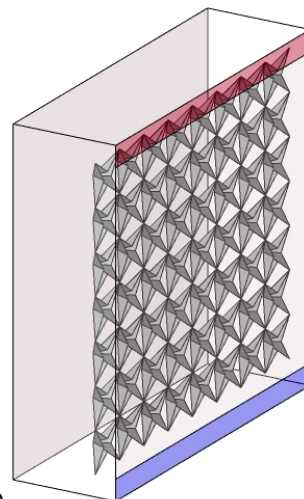


(Case D)

Origami shaded cavity



(Case E)



(Case F)

Figure 6-11: Domain Size of non-shaded, integrated flat shading and integrated folded shading.

### 6.2.3. The Materials

Semi-transparent solids are used for solid glazing materials and opaque solids for solar-shadings and passive walls. Physical and optical properties for solid materials are shown in Table 6-5 and Table 6-6. The air is set as a transparent medium, and air density is set as a function of temperature using the Boussinesq approximation method (Coussirat et al., 2008; Hazem et al., 2015; Parra et al., 2015). The shading material is lightweight, light-coloured and high reflection. The SMMs are not modelled as they are actuators with small surface areas and minimal effect on heat transfer in the cavity.

Table 6-4: Air properties.

Air	
Cp (Specific Heat)	1006.43 J/kg.k
Thermal conductivity	0.0242 W/mk
Viscosity	$1.7894 \times 10^{-5}$ kg/m.s

Table 6-5: Physical properties of DSF elements (Iyi, 2013; Iyi et al., 2014; Ji et al., 2007, 2008).

	Single glazing (outer)	Double glazing (inner)	Grills	Solar- shadings	Passive walls
$\rho$ (kg/m <sup>3</sup> )	2500	2500	2719	2719	2100
Cp (J/kg·K)	840	840	871	871	1100
K (W/m·K)	1.7	1.7	202.4	202.4	0.8
Absorption coefficient	30*	30*	-	-	0.58
	3000**	1285.7**	-	-	
Emissivity	0.84	0.84	0.7	0.7	0.58
Refractive index	1.5	1.5	1.4	1.4	1

\*\* For wavelength 0–2.7 micrometers and \* for wavelength 2.7–1000 micrometers

Table 6-6: Solar radiation properties of materials (Iyi, 2013; Iyi et al., 2014; Ji et al., 2007, 2008).

		Absorptivity ( $\alpha$ )	Transmissivity ( $\tau$ )
Outer glass	Visible	$\alpha_V = 0.09$	$\tau_V = 0.83$
	Infrared	$\alpha_{IR} = 0.09$	$\tau_{IR} = 0.83$
	Diffuse hemispherical	$\alpha_D = 0.1$	$\tau_D = 0.75$
Inner glass	Visible	$\alpha_V = 0.49$	$\tau_V = 0.3$
	Infrared	$\alpha_{IR} = 0.49$	$\tau_{IR} = 0.3$
	Diffuse hemispherical	$\alpha_D = 0.49$	$\tau_D = 0.32$
Solar Shading	Visible	$\alpha_V = 0.5$	-
	Infrared	$\alpha_{IR} = 0.75$	-



### 6.3. The Meshing

Non-shaded and shaded cases are modelled in AutoCAD and exported as step files to be further processed in Ansys software package. The meshing is built within ANSYS Meshing application and different parts are given named selection without any overlapping to guarantee successful mesh transformation to fluent. The mesh type depends on the complexity of the model. The hexahedral cells are selected for the non-shaded cavities, which is considered faster and have better results, as shown in Figure 6-12. The DSFs integrated with solar-shading devices are meshed using a hybrid mesh, the flat solar-shading as shown in Figure 6-13, and the folded solar shading, is meshed as shown in Figure 6-14, where hexahedral cells are used for solids and tetrahedral for fluid zones. Meshing complex forms needs refinement of cell sizes near complex parts to capture geometry details. Therefore, inflation layers around all solid surfaces are modelled to capture the thermal boundary layers created at the solid-fluid surface contacts. For the glazing, a boundary-layer mesh accomplishing a  $y^+ \approx 1$  is set. The conformal mesh is used to create proper contact layers where bodies share common nodes at the interface to enable solar ray-tracing analysis. A modelling modification is done for the shaded cases. The shading devices reach both side ends of the cavity to be able to define the material reflection and absorption properties of the solar-shading.

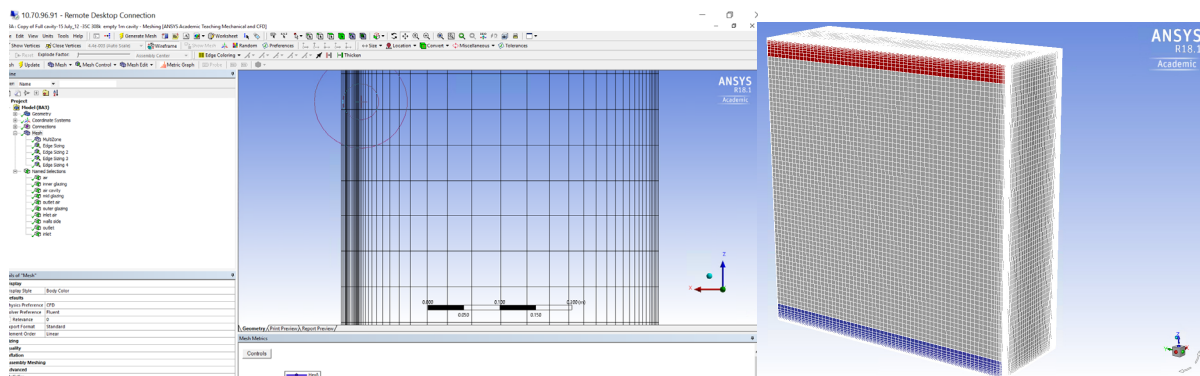


Figure 6-12: Hexahedral Meshing of Non-shaded case model.

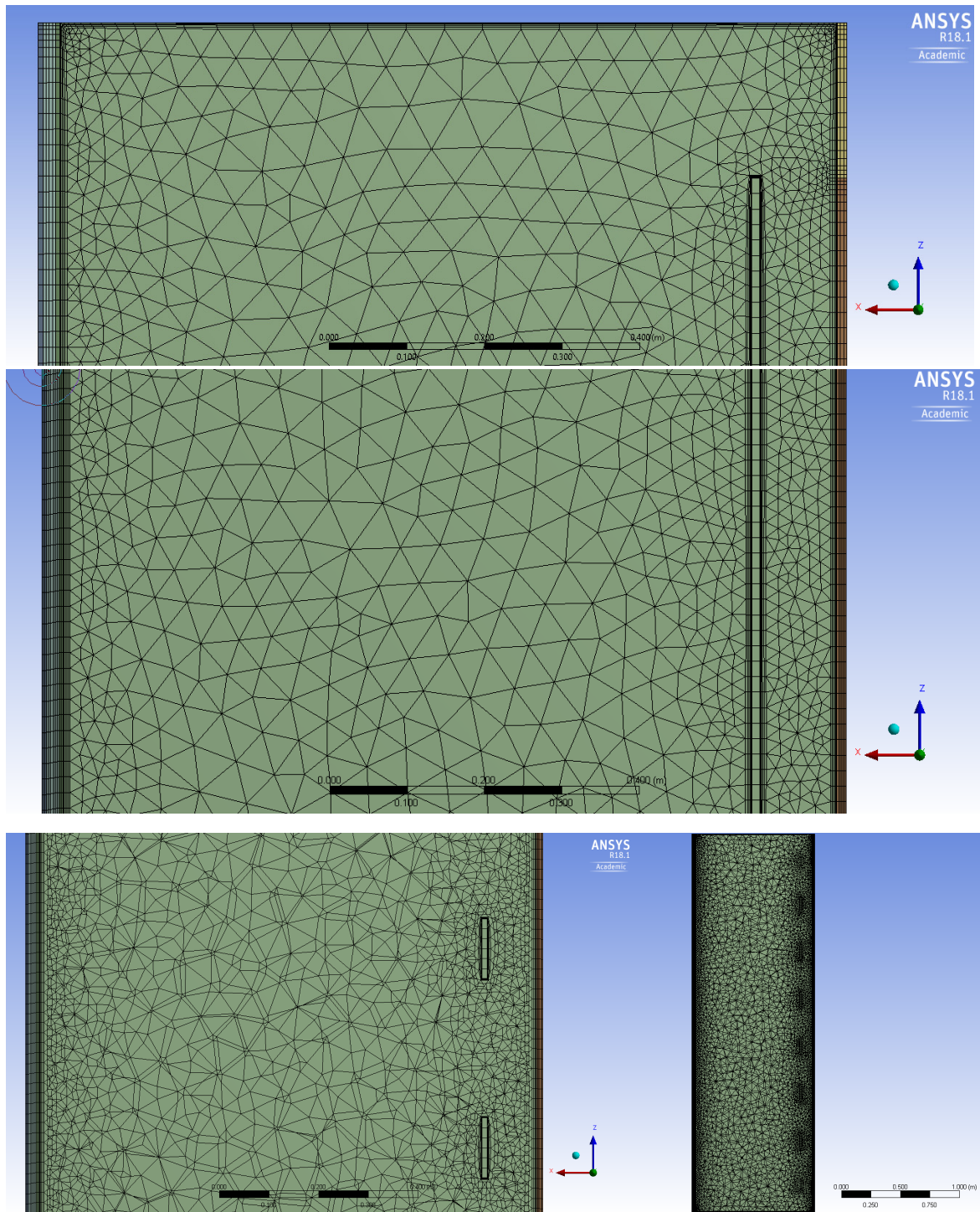


Figure 6-13: The hybrid meshing of flat solar shading cavities using proximity near solid surfaces and inflation layers.



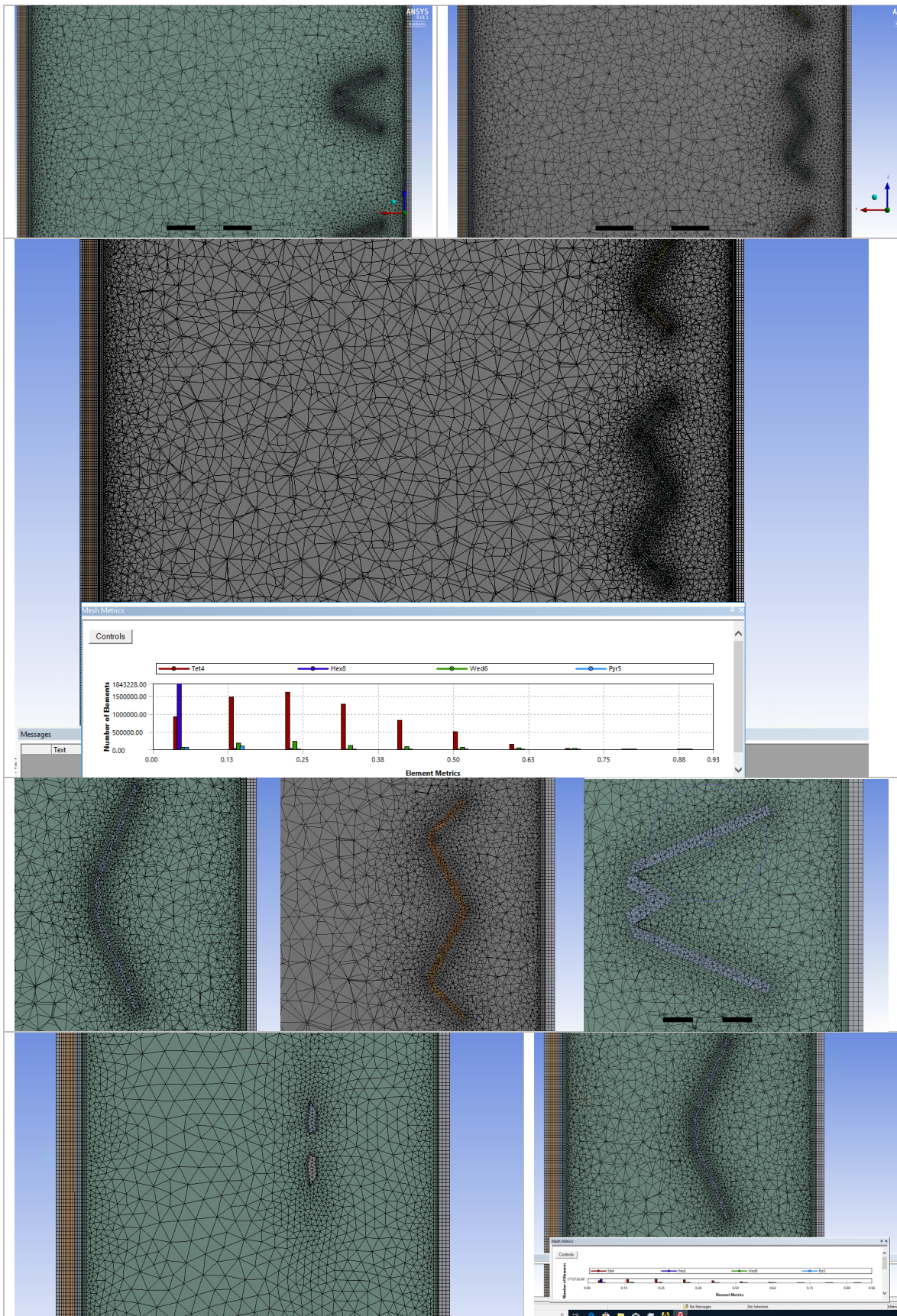


Figure 6-14: Hybrid meshing of folded solar shading cavities using proximity near solid surfaces and inflation layers.

### 6.3.1. Mesh independence test

The number of cells affects the simulation accuracy and computational time. Therefore, mesh independency tests are done through series refinements to select the optimal size taking in consideration recommended  $Y^+$  value (Pasut and De Carli, 2012). The mesh independency tests on the flat-shaded cavity are presented here while monitoring temperature profiles. Three different mesh densities are tested for the flat-shaded cases in the 0.4m vertical section domain size (mesh 1=12,000 cell, mesh 2=85,000 cell and mesh 3=715,000 cell). The two finer meshes obtain similar results in terms of temperature. Figure 6-15 and Figure 6-16 present the results obtained for the mesh independency test of this case where the cavity mesh of 85,000 cells (mesh 2) is selected for the purposes of this work.

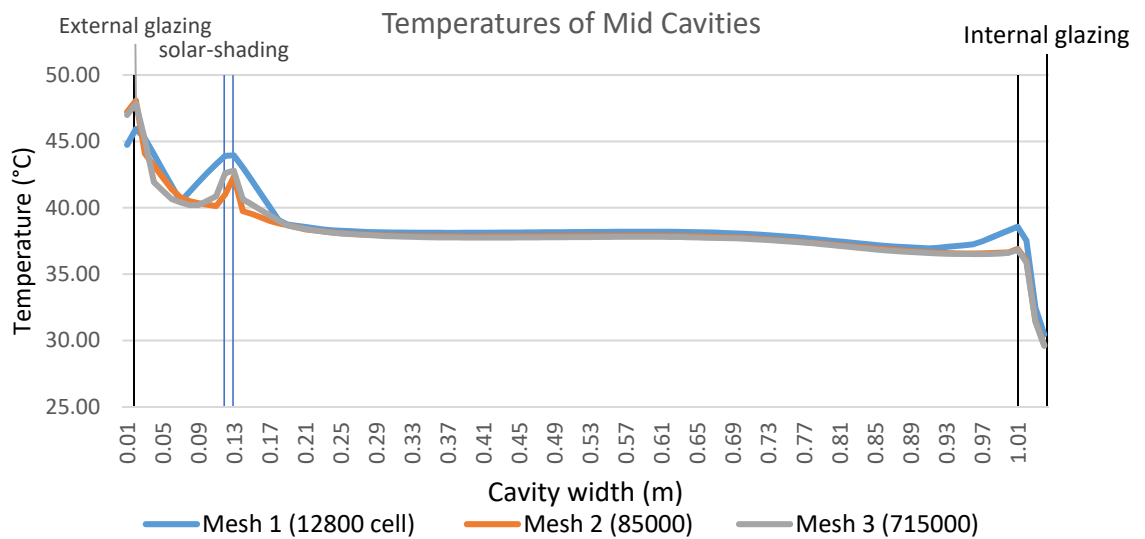


Figure 6-15: Graph compares mid cavity temperatures with the Flat-shading 30% for three mesh sizes.

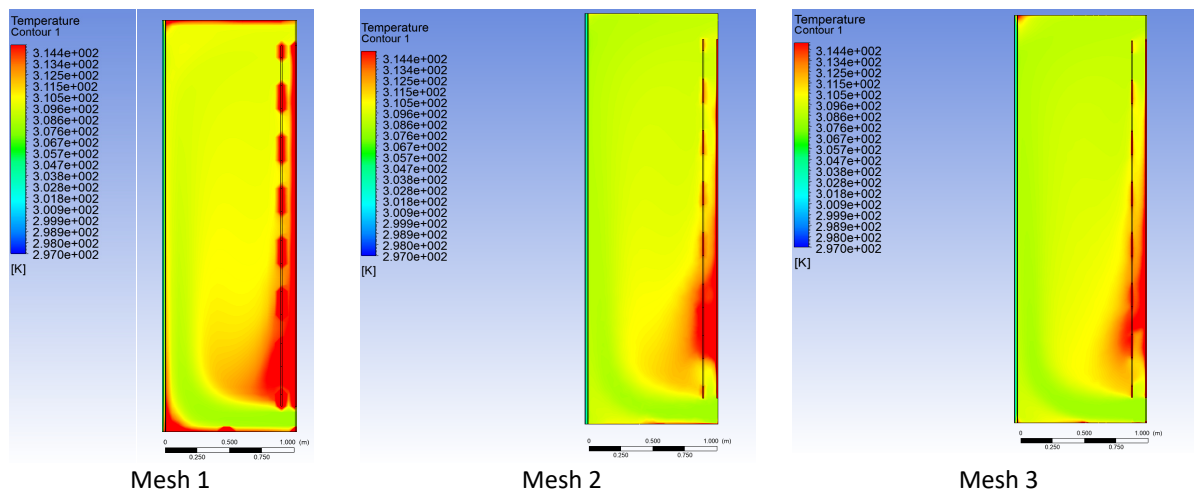


Figure 6-16: Temperature profile of the Flat-shaded cavity 30% for three mesh sizes.

For complex geometries, meshing is of high importance. The curvature and proximity sizing option is set to a minimum of 0.01 m and 0.004 m for proximity near solid surfaces. Five layers of inflations are set for all glazing surfaces with a growth rate of 1.3 and total thickness of (0.006) and 3 inflation layers for shading units with a growth rate of 1.3 and total thickness of (0.004) as shown in Figure 6-14. Skewness is checked for all meshes to avoid solution divergence. Table 6-7 presents the summary statistics for meshes in terms of the number of cells, time and number of runs taken to reach a converged solution of different studied cases. Case A convergence is attached in Appendix H.

*Table 6-7: Computational efforts for all modelling strategies studied cases.*

Case	Case description	No. of cells	Time (hours) to reach converged solution	No. of runs to reach converged solution
Case A	0.4m Vertical Section (Non-shaded case)	99,900	7 h	4500 run
Case B	Full Cavity (Non-shaded case)	582,540	14h	6000 run
Case C	0.4m Vertical Section (Flat-shaded case)	715,282	14h	4500 run
Case D	Full Cavity (Flat-shaded case)	3,844,101	24 h	6000 run
Case E	0.4m Vertical Section (Origami-shaded case)	9,385,695	48h	6000-7000 run

#### 6.4. Numerical Modelling

The study is conducted through 3D modelling using CFD code Ansys Fluent package to simulate the airflow and associated heat transfer (coupled convective, conductive and radiative) through the DSF. In order to simulate the studied cases, Navier-Stokes equations together with the energy conservation equation are solved using CFD code Ansys Fluent® v18.1. The velocity and temperature fields in the channel are governed by three basic equations: 1) the continuity equation (mass conservation); 2) the motion or transport equation and 3) the energy equation. CFD code couples thermo-fluid-dynamics problems using RNG k-epsilon turbulence and DO radiation models as recommended from Chapter Five. The full buoyancy effect in the RNG k-epsilon turbulence model is attached to the simulations, and the gravity is set to  $-9.81\text{m/s}^2$  with z-direction. Furthermore, Enhanced Wall Treatment is chosen under the options for Near-Wall Treatment. The air was chosen as the simulation fluid.

The fluid is set to be incompressible ideal gas and in a turbulent flow regime to make variables temperature-dependent. The buoyancy effect of air is simulated with Boussinesq approximation (Y. Li et al., 2017). Discrete Ordinate (DO) radiation model with non-gray specification and solar ray-tracing is used. Two bands 'Solar' and 'Thermal' are set with non-gray option. The solar band corresponds to wavelengths smaller than 2.7  $\mu\text{m}$ , and the thermal band to wavelength larger than 2.7  $\mu\text{m}$ . 6x6 divisions are set for all cases except the complex cases which are set to 4x4 to work with the available CPU. Besides, the setting of 3x3 pixilation is applied. All glazing surfaces are set as participating in radiation. Since radiation is the dominant mode of heat transfer in the computational domain, therefore, the flow iterations per radiation iteration are specified as 5 (Iyi et al., 2014).

#### *6.4.1. Boundary Conditions*

Thermal boundary conditions for the exterior and interior layers are imposed as a mixed condition (radiation and convection). Convection coefficients were set to 12  $\text{W}/\text{m}^2\text{K}$  and 8  $\text{W}/\text{m}^2\text{K}$  for the outdoors and indoors glazing surfaces respectively similar to previous research carried in the Mediterranean region in Barcelona (Spain) (Coussirat et al., 2008; Parra et al., 2015; Velasco et al., 2017). As the DSF is attached to an air-conditioned office zone, the internal boundary zone was treated as a single volume of air at a constant temperature of 22°C and an average velocity in z of 0.1  $\text{ms}^{-1}$  to reflect a typical mean air velocity for an air-conditioned space. The upper and lateral walls are considered adiabatic and they do not participate in the solar raytracing. The temperature of the internal air-conditioned office was set to 22 °C during the winter and 24°C during the summer following Egypt's regulations on energy efficiency in buildings. The ambient temperature was set to 35 °C (July/Summer) or 17 °C (January/Winter) as per the selected dates with weather data. Table 6-8 shows the external radiation values extracted from Ansys Fluent solar calculator as a function of the fed time and location.

Table 6-8: Location settings and external radiation values.

Design Day	Summer Peak Day			Winter Peak Day		
Date	15th July			15th of January		
Time	9 am	12 pm	15 pm	9 am	12 pm	15 pm
Direct Normal Solar Irradiation (at Earth's surface) [W/m <sup>2</sup> ]:	824.7	1320.4	825.6	832.6	970.6	849.7
Sun Direction Vector	X: -0.0113, Y: -0.6594, Z: 0.7518	X: -0.1487, Y: -0.0024, Z: 0.9888	X: -0.0136, Y: 0.6561, Z: 0.7545	X: -0.6358, Y: -0.6711, Z: 0.3813	X: -0.7781, Y: -0.0167, Z: 0.6279	X: -0.6470, Y: 0.6477, Z: 0.4023
Diffuse Solar Irradiation-Vertical Surface [W/m <sup>2</sup> ]	109.0	111.4	108.8	64.9	66.9	65.7
Diffuse Solar Irradiation-Horizontal surface [W/m <sup>2</sup> ]	111.8	179.0	111.9	53.1	61.9	54.2
Outer temperature (Ambient temperature)	31 Celsius 304 Kelvin	35 Celsius 308 Kelvin	35 Celsius 308 Kelvin	12 Celsius 285 Kelvin	17 Celsius 290 Kelvin	17 Celsius 290 Kelvin
Inner temperature	24 Celsius 297 Kelvin	24 Celsius 297 Kelvin	24 Celsius 297 Kelvin	22 Celsius 295 Kelvin	22 Celsius 295 Kelvin	22 Celsius 295 Kelvin

At the inlet, the boundary condition was set as velocity inlet in which the air enters the channel with a constant velocity ( $V = 0.4$  m/s). This is an average velocity value for inlet condition, which would change relative to inlet height as reported by Hamza and Qian (2016). A similar study carried in china by Y. Li et al. (2017) set a velocity inlet for DSF equal to 0.45 m/s for the hottest month (July). Additionally, Liao et al. (2005) found that the heat transfer coefficients are well-validated for the velocity range from 0.3 m/s to 0.6 m/s. However, Guardo et al. (2011) argued that the increase in the turbulence intensity of the inlet flow in the range between 0.4–4 m/s does not reduce the solar load gains. At the outlet of the domain, the outflow boundary condition was set as a pressure outlet, and the flow rate weighting factor is set to 1.



The inlet and outlet specification method for turbulence is set using Intensity and hydraulic diameter, as shown in Table 6-9. It was calculated using the Engineering Equation Solver (EES) software (Klein & Alvarda, 2007) with the following equation. The Hydraulic diameter is defined as four times the inlet/outlet area divided by its perimeter.

To specify Hydraulic diameter

$$\text{Hydraulic diameter} = 4 \text{ Area} / \text{Perimeter}$$

$$\text{Area} = (W \times H)$$

$$\text{Perimeter} = (W + H) \times 2$$

To specify turbulence intensity

$$I = 0.16 \text{Re}^{-1/8}$$

- The Reynolds number is defined as

$$\text{Re} = \frac{\rho u L}{\mu} = \frac{\rho u (D - \text{Hydraulic})}{\mu}$$

where:

- $\rho$  is the density of the fluid = 1.2047 kg/m<sup>3</sup>
- $u$  is the velocity of the fluid with respect to the object (m/s)
- $L$  is a characteristic linear dimension (m) taken as  $D - \text{Hydraulic}$
- $\mu$  is the dynamic viscosity of the air = 1.821 or kg/m·s)
- The Reynolds number (Re) is an important dimensionless quantity in fluid mechanics used to help predict flow patterns in different fluid flow situations.

*Table 6-9: Hydraulic diameter and Intensity inputs*

Input	Value
Initial inlet velocity	0.4
Hydraulic diameter	0.3765
Intensity	0.05065

**6.4.2. Solver set-up**

All the cases are solved using Fluent code with double precision for better accuracy. The SIMPLE algorithm is used for coupled pressure and velocity. The PRESTO! discretization scheme is adopted for pressure and Second order upwind discretization schemes are imposed on all the transport equations. Low values for Under Relaxation Factors (URF=0.2) for the energy equations are initially set until convergence to achieve good solution stability and then default URF values are set for fast convergence as discussed in chapter five page 202. All residuals dropped for less than  $1 \times 10^{-3}$  for all solved equations except energy to  $1 \times 10^{-6}$ .

All heat fluxes recorded are integrated, and area-weighted averaged to compute the incident radiation, surface temperature and the solar heat gains through the interior face of the inner glazing. This section explained the numerical CFD setup carried for the CFD simulations. The next section will discuss the results of the three scenarios, *non-shaded DSF*, *integrated DSF with flat solar-shadings* and *integrated DSF with origami solar-shadings*.

## 6.5. Results

For all studied cases, airflow and temperature fields are obtained to assess the DSF thermal performance. The temperature and velocity profiles are studied on a longitudinal mid-section of the DSF for a peak summer day (15<sup>th</sup> of July) and a peak winter day (15<sup>th</sup> of January), three times a day at (9:00 am, 12:00 pm and 15:00 pm). The effect of the solar shading devices on the indoor solar heat gain is evaluated using a set of numerical simulations. Incident total radiation and heat flux through the DSF interior surfaces are recorded as a point in time simulations at three times a day. These analyses are area-weighted averaged.

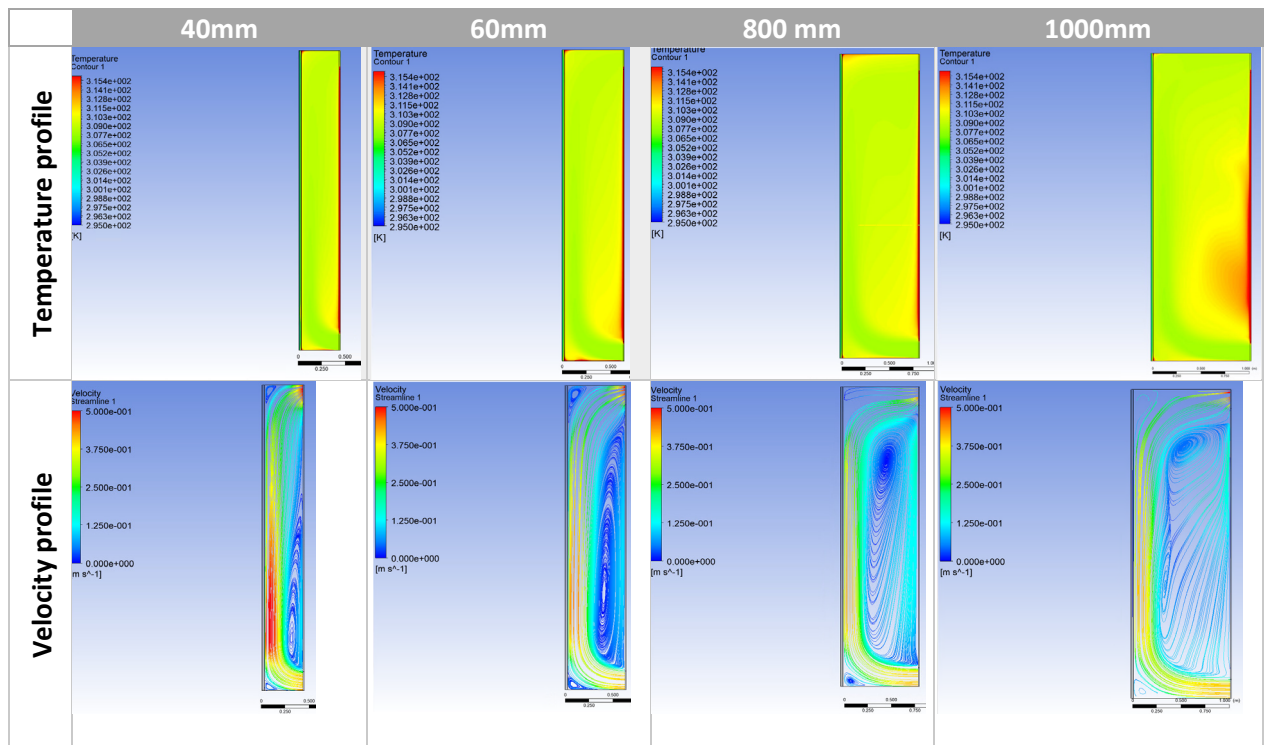
### 6.5.1. Scenario 1: Non-shaded DSF

The geometrical variables of the non-shaded DSF cavity are the DSF cavity width, the façade layering, and the domain size. These geometrical variables are compared at the Midday of the 15<sup>th</sup> of July (peak summer day).

#### 6.5.1.1. DSF cavity width

Temperature and velocity profiles inside the cavity are obtained to qualitatively assess the DSF thermal performance. Table 6.10 shows the cavity temperatures and airflow comparing the four cavity widths (0.4 m, 0.6 m, 0.8 m & 1.0 m) at 12:00 pm 15<sup>th</sup> of July, around peak solar radiation is expected. Both external and internal surface temperatures for all the cavity widths are calculated to compare the cavity performances.

Table 6-10: Mid-cavity Temperature and Velocity profiles comparing the four cavity widths (0.4, 0.6 m, 0.8 m & 1.0 m) at 15th July (12:00 pm).



The results show that the 1 m cavity width resulted in a drop of 17.5°C between single external glazing with temperature 47.8°C and internal double glazing with temperature 29.5°C as shown in Figure 6-17. All the smaller cavities recorded higher internal glazing temperatures. The 0.8, 0.6 and 0.4m cavities resulted in 30°C, 30.3°C and 30.5°C at internal double glazing surface temperature. By monitoring total heat flux of internal surface, it was found that heat gains are reduced from 74.36 to 63.54 w/m<sup>2</sup> by increasing the cavity width from 0.4m to 1m as shown in Figure 6-19. The results of this section indicate that increasing the cavity width can improve the thermal performance of the DSF where the 1m cavity reduces the heat gain by 15%. By analysing the airflow, it is found that the successive decrease in cavity width, leads to a significant increase in the average air velocity. As shown in Figure 6-18, the 0.4m wide cavity recorded 0.22 m/s average air velocity compared to 0.16 m/s recorded by the 1m wide cavity. Although the increase of air velocity in narrow cavities can extract warmer air to outlet section as shown, it doesn't offset the impact of the direct radiation heating on the inner glazing surface as shown in Figure 6-17 and Figure 6-18. Therefore, the 1 m wide DSF cavity is recommended.

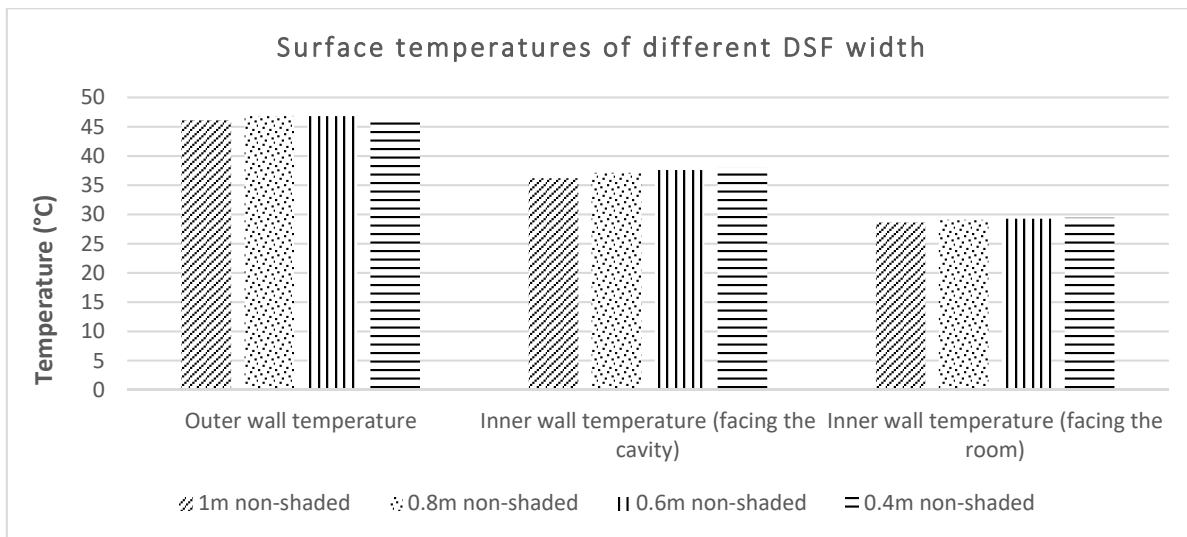


Figure 6-17: Inner and outer surface temperatures comparing the four cavity widths (0.4, 0.6 m, 0.8 m & 1.0 m) at 15th July (12:00 pm).

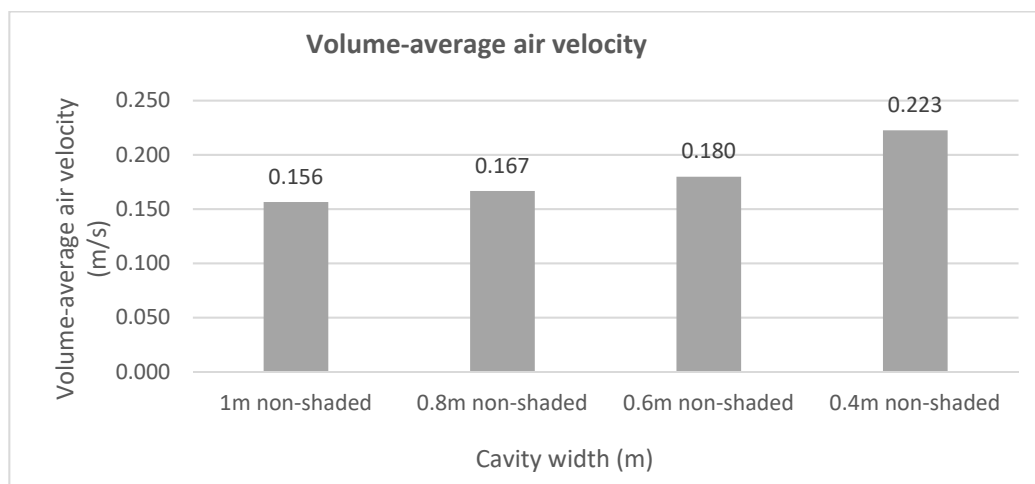


Figure 6-18: Volume-average air velocity comparing the four cavity widths (0.4, 0.6 m, 0.8 m & 1.0 m) at 15th July (12:00 pm).

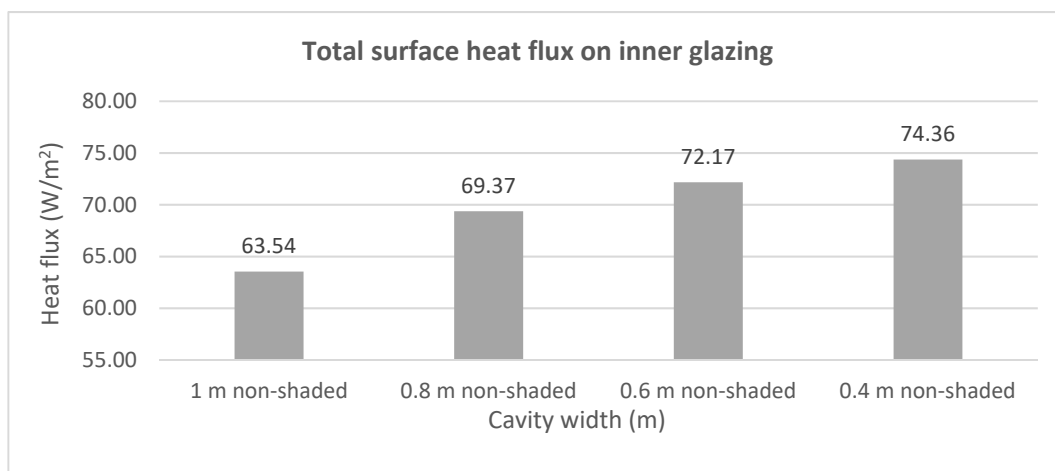


Figure 6-19: Total heat flux on inner glazing for the four cavity widths (0.4, 0.6 m, 0.8 m & 1.0 m) at 15th July (12:00 pm).

### 6.5.1.2. DSF Façade layering

Temperature and velocity profiles inside the 1 m wide cavity are obtained for the single and double inner glazing to compare their impact on the DSF thermal performance qualitatively. Table 6-11 shows the temperature and velocity comparing the two configurations at 12:00 pm on the 15<sup>th</sup> of July. The internal double glazing lowered the internal surface temperature by 24% from 39.4°C recorded by single glazing to 29.5°C recorded by the double glazing.

Table 6-11 Comparison of single and double inner glazing configuration.

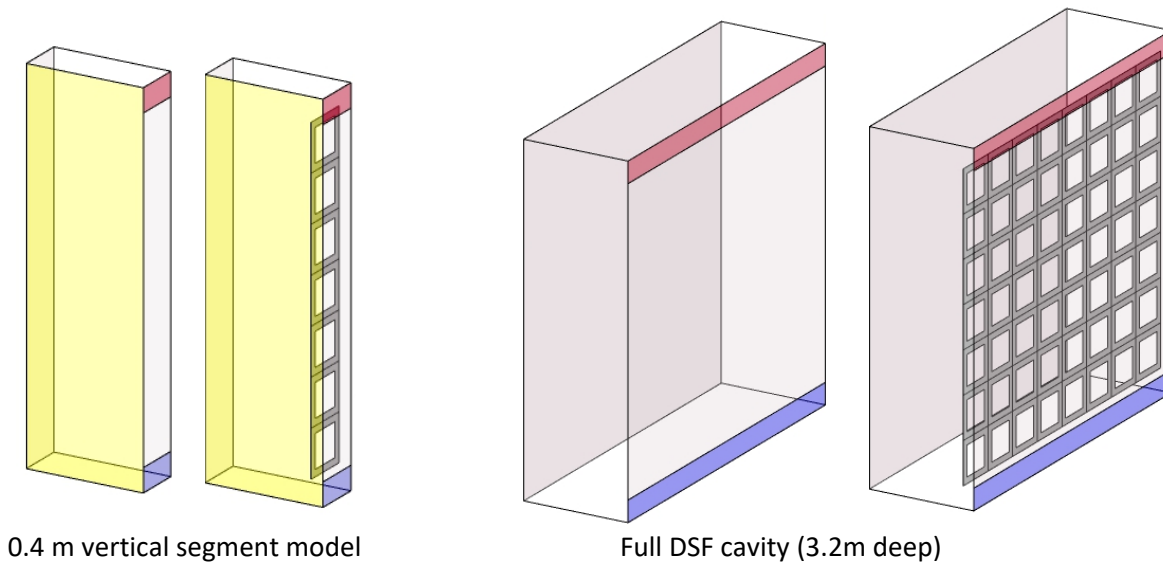
	Internal Single glazing	Internal double glazing
Temperature Profile		
Velocity Profile		

### 6.5.1.3. DSF domain size.

Two 3D models are compared; 0.4m vertical segment model and full DSF cavity (3.2m deep). Similar to the validated case, the 3D approach is adopted to enable the use of the solar load model (solar-raytracing), asses more complex solar-shading forms, and the thermal stratification behaviour. Initially, a vertical section with 0.4 m deep was used to fit the average dimension of the light-weight solar shading module. The bottom and the top boundary

conditions are set as adiabatic walls while the lateral walls are set as a symmetric boundary as recommended by (Coussirat et al., 2008) as shown in Figure 6-20 (a).

Although this method allows for complex form assessment with reduced computational cost, it has some limitations. Difficulties arose when modelling different timings such as; (9:00) and (3:00 pm). The symmetry boundary condition let the solar radiation directly into the DSF domain, which affects the internal glazing directly. This method works effectively when the solar direction is not directed towards the side walls, in conditions such as July midday. Further modelling of a full DSF cavity (3.2m deep), which can take eight solar shading modules is modelled to compare the two methods, as shown in Figure 6-20 (b). In case of full cavity model, the lateral walls are set as adiabatic walls instead of symmetric boundary conditions. The geometrical representation of the two models; 0.4 m vertical segment model and full DSF cavity (3.2m deep) are presented as shown in Figure 6-20.



*Figure 6-20: Domain Size.*

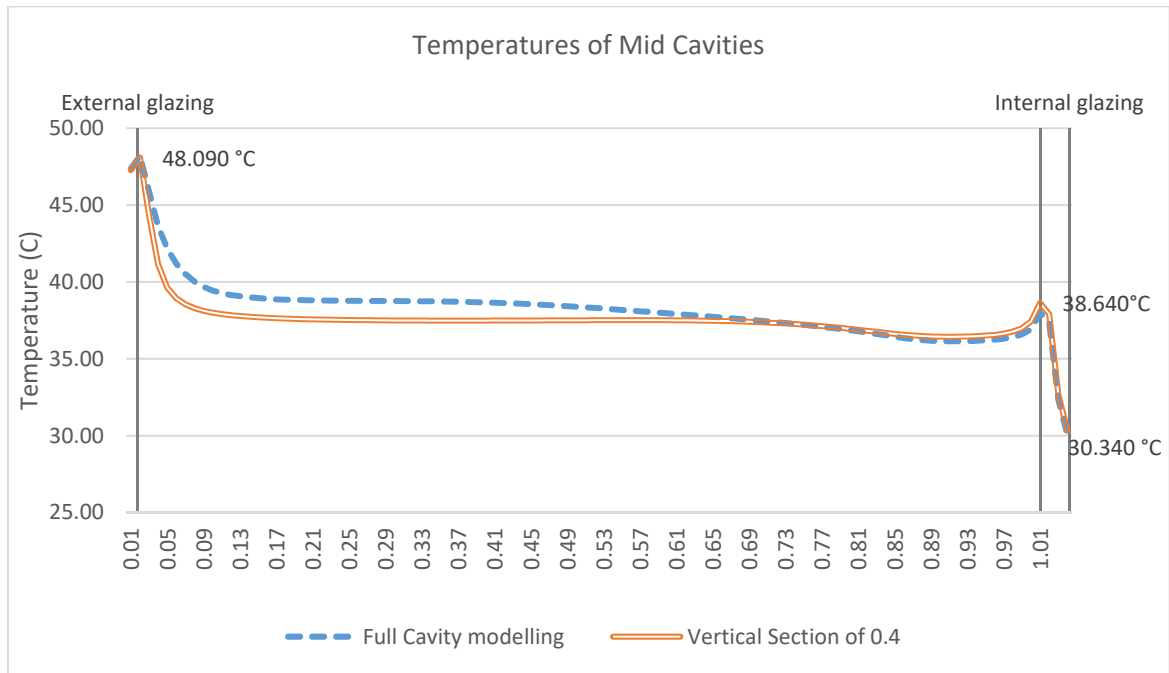


Figure 6-21: Temperature profile of non-shaded 1m DSF at mid cavity comparing Full width and 0.4 m vertical segment model.

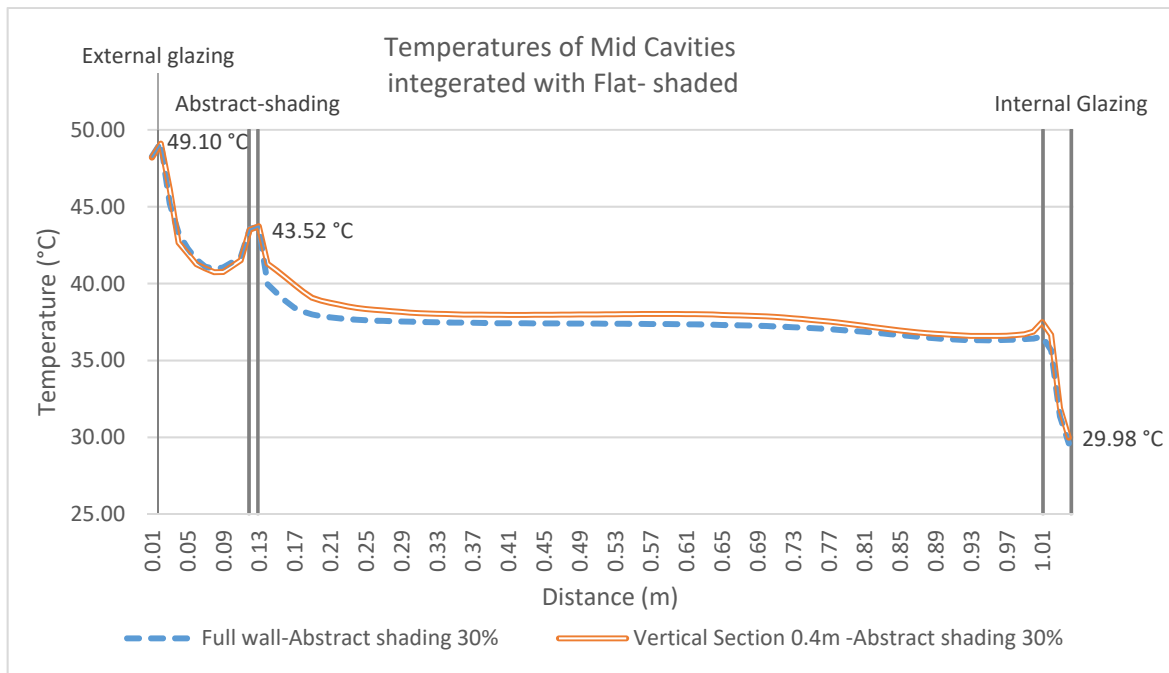


Figure 6-22: Temperature profile of Flat-shaded 30% DSF at mid cavity comparing Full width and 0.4 m vertical segment model.

As shown in Figure 6-21 and Figure 6-22, the temperature profile at the mid cavity of both methods is similar with less than 5% variation. Both methods are valid for summer middays, but full cavity model is used in case of side components of sun angles at morning times and late afternoon times; (9:00 am) and (3:00 pm). Accordingly, a full cavity 3.2m deep is used for further experimentation of DSF with and without shading. One major drawback of this full cavity model is the extra computational power demand. Therefore, for assessment of



the folded origami shading, the 0.4 depth method is used to assess the DSF structure on July midday.

So far, this chapter has discussed the impact of the *cavity's width, façade layering* and *domain size* on the non-shaded DSF thermal performance. The 1m wide cavity glazing is selected as it reduces the heat gain by 15% compared to the 0.4m wide cavity. The inner double glazing is selected as it decreased the internal surface temperature by 24% compared to single glazing. Full DSF cavity (3.2m deep) is recommended as the symmetry boundary condition of the 0.4 m vertical segment model let the solar radiation directly into the DSF domain at morning and late afternoon times. Having discussed the effect of the geometrical variables on the non-shaded case, it is now necessary to simulate the non-shaded DSF at different times of a peak summer and winter day.

#### 6.5.1.4. Non-shaded DSF with time

This set of analysis examines the non-shaded DSF cavity as a base case on 15<sup>th</sup> of July and 15<sup>th</sup> of January at 9:00, 12:00 pm and 3:00 pm respectively. After testing different cases for a non-shaded cavity, this phase will proceed with 1 m wide non-shaded DSF, internal double glazing and full cavity 3.2 deep model.

Temperature profiles inside the cavity are obtained to qualitatively assess the non-shaded DSF thermal performance at different times of a peak summer and winter day. Both external and internal surface temperatures for the non-shaded cavity are calculated, as shown in Figure 6-24, and mid cavity temperature, as shown in Figure 6-23.

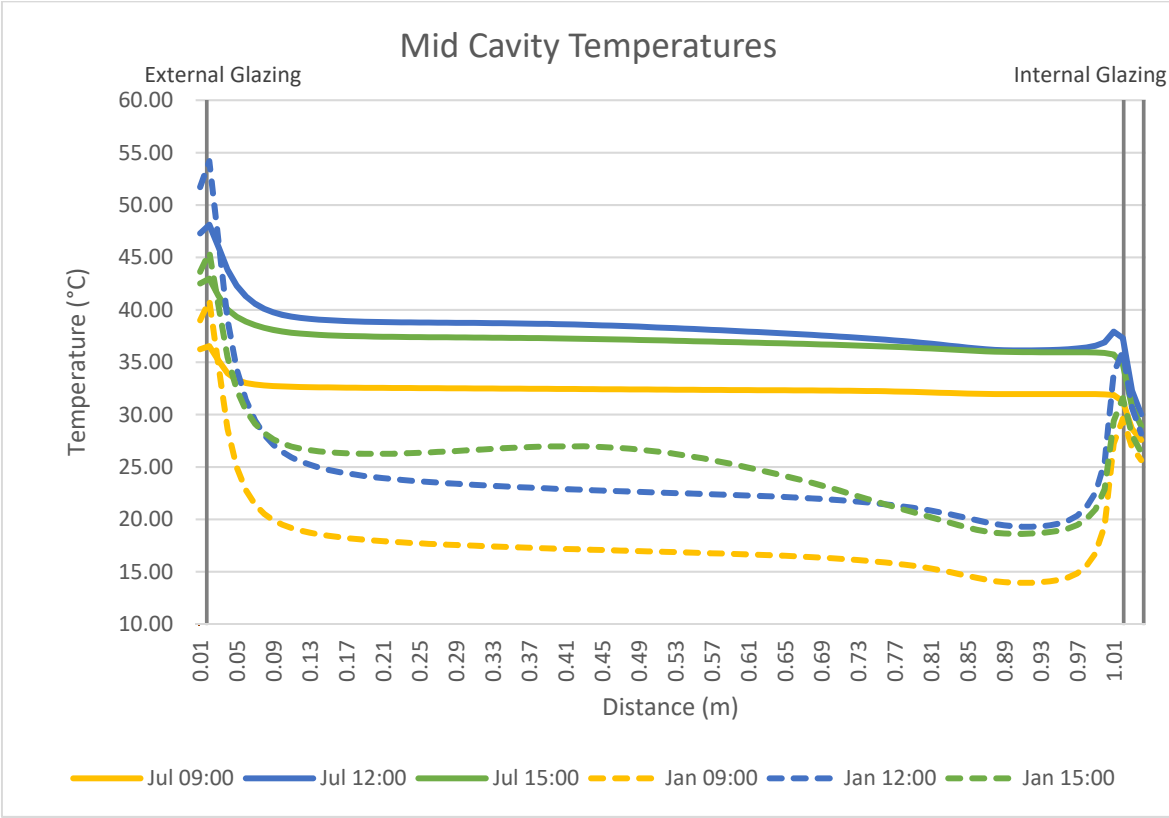


Figure 6-23: Mid cavity temperature for the non-shaded DSF.

Table 6-12: Cavity temperature profile during 15<sup>th</sup> July and 15<sup>th</sup> January.

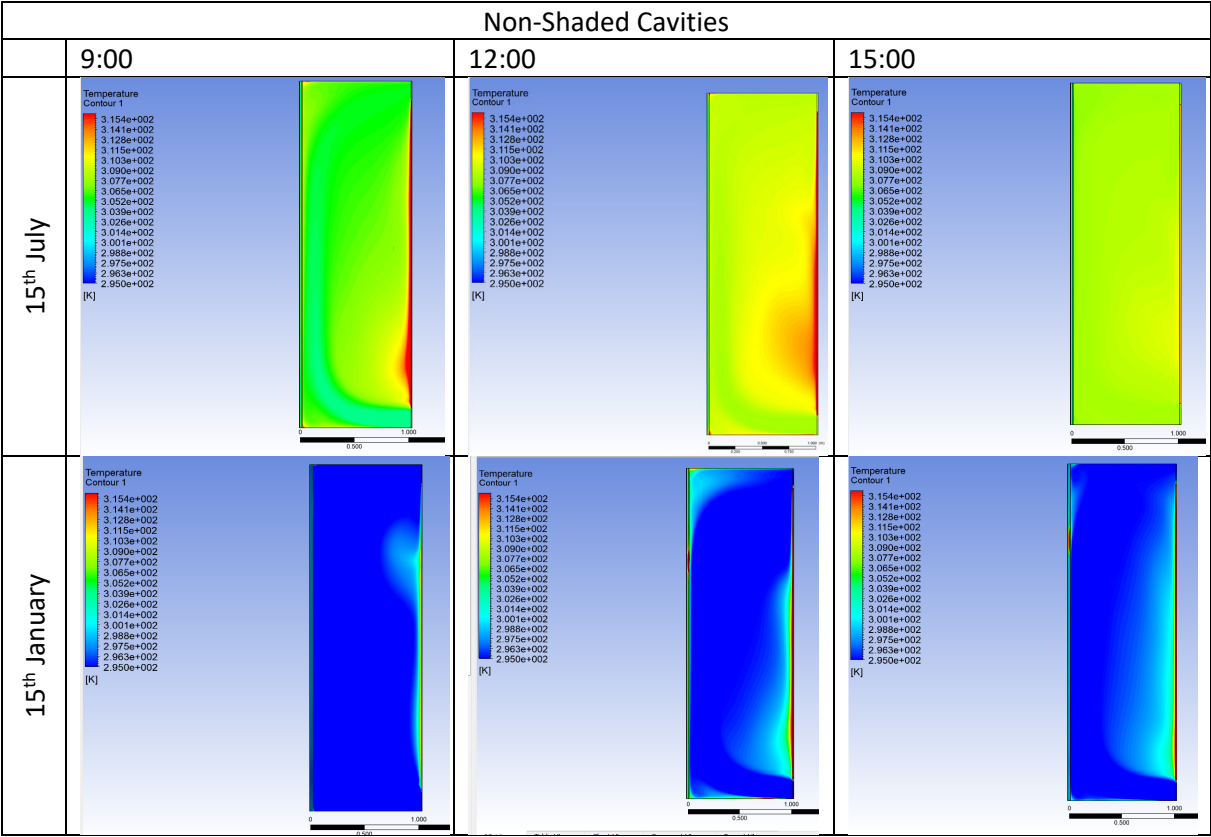


Table 6-12 shows the cavity temperature evolution during the 15<sup>th</sup> of July and 15<sup>th</sup> of January. The temperature inside the cavity increases until the peak solar radiation. After midday, the cavity temperature decreases due to the lower solar radiation level. Temperature profiles, as shown in Table 6-12 and Figure 6-24, indicate that the interior glazing is consistently lower than the exterior glazing. In summer, the highest profiles are found to be at 12:00 and 15:00 pm of the summer's peak day. In the midday of July, the external glazing reached a maximum temperature of 48°C. The non-shaded DSF obtains a difference in temperature between the external glazing and the internal double glazing facing the cavity by around 11°C (22.5%) to be 27.59 °C. The internal double glazing facing the room resulted in an extra temperature drop of 7°C, which represents 37.6% in total and reaches a temperature of 30°C. In winter, the low solar angles in the south direction resulted in increasing the external glazing temperature to reach 54.2°C at 12:00 pm, and the internal glazing reaches a temperature of 28.21° resulting in a 26°C difference in temperature.

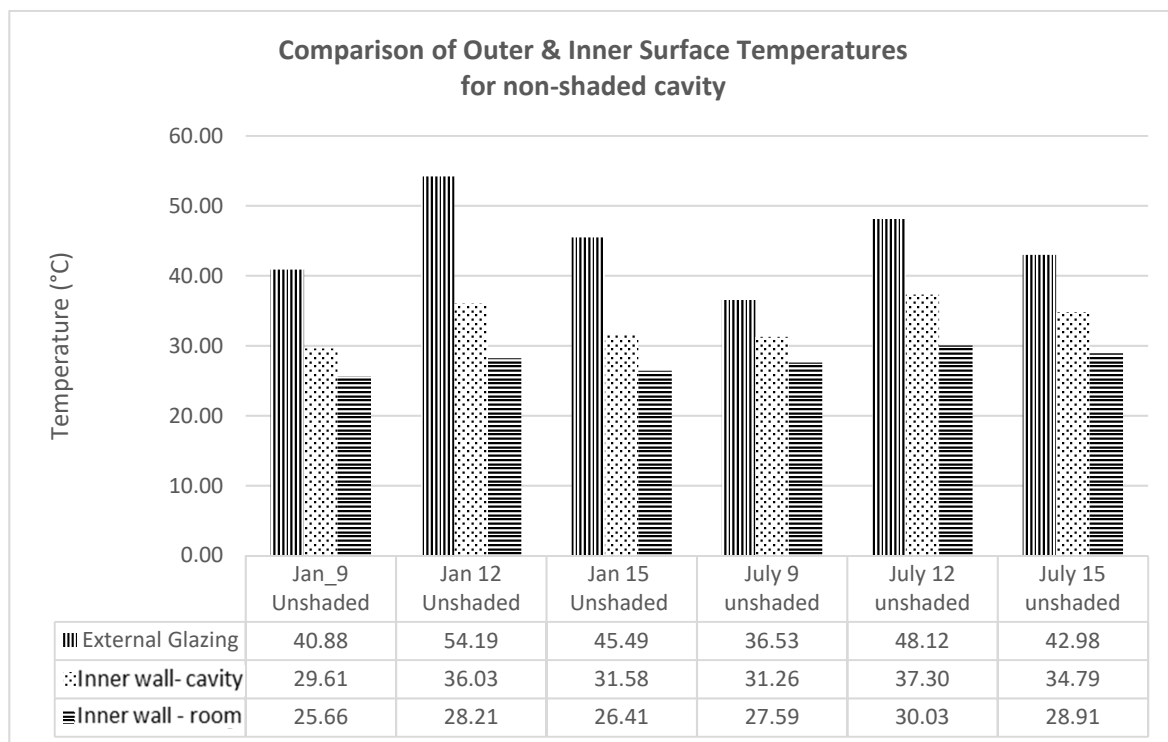


Figure 6-24: Comparison of outer & inner surface temperatures for the non-shaded cavity.

Velocity profiles and Air velocity average inside the cavity are obtained at different times of a peak summer and winter day. Results are recorded, as shown in Figure 6-25 and Table 6-13.

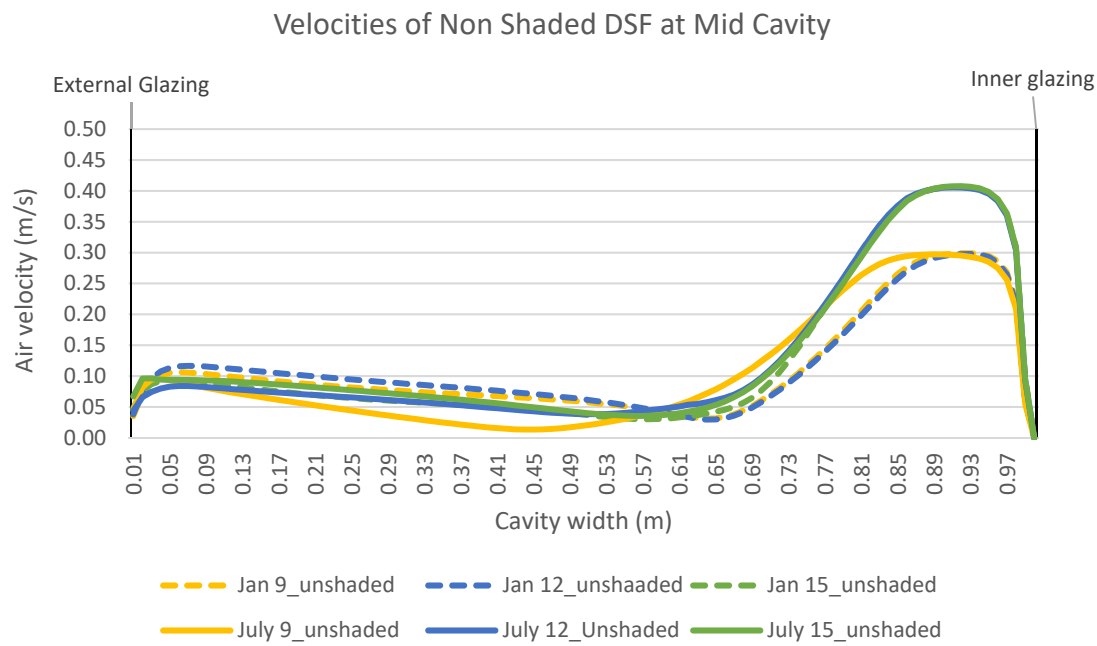
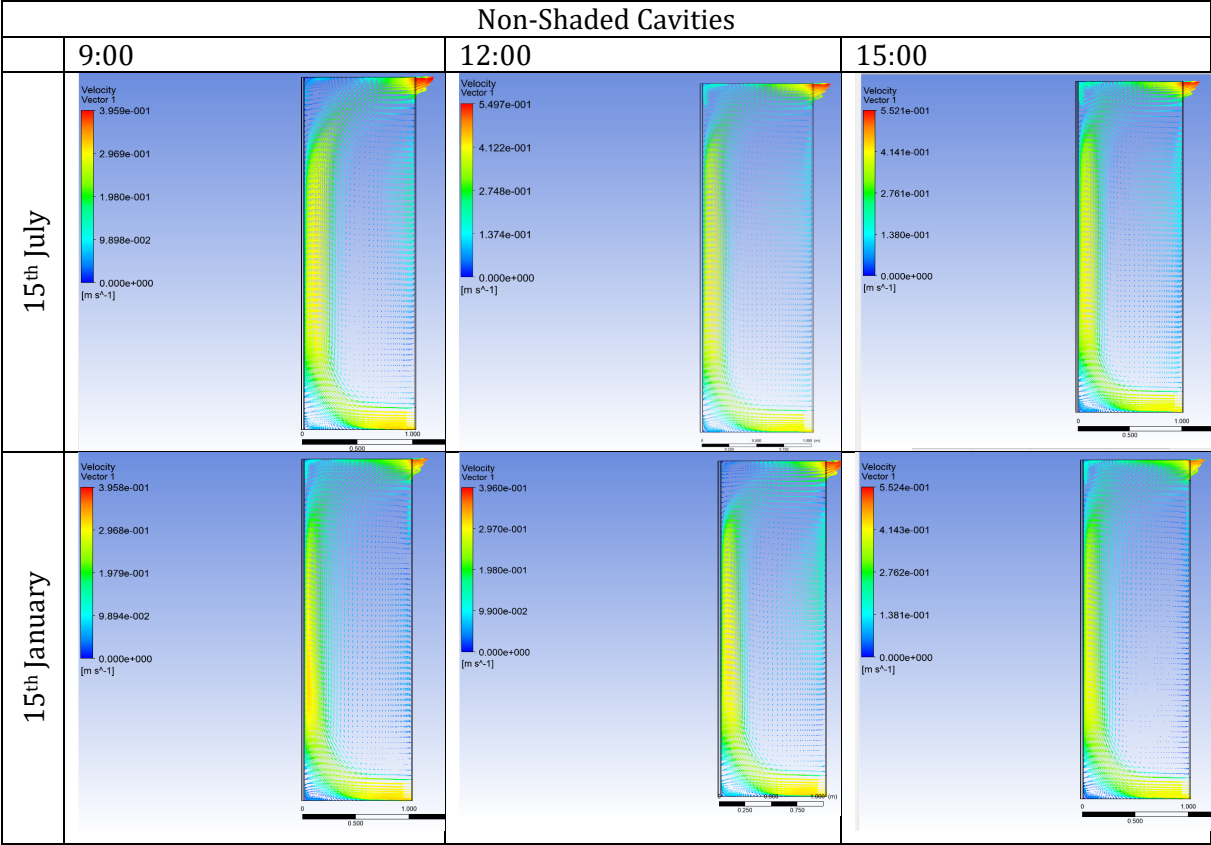


Figure 6-25: Velocity profile of non-shaded DSF

Table 6-13: Airflow of non-shaded DSF at 15th July and 15th January.



Air velocity average reaches a maximum of 0.15 m/s and a minimum of 0.11 m/s for the non-shaded cavity (3.2m-high and 1.00m-wide). Figure 6-25 shows the velocity profile at mid cavity. The maximum airflow for all cases is close to the internal glazing surface and their peaks are at 0.08m away from the glazing element, as shown in Figure 6-25. The highest velocity is 0.41m/s occurs at 12:00 h and 15:00 h of 15<sup>th</sup> of July corresponding to solar radiation 1320.36 W/m<sup>2</sup>. The lowest peak of 0.30 m/s occurs at 9:00 h, which corresponds to solar radiation 832.57 W/m<sup>2</sup>. The range of mean velocities concurs with Hamza and Underwood (2005) DSF studies in hot arid areas. Hamza and Underwood (2005) found that mean velocities are in the range between 0.045 m/s – 0.84 m/s.

Having discussed the non-shaded DSF cavity as a base case, the coming sections will study the performance of the DSF with integrated solar shadings; abstracted flat and folded origami.

#### *6.5.2. Scenario 2: Flat solar shading*

The proximity of the solar shading devices to the external glazing is chosen in the range between 0.1 to 0.2 m to benefit from the temperature rise from direct solar radiation in this cavity zone for the activation of the SMM actuators. Also, this position helps the solar-shading to block the direct solar radiation from affecting the back zone. This position creates a large buffer space between the solar shading and the internal double glazing resulting in the negligible effect of the heated solar shading on internal surfaces. The large buffer space between the solar shading and the internal double glazing allows any maintenance work needed for the façade or the solar-shading. This decision concurs with Safer et al. (2005) and Gratia and De Herde (2007) findings. Safer et al. (2005) demonstrated that positioning the blind at 15cm from the external glazing is the best configuration for the external ventilation of the channel, particularly in summer condition. Gratia and De Herde (2007) recommended positioning the solar-shading device in the range between the mid of the cavity and the external skin.

The position of origami folded solar shading modules sits 0.2m away from the external surface of the DSF to give the unit the freedom to move and fold forward. The position of the abstracted flat solar-shading is chosen at 0.1m away from the external glazing as an average position of the origami folded unit range of motion, as shown in Figure 6-26. In the coming section; the performance of DSF integrated with flat solar-shading devices is studied in terms of surface and air temperatures, airflow and heat flux.

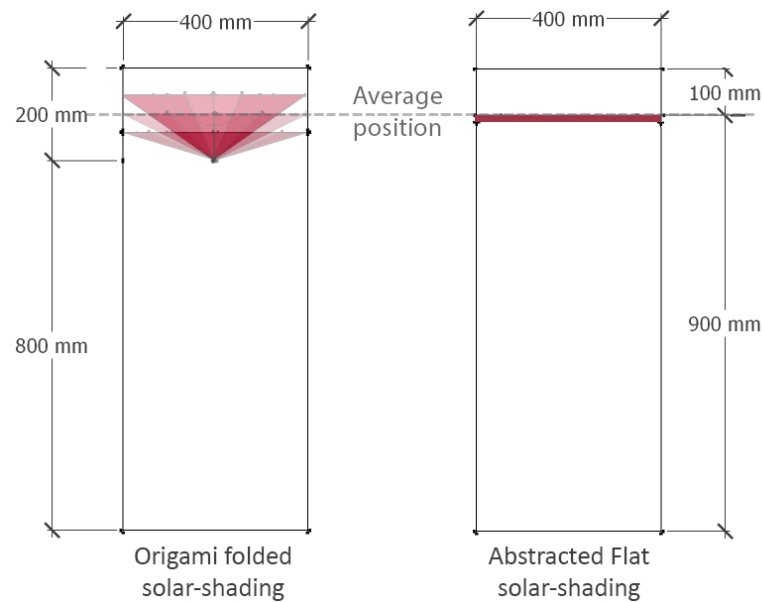


Figure 6-26: Position of solar shading in plan view, Origami folded and abstract flat.

#### 6.5.2.1. Temperature Contours

Surface and air temperatures inside the flat-shaded cavity are tested numerically with the three aperture sizes (30%, 50%, & 70%) and compared with the non-shaded base case at 15<sup>th</sup> of July and 15<sup>th</sup> of January at 9:00, 12:00 pm and 3:00 pm respectively as shown in Table 6-14, Table 6-15 and Figure 6-16. Table 6-14 shows the cavity temperature evolution of the flat-shaded cavity during 15<sup>th</sup> of July and 15<sup>th</sup> of January. The flat solar shading device proximity to the outer glazing results in heating the frontal zone and external glazing, especially at peak solar radiation cases. The solar shading heats up as a result of solar radiation and affects the surrounding area.

Table 6-14: Cavity temperature profile during 15<sup>th</sup> July.

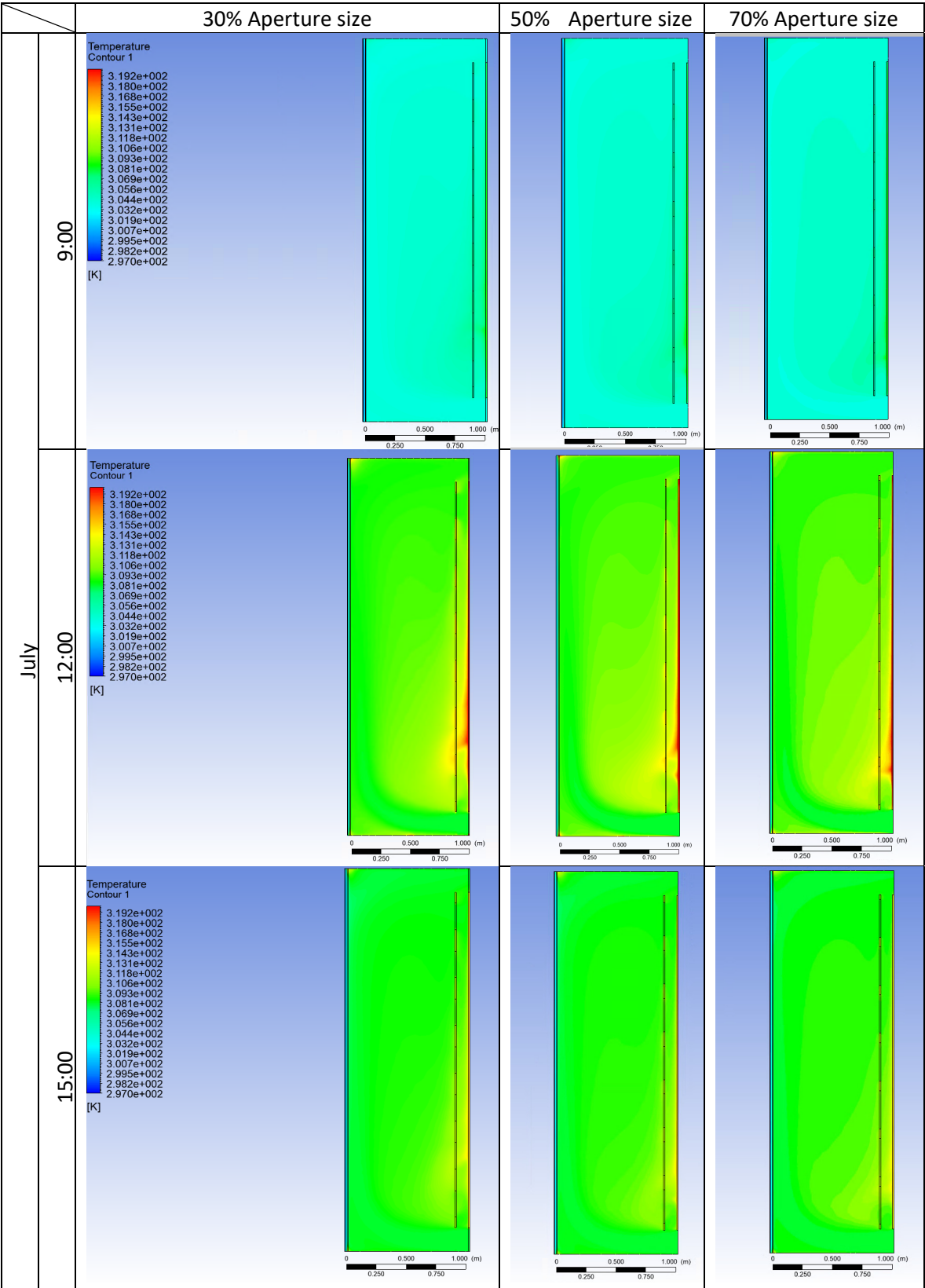




Table 6-15: Cavity temperature profile during 15<sup>th</sup> January.

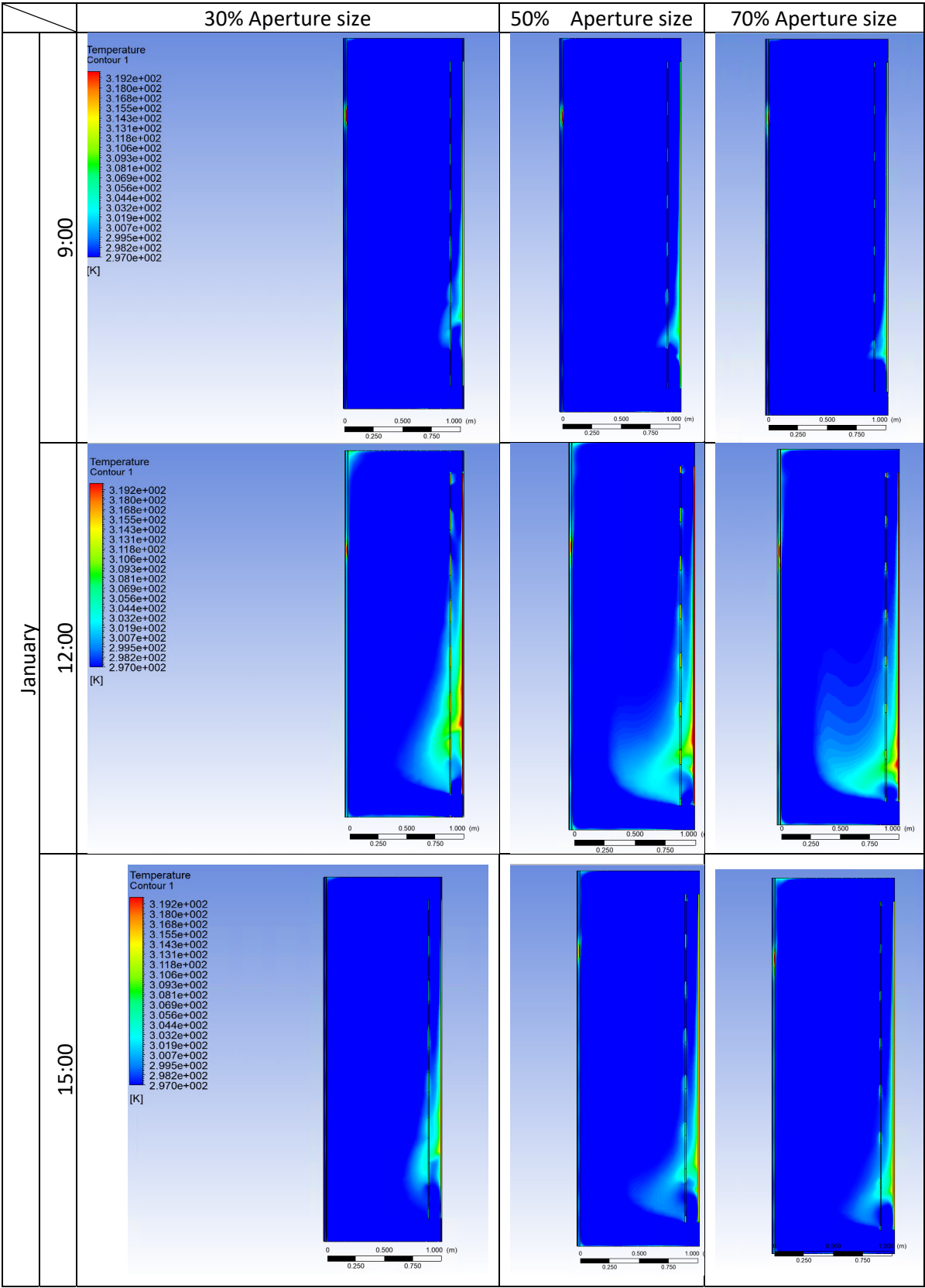
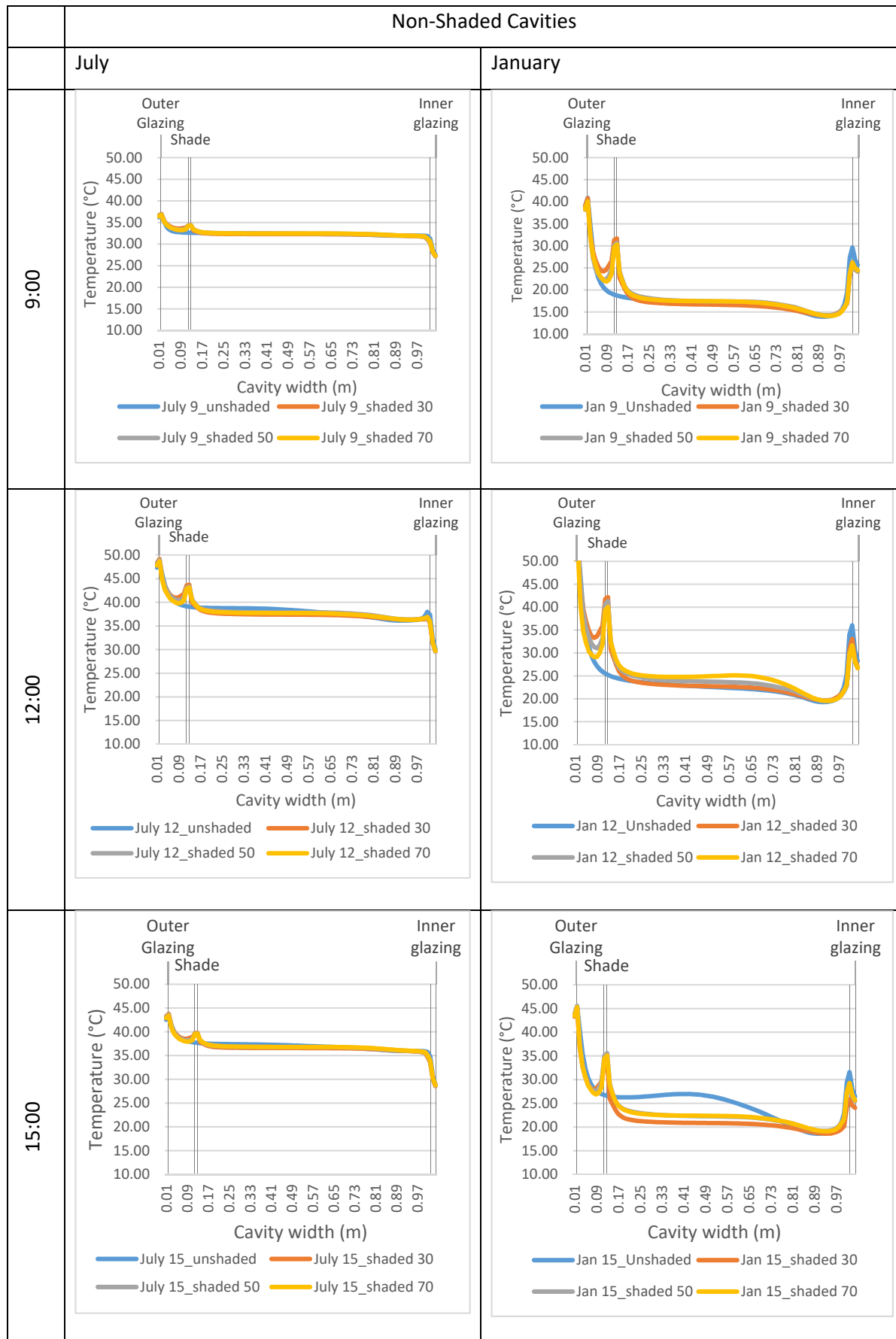


Table 6-16: Temperature profile at mid-cavity for Flat-Shaded Cavities Vs non-shaded cavities.



The obtained average inner surfaces and cavity temperatures for the integrated DSF are in all cases lower than the values reported for non-shaded DSF in the same dates as shown in Table 6.16. Records of the surface temperatures of the non-shaded and flat-shaded cases are attached in Appendix F. The proximity of the solar-shading devices to the external glazing resulted in increasing the temperature in the frontal zone. In midday of peak summer, the solar-shading devices result in 1°C increase in the external glazing temperature, which varies according to the aperture size. The (30%) screen aperture raised the 'frontal zone' and external glazing temperatures due to the heat trapped in the frontal zone compared to the (70%) screen aperture. On the other hand, the 'back zone' and internal glazing temperatures are reduced as the closed configuration tends to contain the heat in the frontal zone. The small apertures reduced the 'back zone' air temperature, and the surface temperature of the internal glazing. In contrast, the opened configuration (70%) resulted in a higher air temperature in the 'back zone'. The external glazing surface temperature increases proportionally with the aperture size. Therefore, this section revealed an apparent correlation between aperture size and external glazing temperature. The smaller the aperture size, the more heat trapped in the outer chamber, hence the external glazing temperature increased while the internal decreased.

Tables of detailed results are attached in Appendix F. On the 15<sup>th</sup> of July at 15:00h, the integration of the 30% aperture flat shading reduced the surface temperature of the internal glazing facing the cavity from 34.8°C to 32.3°C and surface temperature for the internal glazing facing the room from 28.9°C to 27.8°C. The other aperture sizes of 50% and 70% achieved less reductions on the internal glazing facing the room, which are 28.6°C and 28.8°C respectively. In summer, the integration of 30% aperture flat shading resulted in 15.4°C reductions in temperature between the external glazing (43.2°C) and the internal double glazing (27.8°C) which represents 40%. These lower surface and cavity temperatures have a direct impact on the overall heat transfer toward the building, reducing the convective and radiative fluxes due to the reduction of temperature. Although different apertures don't show an extreme difference in the temperature profiles, this is due to the relatively high ambient air temperatures in summer. The solar heat gains and heat flux of the internal glazing surface would be better indicators for blocking the direct solar radiation.

Velocity profiles inside the flat-shaded cavity are obtained at 9:00, 12:00 pm and 15:00 pm of peak summer and winter day for the three aperture sizes (30%, 50%, & 70%) and compared with the non-shaded cases as shown in Figure 6-27, Figure 6-25 and Table 6-17.

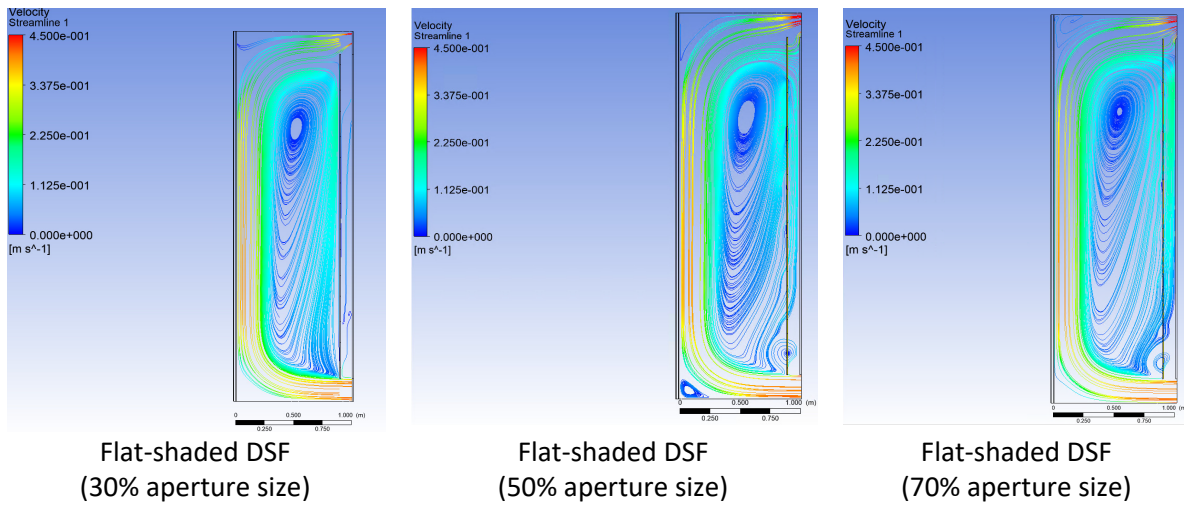
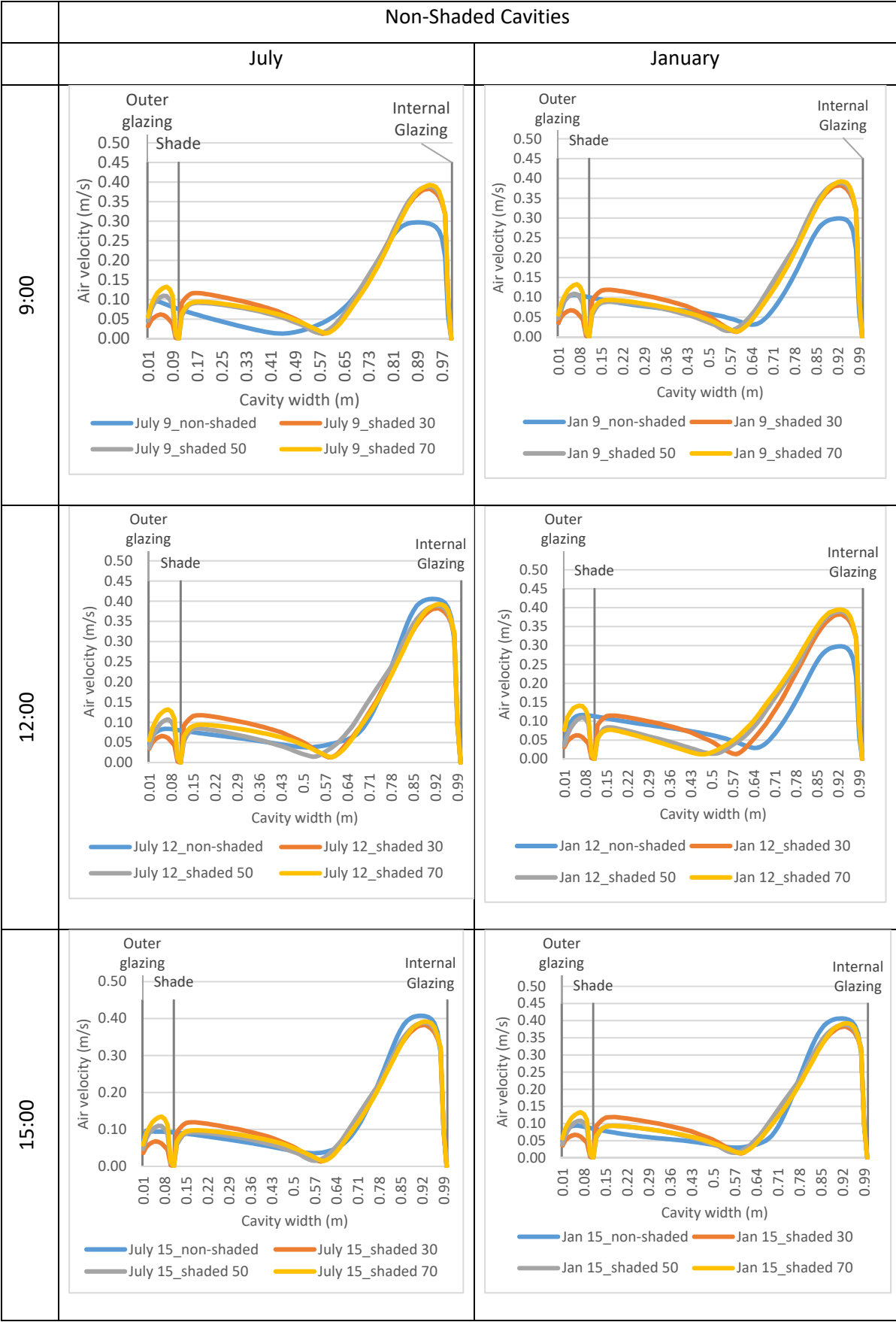


Figure 6-27: Velocity profile at mid cavity equipped with Flat-shading at 15<sup>th</sup> July 12:00.

The solar shadings increase the airflow in the frontal zone due to its high surface temperature and high air temperature in the frontal zone. The flow velocities obtained are low for all case studies. At high temperatures, the solar-shadings reduced the air velocity close to the internal glazing surface from 0.41m/s to 0.39 m/s occurs at 12:00h and 15:00h of 15<sup>th</sup> of July and 15:00 of 15<sup>th</sup> of Jan (Table 6-17). On the other hand, the solar-shading raised the lowest peak of 0.30 m/s recorded by the non-shaded cavity to 0.39 m/s occurs at 9:00h of 15<sup>th</sup> of July and 9:00h and 12:00h of 15<sup>th</sup> of Jan. Solar shading enhance the airflow around the shading system. However, the enhancement of the solar-shading in the 1m wide DSF cavity is relatively minimal due to the large air volume.

Table 6-17: Velocity profile at mid-cavity for flat-shaded cavities vs non-shaded cavities.



The velocity fields indicate that the shading has little effect on the back zone. The solar shading devices increase the airflow in the frontal zone compared to the non-shaded cases. Also, the solar shading results in an increase in the airflow due to its high surface temperature. As seen in the graphs in Table 6-17, the flow velocities obtained are low for all case studies. The 30% aperture solar shading increases the airflow around the shading.

### 6.5.2.3. Heat Flux

Heat flux through the interior surfaces of a flat solar-shaded DSF is recorded on the 15<sup>th</sup> of July and 15<sup>th</sup> of January at 9:00, 12:00 pm and 15:00 pm as shown in Figure 6-28. These heat fluxes were integrated, and area-weighted averaged to compute the solar heat gains.

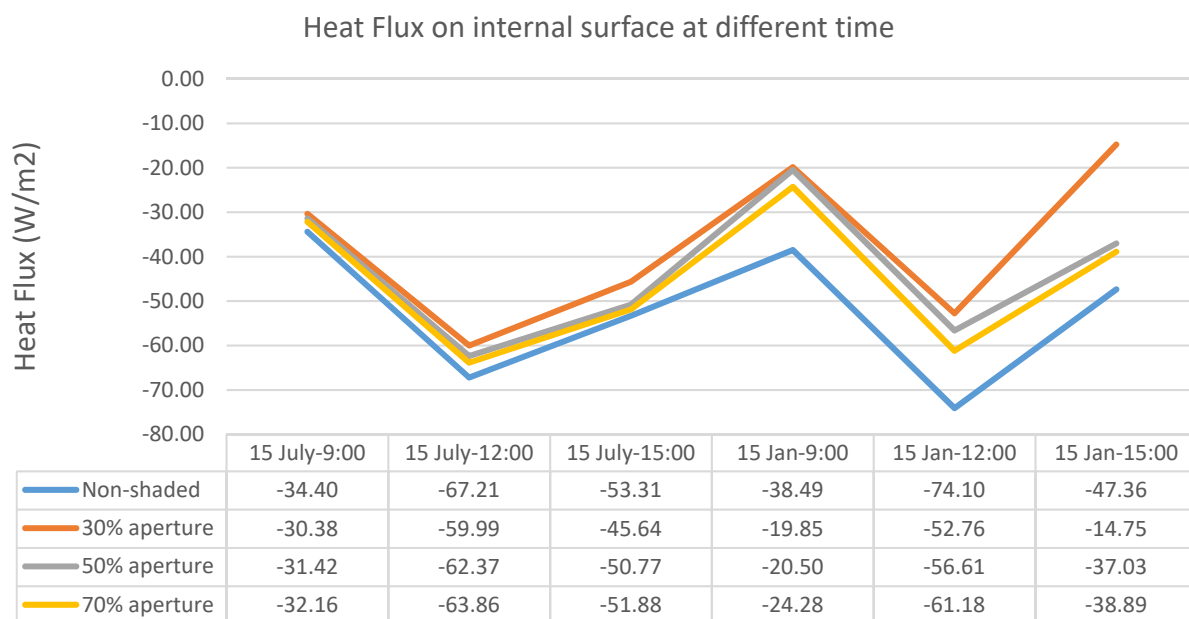


Figure 6-28: Heat Flux on the internal surface at different time.

Figure 6-28 shows the heat flux recorded for the solar-shaded modelled cases. The heat flux entering the building shows a maximum peak in sunny summer day (15<sup>th</sup> July) at 12:00 pm and 15:00 pm, when theoretical maximum values for solar radiation are applied. The best significant role of the closed aperture is found on the 15<sup>th</sup> of July at 15:00 pm by reducing the internal space total heat gains by 15% compared to the non-shaded cavity. The results showed that the small aperture solar shading (30°), resulted in a minimum value of transmitted heat flux with the value of 30.4 W/m<sup>2</sup>. In winter, when the sun has low angular directions, solar shadings cause a high difference in solar heat gains that reach 45% compared to the non-shaded DSF.

The significant role of solar shading devices appears at lower sun angles. This finding is consistent with that of Mei et al. (2007) who used the solar simulator directly normal to external glazing. The solar shading shows high efficiency at lower solar angles occurring at 15:00 pm, while the DSF ventilated cavity plays a bigger role as a shading device in higher solar angles.

In summary, a closed aperture is highly recommended at 12:00 h and 15:00 h of summertime when the solar irradiance has maximum values. Although results can show that open aperture is recommended in the winter to enable part of the direct solar radiation to heat up the internal space, it is recommended to maintain closed aperture at 12:00 h of wintertime to prevent glare.

Lower solar heat gains and internal glazing temperatures can be obtained in peak hours by optimizing the solar-shading devices aperture size as shown in Table 6-18. This is a result of two conditions; the higher airflow rate that circulates inside the DSF, and the lower exposition of inner glazing to solar radiation. Reductions in solar gains and internal glazing temperatures lead to a decrease of the buildings' primary energy consumption and improving the building's carbon footprint.

*Table 6-18: Optimized aperture size with corresponding air and surface temperatures.*

Month	Time	Optimized aperture	Temperature of inner glazing
July	9:00	Aperture 70	27.3°C
	12:00	Aperture 30	29.6°C
	15:00	Aperture 30	28.5°C
January	9:00	Aperture 70	24.5°C
	12:00	Aperture 30	26.9°C
	15:00	Aperture 70	25.6°C

Having discussed the non-shaded DSF cavity and the flat shaded cavities, next section will study the DSF integrated with folded origami solar-shadings devices to test the effect of the change of form from flat to folded shading.



### 6.5.3. Scenario 3: Origami Folded solar-shading

The position of the folded solar shading modules sits 0.2m away from the external surface of the DSF to give the unit the freedom to move and fold forward. The vertex is fixed, and the unit's corners move forward in the frontal zone. This concave form tends to contain the heat inside for material activation.

The set of analysis for the origami solar shading is carried at the 15<sup>th</sup> of July 12:00 pm using the 0.4m vertical segment domain size. The folding units mesh requires fine mesh to reach accepted quality in addition to the number of inflation layers. The full wall cases can reach eight multiples the number of cells of the 0.4m vertical segment to reach (9,385,695), which the available computational power can't process. According to this limitation, 0.4 m vertical segment is used for the following simulation. The results of origami solar-shading at (30%, 50%, & 70%) is compared with the flat solar-shading and non-shaded cases using the same 0.4m 3D vertical section method at the 15<sup>th</sup> of July 12:00 pm.

#### 6.5.3.1. Temperature Contours

Surface and air temperatures, are tested numerically for the origami shaded cavity with the three aperture sizes (30%, 50%, & 70%) and compared with the flat solar-shaded and non-shaded cavities at 12:00pm 15<sup>th</sup> of July as shown in Figure 6-29 and Figure 6-30.

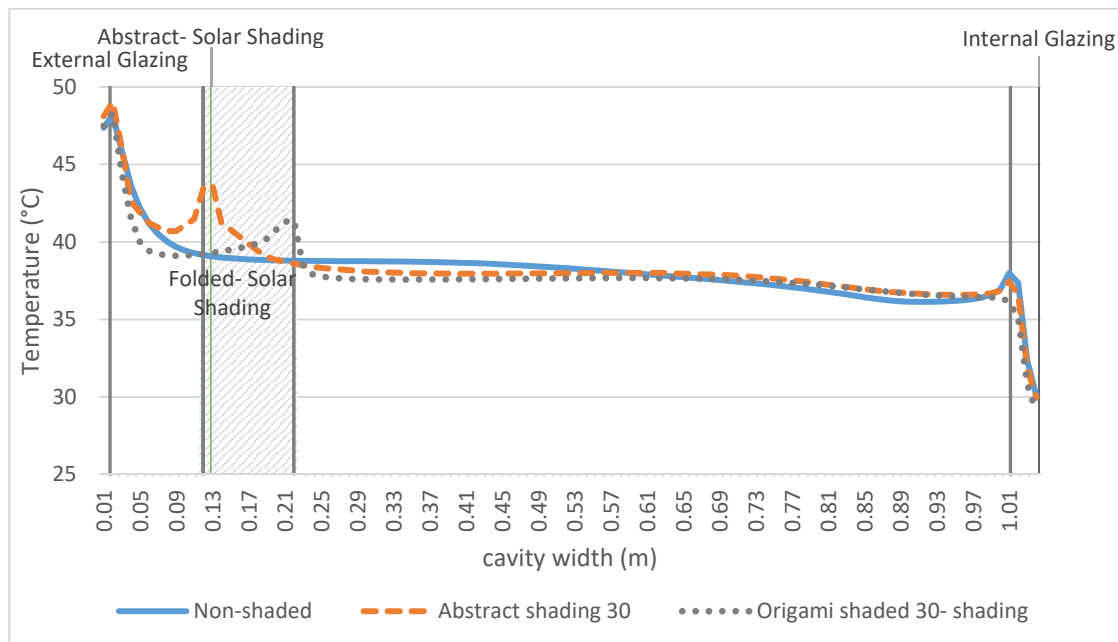


Figure 6-29: Mid cavity temperature comparing 30% Origami shaded, 30% flat shaded and non-shaded DSF at 12:00 pm 15<sup>th</sup> of July.

The folded solar-shadings obtained slightly lower cavity temperatures compared to flat solar shadings. All the origami-shading apertures resulted in more reductions on inner glazing surface temperatures compared to the corresponding apertures of flat shading. For example, the 30% aperture origami solar-shading recorded 1°C temperature drop on the internal surface of the inner glazing than the flat shading, which represents a 3% temperature reduction. It can be seen from the data in Figure 6-29 that the location of the folded solar shading at 0.2m from the external glazing increased the external glazing temperature by 0.4°C compared to the non-shaded cavity. This value is lower than the external glazing temperature recorded using the 30% aperture of the flat shading by 0.6°C which is obviously due to the proximity of the flat shading to the external glazing.

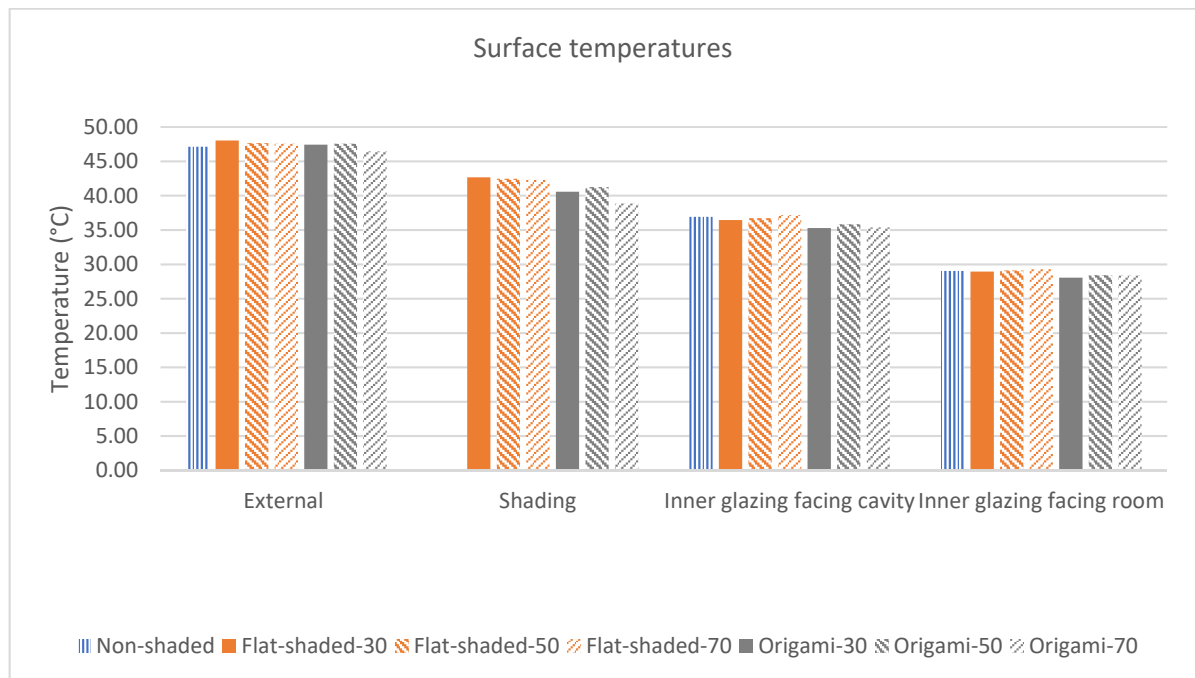


Figure 6-30: Comparison of surface temperatures between 30% Origami shaded, 30% flat shaded and non-shaded DSF at 12:00 pm 15th of July.

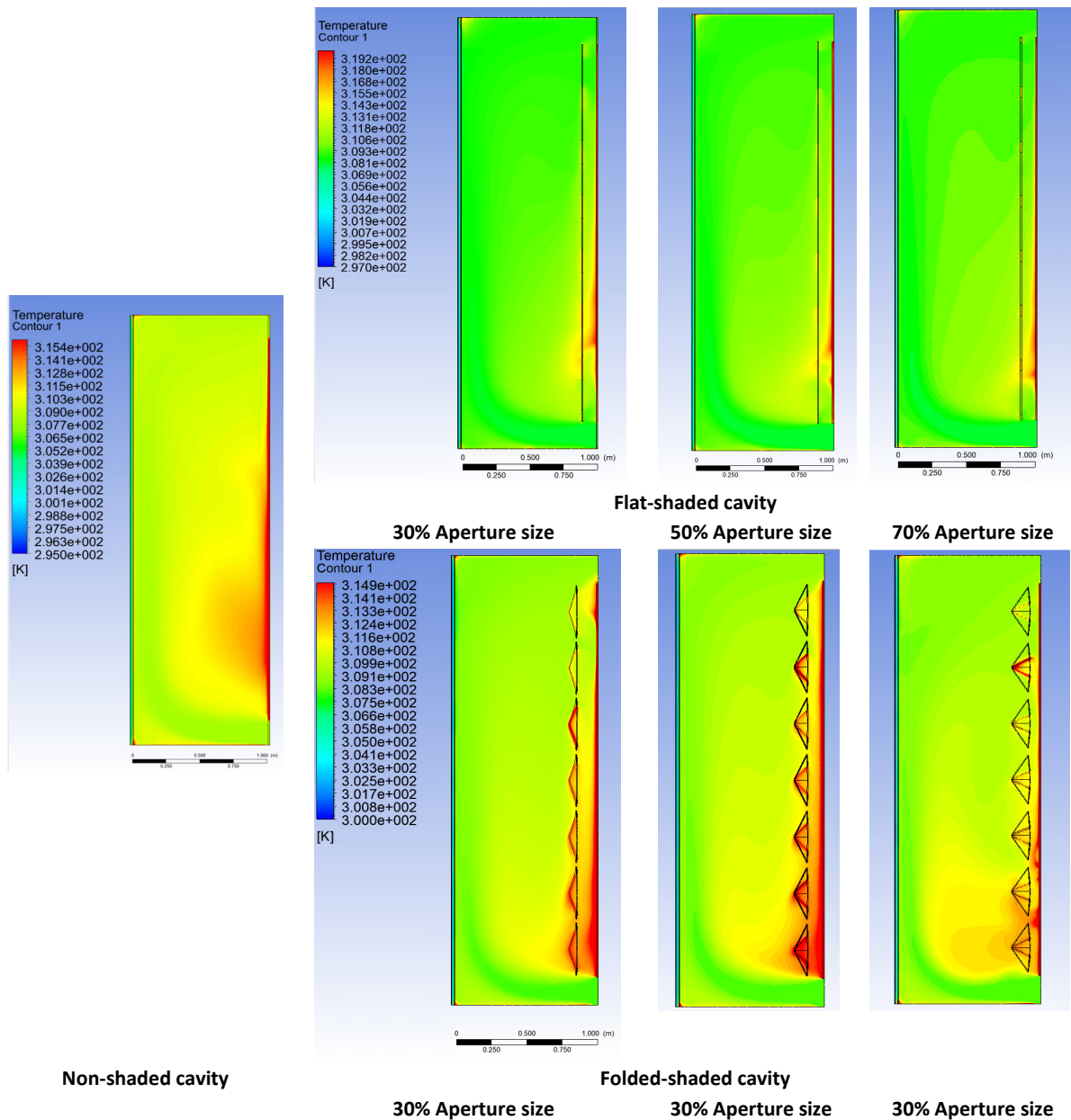


Figure 6-31: Comparison of temperature profiles for the non-shaded flat-shaded and origami-shaded cavities at 12:00h on the 15<sup>th</sup> of July.

The closed configuration (30%) resulted in a high air temperature (38°C) in the ‘frontal zone’ and lower air temperature in the ‘back zone’ as well as lower internal glazing temperature. On the other hand, the opened configuration (70%) resulted in a higher air temperature in the ‘back zone’ along with higher internal glazing temperature compared to the 30% aperture.

#### 6.5.3.2. Airflow rates and velocity profiles

Velocity profiles inside the origami shaded cavity are obtained at 12:00 pm 15<sup>th</sup> of July for the three aperture sizes (30%, 50%, & 70%) and compared with the non-shaded cases as shown in Figure 6-32.

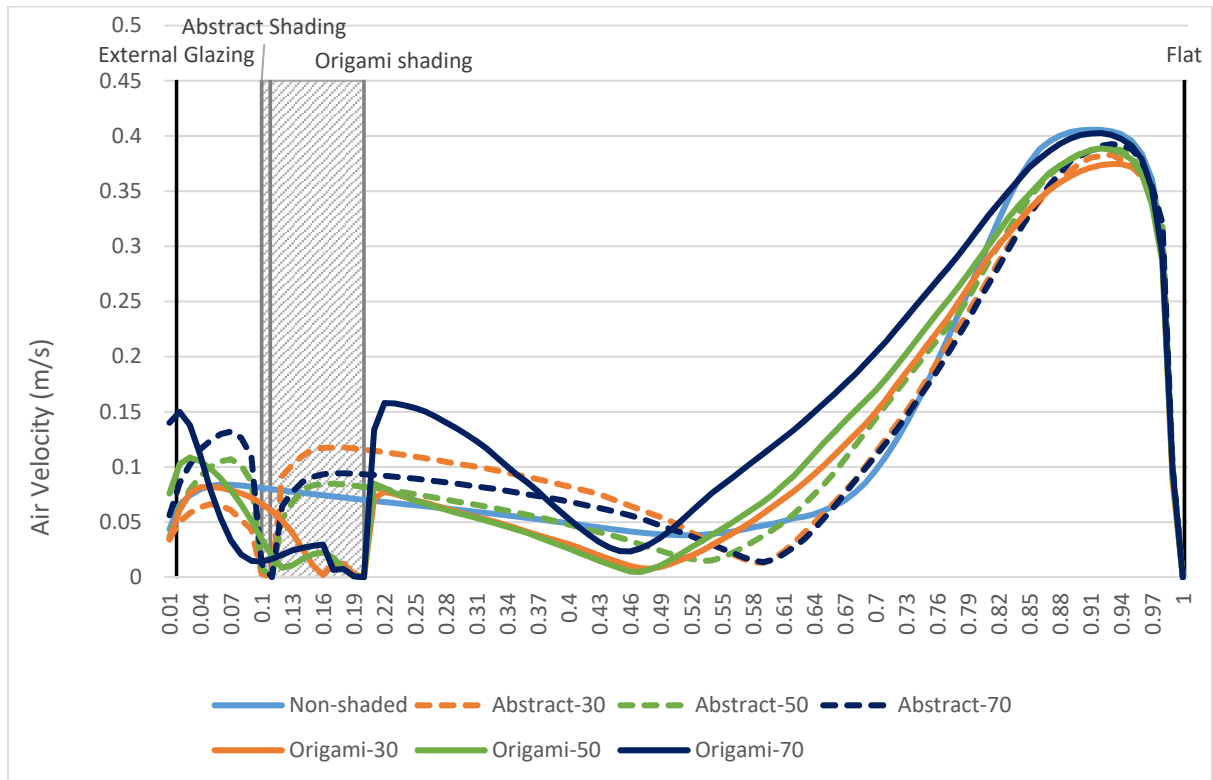


Figure 6-32: Velocity profile at mid-cavity comparing 30% Origami shaded, 30% flat shaded and non-shaded DSF at 12:00 pm on the 15th of July.

As shown in Figure 6-33, the origami shading is more geometrically complex than the flat shading which result in more turbulent flow around the solar-shading and increase the airflow in the mid cavity. The complexity of the origami solar-shadings of the 70% aperture resulted in more turbulence around the solar-shading that reach 0.15m/s compared to 0.11m/s for the 30% aperture.

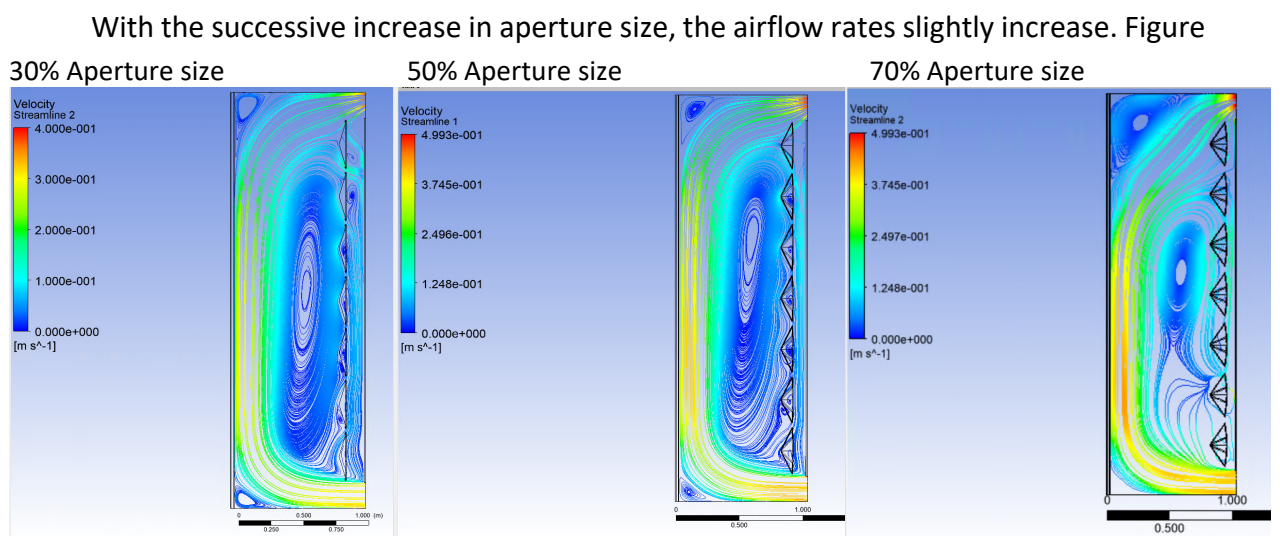


Figure 6-33: Velocity profile at mid cavity equipped with folded origami-solar-shading on 15th of July at 12:00pm.

6-32 shows the velocity profile at mid cavity, which illustrates that the behaviour near the

inner glazing is similar in all cases but differs around the shading and mid cavity. The maximum airflow for all cases is close to the surface of the internal glazing and their peaks are at 0.08m from the glazing element. The highest velocity is 0.41m/s occurred in the non-shaded cavity followed by 0.4 m/s for the 70% origami solar-shaded and 0.39 for the flat-shaded cavity at 12:00 h on the 15<sup>th</sup> of July.

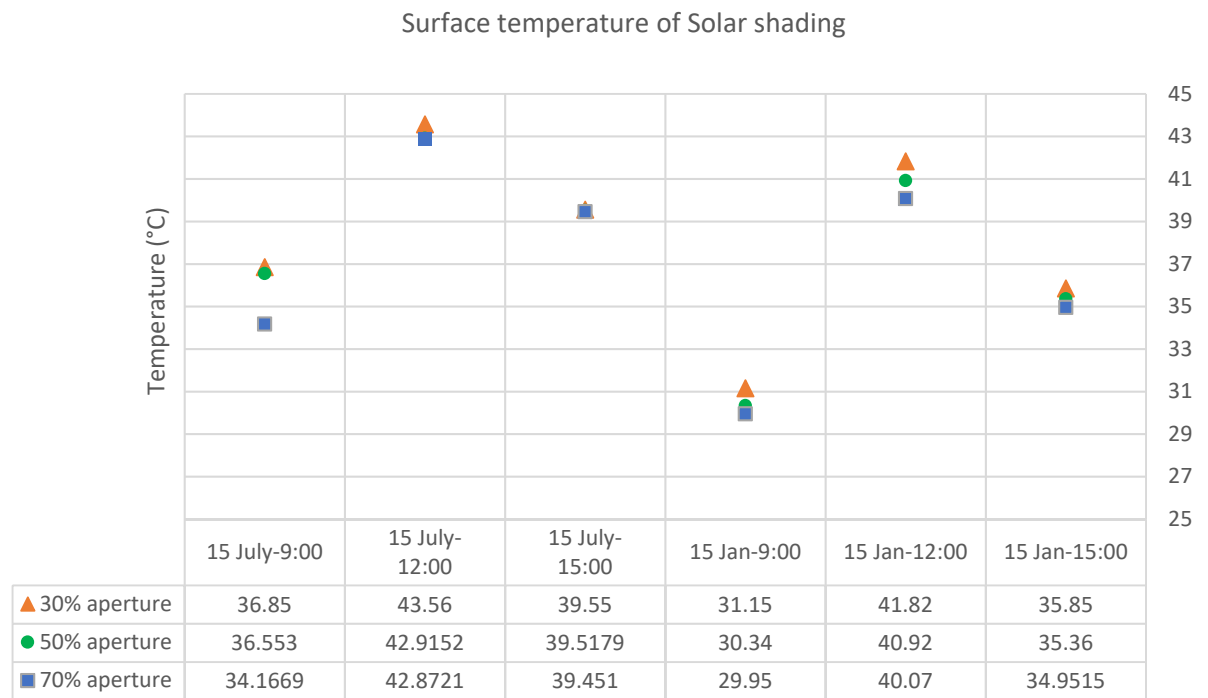
#### 6.5.3.3. Heat Flux

Strong evidence regarding the efficiency of the folded solar shading is found on the 15<sup>th</sup> of July 12:00 by reducing the total heat gains by 21.5% compared to the non-shaded cavity and 12% compared to the flat-shaded cavity. This difference between the origami solar-shading and flat solar-shading groups presents a significant heat gain reduction. The results show that the 30% aperture origami-solar-shading is the optimal configuration at 15<sup>th</sup> of July 12:00 as it reduced the total heat flux at the internal glazing from 67.2 W/m<sup>2</sup> to 52.75 W/m<sup>2</sup> compared to the non-shaded cavity. This result may be explained by the fact that the concave form contained the heat inside and raise the temperature in the frontal zone while lowering the back zone temperature affording extra protection for the internal glazing resulting in less solar gain and extra energy savings.

In summary, this section has analysed the DSF conditions using three aperture sizes for both flat and origami solar-shadings. The next part of this chapter will look at the heat distribution on the solar shading device for informing the design of the module and material.

#### 6.5.4. *Analysis of solar shading*

The solar-shadings' surface temperatures are recorded inside the full cavity model integrated with the flat shading. Flat-shading screen with three aperture sizes (30%, 50%, & 70%) are tested on the 15<sup>th</sup> of July and 15<sup>th</sup> of January at 9:00 am, 12:00 pm and 15:00 pm respectively as shown in Table 6-14 and Figure 6-34. Moreover, surface temperatures of folded origami solar-shadings are analysed on the 15<sup>th</sup> of July at 12:00 pm to inform the range of activation required for the actuators and their preferable location.

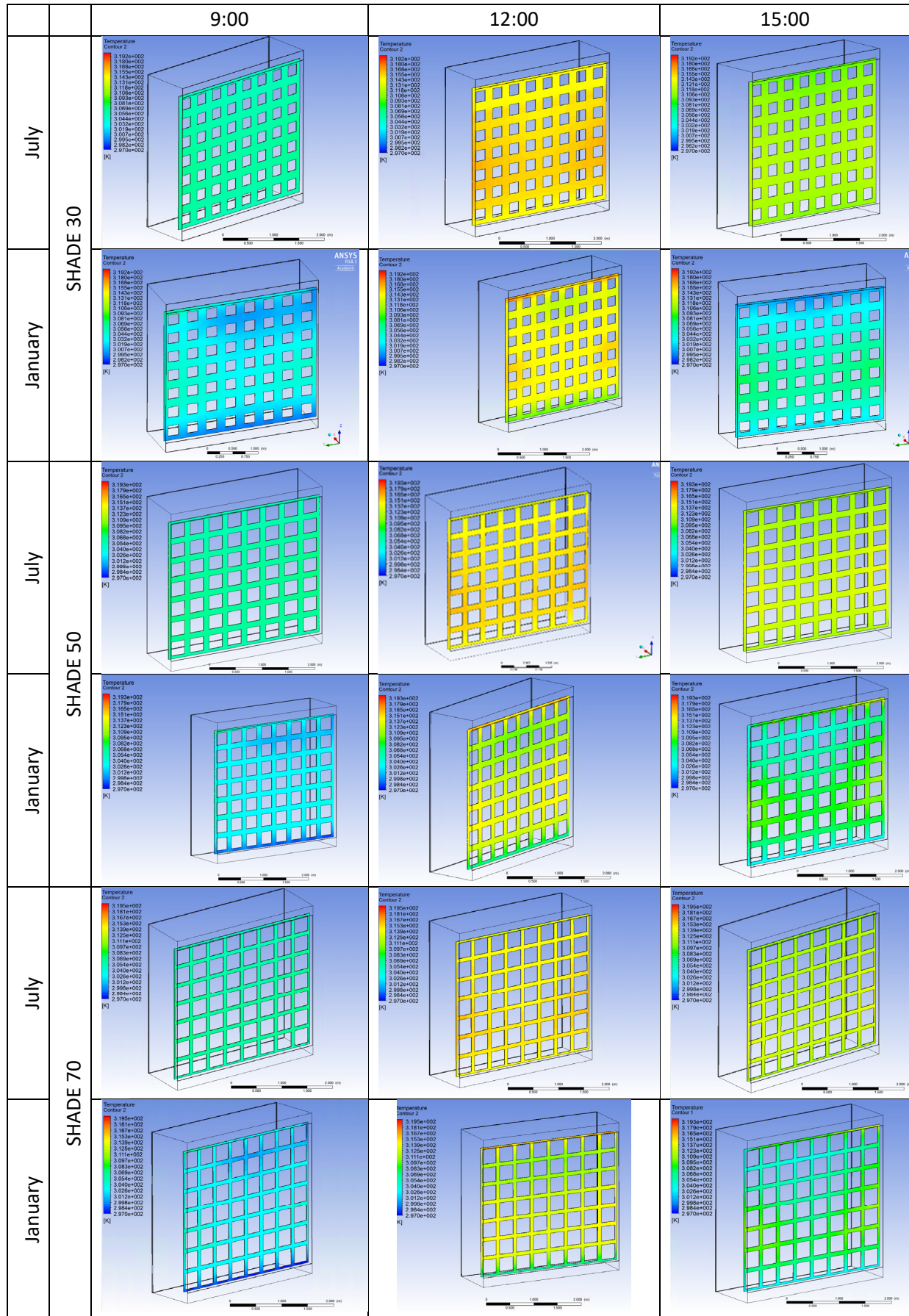


*Figure 6-34: Average surface temperature of flat solar shading.*

In summer, solar-shading temperature increases during the day, due to the high exposition to solar radiation and heat absorbed from the cavity. This behaviour is reverted quickly after sunset, with no incident radiation. The solar shading with closed configuration (30%) has the highest temperature of all due to the large exposed area of the solar-shading and the heat trapped in the frontal zone. The obtained average surface temperature of the (30%) solar shading reached a maximum of 43.6°C at the midday of July and a minimum of 31.15°C on the morning of January. A maximum temperature difference of about 12.5°C at the solar shading surface is observed as shown in the above graph. This thermal energy harvested on the solar shading surface is used to activate the SMM actuators.

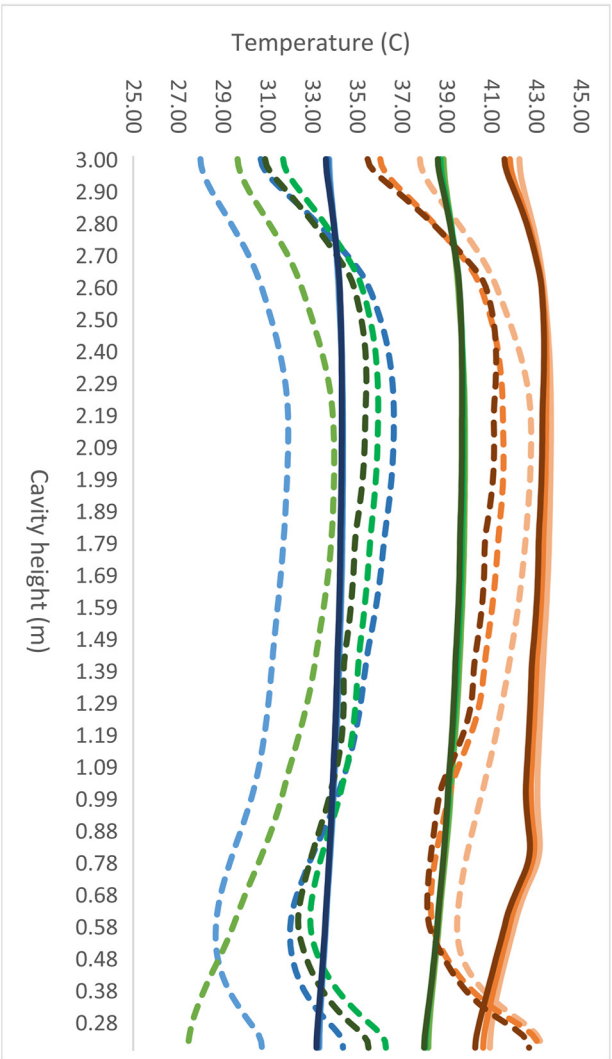


Table 6-19: Surface temperature distribution of solar shading.

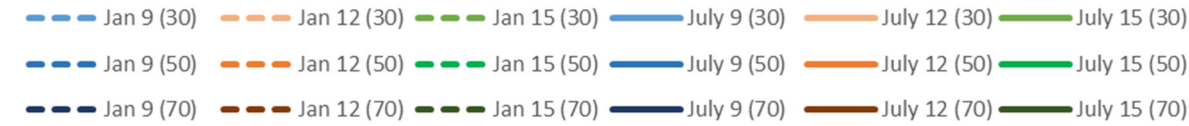




From Table 6-19, the surface temperature of the solar-shading screen gives a slightly different gradient as a result of the solar angle and the proximity to the inlet and outlet. A minimal temperature difference of about 2°C at the solar shading surface takes place at 9:00 and 15:00 July where the temperature is almost uniform among the surface and reaches, 34 °C and 40 °C respectively as shown in Figure 6-34 and Table 6-19. The 3D full cavity model has the ability to predict the temperature distribution among the shading surface. Each actuator has a specific location in the system arrangement which could be exposed to a different amount of radiation and have a slightly different surface temperature that may result in a



different response.



From Figure 6-35, it is observed that the three aperture sizes didn't have much impact on the solar-shading surface temperature in summertime. The solar-shading surface temperature reports 34°C, 42°C and 40°C at (9:00, 12:00 and 15:00 h) respectively. On the contrary, different aperture sizes affect the solar shading temperature widely in winter. At midday, the 30% aperture size has the highest temperature as a result of trapped heat and convection effect.

At the midday of the 15<sup>th</sup> of July, the direct radiation coming through the outlet opening affected the 2<sup>nd</sup> and 3<sup>rd</sup> origami units and raised their temperature by 3°C unit, as shown in Figure 6-36. Additionally, as seen in Table 6-19, the temperature distribution on the flat solar-shading screen was non-uniform as a direct effect of solar angle and value of solar radiation. All these factors would affect those arrayed units to slightly vary vertically and horizontally. These variations would affect the individual response of each actuator, SMA or SMP, to act on its own, resulting in a slightly different aperture as a function of spring elongation or polymer sheet contraction. Detecting these variations and customizing the material accordingly would minimize the consequent differentiation to help the unit to act as planned. Having each unit as a robot that moves on its own with its embedded actuator gives it the benefit of freedom and individuality. Despite of the individual reaction of each actuator to the local thermal heat gains, they all move in a very close range.

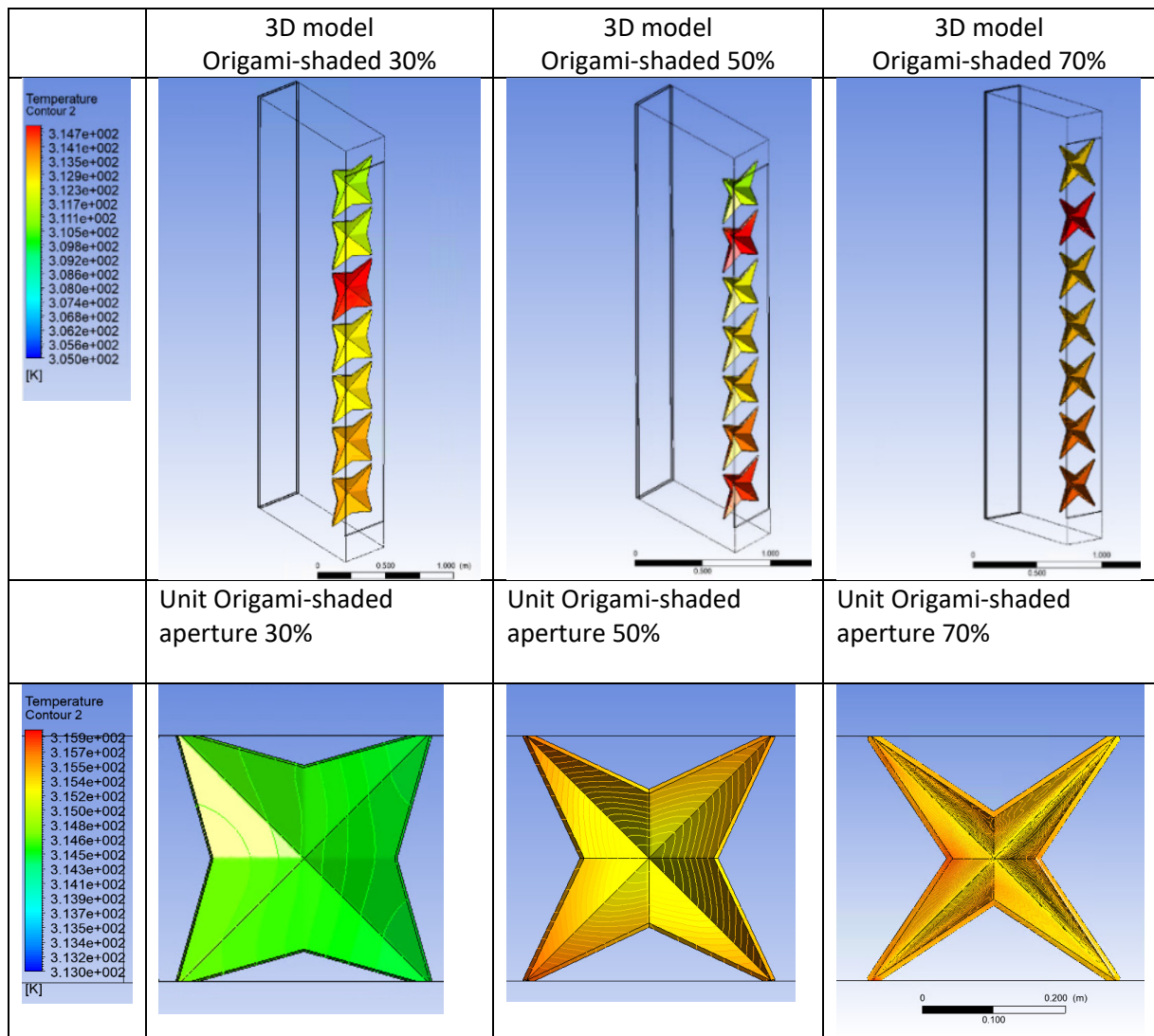


Figure 6-36: Folded solar-shading 3D analysis recorded at 12:00 pm on the 15<sup>th</sup> of July.

While zooming in onto the single origami unit as shown in Figure 6-36, it was found that the tips and edges moving forward towards the external glazing have higher temperature than the inner valleys. The solar shade of the closed configuration (30% aperture) sits back from the external glazing having a lower temperature of 41°C. When moved forward, the unit heats up, and the tips' temperature is raised to 43°C.

In conclusion, the preferred configuration for summer peak time (12:00 pm and 15:00 pm) is the closed configuration (30% aperture). The 30% aperture for the midday of the peak winter protects the inner glazing from the glare effect and results in higher inner temperature due to the effect of the heated solar-shading surface. The 70% aperture should be maintained at all other low direct radiation values and ambient temperatures, as shown in Table 6-20.

Table 6-20: Activation temperatures and aperture size required at peak summer and winter days.

Month	Time	Optimized aperture	State	Average Temperature at the solar shading	Temperature of inner glazing	Ambient temperature
July	9:00	Aperture 70	Opened	34.5°C	27.3°C	31°C
	12:00	Aperture 30	Closed	43°C	29.6°C	35°C
	15:00	Aperture 30	Closed	40°C	28.5°C	35°C
January	9:00	Aperture 70	Opened	31°C	24.5°C	12°C
	12:00	Aperture 30	Closed	40°C	26.9°C	17°C
	15:00	Aperture 70	Opened	35°C	25.6°C	18°C

In order to ensure robust sun protection in the hot arid climate of Cairo, the responsive shading system should be programmed to be in a closed state between 40-50°C, which is the highest threshold to be expected throughout the entire year as shown from climatic meteorological data for Cairo, Egypt included in Appendix C (Liggett et al., 2016). The temperature of the solar shading surface at the highest solar radiation represented at the peak summer day is the most important. A closed configuration represented by an aperture of 30% should occur above 39/40°C detected at the solar shading or at 37°C in case the actuators are located in between the units. An aperture of 50% would occur between 37°C and 39°C and an aperture 70% between 31°C and 36°C. The kinetic module should be fully opened below 30°C detected at the solar shading. Thus, It is recommended to use the embedded SMMs with activation temperature from 35-40°C which can be programmed to reach intermediate shapes or positions at these temperature ranges.

- Fully opened - Below 30°C
- Aperture 70 - Between 31°C-36°C
- Aperture 50 - Between 37°C-39°C
- Aperture 30 - Above 40°C

The environmental feedback provides informative data by measuring the surface and cavity temperatures to detect the *activation temperatures* required to actuate the responsive solar shading system.

The data obtained from the surface temperature analysis of solar shading can also inform the actuators' location. Some techniques and locations are preferable in terms of material consumption of SMM, acquisition of maximum motion and sun exposure. The two-way exposed springs with intrinsic return mechanism have the benefits of maximum sun exposure, high range of motion and allows the solar-shading unit to act individually as a robot. By looking at the tested origami unit, the tips and edges are closer to the external glazing and have a higher temperature than the inner valleys, as shown in Figure 6-37. As discussed in Chapter Four, suspension of spring actuators with fixations at the ends, offers the highest solar radiation exposure without material insulation. Four two-way actuators can be located near the tips, as shown in Figure 6-37. Upon activation at 40°C, the two-way SMA springs can elongate from 1.5cm to 4.5cm to transform the unit from opened configuration (70% aperture) to closed configuration (30% aperture).

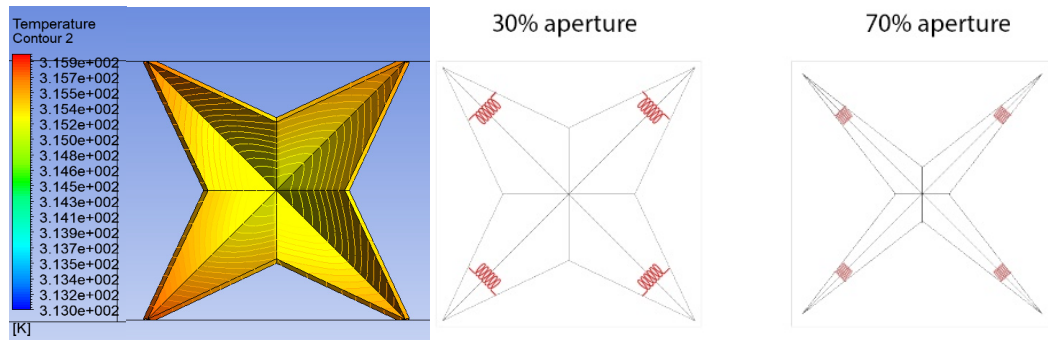


Figure 6-37: Linear two-way actuators located at the four wings of the simulated Origami solar-shading.

From this chapter, the data obtained from the surface and air temperature analysis, airflow and heat flux inform the selection of aperture sizes and preferable forms that protect the inner glazing systems. While, the data obtained from the surface temperature analysis of solar shading informs the range of activation required for the actuators and their location.

## 6.6. Conclusion

This chapter used computational fluid dynamics (CFD) to model the heat transfer problem taking place inside a south-oriented ventilated DSF located in Cairo, Egypt. A corridor single storey double skin cavity is modelled. The cavity is studied in non-shaded conditions, integrated with flat and folded solar shading devices to inform the responsive system design.

### - Non-shaded DSF cavities

The effects of several DSF geometrical variables, which includes the cavity's width, the façade layering, and the domain size, showed a significant role in controlling DSF's performance.

Regarding the **cavity's width**, it was found that increasing the cavity width can improve the thermal performance of the DSF. Narrow cavities allow the direct radiation to affect the inner glazing surface strongly. The 1m wide cavity reduces the heat gain by 15% compared to the 0.4m wide cavity.

Regarding the **façade layering**, the internal double glazing lowered the internal surface temperature by 24% compared to single glazing when studied at 12:00 pm 15th of July. Accordingly, the inner double glazing is recommended as they allow considerable cooling load reduction in summer.

Regarding the **domain size**, the 3D vertical segment method with side symmetry boundary conditions successfully assessed the DSF structure behaviour on July midday with less than 5% variation compared to the full cavity modelling. It has the advantages of using the solar load model, which is only available in the ANSYS Fluent 3D solver, assesses more complex forms than 2D, and compute the turbulent mixing appropriately with the proposed geometry. Moreover, the 3d model has the ability to predict the temperature distribution among the shading surface. This method allows for a complex form assessment with reduced computational cost compared to the full model method. However, the most important limitation lies in the fact that the source of solar radiation is direct toward the external glazing without side vector components that may affect the symmetry surfaces. On the other hand, the full cavity modelling is more accurate and has all above-mentioned benefits but needs huge computational power. Additionally, the 3D full cavity model has the ability to predict the temperature distribution among the shading surface.

It was found that the highest air cavity temperatures are near the outer glazing. The closer the solar-shading screen to the outer glazing, the higher the surface temperature of the shading devices which facilitate the activation of the actuators. A responsive solar-shading system is recommended to be integrated into a 1m wide DSF cavity in the range between 0.1 to 0.2m away from the outer glass to activate the smart material.

- **Flat-shaded DSF cavities**

Ventilated DSF proves to act effectively in summer, and the integration of flat-solar shading has an added value of 12 and 15 %. The net heat gain to the indoor environment is reduced considerably with solar shading devices in DSF. A 30% aperture is highly recommended when the solar irradiance has maximum values of 1320 W/m<sup>2</sup> and at 12:00h of

wintertime to protect the inner space from the glare effect. The 70% aperture should be maintained at all other low direct radiation values below 850 W/m<sup>2</sup>.

- **Origami-shaded DSF cavities**

The origami folded solar shading devices are more efficient by reducing the solar heat gain by 21.5% compared to the non-shaded cavity and 12% compared to the flat-shaded cavity in peak summertime. This result may be explained by the fact that origami folded shading has more depth than the flat solar-shading, which contributes to further refractions of the direct solar radiation and a larger absorption surface for direct solar radiation. The method of simplification of complex solar-shading forms into a flat screen with the same aperture size succeeded to give us guidance of the general system performance in peak summer and winter days with less computational power. Nevertheless, the detailed modelling of origami-shaded DSF showed more energy reductions.

- **Solar shading Analysis**

The positioning of the solar-shading screen close to the outer glazing results in increasing the exposure of smart material actuators (SMA) to direct solar radiation and conductive transfers which facilitates its activation. It is recommended to use SMAs with actuation temperature from 35-40°C. This range of temperature can be achieved on the surface of the solar shading and the surrounding zone when the solar irradiance has high values. The integration of responsive solar-shadings into the external envelope of buildings, provides architects with more freedom to integrate advanced technologies in their designs with all its embedded aesthetics reaching new versions of solar screens, thus adding new tools for *Green Buildings'* design.

This study lays the groundwork for future research into performance-based designs of responsive skins. It provides informative data that guides the design decisions, customizes the motion and tailors the smart material properties. This study provided an important opportunity to understand the link between the geometry selection and range of motion along with the thermal conditions of the cavity. The synchronization between the activation temperatures of the smart material actuators and the thermal conditions of the cavity is crucial for proper operation of the system.



## Chapter 7 . THE DESIGN FRAMEWORK

### 7.1. Introduction

This chapter integrates and reflects on the design experiments and the environmental data from CFD analysis using an open-ended design approach in order to develop a framework for responsive solar-shading design and decision-making process informed by experimental and environmental feedback. By doing so, different design parameters for responsive solar-shading systems in specific and responsive systems in general, are related in a way that guides students and researchers in the kinetic field for future development. The design framework aims to open up possibilities by leaving spaces of freedom for designers to re-appropriate the design of the responsive system by changing their context of operation and design approach. Testing this framework with designers and students would add to its validity and could help shaping educational activities in the field.

As shown in Figure 7-1, the framework reflects the feedback from hands-on explorations in chapter 4 and environmental performance in chapter 6 on the design of responsive solar-shadings to guide further decision-making processes.

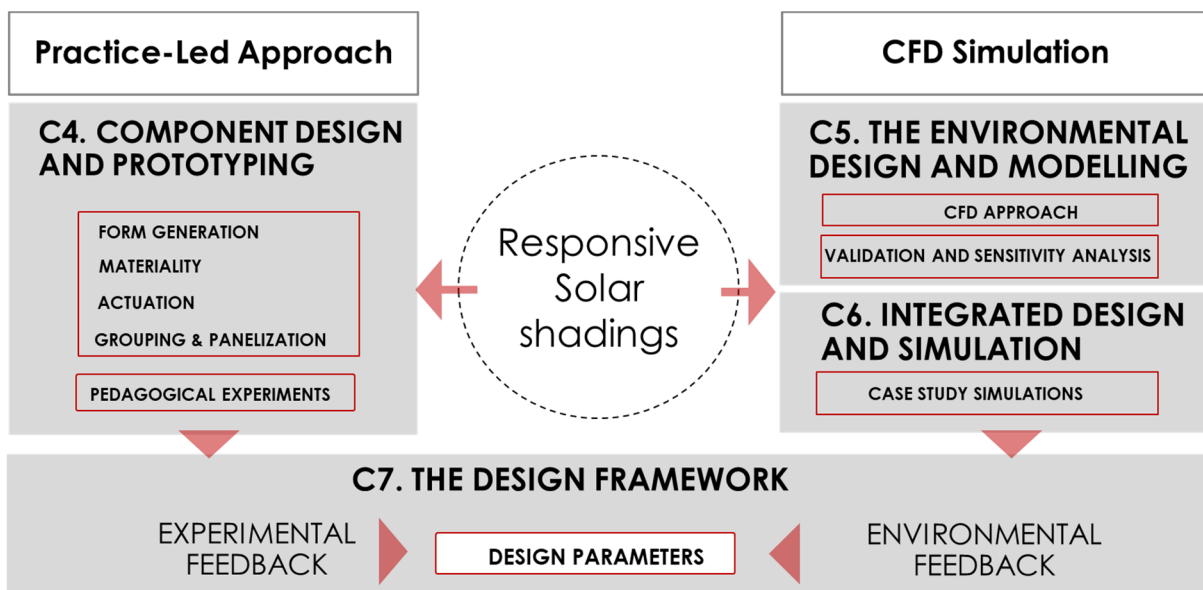


Figure 7-1: The design framework as an integrative process linking design and performance.

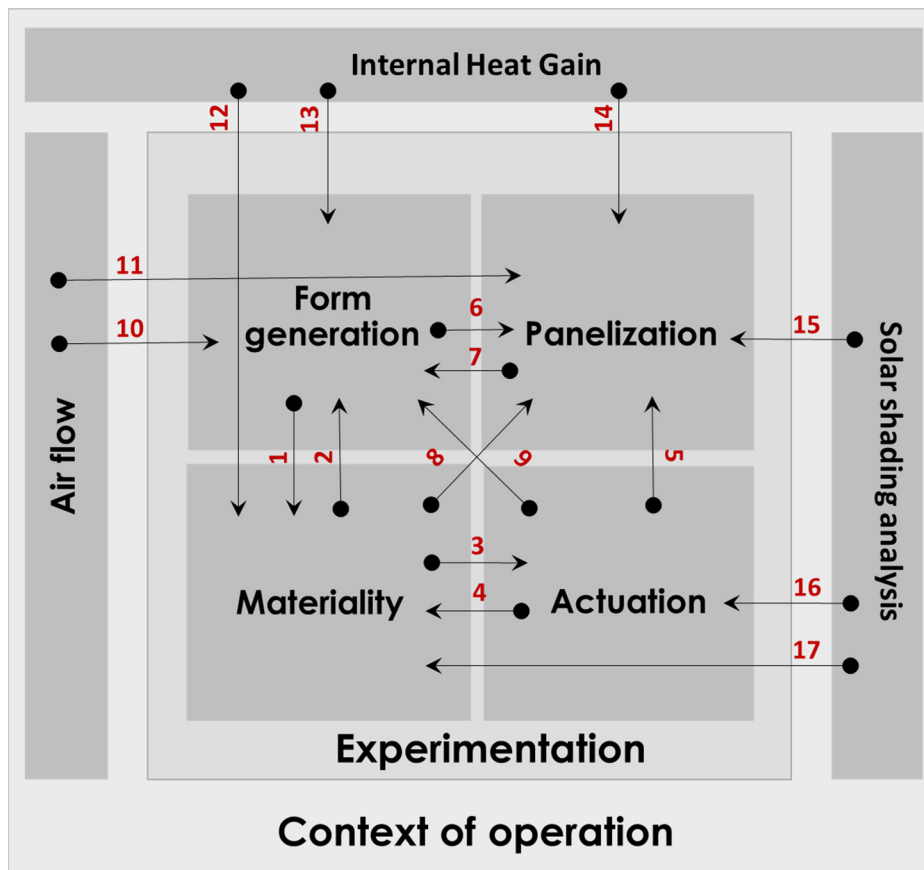
### 7.2. The Design Framework

The design framework discusses the relationships between the key aspects that the design process of responsive solar-shading systems should cover. Interestingly, the creative practice unfolds the relation between these aspects, which was found to be working not only in one-

way in which one aspect informs the other but also sometimes it works in both ways. It is not rigid and can be approached from any of these aspects as a starting point as long as all aspects are taken into consideration.

This chapter is zooming out from the very specifics of the researcher's own experience to the generality of the framework which may afford different perspectives of how the design could be approached as long as each aspect is studied at a specific point during the design process. This framework move towards a more collective approach which focuses on tying different forms, material diversities, actuation means and grouping strategies rather than a linear design process. The framework aims to reach an understanding of how each change in one parameter would affect the other. The study of these responsive systems within their context of operation not only affect their workability/ operability but more importantly define their role.

The framework shown in Figure 7-2 illustrates the relation between experimental and environmental performance, the interrelated parameters of form generation, materiality, actuation, and panelization work collectively to shape the system which as a facade serves more than one environmental function. Part of these decisions are made during the different phases of the experimental design process, while others are part of the reflection of the surrounding context.



#### Internal

##### 1- Form to materiality

Plants can inspire actuators allocation. Folded surfaces can be actuated using linear actuators.

##### 2- Materiality to form

Material generates the form. Exploration with passive soft materials presents a wide range of hinge-less soft deformation and encourage curved folding forms. The actuators' type, their direction and range of motion can generate the form.

##### 3- Materiality to actuation

Selection of Activation range and Exposure of actuator to facilitate actuation

##### 4- Actuation to materiality

System reversibility can use materiality (by passive elastic materials or two-way actuators)

##### 5- Actuation to panelization

System reversibility can use gravity (unit positioning)

##### 6- Form to panelization

The shape of unit arrayed can guide the ways of clustering

##### 7- Panelization to form

Geometrically tessellated

##### 8- Materiality to panelization

Actuators or passive springs could be located between units

##### 9- Actuation to form

System reversibility can use curved folding

#### External

##### 10- Airflow to form

Selection of form that optimizes airflow in the cavity

##### 11- Airflow to panelization

Airflow analysis would define how Selection of the shading units position the that optimizes airflow in the cavity.

##### 12- Internal heat gain to materiality

Selection of actuators' range of motion that fulfils the required aperture range optimizing the internal heat gain

##### 13- Internal heat gain to form

Selection of form that optimizes heat gain

##### 14- Internal heat gain to panelization

Selection of relative positioning of solar shading that affords maximum exposure for smart material actuation

##### 15- Solar shading temperature analysis to panelization

Selection of relative positioning of solar shading that optimizes internal heat gain

##### 16- Solar shading temperature analysis to actuation

Synchronize the smart materials' activation ranges with the surface temperature of the solar shading

##### 17- Solar shading temperature analysis to materiality

Selection of actuator types that could be activated with direct solar radiation and positioning the actuators in the highest temperature spots.

*Figure 7-2: A design framework for responsive solar-shadings.*

The relation between experimental and environmental performance will be discussed in the following sections.

The presented framework would shed light on different approaches to the design of responsive solar shading system. As shown in Figure 7-3, the design could begin by the experimental parameters and test their environmental role or could begin by the contextual information that defines their environmental role then move on to design their experimental specifics.

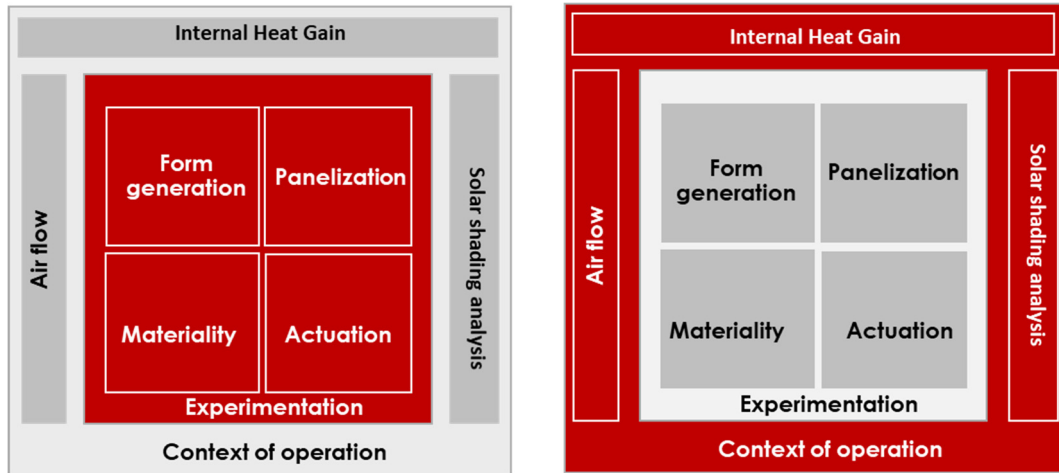


Figure 7-3: Responsive solar-shading system designs as In-out or out-in design process

Having presented a helicopter view of the framework, the next two sections describe the relationship between different aspects in experimental and environmental domains.

### 7.3. Experimental Feedback

The experimental exploration not only leads the design decisions based upon technical aspects that ensure the workability of the system but also the aesthetic qualities of materials and movements. To design a working deployable responsive solar-shading system, these four aspects need to be thought thoroughly; form generation, materiality, actuation and panelization. The presented framework argue that the design process could not be a linear process. Through the experimentation, the same parameter can be revisited multiple times to make adjustments and refine the system in case it is receiving feedback from multiple domains. The responsive solar shading design can be approached from any of these four aspects as a starting point following this relationship network shown in Figure 7-4. The thesis recommends performing these four phases of exploration using the hands-on exploration and tinkering materials to explore the resulting motion with time in space.

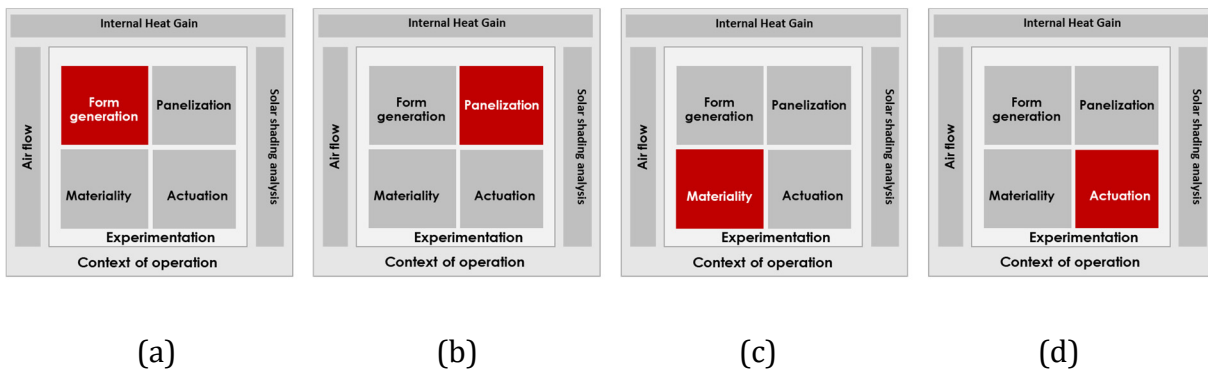


Figure 7-4: Responsive solar-shading system design from different start points in the experimental design process

- (a) Starting with *FORM GENERATION* - One approach is to design a fully deployable single component and then group or cluster it. The responsive component can behave as a single organism or robot through using some actuator types and locations which enables it to acquire a standalone reversible motion. This strategy allows more flexibility for patterns of grouping. Moreover, starting from bioinspiration as form generator can inform multiple actuation methods, material selections and pliable systems grouping.
- (b) Starting with *PANELIZATION* - The designer can begin with the strategy of panelization and positioning. Panelization can lead the form-generation allowing the designer to think about the movement and actuation directly to the geometrically tessellated surface. In this case, there is a different way of thinking about actuation and active material allocation. The component is perceived as a unit of the grid where the actuators or counterweight elements can be located in-between components or grouped in a highly exposed location.
- (c) Starting with *MATERIALITY* - Materiality is considered a strong driving force for the design. The approach of materiality or materiability is one of the recent approaches that many designers would be curious about. As shown in Figure 7-4, materiality is found to be highly related to almost all the other aspects. By focusing on materiality as the driving force of design, their material properties and fabrication techniques are so important for the form and function of the solar-shading system. This includes material thinking of active and passive materials. By exploring their characteristics, many ideas can be generated. For example; their flexibility can result in material deformation movements, their elasticity can represent a return mechanism, their strength and durability can inform their appropriateness for use in building

constructions, their colour, emissivity, absorptivity and reflectivity affect their environmental thermal performance, and their availability in the specific context can guarantee their sustainability.

- (d) Starting with *ACTUATION*- Actuation and system reversibility inform both the selection of material; active or passive as well as the location of actuators by considering the stimulus which the structure need to respond to; its value and direction. The location of the solar-shading system itself, the allocation of the smart material and the actuators' activation ranges are all design decisions related to actuation that can generate the design of the system. The design should consider the system reversibility of how the structure returns to its memorized form as soon as the stimulus has gone below the activation temperature to ensure the balance of the system. It can affect the form by using curved folding, the passive material selection by using elastic materials, and the type of actuator by using two-way actuators or using counter-weight elements.

This section has attempted to provide a brief overview of the different experimental approaches to the design of responsive solar shading systems. The next section will go on to illustrate the specific internal relationships between the four aspects, as shown in the main design framework in Figure 7-4.

#### *7.3.1. Form and materiality*

The form and materiality of responsive structures need to be studied inseparably. They together specify the system deployability. The form of kinetic structures depends on the geometry of the components, how they move and how various materials connect.

- Connector 1 - (Form to materiality) - Single units can rotate or slide to create a simple kinetic pattern; however, the selection of internal crease pattern, straight or curved lines, enables the unit to perform the more complex folding motion. The selection of materials, passive and active, facilitates the animation of the designed forms. Moreover, Bio-inspiration as form generator, not only inspires selections of geometrical forms, but also extends to inform the flexibility of the materials used, the way the structures can be actuated, the type and location of actuators needed to move, roll and fold the deployable structure. The resemblance of the motion triggers in some plants can inspire the allocation of actuators within the passive material to fold or change the surface curvature upon expansion.

- Connector 2 (Materiality to form)- The exploration within passive soft materials presents a wider range of hinge-less soft deformation and encourage curved folding forms. By supporting the concepts of materiality and materiability, the material abilities can guide and drive the form. The selected materials need to be strong but can be either flexible or rigid, passive and/or active and how these various materials can be fixed together to generate a dynamic form.

- Passive materials

Flexible and rigid materials can achieve deployability with different means. Rigid materials can be precisely shaped into deployable foldable units that can be easily reconfigured by linear actuation. Rigid thin materials; can be connected with flexible joints or hinges to be able to fold. At the same time, the flexibility and deformation properties of elastic materials such as polymers and textiles can present a new generation of soft robotics. The stretching, bending, twisting and rolling movements of soft materials open up more design options. It offers a high range of transformation similar to folding movements which can achieve high openness percentage.

- Active materials

The selection of the smart materials' type, their direction and range of motion highly affect the overall solar-shading component deployability. The designer can select from the wide palette of smart materials and whether to work as standalone active material or as an actuator attached with a passive material. In the case of actuators, the type of fixation impacts how powerful the actuator can animate a structure to achieve a high range of transformation. The designer can begin with investigations about fixation patterns, hinged or bilayered, to generate interesting forms. The selection from the different types of actuators is based on their ability to amplify the motion and achieve a high range of motion, thus an aperture size.

### *7.3.2. Materiality and actuation*

The linkage between materiality and actuation lies in the process of animation of the structure or the activation of the material to achieve forward and backward motion.

-Connector 3 (Materiality to actuation) - Different types of actuators and their way of fixation allow them to different degrees of exposure and freedom of motion that relate to the direction of stimulus it needs to respond to. The selection of materials' locations should be based on actuation direction and activation temperatures.



-Connector 4 (Actuation to materiality)- The system reversibility informs both the selection of material, active or passive, as well as the location of actuators or counterweight elements that brings the structure back to its memorized form as soon as the stimulus has gone below the activation temperature. The experimentation feedback, in this case, is technical to insure the workability and balance of the system. The system reversibility affects the choice of passive and smart materials. Passive elastic materials can be used as an efficient return mechanism. Some plastics; such as polypropylene, are considered materials with high elasticity and could help in returning the unit to its initial form. The *type of actuator* is also informed by the system reversibility. Two-way SMMs can be used. They remember the two different shapes; one at low temperatures, and one at the high-temperature. They have a standalone reversible action which are able to bring the structure back to its memorized position upon cooling.

#### 7.3.3. *Actuation and panelization*

Connector 5 - (Actuation to panelization) - The actuators can be grouped and located where maximum sun exposure is present. The direction of the triggering stimulus can inform the way the units can be clustered to reach maximum exposure without preventing each other from reaching their required activation temperature.

#### 7.3.4. *Panelization and form*

- Connector 6- (Form to panelization) Grouping and panelization of simple cell movements by any of the three key manipulations: translation, reflection, and rotation would change the created patterns and accordingly the form of the envelope as a whole. The elegance of the structure can be perceived in the way it moves, slides, bends or folds. It is also perceived in the way the units are grouped together to create sublime patterns that resonate over time and the way the motions propagate over the facade. It can also be seen in the individuality and slight variation in the movement of each solar-shading component that gives the structure a natural sense.

- Connector 7 - (Panelization to form) Panelization can lead the form-generation allowing the designer to think about the movement and actuation directly to the geometrically tessellated surface.

### *7.3.5. Materiality and panelization*

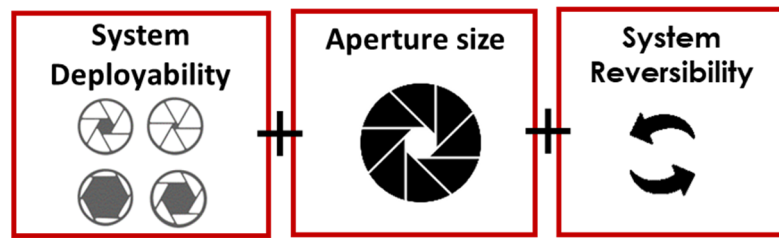
- Connector 8 - (Materiality to panelization) One of the actuation strategies deals with the solar shading system as a whole depending on the in-between connections. This is similar to the connectivity principle in pliable systems, where the deformation behaviour of the individual elements is constrained by their neighbouring elements. The linking of these elements allows the transmission of forces and torque (Schleicher et al., 2011). Thus the deformation of one element will result in the deformation of the adjacent element. This relationship can be used to build up a cascading deformation movement. Connectors or actuators can be located in-between the components. Intermediate actuators can be located to move more than one component. Similarly, counterweight elements which are responsible for the reverse mechanism can be connected to in-between units. This method requires a sensitive design of coupled members of equal forces to guarantee a reversible motion.

### *7.3.6. Form and actuation*

Connector 9 - (Actuation to form) - The principles of curved-line folding can be used to create bending-active kinetic systems. They have inherited return mechanism characteristics that help shape memory performance. When the curved folding is applied over an elastic material they work together to help the return mechanism. Curved-line folding alters 3D interesting double-curved forms that might be complex, aesthetically pleasing but simple in fabrication and deployed by simple actuation means.

### *7.3.7. Key factors of experimental performance*

On the whole, from the hands-on experimental investigation, it was found that the system deployability and system reversibility are the key factors for the workability of responsive solar shading structures. In order to effectively maximize the deployability of a structure, specific relative selections to its form, its motion, its material settings and grouping strategies have to be made which directly affect the resulting aperture size. The aperture size is the main parameter that affects environmental performance. The thesis recommends designers to take these three key concepts as criteria for evaluation.



*Figure 7-5: System deployability, system reversibility and aperture size are the key factors for the workability and operability of responsive solar shading systems*

This section has attempted to provide a brief summary of the internal experimental relationships. It is now necessary to explain the external relationships between the context of operation and the experimental aspects.

#### **7.4. Environmental Feedback**

The findings of thermal and airflow environmental analysis in Chapter Six can inform the design of the responsive solar shading with recommended forms, materiality and aperture sizes, while the analysis of solar-shading surface temperature informs positioning of the solar-shading location and the actuators' location and activation ranges. The context of operation not only leads design decisions on where and how the screen should be positioned to appropriately function but also when they open and close, the dense of grouping and the aperture sizes to control thermal gain and daylighting. Rather than finding a form that is deployable and reversible with minimal energy use, the form can be alternatively approached by looking at the broader surrounding context of the responsive system to find which design decisions of form, morphology and aperture size can optimize the inner solar gain and airflow in the cavity. Designers can find the component form and grouping strategies that exactly achieve the required aperture size variation all the year-round to optimize both thermal and daylighting performance. They can allocate actuators in a way that maximize their solar exposure.

This section focuses on how the obtained environmental data can inform design decisions of responsive solar shading system. The environmental feedback provides informative data that guide the design decisions, customize the motion and tailor the smart material properties. This study provides an opportunity to understand the link between the different parameters of responsive solar shading in relation to the conditions of the context of operation.

#### *7.4.1. Airflow analysis and form*

Connector 10- Airflow analysis would define how the 3D form and depth of the shading unit affects the air movement in the channel since the solar-shading devices with large depth result in higher airflow in the cavity and act as better shades.

#### *7.4.2. Airflow analysis and panelization*

Connector 11- Airflow analysis would define how the position of the shading unit affects the air movement in the channel.

#### *7.4.3. The internal thermal solar gains and materiality*

Connector 12- The solar gain analysis affects the actuation by the decided aperture size and hence the range of motion for the actuator. Moreover, environmental feedback informs the colour and reflectivity of the solar-shading material, which affects the internal solar gain and may contribute to cooling load reduction. The coefficient of solar absorptance and reflectivity defines the colour characteristics of solar shading units. The material emissivity control heat flux transmitted into the interior environment.

#### *7.4.4. The internal thermal solar gains and form*

Connector 13- The internal thermal solar gains can guide decisions related to the form generation (form and depth) of the shading, and the aperture size. These environmental analyses inform how the form can trap the heat in the frontal zone of the cavity. Designers can select from 3D forms resulting from fold, swivel or swing motion. The three-dimensional forms of shading systems provide physical depth to the configuration and provide self-shading, which can contribute to further energy reductions.

#### *7.4.5. The internal thermal solar gains and panelization*

Connector 14- The solar gain analysis informs the required aperture sizes at different hours and seasons. The aperture size is a result of the range of motion of the components in a specific position and their grouping strategy. It is produced as a result of grouping multiple deployable components. Thus, the change in the tilting behaviour, positioning of units, and overlapping would affect the aperture size. Moreover, the internal heat gain informs the relative positioning of the solar shading to eliminate the effect of heat exchange between the solar shading system and the inner glazing.

#### *7.4.6. Solar shading temperature analysis and panelization*

Connector 15- The solar-shading temperature analysis informs the relative positioning of solar shading to maximize the exposure of actuators to the stimulus and the direct solar radiation.

#### *7.4.7. Solar-shading thermal analysis and actuation*

Connector 16- The synchronization between the activation temperatures of the smart material actuators, the surface temperature of the solar shading materials and thermal conditions of the context is crucial for optimizing the operation of the responsive solar-shading system passively. Since the thermally responsive actuators are responding to solar radiation and changes in ambient temperature, the direction and value of the free directional source of solar energy need to be sufficient to activate the material. Therefore, the thermal analysis at the solar shading surface informs not only the location and exposure of the smart material but also the activation temperatures required.

#### *7.4.8. Solar-shading thermal analysis and materiality*

Connector 17- The solar-shading thermal analysis impacts the location of actuators and their activation ranges rather than the actuator type. The environmental performance doesn't have direct recommendation of the actuator type but rather recommends the location of most sun exposure or highest temperature on the surface of the solar shading. On the other hand, the actuator type should be decided according to the success of reaching the full capacity of transformation or the environmentally recommended aperture size. So, the selected type of actuator should ensure the most efficiency and workability of the system in the temperature ranges advised by environmental feedback. The *location of the actuator* is meant to be in maximum exposure to the direct solar radiation and in a strategic location to efficiently move the shading unit. Some techniques and locations are preferable in terms of material consumption, acquisition of maximum motion and sun exposure.

### **7.5. Conclusion**

Experimental and environmental feedback can inform the design of the responsive solar-shading system. Weaving these two approaches of exploration to test the functionality of responsive solar-shading systems, highlighted the relationships between parameters that shape the system. Integrating all these aspects of responsive solar-shadings for decision making is a complicated problem that needs to be studied collectively in one domain. Putting together all these aspects could be the key to a real successful application of responsive systems.

The framework presented in this chapter discussed the relation between these aspects which was found to be working in one-way or two-ways and can be approached from any of these aspects as a starting point as long as all aspects are taken in consideration. Some parameters need to balance between more than one decision due to receiving feedback from different aspects. These are where some design loops are found.

From the experimental investigation, it was found that the deployability and system reversibility are the key factors for the workability of responsive solar shadings structure. The aperture size is the main parameter that affects environmental performance. Designers using experimentation or new software design tools need to take these three key concepts as criteria for evaluation. Materiality was found to be a promising approach and a start point for the design process as it is related to almost all other aspects and can be the main driving force of design using material-based actuation.

From the environmental investigation, it was found that thermal and airflow analysis can inform the design of the responsive solar shading with recommended forms, aperture sizes, solar- shading positioning while the analysis of solar-shading surface temperature informs actuators location and activation ranges.

Overall, the experimental investigations recommend solutions that allow a high range of deployability and reversibility. The environmental analysis, determine the value the optimum aperture size at specific times to optimize internal heat gain and recommend the form that optimizes airflow and heat gain.

## Chapter 8 : CONCLUSIONS AND FUTURE OUTLOOK

### 8.1. Introduction

This research, through its different parts, has illustrated the potential of applying smart materials in responsive solar shading systems. The interdisciplinary mixed approach of hands-on exploration and CFD simulations provided an understanding of the behaviour and performance of responsive solar shading systems experimentally and environmentally and identified the correlations between design, materiality, and environmental performance which was discussed in Chapter Seven.

This chapter represents the thesis conclusions in terms of a summary, limitations and proposed future work in the field. Thus, it is divided into three main sections. The first section focuses on the summary of this research which tackles six main points each is mapped to an objective:

- Material-based design approach for responsive solar shading systems (*objective 1*),
- The mixed interdisciplinary methodology (*objective 2*),
- Hands-on exploration for Responsive Solar-shading Components' Design(*objective 3*),
- CFD as a Tool for Assessing Integrated DSF(*objective 4*),
- Simulation of DSF integrated with Solar-shading System(*objective 5*),
- Developed framework (*objective 6*).

The second section discusses the limitations of the work. The third section focuses on the recommendations for future work in the field, which focuses on an overview of potential applications and new software tool.

### 8.2. Summary

This section presents a summary and a conclusion of the main five chapters of the thesis where every chapter builds on one another.

#### 8.2.1. *Material-based design approach for responsive solar shading systems (objective 1)*

Overall, this study strengthens the idea that smart materials can present a possible alternative for conventional building solar-shading systems and envisions the concept of a futuristic, soft, and flexible architecture. This is due to their distributed deformation with a relatively large number of degrees of freedom which can be achieved through controllable



variance in material properties. Origami and bio-inspired principles presented a rich source of inspiration for the understanding of folding mechanisms that can guide the design of responsive modular systems which respond to environmental stimuli. As the aim of chapter two was to triangulate the intersection between bio-inspiration, folding principles, and material science development (smart materials), and study the underlying mechanisms and generative techniques of responsive reversible motion (Objective 1). Some mechanisms for deployable and responsive structure are revealed.

Biology, especially plants, is a rich source of inspiration for hinge-less responsive solar-shadings on macro and micro scales. Plant flexibility is achieved through the adaptive behaviour that changes its morphological features by acting as living hinges and allowing for elastic deformations. The most inspiring concept is how they perform mobility with minimal energy by making use of geometrical forms, complex embedded actuation system, folding techniques and system reversibility. General concepts which are common in some plant species such as bi-layering, bi-stability and pliability can drive plenty of ideas. It was found that biomimicry can be inspiring at any of the four discussed aspects. On the geometrical form level, straight folding were found in the hornbeam leaves by applying Miura-ori folded pattern to achieve significant contraction while curved folding can create bending-active kinetic systems. On the material selection level, the strong but flexible, pliable and elastic properties of plant leaves lead to specific material selections. On the actuation level, the way the plants are actuated guides the type and location of actuators needed to move, roll and fold the deployable structure. Also, the hygroscopic shrinking or swelling mechanism proposes bilayering as an actuation mean. On the grouping level, the concept of pliability can have a major benefit for deployable systems based on elastic deformation.

Origami-inspired structures have great potential for reconfigurable structures, especially self-folding robots, due to their predictability, controllability, and scalability. Origami has the advantages of reduced material consumption, creation of structures with improved strength-to-weight ratios, reduction in manufacturing complexity in addition to methods of production. Folded geometrical forms vary according to the type of crease lines; whether 'straight' or 'curved'. The type and pattern of crease lines and their relationship are the main factors that define the behaviour of the folded surface. It was found that most of the self-folding examples coupled simple straight crease folding with material actuation. Straight folding can achieve a high range of deployability and aperture sizes. However, folded

geometries using curved folds inherit a structural strength and show better performance compared to straight folded geometries. The principles of curved-line folding can be used to create bending-active kinetic systems despite being relatively underexplored. Studying Origami and bio-inspired principles together led to an understanding of folding mechanisms.

Materials with embedded responsiveness can be used to mimic reversible plant motions. SMA wires and springs can be embedded within lightweight materials using hinged or bilayer fixation types to activate the solar-shading systems. Chapter two identified the potential of using SMMs in conjunction with light-weight structures using folding mechanisms to develop responsive solar shading system applications.

### *8.2.2. The mixed interdisciplinary methodology (objective 2)*

The mixed interdisciplinary methodology and integrated methods drove the design parameters formulating the framework by the end of the thesis. It shows how they are affected by each other when studied collectively. It opens the discussion of the importance of examining all these aspects relative to each other and looking for tools to achieve this goal for more sustainable futures. The Interdisciplinary Research Methodology was built on a process approach where the research aim about testing the performance of responsive solar-shadings is leading for decisions in the various stages of the research. It puts the common goal of developing kinetic responsive systems at the centre of the research. The design framework described how the input from the different methods are synthesized to achieve the overall research aim bringing the experimental and environmental feedback together in the integration stage which benefited from the research being interdisciplinary. In the experimental study, different parts of the research were distinguished to stimulate the researcher to consider the case study design based on quantitative information such as the aperture size. While different components of the environmental design were distinguished to consider the experimental design with qualitative data such as the form and the actuator location.

The experimental and environmental investigations depend on one another for data collection and analysis, and synthesis was planned after the completion of the investigations.

### *8.2.3. Hands-on exploration for responsive solar shading components (objective 3)*

As the aim of chapter four was to explore the potential of SMMs, in order to understand their immanent dynamic activity, and use bio-inspiration and folding principles to alter complex deployable forms using simple actuation strategies (Objective 3), the creative design processes, which were carried by the researcher or the students, led to a deeper understanding of responsive system potentials and parameters. The creative practice recommended specific techniques, design process and set of design parameters of responsive solar shadings that can generate a range of design options. The researcher's actions and decisions through the open exploration generated a design process that can be further applied in similar educational courses and workshops. The study unfolded layered investigation of façade kinetics based on form generation, materiality, actuation and panelization.

#### **- FORMS:**

By testing various deployable forms, origami-inspired structures showed a great potential for reconfigurable structures, especially self-folding structures. The straight crease folding proved to achieve better contractions and higher ranges of motion. Adding extra folds helps the module to achieve more contractions and improve rigidity. Great potential lies in curved-line folding which can be used to create bending-active kinetic systems. They have significant potential as kinetic applications for their simplicity and inherited return mechanism characteristics when the curved folding is applied over an elastic material they work together to help the return mechanism.

#### **- MATERIALITY:**

Through the material tinkering process with lightweight passive materials, two materials showed high potential for their performance, polypropylene and felt. Polypropylene is a lightweight, flexible material with good resistance to fatigue. It has the advantage of being moisture-resistant and can be safely laser-cut, marked, engraved and creased using a cold or hot creasing technique. The resulting 'hinges' can be folded many times without the material breaking, which makes it possible to create living hinges. It has high elasticity which allows it to work as a return mechanism. On the other hand, the flexibility and deformation properties of textiles present a new generation of soft robotics. Felt proved to have a great potential to be used for bending and soft deformation. It has good potential for responsive solar-shading systems due to its durability and resistance to wear and tear. It is an excellent insulator for

both temperature and sound. As a non-woven fabric, it holds its edges and does not unravel when laser-cut. Felt proved to act efficiently in bending and soft deformation. These advantages make polypropylene and felt promising materials for dynamic solar-shading systems.

The hands-on experimentation which was conducted to explore the potential of shape memory materials SMMs and predict their immanent dynamic activity highlighted their ability to morph complex self-deployable structures using simple actuation strategies repetitively and continuously. SMMs; specifically SMAs (NiTi-based alloys) and SMPs, can be used to mimic reversible plant motions. NiTi-based SMAs are more reliable and have unique thermomechanical characteristics, good output/weight ratio, sensing and actuating capability and reasonable damping properties. They are typically energy-dense, geometrically simple and silent. They can be clamped at one or both ends, installed as endless, and weaved manually or mechanically. They are simple to attach and easy to create in quantities of tens or hundreds. Thus, they have great potential to act as servo-actuators. Also, SMP can be considered taking into consideration their low density and limited SME, which means they are only capable of a certain level of shape recovery. Both SMAs and SMPs can be used in conjunction with light-weight structures and tensile skins. SMA spring actuator with variable length has a great potential to work as living hinges. The freedom of the hinged or suspended actuators can better sense environmental conditions and trigger motion. Springs proved to achieve the best travel distance. The fully exposed SMA springs are found to be the simplest and most successful technique. Zigzag trained wires or flat springs achieved a linear contraction from 15 cm to 5 cm. Similarly, the trained helical springs achieved a contraction third their original length from 15 cm to 5 cm. The longest travel distance was achieved by the manufactured helical springs from 15 cm to 2 cm at activation temperature (original length). The linear shrinkage of the SMA spring can result in the rotation of horizontal surfaces to a deformed double curved surface upon the existence of a curved-line fold.

- **ACTUATION:**

Due to practical constraints, the models were activated using electric current and heat gun. Future work can investigate their performance in a real context of direct sun exposure. By studying the fixation methods, the weaving technique failed to achieve major motion changes as the wire is slightly fixed to the unit material and the pre-trained motion of the wire is not transferred to the material. The Knitting technique added a degree of insulation and

relatively restricted the movement of the wire. On the other hand, a fully suspended SMA spring actuator that has variable length has a great potential to work as living hinges. The freedom of the hinged or suspended actuators can better sense environmental conditions and trigger motion. Springs proved to achieve the best travel distance. Zigzag trained wires or springs work better in this case with maximum deformation or contraction. Regarding the system reversibility, four return mechanisms were proposed and tested. These mechanisms are (a) the gravity, (b) coupling passive and active elements, (c) the passive elastic material, and (d) the two-way training for SMM. The gravity and material as return mechanisms are simple and promising. Gravity can be only considered in the horizontal position of the deployable structures. Two-way springs were able to extend from their original length of 1.5 cm (at room temperature) to 4.5 cm (at austenite temperature) in less than 4 sec and reversed back in 70 sec upon cooling. The use of polypropylene material with high elasticity is found to be slower but efficient. The SMA spring contracts from 10cm to 3cm in 14sec and the polypropylene material stretched the spring back from 3cm to 8cm in 360 sec upon cooling. The thesis argues that the most successful return mechanism is the one that serves a standalone reversible action. The material as a return mechanism proved to be the most efficient either by using two-way actuators or passive elastic materials, such as polypropylene or silicone.

- **PANELIZATION:**

The arrangement of the responsive units has a huge impact on their functionality and efficiency. Changing the references allows for three key manipulations: translation, reflection, and rotation to create patterns. The method of actuation and location of actuators highly affect the resulting pattern, its aesthetical qualities and workability. In case of using gravity, elastic material or two-way SMM as a return mechanism, each unit can move independently from any neighbour unit. On the other hand, connecting smaller components enables the system to work collectively. This takes place by allocating actuators or counter elements in-between the components or joining them with solid connectors. Panelization has a major role in defining the aperture size of the system, along with the component's form. Aperture size can be customized by controlling some factors; such as layering of units in both directions, using straight or staggered pattern and using in-between solid or void connections.

Experimentally, systems that allow high deployability and reversibility are recommended. Recommendations from Experimental Feedback are as follows:

- Bending-active structures are structural forms that can facilitate the motion and the reversibility of the motion as found in section 4.8.2 and 4.8.3.
- The straight crease folding proved to achieve better contractions and higher ranges of motion as found in section 4.11
- Curved-line folding has inherited return mechanism characteristics which enhances the shape memory performance. It can be coupled with the passive elastic material to help the return mechanism as found in section 4.8.2 and 4.8.3.
- Linear actuators, especially springs, proved to achieve the best travel distance. The fully exposed hinged SMA springs are found to be the simplest and most successful technique as found in section 4.5.
- The material as a return mechanism proved to be the most efficient either by using a two-way actuator or a passive elastic material, such as polypropylene or silicone as found in section 4.6.
- Fabrics especially felt have the potentials of soft deformation movements using fabrics. Felt is an excellent insulator for both temperature and sound. It is durable and resistant to wear and tear as found in section 4.8.4.

Smart materials and bio-inspired are capable of replacing the complex mechanical systems principles through the previously discussed mechanisms. Soft structures using smart materials can alter their shape under thermal stimulus giving large range of deformation and aperture size as demonstrated in sections 4.8.3 and 4.8.4. The soft deployable structures are very simple yet aesthetically pleasing. It can alter complex deployable forms using linear actuators. The flexibility of soft materials enable them to produce soft deformation movements like bending, swelling and curling motion which are not possible with rigid materials. Soft structures realized with smart materials can work autonomously in respond to thermal stimulus and represent a passive system or can be controlled, computerized, and connected to intelligent network of electronic devices to work as a soft robot representing an active system.

Based on the hands-on explorations and the six-week course, an actual actuated prototype was selected to bring experimental and environmental together through the integration of material thinking and simulation of real environment performance. Folded origami unit is investigated in this research as they have a high potential as deployable structures similar to

the '*folded flowers*' in section 4.10.2 and '*Umbrella units*' in section 4.8.1. It has the ability to be actuated individually or work in clusters. It can achieve high ranges of aperture size between fully closed to 91% opening.

The proposed integrated DSF system with responsive shading protects this soft notion of solar shadings from weather and air pollution. The cavity-integrated responsive solar-shadings present an eco-friendly low-tech alternative to conventional or mechanized solutions. Cavity-Integrated responsive shading devices, is a sustainable solution, with the double benefits of a responsive façade under a controlled environment. DSF can help in achieving the activation temperatures needed to activate the SMMs, decreasing the cooling loads by lowering the temperature via ventilation and acting as an acoustic barrier. Despite all the previously stated benefits of the integrated system, the responsive solar shadings might be applied externally to achieve more aesthetical appearance and freedom of form. The NiTi-based SMA's reliability, high corrosion resistance and reasonable damping properties allow them to be applied externally. But, the selection of the external passive material will be of great importance as well as the structural and wind load considerations.

#### *8.2.4. CFD as a tool for assessing integrated DSF (objective 4)*

The proposed responsive solar-shading system is integrated within a DSF to protect the fragile mechanics from harsh weather conditions. The behaviour of DSF is complex due to the multiple coupled physical phenomena that take place inside the cavity. CFD analysis is one of the most significant tools to predict DSF behaviour. In DSFs with differentially heated walls, the turbulence modelling should be coupled with radiation modelling as the radiation is considered the main contributor to the heat transfer problem because of the large exposed glass areas. As the aim of chapter 5 was to set guidelines for the Computational fluid dynamics (CFD) numerical modelling setup of a DSF integrated with solar-shading system and validate this CFD modelling setup against an experimental case (Objective 4), the CFD modelling work was validated using real physical experimental results from Mei et al. (2007).

Through the validation of CFD modelling using experimental results of Mei et al. (2007), guidelines for the CFD simulation setup are set to reach results with high accuracy, which are:

- RNG k- $\epsilon$  turbulence model with full buoyancy effect resulted in the best agreement for the simulations. The Enhanced Wall Treatment should be adopted



for the RNG k- $\epsilon$  model. It proved to have better simulation stability and achieve convergence faster than SST k- $\omega$  turbulence model.

- The DO radiation model is more accurate than P1 radiation but requires high computational facilities. P-1 radiation models resulted in around 11% error on external and internal surface temperatures. P-1 radiation underestimates the air temperature in the cavity by 3°C compared to DO model. Discrete Ordinates radiation model should be implemented in conjunction with the Solar Ray-tracing options of the solar load model.
- Two bands 'Solar' and 'Thermal' should be set for the Non-Gray Discrete Ordinates (DO) model. The solar band corresponds to wavelengths smaller than 2.7  $\mu\text{m}$ , and the thermal band to wavelength larger than 2.7  $\mu\text{m}$ . A fine angular discretization of 6x6 and a pixilation of 3x3 are recommended.
- The extension of the computational domain to include part of the external environment allows proper modelling of the ambient environment. A slightly higher cavity temperature was recorded but almost the same surface temperatures for the solid surfaces. However, the difference is small and can be negligible.
- Level of complexity of the model directly affects the computational timing and the problem resolved. The full detailed model resulted in a more accurate airflow analysis, while the abstracted model predicted the exact same external and internal glazing surface temperatures. Adding the grills details does not show an appreciable difference in the results. It means that it is not worthy of making a full detailed model.

The CFD coupled thermo-fluid-dynamics models are able to predict airflow, heat flux, air and surface temperatures close to the experimental data. CFD proves to be a useful tool when modelling conductive/ convective/ radiative heat transfer in integrated DSF.

#### *8.2.5. Simulation of DSF integrated with responsive solar shading system (objective 5)*

As the aim of chapter 6 was to environmentally asses the responsive solar shading system performance within their potential context of operation and use environmental feedback as a guidance to customize the material and design of the responsive system; form and aperture size (Objective 5), the above mentioned CFD setup guidelines was applied. This study provided an important opportunity to understand the link between the form selection

and aperture size along with the thermal conditions of the cavity. The synchronization between the activation temperatures of the smart materials actuators and the thermal conditions of the cavity is crucial for the proper operation of the system. The findings of the non-shaded and shaded DSF cavities will be discussed below

- **The non-shaded cavities**

Parameters of non-shaded DSF cavities were studied for two reasons. The first is to select the optimized cavity to be integrated with the responsive solar shading, and the second is to be used as a base case for comparative studies with shaded cavities. The parameters are the cavity's width, façade layering, and domain size. Increasing the cavity width can improve the thermal performance of the DSF. The 1m wide cavity reduces the heat gain by 15% compared to the 0.4m wide cavity. The internal double glazing lowered the internal surface temperature by 24% compared to single glazing when studied at 12:00 pm 15th of July. The 3D vertical segment method with side symmetry boundary conditions successfully assessed the DSF structure behaviour on July midday with less than 5% variation compared to the full cavity modelling. It has the advantages of using the solar load model, which is only available in ANSYS Fluent 3D solver. The 0.4m vertical section model allows for complex form assessment with reduced computational cost compared to the full model method. However, the most important limitation lies in the fact that the source of solar radiation should be directed towards the external glazing without side vector components that may affect the symmetry surfaces.

- **The shaded cavities**

- *Flat and Folded solar-shading were studied* to evaluate the effects of different aperture sizes and forms of solar-shading system. The folded solar shading is the digital replication of the actual actuated prototype previously selected in the experimental work of Chapter Four. The temperature on the solar shading is recorded to customize the temperature needed by the smart material to be activated and perform responsively.

- **The aperture size**

A 30% aperture is highly recommended at peak summertime hours between 12:00h and 15:00h when the solar irradiance has maximum values of 1320 W/m<sup>2</sup> and at 12:00h of wintertime to protect the inner space from the glare effect. The 70% aperture should be maintained at all other low direct radiation values below 850 W/m<sup>2</sup>.

- **The Form**

The origami folded solar shading devices are more efficient by reducing the solar heat gain by 21.5% compared to the non-shaded cavity and 12% compared to the flat-shaded cavity in the peak summertime. This result may be explained by the fact that origami folded shading has more depth than the flat solar-shading, which contributes to further refractions of the direct solar radiation and a larger absorption surface for direct solar radiation. The method of simplification of complex solar-shading forms into a flat screen with the same aperture sizes provided us with the general system performance in peak summer and winter days with less computational power. Nevertheless, the detailed modelling of origami-shaded DSF showed more energy reductions.

- **Customize the smart material**

The responsive solar-shading system is recommended to be integrated close to the outer glazing, where the highest air cavity temperatures are expected. It is integrated in the range between 0.1 to 0.2m away from the outer glass in a 1m wide DSF cavity to activate the smart material. The positioning of the solar-shading screen close to the outer glazing results in increasing the exposure of smart material actuators (SMA) to direct solar radiations and conductive transfers from within the cavity which facilitates its activation. It is recommended to use SMAs with actuation temperature from 35-40°C. This range of temperature is achieved on the surface of the solar-shading and the surrounding zone. In order to ensure robust sun protection in the hot arid, climate of Cairo, the responsive shading system should be programmed to be in a closed state between 40-50°C which is the highest threshold to be expected throughout the entire year as shown in Appendix C (Liggett et al., 2016). The temperature of the solar-shading surface at the highest solar radiation represented at the peak summer day is the most important. A closed configuration represented by an aperture of 30% should occur above 39/40°C detected at the solar shading or at 37°C in case the actuators are located in between the units. An aperture of 50% would occur between 37°C and 39°C and an aperture 70% between 31°C and 36°C. The kinetic module should be fully opened below 30°C detected at the solar shading.

Environmentally, the value of optimum aperture size at specific times to reduce internal heat gain and the form that increases airflow and minimizes heat gain are the main parameters. Recommendations from Environmental Feedback are as follows:

- Three dimensional solar-shadings with larger depth result in higher airflow in the cavity and acts as better shading units that prevent direct solar radiation and glare.
- Concave forms tend to contain the heat inside it for better material activation.
- Concave forms raise the temperature in the frontal zone and lower the back zone temperature.
- The planar surface change has less protection for the internal glazing and result in less air movement in the cavity
- Positioning the solar-shading screen close to the outer glazing to activate the smart material

All the above tested parameters from the experimental and environmental domains through the actual actuated prototype are tied up in the framework moving from the specifics of the tested case to a more general perspective of the thermally responsive solar-shading systems.

#### 8.2.6. *The design framework (objective 6)*

As the aim of chapter 7 was to develop a framework for the design of responsive solar shading systems which can be used to generate open-ended design possibilities (Objective 6), reflections on the design experiments and the environmental data from CFD analysis were carried and integrated. Weaving these two approaches of exploration to test the functionality of responsive solar-shading systems, highlighted the relationships between parameters that shape the system. The design framework aims to open up possibilities by leaving spaces of freedom for designers to re-appropriate the design of the responsive system by changing their context of operation and design approach.

From the hands-on experimentation, the framework focused on the *system deployability* and *system reversibility* as the key factors for the workability of responsive solar shading structures. The *system reversibility* informs both the selection of material; active or passive as well as the location of actuators or counterweight elements that brings the structure back to its original form. The *system deployability* depends on the geometry of the surface, its material and actuation in a specific position. In order to effectively maximize the *system deployability*, changes to its form, its motion or its material settings have to be made. By changing these parameters, an appropriate system can be selected to match the environmentally required aperture size that reduces the internal solar gain. The resulting changeable patterns of openings generate the core performance and aesthetics of kinetic

systems. The study claims that the most environmentally significant parameter is the aperture size.

Environmental feedback leads design decisions mainly on the aperture size that is required on a different daily and seasonal conditions.

- The *Internal heat gains analysis* can inform the design of the responsive solar shading with recommended forms, depths and aperture size, as well as solar-shading position.
- The airflow analysis informs the components forms and position than enhances ventilation in the cavity.
- The analysis of solar-shading surface temperature informs actuators location, which should be at maximum sun exposure and detect the required activation temperature ranges.

Figure 8-1 elaborates in specific how external environmental factors impact the set of parameters of a responsive solar-shading system.

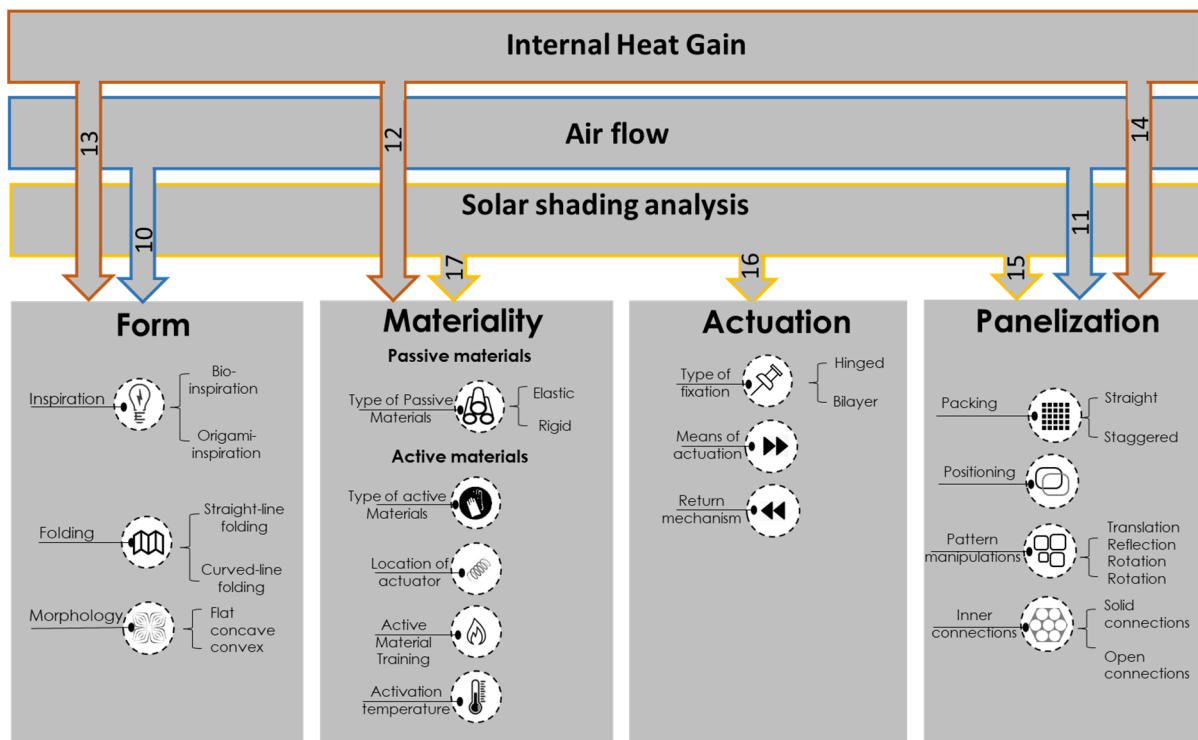


Figure 8-1: Impact of environmental aspects of the system parameters.

This study provided an important opportunity to understand the relationships between the system parameters within their context of operation and the thermal conditions of the cavity. The synchronization between the activation temperatures of the smart materials actuators and the thermal conditions of the cavity is crucial to the proper operation of the system. Integrating all these aspects of facades for decision making and assessing it with the

whole building performance is a complicated problem that needs to be studied collectively in one domain. Putting together all these aspects could be the key to a real successful application of responsive systems.

### **8.3. Limitations of the Study**

Despite these promising results of responsive solar-shadings, questions remain. Looking at the investigated parameters of responsive facades for the experimental and environmental performance, the scope of this study was limited to some parameters that can be widened and integrated. The experimental exploration in this study focused on shape memory alloys, other developed or under smart development materials can be tested to widen the implementation of the materiability approach in the architectural field. The scope of this study was limited to ventilated cavities and air-conditioned spaces. Future studies can extend to include ventilated spaces as some studies reported that it is preferable to open the windows in some seasons to introduce warmer air when they felt cold from the air conditioning system. In the research, all the solar-shading devices are positioned inside the cavity, however the external positioning of the solar shading is effective in hot countries and it would be helpful to compare the impact of changing the location of solar-shading devices. Staggering inlets and outlets may be further tested as reported by (Oesterle, 2001) to increase the vertical distance to the maximum and avoid vitiated air entering through the upper floor inlets. Moreover, different solar-shading materials can be simulated to test the effect of different material emissivity on heat transfer.

CFD is the tool used for integrated DSFs assessment in this research. The available computing power is one of the factors influencing the selection of the tested variables using the CFD technique. It should be noted that this study was limited by the available computational power. According to the available computational power, 0.4 vertical section was simulated instead of full models for origami-shaded and Point in time simulations which are limited to a peak summer and a peak winter day. The behaviour through the rest of the year needs to be tested. Moreover, the study of façade systems in attachment to the internal and external domains would help to ensure internal thermal comfort. Simulations of adaptive façade performance are still at an early stage of progress, with several more aspects are still needed to be explored.

The immediate response of the designed system in higher temperature ranges which is most likely with the global warming taking over needs to be tested. Although, the study was carried for hot arid climate, introducing different contexts can be investigated to test the framework and its applicability for different contexts.

The study was limited to analysing the coupled thermo-fluid-dynamics model. Daylighting performance needs to be further studied to optimize the aperture size. Daylighting studies can be coupled with thermal performance simulations to give an extra dimension to the façade performance.

In this study, three aperture sizes (30, 50 and 70 %) were modelled to represent the responsive solar-shadings' different states. Although the study used a minimum aperture size of 30% to allow minimum required daylighting for office spaces and to maintain an indoor and outdoor visual relationship, but the kinetic system can be tested further for smaller and larger apertures ranging from 0 to 100. Comparison of optimized fixed and kinetic solar-shading systems is recommended to give clear evaluation of the effect of responsive shading on the internal thermal comfort.

Moreover, the study was limited to analysing the performance of south-oriented facades but different orientations; like east and west can be further environmentally analysed. Applying responsive systems on the east and west façades in Cairo, Egypt would be even more interesting due to their exposure to solar energy at lower angles than the southern orientation.

The investigated DSF case study located in Cairo, Egypt was hypothetical. Building a real physical prototype might have many benefits. It would be a validation for both concepts and simulations results. The exact movement of solar-shading units can be tracked and recorded in response to daily and seasonal conditions. The durability and hysteresis of smart actuators would be tested. The collected experimental data and measurements can be compared with the data collected from CFD simulations.

The studied façade components developed a smart system that has an embedded responsive reaction on its own; in other words, an autonomous system which is not automated. Nevertheless, these actuators can be automated and controlled electronically through Arduino coding and central building management systems. This can be for reasons of

affording system and occupants overriding. Arduino coding may offer programmed more sophisticated movements and complex forms but with more complex and high-tech systems.

#### **8.4. Future Work**

This section discusses the recommendations for future work on responsive solar shading systems which focuses on possibilities for the design of responsive systems, an overview of potential applications and new software tool.

##### *8.4.1. Materiality and Prototyping*

Promising groups of materials and fabrication processes are already available in the market or are about to be in the near future. The group of plastics and polymers are well suited for elastic kinetic structures due to their high values in strength-to-modulus ratio. Plastics, like polypropylene, have relatively low Young's modulus which indicates that small external forces can cause large deflections. This is considered a disadvantage for large-scale architectural applications. Thermoplastics and fibre reinforced polymers could be more promising. Research on light metals, such as Graphene can be very promising for solar-shading application due to its strength, elasticity and lightness. The thesis encourages ongoing research on smart material composites and applications that can work on its own or as actuators, such as Thermobimetals (TB), Shape Memory Materials (SMM), and Electroactive Polymers (EAP) which have large active deformation potential. Future work can include investigations and improvements on the hysteresis of SMA and the Life Cycle behaviour of SMA actuators and the systems integrated with smart materials.

Future studies can cover production methods which fit large-scale architectural applications and overcome any issues of scalability. The study recommends wide range production of actuator sizes and powers to be available in the market. Different upscaling strategies should be tested, such as increasing the number of embedded or attached actuators which are needed to acquire the required motion and achieve the system balance at larger scale.

In case of the external positioning of solar-shadings, the system faces a serious combination of dead loads, live loads, and environmental loads, and therefore it is more reasonable to choose materials with a higher Young's modulus, as provided by some woods or fiber composites.

Digital fabrication and Rapid prototyping techniques would be a fruitful area for further work. It will allow for the development of different techniques. One technique could



be printing smart materials by three-axis CNC machine which transfers the patterns onto lightweight materials; like plastic, paper or fabric; either by layering or knitting. This technique can result in self-folding planar forms into three-dimensional forms. Another technique is the 4D printing for different elastomers and SMPs in addition to the moulding and casting processes of smart materials sheets.

Different design possibilities and scales can be further fabricated for system development. Considerably, more work will need to be done for upscaling techniques. Collaboration with manufacturers to investigate large-scale architectural applications of the technology can be carried. Issues of scalability might be preventing the application of smart materials on a large architectural scale.

#### *8.4.2. Overview of potential applications*

This part question whether the previously described responsive systems may actually have a practical use and can exhibit potential to new and enriching fields of applications. This research opens the research potential to far-ranging possibilities of responsive structures, particularly in the field of responsive architecture, responsive clothing and soft robotics. This concept can be applied to any responsive surfaces that need to be adaptable to different conditions.

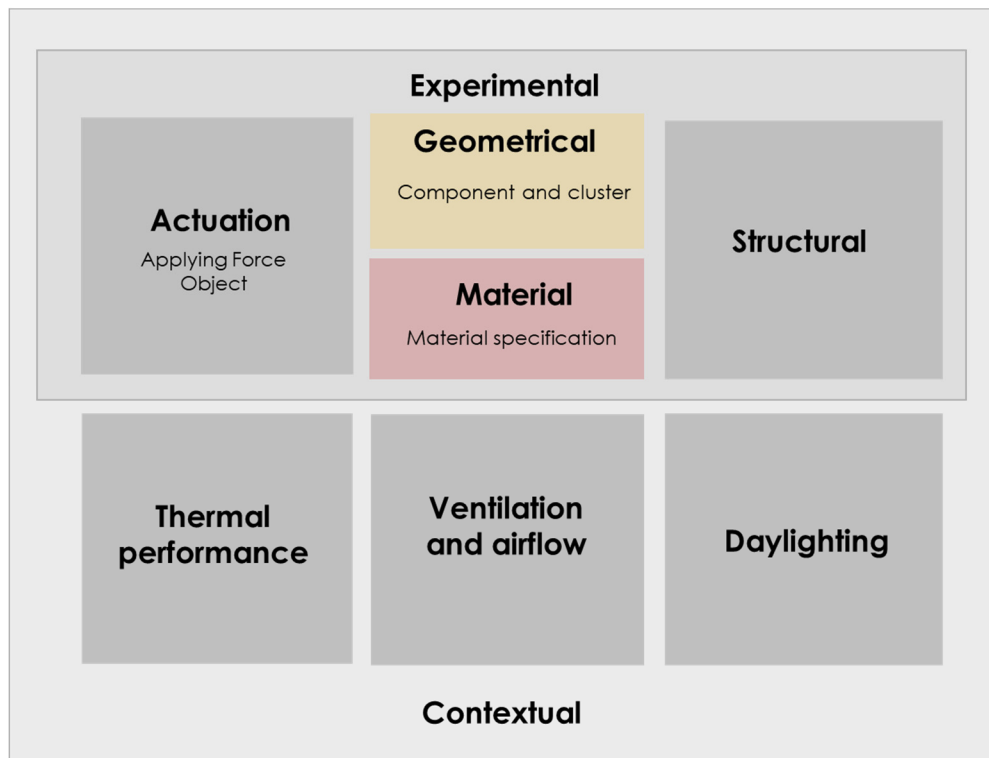
On the architectural level, the application of smart actuators is promising for convertible surfaces; building skins and roofs. It is not limited to shading functions. The skin could be programmed to open under high temperature to afford ventilation. In addition to roofs and facades applications, it can contribute to the development of interactive interiors, moving furniture, art installations, smart textiles, robotic toys and display ornaments.

Interior designs, can be responsive to inhabitants' proximity or temperature and reconfigure accordingly. The smart materials can be connected to any type of sensors to create an interactive structure. For example, a proximity sensor can be connected to the actuator to trigger the responsive action when visitors pass by. It can display different aperture sizes in response to people using the space, which changes over time or display a coloured imprint of visitors to invite them to interact. Furthermore, furniture can achieve changes in the interior space. Reconfigurable smart furniture can comprise sensing proximity or motion or respond to body temperatures. Furniture can change from a state to another, from compressed to full size.

#### 8.4.3. *New software tool*

Parametric and generative design tools, as well as computational optimization, have high potential to integrate different streams and receive feedback from multiple domains. Parametric tools using Dynamo/ Revit or Grasshopper/Rhino platforms as an open-source can be promising to customize a design tool for responsive solar-shading system design. This design tool should move towards a more collective approach which focuses on tying different forms, material diversities, actuation means and grouping strategies rather than a linear design process. It should be programmed to study how each change in one parameter would affect the other through defined geometrical, mathematical and physical relationships. The study of responsive systems within their context of operation not only affect their operability but more importantly define their environmental role. Integrating all these aspects of responsive solar-shadings for decision making is a complicated problem that needs to be studied collectively in one domain. Putting together all these aspects could be the key to a real successful application of responsive systems.

The design tool could be a new standalone software simply a new plugin or an algorithmic script within the current algorithmic tools. The algorithmic script can be constructed within the parametric platforms grouped in components and linked with common parameters or mathematical and physical relationships as shown in Figure 8-2. The algorithm script should be built on parametric geometrical modelling based either on components or tessellated surface. Similar to the discussion of the framework, the component can be designed first and then arrayed and clustered, or the script can start by tessellating the surface and work on a single cell which is replicated in this order. The geometrically constructed cell or group of cells are defined by a series of points and connected by curves or lines and may add creases using origami module. The geometry should be linked with materials that can be changed using a drop-down list or customized with material properties. The components' behaviour should be tested using Live physics upon actuation for motion and structural stability as well as their environmental performance.



*Figure 8-2: Several components to be integrated into a parametric platform*

Great potential in simulating kinetic responsive structures is through Kangaroo, which is a Live Physics engine for interactive simulation, form-finding, optimization and constraint solving. Not only kangaroo can be used to study the system structurally, but also it has some applications with folding origami. Moreover, kangaroo can be used to simulate the motion in response to heat sources and optimize the location of sensors/actuators to exactly achieve the required motion. The actuators can be defined digitally as “Force Object” using Kangaroo which can simulate actuators rods, springs and sheet materials. Kangaroo contains various ways of generating forces which affect the particles in the simulation. The parametric design can parametrize the form, the folding pattern, the size of the units and the aperture size. Moreover, many parameters related to materials and actuators can be tested and optimized; such as:

- The type of passive material
- The type of actuators
- The location of actuators
- The activation range of actuators
- The range of transformation of actuators

The components' and actuators' location in relation to gravity and heat source is highly important. The components' position should optimize solar gains while the location of the actuators needs to be optimized to reach activation temperature. In the same time, the location of the actuators should be tested for their workability with materials weight and size for their forward and backward motion. The system deployability, system reversibility and aperture size as key factors of the system workability can be quantified through components embedded in the script to assure some sort of functionality before moving to the contextual analysis. All these parameters are linked with their context of operation.

The environmental simulation of responsive solar shading systems can be integrated to improve the decision-making process using integrated *simulations of daylighting*, thermal performance and natural ventilation. Daylighting analysis can be run through Diva or honeybee and ladybug. Diva is an environmental analysis plugin which integrates daylighting analysis using radiance/DAYSIM with thermal simulations using EnergyPlus. Honeybee is capable of simulating thermal performance and energy consumption. The Butterfly is an add-on which allows users to work with OpenFoam and run CFD simulation, but it is under development. Although this might seem very promising, it is still under development and doesn't allow the simulation of complex geometries compared to ANSYS CFD capabilities. The main limitation with it so far is the limited ability to simulate complex forms and thin materials which require different models and thus lose the integrative potential of the model. Integrating all these aspects of facades for decision making and studying it within the whole building performance is a complicated problem that can be studied separately and then collectively in one domain. The early investigation of these systems has a great value rather than further retrofitting.

The integration of the responsive solar shading system in DSF may have many benefits as previously stated; however, the selection of DSF as part of the solution adds to the complexity of the simulation problem. The responsive solar shading systems might be applied externally to achieve more aesthetical appearance and freedom of form. In case of external application of the system, the analysis of the cavity's airflow that requires CFD or OpenFOAM would be replaced by simulations of external forces. In this case, a lot of material testing will be of great importance for the system's durability, maintenance and protection from malfunctions. Additionally, the structural and wind load considerations may need another set of simulation.

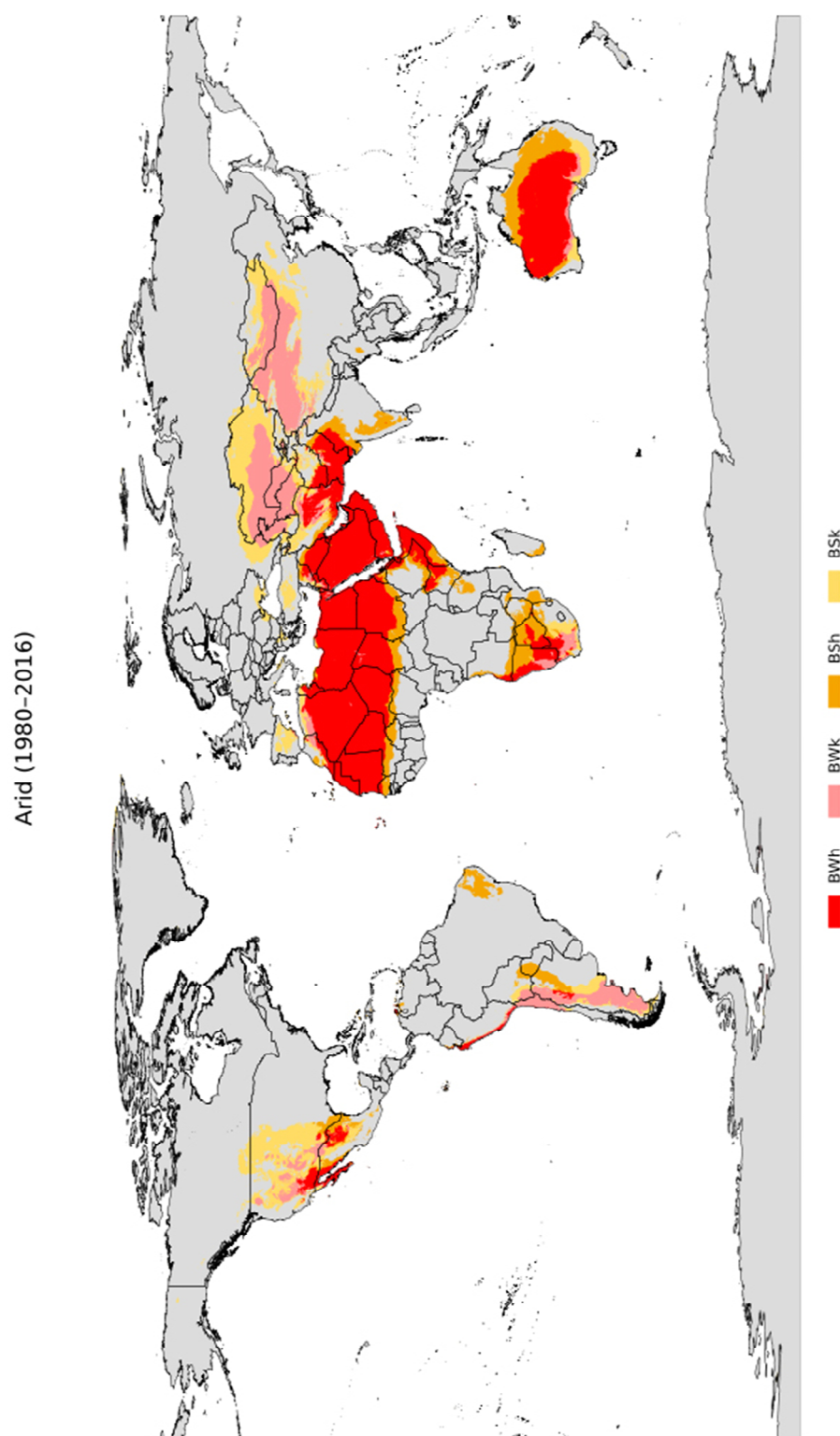
One of the main problems of simulations is the geometry simplification. It was hard to mesh double-curved surfaces using Ansys as it requires a large number of mesh cells, thus more computational time. This problem might be solved by designing software with embedded simplifications. Simplifications of curved geometries into fragments of flat surfaces and simplifying thicknesses of materials could be programmed in the tool. For specific simulations like thermal analysis, single-layered surfaces are required while double-layered surfaces are required for daylighting simulations which needs to model and run separate models. The software may do these simplifications automatically in association with some simulations by simplifying the surface details but keeping the general morphology and materials' properties. Simplification of aperture sizes can be processed for thermal and daylighting analysis when working on the large scale of the building.

Additionally, studies need to be carried on the scale of the whole building, not on a space-by-space basis as part of the holistic approach. The smooth integration between the solar-shading component, the solar shading system, the internal space and the building needs to be processed. All façade systems at different orientations should be linked to ensure the system smartness. The software needs to connect the material smartness, the component smartness and the whole building or system smartness.

This multifaceted design process could produce an entirely new category of responsive facade design outcomes. It blurs the lines between the physical, digital, and biological spheres. The continuity of research in the direction of novel approaches of soft robotics and smart materials, on the architectural scale, can reshape our contemporary sustainable architecture solutions and opens the research potential to far-ranging possibilities. It is a step towards the Fourth Industrial Revolution, which can reshape our future with the advances in artificial intelligence (AI), robotics, 3D printing, genetic engineering, and other technologies.

## APPENDICES

APPENDIX A: *Koppen Climate Classification Map World (Beck et al., 2018)*



*APPENDIX B: MArch Vertical Technology Studios 2018-19*

Homeostasis (12 students)



## Stage 5: Experimentation Studio: **Homeostasis**

Teaching team: **Neveen Hamza and Yomna Elghazi**

The definition of **homeostasis** is the ability or tendency to maintain internal stability in an organism to compensate for external environmental changes. Both buildings and natural systems are exposed to changing environmental conditions, which often require management of heat, air, water, and light. *We would like the intelligent building of a future generation to open its windows like eyelids to the dawn, to sense the heat of the rising sun or respond to the chill of a breeze by raising the hairs on its back for insulation.* Aldersey-Williams(2003)

In some organisms, adaptation to provide a stable body function is accomplished through their skin functioning as an environmental filter, whereas in others, it is achieved through their built structures (i.e. penguins changing their body fat depending on the weather). Considering the building envelope as a medium, rather than a barrier, opens new avenues in design, where functional attributes can be designed to provide indoor comfortable thermal and visual conditions with less impact on energy demand.

**Homeostasis** of the external skin is built on principles of combining lessons from nature into material science, electronics and soft mechanics. This led to a number of architectural configurations termed 'Kinetic facades, biomimetics and deployable architecture'. A combination of understanding how nature responds intelligently to its environment (Figure 1).

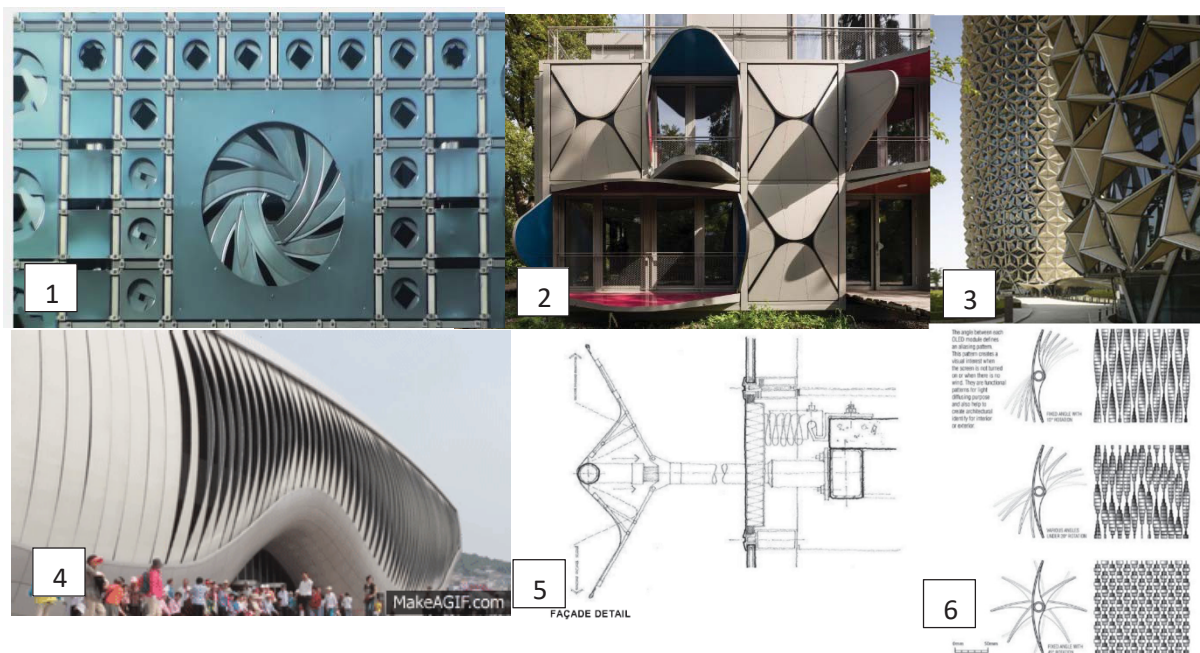


Figure 1:

1- *Instutite du Monde Arabe Jean Nouvel*

2- *Ballet mecanique Flats Zurich- Manuel Herz Architects*

<https://www.dezeen.com/2018/09/03/ballet-mecanique-moving-walls-manuel-herz-architects-balconies/> 3- *Burg Albahr- Abu Dhabi*

4- *Seoul Expo 2012, SOMA Architecture*

5- *Umbrella mechanics with responsive*

*materials 6- Pivotal movement of a shading system*

The challenge of these systems is always the weather conditions themselves that would lead to the various small parts of the system malfunctioning and needing extra maintenance. The idea of protecting the moveable parts into a double skin façade offers an opportunity to design responsive

shading systems with shape memory alloys combined with principles of soft mechanics lead to reducing stresses of wind loading, shear and frictions between the moving elements.

Some of the earliest examples of these systems were Jean Nouvel's institute du Monde Arab building in Paris, offering an imitation of the iris of the eye's movement but in various metallic parts. Although enclosed between two layers of glass maintenance and energy demand still proved a challenge.

This studio will look into the principle of Homeostasis through deployable architecture mechanisms depending on various material properties, shapes and movements that can passively maximize the response to weather conditions.

In general these systems can move in a 2D, 3D, by folding, twisting, scissors or in a rotation action

### **Your brief:**

Look into materials and mechanisms that maybe actuated by the thermal conditions inside a double skin and provide a deployable shading system that responds to the variability of daylight conditions to provide a visual indoor environment that is variable yet within comfort limits.

The configuration needs to be light, provide the least friction possible and move either with the least mechanical effort or with an actuation system that depends on the thermal conditions, such as direct solar radiation.

-The configuration will be enclosed in a double skin façade system of a unit of maximum dimensions 0.5\*0.5m.

-The panel is expected to be part of a modular system and can explore various fixation methods to a timber frame structure.

-This will be part of an exhibition with the other groups to share ideas.

### **Our teaching team perspective**

The success of your experiment will be judged based on Benyus (2002) lists of Nature's characteristics from which we can learn:

- runs on sunlight;
- uses only the energy it needs;
- fits form to function;
- recycles;
- rewards cooperation;
- banks on diversity;
- demands local expertise;
- is aesthetically interesting and attracts curiosity to explore how it moves
- realises the power of limits- so enjoy the exercise and the journey

### **Schedule:**

Week 1: work in small groups to experiment with different shading mechanisms and materials, you can choose one or more of these techniques or come up with your own innovative ideas

- a- A planar system moving in 2D
- b- 3 D movement
- c- origami-folding structures
- d- Twisting
- e- Scissor movement
- f- pivots

Week 2,3,4 and 5 Develop your design and build the model, test and film the various movements of

your systems in response to various lighting conditions

Week 6: work with other groups to provide a single timber framework that would take on all façade modules from all groups and curate your exhibition

<b>Week no. 1</b>	Introduction to course objectives and outline.	Introduction
	5m Lecture: Building envelopes and shading systems	
<b>Week no. 2</b>	Lecture: Responsive facades: FORM+MECHANISM+MATERIAL/ Origami and Biomimcry as Generative techniques <b>Homework:</b> Design kinetic modules in groups- mechanisms-inspired by Origami and Biomimcry (3 to 4 ideas each group)- 15 cm models	Design
<b>Week no. 3</b>	Lecture: Smart Materials and Actuation <b>Homework:</b> Design actuated kinetic modules	
<b>Week no. 4</b>	Designing kinetic modules- Individual desk critiques for designs and proxies- Select Best of idea for each group <b>Homework:</b> Developing the final 1:1 model	
<b>Week no. 5</b>	Developing the final 1:1 model fixed on structural frame combined façade for all groups -A5 booklet (process of material experimentation and a section)	1:1 prototype building
<b>Week no. 6</b>	Submission of final presentation. Final Jury.	
		Final Crit

### Outputs:

- 1- co-ordinated publication for all groups:  
A5 booklet (mainly images, small amount of text) from each sub-group documenting the process of material experimentation and a sectional drawing approx. 1:5 - 1:10.
- 2- A 1:1 fixed on structural frame combined façade for all groups  
  
1:1 refined prototype of the façade module and its connections to the structure clearly demonstrating how the various parts respond to environmental stimuli (Note that if you can't have an electrical input you may choose to mimic this by manual movement)
- 3- A film documenting the process and final output recording its response to various daylight or thermal actuations

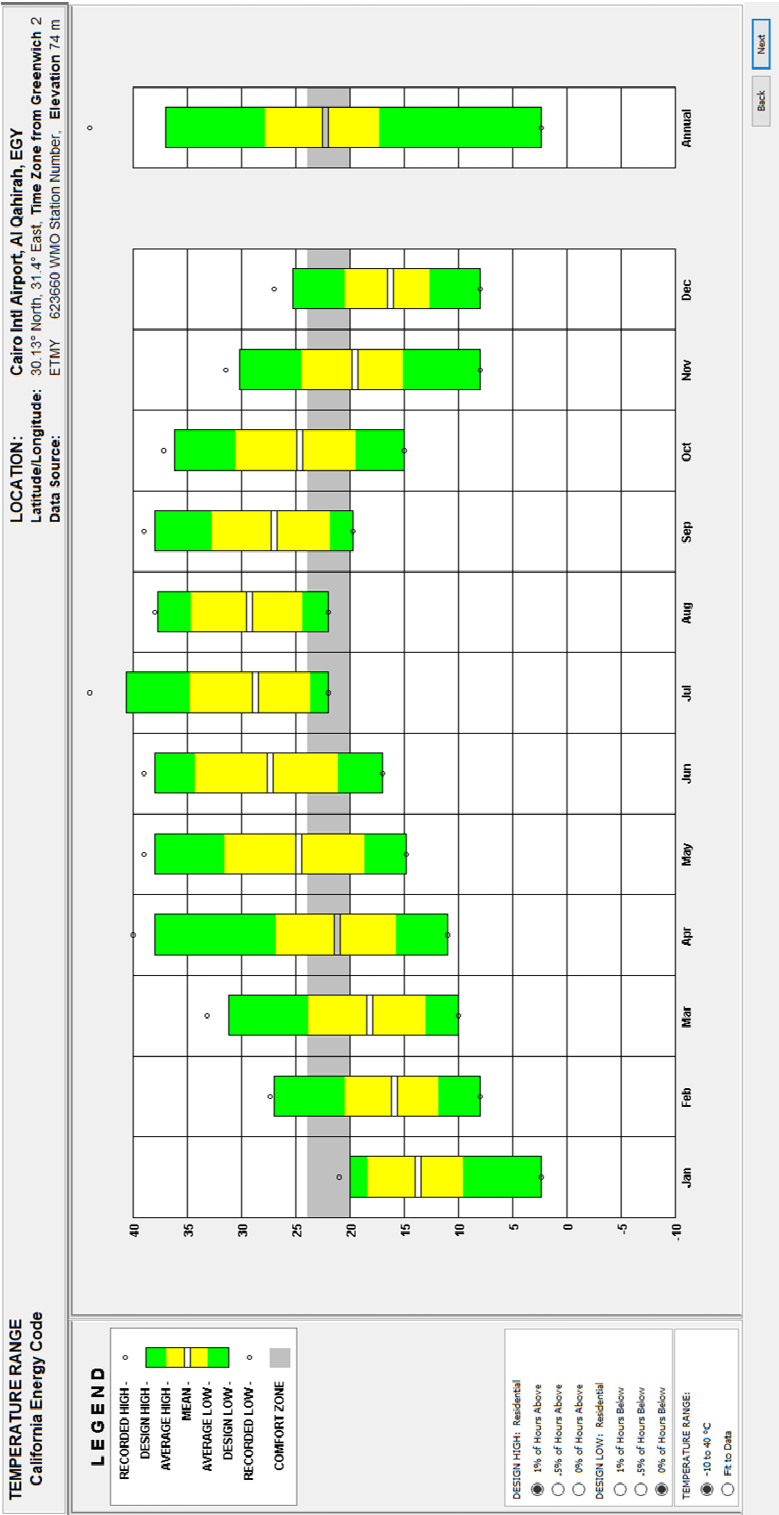
### References and a reading list:

1. Benyus J M 2002 *Biomimicry* (Harper Perennial)
2. Aldersey-Williams H 2003 *Zoomorphic* (Laurence King)

3. ElGhazi, Y., Hamza, N. and Dade-Robertson, M. (2017) *Passive and Low Energy Architecture (PLEA2017): Design to thrive*. Edinburgh, United Kingdom, pp. 3636-3643. Available at: <https://plea2017.net/>.
4. Kellert S R Heerwagen J H Mador M L 2008 *Biophilic Design: The Theory , Science and Practice of Bringing Buildings to Life* (Hoboken NJ: Wiley)
5. Derek Clemets Crome Lessons from Nature for sustainable architecture, Chapter 2: in Learning from Nature
6. Edwin, A.P.-H., Darren, J.H., Richard, J.M., Jr. and Dimitris, C.L. (2014) 'Origami-inspired active structures: a synthesis and review', *Smart Materials and Structures*, 23(9), p. 094001.
7. Fiorito, F., Sauchelli, M., Arroyo, D., Pesenti, M., Imperadori, M., Masera, G. and Ranzi, G. (2016) 'Shape morphing solar shadings: A review', *Renewable and Sustainable Energy Reviews*, 55, pp. 863-884.
8. Schaeffer, O. and Vogt, M.-M. (2010) *Move: architecture in motion-dynamic components and elements*. Walter de Gruyter.
9. Schleicher, S., Lienhard, J., Poppinga, S., Speck, T. and Knippers, J. (2015) 'A methodology for transferring principles of plant movements to elastic systems in architecture', *Computer-Aided Design*, 60, pp. 105-117.
10. Sun, L., Huang, W.M., Ding, Z., Zhao, Y., Wang, C.C., Purnawali, H. and Tang, C. (2012) 'Stimulus-responsive shape memory materials: A review', *Materials & Design*, 33, pp. 577-640.
11. Vergauwen, A., Laet, L.D. and Temmerman, N.D. (2017) 'Computational modelling methods for pliable structures based on curved-line folding', *Computer-Aided Design*, 83, pp. 51-63.

APPENDIX C: Temperature Range of Cairo, Egypt

Generated Using 'Climate consultant version 6.0' (Liggett et al., 2016)



APPENDIX D: The Nature of Coupled Fluid Dynamics and Heat Transfer

The DSF rectangular cavity with differentially heated walls is the basic set up of buoyancy-driven flow in indoor environments. The heat exchange between the glazing elements and the surrounding occurs by conduction, convection and radiation. It occurs from higher temperature to lower temperature, and is not bound to a medium. The process depends on the temperature distribution, the optical properties and the surface geometry (Knaack & Koenders, 2018).

The heat transfer for building facades has been defined by (Knaack & Koenders, 2018) as the transport of thermal energy through a construction element, such as the glazing elements, through which this process is affected by the climate of external and internal boundary conditions. Commenting on heat transfer in DSF, Mei concludes: 'the net heat gain to indoor environments is dominated mainly by transmitted solar radiation, with a small contribution from the radiative and convective fluxes' (Mei et al., 2007). It considers the heat transport within material-specific construction element and the heat transfer between its inner surface and the interior environment as well as its exterior surface and the exterior environment. The coming section presents the definitions of these types of heat transfer (conduction, convection, and radiation) to describe the phenomenon taking place in DSF.

**Heat conduction** is a mechanism of heat transfer facilitated by microscopic particles without bulk movement of particles. This mechanism is typical for solids. Conduction is facilitated by stationary particles, so it primarily occurs in the solid state (Pinterić, 2017). The measure of the material's ability to transfer heat is thermal conductivity  $\lambda$  [W/m·K]. According to a definition provided by Knaack and Koenders (2018): 'thermal conductivity determines how much thermal energy is transported per unit of length of a material layer and a temperature delta of 1 Kelvin'. For example, Materials with high density atom and closely packed molecules have high thermic conductivity whereas the thermic conductivity of materials with low density packing is low (Knaack & Koenders, 2018). This principle applies to *DSF surfaces* where heat passes straight through *glazing surfaces, grills* and frame.

**Heat transmission through convection** occurs when the thermal energy of a body is transmitted to a passing medium, such as air, or transmitted from a passing medium to a body. Warm body surfaces can transfer thermal energy to adjacent air molecules, which in turn creates a flow. This process based on different densities is called convection (Knaack & Koenders, 2018). It is facilitated by travelling particles; therefore, it occurs in liquid and gaseous states. Convection can be classified into

two groups; Natural convection and Forced convection. Natural convection appears when the bulk movement of particles is facilitated by some natural process, for example, buoyancy. While, Forced convection appears when the bulk movement of particles is facilitated by a device, for example, a fan (Pinterić, 2017). The resulting heat flux density  $q$  between a body and an adjacent gaseous or liquid medium depends on the temperature of the flowing medium  $\theta_u$  and the body surface temperature  $\theta_s$ . The convective heat flux density  $q$  is generated by the multiplication of the heat transmission coefficient  $h_f$  with the temperature difference between the flowing medium  $T_f$  and the body surface temperature  $T_w$ . The greater the temperature difference and the heat transmission coefficient, the greater the resulting heat flow and the better the heat transmission (Knaack & Koenders, 2018).

## APPENDIX E: The Mathematical Model

The general governing equations for the fluid domain are developed by using Navier-Stokes equations. The velocity and temperature fields in the channel are governed by three basic equations: the continuity equation (mass conservation); the motion / transport equation and the energy equation.

For modelling expected turbulent airflow, the viscous model was set to RNG k-epsilon ( $k - \epsilon$ ). Furthermore, Enhanced Wall Treatment was chosen under the options for Near-Wall Treatment. The Transport equations of the RNG k- $\epsilon$  Model is given by equations (1) to (8) as shown in ANSYS FLUENT User's Guide. Equation (1) presents the turbulent kinetic energy with different terms.

$$\frac{\partial}{\partial t}(\rho k) + \frac{\partial}{\partial x_i}(\rho k u_i) = \frac{\partial}{\partial x_j} \left( \alpha_k \mu_{eff} \frac{\partial k}{\partial x_j} \right) + G_k + G_b - \rho \epsilon - Y_M + S_k \quad (1)$$

Equation (2) presents the turbulent energy dissipation Equation.

$$\frac{\partial}{\partial t}(\rho \epsilon) + \frac{\partial}{\partial x_i}(\rho \epsilon u_i) = \frac{\partial}{\partial x_j} \left( \alpha_\epsilon \mu_{eff} \frac{\partial \epsilon}{\partial x_j} \right) + C_{1\epsilon} \frac{\epsilon}{k} (G_k + C_{3\epsilon} G_b) - C_{2\epsilon} \rho \frac{\epsilon^2}{k} - R_\epsilon + S_\epsilon \quad (2)$$

$C_{1\epsilon}$  and  $C_{2\epsilon}$  are model constants derived analytically by the RNG theory. These values, used by default in ANSYS Fluent, are  $C_{1\epsilon} = 1.42$  and  $C_{2\epsilon} = 1.68$

The shading screen increases airflow through the gap with a strong buoyancy effect. The buoyancy effect of air is simulated with Boussinesq approximation (Y. Li et al., 2017). To Model the Effective turbulent Production in the k- $\epsilon$  Models with Boussinesq approximation, the generation of K ( $G_k$ ) is evaluated in a manner consistent with the Boussinesq hypothesis.

$$G_k = \mu_t S^2 \quad (3)$$

where  $S$  is the modulus of the mean rate-of-strain tensor, defined as

$$S \equiv \sqrt{2 S_{ij} S_{ij}} \quad (4)$$

To Model the Effective (turbulent) Viscosity the following differential equation is used in the RNG k- $\epsilon$  Model, where the turbulent transport varies with the effective Reynolds number. In low-Reynolds number and near-wall flows the following equation is used.



$$d\left(\frac{\rho^2 k}{\sqrt{\varepsilon \mu}}\right) = 1.72 \frac{\hat{v}}{\sqrt{\hat{v}^3 - 1 + C_v}} d\hat{v} \quad (5)$$

$$\hat{v} = \frac{\mu_{eff}}{\mu} \quad (6)$$

$$C_v \approx 100$$

While in the high-Reynolds number limit, the following equation of turbulent eddy viscosity is used.

$$\mu_t = \rho C_\mu \frac{k^2}{\varepsilon} \quad (7)$$

$C_\mu$  is a constant equals to 0.0845 for RNG k- $\varepsilon$  Model

To Calculate the Inverse Effective Prandtl Numbers, the following equation is used in the RNG k- $\varepsilon$  Model

The inverse effective Prandtl numbers,  $\alpha^k$  and  $\alpha^\varepsilon$ , are computed using the following formula derived analytically by the RNG theory:

$$\left| \frac{\alpha - 1.3929}{\alpha_0 - 1.3929} \right|^{0.6321} \left| \frac{\alpha + 2.3929}{\alpha_0 + 2.3929} \right|^{0.3679} = \frac{\mu_{mol}}{\mu_{eff}} \quad (8)$$

where  $\alpha_0 = 1.0$  In the high-Reynolds number limit ( $\frac{\mu_{mol}}{\mu_{eff}} \ll 1$ ),  $\alpha_0 = \alpha_0 \approx 1.393$

An additional equation for energy conservation is solved in ANSYS Fluent when flows involving heat transfer. The flow in the DSF domain is mainly taking place through natural convection that occurs as a result of buoyancy-driven flow. The steady-state calculation performed using the Boussinesq model which is applicable in small temperature differences in the domain. This model treats density as a constant value in all solved equations, except for the buoyancy term in the momentum equation.

$$(\rho - \rho_0)g \approx -\rho_0 \beta (T - T_0)g \quad (9)$$

This Boussinesq approximation is valid when  $\beta(T - T_0) \ll 1$ . As, the Thermal expansion coefficient  $\beta$  for air ranges from 0.0035 at 15°C to 0.0031 at 50°C  $\beta(T - T_0)$  is much less than 1.

Usually, the most important physical quantity of interest is the total density of heat flow rate. We can get its value for the black body by integrating Planck's law for all wavelengths. This expression is called the Stefan-Boltzmann law, and constant  $\sigma = 5.670 \times 10^{-8}$  is called the Stefan-Boltzmann constant (Pinterić, 2017).

In this kind of problems, the radiation exchange between the wall surface (façade) and its adjacent environment is the main focus. The external radiation boundary condition is calculated from equation (10).

$$Q_{rad} = \sigma \times (T_{max}^4 - T_{min}^4) \quad (10)$$

Uncoupled options are used with the DO model for the given case, assuming low optical thickness and negligible scattering coefficients for its medium (air), where energy and radiation intensity equations are solved one by one (sequential not simultaneous approach). For DO model with non-gray option, RTE for spectral intensity  $I_\lambda(\vec{r}, \vec{s})$  could be written as following

$$\nabla \cdot (I_\lambda(\vec{r}, \vec{s}) \vec{s}) + (a_\lambda + \sigma_s) I_\lambda(\vec{r}, \vec{s}) = a_\lambda n^2 I_{b\lambda} + \frac{\sigma_s}{4\pi} \int_0^{4\pi} I_\lambda(\vec{r}, \vec{s}') \phi(\vec{s}, \vec{s}') d\Omega'$$

Where:

$\lambda$ : The wavelength.

$\vec{s}$ : assigned direction.

$\vec{r}$ : assigned position.

$a_\lambda$ : The spectral absorption coefficient.

$I_{b\lambda}$ : The black body intensity given by the Planck function.

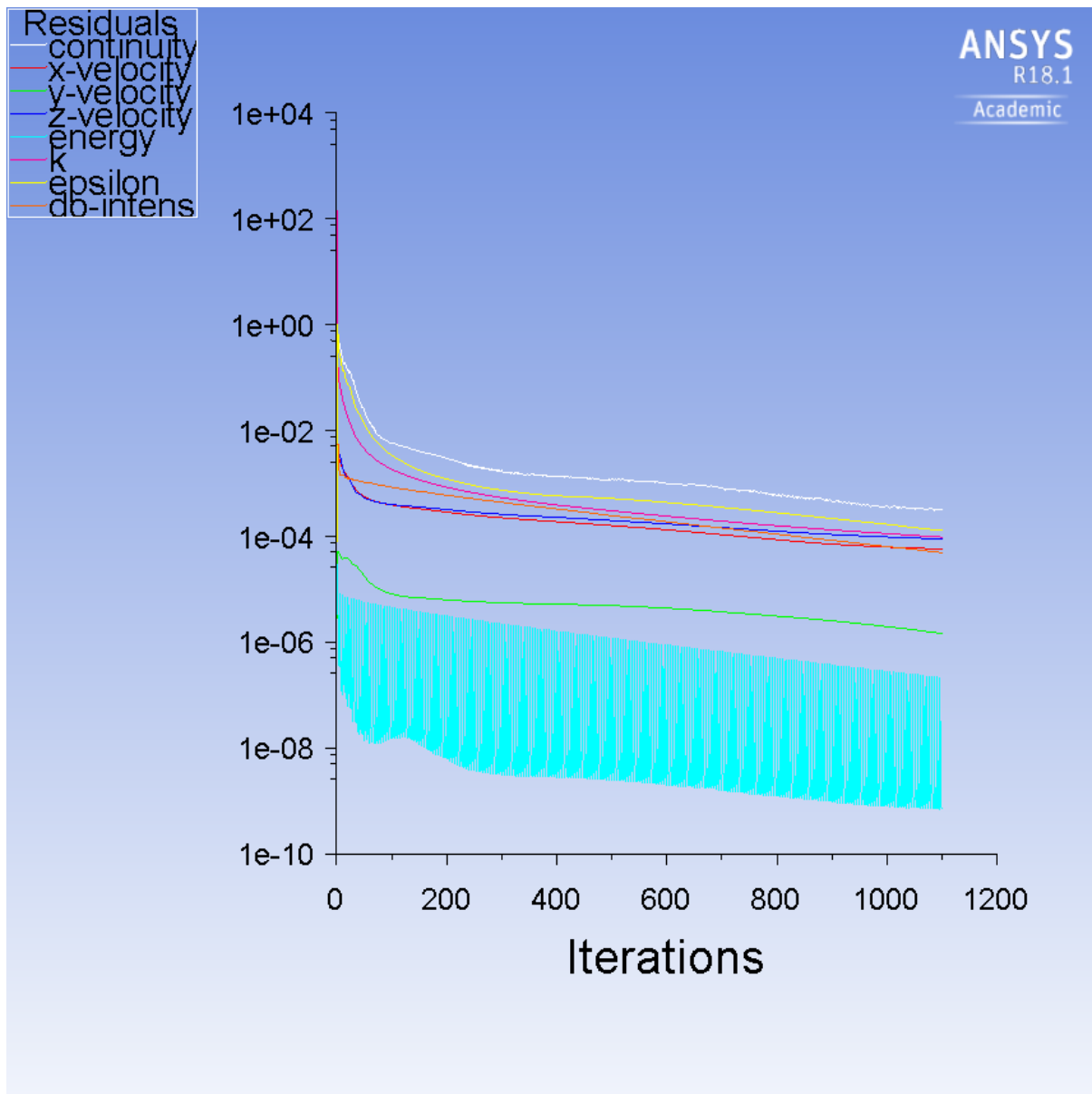
$n$ : The refractive index.

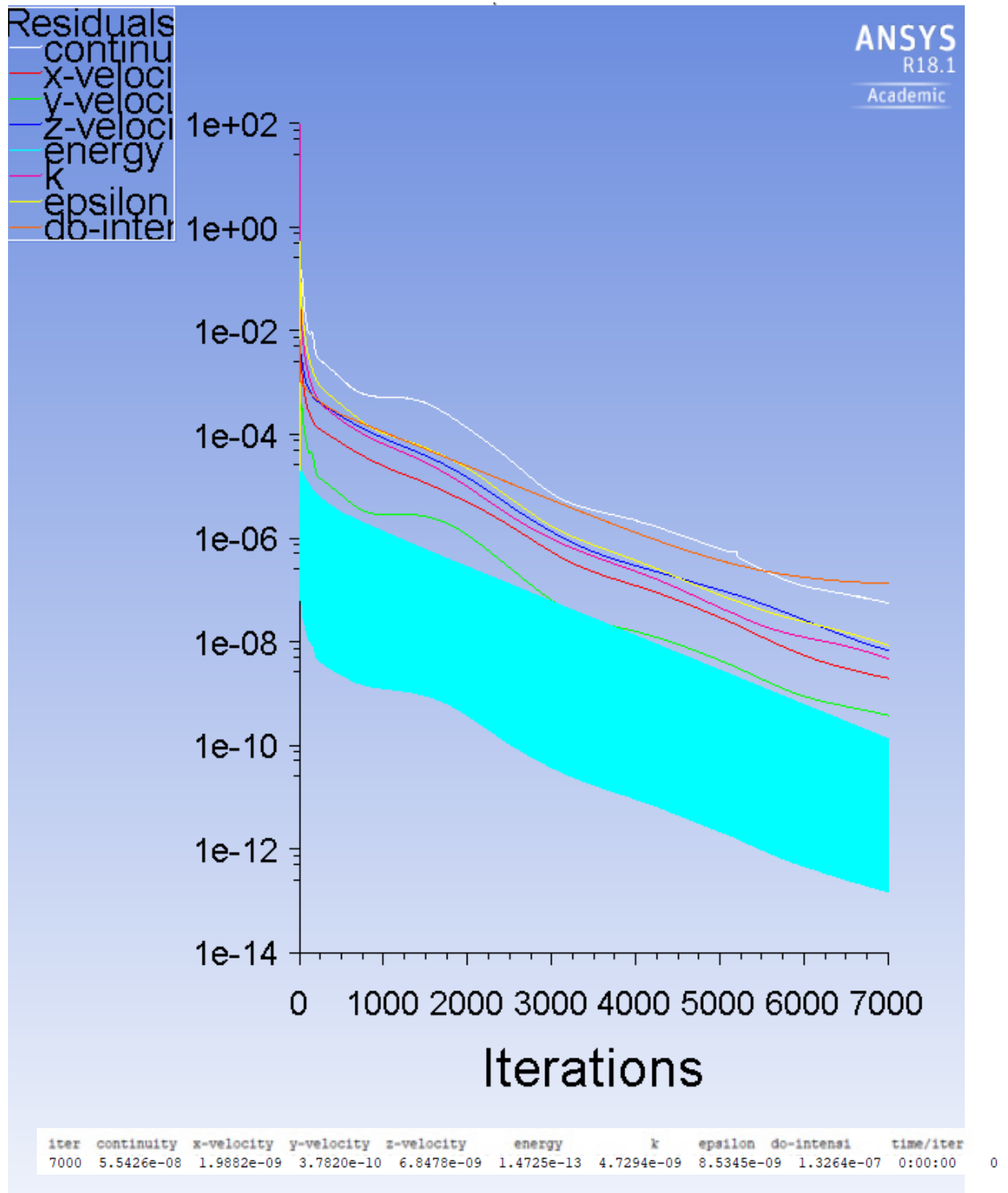


Temperatures of Mid Cavities																								
	January												July											
	09:00						12:00			15:00			09:00			12:00			15:00					
	Non-shaded	shaded			Non-shaded	shaded	Non-shaded	shaded	Non-shaded	shaded	Non-shaded	shaded	Non-shaded	shaded	Non-shaded	shaded	Non-shaded	shaded	Non-shaded	shaded	Non-shaded	shaded		
		30%	50%	70%																			30%	50%
outer Glazing	40.9	39.7	40.0	40.1	54.2	54.7	52.9	52.9	45.5	45.1	45.5	45.3	36.5	36.9	36.9	36.8	48.1	49.2	48.9	48.6	43.0	43.2	43.6	43.4
Internal Glazing (facing cavity)	29.6	24.9	25.8	26.3	36.0	33.0	30.3	31.6	31.6	25.8	28.9	29.3	31.3	30.3	30.5	30.6	37.3	35.7	35.7	35.8	34.8	32.3	33.7	33.9
Internal Glazing (facing room)	25.7	23.8	24.2	24.4	28.2	26.9	26.1	26.7	26.4	24.1	25.5	25.7	27.6	27.1	27.3	27.3	30.0	29.6	29.6	29.6	28.9	27.9	28.7	28.8
Reduction outer & inner (room)	15.2	16.0	15.8	15.6	26.0	27.8	26.8	26.2	19.1	21.1	20.1	19.6	9.0	9.7	9.6	9.4	18.1	19.6	19.3	19.0	14.1	15.4	14.9	14.6
Reduction Bet. outer & inner (cavity)	11.3	14.9	14.2	13.8	18.2	21.7	22.6	21.3	13.9	19.3	16.7	16.0	5.3	6.6	6.4	6.2	10.8	13.5	13.2	12.8	8.2	10.9	9.9	9.5
Percent outer & inner (room)	37.2	40.2	39.5	39.0	47.9	50.8	50.7	49.5	41.9	46.7	44.0	43.3	24.5	26.4	26.1	25.7	37.6	39.8	39.5	39.1	32.7	35.5	34.2	33.7
Percent mid outer &	27.6	37.4	35.6	34.5	33.5	39.6	42.8	40.2	30.6	42.8	36.6	35.4	14.4	18.0	17.4	16.7	22.5	27.5	27.0	26.3	19.0	25.3	22.6	21.8

60.00







## REFERENCES

- Addington, D. M. (2005). *Smart materials and new technologies : for the architecture and design professions*. Oxford: Oxford : Architectural Press.
- Adrover, E. R. (2015). *Deployable Structures*: Laurence King Publishing Ltd.
- Air Flow(er). (2018). Retrieved from <http://www.liftarchitects.com/#/air-flower>
- Aksamija, A. (2016). Design methods for sustainable, high-performance building facades. *Advances in Building Energy Research*, 10(2), 240-262.
- Aljofi, E. (2005). *The potentiality of reflected sunlight through Rawshan screens*. Paper presented at the Proceedings of the International Conference Passive and Low Energy Cooling for the Built Environment, Santorini, Greece.
- Amaireh, I. (2017). *Numerical investigation into a double skin façade system integrated with shading devices, with reference to the city of Amman, Jordan*. (PhD), University of Nottingham,
- ANSYS Meshing Solutions. (2014). In.
- Aouf, R. S. (2017). Aeromorph inflatables fold themselves from flat sheets into complex origami.
- Aouf, R. S. (2019). Thermobimetal shutters by Doris Sung self-regulate the temperature of buildings. Retrieved from <https://www.dezeen.com/2019/04/19/doris-sung-invert-thermobimetal-shutters/>
- Armstrong, A., Buffoni, G., Eames, D., James, R., Lang, L., Lyle, J., & Xuereb, K. (2013). The Al Bahar towers: multidisciplinary design for Middle East high-rise. *Arup J*, 2, 90-95.
- Arnold, J. G., Moriasi, D. N., Gassman, P. W., Abbaspour, K. C., White, M. J., Srinivasan, R., . . . Van Liew, M. W. (2012). SWAT: Model use, calibration, and validation. *Transactions of the ASABE*, 55(4), 1491-1508.
- Attia, S. (2018). Evaluation of adaptive facades: The case study of Al Bahr Towers in the UAE. *QScience Connect*, 2017(2, Special Issue on Shaping Qatar's Sustainable Built Environment- Part I), 6.
- Attia, S., Beltrán, L., De Herde, A., & Hensen, J. (2009). "Architect friendly": A comparison of ten different building performance simulation tools. Paper presented at the Proceedings of 11th International Building Performance Simulation Association Conference and Exhibition.
- Babaizadeh, H., Haghighi, N., Asadi, S., Broun, R., & Riley, D. (2015). Life cycle assessment of exterior window shadings in residential buildings in different climate zones. *Building and Environment*, 90, 168-177. doi:10.1016/j.buildenv.2015.03.038



- Baldinelli, G. (2009). Double skin façades for warm climate regions: Analysis of a solution with an integrated movable shading system. *Building and Environment*, 44(6), 1107-1118.  
doi:10.1016/j.buildenv.2008.08.005
- Barozzi, M., Lienhard, J., Zanelli, A., & Monticelli, C. (2016). The Sustainability of Adaptive Envelopes: Developments of Kinetic Architecture. *Procedia Engineering*, 155, 275-284.  
doi:10.1016/j.proeng.2016.08.029
- Barth, R. S. (2002). *Learning by heart*: John Wiley & Sons.
- Baseta, E., Tankal, E., & Shambayati, R. (2014). Translated Geometries. Retrieved from <https://iaac.net/project/translated-geometries/>
- Beck, H. E., Zimmermann, N. E., McVicar, T. R., Vergopolan, N., Berg, A., & Wood, E. F. (2018). Present and future Köppen-Geiger climate classification maps at 1-km resolution. *Scientific data*, 5, 180214.
- Begle, M., Luna, D., Luna, I., & Ardila, J. D. (2013). Advanced Materials – Shape Memory Alloy – Nitinol. Retrieved from <http://legacy.iaacblog.com/maa2012-2013-advanced-materials/2013/06/advanced-materials-shape-memory-alloy/>
- Bell, V. B. (2014). *Materials for design 2*: New York, New York : Princeton Architectural Press.
- Bellia, L., Marino, C., Minichiello, F., & Pedace, A. (2014). An Overview on Solar Shading Systems for Buildings. *Energy Procedia*, 62, 309-317. doi:10.1016/j.egypro.2014.12.392
- Bende, N. P., Evans, A. A., Innes-Gold, S., Marin, L. A., Cohen, I., Hayward, R. C., & Santangelo, C. D. (2015). Geometrically controlled snapping transitions in shells with curved creases. *Proc Natl Acad Sci U S A*, 112(36), 11175-11180. doi:10.1073/pnas.1509228112
- Bengisu, M., & Ferrara, M. (2018). *Materials that Move: Smart Materials, Intelligent Design*: Springer.
- Böke, J., Knaack, U., & Hemmerling, M. (2018). State-of-the-art of intelligent building envelopes in the context of intelligent technical systems. *Intelligent Buildings International*, 11(1), 27-45.  
doi:10.1080/17508975.2018.1447437
- Boudaoud, A. (2010). An introduction to the mechanics of morphogenesis for plant biologists. *Trends in plant science*, 15(6), 353-360.
- Bryan, H. J., & Clear, R. D. (1981). Calculating interior daylight illumination with a programmable hand calculator. *Journal of the Illuminating Engineering Society*, 10(4), 219-227.
- Burgert, I., & Fratzl, P. (2009). Actuation systems in plants as prototypes for bioinspired devices. *Philos Trans A Math Phys Eng Sci*, 367(1893), 1541-1557. doi:10.1098/rsta.2009.0003

- Burrows, L. (2017). Artificial muscles give soft robots superpowers. Retrieved from <https://www.seas.harvard.edu/news/2017/11/artificial-muscles-give-soft-robots-superpowers>
- Calcerano, F., & Martinelli, L. (2016). Numerical optimisation through dynamic simulation of the position of trees around a stand-alone building to reduce cooling energy consumption. *Energy and Buildings*, 112, 234-243.
- Callens, S. J. P., & Zadpoor, A. A. (2018). From flat sheets to curved geometries: Origami and kirigami approaches. *Materials Today*, 21(3), 241-264. doi:10.1016/j.mattod.2017.10.004
- Candy, L. (2006). Practice based research: A guide. *CCS report*, 1, 1-19.
- Carpi, F., Kornbluh, R., Sommer-Larsen, P., & Alici, G. (2011). Electroactive polymer actuators as artificial muscles: are they ready for bioinspired applications? *Bioinspiration & Biomimetics*, 6(4), 045006. doi:10.1088/1748-3182/6/4/045006
- Cermak-Sassenrath, D., & Møllenbach, E. (2014). *Teaching to tinker: making as an educational strategy*. Paper presented at the Proceedings of the 8th Nordic Conference on Human-Computer Interaction: Fun, Fast, Foundational.
- Chan, A., Chow, T. T., Fong, K., & Lin, Z. (2009). Investigation on energy performance of double skin façade in Hong Kong. *Energy and Buildings*, 41(11), 1135-1142.
- Choi, K.-H. (2016). Practice-led origami-inspired fashion design: out of the frame: flight by paper plane. *International Journal of Fashion Design, Technology and Education*, 9(3), 210-221. doi:10.1080/17543266.2016.1158872
- cilento, K. (2012). Al Bahar Towers Responsive Facade / Aedas Retrieved from <https://www.archdaily.com/270592/al-bahar-towers-responsive-facade-aedas>.
- . Computational Domain. (2008). In D. Li (Ed.), *Encyclopedia of Microfluidics and Nanofluidics* (pp. 275-275). Boston, MA: Springer US.
- Coussirat, M., Guardo, A., Jou, E., Egusquiza, E., Cuerva, E., & Alavedra, P. (2008). Performance and influence of numerical sub-models on the CFD simulation of free and forced convection in double-glazed ventilated façades. *Energy and Buildings*, 40(10), 1781-1789.
- Crawley, D. B., Hand, J. W., Kummert, M., & Griffith, B. T. (2008). Contrasting the capabilities of building energy performance simulation programs. *Building and Environment*, 43(4), 661-673. doi:10.1016/j.buildenv.2006.10.027
- Cross, N. (1982). Designerly ways of knowing. *Design studies*, 3(4), 221-227.
- Cross, N. (2001). Designerly ways of knowing: Design discipline versus design science. *Design issues*, 17(3), 49-55.

- Dabaieh, M., Wanas, O., Hegazy, M. A., & Johansson, E. (2015). Reducing cooling demands in a hot dry climate: A simulation study for non-insulated passive cool roof thermal performance in residential buildings. *Energy and Buildings*, 89, 142-152. doi:10.1016/j.enbuild.2014.12.034
- Datta, G. (2001). Effect of fixed horizontal louver shading devices on thermal performance of building by TRNSYS simulation. *Renewable Energy*, 23(3-4), 497-507.
- De Wilde, P. (2018). *Building performance analysis*: John Wiley & Sons.
- Doumptioti, C., Greenberg, E. L., & Karatzas, K. (2010). *Embedded intelligence: material responsiveness in façade systems*.
- Drew, L. (2007). Designing the interface between research, learning and teaching. *Design Research Quarterly*, 2(3), 1-5.
- Drozdowski, Z., & Gupta, S. (2009). *Adaptive fritting as case exploration for adaptivity in architecture*. Paper presented at the Proceedings of the 29th Annual Conference of the Association for Computer Aided Design in Architecture (ACADIA).
- Dubois, M.-C. (2001). Solar shading for low energy use and daylight quality in offices: simulations, measurements and design tools.
- Edwin, A. P.-H., Darren, J. H., Richard, J. M., Jr., & Dimitris, C. L. (2014). Origami-inspired active structures: a synthesis and review. *Smart Materials and Structures*, 23(9), 094001.
- El Ahmar, S., & Fioravanti, A. (2015). *Simulating the thermal and daylight performances of a folded porous double façade for an office building in Cairo*. Paper presented at the International Conference of the Architectural Science Association (ASA).
- El Sheikh, M., & Kensek, K. (2011). *Intelligent skins: Daylight harvesting through dynamic light-deflection in office spaces*. Paper presented at the En ARCC 2011 Conference proceedings.
- Elarga, H., Zarrella, A., & De Carli, M. (2016). Dynamic energy evaluation and glazing layers optimization of façade building with innovative integration of PV modules. *Energy and Buildings*, 111, 468-478. doi:10.1016/j.enbuild.2015.11.060
- ElGhazi, Y., Hamza, N., & Dade-Robertson, M. (2017). *Responsive Plant-inspired skins A review*. Paper presented at the Passive and Low Energy Architecture (PLEA2017): Design to thrive, Edinburgh, United Kingdom.
- Eltaweel, A., & Su, Y. (2017). Parametric design and daylighting: A literature review. *Renewable and Sustainable Energy Reviews*, 73, 1086-1103. doi:10.1016/j.rser.2017.02.011
- Epps, G., & Verma, S. (2013). Curved Folding: Design to Fabrication Process of Robofold. *Shape Modeling International 2013*, 75.

- Esquivel, G., Weiser, D., Hartl, D. J., & Whitten, D. (2013). POP-OP: A shape memory-based morphing wall. *International Journal of Architectural Computing*, 11(3), 347-362.
- Felton, S. M., Becker, K. P., Aukes, D. M., & Wood, R. J. (2015). Self-folding with shape memory composites at the millimeter scale. *Journal of Micromechanics and Microengineering*, 25(8). doi:10.1088/0960-1317/25/8/085004
- Felton, S. M., Tolley, M. T., Shin, B., Onal, C. D., Demaine, E. D., Rus, D., & Wood, R. J. (2013). Self-folding with shape memory composites. *Soft matter*, 9(32). doi:10.1039/c3sm51003d
- Fiorito, F., Sauchelli, M., Arroyo, D., Pesenti, M., Imperadori, M., Masera, G., & Ranzi, G. (2016). Shape morphing solar shadings: A review. *Renewable and Sustainable Energy Reviews*, 55, 863-884. doi:10.1016/j.rser.2015.10.086
- Fox, M., & Kemp, M. (2009). Interactive architecture. In: New York: Princeton Architectural Press.
- Frecker, M. I. (2003). Recent advances in optimization of smart structures and actuators. *Journal of Intelligent Material Systems and Structures*, 14(4-5), 207-216.
- Gadelhak, M. (2013). High Performance facades: designing office building facades to enhance indoor daylighting performance. *M. Sc. department of Architecture, faculty of Engineering, Ain University, Egypt*.
- Ghaffarianhoseini, A., Ghaffarianhoseini, A., Berardi, U., Tookey, J., Li, D. H. W., & Kariminia, S. (2016). Exploring the advantages and challenges of double-skin façades (DSFs). *Renewable and Sustainable Energy Reviews*, 60, 1052-1065. doi:10.1016/j.rser.2016.01.130
- Gianluca, R., Fiorito, F., & Vallati, O. (2018). *Development of an Adaptive Shading Device Based on Flexible Structural Elements and SMA Springs*. Paper presented at the In Facade 2018 - Adaptive! Proceedings of the COST Action TU1403 Adaptive Facades Network Final Conference,, Luzern: TU Delft Open.
- GlobalABC, I., UNE. (2019). Global status report for buildings and construction: towards a zero emissions, efficient and resilient buildings and construction sector.
- Goia, F., Haase, M., & Perino, M. (2013). Optimizing the configuration of a façade module for office buildings by means of integrated thermal and lighting simulations in a total energy perspective. *Applied Energy*, 108, 515-527. doi:<https://doi.org/10.1016/j.apenergy.2013.02.063>
- Gratia, E., & De Herde, A. (2004). Optimal operation of a south double-skin facade. *Energy and Buildings*, 36(1), 41-60. doi:10.1016/j.enbuild.2003.06.001
- Gratia, E., & De Herde, A. (2007). The most efficient position of shading devices in a double-skin facade. *Energy and Buildings*, 39(3), 364-373. doi:10.1016/j.enbuild.2006.09.001

- Gray, C., & Burnett, G. (2009). *Making sense: An exploration of ways of knowing generated through practice and reflection in craft*. Paper presented at the Proceedings of the Crafticulation and Education Conference.
- Guardo, A., Coussirat, M., Valero, C., Egusquiza, E., & Alavedra, P. (2011). CFD assessment of the performance of lateral ventilation in Double Glazed Façades in Mediterranean climates. *Energy and Buildings*, 43(9), 2539-2547. doi:10.1016/j.enbuild.2011.06.008
- Guo, Q., Dai, E., Han, X., Xie, S., Chao, E., & Chen, Z. (2015). Fast nastic motion of plants and bioinspired structures. *Journal of the Royal Society Interface*, 12(110), 20150598.
- Hamza, N. (2004). *The Performance of Double Skin Facades in office building refurbishment in hot arid areas*. (PhD Thesis), University of Newcastle upon Tyne,
- Hamza, N., Cook, M., & Cropper, P. (2011). *Comparative Analysis of Natural Ventilation Performance in Non-Uniform Double Skin Facades in Temperate Climates*. Paper presented at the Proceedings of Building Simulation.
- Hamza, N., & Qian, Z. (2016). *Validating the performance of a Double Skin Facade in winter in an hot arid climate*. Paper presented at the PLEA 2016 Los Angeles - 36th International Conference on Passive and Low Energy Architecture. Cities, Buildings, People: Towards Regenerative Environments, Los Angeles.
- Hamza, N., & Underwood, C. (2005). *CFD supported modelling of double skin facades in hot arid climates*. Paper presented at the Proceedings of 9th International Building Performance Simulation Association Conference (IPBSA), Montreal, Canada.
- Hashemi, N., Fayaz, R., & Sarshar, M. (2010). Thermal behaviour of a ventilated double skin facade in hot arid climate. *Energy and Buildings*, 42(10), 1823-1832. doi:10.1016/j.enbuild.2010.05.019
- Hassanli, S., Hu, G., Kwok, K. C. S., & Fletcher, D. F. (2017). Utilizing cavity flow within double skin façade for wind energy harvesting in buildings. *Journal of Wind Engineering and Industrial Aerodynamics*, 167, 114-127. doi:10.1016/j.jweia.2017.04.019
- Hasselaar, B. (2006). Climate Adaptive Skins: towards the new energy-efficient façade. *Management of Natural Resources, Sustainable Development and Ecological Hazards*, 99, 351.
- Hawkes, E., An, B., Benbernou, N. M., Tanaka, H., Kim, S., Demaine, E., . . . Wood, R. J. (2010). Programmable matter by folding. *Proceedings of the National Academy of Sciences*, 107(28), 12441-12445.
- Hazem, A., Ameghchouche, M., & Bougriou, C. (2015). A numerical analysis of the air ventilation management and assessment of the behavior of double skin facades. *Energy and Buildings*, 102, 225-236. doi:10.1016/j.enbuild.2015.05.057

- Holstov, A. (2018). *Wood-based hygromorphic materials for sustainable responsive architecture*. Thesis (Ph. D.)--Newcastle University, 2018., Newcastle upon Tyne, England.
- Holstov, A., Bridgens, B., & Farmer, G. (2015). Hygromorphic materials for sustainable responsive architecture. *Construction and Building Materials*, 98, 570-582.  
doi:10.1016/j.conbuildmat.2015.08.136
- Hovestadt, L., & Kretzer, M. (2014). *ALIVE : Advancements in adaptive architecture*: Basel/Berlin/Boston : Birkhäuser.
- Howell, L. L. (2001). *Compliant mechanisms*: John Wiley & Sons.
- Huang, W. (2002). On the selection of shape memory alloys for actuators. *Materials & Design*, 23(1), 11-19.
- Huang, W., & Toh, W. (2000). Training two-way shape memory alloy by reheat treatment. *Journal of materials science letters*, 19(17), 1549-1550.
- Huang, W. M., Ding, Z., Wang, C. C., Wei, J., Zhao, Y., & Purnawali, H. (2010). Shape memory materials. *Materials Today*, 13(7), 54-61.
- Huang, W. M., Goh, H. B., & Li, C. (2002). Effects of reheat treatment conditions on two-way shape memory. *Journal of materials science letters*, 21(13), 991-993.
- Ilievski, F., Mazzeo, A. D., Shepherd, R. F., Chen, X., & Whitesides, G. M. (2011). Soft robotics for chemists. *Angewandte Chemie International Edition*, 50(8), 1890-1895.
- Ioannidis, Z., Buonomano, A., Athienitis, A. K., & Stathopoulos, T. (2017). Modeling of double skin façades integrating photovoltaic panels and automated roller shades: Analysis of the thermal and electrical performance. *Energy and Buildings*, 154, 618-632.  
doi:10.1016/j.enbuild.2017.08.046
- Iyi, D. (2013). *A Study on Buoyancy Driven Turbulent Flow Associated with Radiation in Cavities Partially Filled with Blockages*. Northumbria University Retrieved from <http://nrl.northumbria.ac.uk/15246/>
- Iyi, D., Hasan, R., Underwood, C., & Penlington, R. (2014). Double skin façade: modelling technique and influence of venetian blinds on the airflow and heat transfer. *Applied Thermal Engineering*.
- Jacobsson, M. (2013). *Tinkering with interactive materials-Studies, concepts and prototypes*. KTH School of Computer Science and Communication (CSC),
- Jaksch, S., & Sedlak, V. (2011). A Foldable Umbrella Structure—Developments and Experiences. *International Journal of Space Structures*, 26(1), 1-18.

- Ji, Y., Cook, M. J., Hanby, V., Infield, D. G., Loveday, D. L., & Mei, L. (2007, 2007-09-03). *CFD modelling of double-skin facades with venetian blinds*. Paper presented at the Building Simulation 2007.
- Ji, Y., Cook, M. J., Hanby, V., Infield, D. G., Loveday, D. L., & Mei, L. (2008). CFD modelling of naturally ventilated double-skin facades with Venetian blinds. *Journal of Building Performance Simulation*, 1(3), 185-196. doi:10.1080/19401490802478303
- Jiru, T. E., Tao, Y.-X., & Haghighat, F. (2011). Airflow and heat transfer in double skin facades. *Energy and Buildings*, 43(10), 2760-2766.
- Johnsen, K., & Winther, F. V. (2015). Dynamic Facades, the Smart Way of Meeting the Energy Requirements. *Energy Procedia*, 78, 1568-1573. doi:10.1016/j.egypro.2015.11.210
- Joseph, J. (2018). Facility Design and Process Utilities. In *Biopharmaceutical Processing* (pp. 933-986): Elsevier.
- Kapsali, V. (2016). *Biomimetics for Designers*: Thames & Hudson.
- Karanouh, A., & Kerber, E. (2015). Innovations in dynamic architecture. *Journal of Facade Design and Engineering*, 3(2), 185-221. doi:10.3233/fde-150040
- Kelloggs Research Labs. (USA). Retrieved from [www.kelloggsresearchlabs.com](http://www.kelloggsresearchlabs.com)
- Khoo, C. K., & Salim, F. (2013). Responsive Materiality for morphing architectural skins.
- Khoo, C. K., & Salim, F. D. (2013). *Lumina: a soft kinetic material for morphing architectural skins and organic user interfaces*. Paper presented at the Proceedings of the 2013 ACM international joint conference on Pervasive and ubiquitous computing.
- Kim, D.-W., & Park, C.-S. (2011). Difficulties and limitations in performance simulation of a double skin façade with EnergyPlus. *Energy and Buildings*, 43(12), 3635-3645.
- Kirimtat, A., Koyunbaba, B. K., Chatzikonstantinou, I., & Sariyildiz, S. (2016). Review of simulation modeling for shading devices in buildings. *Renewable and Sustainable Energy Reviews*, 53, 23-49. doi:10.1016/j.rser.2015.08.020
- Klein, S., & Alvarada, S. (2007). Engineering equation solver (EES). In: F-chart software, WI.
- Knaack, U., & Koenders, E. (2018). *Building Physics of the Envelope : Principles of Construction*: Basel : Birkhäuser.
- Kobayashi, H., Kresling, B., & Vincent, J. F. V. (1998). The geometry of unfolding tree leaves. *Proceedings of the Royal Society of London B: Biological Sciences*, 265(1391), 147-154.
- Kolarevic, B., & Parlac, V. (2015). *Building dynamics : exploring architecture of change*: London : Routledge, Taylor & Francis Group.
- Koschitz, D., Demaine, E. D., & Demaine, M. L. (2008). Curved crease origami.

- Kottek, M., Grieser, J., Beck, C., Rudolf, B., & Rubel, F. (2006). World map of the Köppen-Geiger climate classification updated. *Meteorologische Zeitschrift*, 15(3), 259-263.
- Kretzer, M. (2017a). *Information Materials Smart Materials for Adaptive Architecture*: Cham : Springer International Publishing : Imprint: Springer.
- Kretzer, M. (2017b). Towards a new softness. In *Information Materials* (pp. 167-179): Springer.
- Kretzer, M., & Damjanovic, I. (2012). Animated textiles.
- Kretzer, M., & Hovestadt, L. (2014). *ALIVE: Advancements in adaptive architecture* (Vol. 8): Birkhäuser.
- Kretzer, M., & Rossi, D. (2012a). ShapeShift. *Leonardo*, 45(5), 480-481.
- Kretzer, M., & Rossi, D. (2012b). ShapeShift. *Leonardo*, 45(5), 480-481. doi:10.1162/LEON\_a\_00451
- Krymsky, Y. (2011). CJ R&D Center Kinetic Facade. Retrieved from <https://yazdanistudioresearch.wordpress.com/2011/11/15/cj-rd-center-kinetic-facade/>
- Lamnatou, C., Mondol, J. D., Chemisana, D., & Maurer, C. (2015). Modelling and simulation of Building-Integrated solar thermal systems: Behaviour of the system. *Renewable and Sustainable Energy Reviews*, 45, 36-51. doi:10.1016/j.rser.2015.01.024
- Lauff, C., Simpson, T. W., Frecker, M., Ounaies, Z., Ahmed, S., von Lockette, P., . . . Lien, J.-M. (2014). *Differentiating bending from folding in origami engineering using active materials*. Paper presented at the ASME 2014 International Design Engineering Technical Conferences and Computers and Information in Engineering Conference.
- Lauder, B. E., & Sharma, B. (1974). Application of the energy-dissipation model of turbulence to the calculation of flow near a spinning disc. *Letters in heat and mass transfer*, 1(2), 131-137.
- Li, S., & Wang, K. W. (2016). Plant-inspired adaptive structures and materials for morphing and actuation: a review. *Bioinspir Biomim*, 12(1), 011001. doi:10.1088/1748-3190/12/1/011001
- Li, Y., Darkwa, J., & Kokogiannakis, G. (2017). Heat transfer analysis of an integrated double skin façade and phase change material blind system. *Building and Environment*, 125, 111-121. doi:10.1016/j.buildenv.2017.08.034
- Liao, L., Athienitis, A., Park, K.-W., Collins, M., & Poissant, Y. (2005). *Numerical study of conjugate heat transfer in a BIPV-Thermal system*. Paper presented at the 2005 International Solar Energy Conference.
- Lienhard, J. (2014). *Bending-active structures form-finding strategies using elastic*. Universität Stuttgart - Institut für Tragkonstruktionen und Konstruktives Entwerfen,;
- Lienhard, J., Poppinga, S., Schleicher, S., Speck, T., & Knippers, J. (2010). Elastic architecture: nature inspired pliable structures. 1, 469-477. doi:10.2495/dn100421



- Lienhard, J., Schleicher, S., Poppinga, S., Masselter, T., Milwich, M., Speck, T., & Knippers, J. (2011). Flectofin: a hingeless flapping mechanism inspired by nature. *Bioinspiration & Biomimetics*, 6(4), 045001. doi:10.1088/1748-3182/6/4/045001
- Liggett, R., Milne, M., Gomez, C., Leeper, D., BENSON, A., & BHATTACHARYA, Y. (2016). Climate Consultant 6.0. *California, Los Angeles: Murray Milne*.
- Lignarolo, L. E. M., Lelieveld, C., & Teuffel, P. (2011). *Shape morphing wind-responsive facade systems realized with smart materials*. Paper presented at the Adaptive Architecture: An International Conference, London, UK, March 3-5, 2011.
- Liu, Y., Boyles, J. K., Genzer, J., & Dickey, M. D. (2012). Self-folding of polymer sheets using local light absorption. *Soft matter*, 8(6), 1764-1769.
- Liu, Y., Genzer, J., & Dickey, M. D. (2016). "2D or not 2D": Shape-programming polymer sheets. *Progress in Polymer Science*, 52, 79-106. doi:10.1016/j.progpolymsci.2015.09.001
- Loonen, R. (2010). Overview of 100 climate adaptive building shells.
- Loonen, R. C., Favoino, F., Hensen, J. L., & Overend, M. (2017). Review of current status, requirements and opportunities for building performance simulation of adaptive facades. *Journal of Building Performance Simulation*, 10(2), 205-223.
- Loonen, R. C., Trčka, M., Cóstola, D., & Hensen, J. L. (2013). Climate adaptive building shells: State-of-the-art and future challenges. *Renewable and Sustainable Energy Reviews*, 25, 483-493.
- Loonen, R. C. G. M., Favoino, F., Hensen, J. L. M., & Overend, M. (2016). Review of current status, requirements and opportunities for building performance simulation of adaptive facades. *Journal of Building Performance Simulation*, 10(2), 205-223. doi:10.1080/19401493.2016.1152303
- Loschke, S. K. (2016). *Materiality and architecture*: Routledge.
- Mabermann, C., & Kroschwitz, J. (1991). Encyclopedia of Chemical Technology. *John Wiley & Sons, New York*, 1, 251.
- Mahadevan, L., & Rica, S. (2005). Self-organized origami. *Science*, 307(5716), 1740. doi:10.1126/science.1105169
- Mahmoud, A. H. A., & Elghazi, Y. (2016). Parametric-based designs for kinetic facades to optimize daylight performance: Comparing rotation and translation kinetic motion for hexagonal facade patterns. *Solar Energy*, 126, 111-127. doi:10.1016/j.solener.2015.12.039
- Mäkelä, M. (2007). Knowing through making: The role of the artefact in practice-led research. *Knowledge, Technology & Policy*, 20(3), 157-163.

- Makonin, S. (2016). App programming and its use in smart buildings. In *Start-Up Creation* (pp. 451-463): Elsevier.
- Malkawi, A. M. (2004). Developments in environmental performance simulation. *Automation in Construction*, 13(4), 437-445.
- Manz, H., Schaelin, A., & Simmler, H. (2004). Airflow patterns and thermal behavior of mechanically ventilated glass double façades. *Building and Environment*, 39(9), 1023-1033.  
doi:10.1016/j.buildenv.2004.01.003
- Maragkoudaki, A. (2013). No-Mech Kinetic Responsive Architecture: Kinetic Responsive Architecture with No Mechanical Parts. 145-150. doi:10.1109/ie.2013.23
- Meagher, M. (2015). Designing for change: The poetic potential of responsive architecture. *Frontiers of Architectural Research*, 4(2), 159-165. doi:10.1016/j.foar.2015.03.002
- Meerbeek, B., te Kulve, M., Gritti, T., Aarts, M., van Loenen, E., & Aarts, E. (2014). Building automation and perceived control: A field study on motorized exterior blinds in Dutch offices. *Building and Environment*, 79, 66-77. doi:10.1016/j.buildenv.2014.04.023
- Mei, L., Loveday, D., Infield, D., Hanby, V., Cook, M., Ji, Y., . . . Bates, J. (2007). *The influence of blinds on temperatures and air flows within ventilated double-skin façades*. Paper presented at the Proceedings of Clima 2007 WellBeing Indoors.
- Menges, A. (2012). *Material computation : higher integration in morphogenetic design*. London: London : Wiley.
- Menter, F. R. (1994). Two-equation eddy-viscosity turbulence models for engineering applications. *AIAA journal*, 32(8), 1598-1605.
- Mestre, O., Riofrio, J., & Shin, M. (2014). *Characterization of Nitinol as a Servo-Biomimetic for Facial Muscles*. Paper presented at the ASME 2014 International Mechanical Engineering Congress and Exposition.
- Mingallon, M., & Ramaswamy, S. (2012). *Bio-inspired self-actuating composite materials*: INTECH Open Access Publisher.
- Minoli, D., Sohraby, K., & Occhiogrosso, B. (2017). IoT Considerations, Requirements, and Architectures for Smart Buildings—Energy Optimization and Next-Generation Building Management Systems. *IEEE Internet of Things Journal*, 4(1), 269-283.  
doi:10.1109/jiot.2017.2647881
- Mirrahimi, S., Mohamed, M. F., Haw, L. C., Ibrahim, N. L. N., Yusoff, W. F. M., & Aflaki, A. (2016). The effect of building envelope on the thermal comfort and energy saving for high-rise buildings in hot–humid climate. *Renewable and Sustainable Energy Reviews*, 53, 1508-1519.

- Moloney, J. (2006). *Between Art and Architecture: The Interactive Skin*. Paper presented at the Tenth International Conference on Information Visualisation (IV'06).
- Moloney, J. (2011). *Designing kinetics for architectural facades: state change*: Taylor & Francis.
- Mueller, S., Kruck, B., & Baudisch, P. (2013). *LaserOrigami: laser-cutting 3D objects*. Paper presented at the Proceedings of the SIGCHI Conference on Human Factors in Computing Systems.
- Nagy, Z., Svetozarevic, B., Jayathissa, P., Begle, M., Hofer, J., Lydon, G., . . . Schlueter, A. (2016). The Adaptive Solar Facade: From concept to prototypes. *Frontiers of Architectural Research*, 5(2), 143-156. doi:10.1016/j.foar.2016.03.002
- Niedderer, K., & Roworth-Stokes, S. (2007). *The role and use of creative practice in research and its contribution to knowledge*. Paper presented at the IASDR International Conference.
- Nielsen, M. V., Svendsen, S., & Jensen, L. B. (2011). Quantifying the potential of automated dynamic solar shading in office buildings through integrated simulations of energy and daylight. *Solar Energy*, 85(5), 757-768. doi:10.1016/j.solener.2011.01.010
- Nimkulrat, N. (2012). Hands-on intellect: Integrating craft practice into design research. *International Journal of Design*, 6(3).
- Nimkulrat, N. (2013). Situating creative artifacts in art and design research. *FormAkademisk-forskningstidsskrift for design og designdidaktikk*, 6(2).
- Oesterle, E. (2001). *Double skin facades: integrated planning; building physics, construction, aerophysics, air-conditioning, economic viability*: Prestel.
- Ostuzzi, F., De Couvreur, L., Detand, J., & Saldien, J. (2017). From Design for One to Open-ended Design. Experiments on understanding how to open-up contextual design solutions. *The Design Journal*, 20(sup1), S3873-S3883. doi:10.1080/14606925.2017.1352890
- Oxford dictionary of English*. (2005). Oxford University Press.
- Oxman, N. (2010). *Material-based design computation*. Massachusetts Institute of Technology,
- Oxman, N., & Rosenberg, J. (2007). Material computation. *International Journal of Architectural Computing*, 1(5), 21-44.
- Palmero-Marrero, A. I., & Oliveira, A. C. (2010). Effect of louver shading devices on building energy requirements. *Applied Energy*, 87(6), 2040-2049. doi:10.1016/j.apenergy.2009.11.020
- Parisi, S., Rognoli, V., & Sonneveld, M. (2017). Material Tinkering. An inspirational approach for experiential learning and envisioning in product design education. *The Design Journal*, 20(sup1), S1167-S1184. doi:10.1080/14606925.2017.1353059
- Parra, J., Guardo, A., Egusquiza, E., & Alavedra, P. (2015). Thermal Performance of Ventilated Double Skin Façades with Venetian Blinds. *Energies*, 8(6), 4882-4898. doi:10.3390/en8064882

- Pasut, W., & De Carli, M. (2012). Evaluation of various CFD modelling strategies in predicting airflow and temperature in a naturally ventilated double skin façade. *Applied Thermal Engineering*, 37, 267-274. doi:10.1016/j.applthermaleng.2011.11.028
- Pelaz, B., Blanco, J. M., Cuadrado, J., Egiluz, Z., & Buruaga, A. (2017). Analysis of the influence of wood cladding on the thermal behavior of building façades; characterization through simulation by using different tools and comparative testing validation. *Energy and Buildings*, 141, 349-360. doi:10.1016/j.enbuild.2017.02.054
- Pesenti, M., Masera, G., & Fiorito, F. (2015). Shaping an Origami Shading Device through Visual and Thermal Simulations. *Energy Procedia*, 78, 346-351. doi:10.1016/j.egypro.2015.11.663
- Pesenti, M., Masera, G., Fiorito, F., & Sauchelli, M. (2015). *Kinetic solar skin: a responsive folding technique*. Paper presented at the International Conference on Solar Heating and Cooling for Buildings and Industry, SHC 2014.
- Pinterić, M. (2017). *Building Physics From physical principles to international standards*: Cham : Springer International Publishing : Imprint: Springer.
- Poppinga, S., Masselter, T., Lienhard, J., Schleicher, S., Knippers, J., & Speck, T. (2010). Plant movements as concept generators for deployable systems in architecture. *Design and Nature* V, 403-409.
- Poppinga, S., Zollfrank, C., Prucker, O., Ruhe, J., Menges, A., Cheng, T., & Speck, T. (2017). Toward a New Generation of Smart Biomimetic Actuators for Architecture. *Adv Mater*. doi:10.1002/adma.201703653
- Pourmohammadi, A. (2013). Nonwoven materials and joining techniques. In *Joining Textiles* (pp. 565-581): Elsevier.
- Premier, A. (2012). dynamic façades and smart technologies for building envelope requalification. *Screencity-International Academic journal*, 1, 65-69.
- Prowler, D. (2016). Sun control and shading devices. *Whole Building Design Guide*.
- Qingyan, C., & Van der Kooi, J. (1988). Accuracy—A program for combined problems of energy analysis, indoor airflow, and air quality. *ASHRAE Transactions*, 94, 196-214.
- Quinn, A. K. (2018).
- Reichert, S., Menges, A., & Correa, D. (2015). Meteorosensitive architecture: Biomimetic building skins based on materially embedded and hygroscopically enabled responsiveness. *Computer-Aided Design*, 60, 50-69. doi:10.1016/j.cad.2014.02.010
- Reyssat, E., & Mahadevan, L. (2009). Hygromorphs: from pine cones to biomimetic bilayers. *J R Soc Interface*, 6(39), 951-957. doi:10.1098/rsif.2009.0184

- Ritter, A. (2007). *Smart materials in architecture, interior architecture and design*: Walter de Gruyter.
- Rognoli, V., Ayala-García, C., & Parisi, S. (2016). *The emotional value of Do-it-yourself materials*. Paper presented at the Proceedings of 10th International Conference on Design & Emotion.
- Rossi, D., Nagy, Z., & Schlueter, A. (2012). Adaptive distributed robotics for environmental performance, occupant comfort and architectural expression. *International Journal of Architectural Computing*, 10(3), 341-359.
- Roudsari, M. S., Pak, M., & Smith, A. (2013). *Ladybug: a parametric environmental plugin for grasshopper to help designers create an environmentally-conscious design*. Paper presented at the Proceedings of the 13th international IBPSA conference held in Lyon, France Aug.
- Ruck, N. C. (1989). Building design and human performance.
- Rus, D., & Tolley, M. T. (2015). Design, fabrication and control of soft robots. *Nature*, 521(7553), 467-475. doi:10.1038/nature14543
- Sadineni, S. B., Madala, S., & Boehm, R. F. (2011). Passive building energy savings: A review of building envelope components. *Renewable and Sustainable Energy Reviews*, 15(8), 3617-3631. doi:10.1016/j.rser.2011.07.014
- Safer, N., Woloszyn, M., & Roux, J. J. (2005). Three-dimensional simulation with a CFD tool of the airflow phenomena in single floor double-skin facade equipped with a venetian blind. *Solar Energy*, 79(2), 193-203. doi:10.1016/j.solener.2004.09.016
- Salakij, S., Yu, N., Paolucci, S., & Antsaklis, P. (2016). Model-Based Predictive Control for building energy management. I: Energy modeling and optimal control. *Energy and Buildings*, 133, 345-358. doi:10.1016/j.enbuild.2016.09.044
- Sauchelli, M., Lobaccaro, G., Masera, G., & Fiorito, F. (2013). *Smart Solutions for Solar Adaptive Façade Preliminary studies for an innovative shading device*. Paper presented at the XIX IAHS World Congress,, Milan, Italy.
- Schaeffer, O., & Vogt, M.-M. (2010). *Move: architecture in motion-dynamic components and elements*: Walter de Gruyter.
- Schielke, T. (2014). Light Matters: Mashrabiya—Translating Tradition into Dynamic Facades. In: ArchDaily.
- Schleicher, S. (2016). *Bio-inspired Compliant Mechanisms for Architectural Design: Transferring Bending and Folding Principles of Plant Leaves to Flexible Kinetic Structures*. University of Stuttgart, Germany,

- Schleicher, S., Lienhard, J., Poppinga, S., Speck, T., & Knippers, J. (2011). *Adaptive façade shading systems inspired by natural elastic kinematics*. Paper presented at the Proceedings of the International Conference on Adaptive Architecture.
- Schleicher, S., Lienhard, J., Poppinga, S., Speck, T., & Knippers, J. (2015). A methodology for transferring principles of plant movements to elastic systems in architecture. *Computer-Aided Design*, 60, 105-117. doi:10.1016/j.cad.2014.01.005
- Scott, J. (2013). Hierarchy in knitted forms: environmentally responsive textiles for architecture.
- Scott, J. (2016). *Programmable Knitting*. Paper presented at the Acadia 2016 Posthuman Frontiers: Data, Designers, and Cognitive Machines: Projects Catalog of the 36th Annual Conference of the Association for Computer Aided Design in Architecture.
- Scrivener, S. (2002). The art object does not embody a form of knowledge.
- Scrivener, S., & Chapman, P. (2004). The practical implications of applying a theory of practice based research: a case study. *Working papers in art and design*, 3(1).
- Selkowitz, S., Papamichael, K., & Wilde, G. (1986). A concept for an advanced computer-based building envelope design tool.
- Shameri, M. A., Alghoul, M. A., Sopian, K., Zain, M. F. M., & Elayeb, O. (2011). Perspectives of double skin façade systems in buildings and energy saving. *Renewable and Sustainable Energy Reviews*, 15(3), 1468-1475. doi:10.1016/j.rser.2010.10.016
- Sharaidin, M. (2014). Kinetic facades: towards design for environmental performance.
- Sherif, A., El-Zafarany, A., & Arafa, R. (2012). External perforated window Solar Screens: The effect of screen depth and perforation ratio on energy performance in extreme desert environments. *Energy and Buildings*, 52, 1-10. doi:10.1016/j.enbuild.2012.05.025
- Sherif, A., Sabry, H., & Rakha, T. (2012). External perforated Solar Screens for daylighting in residential desert buildings: Identification of minimum perforation percentages. *Solar Energy*, 86(6), 1929-1940. doi:10.1016/j.solener.2012.02.029
- Sinibaldi, E., Argiolas, A., Puleo, G., & Mazzolai, B. (2014). Another Lesson from Plants: The Forward Osmosis-Based. *PLoS ONE*, 9(7).
- Sinopoli, J. M. (2009). *Smart buildings systems for architects, owners and builders*: Butterworth-Heinemann.
- Speck, T., & Speck, O. (2008). Process sequences in biomimetic research. I, 3-11. doi:10.2495/dn080011
- Stec, W., Van Paassen, A., & Maziarz, A. (2005). Modelling the double skin façade with plants. *Energy and Buildings*, 37(5), 419-427.

- Sterling, B. (2016). Diffusion Choir. Retrieved from <https://www.wired.com/beyond-the-beyond/2016/10/diffusion-choir/>
- Sterman, Y., Demaine, E. D., & Oxman, N. (2013). PCB origami: A material-based design approach to computer-aided foldable electronic devices. *Journal of Mechanical Design*, 135(11), 114502.
- Summers, D., Hanson, T., & Wilson, C. (1986). Validation of a computer simulation of wind flow over a building model. *Building and Environment*, 21(2), 97-111.
- Sun, L., Huang, W. M., Ding, Z., Zhao, Y., Wang, C. C., Purnawali, H., & Tang, C. (2012). Stimulus-responsive shape memory materials: A review. *Materials & Design*, 33, 577-640.  
doi:10.1016/j.matdes.2011.04.065
- Sung, D. (2016). Smart Geometries for Smart Materials: Taming Thermobimetals to Behave. *Journal of Architectural Education*, 70(1), 96-106. doi:10.1080/10464883.2016.1122479
- Tadayyon, G., Mazinani, M., Guo, Y., Zebarjad, S. M., Tofail, S. A. M., & Biggs, M. J. (2016). The effect of annealing on the mechanical properties and microstructural evolution of Ti-rich NiTi shape memory alloy. *Materials Science and Engineering: A*, 662, 564-577.  
doi:10.1016/j.msea.2016.03.004
- Toffoli, T., & Margolus, N. (1991). Programmable matter: concepts and realization. *Physica. D, Nonlinear phenomena*, 47(1-2), 263-272.
- Tolley, M. T., Felton, S. M., Miyashita, S., Aukes, D., Rus, D., & Wood, R. J. (2014). Self-folding origami: shape memory composites activated by uniform heating. *Smart Materials and Structures*, 23(9). doi:10.1088/0964-1726/23/9/094006
- Trivedi, D., Rahn, C. D., Kier, W. M., & Walker, I. D. (2008). Soft robotics: Biological inspiration, state of the art, and future research. *Applied Bionics and Biomechanics*, 5(3), 99-117.  
doi:10.1080/11762320802557865
- Tsoka, S., Leduc, T., & Rodler, A. (2021). Assessing the effects of urban street trees on building cooling energy needs: The role of foliage density and planting pattern. *Sustainable Cities and Society*, 65, 102633.
- Tzempelikos, A., & Athienitis, A. K. (2007). The impact of shading design and control on building cooling and lighting demand. *Solar Energy*, 81(3), 369-382.  
doi:10.1016/j.solener.2006.06.015
- Tzempelikos, A., Athienitis, A. K., & Karava, P. (2007). Simulation of façade and envelope design options for a new institutional building. *Solar Energy*, 81(9), 1088-1103.

- Ueda, M., & Nakamura, Y. (2006). Metabolites involved in plant movement and 'memory': nyctinasty of legumes and trap movement in the Venus flytrap. *Nat Prod Rep*, 23(4), 548-557.  
doi:10.1039/b515708k
- Varughese, J. P., & John, M. M. (2016). *Effect of emissivity of shading device and air flow inside cavity of Double Skin Facade for energy saving and Thermal Comfort in buildings: A CFD modeling*. Paper presented at the Energy Efficient Technologies for Sustainability (ICEETS), 2016 International Conference on.
- Velasco, A., Jiménez García, S., Guardo, A., Fontanals, A., & Egusquiza, M. (2017). Assessment of the Use of Venetian Blinds as Solar Thermal Collectors in Double Skin Facades in Mediterranean Climates. *Energies*, 10(11). doi:10.3390/en10111825
- Vergauwen, A., Alegria, M. L., Roovers, K., & De Temmerman, N. (2013). *Parametric design of adaptive shading elements based on Curved-line Folding*. Paper presented at the Proceedings of the first conference transformables, Seville, Spain.
- Vergauwen, A., De Temmerman, N., & Brancart, S. (2014). The design and physical modelling of deployable structures based on curved-line folding. 1, 145-155. doi:10.2495/mar140121
- Vergauwen, A., De Temmerman, N., & De Laet, L. (2014). *Digital modelling of deployable structures based on curved-line folding*. Paper presented at the Proceedings of the IASS-SLTE 2014 Symposium "Shells, Membranes and Spatial Structures: Footprints.
- Vergauwen, A., Laet, L. D., & Temmerman, N. D. (2017). Computational modelling methods for pliable structures based on curved-line folding. *Computer-Aided Design*, 83, 51-63.  
doi:10.1016/j.cad.2016.10.002
- Wagdy, A., Elghazi, Y., Abdalwahab, S., & Hassan, A. (2015). The Balance between Daylighting and Thermal Performance Based on Exploiting the Kaleidocycle Typology in Hot Arid Climate of Aswan, Egypt. In *AEI 2015* (pp. 300-315).
- Wang, J., Beltrán, L. O., & Kim, J. (2012). *From static to kinetic: A review of acclimated kinetic building envelopes*. Paper presented at the World Renewable Energy Forum, WREF 2012, Including World Renewable Energy Congress XII and Colorado Renewable Energy Society (CRES) Annual Conferen.
- Wang, L., & Wong, N. H. (2009). Coupled simulations for naturally ventilated rooms between building simulation (BS) and computational fluid dynamics (CFD) for better prediction of indoor thermal environment. *Building and Environment*, 44(1), 95-112.  
doi:10.1016/j.buildenv.2008.01.015



- Werner, C. (2013). *Transformable and transportable architecture: analysis of buildings components and strategies for project design*. Paper presented at the Universidad Politécnica de Cataluña, Barcelona, España.
- Wetter, M. (2009). Modelica-based modelling and simulation to support research and development in building energy and control systems. *Journal of Building Performance Simulation*, 2(2), 143-161.
- Wick, R., & Grawe, G. D. (2000). *Teaching at the Bauhaus*: Univerza v Ljubljani, Akademija za likovno umetnost in oblikovanje.
- Wigginton, M., & Harris, J. (2013). *Intelligent skins*: Routledge.
- Winters, A. (2017). *Why does soft matter? Exploring the design space of soft robotic materials and programmable machines*. Royal College of Art,
- Wong, P. C., Prasad, D., & Behnia, M. (2008). A new type of double-skin façade configuration for the hot and humid climate. *Energy and Buildings*, 40(10), 1941-1945.  
doi:10.1016/j.enbuild.2008.04.014
- Wood, A., & Henry, S. (2014). Best Tall Buildings. *Proceedings of the CTBUH Award Ceremony*, 2.
- Yakhot, V., & Orszag, S. A. (1986). Renormalization group analysis of turbulence. I. Basic theory. *Journal of scientific computing*, 1(1), 3-51.
- Ye, P., Harrison, S., Oosthuizen, P., & Naylor, D. (1999). Convective heat transfer from a window with a venetian blind: detailed modeling. *ASHRAE Transactions*, 105, 1031.
- Yoon, S.-H., Park, C.-S., & Augenbroe, G. (2011). On-line parameter estimation and optimal control strategy of a double-skin system. *Building and Environment*, 46(5), 1141-1150.
- Zanaboni, E. (2008). One Way and Two Way-Shape Memory Effect: Thermo-Mechanical Characterization of Ni-Ti Wires. *Universita degli Studi di Pavia, Pavia, Italy*.
- Zanghirella, F., Perino, M., & Serra, V. (2011). A numerical model to evaluate the thermal behaviour of active transparent façades. *Energy and Buildings*, 43(5), 1123-1138.
- Zhai, Z., Chen, Q., Haves, P., & Klems, J. H. (2002). On approaches to couple energy simulation and computational fluid dynamics programs. *Building and Environment*, 37(8-9), 857-864.
- Zhai, Z., & Previtali, J. M. (2010). Ancient vernacular architecture: characteristics categorization and energy performance evaluation. *Energy and Buildings*, 42(3), 357-365.  
doi:10.1016/j.enbuild.2009.10.002
- Zhai, Z. J., Zhang, Z., Zhang, W., & Chen, Q. Y. (2007). Evaluation of Various Turbulence Models in Predicting Airflow and Turbulence in Enclosed Environments by CFD: Part 1—Summary of

Prevalent Turbulence Models. *HVAC&R Research*, 13(6), 853-870.

doi:10.1080/10789669.2007.10391459

Zhang, Z., Zhang, W., Zhai, Z. J., & Chen, Q. Y. (2007). Evaluation of Various Turbulence Models in Predicting Airflow and Turbulence in Enclosed Environments by CFD: Part 2—Comparison with Experimental Data from Literature. *HVAC&R Research*, 13(6), 871-886.

doi:10.1080/10789669.2007.10391460

Zhao, J., Zhao, X., Jiang, Z., Li, Z., Fan, X., Zhu, J., . . . Pan, F. (2014). Biomimetic and bioinspired membranes: preparation and application. *Progress in Polymer Science*, 39(9), 1668-1720.

Zirkelbach, D., Schmidt, T., Kehrner, M., & Künzeli, H. (2007). Wufi® Pro—Manual. *Fraunhofer Institute*.